UNIVERSITA' DEGLI STUDI DI PARMA

Dottorato di Ricerca in Scienze della Terra

Ciclo XXII

MASS TRANSPORT COMPLEXES IN BACINI CONFINATI A CONTROLLO STRUTTURALE: L'UNITA' EPILIGURE DI SPECCHIO (APPENNINO SETTENTRIONALE)

Coordinatore:
Prof. Luigi Torelli

Tutor:
Dr. Roberto Tinterri

Dottorando: Kei Ogata

MASS TRANSPORT COMPLEXES IN STRUCTURALLY CONTROLLED BASINS: THE EPILIGURIAN SPECCHIO UNIT (NORTHERN APENNINES, ITALY)

A Dissertation

by

KEI OGATA

Submitted to the University of Parma

in fulfillment of the requirements for the degree of

DOCTOR OF PHILOSOPHY

Tutor:

Dr. Roberto Tinterri (University of Parma, Italy)

Co-tutors:

Prof. Emiliano Mutti

Prof. Gian Andrea Pini (University of Bologna, Italy)

March 2010

CONTENTS

Abstract……..……p. 9

1. Introduction……..……..……..p. 13

1.1 Objectives

1.2 Mass Transport Deposits and Complexes (MTDs and MTCs): an overview

1.3 Note on sedimentary chaotic units in the field

1.4 Note on tectonic chaotic units in the field

1.5 List of figures

2. Methodology……..…….....….p. 31

2.1 List of figures

3. Geologic setting: Northern Apennines……..……...……..p. 41

3.1 Epiligurian Units outline

3.2 Ranzano Unit outline

3.3 Specchio Unit outline

3.4 List of figures

4. Pessola Valley outlier..……..……...p. 73

4.1 Previous studies

4.2 Stratigraphy

4.3 Tectonic setting

4.4 List of figures

5. Mt. Roccone outlier……..……...p. 169

5.1 Previous studies

5.2 Stratigraphy

5.3 Tectonic setting

5.4 List of figures

6. Caffaraccia section (Mt. Barigazzo outlier)…….……p. 193

6.1 Previous studies

6.2 Stratigraphy

6.3 Tectonic setting

6.4 List of figures

7. Specchio Unit (R2) anatomy……..……p. 205

7.1 Matrix

7.2 Blocks

7.3 Structures

7.3.1 Folds
7.3.2 Ductile syn-sedimentary shear zones
7.3.3 Structure associations

7.4 Internal subdivisions of the Specchio Unit (R2)

7.5 Pessola Valley outlier……...…...p. 215

7.5.1 Sub-unit R2/a
7.5.2 Sub-unit R2/b
7.5.3 Sub-unit R2/c
7.5.4 Sub-unit R2/d
7.5.5 Sub-unit R2/e

7.6 Mt. Roccone outlier……..…p. 223

7.6.1 Sub-unit R2/d
7.6.2 Sub-unit R2/e

7.7 Caffaraccia Section (Mt. Barigazzo outlier)……..……..……p. 225

7.7.1 Sub-unit R2/c
7.7.2 Sub-unit R2/d

7.8 List of figures

8. Integration with modern examples…….....p. 343

8.1 Physical characteristics of a submarine landslide deposit

8.1.1 Triggering mechanisms
8.1.2 Transport mechanisms
8.1.3 Accumulation mechanisms

8.2 MTDs in modern convergent/collisional margin settings

8.3 General physiographic setting of an “active” margin

8.3.1 Nankai (SW Japan)
8.3.2 Cascadia (NW North America)
8.3.3 Sunda-Banda (S Indonesia)

8.4 Possible analogs for comparison purposes

8.4.1 NW Borneo
8.4.2 SW Taiwan
8.4.3 SW and NE New Zealand

8.5 List of figures

9. Results and Discussion……..……..p. 423

9.1 Kinematic models of emplacement for the R2 Specchio Unit

9.1.1 Matrix significance and blocky-flow deposits
9.1.2 Confining effects on MTD emplacement

9.2 Local basin characterization

9.2.1 Basin characteristics and MTDs significance
9.2.2 Hosting sedimentary successions depositional style

9.3 Regional implications for the Epiligurian succession

9.4 List of figures

10. Conclusions……..……...…….p. 441

Acknowledgments

Credits

References…….……p. 449

ATTACHMENTS:

I. PANEL n. 1: Geologic maps and cross sections (1:10.000 scale)
II. PANEL n. 2: Specchio Unit R2 structural data
III. PANEL n. 3: General stratigraphic logs
IV. PANEL n. 4: Detailed stratigraphic logs of the Specchio Unit R2 lower and upper contacts

Abstract

The recent increasing in geophysical exploration of continental margins and the concomitant progress of increasingly more sophisticated seismic- and acoustic-imagery technologies have shown the widespread occurrence of large accumulations of remolded sediments generated by submarine landslides, and commonly referred to as Mass Transport Deposits or Complexes (MTD and MTC, respectively).

These units are being intensively investigated, not only for strictly scientific reasons, such as their environmental significance, understanding of triggering processes, and their role in the transformation of density flows, but also because of economic and social implications, mainly in terms of hydrocarbon exploration and production, and geohazards.

On the other hand, field-based studies on ancient examples of MTDs are relatively scarce with respect to the huge amount of data derived from marine geology. Many problems arise from the tentative comparison of the data derived from these two different approaches, mainly because of the resolution limits and scaling problems between these methods, and for the limited occurrences of comparable geodynamic contexts and relative unambiguous interpretations (*i.e.* collisional/convergent *versus* divergent margin settings). This is particularly evident for accretionary systems, where several controlling factors combine to produce "chaotic units" at different scales.

This kind of situation highlights the need of a systematic comparison and an integrated approach to the study of such units for a better understanding of their geologic significance, especially for those depositional environments located on top of accretionary prisms, which represent an ideal setting for studying the role of mass transport deposits in the wedge evolution, in spite of their yet relatively poor recognition in the modern and ancient rock record.

Keeping in mind the above problems and in order to partly fill this gap, this study has been carried out through a field-based work carried on an ancient example of MTC, known as the Specchio Unit among the Apennine geologists, and typically developed on top of an accretionary prism. This unit occurs within the lower Rupelian rocks of the syn-orogenic sedimentary record of the Eocene-Oligocene Epiligurian succession, cropping out in the eastern side of the Northern Apennines (Italy) as isolated sedimentary remnants (*i.e.* outliers), representing the fill of local intra-slope basins developed on top of the translating Ligurian Nappe (*i.e.* proto-Apenninic accretionary wedge).

This study has been developed through cartographic- to microscopic-scale stratigraphic and structural analyses, collected directly on the slide bodies and on the over- and under-lying

sedimentary succession, along with an attempt of systematic comparison with so far recognized modern analogs, focusing on both the slide-related features and the overall physiography of the original depositional setting.

The first important result coming out from these detailed outcrop studies, is the subdivision of this MTC into five sub-units, representing at least four distinct MTDs: the lower ones, of local significance, derived from the southern sectors, and the upper ones, of basin-wide extent, derived from the northern sectors. The largest MTD reaches an inferred volume of involved material of about 150 km^3. The vertical stacking of these MTDs and the progressively "shallower water nature" of the internal components, seems to represent the deposition from closely spaced events, originated through a retrogressive failure process, involving progressively more proximal areas.

Careful observations carried on the internal elements of these units (*i.e.* matrix and blocks) allow considerations on slide mechanics, with the detailed characterization of sedimentary bodies generated by catastrophic processes, which include both slump- and debris flow-like facies (*i.e.* blocky-flow deposits of Mutti *et al*., 2006), and the influence exerted by structural confinement on the slide emplacement, mainly in term of forced slide direction, localized over-thickening, substrate coupling (bed erosion in a sedimentological sense) and margin-induced strain partitioning. In particular, this study highlights the likely occurrence of a generalized lateral buckling (compression + transpression), transversally to the main sliding direction, and an overall unidirectional shearing in the longitudinal sense, giving important information on the slide kinematics.

This study also contributes to the understanding of the local intra-slope basin configuration, highlighting the differences in facies associations between pre- and post-slide emplacement sedimentary successions, and the possible existence of an overall shallow level tectonism (gravity-related?). This kind of "slope-tectonics"-type regime forecasts the synergic development of thrust- and strike slip-related shale diapirism and local, small-scale MTDs, affecting basin margins and intrabasinal highs, and contributing to the development of an overall above-grade slope physiography.

Moreover, some regional considerations on the palaeogeograhic setting of the lower Rupelian Epiligurian succession can be made, integrating the so far accepted hypothesis from the literature with the results of this study, mainly in terms of transport directions, provenance and environmental significance of the involved material. The evidence of a far-located calcalkaline volcanism (in particular here I report the first recognition of resedimented volcaniclastic beds in the sedimentary succession on top of the Specchio unit, in the Pessola Valley outlier), along with the climatic- and tectonic-related signatures characterizing the restored sedimentation, could contribute in

constraining the possible triggering mechanisms and preconditioning factors of slide development, thus giving indirect information on the general configurations of source areas.

These observations demonstrate that further specific studies on previously overlooked "chaotic" units may significantly contribute to a better understanding of the Apenninic orogenic system, and, at the same time, introducing new challenges for their application into other orogenic belts worldwide.

Part of these conclusions are in contrast with the nowadays-generalized belief that seismically active convergent margins are characterized by the occurrence of relatively few and smaller scale MTDs, if compared to divergent margin settings. In such contexts, submarine landslides are thought to develop close to the main deformation front, commonly located in deep-water settings.

Apart from some specific convergent margins (*e.g.* southern Cascadia, NE New Zealand, western Aleutinian Arc), particularly those involving a continental collision (*e.g.* NW Borneo), where some catastrophic, large-scale MTDs are observed to occur, in typical convergent margin settings (particularly those involving oceanic crust consumption; *e.g.* offshore Perù, Costa Rica), MTDs sharing huge dimensions with those of divergent margins are instead characterized by overall slow-rate motion, and are thought to be commonly linked to subduction dynamics (*e.g.* colliding seamount).

In spite of these interpretations, this work seems to confirm the possible occurrence of catastrophic, large-scale MTDs on the internal depositional domains of an accretionary prism (*i.e.* internally from the main tectonic front), which may originate from shallow-water regions, also possibly involving near-shore areas, with consequent important implications, for example, in terms of geohazard purposes.

In summary, it is possible to suggest that an integrated field-based approach to the study of MTDs may significantly contribute to solve some scaling problems about submarine landslide deposits. In particular, this approach should be useful in facing the difficulties regarding the interpretation of "chaotic" units cropping out in orogenic belts, as well as those characterizing modern submarine collisional belts.

1. INTRODUCTION

Chaotic sedimentary bodies originated by submarine mass-wasting processes are widely recognized in both the sedimentary record of ancient basins and in the present-day seafloor in continental margin setting.

During the last three decades these bodies have received significant consideration from the scientific community, mainly in term of specific academic interests, such as the distinction between different genetic processes (*i.e.* slides, slumps, debris avalanches and flows) and the flow evolution with respect to the generation of density flows (*i.e.* grain flows and turbidites) (*e.g.* Hampton, 1972; Middleton and Hampton, 1973; Lowe, 1982; Stow, 1986; Mutti, 1992; Mulder and Cochonat, 1996; Piper *et al.*, 1999; Mohrig and Marr, 2003).

Characterization of these bodies in exhumed sedimentary successions is a useful tool for stratigraphic analysis in that they represent excellent markers, helping to delineate basin morphologies and syn-sedimentary tectonic movements (*e.g.* Rupke, 1976; Woodcock, 1976, 1979; Ori *et al.*, 1986; Lucente, 2000; Mutti *et al.*, 2002; Roveri *et al.*, 2003).

The detailed knowledge of these deposits can help in distinguishing between superficial soft-sediment deformation due to mass transport and shallow deformation induced by tectonics in un-consolidated sediments (Elliot and Williams, 1988; Steen and Andersen, 1997). Therefore such studies are useful to understand the complex relationships between mass wasting and tectonic processes in the origin of stratally disrupted rock units (*i.e. mélanges*) representing considerable part of accretionary wedges (Raymond, 1984; Cowan, 1985; Orange and Underwood, 1995) (fig. 1.1).

Moreover, these studies have important applications to the study of submarine geohazards both in deepwater and coastal settings: submarine landslides can destabilize offshore-engineered structures (*i.e.* platforms, pipelines, submarine cables) and cut back through the shoreline in populated areas, also generating tsunamis which wave-forms seem to be controlled by landslide kinematics (Prior and Coleman, 1982; Moore and Moore, 1984; Von Huene *et al.*, 1989; Harbitz, 1992; Jiang and LeBlond, 1992; Hampton *et al.*, 1996; Masson *et al.*, 2002; Trifunac *et al.*, 2002; Shipp *et al.*, 2004) (fig. 1.2).

Another important aspect in this research field is the linkage between these events and the release of huge quantities of methane, with possible global climatic implications (Nisbet and Piper 1998; Nisbet, 2002) (fig. 1.3).

Finally, the correct understanding of such deposits has also economic repercussions for hydrocarbon exploration in offshore areas, mainly because of operative security purpose and seal/reservoir distributions (Weimer and Shipp, 2004; Amerman, 2004).

The huge amount of data coming from marine geology of modern continental margins strongly enhanced our understanding of the overall morphology of mass transport deposits. Side-scan images, multi-beam morpho-bathymetry, 2D and 3D high resolution seismic and sub-bottom profiles provide detailed outlining of the external geometries, vertical/lateral extension and surface/basal attitude of these deposits (*e.g.* Dingle, 1977; Embley and Jacobi, 1977; Prior *et al.*, 1982a, 1984; Normark and Gutmacher, 1988; Trincardi and Normark, 1989; Trincardi and Argnani, 1990; Huvenne *et al.*, 2002, Canals *et al.*, 2004). These studies however provide only partial information about the internal anatomy of these bodies, mainly because of the resolution limit of the geophysical method, the ambiguity of interpretation (*e.g.* Gardner *et al.*, 1999; Lee *et al.*, 2004) and the common presence of transparent zones (Coleman and Garrison, 1977).

By contrast, ancient mass transport deposits exposed in orogenic belts provide detailed information on the internal and external structures (*i.e.* upper and lower contacts, lateral relationships with encasing sediments), and thus allowing important considerations on triggering mechanisms, sediment transport/erosion and depositional processes.

Field-based approach is thus a fundamental tool for this task, even though some problems still remain: for example, relating vertical and lateral changes of internal deformations to the overall geometry of the deposits is limited by the detailed character of certain studies, often focused on small-scale bodies or single outcrops of larger bodies (*e.g.* Vries Klein *et al.*, 1972; Woodcock, 1976; Farrel, 1984; Gawthorpe and Clemmey, 1985; Pickering, 1987; Martinsen, 1989; Tarquin Teale and Young, 1987; Martinsen and Bakken, 1990; Leigh and Hartley, 1992). The evident limit of this kind of study is the overall scarcity (or missed recognition) of extensive, widely distributed and clearly correlatable exposures of well-preserved large-scale mass transport deposits (Ineson, 1985; Macdonald *et al.*, 1993).

Another stimulating problem arising from integration of geophysical and outcrop data is that modern active and convergent margins don't show evidence of widespread large-scale submarine landslides as instead observable in exposed orogenic belts (Camerlenghi *et al.*, 2009).

The recent increase of field-based studies on ancient mass transport deposits highlights the need for a modern integrated methodological approach to completely fill theses conceptual gaps that still separates interpretations concerning ancient and modern mass transport deposits (Lucente and Pini, 2003, 2008; Lucente *et al.*, 2006; Callot *et al.*, 2008a, 2008b; Draganits *et al.*, 2008; Van der Merwe *et al.*, 2009).

1.1 Objectives

The aim of this work is the wide-ranging study of MTDs occurring in confined basins on top of accretionary prisms, and the selected case study for field-based investigations is the Specchio Unit, a thick mass transport complex emplaced in the Eocene-Oligocene syn-orogenic Epiligurian sedimentary succession of the Northern Apennines (Italy).

Detailed geo-structural and stratigraphic analyses, integrated with observations on present day geophysical analogs from marine geology, are herein used to characterize the anatomy of the Specchio Unit and its relationships with the hosting sediments. This approach is herein used to test some hypothesis regarding:

- Mass transport driving mechanisms (*i.e.* triggering, sliding, accumulation and post-depositional processes) leading to the origin of the Specchio Unit and its component;
- Local basin configuration (*i.e.* stratigraphic character and relationships with over- and underlying bedded sediments, number and provenance of every single event which compose the whole Specchio Unit and relationships between structures and basinal morphologies);
- Regional paleogeographic configuration of Epiligurian mini-basins.

1.2 Mass Transport Deposits and Complexes (MTDs and MTCs): an overview

The huge amount of new data coming from study of present-day continental margins and the consequent over-production of models and classifications are quite congesting the inherent literature, well exceeding the assimilation potential of the scientific community. This fact is also highlighted by the overwhelming use of ambiguous terms to define such deposits, in both marine and field-based geology.

In this context, the terms MTD and MTC, which are originally seismo-stratigraphic definitions (Weimer, 1989), have been recently used to identify ancient submarine landslide-related chaotic sedimentary bodies, spanning from slide/slumps to debris-flow deposits (*e.g.* Pickering and Corregidor, 2005).

For reason of simplicity here I refer to Mass Transport Deposits (MTD) as sedimentary accumulation emplaced during a single Mass Transport Event (MTE; *sensu* Amerman, 2004). Close association of genetically and evolutionary related MTD constitutes a Mass Transport Complex (MTC); in other words, an MTC is intended as the product of more linked MTE.

1.3 Note on sedimentary chaotic units in the field

Here I briefly discuss the state-of-the-art concerning submarine sliding-related chaotic bodies from an outcrop perspective (for an extensive review, see Pini, 1999; Dykstra, 2005a, 2005b).

The current field-based terminology regarding sedimentary chaotic units is quite overwhelmed and confused, mainly because of several factors:

1) possible occurrence of more than one genetic process;
2) high diversification and the strong morphologic convergence of products;
3) world-wide distribution, generally un-related to geodynamic setting;
4) general lacking of well exposed examples and/or missed recognition due to limited outcrops;
5) different and unlinked static classifications used for both marine geology surveys and outcrop-based studies.

From a strictly field-based sedimentological approach these deposits can be differentiated on the basis of their mesoscopic appearance, texture and composition. An attempt to define these chaotic facies has been made by Mutti (1985, unpublished data; fig. 1.4).

The classical subdivision of submarine mass wasting deposits were made by Dott (1963), Carter (1975) and Nardin *et al.* (1979) (fig. 1.5).

Generally speaking, deposits produced from various gravitational mass transport processes are defined in the literature with terms as “slump” and “slide” (Woodcock, 1979; Prior and Coleman, 1982; Gawthorpe and Clemmey, 1985; Pickering *et al*., 1986). There is the overall agreement in making a clear distinction between slump and slide mechanisms: slump masses move upon an upwards-concave basal detachment surface (rotational movements), developing a wide range of internal deformational structures, whereas slide masses glide over a planar detachment surface (translational movements), showing no or little internal deformation (Stow, 1986; Nemec, 1990; Shanmugan *et al.*, 1995) (Fig. 1.6).

As already pointed out by Lucente and Pini (2003, 2008) and Lucente *et al.* (2006), within large mass transport bodies, slide-like deposits (*i.e*. associations of relatively undeformed slide blocks of either intra- ad extra-basinal origin) usually coexist (especially in foredeep settings) in close association with slump-like deposits, and progressive stratal disruption (*i.e.* downslope increases of mass desegregation) is interpreted as the primary cause for the transformation of slumps into debris flows (Mutti *et al.*, 2006).

Similar mass wasting associations have been documented from present day seafloor examples (*e.g.* Jacobi, 1976; Prior *et al.*, 1984; Normark and Gutmacher, 1988; Masson *et al*., 2002; Minisini,

2007). The exponential increase of deep-water geophysical imagery of modern continental margins, especially due to hydrocarbon exploration, unravels several different seismic facies coexisting within huge submarine landslide accumulations; these deposits has been classically referred as large-scale *Mass Transport Deposits* or *Complexes* (MTD or MTC; Weimer, 1989; Weimer and Shipp, 2004; McGilvery *et al.*, 2004).

In the classical concerning literature, another controversial term is *olistostrome*. This term was firstly introduced by Flores (1955, 1959) to indicate polymictic (*i.e.* extrabasinal, exotic in respect to hosting sediments) sedimentary chaotic bodies, characterized by block-in-matrix fabric, and comprised inside layered sequences of normal marine deposits. This definition, originally used by the above-mentioned author for the Tertiary succession of Sicily, has been extended to similar bodies in the rest of Apennines (*e.g.* Abbate *et al.*, 1970, 1981; Elter and Trevisan, 1973; Ricci Lucchi, 1975; Naylor, 1981, 1982; Pini, 1999) and in other orogenic belts worldwide (Page, 1978; Aalto, 1981; Díaz-del-Río *et al.*, 2003).

This term doesn't include any size information (Abbate *et al.*, 1981) and the currently accepted broad definition includes the following types of sedimentary chaotic bodies (Abbate *et al.*, 1981; Pini, 1999; Cowan and Pini, 2001; Lucente and Pini, 2003):

- bodies with cm- to m-sized blocks dispersed in a clay and/or sand-silt matrix (type A olistostromes; Pini, 1999);
- bodies with tens to hundreds of meters-sized blocks (*i.e.* olistoliths), contained in a matrix with the same features of the type A olistostrome (type B olistostrome; Pini, 1999);
- bodies almost completely composed of blocks (*i.e.* olistoliths swarms), without a significant amount of matrix (type C olistostrome; Lucente and Pini, 2003).

The origin of these bodies is due to different types of gravitational mass movements, such as block slides, debris avalanches, debris flows and hyper-concentrated flows (fig. 1.7).

It's also important to note that, even if the term *mélange* (Greenly, 1919; Hsü, 1968, 1974; Silver and Beutner, 1980; Raymond, 1984) has been classically used in the international literature to indicate tectonic product, the term olistostrome has been actually applied to mélange in many orogenic belts, implying a possible origin from mass wasting processes (*e.g.* among many others, Cowan, 1985; Page, 1978; Hibbard and Williams, 1979; Swarbrick and Naylor, 1980; Page and Suppe, 1981; Brandon, 1989; Taira *et al*., 1992; Bader and Pubellier, 2000; Kuzmichev *et al.*, 2001; Alonso *et al.*, 2006; Vollmer and Bosworth, 1984, Festa *et al.*, 2009).

The conceptual subdivision used in this work is based on the dynamic classification of MTD recently proposed by Mutti *et al.* (2006, unpublished data), based on field observations mainly collected from the Apennines (Italy), the Pyrenees (Spain) and the Néuquen basin (Argentina), and

preliminarily integrated with geophysical data coming from South America Atlantic continental margin (offshore Brazil).

This classification focuses on general rheologic behaviour, downslope desegregation and consolidation degree of the involved material. The deposits and related processes are thus defined by six linked end-members, which are arranged in a broad spectrum spanning from block falls and avalanches to the classical turbidity current. These authors (*i.e.* Mutti and Carminatti, oral presentation from Mutti *et al.*, 2006) also suggest the introduction of a new category of mass transport body termed *blocky-flow deposit*, conceptually representing an intermediate member between slump and debris flow deposits (fig. 1.8).

This kind of deposit has been interpreted as product of a complex flow that is similar to a debris flow, or hyper-concentrated flow, except for carrying out-size coherent and internally deformed blocks (meters to hundreds of meters across) usually arranged in isolated slump folds. The origin of blocky flows is still difficult to understand only with presently available data, particularly because of the contemporary developing of coherent slide blocks and a plastic flow that carry them as floating elements over long distance.

During the last ten years field-based works on these topics have been considerably improved, mainly because of the significative contribution given by marine geology and the needed of a modern integrated approach for studying large-scale fossil submarine landslides (Lucente and Pini, 2003, 2008; Pickering and Corregidor, 2005; Dykstra, 2005a, 2005b; Yamamoto *et al.*, 2007; Strachan, 2002, 2008; Callot *et al.*, 2008a, 2008b; Draganits *et al.*, 2008; Van der Merwe *et al.*, 2009).

1.4 Note on tectonic chaotic units in the field

These kinds of units as commonly referred to as *tectonosomes*, *tectonites*, (tectonic) *mélanges* and *broken formations* (Hsü, 1974; Vollmer and Bosworth, 1984; Cowan, 1985; Byrne, 1985; Castellarin *et al.*, 1986; Bettelli *et al.*, 1994, 1996a, 1996b; Pini, 1999).

On the field, these bodies generally present a marked *in situ* tectonic desegregation of the primary internal structures (*i.e.* sedimentary), without clear evidences of incipient metamorphism. Usually, these units share different degrees and styles of deformation, spanning from the simple *boudinage* (*i.e.* layer-parallel deformational process enucleating separate elements through the generalized extension of bed packages characterized by different rehologic behaviours) to the block-in-matrix fabric in extreme cases, mostly depending on timing and entity of the tectonic deformation.

The classical diagnostic indicator for discrimination of these units from sedimentary ones is the missing of depositional upper contacts with the background lithologies and clear tectonic-induced structures (*i.e.* mineralized veins, generalized brittle deformations, cathaclasis and grain-breakage, etc.). Also the recognition of a brecciated texture in the fine-grained lithologies (*i.e.* matrix) may be indicative of a mass wasting process instead of a tectonic one (Bettelli *et al.*, 1996a; Pini, 1999).

Moreover, these bodies seem to share an apparent internal structural order, usually highlighted by a common planar orientation of bodies, blocks and textural characteristics, virtually recognizable at different scales. Particularly, the matrix generally show evidence of a more or less pervasive scaly fabric, represented by an oriented foliation caused by simple shear mechanisms: the foliated appearance is due to the presence of prismatic-lenticular flakes, usually with slickenside striations and polished surfaces, recognizable at the micro- and meso-scale (*i.e.* microlithons and lithons, respectively), developed through the intersection of two or more shear planes with curvilinear and anastomosing trends (Maltman *et al.*, 1997; Vannucchi and Maltman, 2000; Vannucchi *et al.*, 2003).

In the most of the studied examples, the scaly fabric marks a type of pseudo-stratification often roughly parallel to the main tectonic contacts bounding these units; as observable from a cartographic point of view, this kind of oriented trend shows a significant concordance with the geometrical disposition of the unit and the main local tectonic structures.

Following criteria proposed by Pini (1999), these tectonosomes should be identified from some features as: 1) fault-bounded units or bodies with different dimensions (meters- to tens of kilometers-sized); 2) monomyctic (*i.e.* intraformational) lithologies; 3) common planar orientations of elements (*i.e.* still stratified or fragmented beds), giving some kind of internal order; 4) multi-scale coincident structural order of deformational features as *boudins*, fold axial surfaces, element stacking, thrusts, pinch-and-swell structures and scaly fabric; 5) cartographic-scale evidence of development of elongated “belts” and “bands”, cross-cutting adjacent stratigraphic successions and sharing common orientation with main tectonic lineaments (fig. 1.9).

Deformational mechanisms proposed for the origin of such units in accretionary settings are essentially attributed to extensional flattening processes linked to low-angle duplications (Castellarin *et al.*, 1986) and tectonic-gravitative spreading developed through progressive simple shearing (Cowan, 1985). These deformations are characterized by a generalized mesoscopic ductile behaviour, developed at low confining pressure (*e.g.* shallow-level tectonics), in poorly- or un-lithified sediments with high contrast of competence between lithotypes and high fluid content (*i.e.* excess pore pressure regimes).

According to these interpretations, besides the lacking of syn-kinematic metamorphism, evidence of hydro-fracturing are also documented (*i.e.* fragmentation of rock *continuum* due to overpressured fluids migration). The scaly fabric recorded within the matrix is thus interpreted as product of a progressive simple shear coupled with slow overpressured fluid expulsion.

Moreover, as confirmed by data coming from SEM and optical microscopy, this mesoscopic ductile behaviour can be attributed to an independent particulate flow without evident granular breakage, highlighting shallow deformational settings.

In extremely tectonized units, block-in-matrix fabric should be developed, without any evidence of an internal structural order. Recent studies carried on the Basal Complexes of Northern Apennines Ligurian Units introduced two main hypothesis regarding this block-in-matrix fabric development: the first one, proposed by Cowan and Pini (2001), avails oneself of a bed-transposition mechanism, characterized by earlier extensional (*i.e. boudinage* and layer-parallel fragmentation of competent beds) and later compressive processes (*i.e.* progressive dislocation and stacking of blocks and *boudins* through mesoscopic thrusting and inverse faults).

The second hypothesis, proposed by Bettelli and Vannucchi (2003), forecasts a dismembering of competent beds through layer-parallel extensions acting in two orthogonal directions, with some kind of “chocolate tablet” fashion; this type of deformation is justified by the superimposition of two co-planar isoclinalic folding events, with orthogonal axial directions (*i.e.* type 2 folds interference pattern of Ramsey, 1967) (fig. 1.10).

1.5 List of figures

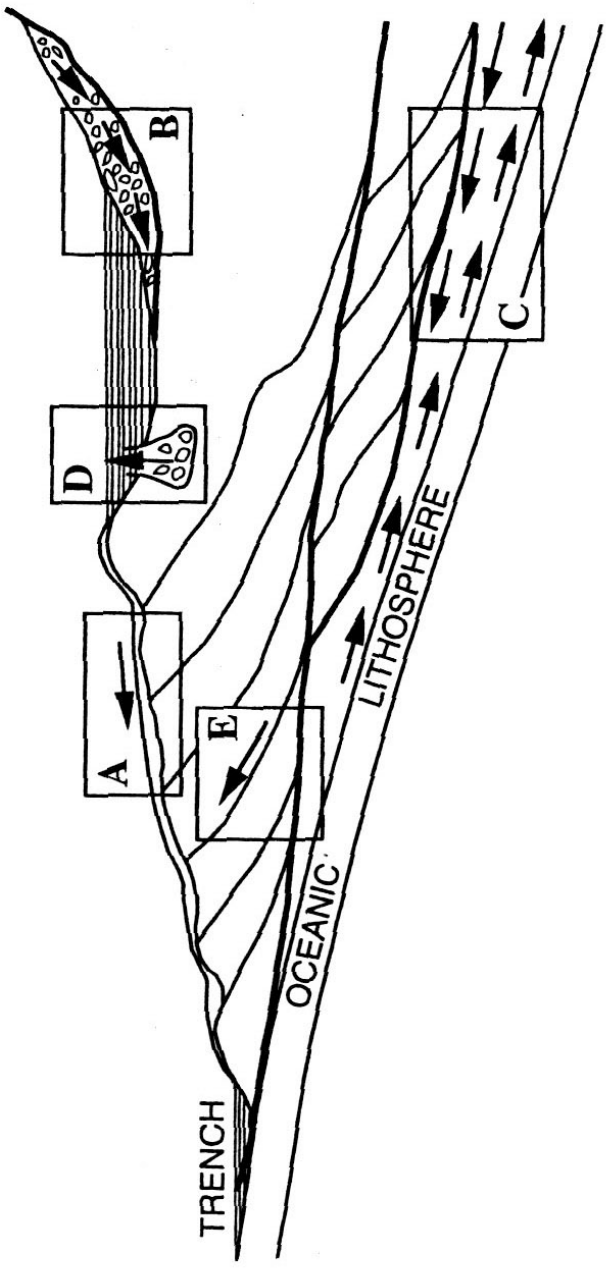

Figure 1.1 - Schematic section of an accretionary prism showing the main localization of sedimentary/tectonic chaotic bodies and inferred stratal-disruption generation zones:

- **A.** Slope tectonics-related units (gravity-induced lateral spreading);
- **B.** Large- and small-scale mass transport deposits;
- **C.** Subduction channels (flow-*mélanges*);
- **D.** Intrusions and extrusions of remobilized material (mud diapirs and mud volcanoes);
- **E.** Shear zone-related *mélanges* (broken-formations)

Modified from Cowan (1985) after Orange & Underwood (1995).

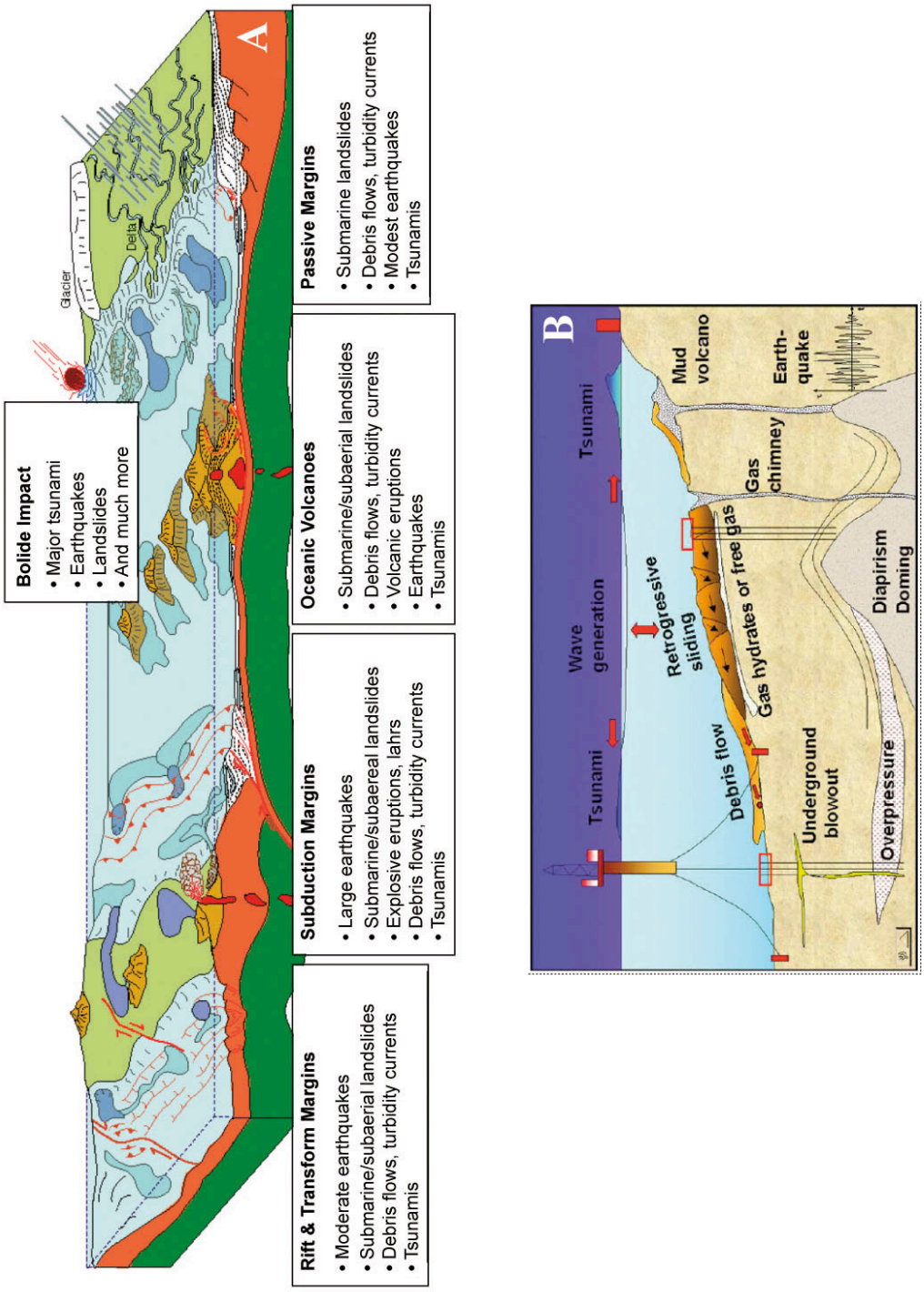

Figure 1.2 - **A.** Schematic representation of typical geohazards occurring in different continental margin settings. Submarine slides are known to occur mainly as a consequence of the natural evolution of continental margins. From Morgan *et al.* (2008; IODP Geohazard Workshop Report), available at http://www.iodp.org/geohazards

B. Cartoon showing offshore geohazards linked to submarine slides generated by human activity. These events are recognized as submarine geohazards for first party (seabed structures) and for third party (population) mainly because of their potential to generate tsunamis.From Camerlenghi *et al.* (2007).

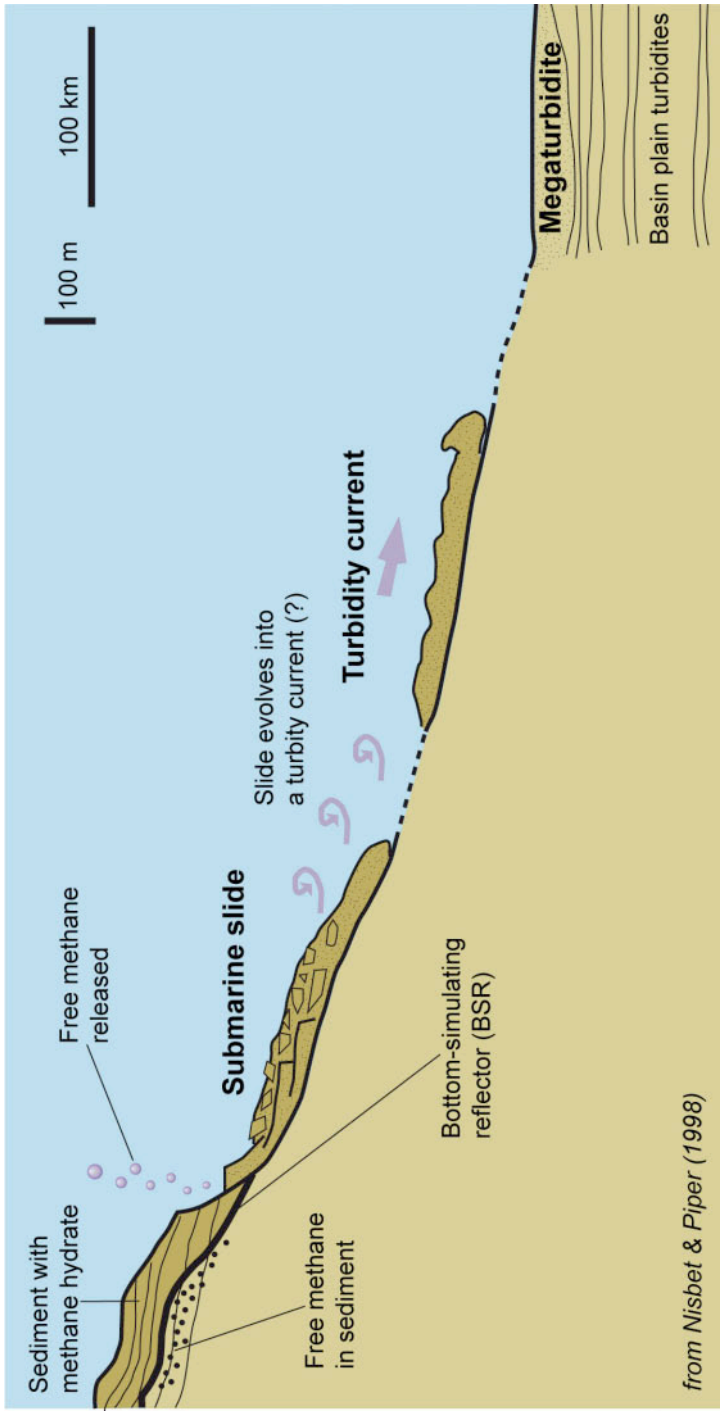

Figure 1.3 - Scheme showing the likely mode of formation of a mega-turbidite deposit (*sensu* Rothwell *et al.*, 1998; 2000). The perturbation and subsequent collapse of unstable sediment accumulations may be associated to strong methane release. The resulting submarine landslide may evolve in a flow of dense current of sediment (turbidity current) downward a continental slope. The final result is a turbidite sequence in the abyssal plain.
Redrawn from Nisbet & Piper (1998).

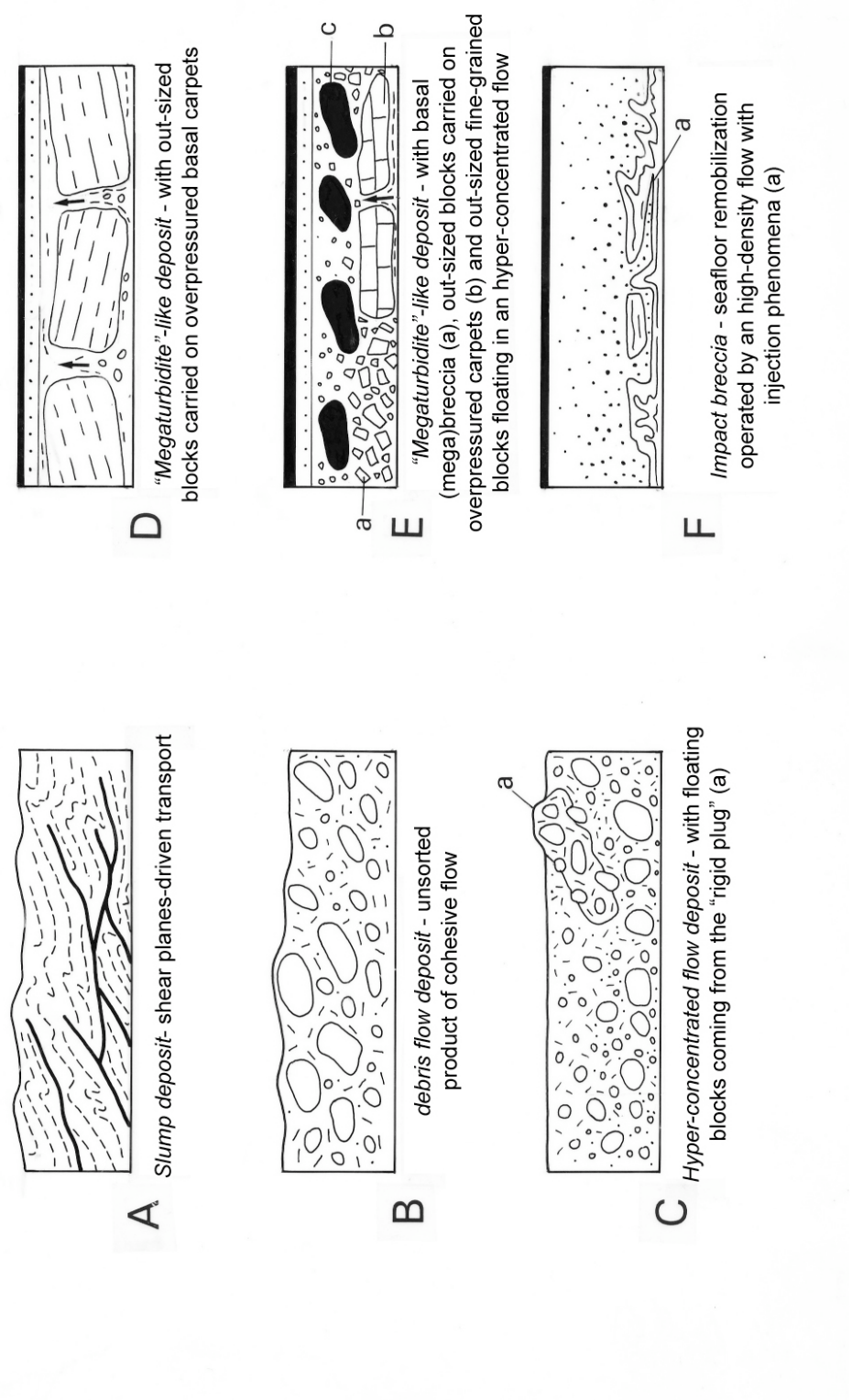

Figure 1.4 - Scheme of sedimentary chaotic units facies based on outcrop observations. From Mutti (1985,unpublished data).

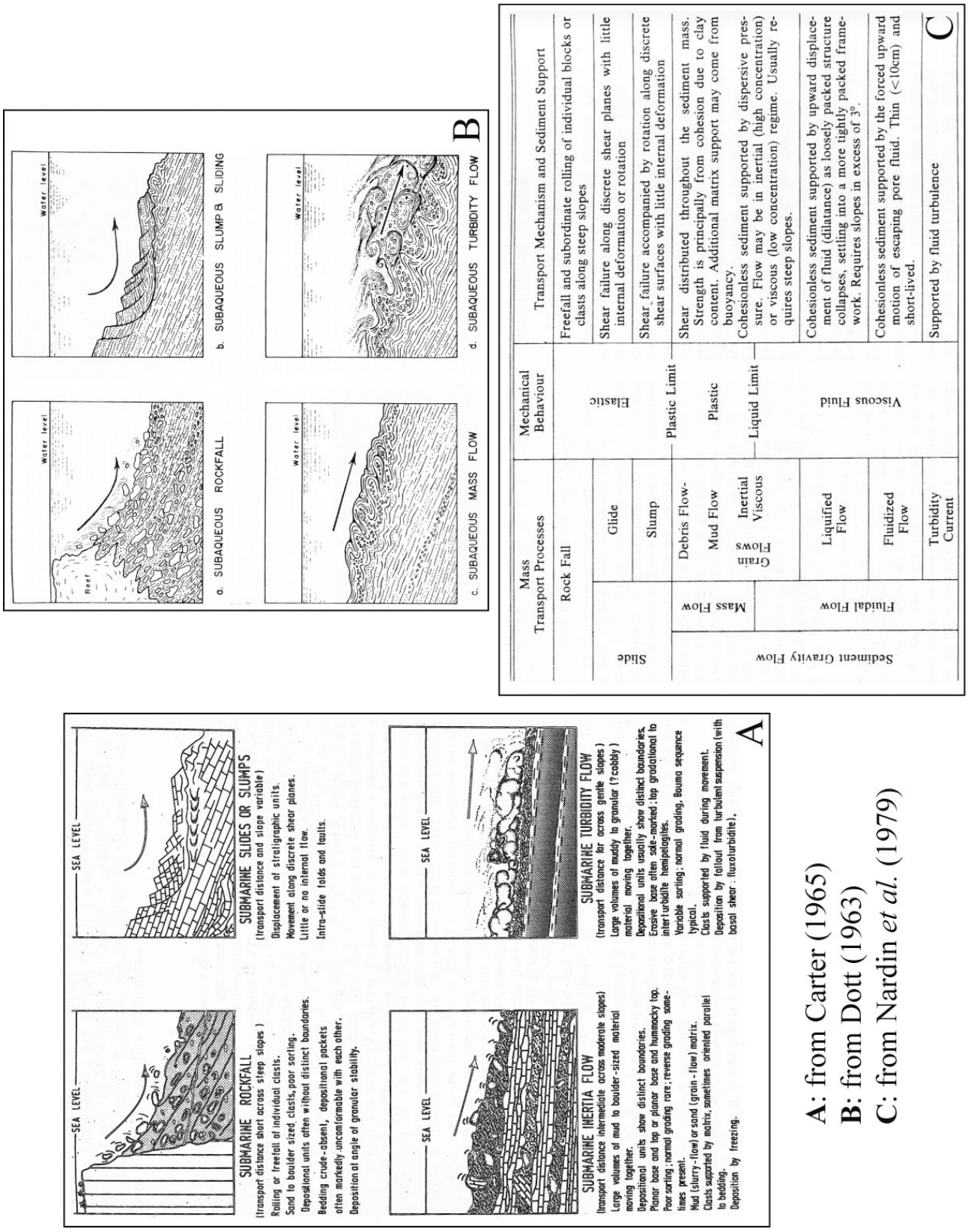

Figure 1.5 - Classical diagrams and schemes depicting the spectrum of submarine mass transport processes. **A.** from Carter (1975), **B.** from Dott (1963) and **C.** from Nardin *et al.* (1979).

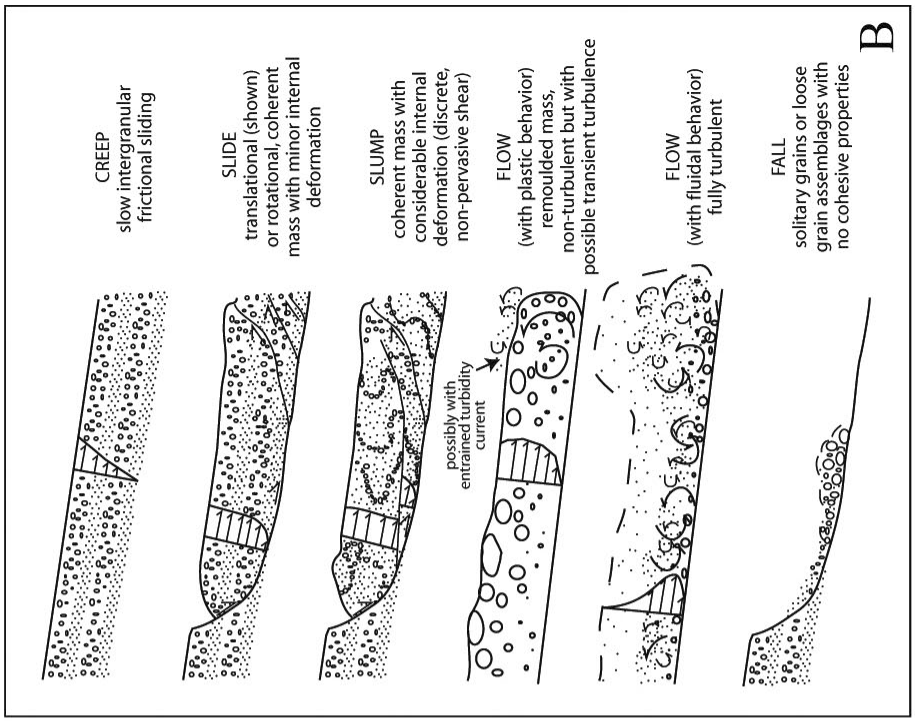

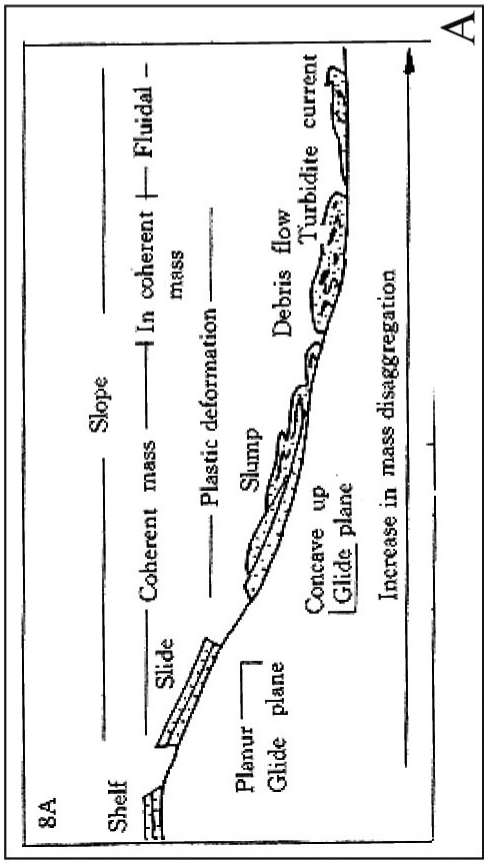

A: from Shanmugan *et al.* (1995)
B: from Nemec (1990)

Figure 1.6 - More recent classification schemes regarding mass transport processes and their possible mutual relationships. **A.** from Shanmugan *et al.* (1995) and **B.** from Nemec (1990).

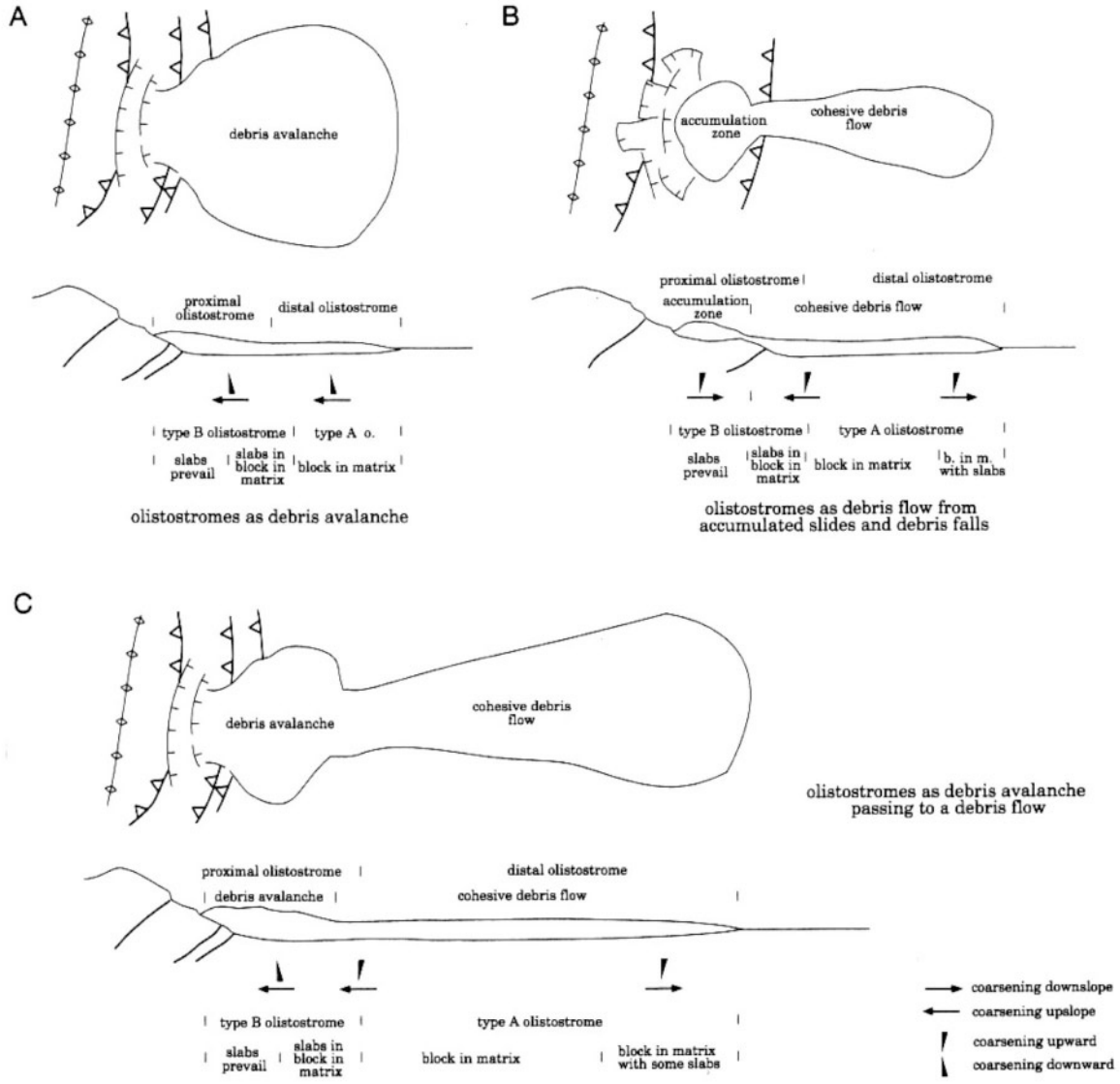

Figure 1.7 - Interpretative diagram showing thrust tectonics-related mass transport deposits development. **A.** single catastrophic event in the frontal slope; **B.** flow-like event coming from accumulationzone of other distinct MTDs; **C.** single catastrophic slope collapse evolving in a flow-like event downslope (from Pini, 1999; see text for details).

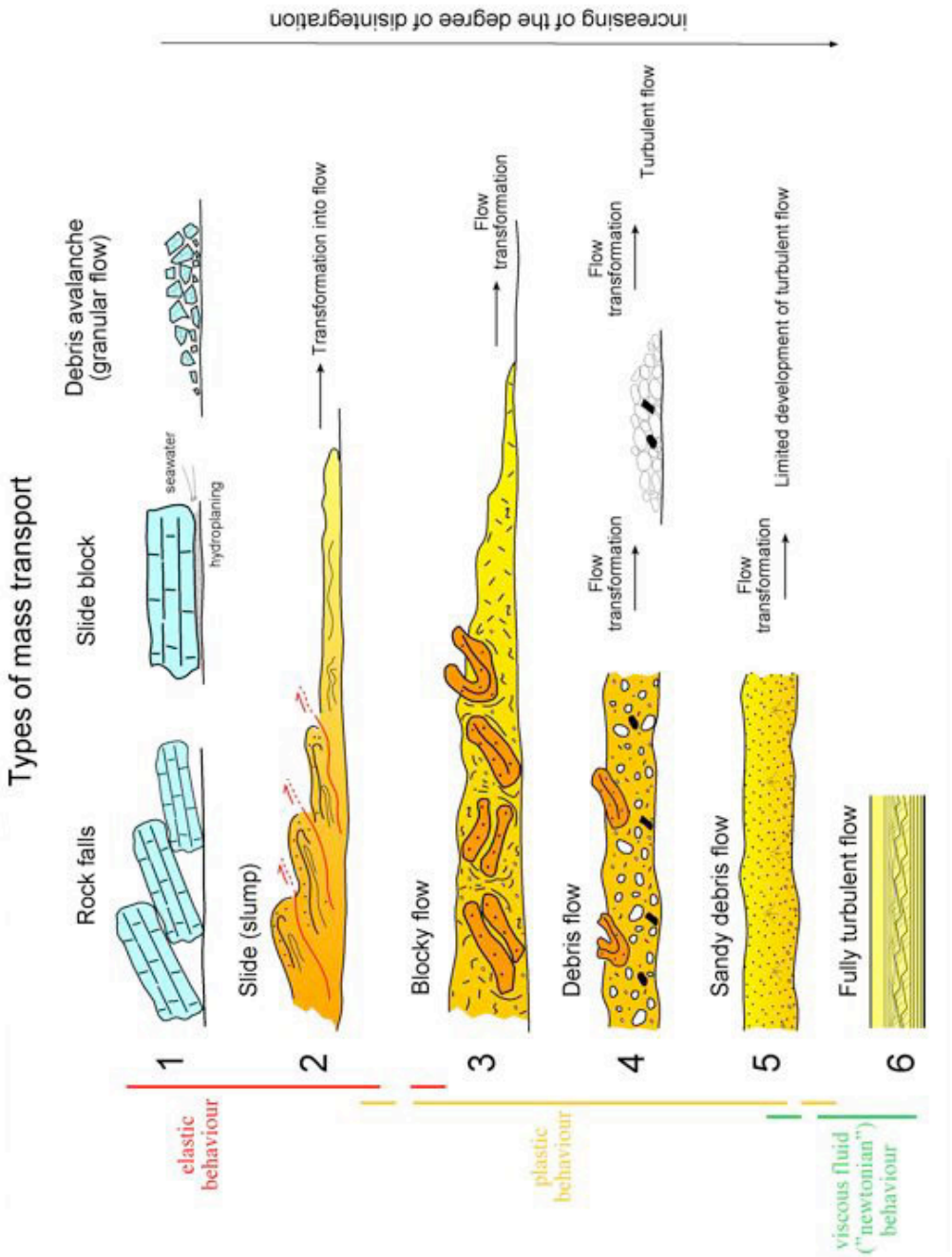

Figure 1.8 - Dynamic classification scheme of mass transport deposits that takes into account genetic and evolutionary relationships between generating processes. Block falls and turbidity currents are intended to represent the end-members of such broad spectrum of processes. Moreover, in this scheme is originally introduced the *blocky-flow* process and related deposit, representing the virtual junction between slump and debris flow products.
From Mutti *et al*. (2006; unpublished data originally presented at the A.A.P.G. Annual Meeting of Houston, Texas).

	CHAOTIC UNIT	
ORIGIN	**SEDIMENTARY**	**TECTONIC**
OVERALL APPEARANCE	- Rock assemblage composed of fine- to coarse-grained, poorly- to un-sorted poly- and/or mono-genic lithologies, with rigid to soft angular- to rounded- multi-sized elements enclosed in a fine-grained matrix (matrix-supported breccia, diamictite, debrite, etc.). - Occurrence of fine-grained micro-clasts (brecciated matrix sensu Bettelli et al., 1996). - Occurrence of not-dissociated out-sized rock masses (slide blocks, olistholiths, stratified rafts, etc.). - Possible presence of variable thick fine-grained covers (mud drapes) or a single thick-bedded turbidite (co-genetic turbidity current) - Occurrence of associated slump deposits	- Rock assemblage composed of fragments of multi-sized and multi-shaped beds and bed-sets of mono-formational lithologies, mechanically enclosed in fine-grained lithologies characterized by scaly fabric. - Occurrence of small-scale fault-bounded blocks - Mesoscale hydro-fracturing evidence - Abundance of mineralized veins - Absence or localized scarce presence of fine-grained un-sorted matrix
TEXTURE	- Presence of fluid-escape structures - Possible presence of reworking evidence of the upper portions - Upper and lower stratigraphic contacts - Generally clastic brecciated texture with a block-in-matrix fabric, which appearance is scale-invariant. - Generally massive appearance, sometimes and in places normal to inverse grading of the clasts.	- General occurence of brittle deformations - General appearance depending on the structural syle, degree of stratal disruption and burial conditions - Boudinage-related structures, preferential alignment of constituents and the scaly fabric trend generally concur to develop a penetrative system of planar structure (tectonic foliation or pseudo-stratification)
PROPOSED OUTCROP ANALYSIS	- Original texture of the elements (blocks) in contrast with that shown by the enclosing matrix. - Generalized presence of ductile simple-shear structures, flowage-related and compaction-related deformations. - Measuring of stratification (or pseudo-stratification) direction and inclination, where expressed by elongated clast iso-orientation, vertical and lateral clast size and compositional variations, alteration color banding,etc. - Detailed characterization of lithologies, shape and clast distribution. - Separate sampling of block, clasts and matrix for palaeontological and microscopical analysis, difrattometry (for pelitic lithologies), etc. - Collecting of structural data on planar (fold axial planes, ductile shear surface, etc.) and linear (fold axis, sheat-fold long axis) structures - Different lithologic units (clast types, matrix and texture) or units characterized by different clast/matrix ratio. - Representation of mappable coeval fine-grained deposits	- Original texture of the elements (blocks) according with that shown by the enclosing matrix. - Measuring of tectonic foliation direction and inclination, where expressed by elongated element iso-orientation, boudinage, scaly fabric, etc. - Detailed characterization of lithotypes and comparation with that ones characterizing less- or un-deformed.bounding units. - Reconstruction of the original lithologic features inferred to characterize the "protoliths" of the unit and cartographic representation test. - Separate sampling of elements and matrix for palaeontological and microscopical analysis, difrattometry (for pelitic lithologies), etc. - Reconstrution of the original local structural arrangement
CARTOGRAPHIC SCALE SUBDIVISIONS	- Representation of mappable blocks and separate bodies (olistholiths, slide blocks, not-dissociated masses). - Recognition of units sharing same lithologies but localized at different geometric and stratigraphic positions. - Recognition of concordant stratigraphic relationships with the over- and under-lying units.	- Mappable bodies identified on the basis of different lithostratigraphic and structural characteristics: interpretable as formal units, if present in other zones within a known stratigraphic succession, otherwise informal units, if the original stratigraphic position is unknown. - Units arrangement in elongated bands, sometimes according to the overall trending of main local tectonic structures. - Cartographic evidence of cross-cutting relationships with surrounding units.

Figure 1.9 - Schematic table reporting a synthesis of recognition methodologies and classification for sedimentary and tectonic chaotic units from an outcrop-based perspective. Compiled after Bettelli *et al.* (1996).

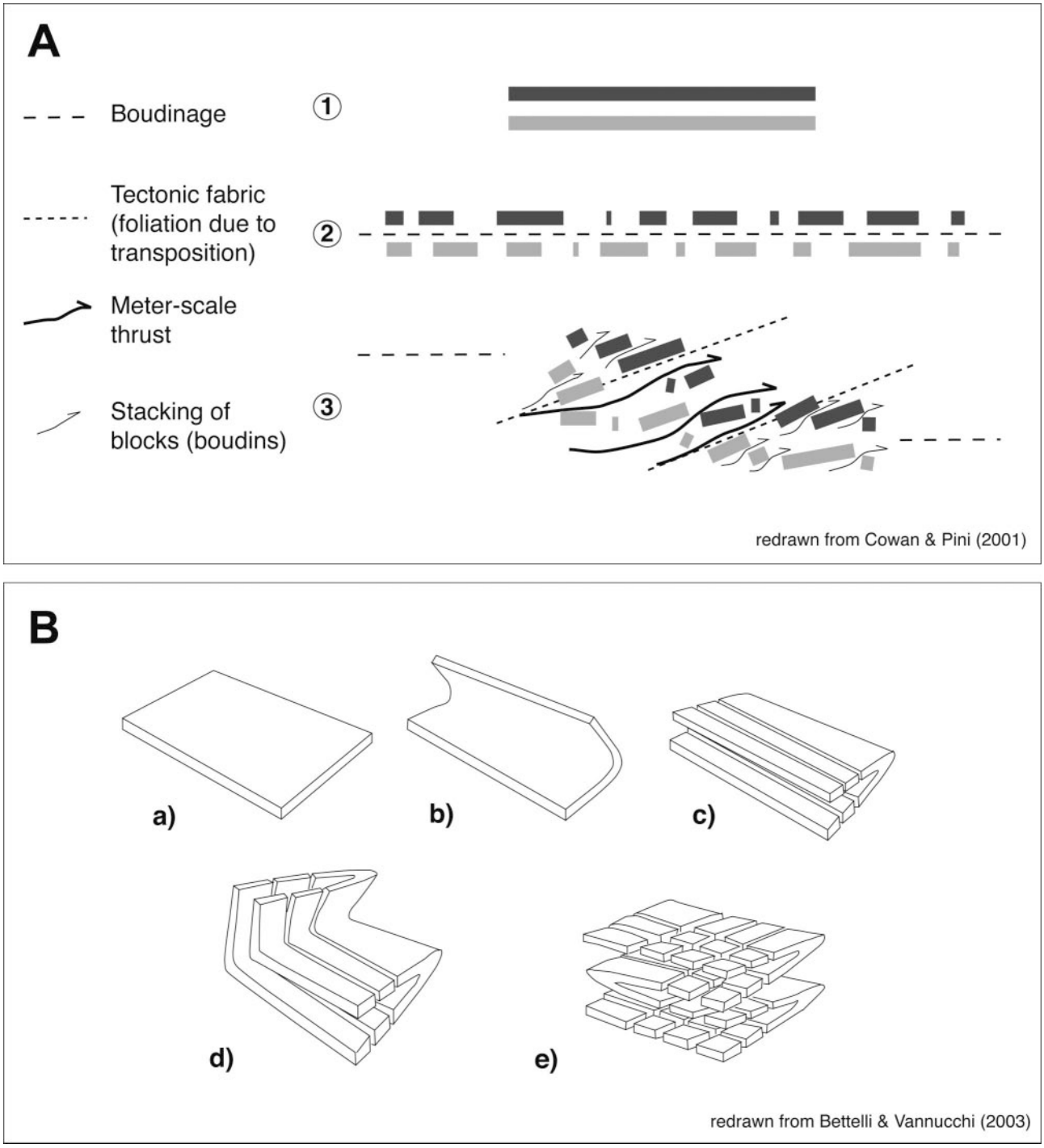

Figure 1.10 - Schemes showing the 2 main possible interpretations for the block-in-matrix fabric development in tectonic chaotic units of the Northern Apennine. **A.** Bed-transposition hypothesis: first fragmentation of a layered sequence through boudinage phenomena followed by an element stacking caused by small-scale thrusting. Redrawn from Cowan & Pini (2001). **B.** Fold-interference hypothesis: progressive strata disruption through the superposition of 2 orthogonal folding events (type 2 interference pattern of Ramsey, 1967) followed by co-planar extension of the fold limbs. Redrawn from Bettelli & Vannucchi (2003).

2. METHODOLOGY

The aim of this work is the detailed study of a consistent set of outcrops belonging to a very large mass transport complex, the Specchio Unit (R2) exposed in Epiligurian outliers (*i.e.* isolated synclinalic sedimentary remnants) scattered on the Padan (*i.e.* eastern) side of the Northern Apennines (fig. 2.1).

The Specchio Unit is interpreted to cover about 1500 square kilometers (assuming the mean distance between hosting outliers), locally reaching more than 400 meters in thickness, and thus resulting comparable with present-day mass transport deposits observed in modern continental margins. By size, the Specchio Unit falls in the field of the largest on-land examples of fossil submarine landslides (fig. 2.2).

In the R2 unit several associations of structures showing different styles of deformation and degrees of stratal disruption can be observed. The presence of relatively clean and continuous selected outcrops allows observations on vertical/lateral relationships of these structures, in some cases also in a three-dimensional way.

This research has been therefore carried on with a field-based approach, integrating stratigraphic, sedimentological and structural, regional- to outcrop-scale observations. The integration of the structural and stratigraphic tools is used to directly and indirectly try to explain the complex external and internal features of the R2 Specchio Unit mass transport complex, in its whole vertical and lateral extent, and from local to regional point of view.

The study of the three selected Epiligurian outliers (*i.e.* Pessola Valley, M. Roccone and Caffaraccia sections; fig. 2.3) hosting the R2 Specchio Unit has been firstly made through a detailed (1:5.000 scale) geological mapping. This reconnaissance has been the fundamental tool for:

- Characterizing internal architecture of the R2 unit;
- Testing the lateral extent of the R2 unit;
- Selection of key-outcrops for specific stratigraphic and structural analyses;
- Identification of upper and lower contacts of the R2 unit;
- Characterization of the hosting sediments and relationships with the substrate and overlying deposits;
- Outline of the local and regional tectonic-stratigraphic framework;

The final product of this research are three 1:10.000 scale geological maps focusing on the internal mappable subdivisions of the R2 Specchio Unit and hosting Ranzano Unit sediments (see Panels n. 1 and n. 2).

Each subdivision has been identified through the analysis of the mean composition, structural style and geometric position in the stratigraphic column.

The structural analyses have been carried out using the criteria defined for the classical slump deposits (Woodcock, 1979; Gawthorpe and Clemmey, 1985; Bradley and Hanson, 1998; Alsop and Holdsworth, 1999, 2004; Strachan and Alsop, 2006; Strachan, 2002, 2008; Lucente and Pini, 2003).

The estimation of the palaeo-transport directions has been primarily achieved through the three-dimensional characterization of the folds (mainly on the basis of their stratigraphic polarity and geometrical asymmetries), and the recognition of the mechanisms responsible for their development (fig. 2.4).

The collected fold data have been plotted using the *separation-arc method*, as defined by Bradley and Hanson (1998), well tested on the field by Lucente and Pini (2003) and Strachan and Alsop (2006).

Given the significant amount of anomalies and dispersions due to the high internal disarticulation and element rotation (*e.g.* Lajoie, 1972) of the R2 unit, more apparent clusters of folds data have been considered within the same plot, highlighting more than one main preferential direction.

For this reason, data other primary structures have been considered, especially those thought to be strongly related to emplacement and accommodation processes, as the overall geometrical element imbrication and the syn-depositional shear zones trend.

Definitively, a structural data set on planar (*i.e.* syn-sedimentary shear surfaces, folds axial planes) and linear (*i.e.* fold axes plunge and trend, sheath folds long axes) has been collected from 22 structural stations, representative of each recognized internal stratigraphic subdivision of the R2 unit: 15 for the Pessola Valley area, 4 for the M. Roccone area and 3 for the Caffaraccia section (fig. 2.5).

These data have been primarily used to unravel average transport directions, but also to identify local differences in deformative styles, potentially useful to discriminate different events/pulses within the same unit, punctual variations in basinal morphologies and emplacement mechanisms.

In the Pessola Valley area, thanks to the favorable outcrop conditions, several detailed (1:20 scale) stratigraphic columns have been measured. Two general logs have been made in the underlying R1 Pessola Unit and overlying R3 M. Roccone Unit, covering a whole thickness of about 500 m. Other punctual stratigraphic logs have been measured across the lower contact (three logs) and across the upper contact of the R2 unit (eight logs) (fig. 2.6).

This approach has been used to highlight the differences between the sediment characteristics of the stratigraphic units above and below the R2 unit, and, consequently, to characterize the external morphologies of the R2 unit through the careful observation of the overlying vertical and lateral facies variations.

This work has been carried out in more than 120 days of field surveys.

To better characterize deformational mechanisms, small-scale textures and compositions, 8 rock samples have been collected in the Pessola Valley outlier (fig. 2.7): 1 from a thrust zone at the base of R1 Pessola unit in the south-eastern sector (LAT1), 6 from different stratigraphic levels of the R2 Specchio unit (R2aEM, R2bEM, R2bIBT, R2cEM, R2dEM and R2eEM, from base to top) and 1 from a distinctive laminated sandstone bed of the R3 Roccone unit (WCBR3). Qualitative microscopic analyses on thin sections and polished rock counter-cuts have been made.

Moreover, these data has been tentatively integrated with published and unpublished geophysical data from modern to recent selected analogs. This latter part has been developed at the *Departament d'Estratigrafia, Paleontologia i Geociències Marines, Facultat de Geologia/Universitat de Barcelona*, under the supervision of the prof. Angelo Camerlenghi.

At the same time, parallel researches has been carried out on other Northern Apennine mixed tectonic-sedimentary chaotic units roughly localized in the basal *decollément* of the Ligurian Nappe above the relative authocthonous Tuscan Units and well exposed in the Bobbio Tectonic Window (Piacenza province). These studies, carried on with drs. Davide Caré and Mario Zèlic of the *Centro di Documentazione per la Geologia dell'Appennino Settentrionale* (Bobbio, Piacenza), have been useful for the characterization of the tectonic overprinting on sedimentary chaotic bodies and the potential role of fluids in the origin of such units (Ogata *et al.*, 2007). These observations, coupled with the literature concerning the long debated olistostrome problem, have been then tentatively exported for the systematic discrimination between the tectonic and sedimentary signal in the analyzed Epiligurian chaotic bodies.

Keeping in mind case studies from other orogenic belts (mainly south-central Pyrenees) and from different situations from the same Northern Apennine chain, I tried to highlight the common features of those bodies, testing interpretations and methodologies already used for similar units.

For this comparing reason, some brief observation concerning shallow level soft-sediment deformation processes acting on active accretionary prism has been made in the Plio-Pleistocene Chikura Group of the Boso Peninsula (Japan), under the guidance of professors Yujihiro Ogawa and Ken-ichiro Hisada of the Tsukuba University.

2.1 List of figures

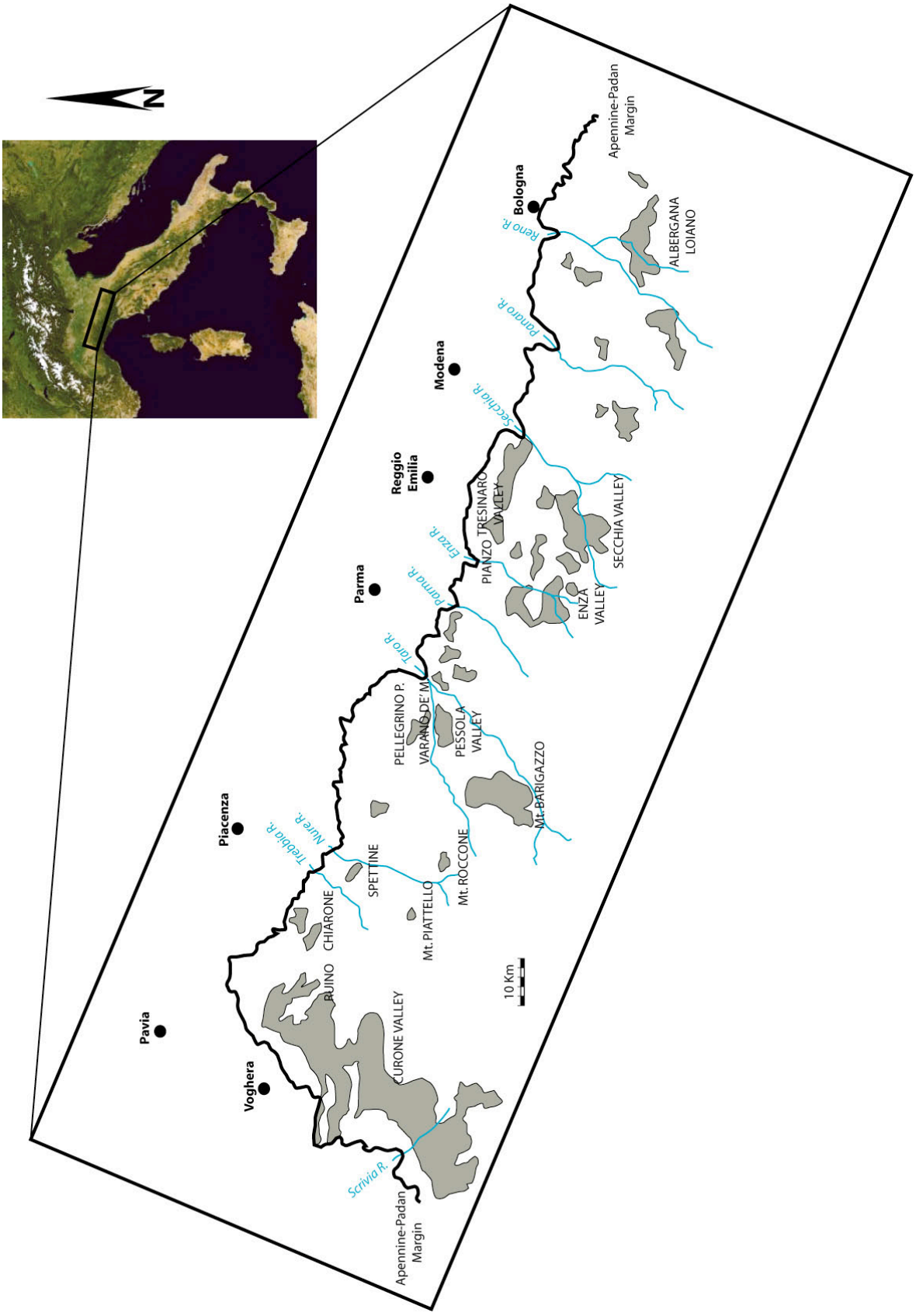

Figure 2.1 - Schematic representation of the Epiligurian succession sedimentary remnants (*i.e.* outliers) scattered across the eastern side of the Northern Apennines. Redrawn and slightly modified from Martelli *et al.* (1998).

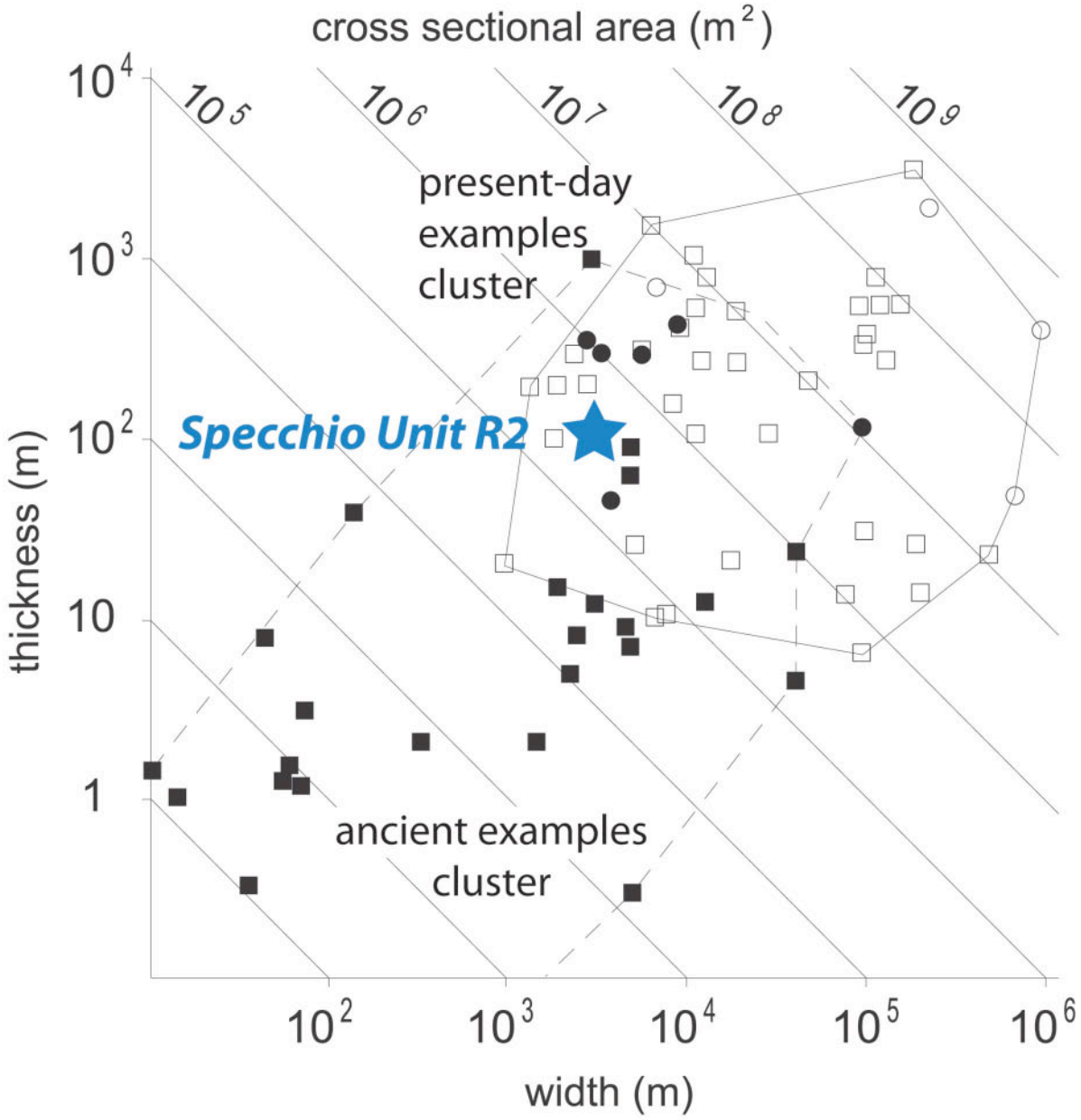

Figure 2.2 - Plot of thickness versus width of ancient (solid squares and circles) and present-day submarine landslides (open squares and circles); relative size of the Specchio unit R2 is plotted. Modified from Woodcock (1979) after the compilation of Lucente and Pini (2003).

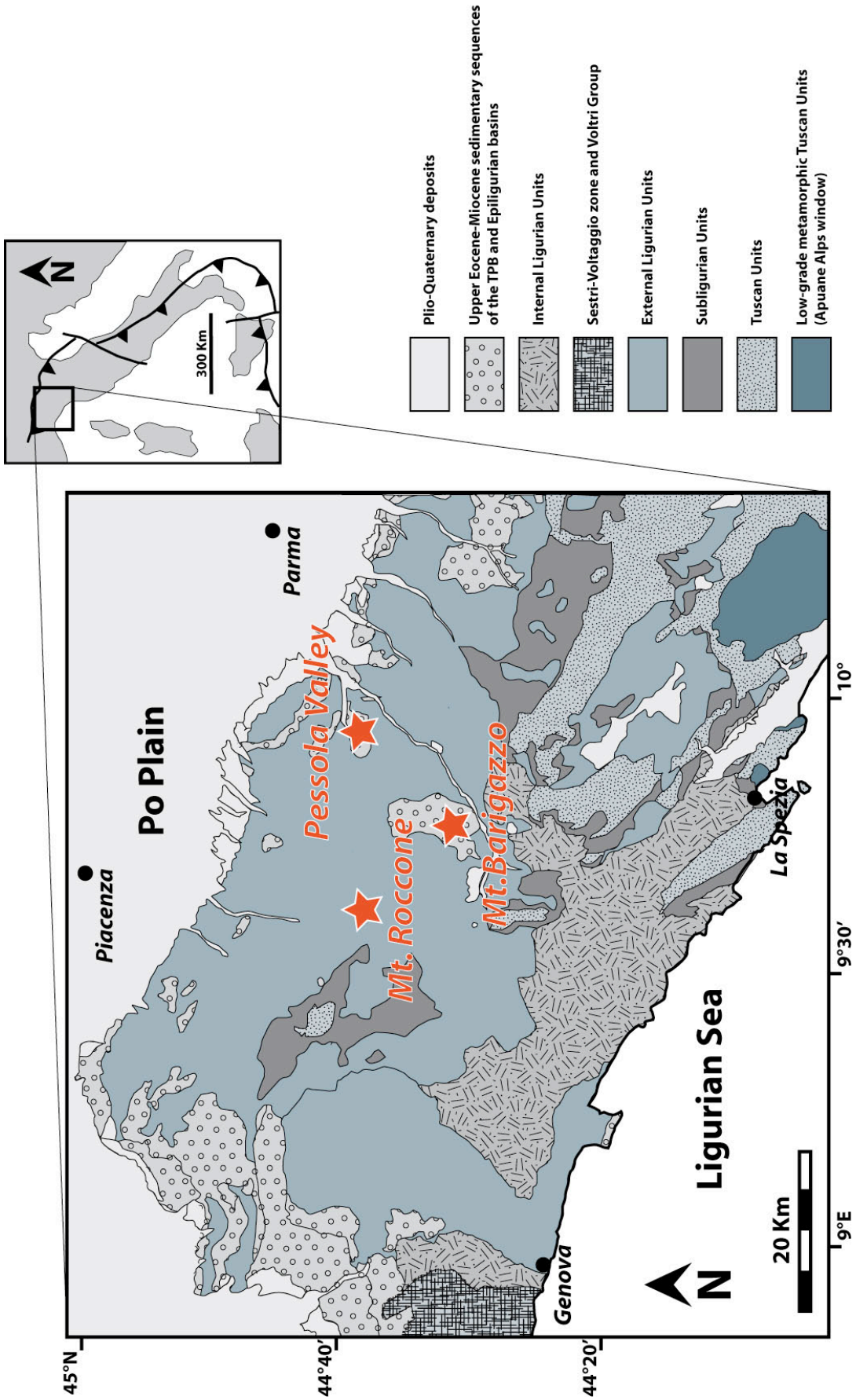

Figure 2.3 - Simplified geological map of the northeastern side of the Northern Apennines with localization of studied areas. Redrawn and slightly modified from Marroni and Pandolfi (2001).

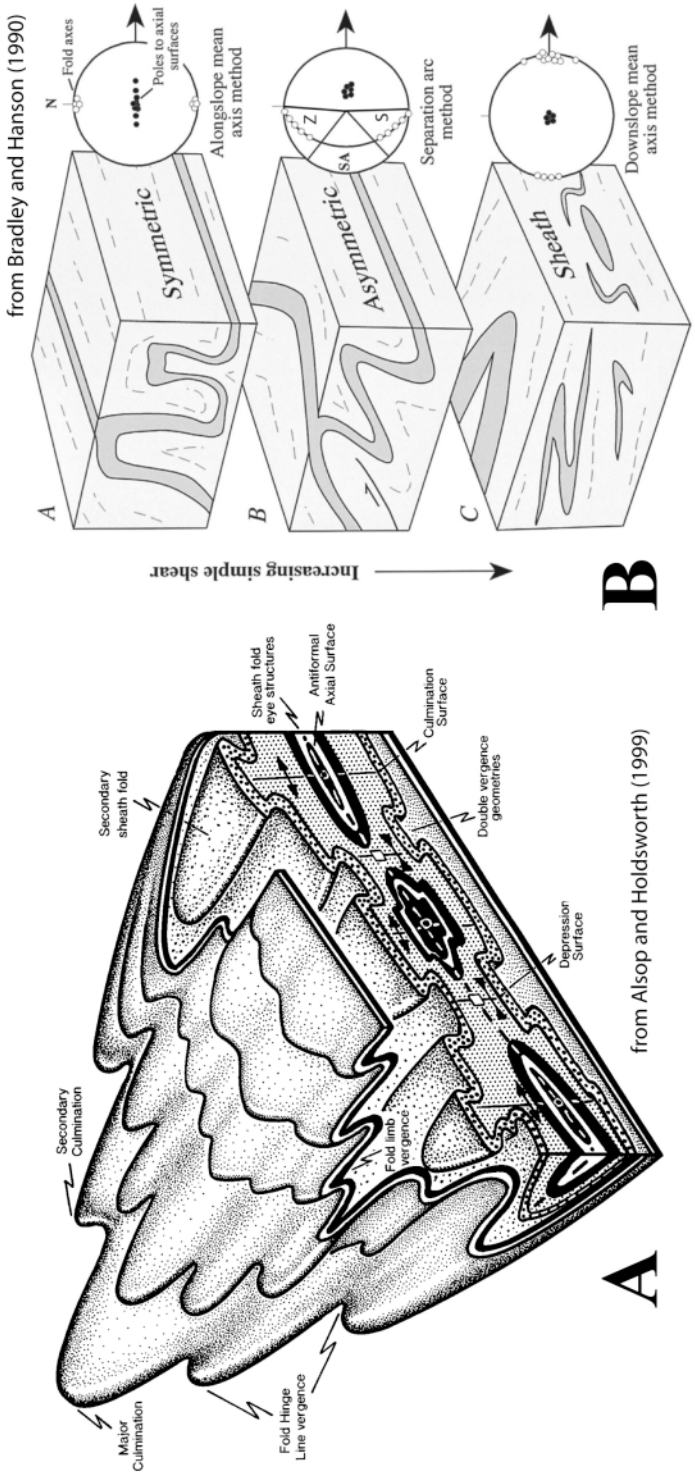

Figure 2.4 - Three structural styles of slump folds stacked from the top down in order of increasing simple shear. Arrows in stereonets show slope direction. **A.** Initially, fold axes show tight clustering normal to slope. Along slope mean-axis method gives the paleoslope direction. **B.** With moderate downslope rotation, fold axes acquire S and Z asymmetry and define two fields along a great circle corresponding to the slope. SA is the separation arc, which gives the paleoslope direction. **C.** With continued downslope rotation, the separation arc narrows and then disappears completely, as fold axes are reoriented toward the downslope direction. Downslope mean-axis method (or better yet, sheath axes) gives the paleoslope direction. From Bradley and Hanson (1998).

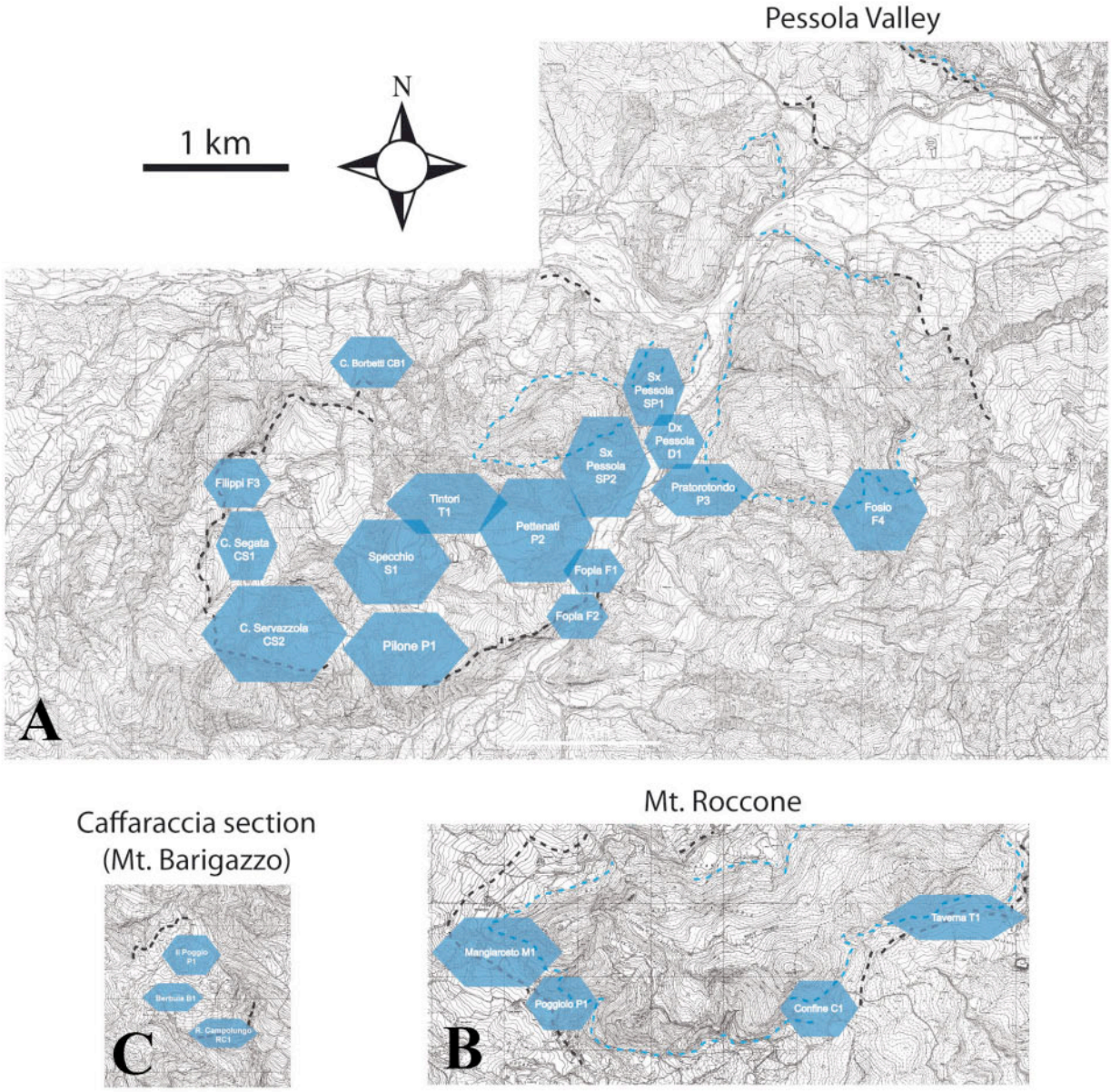

Figure 2.5 - Topographic 1:5.000 map slices (CTR Emilia-Romagna) showing localization of selected structural stations for the Specchio unit R2 analysis. **A.** Pessola Valley outlier. **B.** Mt. Roccone outlier. **C.** Caffaraccia section (Mt. Barigazzo outlier). Black dashed line: Specchio unit R2 basal contact. Blue dashed line: Specchio unit R2 upper contact.

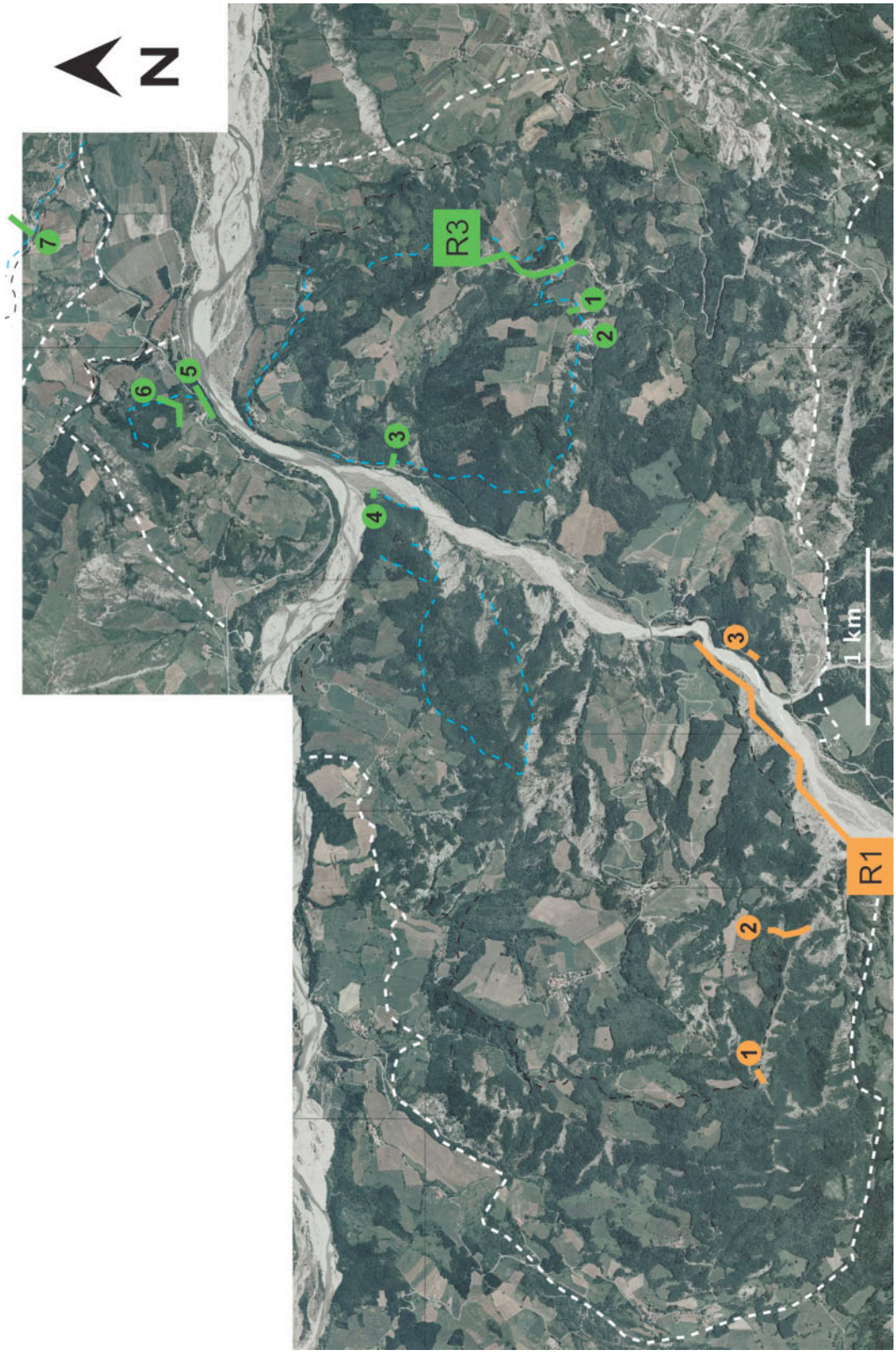

Figure 2.6 - Satellite photo-mosaic of the Pessola Valley outlier with localization of measured stratigraphic log paths. Black dashed line: Specchio unit R2 basal contact. Blue dashed line: Specchio unit R2 upper contact. White dashed line: Epiligurian outlier boundary. Satellite map slices from www.viawindowslive.com/VirtualEarth.aspx.

Figure 2.7 - Satellite photo-mosaic of the Pessola Valley outlier with positions of collected samples for analysis in optical microscopy (thin sections and smear slides). White dashed line: Epiligurian outlier boundary. Satellite map slices from www.viawindowslive.com/VirtualEarth.aspX.

3. GEOLOGIC SETTING: NORTHERN APENNINES

The Northern Apennines is a segment of the Apennine-Maghrebian fold-and-thrust belt, which constitutes the backbone of the Italian peninsula, and developed at the subduction-collisional boundary between the European (*i.e.* Corsica-Sardinia block) and African (*i.e.* Adria micro-plate) plates (for an updated extensive review see Elter *et al.*, 2003; Cerrina Feroni *et al.*, 2004; and reference therein) (fig. 3.1).

Given the high structural complexity and the still ongoing debate on the evolution of the Northern Apennines, in the following I will only briefly describe the tectonic history and the main tectono-stratigraphic components, trying to summarize the huge amount of concerning literature and the so far classically accepted interpretations.

The Northern Apennines has experienced at least three main evolutionary stages during its ~100 M.a. history (Elter, 1973; Boccaletti *et al.*, 1980; Ricci Lucchi *et al.*, 1982; Carmignani and Kligfield, 1990; Zanzucchi, 1994; Marroni and Treves, 1998; Vai and Martini, 2001; Argnani, 2002; and many others), and is nowadays tectonically active, with a general uplift rate of ~1 mm/y at its Padan deformation front (Cyr and Granger, 2008; Picotti and Pazzaglia, 2008).

The first, Cretaceous-Early Palaeogene pre-collisional stage belongs to the Alpine-Himalayan orogenic cycle, and corresponds to an inferred oblique oceanic subduction of the Piedmont-Ligurian Basin under the European plate (Coward and Dietrich, 1989).

The second collisional stage is related to the opening of the Balearic Sea, with the subsequent anti-clockwise rotation of the Corsica-Sardinia microplate (*i.e.* segment of the European plate), from the Oligocene to the Burdigalian.

The third post-collisional stage develops as a generalized extension of the innermost part of the belt since the Late Burdigalian, in response to the opening of the Northern Tyrrhenian Sea and the coeval outward shifting of the thrust front (Castellarin *et al.*, 1992; Finetti *et al.*, 2001). In this framework, the role of transpressive tectonic seems to have played a major role (Vescovi, 1993; Cerrina Feroni *et al.*, 2004).

During the pre-collisional evolution of this convergent system, an orogenic wedge developed, forming the westernmost (*i.e.* innermost) part of the collisional belt (Treves, 1984). This subduction-related orogenic wedge comprises an accretionary complex and a high pressure/low temperature (HP/LT) metamorphic complex (Elter and Marroni, 1991) (fig. 3.2).

The former developed through the accretion of Cretaceous-Paleogene oceanic turbidite units and off-scraped ophiolites, which remnants constitute the Ligurian Units of the Northern Apennines. The latter instead represents an under-plated and then exhumed subduction complex,

formed by HP/LP ophiolite-rich metamorphic units, nowadays exposed in the Ligurian Alps and northeastern Corsica. Evidence of such units has been geophysically detected under the Ligurian Sea (Bartole *et al*., 1991).

The Ligurian Units were thrust eastward during the collision, over the Adriatic continental margin, forming the so-called Ligurian Nappe. This tectonic motion allows the incorporation of ocean-continent transition bounding unit (*i.e.* Subligurian Units) and the progressive involvement of epi-continental cover units of the foreland (*i.e.* Tuscan and Umbro-Marchean Units). These latter units represent relatively authocthonous continental margin successions, bringing on their top thick Upper Oligocene-Miocene siliciclastic turbidite succession, accumulated in the Northern Apennines foredeep developed eastward (*i.e.* outward) to the accreting belt front (fig. 3.3).

Contemporaneously, systems of perched basins developed on top of the over-thrusting Ligurian Units (*i.e.* Epiligurian Units), as well as on the HP/LP metamorphic complex of the orogenic belt suture zone in the Ligurian Alps (*i.e.* Tertiary Piedmont Basin; TPB). These syn-orogenic sedimentary successions are the topic of this work (fig. 3.4).

Given the general tectonic staking of this chain, in the analyzed areas Tuscan and Subligurian Units are not exposed, while the Ligurian Nappe, representing the topmost element of this structural pile, is the depositional substrate of the entire Epiligurian succession (fig. 3.5).

The Ligurian Nappe is made of a strongly dissected complex assemblage of several interrelated components, in which each component has referred to with a different name. Classically, the Ligurian Units have been subdivided into Internal and External ones (in respect to the orogenic polarity) on the basis of the nature of the ophiolitic substratum (according to the classical oceanic succession or being reworked, respectively).

Internal and External Ligurian Units are essentially characterized by thick successions of oceanic siliciclastic (*i.e.* Gottero/Scabiazza Sandstone) and calcareous turbidites (*i.e.* Helminthoid Flysch), respectively, and representing the sedimentary cover of the mesozoic oceanic seafloor.

In the External Ligurian Units, the base of this calcareous turbiditic succession is marked by the so-called Ligurian Basal Complexes, shale-rich and generally chotic units deposited on the oceanic crust (no more exposed) close to the continental margin, and bearing ophiolitic, calcareous and continental crust reworked elements.

Given the strong segmentation of these units, a lot of terms have been used to identify every isolated part of this succession in each outcropping locality (*e.g.* Antola Unit, Caio Unit, Ottone Unit, Morello Unit, Cassio Unit, etc.); for reason of simplicity here I use the generic term of Helminthoid Flysch Units.

3.1 Epiligurian Units outline

The middle Eocene to late Miocene Epiligurian Units are widespread in the Northern Apennines fold-and-thrust belt, scattered as isolated sedimentary remnants (usually corresponding to gentle syncline structures) of siliciclastic successions extending from the eastern sector of the episutural Tertiary Piedmont Basin (TPB) to the NW to the Bologna area to the SE (fig. 3.6).

The term *Epiligurian Succession* was introduced by Ricci Lucchi & Ori (1985) to identify a terrigenous succession unconformably deposited above the tectonized Ligurian Units and contemporarily sedimented in physically independent and relatively small basins.

Classically defined as *semi-authocthonous* (Merla, 1951), *post-geosynclinalic* (Sestini, 1970) and *post-orogenic* (Ogniben, 1972; Zanzucchi, 1982), these units represent the syn-tectonic infilling of migrating and cannibalizing satellite basins localized on top of the Ligurian Nappe (i.e proto-apenninic/Ligurian orogen) during the overthrusting toward the Apenninic foreland, and therefore, from a geodynamic point of view, they share typical characteristics of piggy-back, thrust-top, wedge-top, epi- and peri-sutural basins (Bally and Snelson, 1980; Boccaletti *et al.*, 1980; Ori and Friend, 1984; Ricci Lucchi and Ori, 1985; Ricci Lucchi, 1986; Elter and Marroni, 1991) (fig. 3.7).

The Epiligurian succession is a fundamental element for the reconstruction of the geological evolution of the Northern Apennines and thus it have been extensively investigated in the last 4 decade and the available literature concerning both local and regional approaches is widespread (Pieri, 1961; Braga, 1962, 1965; Radrizzani, 1964; Mutti *et al.*, 1965; Mutti and De Rosa, 1965; Sestini, 1970; Gazzi and Zuffa, 1970; Dallan Nardi and Nardi, 1974; Iaccarino *et al.*, 1974; Braga *et al.*, 1975; Bonazzi and Fazzini, 1979; Vescovi and Rio, 1981; Zanzucchi, 1980; Principi and Treves, 1984; Ricci Lucchi and Ori, 1985; Papani *et al.*, 1987).

Studies focusing on turbidite system stratigraphy and sedimentology (Mutti *et al.*, 1995), bio- and litho-stratigraphy (Martelli *et al.*, 1998; Catanzariti *et al.*, 1997) and petrographical evolution (Cibin *et al*., 2001, 2003), have greatly enhanced the understanding of the Epiligurian succession from a larger-scale point of view.

In spite of different methodologies, these authors converge to the interpretation of the Upper Eocene-Oligocene Epiligurian succession as a basin system elongated in NW-SE direction extending from the eastern part of the TPB to the Bologna area.

They also stressed the high complexity of this sedimentary succession as response to the mesoalpine polyphased tectonics, recorded by sudden modifications in the feeder-depositional systems and basin morphology, occurrence of thick chaotic deposits and sedimentary reworking.

Epiligurian Units has been also adopted as kinematic indicators for the Oligocene to Miocene tectonic evolution of the Northern Apennines for paleo-magnetism (Muttoni *et al.*, 1998) and regional structural geology (Conti, 2002), highlighting the possible consistent rotation of the orogenic deformation front (~ 40° anti-clockwise) (fig. 3.8). Nonetheless evidences of orogenic deformation-induced remagnetizations during Late Miocene are documented for Tuscan and Ligurian Units (Aiello *et al.*, 2004).

The constituent lithostratigraphic units of the Epiligurian Succession include various facies sediments, from deep-water turbidites to shelfal calcarenites, characterized by sharp lateral variations in depositional geometry and style due to complex sea-bottom topography and syn-sedimentary tectonics, and by different clastic composition reflecting contemporaneous evolution of feeding systems.

The classical subdivision used for the Epiligurian succession of the Northern Apennines is that proposed by Bettelli *et al.* (1987) for the Modena-Bologna areas (fig. 3.9).

Recent investigations pointed out the existence of two main depositional cycles corresponding to two different types of basins, late Lutetian to Burdigallian and Burdigallian to early Messinian in age, respectively (Di Giulio *et al.*, 2002; Mancin *et al.*, 2006) (fig. 3.10).

The first depositional cycle (coinciding with the Epimesoalpine sedimentary succession of Mutti *et al.*, 1995) was deposited in a single complex basin about 250 km long and 50 km wide, from the eastern TPB to the Bologna area (Mutti *et al.*, 1995; Martelli *et al.*, 1998; Cibin *et al.*, 2001, 2003).

This complex basin was probably elongated in N-S direction and articulated in three different sectors: a NW sector (i.e. Curone Valley area), an intermediate sector (i.e. the Nizza Valley to the Secchia Valley area), and a SE sector (i.e. the Secchia Valley to the Reno Valley area). Here I take in consideration the intermediate sector, which is characterized by the presence of the analyzed Specchio Unit.

The first depositional cycle of the intermediate sector is classically subdivided into the following main formations, here referred as Units, from the oldest to the youngest: the M. Piano, Ranzano and Antognola Units.

The Monte Piano Unit (Upper Bartonian-Priabonian; Vescovi & Rio, 1981) is composed of mainly pelagic and hemipelagic sediments, characterized by varicoloured mudstones and grey silty-marls in the lower and upper portions, respectively. The base of this unit is gradational or sharp on deformed Ligurian units of the substratum; locally this limit is marked by the presence of mud breccias bodies (Baiso Unit; sedimentary mélange of Bettelli *et al.*, 1987). The upper limit with the

Ranzano Unit is diachronous, younging from late Priabonian to the W to early Rupelian to the E (Cerrina Feroni *et al.*, 2004; Di Giulio *et al.*, 2002)

The Ranzano Unit (Priabonian-Rupelian; Catanzariti *et al*., 1997; Mancin, 1999, 2001; Mancin & Pirini, 2001) is represented by conglomeratic and coarse to fine grained sandstone turbiditic deposits with various prevailing lithologic compositions; this unit represent the stratigraphic interval of interest for the preset work and is therefore extensively discussed in the next session.

The Antognola Unit (Upper Rupelian-Lower Burdigalian) consists mainly of mudstone-dominated sediments with several arenaceous lens-shaped bodies, in some case reaching consistent dimensions (i.e. Lagrimone, Iatica and M. Salso bodies).

The upper part of this unit is characterized by siliceous deposits of the so-called Contignaco Unit, an important time-interval which can be correlated across the whole Northern Apennine chain (Siliceous Lithozone; Amorosi *et al.*, 1995) marking an overall regional to global silica increase during the Burdigalian time (*e.g.* Monterey Formation; Mutti, pers. comm.).

This unit is also characterized by the presence of the Canossa Olistostrome (Papani, 1964, 1971; Bettelli *et al.*, 1987; De Nardo *et al.*, 1991), a huge chaotic ophiolite-bearing argillaceous complex with remarkable areal extent and complex vertical-lateral relationships.

As pointed out by Di Giulio *et al.* (2002), the whole first-cycle sedimentary succession seems to record a general shifting of depositional environment from lower bathyal (basal M.Piano Unit) to lower-middle neritic (lower Bismantova Unit) palaeo-bathimetries (fig. 3.11).

The beginning of the second depositional cycle, extending from the late Burdigalian to the late Messinian, is marked by a regional unconformity, which puts in contact marly deposits of the Antognola Unit with shallow-water limestones and calcarenites of the lower Bismantova Unit (late Burdigalian-early Langhian Pantano Fm.; Papani *et al.*, 1987; Amorosi *et al.*, 1993; 1996).

The upper Bismantova Unit is composed of marls and silty-marls of the Cigarello Fm. (Langhian-Serravallian; Amorosi *et al.*, 1993; 1996). This second depositional cycle ends with the marly deposits of the late Serravallian-early Messinian Termina Unit (Amorosi *et al.*, 1993; Cerrina Feroni *et al.*, 2004).

The relationships between these basins and the external foredeeps are discussed by Ricci Lucchi & Ori (1985) (fig. 3.12).

It is important to note that Mutti *et al.* (1995) considered the Priabonian to late Rupelian portions of this succession (*i.e.* M.Piano-Ranzano succession) as belonging to a truly episutural basin (*i.e.* their Epimesoalpine succession), avoiding the term “Epiligurian” as defined by Ricci

Lucchi and Ori (1985), given its deposition also on Alpine units (*i.e.* Pennidic Units) and the missing of a correspondent foredeep infilling.

3.2 Ranzano Unit outline

Known in the classical regional literature as *Tongriano Appenninico*, this siliciclastic unit was formally defined as Ranzano Sandstone by Pieri (1961), from the type-section located in the Parma Apennine.

It consists mainly of irregular alternations of poorly cemented conglomerates, coarse- to fine-grained sandstones and marls, characterized by a high facies and lithologic variability, and represent the first important siliciclastic input into the Epiligurian basin (see among the others Pieri, 1961; Braga, 1963, 1965; Mutti, 1963; Mutti *et al.*, 1965; Mutti and De Rosa, 1965; Tagliavini, 1968; Sestini, 1970; Bonazzi, 1971; Papani, 1971; Ghibaudo and Mutti, 1973; Fornaciari, 1982).

More recently this unit has been widely investigated from a regional point of view mainly in terms of biostratigraphy (Catanzariti *et al.*, 1997), petrography (Cibin, 1993), lithostratigraphy (Martelli *et al.*, 1998) and turbidite system stratigraphy (Mutti *et al.*, 1995).

Where the basal Epiligurian stratigraphic succession is relatively more preserved (i.e. outer part of Northern Apennines and eastern TPB), the Ranzano Unit is stratigraphically comprised between the fine-grained sediments of the underlying M. Piano Marl and the overlying Antognola Marl, with upper and lower limits marked by regional unconformities (Fornaciari, 1982; Gasperi *et al.*, 1986; Papani *et al.*, 1987; De Nardo *et al.*, 1991) (fig 3.13).

This stratigraphic succession is quite well recognizable along the Padan side of the chain from the Villavernia-Varzi-Ottone-Levanto Tectonic Lineament to the NW, to the Bologna area to the SE, arranged as isolated sedimentary remnants (*i.e.* Epiligurian outliers).

Due to the high complexity of basin morphologies this unit is characterized by local differences on the substratum, resting in the depocentral areas on marly deposits of the M. Piano Unit or on the chaotic deposits of its lower part (i.e. Baiso Mud Breccias), while on inferred structural highs (i.e. basin margins, intra-basinal relieves) it rests directly on deformed Ligurian Units (Bettelli *et al.*, 1987).

As underlined by Braga (1962; 1963), Mutti (1964) and Mutti *et al.* (1965), also regional differences in the substrate relationships are recognizable, marking two distinct alignment of the Epiligurian outliers trend: 1) an inner alignment, where M. Piano Unit unconformably overlies already strongly deformed Ligurian Cretaceous units, and 2) an outer alignment, where the same

units share virtual stratigraphic continuity with the so-called Tertiary Ligurian Flysches (*i.e.* youngest portions of Ligurian domain; Val Luretta, M. Sporno, Viano units).

Despite the lacking of a detailed tectono-stratigraphic constrain, this trend is nonetheless possibly interpreted as expression of the outward migration of the tectonic deformation front, probably started from the Paleogene for inner zones (Mutti, 1964; Elter and Marroni, 1991) and culminating in the Eocene for outer zones (*i.e.* Ligurian Phase *s.s.*).

Detailed regional petrographical studies on the sandstone detritus have shown that particular lithologic and mineralogic associations characterize Ranzano Unit deposits (Gazzi and Zuffa, 1970; Cibin, 1993). Trough these studies 5 petrographical units (i.e. petrofacies) with distinct vertical stacking have been recognized and used to define a regional correlation scheme between Piacenza and Bologna area (Cibin, 1993), highlighting the syn-tectonic evolution of source zones and feeding systems:

- Petrofacies A: continental basement-derived detritus lacking of sedimentary cover (volcanic and plutonic acid rocks, low- to intermediate-grade metamorphic rocks). This petrofacies is present only in the easternmost part of the Epiligurian succession (i.e. to the E of the Secchia Tectonic Lineament), characterizing sandstone deposits coeval to the M. Piano Unit (i.e. Loiano, Rio Giordano, Vesallo Sandstone), and not represented in the intermediate domain considered in this work.
- Petrofacies B: European and/or Insubric crust-derived detritus (metamorphic upper continental basement). It corresponds to the "Ra" petrofacies of Di Giulio (1990, 1991) for the TPB, and characterizes in the intermediate domain the first turbiditic input of the Ranzano Unit (i.e. Pizzo d'Oca Unit).
- Petrofacies C: Ligurian-derived mainly ophiolitic detritus (non- to low-grade metamorphic internal Ligurian Units and related sedimentary cover). It corresponds to the "Rb" petrofacies of Di Giulio (1990, 1991) for the TPB. In the intermediate domain this petrofacies characterizes the bulk of the turbiditic sedimentation (i.e. Val Pessola Unit).
- Petrofacies D: Ligurian-derived mainly calcareous detritus (non- to low-grade metamorphic Ligurian Helminthoid Flysch and related sediments). Important is the presence of some intercalated andesitic volcaniclastic layers, indicative of coeval calcalkaline magmatism, which eruptive centers localization is matter of debate (see below). This petrofacies corresponds in part to the "Rc" petrofacies identified by Di Giulio (1990. 1991) in the TPB.
- Petrofacies E: Alpine-derived HP/LT metamorphic detritus (Ligurian-Piedmont and/or Pennidic domain). It corresponds in part to the "Rc" petrofacies of Di Giulio (1990, 1991) and

in the Epiligurian intermediate domain characterizes the lenticular sandstone bodies intercalated in the Antognola Unit (i.e. Lagrimone body).

In light of above mentioned studies (particularly Bettelli *et al.*, 1987; Cibin, 1993; Mutti *et al.*, 1995; Catanzariti *et al.*, 1997; Martelli *et al.*, 1998) and although some different interpretations, the Ranzano Unit of the investigated intermediate domain (see above) has been subdivided in 3 main unconformity-bounded sub-units, characterized by different compositions and depositional styles (fig. 3.14):

- Pizzo d'Oca unit (upper Priabonian; Catanzariti *et al.*, 1997): coarse- to fine-grained arenaceous unit characterized by B petrofacies of Cibin (1993). This unit presents discontinuous areal extension, locally reaching 200 m or being completely absent, due to erosion of the upper unit and/or basin configuration. The lower limit is represented by sharp unconformable contact with the underlying M. Piano Unit.
- V. Pessola unit (upper Priabonian-lower Rupelian; Catanzariti *et al.*, 1997): conglomeratic to fine-grained arenaceous unit with compositions ascribing to C petrofacies of Cibin (1993). This unit presents strong lateral thickness variations, being however more or less recognizable in all Epiligurian successions of the intermediate domain. The lower limit with the Pizzo d'Oca unit is represented by an angular- to concordant regional unconformity of erosive origin. Locally this unit directly overlies M. Piano Unit or Ligurian substrate.
- Varano de' Melegari unit (lower to upper Rupelian; Catanzariti *et al.*, 1997): this unit corresponds to Specchio and M. Roccone units of Mutti *et al.* (1995). As defined by Martelli *et al.* (1998), the Varano de' Melegari unit represents the intermediate domain expression two other heteropic units, the so-called S. Sebastiano Curone and Albergana units, characterizing the eastern TPB and the Bologna area respectively. This unit shows compositions ascribing to the D petrofacies of Cibin (1993) and is characterized by coarse- to fine-grained (locally conglomeratic) deposits with overall lenticular stratal geometries. Thick sedimentary chaotic bodies are commonly intercalated within this unit, especially in the lower part. The basal Specchio unit, which is the main subject of this work, is the largest among them, in terms of thickness and lateral extent.

By comparison, the Ranzano Unit deposits are classically interpreted as fore-arc sedimentary successions belonging to the NE-verging proto-apenninic accretionary wedge (Reutter *et al.*, 1978; Reutter, 1981; Abbate and Sagri, 1982; Principi and Treves, 1984) (fig. 3.15).

This latter interpretation is quite debatable as there are no geological evidences of volcanic arcs that directly input juvenile material in the Epiligurian basin system. Although there is evidence of fallout-related and reworked volcaniclastic layers of andesitic composition intercalated in the

upper part of the Ranzano Unit (Varano de' Melegari member, Catanzariti *et al.*, 1997; Martelli *et al.*, 1998; Cibin *et al*, 2001), very useful for regional correlation, they only testify sporadic alimentation from far-located eruptive centers (fig. 3.16).

Thick deposits of very coarse to fine-grained reworked andesitic clasts are instead reported from the coeval and more external Subligurian domain (*i.e.* Early Oligocene Aveto-Petrignacola Unit; Elter *et al.*, 1999; Pandolfi *et al.*, 2004).

These deposits have been related to an Early Oligocene andesitic volcanic activity which eruptive centers are difficult to localize with currently available data. Probably these volcanic edifices located relatively far from Epiligurian basin system, in a more external (Periadriatic Volcanic Centers, Mortara well-log data, Cibin *et al.*, 1998; along the Valle Salimbene-Bagnolo Lineament?; Mutti *et al.*, 2002) and/or more internal domains (Oligocene Sardinian Volcanic Centers).

Moreover, aero-magnetic evidence of buried volcanic bodies, confirmed by well-log data (i.e. Pieve S. Stefano well), in Tuscany, Umbria and Romagna Apennines suggest the existence of an external paleogeographic domain characterized by intense calcalkaline volcanic activity during the Oligocene and Miocene (Anelli *et al.*, 1994), which should be taken in account to explain volcaniclastic material of the upper part of the Ranzano Unit and of the coeval Subligurian Aveto-Petrignacola Unit.

These last observations seem to support the existence of one or more short-lived Oligocene volcanic arcs which exact position is however still enigmatic, probably separating very distinct palaeogeographic domains, and suggesting a fore arc- or back arc-like depositional settings for the Epiligurian succession.

Other authors interpreted the Ranzano Unit deposits as part of a large episutural basin, developed in response to the mesoalpine collisional event along the inner margin of the Western Alps (Castellarin *et al.*, 1992; Mutti *et al.*, 1995) (fig. 3.17).

Regarding the paleontological content, it is important to note that in the Ranzano unit of the Mt. Barigazzo outlier, Rovereto (1939) reported the presence of some vertebrate fossil remnants attributed to *Anthracotherium*, intercalated within a wood coal layer. The *Anthracotherium* was an Oligocene-Miocene mammal, typical of fluvial, lacustrine and brackish environments, and the presence of its fossil remnants are also reported in the coeval Molare unit of the Tertiary Piedmont Basin (Kotsakis, 1986).

These evidence, coupled with the abundant shell debris and high content of plant fragments characterizing the Ranzano Unit suggest the relative proximity of these deposits to feeder fluvial

systems, and also strengthen the close relationships with the Tertiary Piedmont Basin as proposed by Mutti *et al.* (1995).

It is important to note that the Ranzano unit does not correspond to any recognized external counterpart (*i.e.* foredeep basin) as shown by the other overlying Epiligurian Units.

Moreover, nonetheless the tectonic influence on the Ranzano Unit sedimentation represents the main controlling factor, the unconformable base of the V. Pessola unit, defined by Mutti *et al.* (1995) as related to a major deformational phase expressed in the TPB with emplacement of the Voltri Group (*i.e.* their Ligurian Phase II), shares a quite good correlation with the oxygen isotope event Oi-1 (early Oligocene glacition; Miller *et al.*, 1987, 1991), recording an eustatic fall-related, basal Oligocene widespread erosional feature (Valle dei Cavalieri erosional event; Catanzariti *et al.*, 1997) and roughly coinciding with the base of the V. Pessola unit of Mutti *et al.* (1995).

The bulk of the Ranzano Unit has been sedimented during the subsequent northward Rupelian transgression, in an overall distensive (or transtensive) geodynamic context related to the coeval Balearic rifting (Mutti *et al.*, 1995).

Regarding the M.Piano-Ranzano succession, Mutti *et al.* (1995) also stressed the time-equivalence and the stratigraphic similarities with the Priabonian-Rupelian sedimentary succession of the western external Alpine domain (*i.e. Grés d'Annot* Formation), also confirmed by the compositional analogies of the volcanoclastic detritus characterizing the upper Ranzano Unit and the Oligocene Alpine foredeep (*i.e.* Taveyanne Unit; Cibin *et al.*, 1998).

3.3 Specchio Unit outline

The Specchio Unit is the most impressive chaotic complex intercalated within the Epiligurian Ranzano Unit and entirely crops out in the Pessola Valley type-location (Northern Apennines, Parma province). The recognition and interpretation of this chaotic unit as an ancient submarine landslide deposit were firstly made in the middle '60 (I.G.G.P Parma, 1965).

Geological mapping and field-based surveys, supported by litho-, petro- and bio-stratigraphic analysis (Mutti *et al.*, 1995; Catanzariti *et al.*, 1997; Martelli *et al.*, 1998; Cibin *et al*, 2001), confirm the presence of this unit in at least 3 Epiligurian sedimentary successions cropping out in the Padan side of the Northern Apennines (in order from NW to SE): Mt. Roccone, Mt. Barigazzo and Pessola Valley areas. Also the Mt. Piattello and Enza Valley outliers are supposed to bear the Specchio Unit, but are only partially discussed in this work given the poor exposures and tectonic complications, respectively (fig. 3.18).

This unit seems to locally crop out also in the Varano de'Melegari-Pellegrino Parmense outlier (exposed to the NE of the Pessola Valley area and partially investigated in this work) as a thin interval (few meters thick) separating R3 unit from the MMP unit.

This chaotic complex has been attributed to the Varano de'Melegari member by Martelli *et al.* (1998), given its basal regional unconformity, while Mutti *et al.* (1995) considered it as a separate member of the Ranzano Unit.

The estimated relative volume of the Specchio Unit is about 150 km^3, calculated in a conservative way assuming the mean distance between outcropping areas: 60 km in length from NW to SE, 25 km in width from SW to NE and considering an average thickness of 100 m.

This unit is therefore an excellent stratigraphic marker for the correlation of the Ranzano Unit through the Epiligurian succession comprised between these Epiligurian outliers (Mutti *et al.*, 1995) (fig. 3.19).

This unit was firstly interpreted as an *endo-olistostrome* (*i.e.* submarine landslide deposit composed by intra-basinal material) by Abbate (1981) and its emplacement age was attributed to the middle Rupelian (Catanzariti *et al.*, 1997).

Actually this chaotic complex encases multi-sized not dissociated elements (*i.e.* slide blocks, olistoliths, slabs) belonging to the underlying Ranzano and M. Piano Unit, but also Ligurian-derived material, thus the original definition of endo-oliststrome results obsolete.

Particularly the intra-basinal elements consist of fluvio-deltaic (*i.e.* fan-delta, delta-slope and pro-delta deposits) and shelfal sediments (*i.e.* glauconitic and bioclastic calcarenites and siltstones); moreover the overall shallow-water origin of these deposits is confirmed by the strong presence of boulders and pebbles with bioerosional hollows (Mutti *et al.*, 1995).

These authors have linked the deposition of this chaotic complex to a major tectonic phase (*i.e.* their Ligurian Phase III), which forecasts the uplift and subsequent destabilization of a Ligurian-related mega-structure (*i.e.* Antola Unit topographic high), representing the separation zone between eastern TPB and the truly apenninic M.Piano-Ranzano basin system, developed by the activation (or re-activation) of the Villavernia-Varzi-Ottone-Levanto Tectonic Lineament (Mutti *et al.*, 1995) (fig. 3.20).

Moreover, Catanzariti *et al.* (1997) tentatively proposed the possible correlation of this mass-wasting complex to a relative eustatic lowering on the basis of the oxygen isotope stratigraphy.

3.4 List of figures

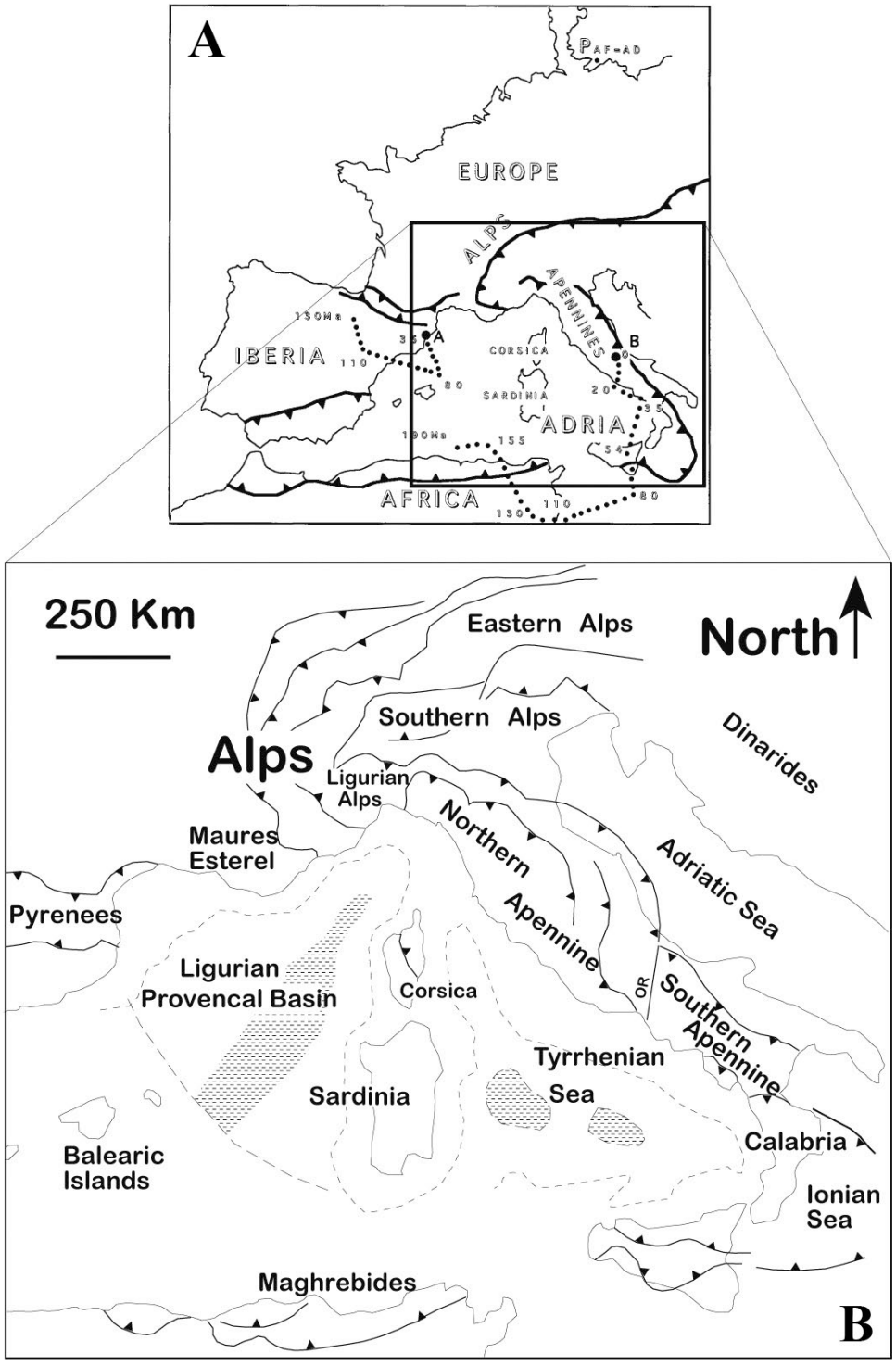

Figure 3.1 - Schematic sketches of the general Mediterranean Alpine-Apenninic orogenic system. **A.** General scheme of the Western Mediterranean area, showing the present position of the orogenic fronts (thick lines). Stippled lines: Late Jurassic to present displacement path of two points within the Adria Plate (B) and Iberia Plate (A), respectively (kinematic data calculated after Savostin *et al.* 1986). From Marroni and Treves (1998). **B.** Tectonic setting of the Northern Apennine within the Maghrebian-Apennine orogenic system and surrounding regions; OR: Ortona-Roccamonfina fault zone. From Cerrina Feroni *et al.* (2004), after Meletti *et al*.(2000), Vai and Martini (2001) and Molli & Tribuzio (2004).

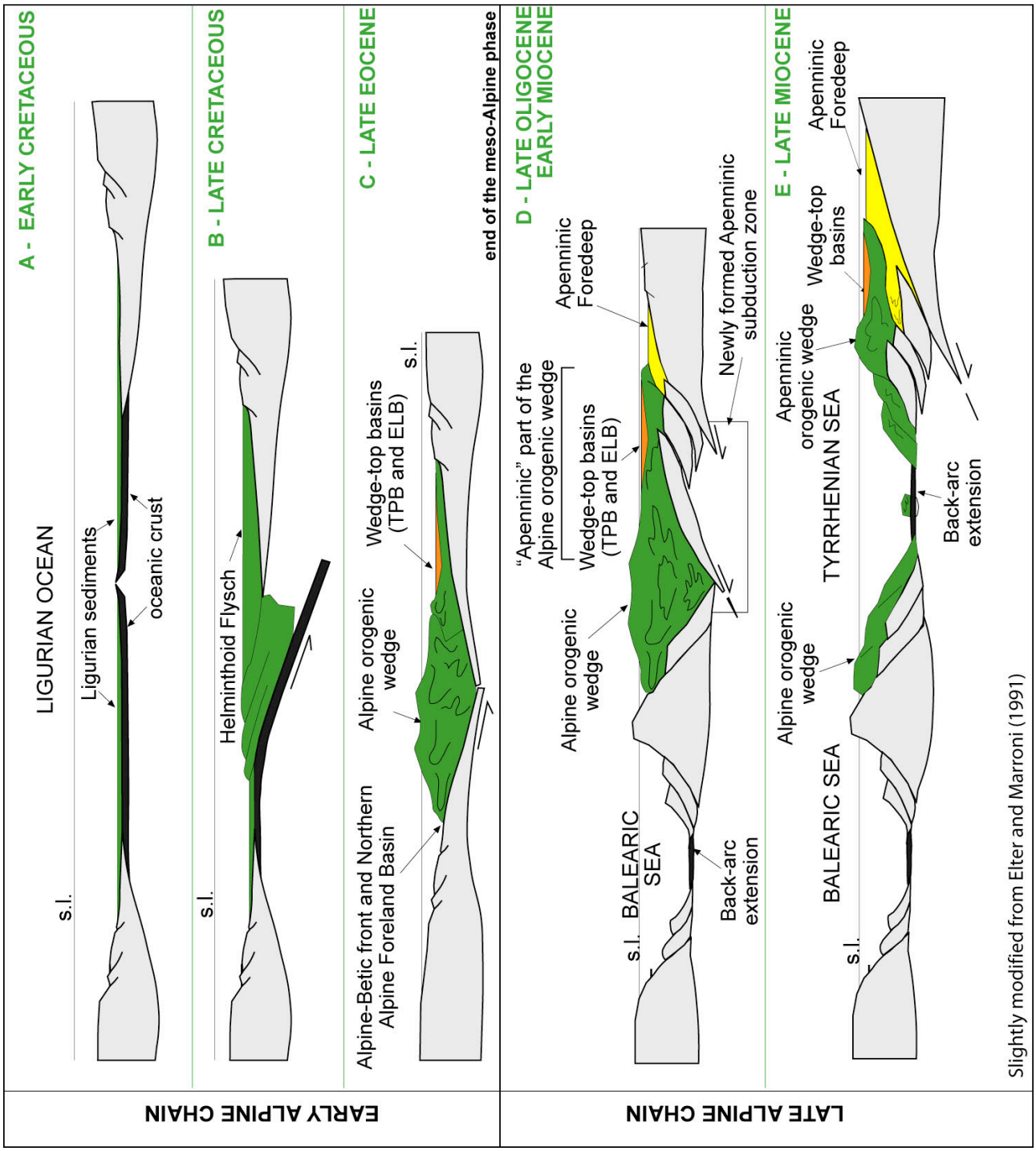

Figure 3.2 - Cartoon showing the main tectonic events of the Alpine-related Northern Apennine evolution. Redrawn and slightly modified from Elter and Marroni (1991).

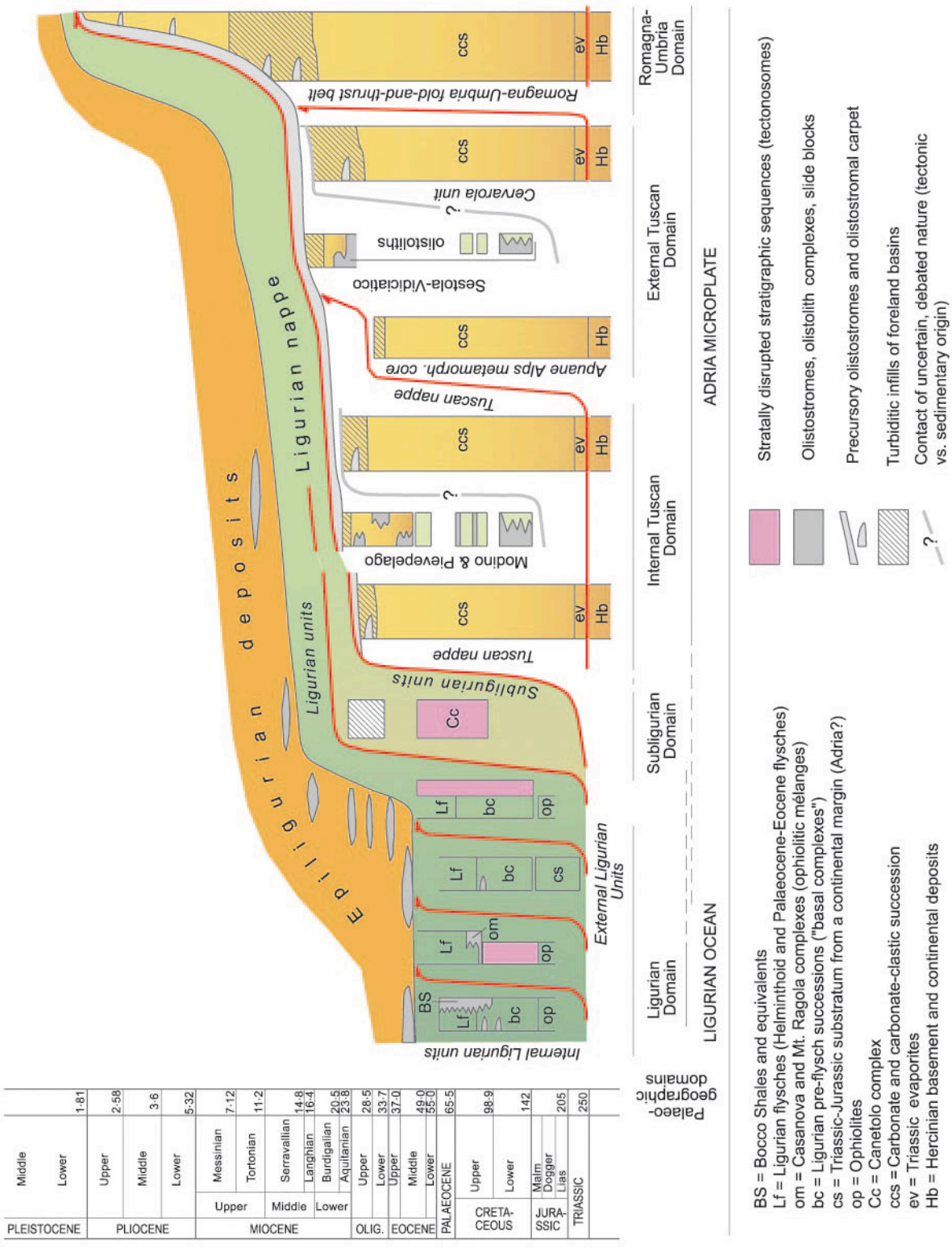

Figure 3.3 - Simplified structural-stratigraphic diagram of the Northern Apennines showing the main structural units, the lithostratigraphic groups and the palaeogeographic domains, with particular emphasis on the distribution of olisthostromes and tectonosomes (*sensu* Pini, 1999). Block letters indicate stratigraphic and palaeogeographic names; structural units are in italics. Note that the olisthostromes in the Epiligurian successions occur mainly within piggy-back sedimentary basins. From Camerlenghi & Pini (2009).

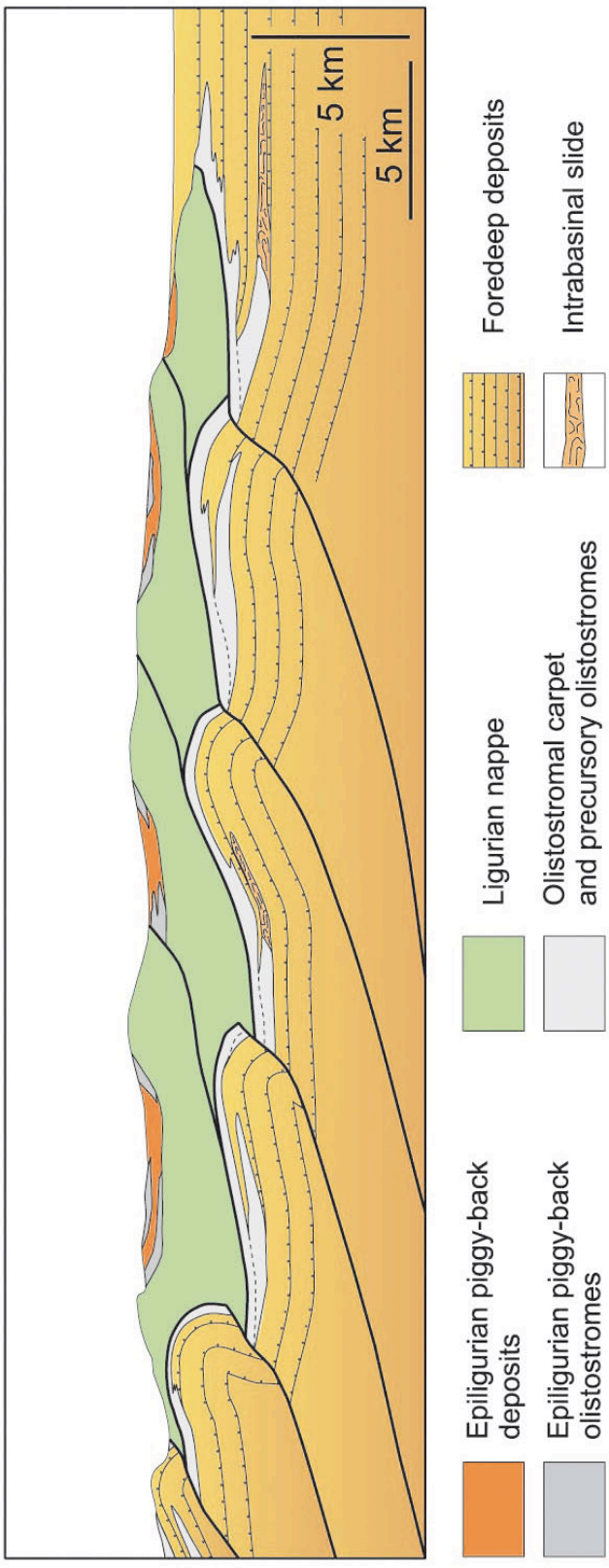

Figure 3.4 - Schematic conceptual geological section (note the small vertical exaggeration) across the northeastern side of the Northern Apennines at the transect of Bologna showing the relationships between the Ligurian Nappe (comprising Subligurian Units), the olistostromal carpet, the precursory olisthostromes and the largest submarine intrabasinal slides into the foredeep basin. The piggy-back olisthostromes on top of the Ligurian Nappe are shown as a part of the Epiligurian deposits.

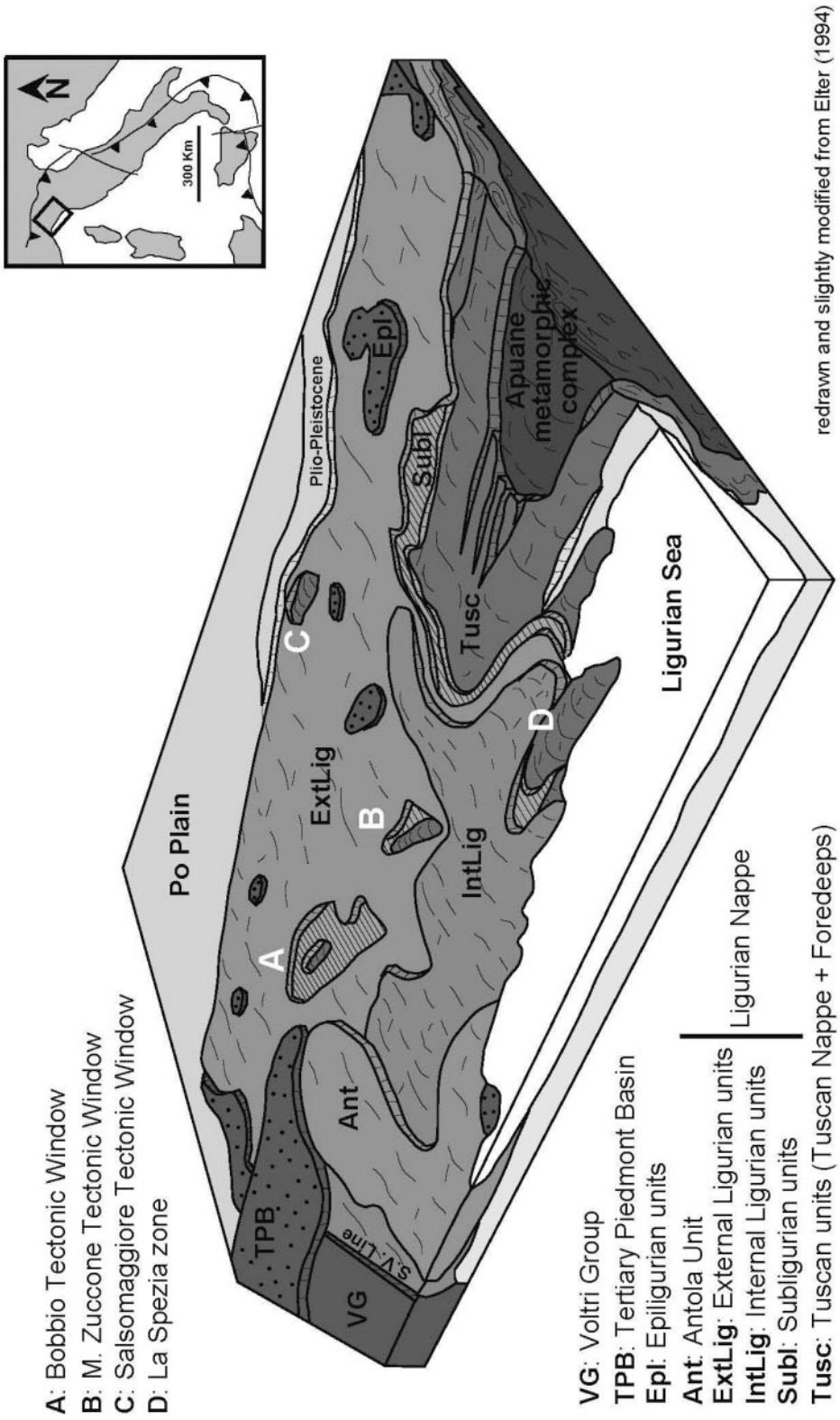

Figure 3.5 - Schematic block diagram showing the general 3D architecture and the main structural units of the Northern Apennine tectonic stacking (redrawn and slightly modified from Elter, 1994).

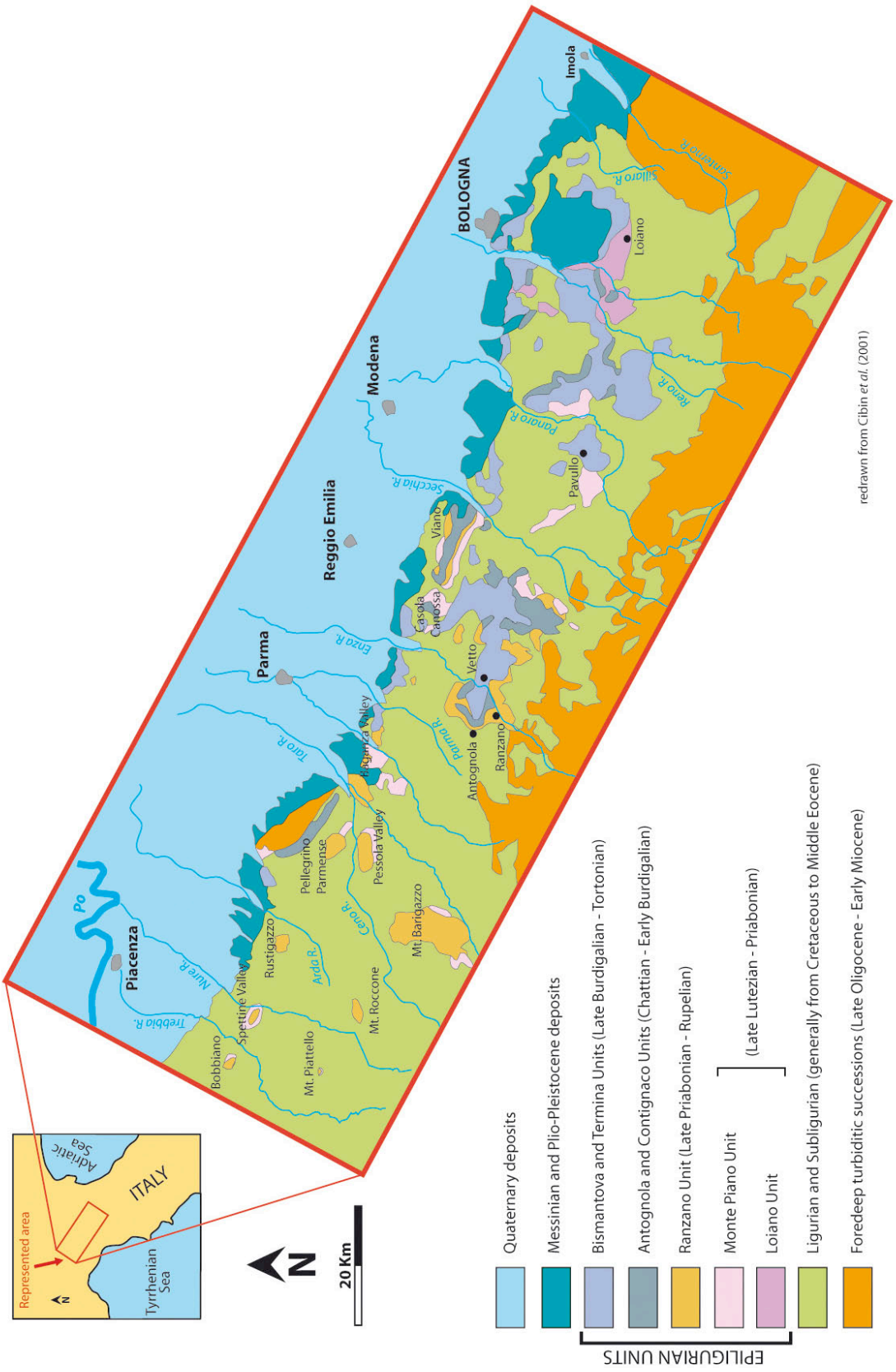

Figure 3.6 - Simplified geological map of the eastern side of the Northern Apennines between the Piacenza and Bologna provinces, to the NW and to the SE, respectively. Particular emphasis is given to the Epiligurian succession stratigraphic units. Redrawn and slightly modified from Cibin *et al.* (2001).

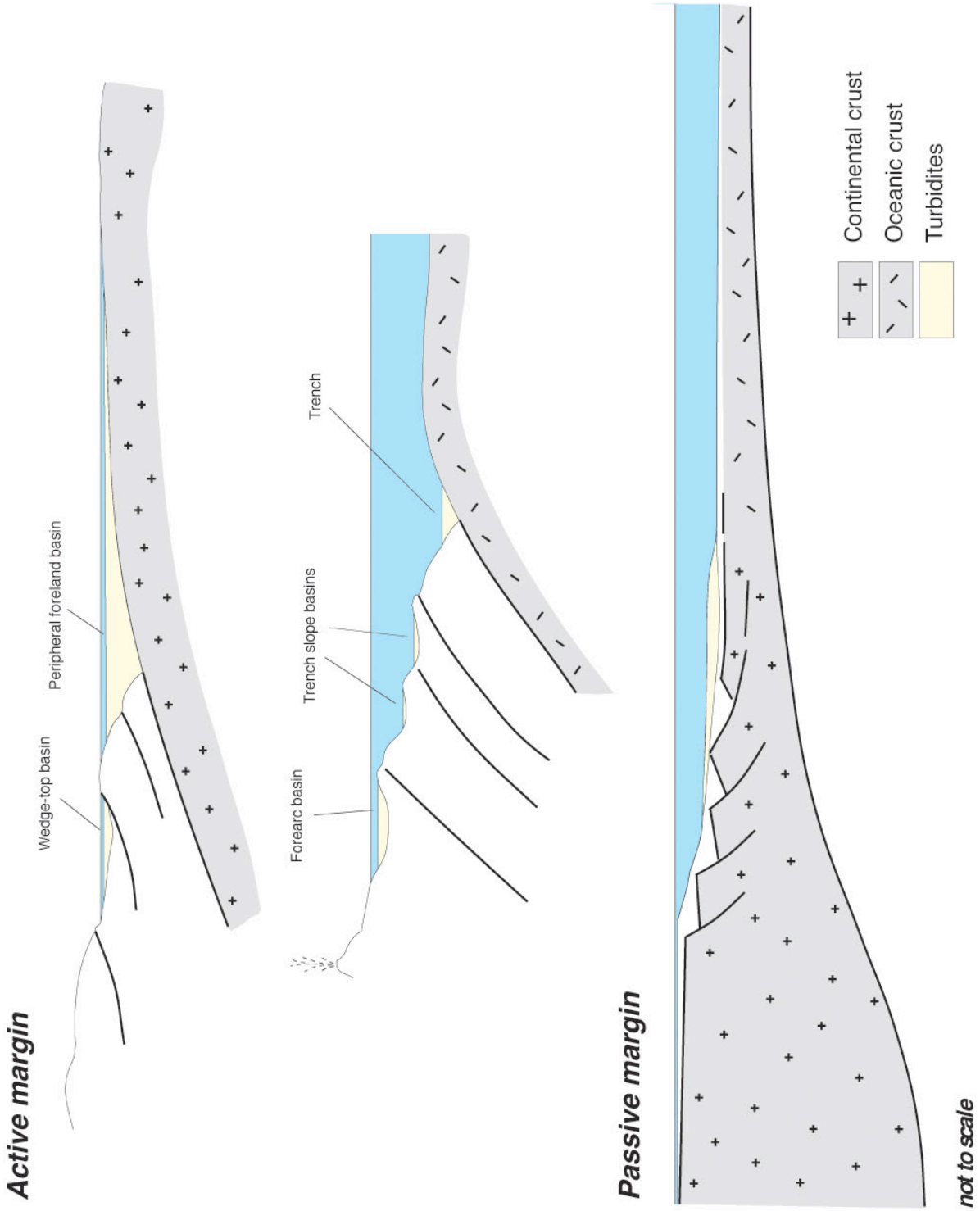

Figure 3.7 - Cartoon showing the main basin types and their localization within different continental margin settings. From Mutti *et al*. (1999).

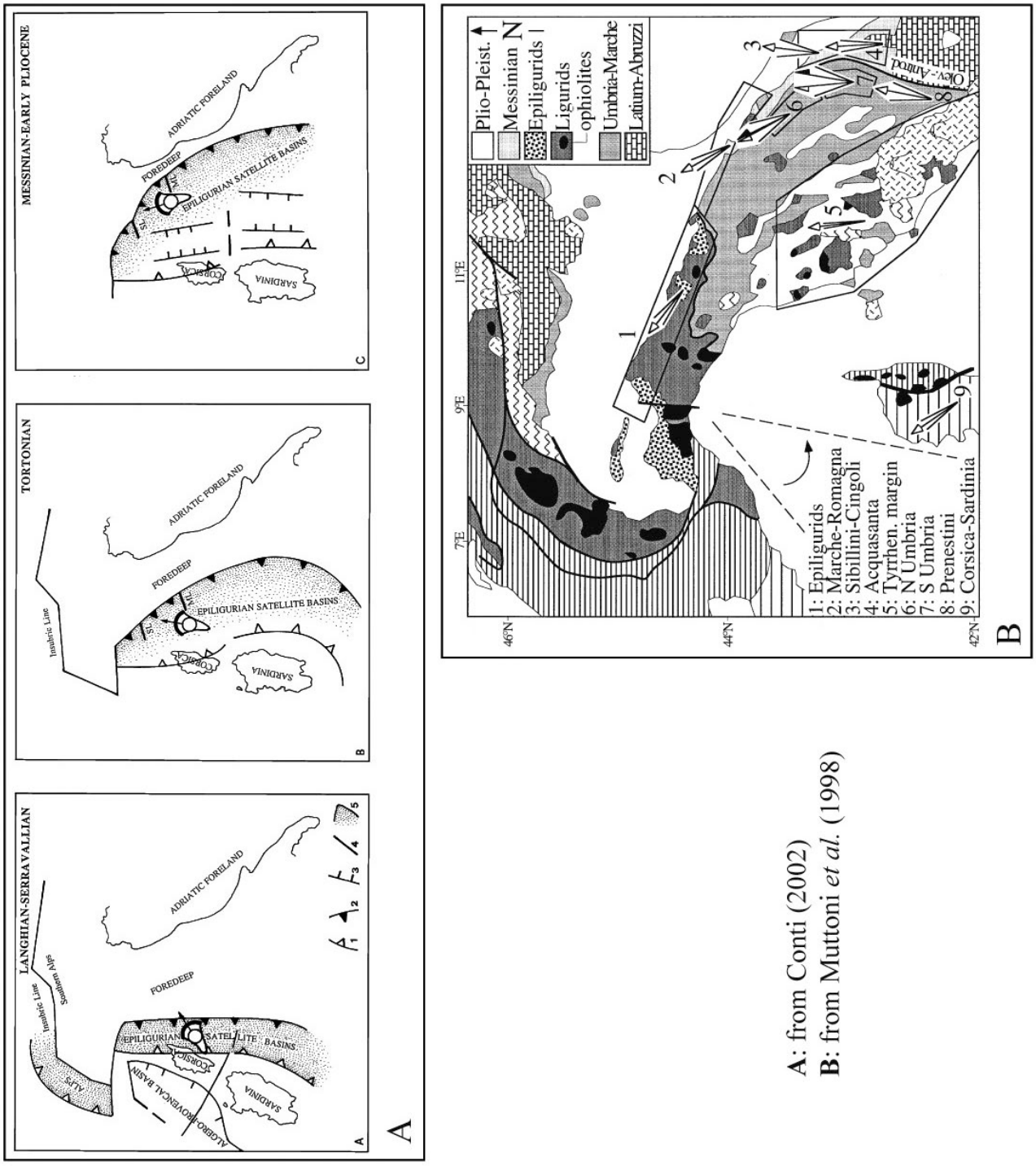

A: from Conti (2002)
B: from Muttoni *et al.* (1998)

Figure 3.8 - Schematic maps representing the anti-clockwise rotation of the Apennine orogenic system. **A.** Palaeogeographic reconstructions of the Northern Apennine deformational front during Langhian-Serravallian (A), Tortonian (B) and Messinian-early Pliocene (C). Various positions and rotations are derived from tectonic transport directions of satellite oroclinal bendings; 1) Alpine front, 2) Apennine front, 3) extensional basins, 4) tear and strike-slip faults (SL=Sillaro Line, ML=Marecchia Line), 5) chain sector under compression. From Conti (2002). **B.** Tectonic map of the Northern and Central Apennines from the *Carta Tettonica d'Italia* 1:50.000. Arrows, with attached reference numbers, represent the angle V between observed and expected paleomagnetic directions. From Muttoni *et al.* (1998).

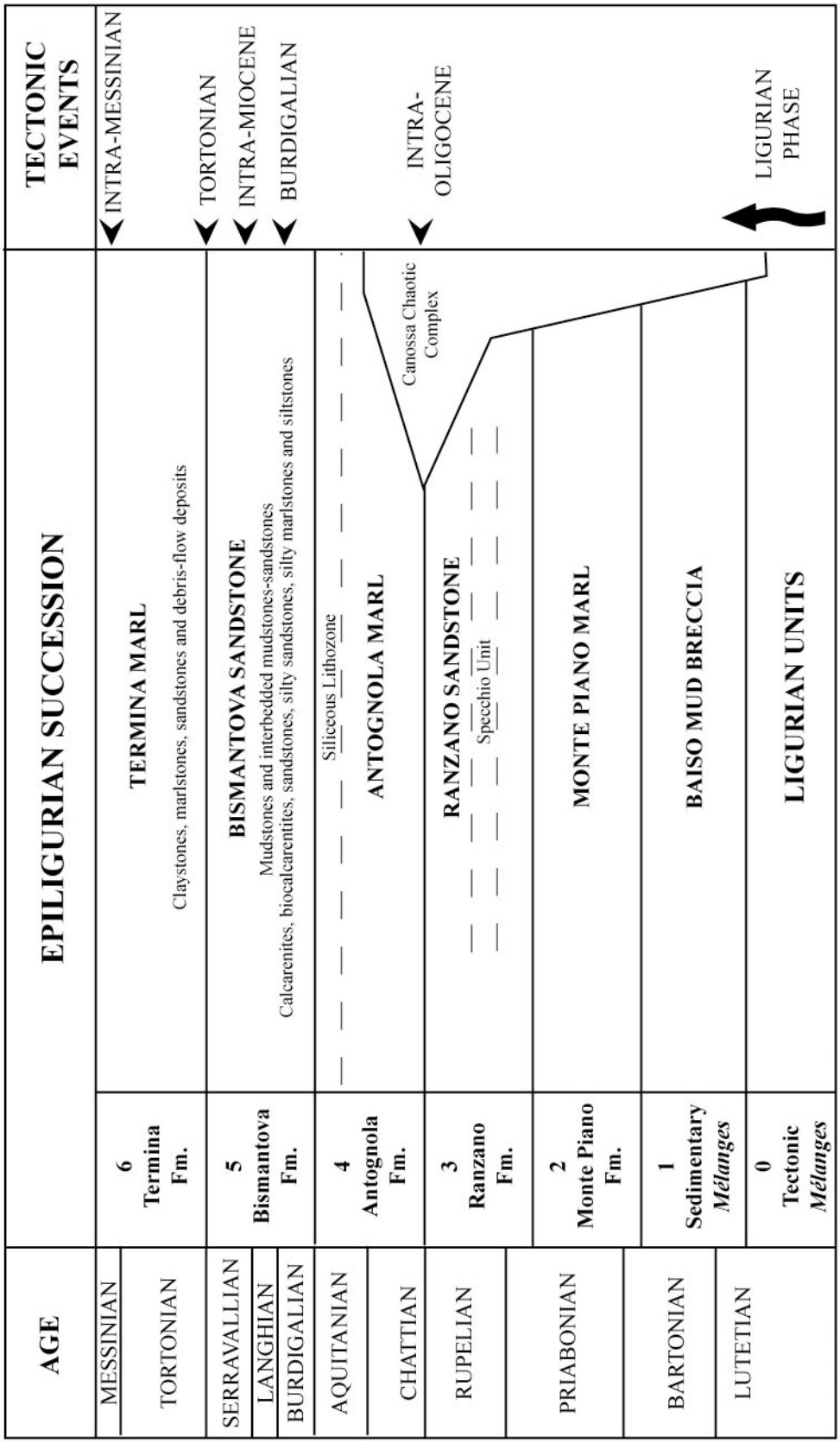

Figure 3.9 - Synthetic table showing the main stratigraphic component units of the Epiligurian succession, their age and the inferred corresponding tectonic events. Redrawn and modified from Bettelli *et al* (1987).

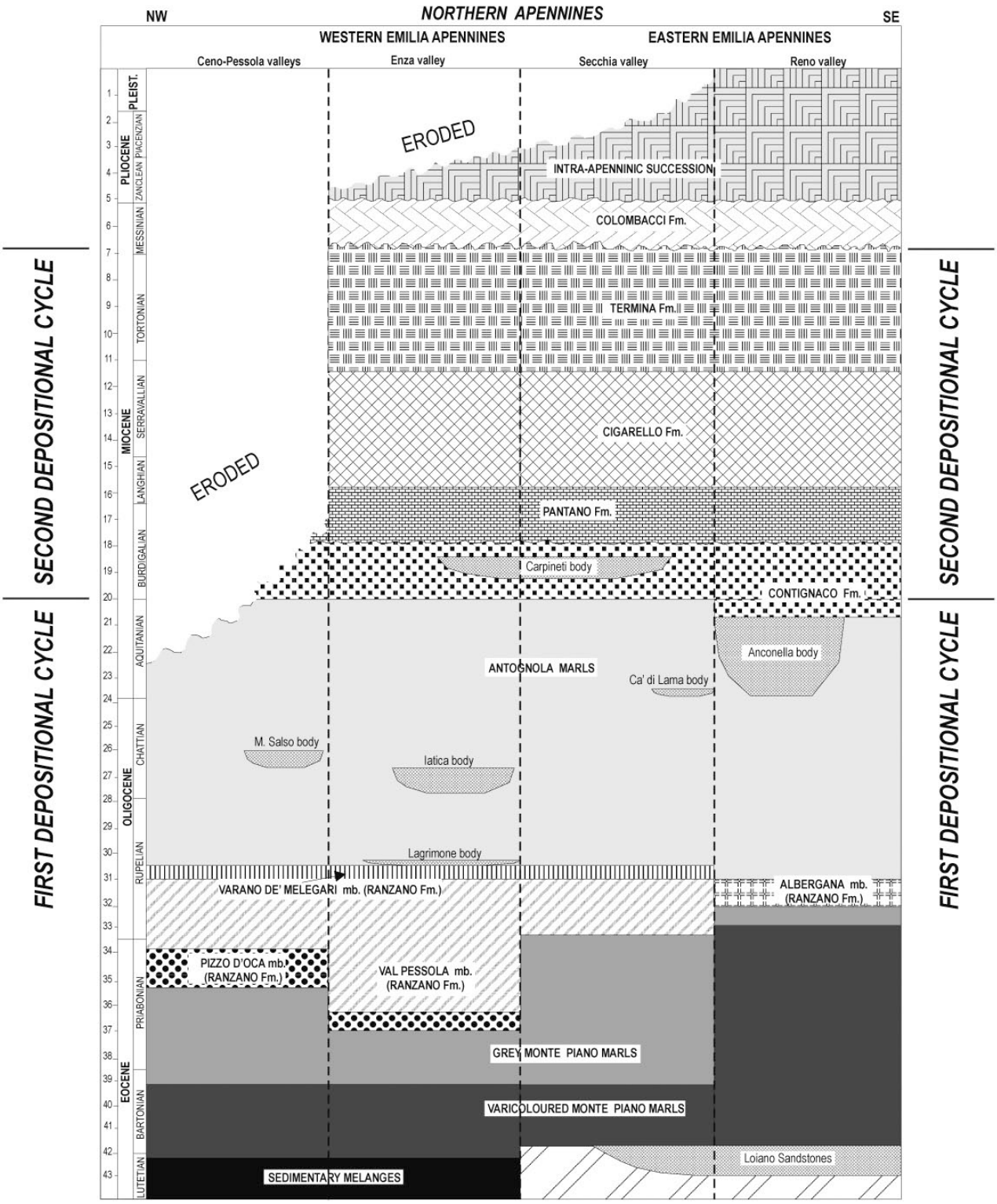

Figure 3.10 - Stratigraphic relationships of the lithostratigraphical units forming the Epiligurian Succession in the Pessola, Enza, Secchia and Reno valleys. Synthesis of the chronostratigraphic data after Mancin & Pirini (2001) and Cerrina Feroni *et al.* (2004 and references therein). From Mancin *et al.* (2006).

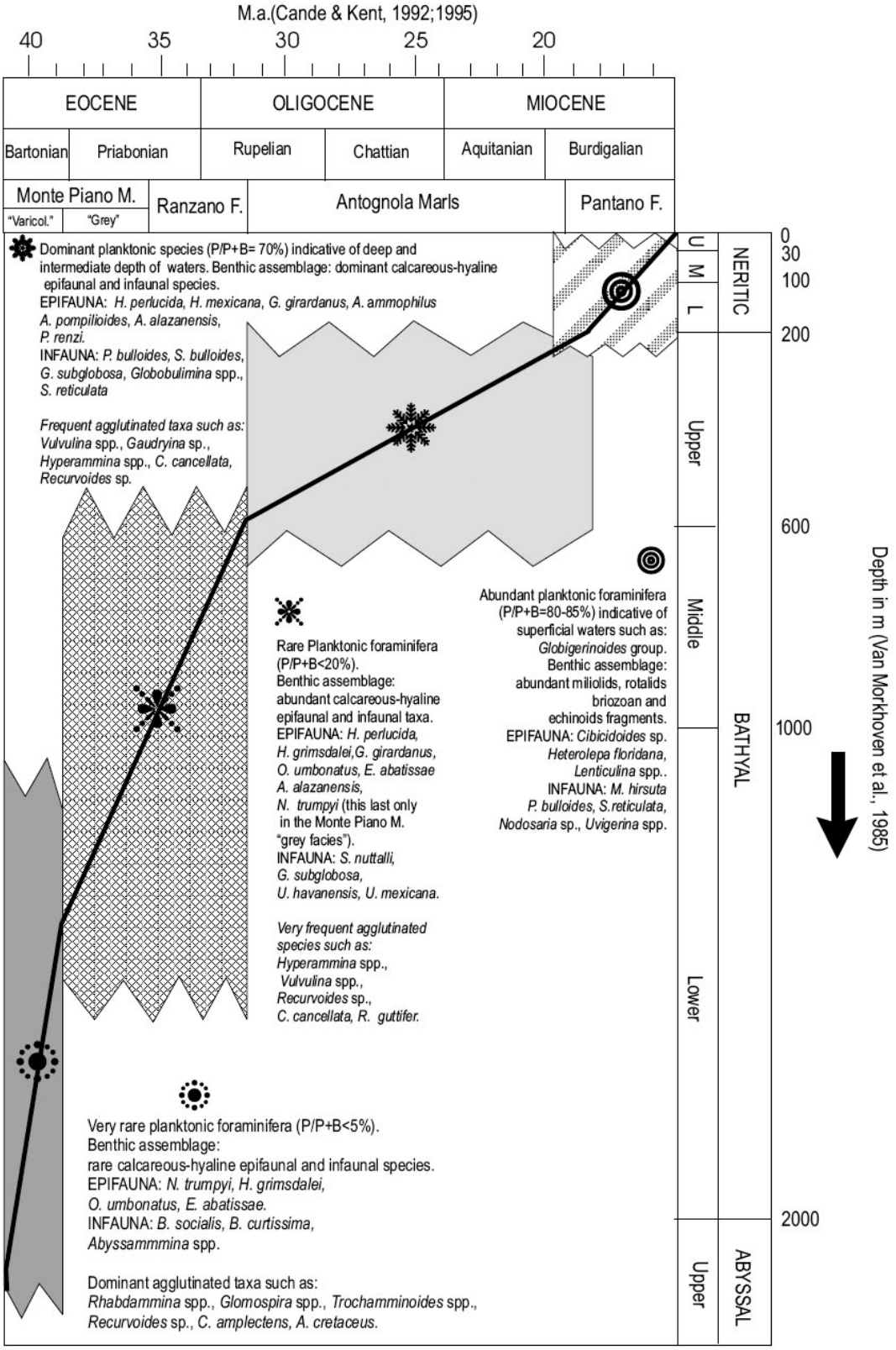

Figure 3.11 - Synthesis of paleobathymetric data concerning the Epiligurian lithostratigraphic units according to planktonic and benthic foraminifer assemblages. From Di Giulio *et al.* (2002).

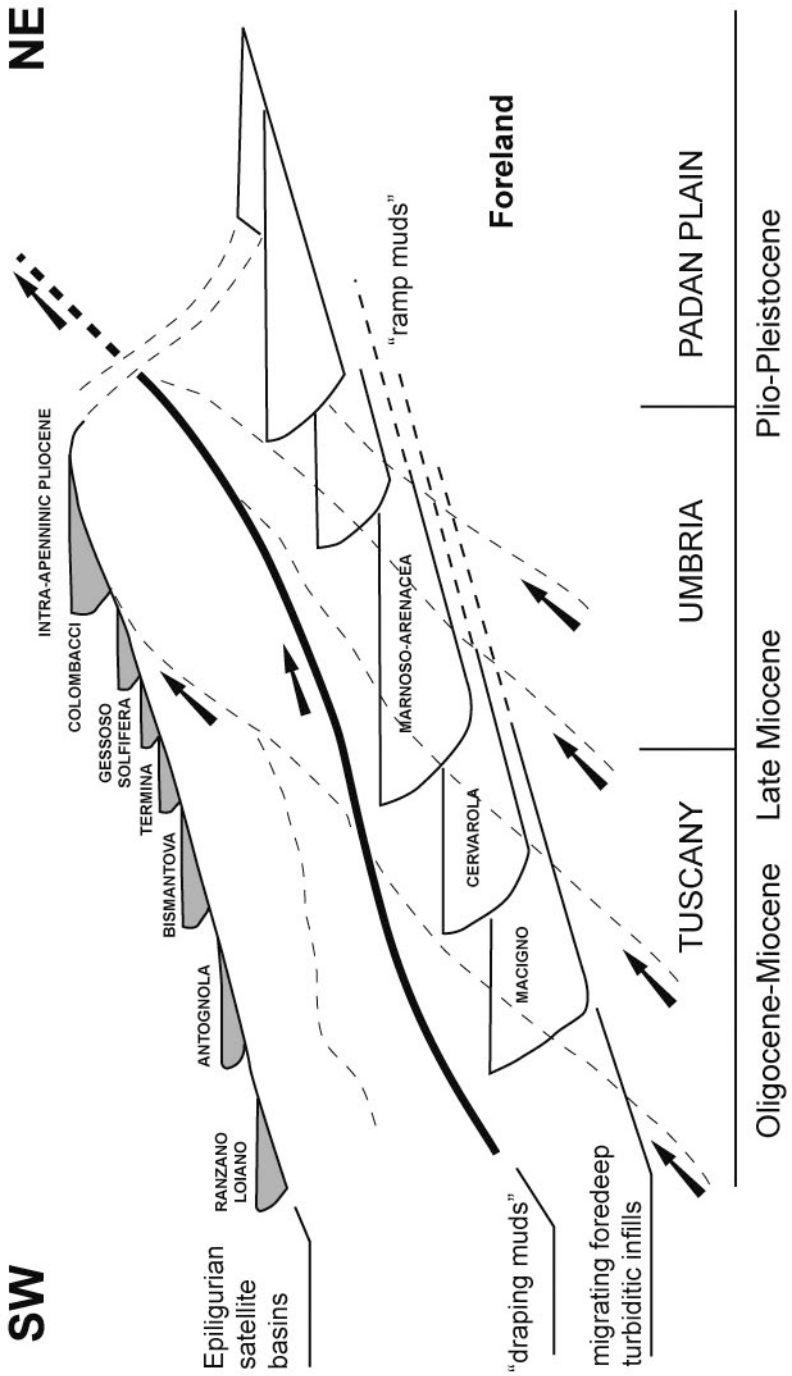

Figure 3.12 - Conceptual scheme of the possible temporal-spatial relationships between Epiligurian satellite basins and the migrating foredeeps. Redrawn from Ricci Lucchi (1986).

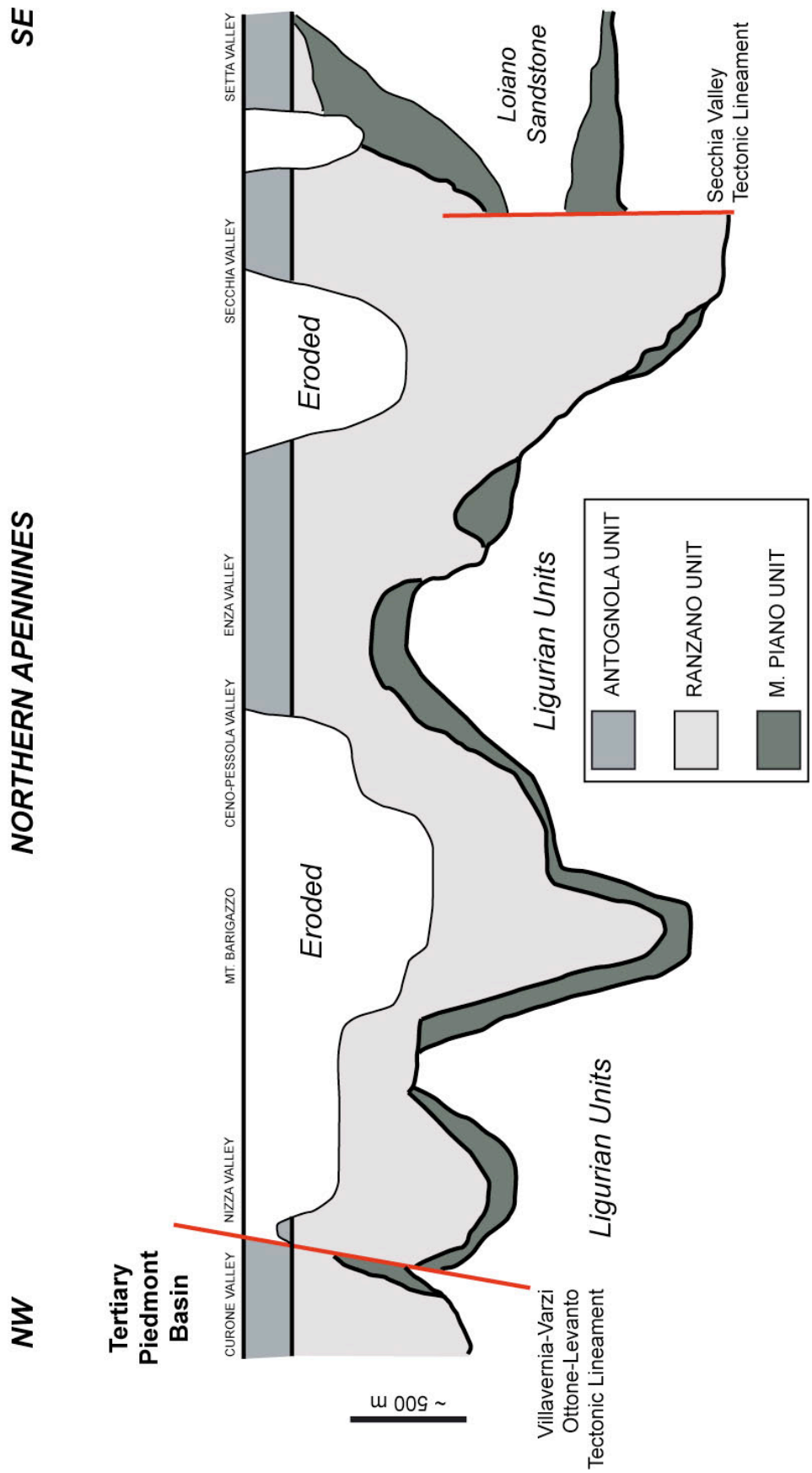

Figure 3.13 - Simplified scheme of the Ranzano unit upper- and lower- stratigraphic relationships in a NW-SE transect throughout the eastern side of the Northern Apennines, from the eastern TPB to the Bologna area. Redrawn and slightly modified from Mancin & Pirini (2001).

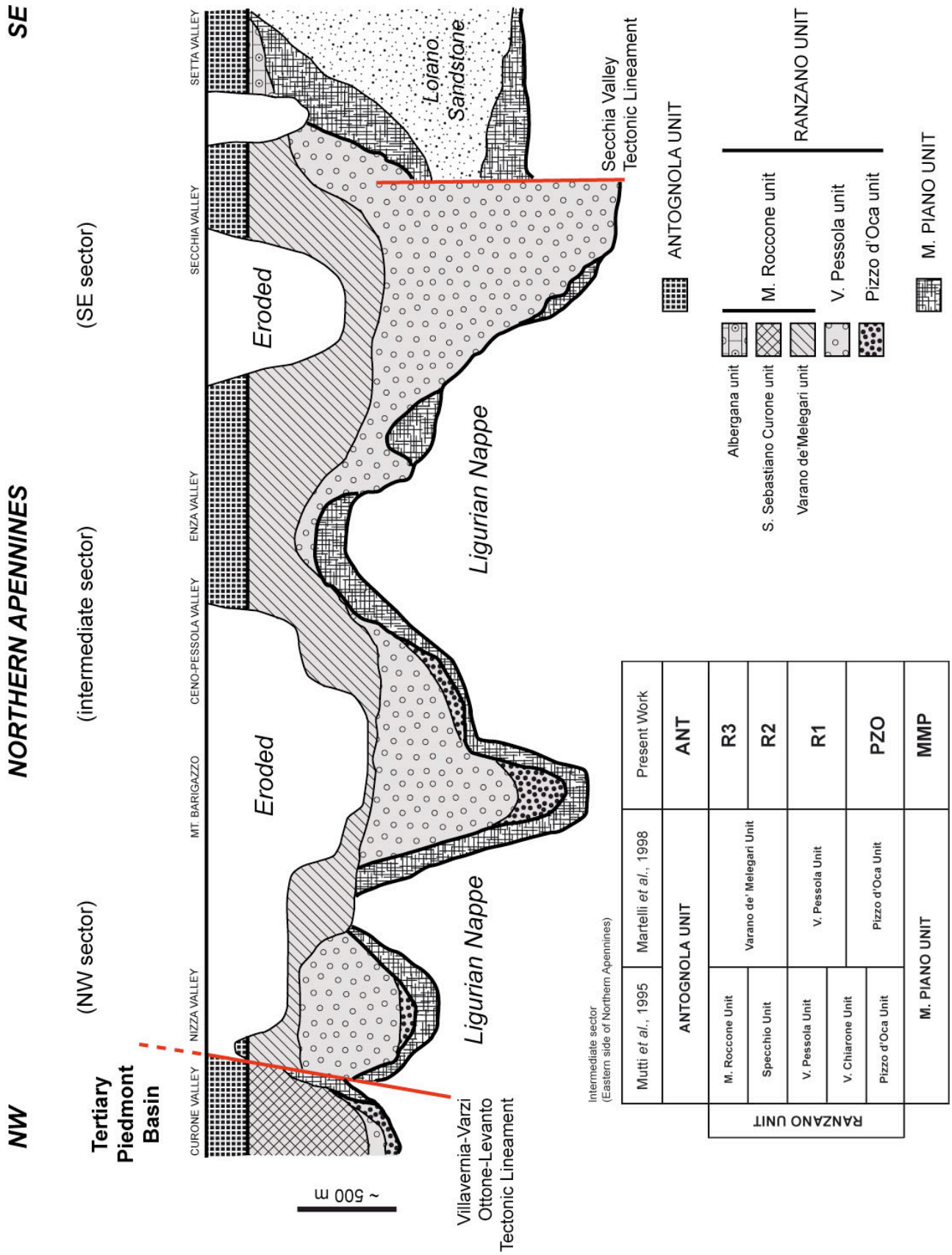

Figure 3.14 - Simplified sketch showing stratigraphic relationships of the Ranzano Unit component members along the same transect of fig. 3.13, with table explaining the correspondent terms used in this work. Redrawn and slightly modified from Martelli *et al.* (1998) and Mancin & Pirini (2001).

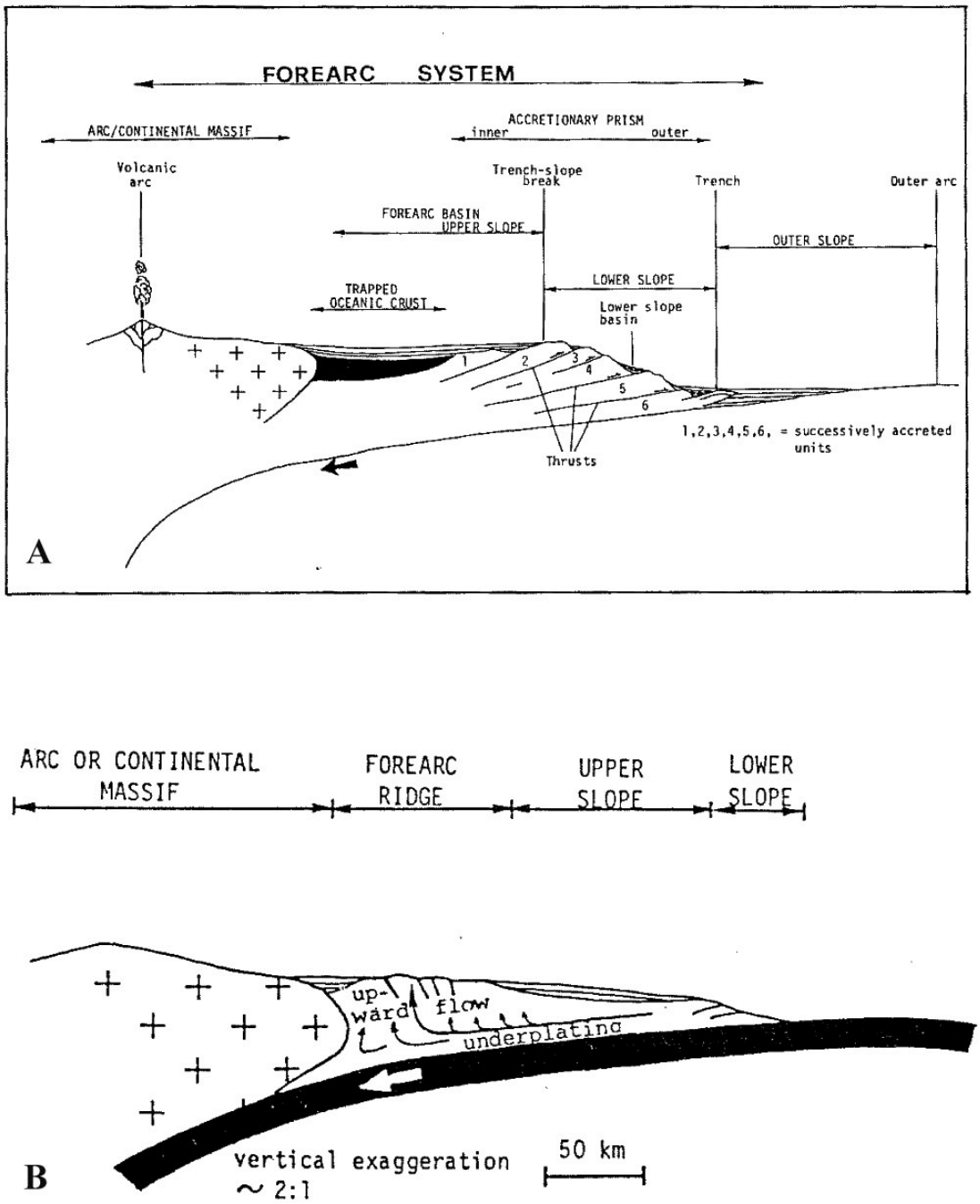

Figure 3.15 - Schematic cross-section trough an accretionary prism with terminology of the characterizing domains. From Principi and Treves (1984). **A.** General model for accretionary prisms characterizing modern trench-arc systems. From Treves (1984). **B.** General model of a more evolved accretionary prism developing underplating and back-stop upward fluid-flow. From Treves (1984).

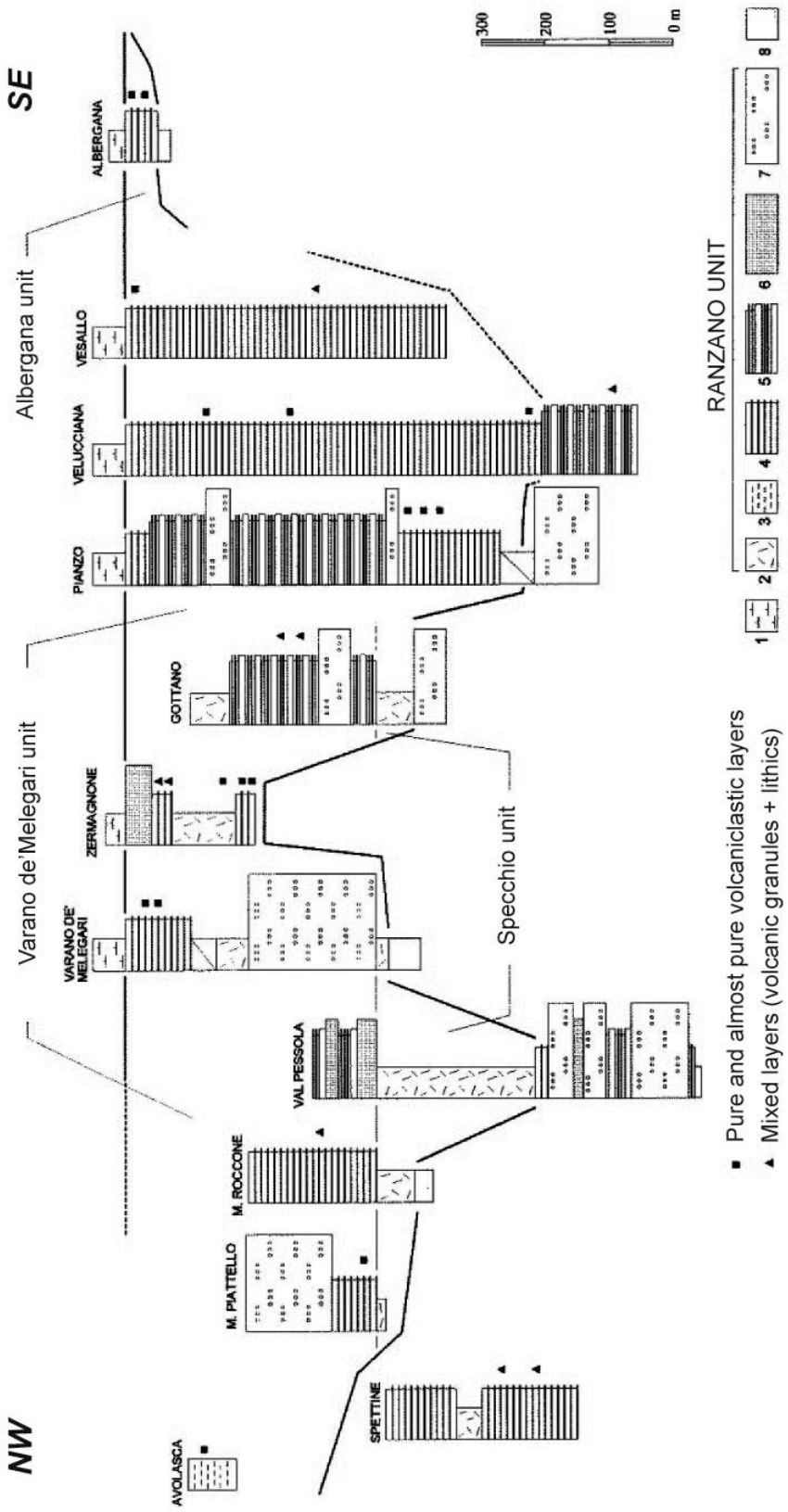

Figure 3.16 - Simplified correlated stratigraphic logs of the upper Ranzano Unit with positions of the volcanoclastic layers. 1. Antognola Unit; 2. sedimentary chaotic bodies; 3. mudstones; 4. mudstone-sandstone beds; 5. sandstone-mudstone beds; 6. sandstones; 7. coarse-grained sandstones and conglomerates; 8. M. Piano Unit. From Cibin *et al.* (1998).

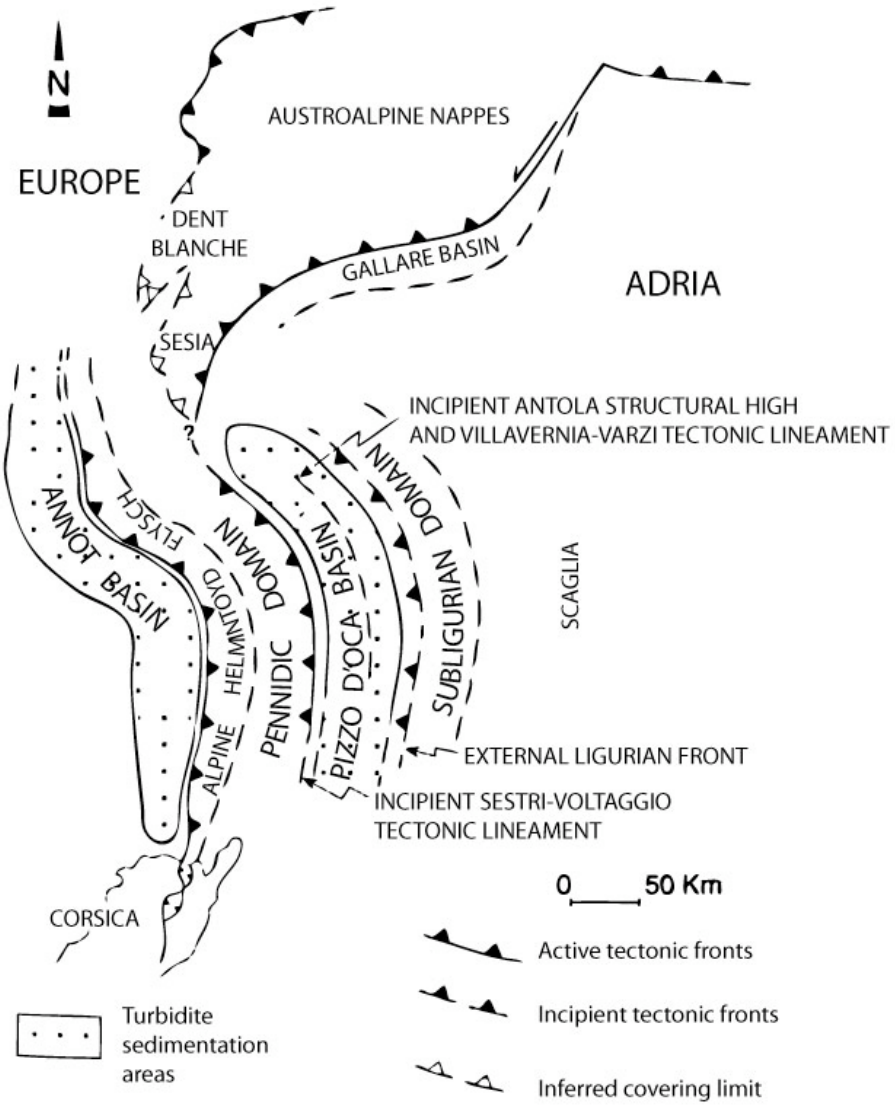

Figure 3.17 - Highly simplified palaeogeographic reconstruction of the Western Alps-Northern Apennine system during the deposition of the Pizzo d'Oca Unit (Priabonian).In the western part of the Alpine prism, the Helminthoyd Flysch Nappe, already thrust over the Briançonnais Domain, represents the tectonically active margin of the Gres d'Annot Basin. In the central sector of the prism, part of the Pennidic Domain is already undergoing sub-aerial erosion (Costa Crevara Breccias); the inner boundary of the Pennidic Domain is represented by an Adria-verging tectonic feature, the future Sestri-Voltaggio Tectonic Lineament. In the inner sector of the Alpine prism, the Pizzo d'Oca Basin overlies Ligurian Units deformed during the Mesoalpine Phase. The Pizzo d'Oca Basin is separated from the Subligurian Domain through the External Ligurian Front, another Adreia-verging tectonic structure. Subsequent thrust-related uplift of this feature will cause emergence and ensuing sub-aerial erosion of Ligurian Units during Ligurian Phase II. From Mutti *et al.* (1995).

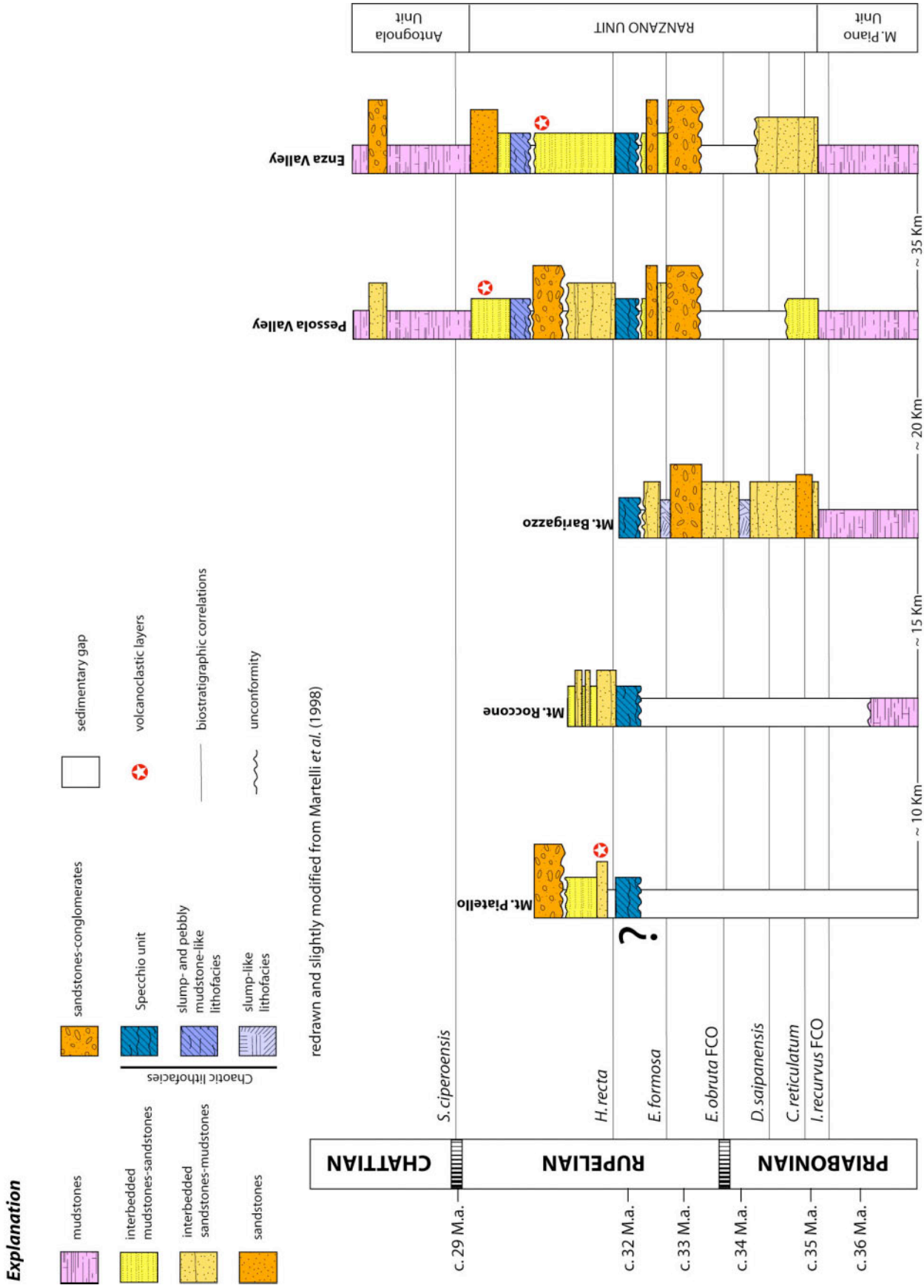

Figure 3.18 - Diagram showing the lithofacies chronostratigraphic distribution of the Ranzano Unit on the basis of calcareous nannoplancton analysis (data from Catanzariti *et al*. 1997). Redrawn from Martelli *et al.* (1998).

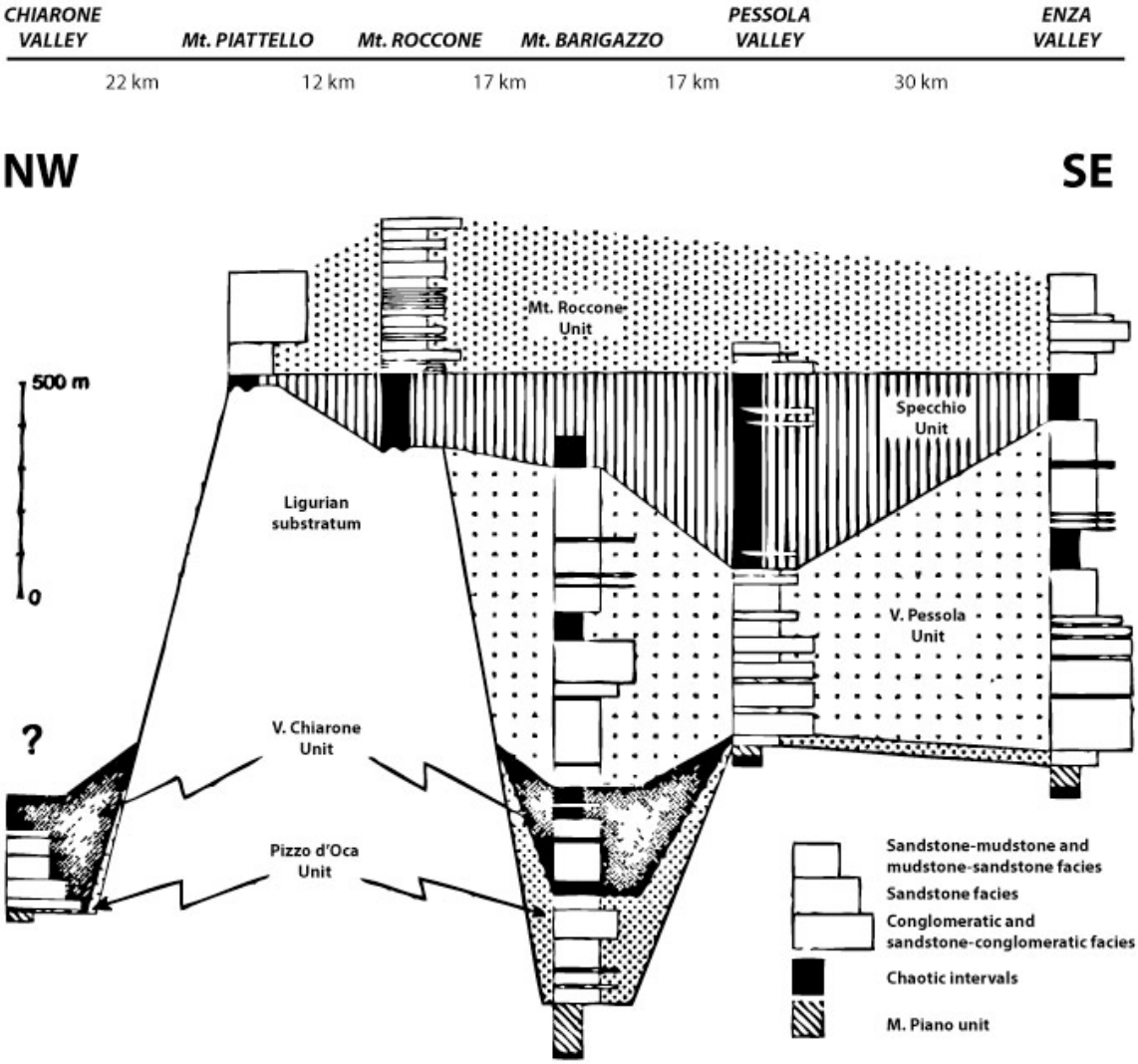

Figure 3.19 - Regional stratigraphic cross section of the Ranzano Unit in the Northern Apennines. The Ranzano Unit is here subdivided in five allostratigraphic units which, from base to top, include: Pizzo d'Oca Unit, V. Chiarone Unit, V. Pessola Unit, Specchio Unit and Mt. Roccone Unit. From Mutti *et al.* (1995).

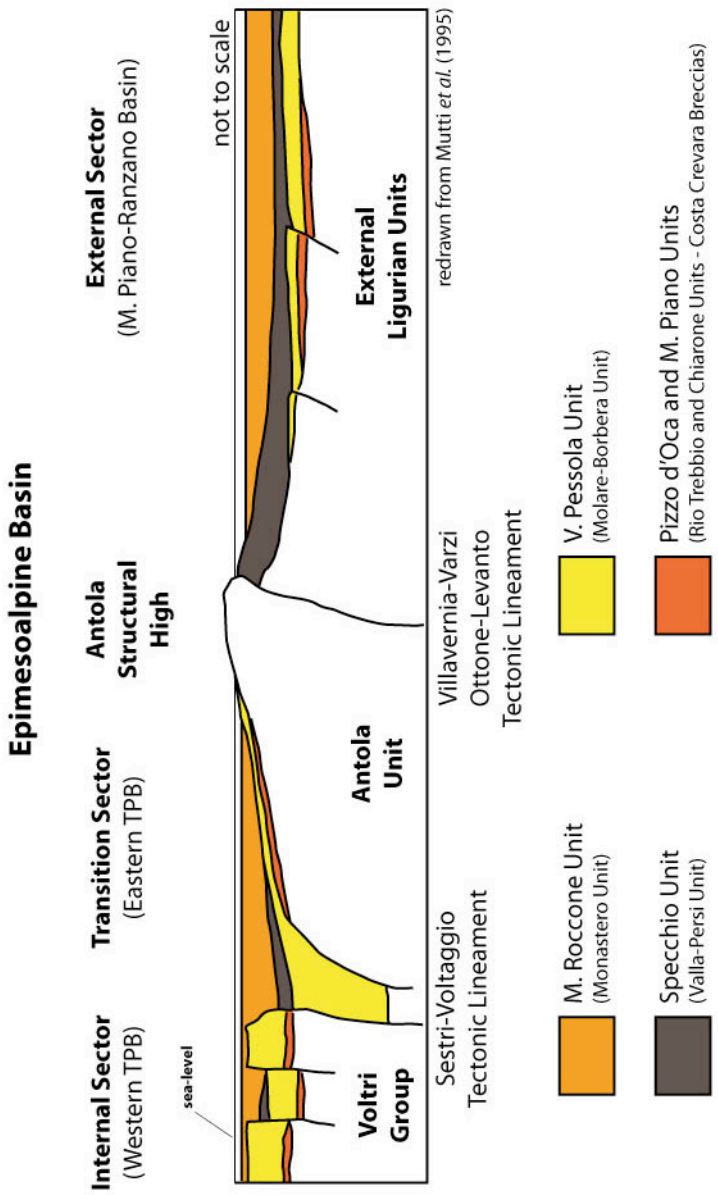

Figure 3.20 - Idealized cross section of the Epimesoalpine Basin at the end of deposition of the Mt. Roccone Unit (Monastero Unit in the TPB). The section is roughly perpendicular to basin axis. Note the influence of the "Antola Structural High" on basin configuration. Redrawn from Mutti *et al.* (1995).

4. PESSOLA VALLEY OUTLIER

This outlier crops out in the lower segment of the Ceno Valley (Parma province; grid n. 198120 and westernmost side of the grid n. 199090 CTR Regione Emilia-Romagna) and covers a surface of ~ 30 km^2. Here, the Pessola river, dextral tributary of the Taro river, cuts this synclinalic outlier in a roughly N-S direction, exposing the whole Epiligurian succession (fig. 4.1).

In this area, the Epiligurian succession represented by the M. Piano Unit and Ranzano Unit, reaches a thickness of ~ 800 m and lies on a substrate mainly composed by calcareous/ophiolite-bearing shaly chaotic complexes, characterizing lower portions of External Ligurian Units (*i.e.* Cassio Unit Basal Complexes and Cretaceous Helmintoyd Flysch; see chap. 3) (fig. 4.2 and 4.3). These units are strongly dismembered by the poly-phased Cretaceous to Quaternary Alpine-Apennine tectonic deformations.

The most prominent tectonic structures affecting the Ligurian substratum and bordering this sector are a NE-vergent kilometric recumbent syncline to the SW (*i.e.* Mt. S. Antonio-Mt. Pareto structure), and a roughly defined tectonic window to the N exposing the Tertiary Helmintoyd Flysch (*i.e.* Mt. Sporno Unit; Vianino tectonic window of Zanzucchi, 1980).

This latter structure roughly separates the Pessola Valley outlier from the Varano de'Melegari-Pellegrino Parmense outlier to the NE, which is composed of younger Epiligurian sediments, and partly represented in the north-easternmost boundary of the studied area.

The Mt. S. Antonio-Mt. Pareto structure can be virtually continued into the Mt. Dosso structure to the W, defining a highly positive tectonic alignment roughly separating the Pessola Valley outlier to the NE and the Mt. Barigazzo outlier to the SW.

4.1 Previous studies

The Epiligurian succession of the Pessola Valley area was firstly characterized and mapped in the middle '60 (I.G.G.P Parma, 1965; Ghelardoni *et al.*, 1965).

Ghibaudo and Mutti (1973) made the first detailed stratigraphic study on the Ranzano Unit of this area, interpreting this succession as the infilling of NE-SW trending large-scale erosional feature (*i.e.* submarine valley) cut into the M. Piano Unit.

Litostratigraphic, sedimentologic, biostratigraphic and petrographic studies on these outcrops were made since the '70 (Gazzi and Zuffa, 1970; Iaccarino *et al.*, 1974; Barbieri, 1978; Masini and Pecchioli, 1988). Other studies aimed to the regional characterization of the Ranzano Unit through

the Northern Apennines are partly based on these rock expositions (Cibin, 1993; Mutti *et al*., 1995; Catanzariti *et al*., 1997; Martelli *et al*., 1998; Cibin *et al*., 2001, 2003).

Other detailed stratigraphic and sedimentologic studies highlight the presence of high-frequency cycles in the depositional trends of the Ranzano Unit in this area (Mutti *et al.*, 1994).

The last geological mapping campaigns of this area were made in the ’90 (Dattilo and Tebaldi, 1991; Mora, 1992; Costa and Frati, 1995).

The Pessola Valley outlier is represented in the sheet n. 198 “Bardi” of the 1:50.000 Geological Map of Italy (Italian Geological Survey, 2000).

4.2 Stratigraphy

In the Pessola Valley Epiligurian basin the sedimentation took place in the middle-upper Eocene over the deformed Basal Complexes of the overturned Mt. Cassio Unit. This succession begins after the meso-alpine phase, with localized Ligurian-derived shale-rich chaotic units characterizing the lower part of M. Piano unit (*i.e.* Baiso mud breccia; BAI), and continues in heteropic relationships with mainly hemipelagic interbedded marls and thin layered turbiditic silty-marls, progressively more abundant upwards (fig. 4.4). In this area the M. Piano unit has a variable thickness of about 40-70 m.

For the strata characterization, here I will use the facies types proposed by Mutti (1992), with a strictly descriptive meaning.

Through a regional unconformity, the sedimentation of the Ranzano Unit begins with the Pizzo d’Oca unit (**PZO**), which takes place over the M. Piano Unit, and represents the first important siliciclastic input of the Pessola Valley basin.

This unit is characterized by fine- to medium-grained, medium- to thin-bedded, graded sandstones (average thickness of ~ 15-20 cm) and mudstones (sand mud ratio; S/M ≈ 1) with a quartz-feldspar lithic composition, giving a diagnostic alteration color. This unit shows an irregular areal distribution (sometimes completely lacking) due to previous basinal morphology and erosion phenomena associated with overlying deposits.

In the analyzed section this unit reaches the maximum thickness of ~ 10 m, with a lower transitional contact with the MMP unit and an upper sharp erosional contact to the R1 unit (fig. 4.5).

The beds show the typical characteristics of the F8-F9 facies of Mutti (1992), with sharp base and more or less laminated transitional top, showing a massive appearance in the lower portions,

except for a rough grading. The rare groove casts present at the base of thicker strata indicate a roughly NE-SW direction.

The **R1** unit, which takes its name from this type-locality (*i.e.* Pessola unit of Mutti *et al*., 1995 and Martelli *et al*., 1998), is well exposed in this area and sharply overlies the Pizzo d'Oca unit, and locally the M. Piano Unit, reaching a maximum thickness of ~ 350 m in the studied section (fig. 4.6).

Due to the favorable exposure conditions of this area, the R1 unit has been studied in detail (1:20 scale) through the measurement of a general log (crossing upper part of MMP and PZO units) and three punctual stratigraphic logs, collected in the southern sector, each one intersecting the R2 unit base.

This unit can be roughly separated into a lower conglomerate-rich portion (S/M >> 1) passing upward into an upper portion made up of coarse- to medium-grained sandstones (S/M > 1). The latter is characterized by localized intercalations of fine-grained and thin-bedded portions (S/M ≈ 1).

The whole succession is generally composed of amalgamated and lenticular thick-bedded (up to 1.5-2 m), coarse-grained (up to granule conglomerate) and poorly cemented sandstone beds, sharing only little evidence of mudstone portions (fig. 4.7).

These strata are mainly massive, in which a more or less evident grading, grain-size breaks (*i.e.* bypass surfaces), traction carpets and faint crude parallel laminae concentrated to the top can be observed (fig. 4.8); their base is usually erosive, showing several evidence of coarse-grained filled scours and loading-related liquefactions and fluid-escape features, roughly concentrated along amalgamation surfaces (fig. 4.9)

Abundant mudstone clasts deriving from both underlying MMP unit and intraformational mudstone beds, sometimes also as cm- to dm-sized "armored balls" (fig. 4.10), and pillar-like fluid escape structures (evidenced by a common "flaking off" appearance) are also common.

In the lowermost portions, thicker beds show evidence of Ligurian-derived clay chips, up to ~ 30 cm across (fig. 4.11). These beds can be ascribed to the F5 facies, sometimes associated to a basal F3 residual deposit (Mutti, 1992; Mutti *et al*., 1999).

From a panoramic view, the general bedding is underlined by the occurrence of aligned diagenetic nodules (created by an incipient cementation around carbonatic and marly elements), usually concentrating in intermediate-upper portion of sandstone beds (fig. 4.12).

The other types of beds characterizing R1 unit are represented by medium- to thin-bedded (from few cm- to dm-thick), coarse- to medium-grained sandstone beds, showing faint grading and crudely developed large- to small- scale oblique laminations, and commonly sharing sharp

undulated tops. These layers show extremely lenticular geometry, wedging out at the outcrop scale (fig. 4.13). These beds share the characteristics defined for the F6 facies of Mutti (1992).

Sometimes, at the base of thicker coarse-grained beds, localized and roughly lens-shaped and usually strongly oxidized intervals of unsorted pebbly sandstones with cm- to ten of cm-sized mudstone intraclasts may occur. These intervals show more or less transitional upper and lower contacts, and have been interpreted as an "impact breccia" due to seafloor erosion operated by overriding flows (fig. 4.14).

These deposits, moreover, are characterized by meters-thick fining- and thinning- upward facies sequences that could be interpreted to record an internal high-frequency cyclicity, usually masked by the evident syn-sedimentary tectonic activity (Mutti *et al.*, 1994).

The R1 unit shows a marked compositional difference in comparison with the underlying Pizzo d'Oca unit ones, sharing a mainly ophiolitic (subordinately carbonatic) Ligurian-derived clastic detritus. Some evidence of bioturbation (*planolites*-like ichnofacies?), scattered shell debris and plant fragment are also present, especially in the upper portions (fig. 4.15).

Approximately in the middle of the R1 succession, a distinctive bed, showing sedimentary characteristics quite different from the over- and under-lying strata, is present. This layer show a well developed T_{a-e} Bouma sequence, with a more or less constant thickness of ~ 1 m across the area, and is composed of medium- to fine-grained sandstone grading upward into a marlstone. The ripples in the upper part upper of this bed show alternating opposite palaeo-currents, probably produced by ponding (*i.e.* flow reflections) phenomena. These features and its basin-wide distribution make this bed a useful stratigraphic marker for the R1 unit, at least for the southwestern sector of this outlier (fig. 4.16).

The uppermost part of this unit is characterized by the localized presence of a ~ 25 m-thick pelitic-arenaceous succession (S/M ≈ 1) essentially composed of thinner, finer grained and more laterally continuous beds than the underlying ones (**R1 thin-bedded facies**), slightly similar to those occurring in the upper R3 unit (fig. 4.17). These beds, that are characterized by a significant increment in the plant fragments content, seem to be organized in intervals in which F6-F8 facies tend to predominate (fig. 4.18), even if some intercalated bed sets (*sensu* Campbell, 1967) of amalgamanted F5 facies (as described by Mutti, 1992), can be present.

This succession, confined in the western sector of the outlier, disappears in the other R1 outcrop, probably being almost completely eroded by the overlying R2 unit.

Sole structures are weakly developed, and the recognized palaeo-current indicators recognized are only some groove and flute casts (where beds are not completely amalgamated),

oblique laminations, asymmetrical scours and some ripple marks in the uppermost portions of finer grained beds (fig. 4.19).

The analysis of inferred palaeo-currents puts in light significant discrepancies (sometimes over the 90°) between primary flow-related features (*e.g.* bottom structures) and secondary flow patterns (*e.g.* traction + fallout structures), with relatively evident dispersions also within groove and flute casts directions, mainly in the R1 unit basal portions. Moreover, there is a quite significant difference between mean palaeo-flow directions characterizing lower R1 unit and the upper R1 thin-bedded facies, with the latter showing a relatively more developed concordance between primary and secondary flow-related structures. Although further analysis are needed, this evidence is here preliminarily attributed to a strong structural control exerted by depocentral margins on the R1 unit basal deposition (*e.g.* flow blocking- and reflection-related features), becoming progressively, and relatively, less important upwards (*i.e.* R1 thin bedded facies) (see attached panels n. 3 and n. 4).

The recurrent high angle in palaeo-current directions shared by F6 oblique laminations with respect to the bottom structures should be tentatively interpreted as marginal *versus* axial flux effects of channelized-like flows, as described by Mutti *et al.* (1994) and Mutti and Tinterri (2004).

On the basis of the sedimentary characteristics mentioned above, the R1 unit shows the typical characteristics of low-efficency turbidite systems characterized by surge-type high-density turbidity currents (as described by Mutti, 1979, 1992; see also Mutti *et al.*, 1999), thought to represent the infilling of localized depocenters belonging to an overall confined mini-basin system.

The chaotic deposits of the **R2** Specchio Unit mass transport complex abruptly truncate this unit. Given the regional unconformity surface represented by its basal contact and its composition, this unit has been considered as a separate member of the Ranzano Unit by Mutti *et al.* (1995), while Martelli *et al.* (1998) attributed it to the overlying Varano de'Melegari unit. This chaotic unit is the topic of this work and it will be discussed in detail in chap. 7.

The fine- to medium-grained (subordinately coarse-grained) sandstone deposits of the **R3** unit (i.e Mt. Roccone unit of Mutti *et al.*, 1995; Varano de'Melegari unit of Martelli *et al.*, 1998) restore the background sedimentation above the irregular surface of the R2 Specchio Unit (fig. 4.20).

The R3 succession of this area has been carefully investigated through the compilation of a general and 8 punctual stratigraphic logs, collected across the R2-R3 contact (one of them measured in the adjacent Varano de'Melegari-Pellegrino Parmense outlier) (see attached panel n. 4).

The basal contact of this unit is marked by the presence of a relatively thick coarse-grained and graded sandstone bed, with an irregular base, usually lying over a discontinuous m-thick interval of an "impact-breccia" facies (foundering into the underlying R2 unit through m-sized

sandstone-filled down-facing cusps), and a relatively sharp top. Given the distinctive features of this bed respecting to the overlying R3 strata, the strong relationship and its common occurrence at the top of the uppermost portion of the R2 unit, its characteristic are described together with the Specchio unit internal subdivisions (see chap. 7).

This unit, reaching a maximum thickness of ~ 100 m, records an overall compositional shift toward more carbonatic detritus. The stratigraphic stacking is generally composed of sandstone lobes (S/M > 1), characterized by evident lateral facies variations in the lower part (fig. 4.21), while in the upper part they show a relatively more tabular geometry with intercalated portions of thin-bedded sandstones (S/M ≈ 1) (fig. 4.22).

The thin-bedded portions are composed of coarse- to medium-grained thin-bedded (average thickness of ~ 5-10 cm) sandstone layers with sharp bases and undulated tops, characterized by well-developed lateral pinch-and-swell geometries. Although the overall facies of these beds is massive, weakly developed grading (sometimes with inverse appearance) and oblique, and subordinately, plane parallel laminations can be observed. These laminations are commonly evidenced by a color banding due to alignments of white clasts, probably because of a different hydraulic behavior (fig. 4.23).

This kind of beds can be ascribed to the F6 facies of Mutti (1992) and are widely represented throughout the entire succession, commonly organized in distinct intervals, especially in the eastern sector.

Other types of beds present in the R3 unit are medium- to thick-bedded (average thickness of ~ 20-30 cm), fine- to coarse-grained sandstones, generally organized in distinct amalgamated bedsets (*sensu* Campbell, 1967), showing an overall upward increasing sheet-like geometry.

These beds, especially where scattered as single beds through the succession, usually have a basal part constituted by massive (liquefied) or roughly graded facies, which can show a crude parallel laminae in the upper part, sometimes also affecting the entire strata (*i.e.* no-traction wispy-type lamination; Mutti pers. comm.) (fig. 4.24). These laminae, which are commonly incurved upward by fluid escapes, appear more spaced in the lower portion of the bed, while in the upper portion are usually much more developed (fig. 4.25).

These beds are also observed to develop an apparent inverse grading in the lower portion of the base, sometimes with distinct grain-size breaks (also possibly due to amalgamation surfaces), that give to the bed an overall bipartite appearance (fig. 4.26). Especially where organized in amalgamated bedsets, these strata may show isolated pebbles and conglomerate lenses along the base (fig. 4.27).

Interestingly, mud-draped scours have been also observed (especially in the lower part of the succession) locally truncating internal laminations of the underlying layer and sometimes, some strata of the lower bedset, resulting in abrupt lateral pinch-out closures (fig. 4.28).

On the basis of these features, these beds can be essentially ascribed to F5 and F8 facies of Mutti (1992), with rare and discontinuous F3 deposits.

Sometimes, the medium- and fine-grained sandstone beds sometimes show an upper plane parallel and oblique laminated portion, in which small-scale hummocky-type geometries can be recognized. The latter are commonly deformed by water escapes (fig. 4.29).

Roughly toward the north, the amalgamated base of thicker strata, is marked by discontinuous lenses of "impact-breccia" facies (fig. 4.30), similar to those observed in the R1 unit (see above).

These strata are also characterized by relatively abundant shell debris, mainly comprising oyster fragments, *nummulites* and sponge spikes (fig. 4.31). Moreover some evidence of bioturbation (*ophiomorpha*- and *planolites*-like ichnofacies) has been also observed (fig. 4.32).

The upper laminated portions of these beds show a diffused reddish alteration colors given by significant accumulations of variously coalified plant fragments, usually disposed with the main planar side parallel to the lamination surfaces (fig. 4.33).

Sometimes, in the basal-intermediate portions of the F5 and F8 beds may occur some clustering of cm-sized clay chips coming from underlying mudstone partings; these clay chips usually share a tubular/cylindrical shape, with their long axes arranged in a parallel way to the layering (fig. 4.34).

In the northernmost analyzed outcrops, formerly in the Varano de'M.-Pellegrino P. outlier (section n. 7; see chap. 2), the R3 unit is almost entirely composed of graded thick bedded conglomeratic- to coarse-grained sandstone beds, arranged in amalgamated bedsets without the intervening of fine-grained interbedded portions. These sandstone-conglomerate beds seem to be organized in thinning- and fining-upward stacking patterns, possibly registering an overall back stepping of the system and a weakly expressed cyclicity.

The clasts contained in these beds (with dimensions up to ~ 50 cm) are mainly composed of well rounded sedimentary (carbonatic and siliciclastic) and, subordinately, ophiolitic pebbles, with diffused evidence of lithodome holes. Some of the larger clasts are made of crystalline gabbro (fig. 4.35).

Within this succession some distinctive oxidized strata commonly occur as F6 and F5 facies. These beds share a strong content of coarse-grained whitish clasts, more or less diluted with the classical grain component, sometimes underlining parallel and oblique laminations in the F6 facies, giving an overall white banded appearance to the whole layer (fig. 4.36).

Microscopic optical analysis carried on an oriented thin section taken from one of these beds (sample R3WCB) confirm that these whitish clasts are made of relatively fresh, angular crystals of zonated plagioclase, well sorted and sharing the same grain-size of the surrounding lithic clasts (fig. 4.37) .

Bed sharing similar characteristics have been observed by Cibin *et al.* (1998) widely distributed throughout the whole Ranzano Unit (*i.e.* Varano de'Melegari unit of Martelli *et al.*, 1998) from the eastern TPB to and over the Secchia Valley Tectonic Lineament, and interpreted as andesitic epiclastic material related the oligocenic calcalkaline volcanism, remobilized from basin margins by gravity flows and then resedimented in these basins. Particularly, these authors have recognized and studied some of these beds in the uppermost part of the near Varano de'Melegari outlier (considered by these authors as the same outlier of the Pessola Valley one).

The present observations, therefore, represent therefore the first recognition of such layers in the Pessola Valley outlier, highlighting their widespread occurrence throughout the entire R3 succession, from base to top.

The sole structures observed in these beds are identified as prod, bounce, flute and groove casts, with the distinct predominance of the latter. These features are concentrated in the lower portion of the unit (fig. 4.38).

The R3 unit succession (as observed in the general stratigraphic log measured in the eastern side of the outlier) shows a slightly evident internal cyclicity, defined by m-sized thickening- and coarsening-upward bedsets, organized in at least 6 cycles. These cycles are quite well recognizable in the field due to the high erosional relief shared by upper thicker beds (fig. 4.39).

These bedsets are characterized by a transitional lower portion which grade upward for alternations to an upper coarse-grained and medium- to thick-bedded portion, showing a sharp upper contact to the next bedset, marked by a localized erosion, sometimes truncating the uppermost strata (see fig. 4.28). The oxidized volcaniclastic layers seem to be concentrated within the middle portions of these strata packages.

In the north-easternmost part of this area is exposed a segment of another Epiligurian outlier (*i.e.* Varano de' Melegari-Pellegrino Permense outlier) made up of a sedimentary succession comprising the MMP unit at the base (resting upon the Ligurian AVV unit through an extensive development of the BAI unit), the R3 unit (mainly composed of thick-bedded coarse-grained facies; F2-F3 and F5 facies of Mutti, 1992), an upper mass transport complex (*i.e.* Varano chaotic unit) and the Antognola unit at the top.

Here the R2 unit is represented by a relatively thin horizon (maximum estimated thickness ~ 20 m) and locally seems to be completely lacking. The vertical order of this stratigraphic succession slightly resembles that cropping out in the Mt. Roccone and Mt. Piattello outliers.

Detailed description and analysis of R1 and R3 units are reported in the attached Panel n. 3 and Panel n. 4.

4.3 Tectonic setting

This Epiligurian outlier is structurally arranged as an open syncline with an axial orientation disposed in a roughly NE-SW direction, gently plunging (~10° to ~20°) toward E-NE. This syncline is bordered to the N-NW by a positive structure exposing the Ligurian Mt. Sporno Unit (*i.e.* Vianino tectonic window; Zanzucchi, 1980) and to the S by Ligurian-derived shale-rich chaotic complexes associated to the Mt. Pareto-Solignano structure. In the NE sector the syncline axis abruptly terminates against a NW-SE-directed belt of shale-rich chaotic complexes separating the Pessola Valley outlier from the Varano de' Melegari one (see attached Panel n. 1).

The Pessola River separates the entire outlier in two quite different sectors: a western one, characterized by relatively little tectonic disturbance, and an eastern one, showing instead a more complex tectonic arrangement (see fig. 4.2). The displacement of tectonic structures, observable in the geomorphology and topography of the area, suggests a relative sinistral component for the NE-SW-directed fault system, possibly related to the tectonic lineaments of the Taro system localized few kilometers toward E (Bernini *et al.*, 1997). The above-mentioned Ligurian lithologies-bearing chaotic complexes, usually recognizable as scaly clays and mud breccias, seem to be concentrated along the main tectonic lineaments, sharing unclear contacts (often disposed at high angle), and seem to characterize the outlier margins, bounding the whole Epiligurian succession as positive structures (fig. 4.40).

There are at least 2 main tectonic directions affecting this zone. These structural lineaments are expressed by major fault and associated minor fault systems, characterized by crosscutting relationships. The whole Epiligurian outlier is incised by a NE-SW-directed fault system, which cuts an E-W-directed one: from a geomorphologic point of view, these 2 tectonic lineaments and their crosscutting relationships are particularly well evidenced by the Pessola and Ceno river waterways, respectively (see fig. 4.2).

Subordinate late tectonic structures (Quaternary?) are represented by minor steep-dipping and closely-spaced normal fault systems oriented in a roughly N-S direction, and characterized by short displacements.

Particularly, the SE sector (*i.e.* Ricodalle section) of this area is characterized by the development of a low-angle thrust system, at present gently dipping toward N-NW, interpreted as being originated and tilted by a growing buried structure affecting underlying Ligurian Units during Late Oligocene time (Costa and Frati, 1995).

This thrust system involves the MMP and R1 units (locally also the PZO unit), duplicating the their lithologic contact and causing a tectonic stacking, which topographically elevates these units at the same altitude of the R3 unit. A ten of m-sized drag syncline is observable in the right side of the Pessola River within the R1 unit and just few tens of meter toward N from the thrust system outcrop, testifying possible associated ramp structures (probably related to the topmost thrust sheet) cutting upwards through the R1 unit (fig. 4.41).

Here it is possible to observe a strong development of both fibrous and spatic calcite vein systems. The former consist of layer-parallel anastomosing and lens-shaped mm-thick veins which are mainly localized within mudstone-rich portions (*i.e.* MMP litholologies) at the base of sandstone beds. The latter are instead more represented within sandstone bed packages, filling cm-sized fractures trending at high-angle in respect to the stratification and tension gashes localized on bedding surfaces. The thrust-bounded portions show evidence of folding and plastic deformations. Evidence of generalized soft-sediment features as meso-scale folds in R1 unit lithologies, "sandstone balls" mainly compose of lithologies belonging to the PZO unit, and patches of pebbly sandstones/mudstones with dominant angular mudstone intraclasts are also present close to main thrust surfaces, indicating possible shallow crustal level conditions of development (fig. 4.42).

Qualitative microscopic analysis carried on two oriented thin rock sections collected within a layer-parallel fibrous vein system at the very base of this thrust system (sample LAT1), confirm evidence of independent particulate flow without grain breakage and thus, no brittle deformation. Moreover its possible to observe a strong development of fibrous micro-vein systems, organized in layering-parallel anastomosing seams, which envelope and separate single particles or elongated particle domains in a layer-parallel pattern, and testifying strong fluid overpressure conditions. The roughly preferred orientation of elongated particles along a faint sigmoidal trend should be taken as kinematic indicator of a movement toward the northern sectors (fig. 4.43).

Another ramp-like structure can be observed along the Rio Molinetto section (south-central sector), marking the boundary between R1 and R2 units. This structure is represented by a low-angle surface (~ 30°), cutting upward the topmost thick-bedded and coarse-grained part of the R1 unit, along the inferred basal contact of the R2 unit (fig. 4.44).

Here, lithologies belonging to the PZO and MMP units are in contact with a strongly disturbed zone representing the locally topmost part of the R1 Unit. This discontinuous interval is

characterized by the presence of deformed blocks belonging to the R1 unit, probably detached by from the underlying ramp structure.

Although there are no evident thrust-sheets recording a possible tectonic stacking, and the R2 unit directly overlies the R1 unit without the occurrence of clear brittle deformations, the scarce amount of matrix, the diffused presence of a scaly-like cleavage, the development of fibrous calcite veining systems and some possible reactivation of the internal contacts of the R2 unit subdivisions (see chap. 7) highlight some relationship to shallow-crustal level deformations (gravity tectonics?), as observable in the above-mentioned Ricodalle section.

Given the strong relationships between the above-described structures and the lower portions of the R2 unit (and the likely overprinting of the upper ones), it is possible to propose a progressive deformation, instead of single punctual tectonic phases, which is thought to develop since Early Oligocene. Nonetheless it is possible that such structures should be related to a slide emplacement-induced deformation of the substrate (see chap. 7 and 9), as described by Lucente and Pini (2003) for the Casaglia-Mt. della Colonna MTD (their "antiformal stack").

In the western outcrops, it is possible to observe the progressive angular unconformities recorded by PZO on MMP unit, and R1 on PZO unit; these onlap relationships and the general stratigraphic expansion (*i.e.* growth strata-like pattern) of R1 sand bodies (coupled with the trend of its internal unconformities) toward southern sectors indicate a progressive syn-sedimetary uplift of the northern margin of this basin (probably related to the Vianino strucure) (fig. 4.45).

A minor and localized inter-stratal shear zone has been recognized ~ 10 m below the upper contact of the R1 unit with the R2 unit in the south-central sector of the area (*i.e.* Fopla section). This shear zone affects a mudstone-rich interval (~ 40 cm thick), inter-bedded within thick- to medium-thick F5 facies bedsets, and developing in a layer-parallel trend. It is composed of an undisturbed lower muddy portion (~ 5-10 cm) separated from a significantly sheared upper portion (~ 25-35 cm) by a relatively laterally continuous, layer parallel, cm-thick vein of fibrous calcite (fig. 4.46).

The sheared portion shows an oxidized appearance, with a relatively poor developed foliation, characterized by the local occurrence of cm- to dm-sized sigmoidal-shaped elements (S-C-like structure?) and small-scale stacking of plastically deformed sandstone bed fragments. The general arrangement of these structures seems to suggest a roughly NE-directed sense of shear. Given the stratigraphic position, the kinematic concordance and the soft sediment character, this structure may be related to the near Ricodalle thrust system (see above), and/or, at least, to the R2 unit basal subdivisions emplacement (see chap. 7).

The R1 unit, and subordinately the R2 unit, are affected by minor normal fault systems and associated fibrous and crystalline calcite veins. These faults share short displacements (~ 1 m of maximum displacement) and oblique components (usually sinistral) of the relative movement, as confirmed by the associated kinematic indicators (*i.e.* striations, calcite steps and growing fibers).

Similar systems of minor steep-dipping normal faults have been also recognized in the R3 unit, although characterized by quite different dipping directions and more closely spaced order (fig. 4.47).

3.4 List of figures

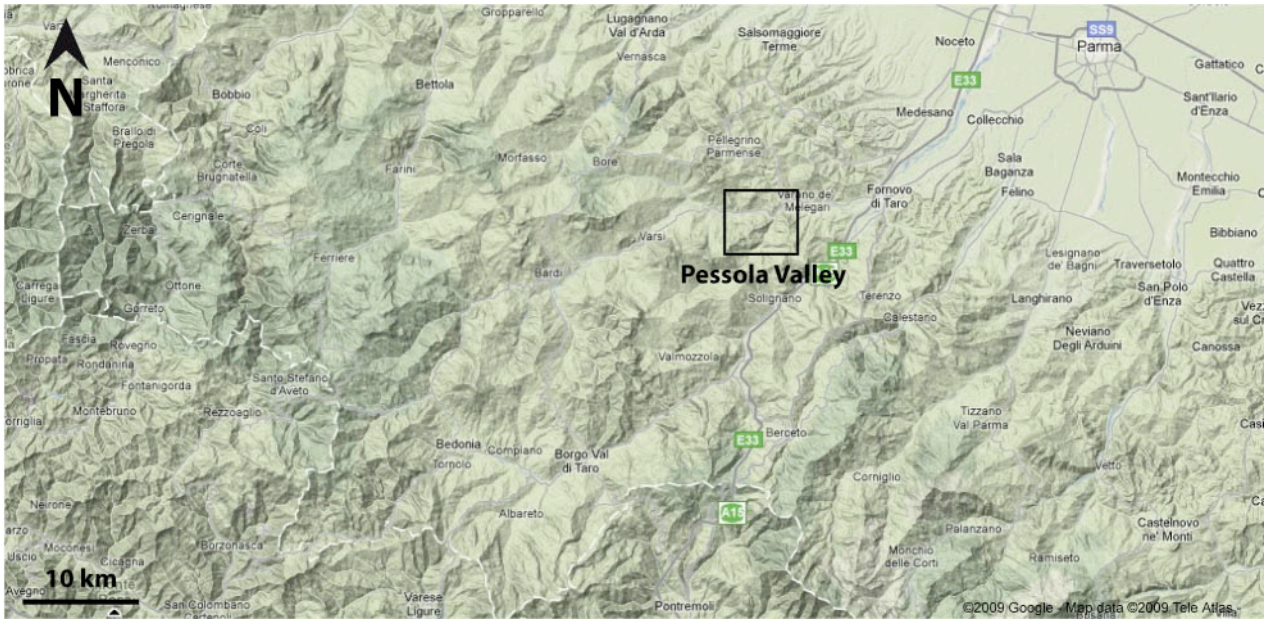

Figura 4.1 - Geographic location of the Pessola Valley area (from GoogleMaps, 2009).

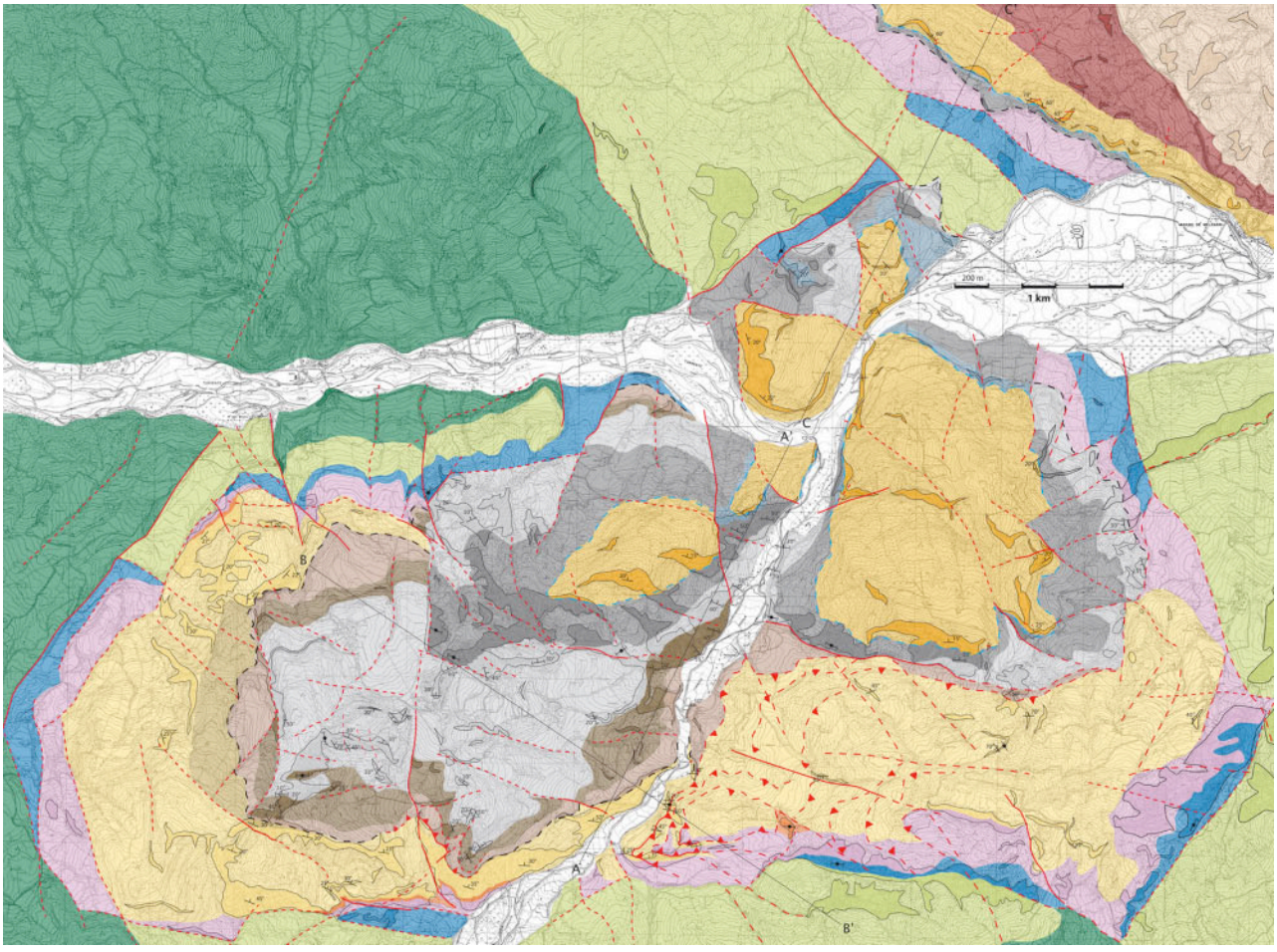

Figure 4.2 - Geologic map of the Pessola Valley area developed in this work (see attached Panel. n.1).

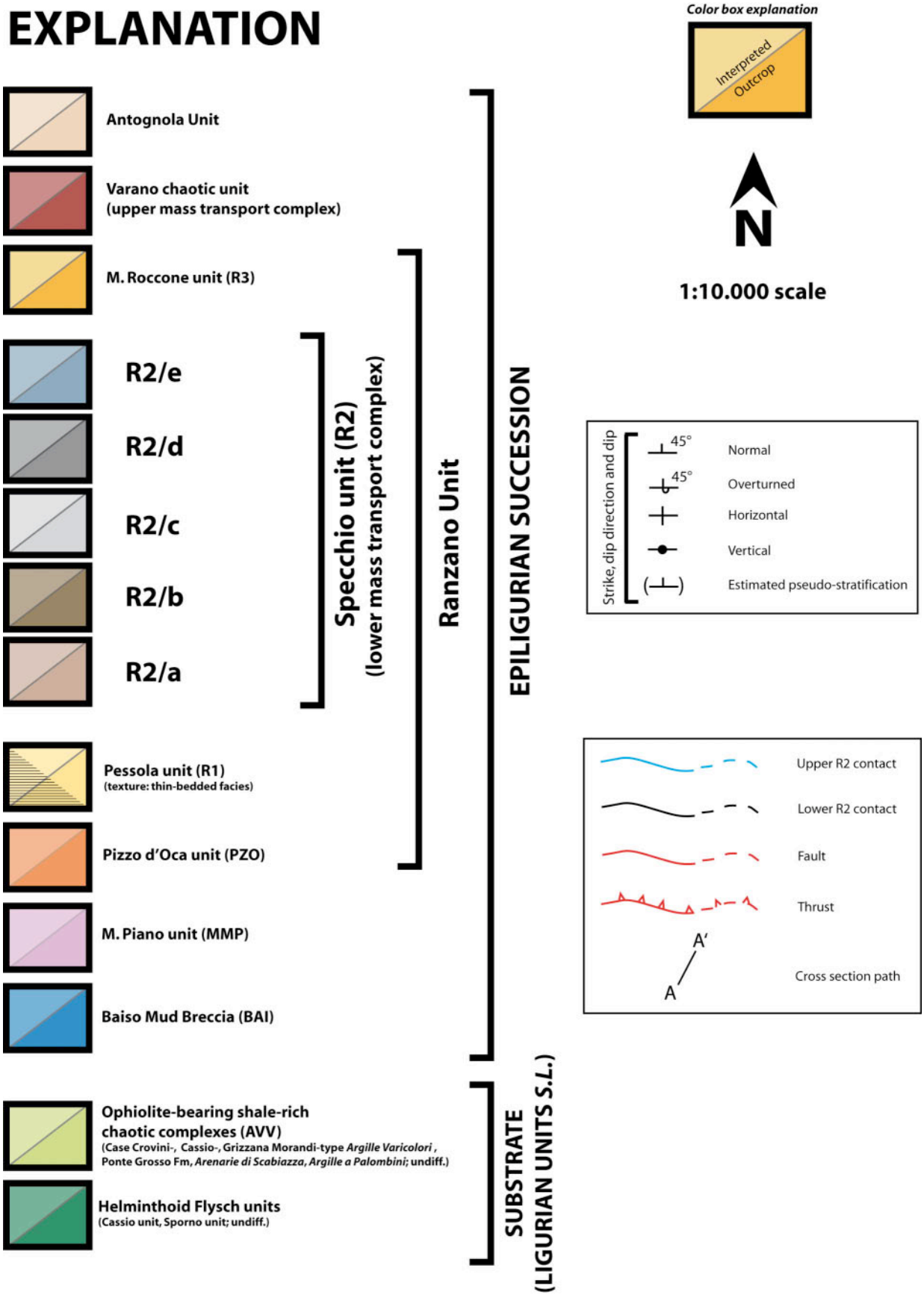

Figure 4.3 - Explanation box for geological maps (see attached Panel n.1).

A
Mt. Pareto
Helmintoyd
Flysch units
(overturned)
SSW
NNE
Pessola V. outlier
R1
BAI
AVV
MMP
PZO
B
C
D
E
F
G
B
MMP
AVV
BAI
C
D
C
D
E
F
G

Figure 4.4 - Panoramic photo-mosaic of the southern margin of the Pessola Valley outlier, showing the Epiligurian succession (to the extreme left) overlying the Ligurian substratum (from the center to the right), represented by the northern flank of the Mt. Pareto tectonic struture. Component photos are taken roughly looking to the E (see fig 4.3 for symbols).

B: Roughly verticalized contact between the Ligurian shale-rich chaotic complexes and the overlying Epiligurian succession, represented by the MMP unit, with the interposition of aligned, lenticular mud-breccia bodies of the BAI unit. Location shown in A.

C: Overall appearance of mud-breccias belonging to the BAI unit. Here the clasts are represented by shaly angular fragments of AVV. Knife for scale, 9 cm long. Location shown in B.

D: Overall appearance of marly deposits belonging to the MMP unit. The general sense of stratification is expressed by compaction-related foliation and alteration color bending. Note the cm-thick fibrous calcite vein roughly developed following the pseudo-stratification trend. Knife for scale, 9 cm long. Location shown in B.

E: Outcrop of tectonized shales and calcareous beds of the Helmintoyd Flysch units. The contact with the AVV unit is located few meters to the left. Location shown in A.

F: Ophiolithic block comprised in the shale-rich chaotic complexes of the AVV unit, localized close to contact with the Helmintoyd Flysch units. Location shown in A. Hammer for scale.

G: Close up of F showing the detailed appearance of the ophiolithic block (ophicalcite-like appearance?). Hammer for scale.

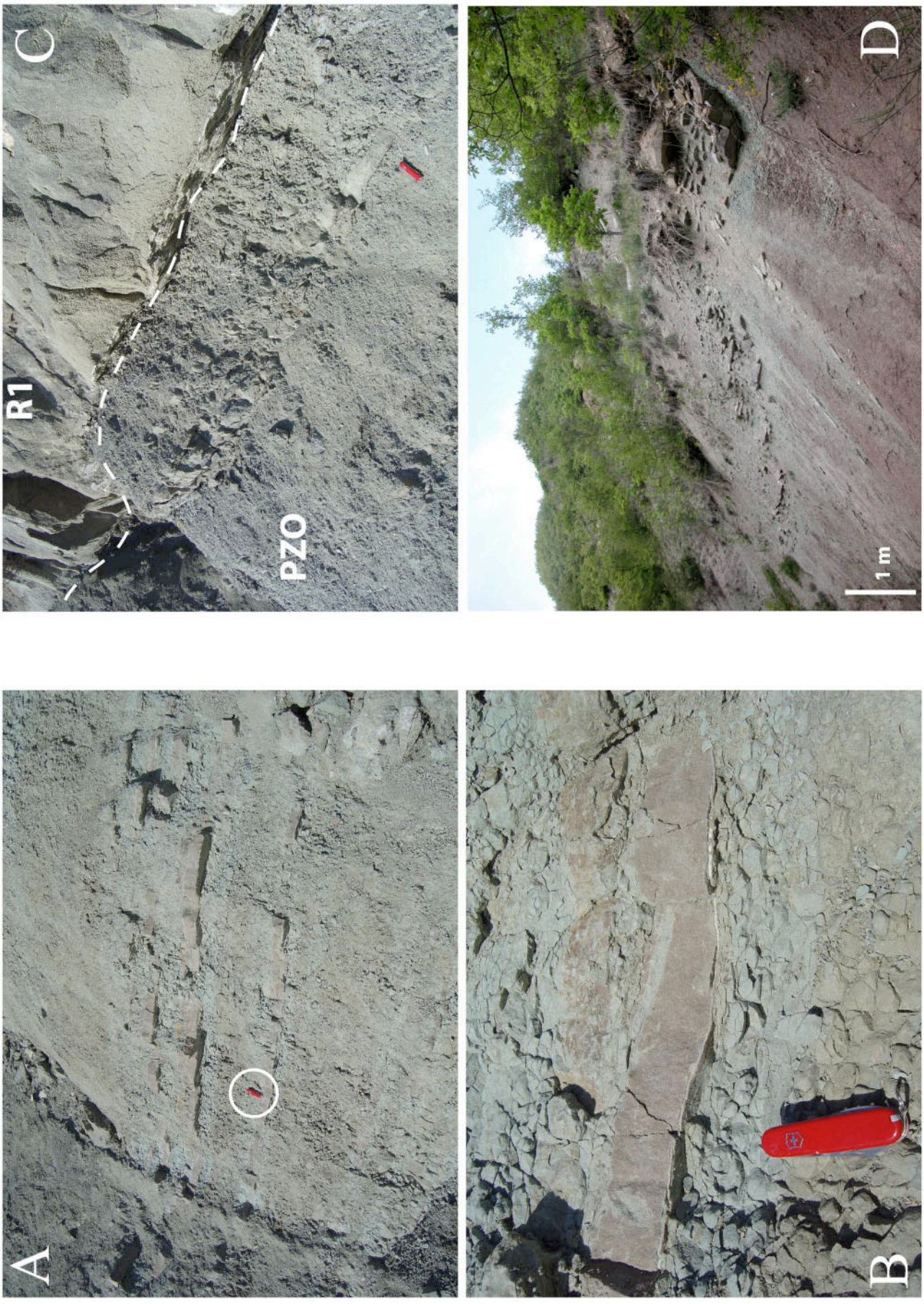
A
B
C
R1
PZ0
D
1 m

Figure 4.5 - A: General outcrop appearance of the PZO unit in the southern sector of the Pessola Valley outlier (left side of Pessola River). Knife for scale, 9 cm long.

B: Close-up of A showing an F9-type bed (*sensu* Mutti, 1992). This kind of facies is representative of the PZO unit in this area. Note the mm-thick fibrous calcite vein developed in layer-parallel trend along the base of the bed; similar features seems to characterize the lower part of the succession, roughly across the contact with the MMP unit. Knife for scale, 9 cm long.

C: Erosive contact between the PZO unit and the overlying R1 unit (left side of Pessola River). Also in this case it is observable a mm-thick, fibrous calcite vein developed along the base of the first coarse-grained, thick bed of the R1 unit. Knife for scale, 9 cm long.

D: Outcrop appearance of PZO unit in the western sector of the Pessola Valley outlier (Rio Molinetto section, see attached Panel n.1). The lower sedimentary contact with the MMP unit is localized few meters below.

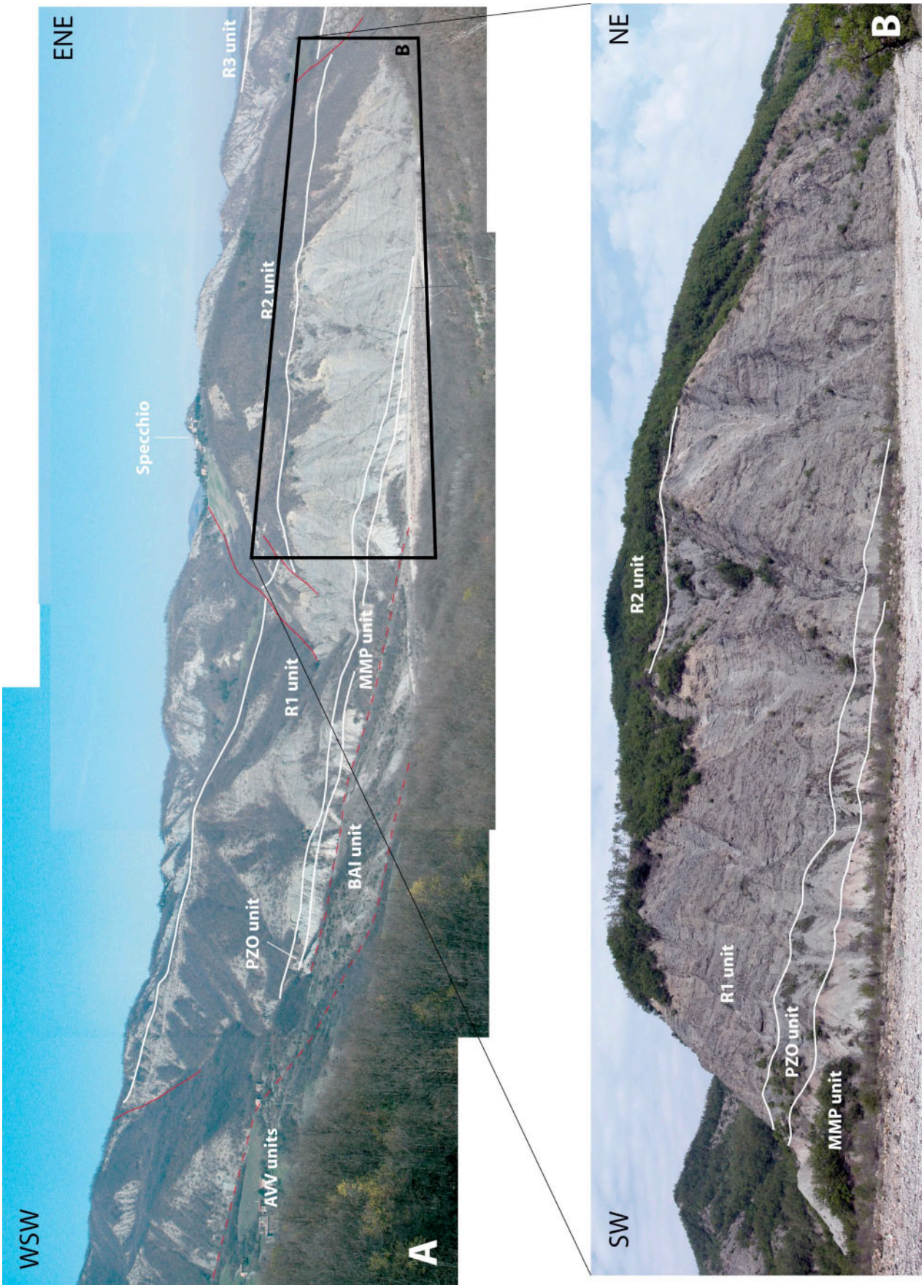
WSW
ENE
A
B
R3 unit
R2 unit
Specchio
R1 unit
MMP unit
BAI unit
PZO unit
AVV units
SW
NE
R2 unit
R1 unit
PZO unit
MMP unit

Figure 4.6 - A: Panoramic photo-mosaic showing the SW margin of the Pessola Valley outlier. Stratigraphic units and major faults are labeled.

B: Close-up of A showing the lower Epiligurian succession and relative component units. Note the complex stratification pattern of the R1 unit and the clear lithlogic contacts with underlying PZO and MMP units.

C
D

D

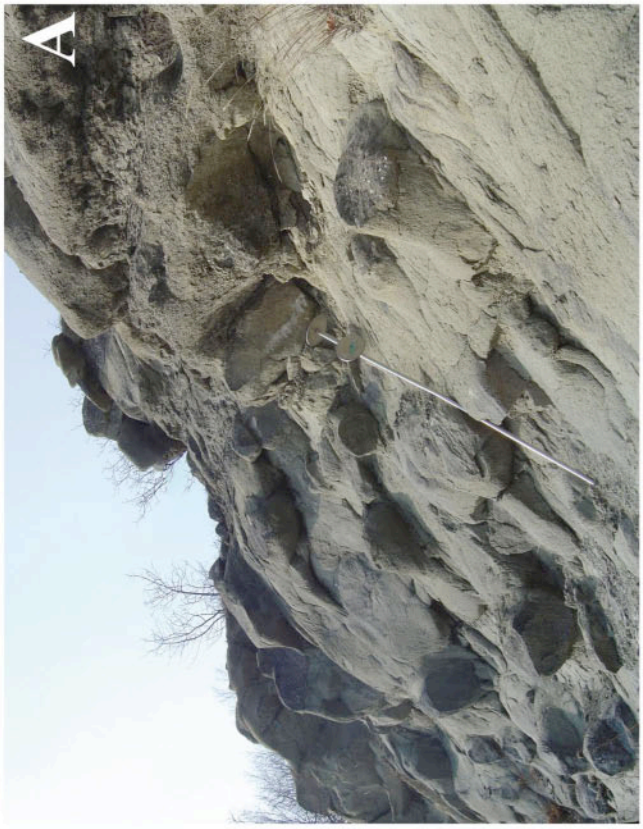
A

B

Figure 4.7 - A: Overall appearance of the R1 unit coarse-grained, thick-bedded facies characterizing the lower portion of the succession (F3-F5 type facies of Mutti, 1992). The general stratification sense is not always clearly discernible, because of the poorly-lithified nature of these sandstones, weak sorting and liquefaction-related disturbance (note the strong presence of diagenetic pseudonodules).

B: Detail of a F5-type bed with erosive base, showing a scour filled with conglomeratic lag accumulation (F3-type). Note the overall ophiolihic nature and well-rounded shape of pebbles. Knife for scale, 9 cm long.

C: Example of F3-F5 type beds succession. Jacob's staff for scale, 1,5 m long.

D: Close up of C showing the F3-type bed. Note the roughly defined bypass top surface and the presence of dm-sized, sub-angular carbonate clasts.

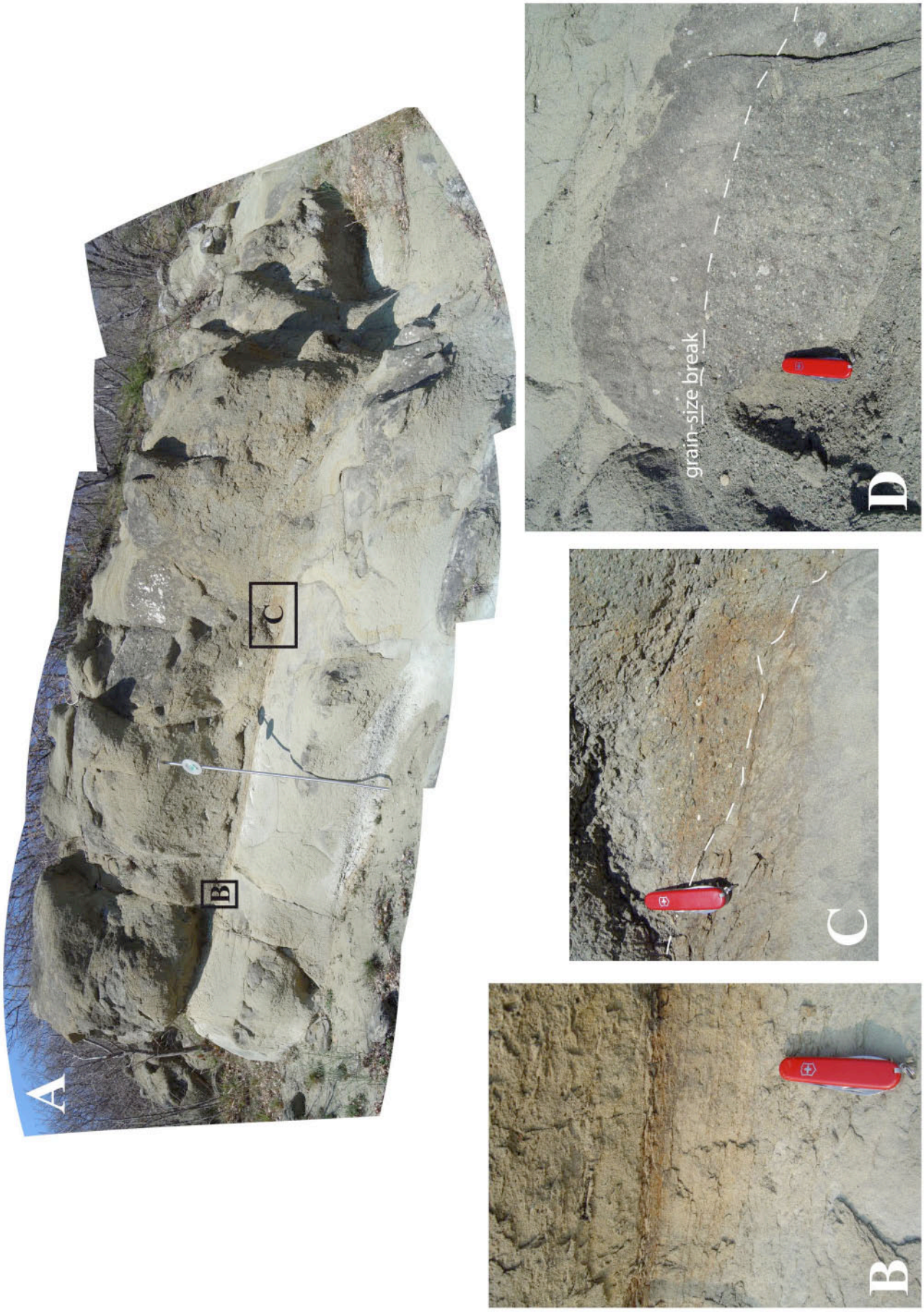
A
B
C
grain-size break
D
C
B

Figure 4.8 - A: Photo-mosaic showing two amalgamated F5-type beds characterizing the middle part of the R1 unit. Jacob's staff for scale, 1,5 m long.

B: Close-up of A showing the upper medium-grained and pseudo-laminated upper part of the F5-bed, and the amalgamation surface between the two. Note the reddish alteration color of the uppermost parting due to organic matter oxidation (*i.e.* plant fragments). Knife for scale, 9 cm long.

C: Close-up of A showing the local lag accumulation of micro-conglomeratic material at the base of the upper F5-type bed. Note the incipient loading-related structures deforming the basal surface. Knife for scale, 9 cm long.

D: Example of bypass-related grain-size break surface sometimes characterizing internal portions of F5-type beds. Knife for scale, 9 cm long.

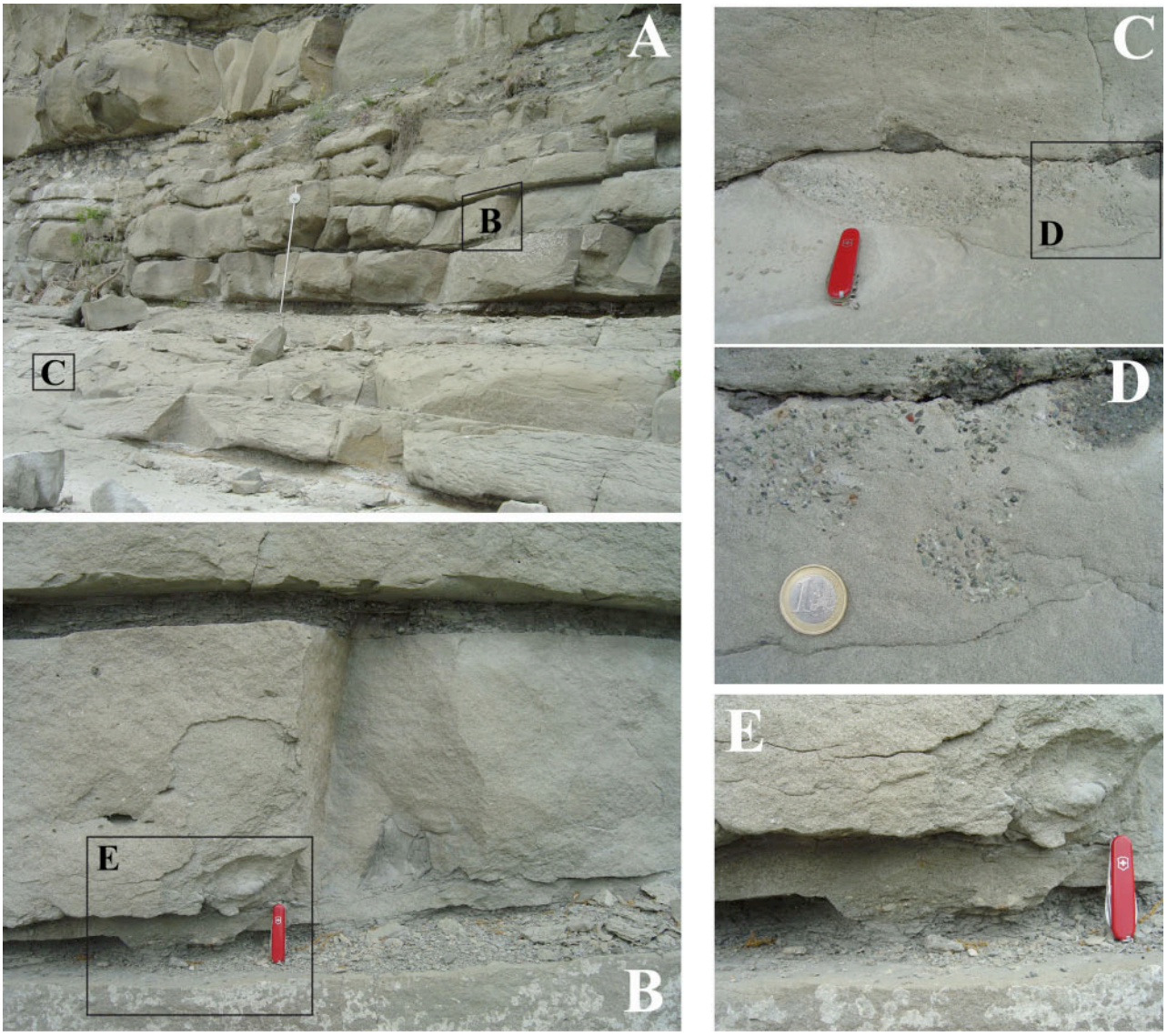

Figure 4.9 - **A**: Overall view of the uppermost part of the R1 unit showing a succession dominated by well defined F5-type beds and subordinate F6-type beds. Note the overall thinning-upward trend of bedsets. Jacob's staff for scale, 1,5 m long.

B: Close-up of A showing two amalgamated F5-type beds characterized by erosive bases and sharp tops. Note the general massive appearance and the presence of roughly aligned clay-chips in the middle part of the upper, thicker bed. Knife for scale, 9 cm long.

C: Close-up of A showing the amalgamation surface between two F5-type beds, underlined by a discontinuous micro-conglomeratic interval. The surface is slightly bended by loading-related structure. Knife for scale, 9 cm long.

D: Close-up of C showing a detail of the loading-related deformations affecting the amalgamation surface. Here it is possible to observe a detached micro-conglomeratic pseudo-nodule "sinking" in the lower liquefied portion of the underlying bed. One Euro coin for scale, 2,2 cm in diameter.

E: Close-up of B showing a tabular-like scour filled with coarse-grained material cutting into the underlying mudstone parting. Note the pebbles alignment along the well-defined amalgamation surface with the overlying bed. Knife for scale, 9 cm long.

Figure 4.10 - Examples of "armored balls" type clay-chips observed in the R1 unit of the Pessola Valley outlier. **A** and **C** are from the left side of the Pessola River (middle-upper R1 unit), while **B** and **D** are from the right side (lower R1 unit). Note the significant size of the example represented in D. Knife (9 cm long), one Euro coin (2,2 cm in diameter) and camera lens cap (7 cm in diameter) for scale.

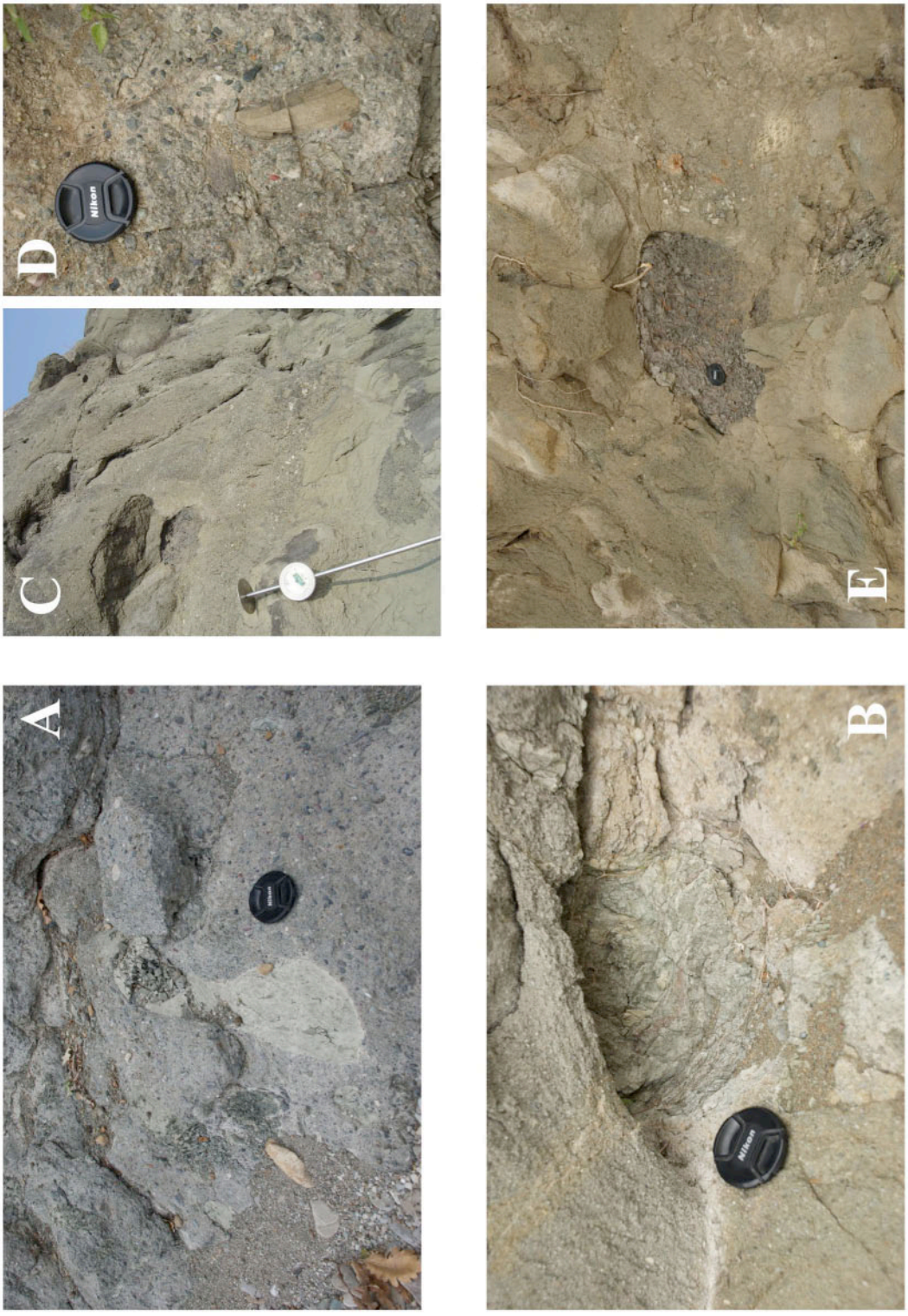

Figure 4.11 - Examples of rip-up clasts observed in the lower portion of the R1 unit in the Pessola Valley outlier.

A: MMP-like mudstone rip-up clast (right side of Pessola River). Camera lens cap, 7 cm in diameter.

B: AVV-like shaly varicolored rip-up clast (right side of Pessola River). Camera lens cap, 7 cm in diameter.

C: AVV-like shaly rip-up clast (left side of Pessola River). Jacob's staff for scale, 1,5 m long (50 cm visible).

D: AVV-like shaly and sandstone rip-up clasts (right side of Pessola River). Camera lens cap, 7 cm in diameter.

E: AVV-like shaly rip-up clast (right side of Pessola River). Camera lens cap, 7 cm in diameter.

Figure 4.12 - Examples of diagenetic pseudo-nodules characterizing midde-upper portion of F3-F5 type beds of the R1 unit in the Pessola Valley area. Note that these pseudo-nodules are always cored with marly and carbonatic elements. The examples represented in **B**, **C** and **D** are from the middle-lower portion of the R1 unit succession of the left side of the Pessola River, while **A** is from the right side. Knife (9 cm long) and camera lens cap (7 cm in diameter) for scale.

A
B

B

D

C

E

Figure 4.13 - A: Outcrop of western R1 unit showing a succession dominated by F6-type beds (Pilone/Rio Molinetto section, see attached Panels n.1 and n.4), stratification surfaces are labeled. Jacob's staff for scale, 1,5 m long.

B: Close up of A showing the three-dimensional strongly lenticular shape of sandstone bodies and their overall pinch-and-swell lateral relationships. Note the internal development of internal large-scale oblique lamination of some sandstone layers. Jacob's staff for scale, 1,5 m long.

C, **D** and **E**: Examples of F6-type beds (same section of A and B); internal oblique lamination is labeled. Camera lens cap (7 cm in diameter), knife (9 cm long) and measuring tape (~ 15 cm visible) for scale.

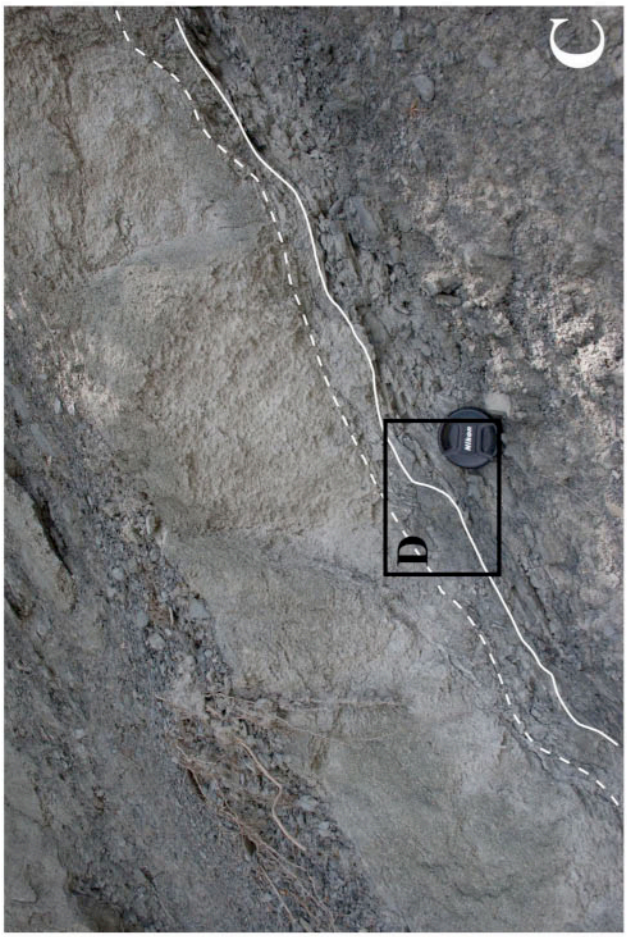
C
D

Nikon
D

A

B

Figure 4.14 - Examples of impact-breccia type intervals characterizing erosive bases of thicker F5-type beds of the middle-lower R1 unit succession of the Pessola Valley outlier.

A: impact-breccia with dm-sized clay-chips (right side of Pessola River). Note the sharp basal contact with a mudstone parting and the coarse-grained lithologies. Field notebook for scale, 14 cm long.

B: impact-breccia with upward clustering of cm-sized clay-chips. Note the overall oxidized appearance (left side of the Pessola River). Knife for scale, 9 cm long.

C: F5-type bed with an erosive base underlined by a cm-thick impact-breccia interval (labeled). Right side of the Pessola River. Camera lens cap for scale, 7 cm in diameter.

D: Close-up of C showing the detailed appearance of the impact-breccia level, characterized by lithologic mixing of pebbles, coarse-grained sand and mud, both from the overlying bed and eroded from the underlying fine-grained parting. Camera lens cap for scale, 7 cm in diameter.

C
D
A
B

Figure 4.15 - Examples of bioturbations and fossils recognized in the R1 unit beds of the Pessola Valley outlier.

A: Example of *planolites*-like ichnofacies sometimes observable on the upper surfaces of R1 unit beds (left side of Pessola River). Knife for scale, 9 cm long.

B: Isolated shell fragment (ostrachod?). Left side of Pessola River. Knife for scale, 9 cm long.

C: Isolated shell fragment. Left side of Pessola River. Twenty cent Euro coin for scale, 2,2 cm in diameter.

D: Scattered shell debris. Northern R1 unit outcrops of the Pessola Valley outlier. One Euro coin for scale, 2,2 cm in diameter.

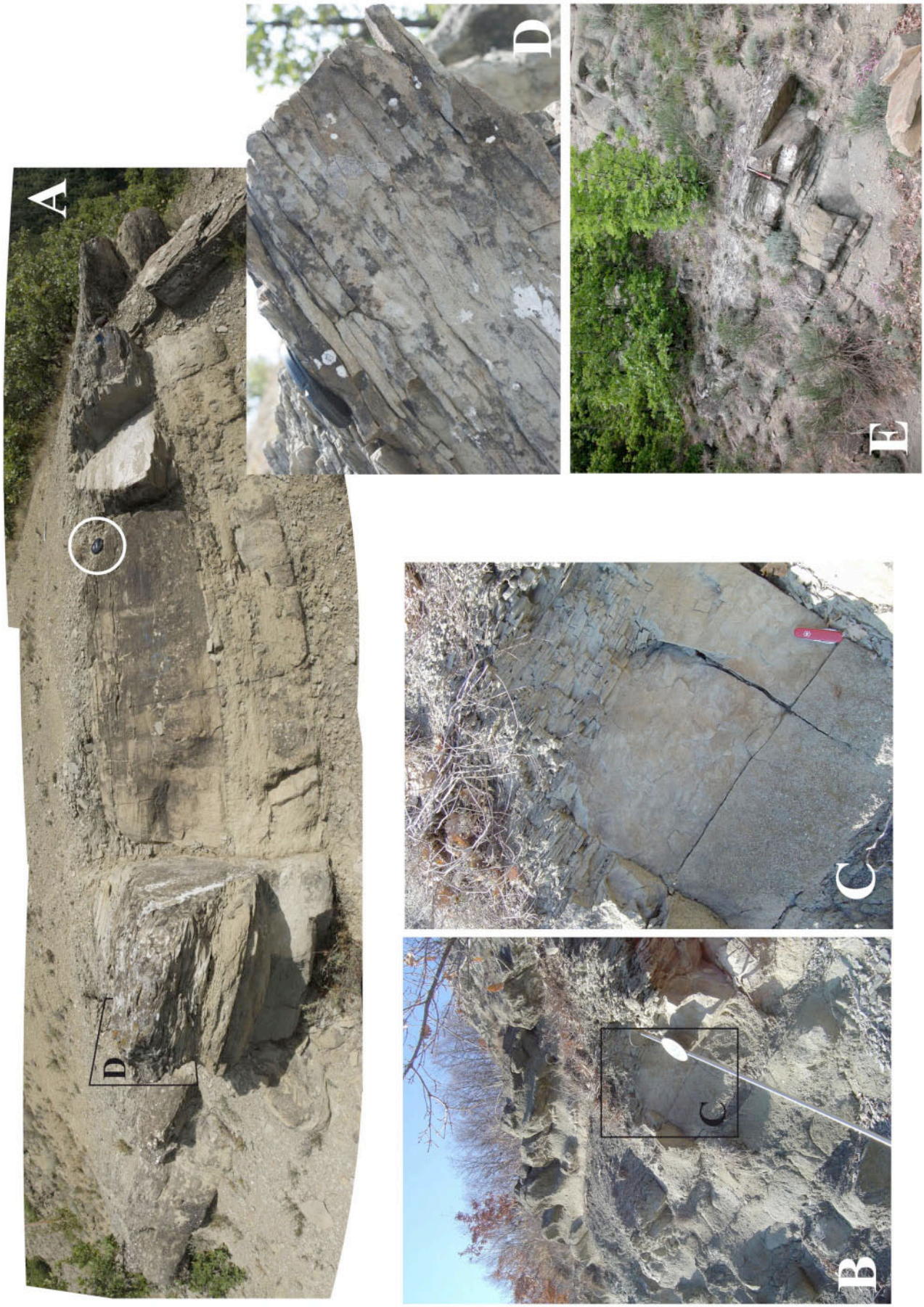
A
D
D
E
C
B
C

Figure 4.16 - A: Overall outcrop appearance of the marly key-bed, representing the unique outlier-wide stratigraphic marker for the middle portion of the R1 unit succession of the Pessola Valley outlier (Pilone/Molinetto section, see attached Panels n. 1 and n. 4). Camera lens cap for scale, 7 cm in diameter.

B: Same key-bed in the left side of the Pessola River section. . Jacob's staff for scale, 1,5 m long (~ 1 m visible).

C: Close-up of B showing the well-developed Bouma T_{a-e} sequence characterizing this key-bed. Knife for scale, 9 cm long.

D: Close-up of A showing the upper oblique laminated portion of the key-bed. In this interval have been observed opposite facing ripples, representing evidences of flow-ponding conditions. Camera lens cap for scale, 7 cm in diameter.

E: Overall outcrop appearance of the key-bed in the Servazzola section (western sector of the Pessola Valley outlier, see attached Panels n.1 and n.4). Hammer for scale.

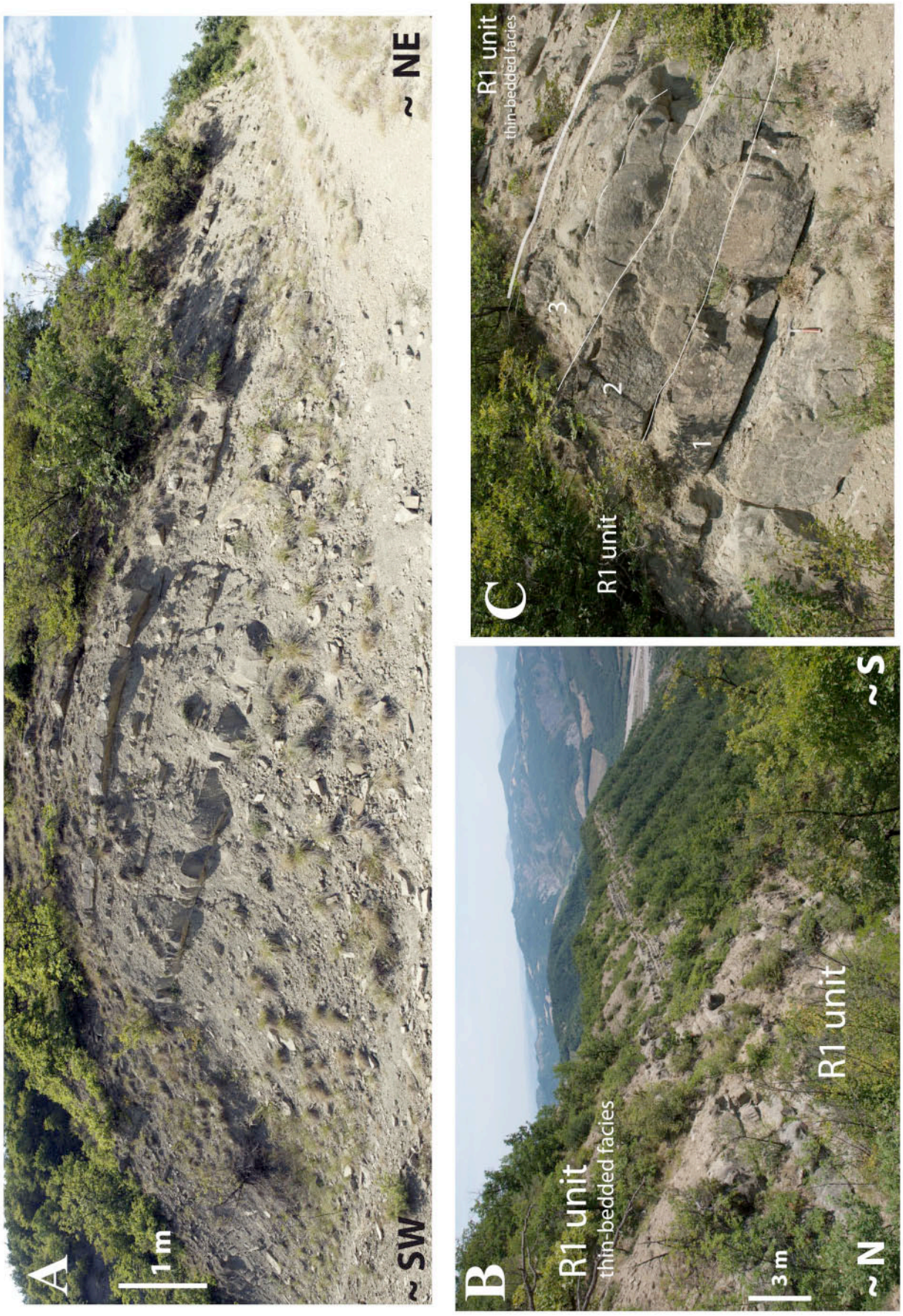
A
~ SW
~ NE
1 m
B
R1 unit
thin-bedded facies
R1 unit
~ N
~ S
3 m
C
R1 unit
thin-bedded facies
R1 unit
1
2
3

Figure 4.17 - A: Outcrop appearance of the R1 unit thin-bedded facies characterizing the wester sector of the Pessola Valley outlier (Servazzola section, see attached Panels n.1 and n.4).

B: Transition between the thick-bedded facies and the overlying thin-bedded facies in the upper portions of the R1 unit (Servazzola section, see attached Panels n.1 and n.4).

C: Last well-defined F5-type amalgamated bedset marking the contact with the thin-bedded facies. Stratification surfaces and component beds are labeled. Note the slight curved stratification surfaces (compensation cycles?) (Servazzola section, see attached Panels n.1 and n.4). Hammer for scale.

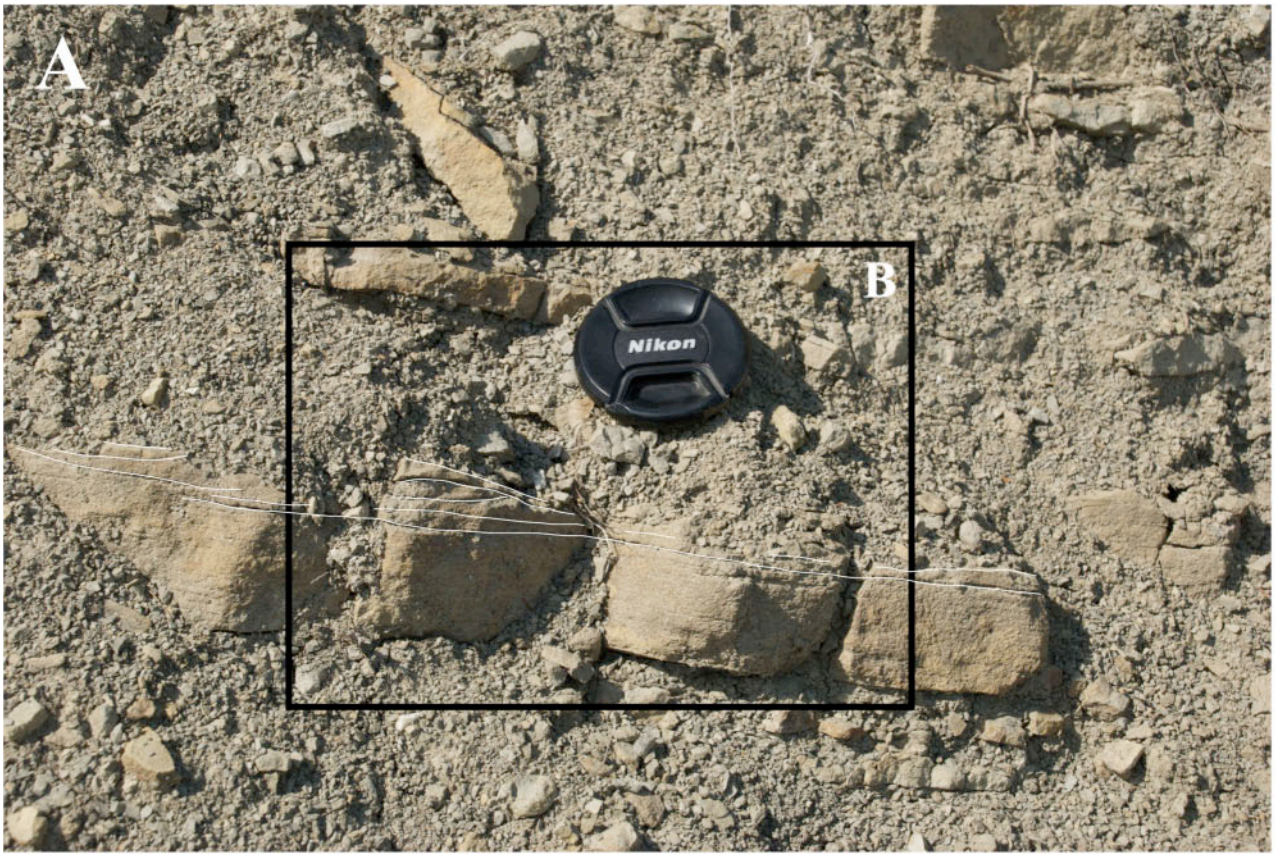
A
B
Nikon

B
Nikon

Figure 4.18 - A: Example of F6-type bed characterizing the thin bedded facies of the uppermost R1 unit (Servazzola section, see attached Panels n.1 and n.4). Camera lens cap for scale, 7 cm in diameter.
B: Close-up of A showing internal parallel-oblique laminations (labeled) characterizing these kinds of beds. Camera lens cap for scale, 7 cm in diameter.

C
D
A
B
Nikon

Figure 4.19 - Examples of sole structures developed in the R1 unit beds of the Pessola Valley outlier.

A: Groove cast developed at the base of an F5-type bed (Pilone section, see attached Panes n.1 and n.4). Measuring tape for scale, 15 cm visible.

B: Flute casts developed at the base of an F5-type bed of the thin-bedded facies of the R1 unit (Servazzola section, see attached Panels n.1 and n.4). Camera lens cap for scale, 7 cm in diameter.

C: Groove cast-type structure developed at the base of an F5-type bed of the thin-bedded facies of the R1 unit (Servazzola section, see attached Panels n.1 and n.4). Measuring tape for scale, 10 cm visible.

D: Loading-related deformations affecting flute casts at the base of a coarse-grained F3/F5-type bed (Pilone section, see attached Panes n.1 and n.4). Knife for scale, 9 cm long.

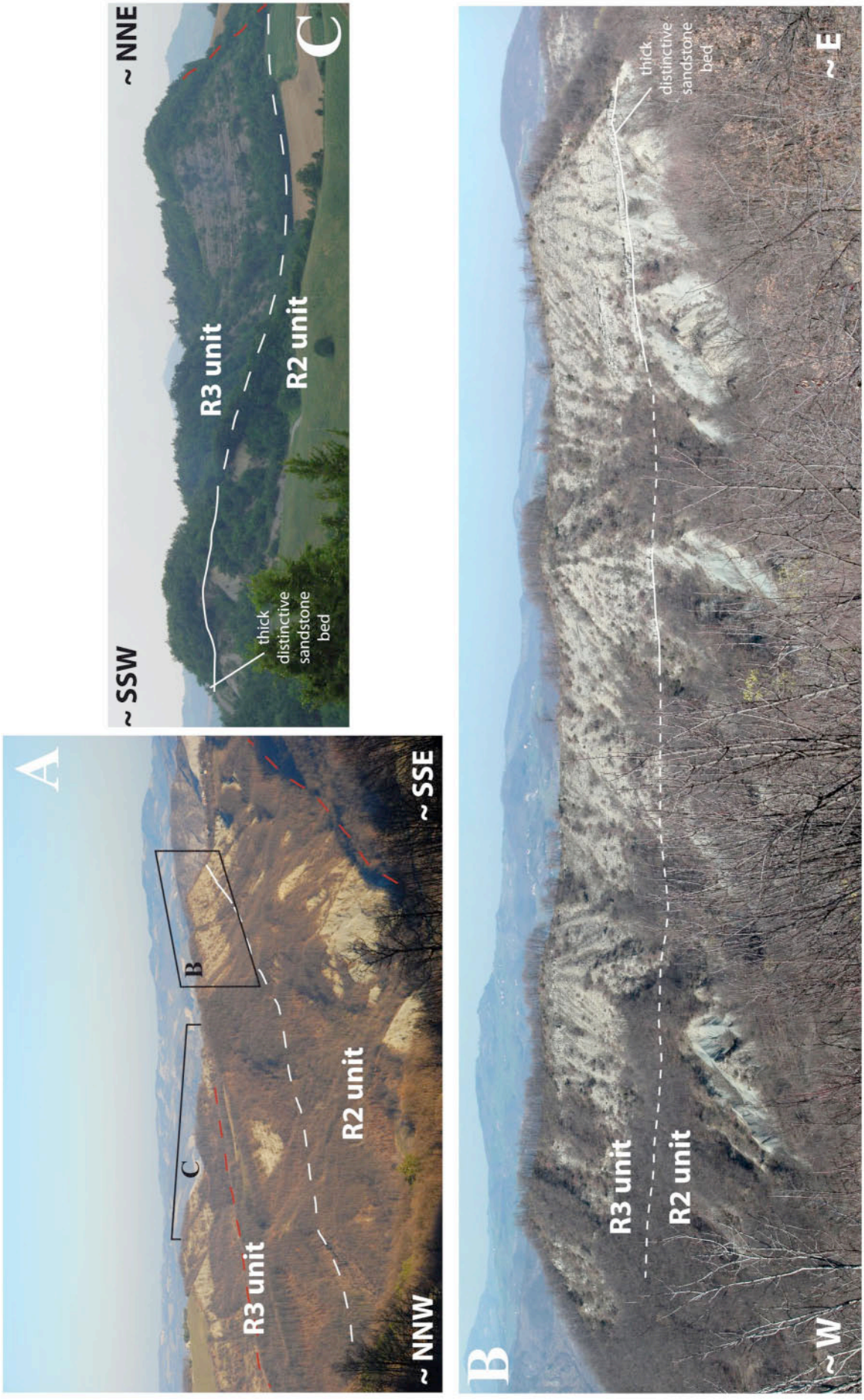
A
~ NNW
~ SSE
R3 unit
R2 unit
C
B
B
~ W
~ E
R3 unit
R2 unit
thick distinctive sandstone bed
C
~ SSW
~ NNE
R3 unit
R2 unit
thick distinctive sandstone bed

Figure 4.20 - A: General view of the R3 unit succession, stratigraphically overlying the R2 Specchio Unit, characterizing the NE sector of the Pessola Valley outlier. Photo is taken roughly looking toward the E.

B: Panoramic photo-mosaic showing the overall appearance of the R3 unit in the Fosio/Faeto section (see attached Panels n.1 and n. 4). Note the distinctive sandstone bed (labeled) marking the contact between R2 and R3 units. Component photos are taken roughly looking toward the N.

C: Panoramic photo-mosaic showing the R3 unit succession and the contact with the underlining R2 unit in the Fosio/Faeto section (see attached Panels n.1 and n. 4). Component photos are taken roughly looking toward the W.

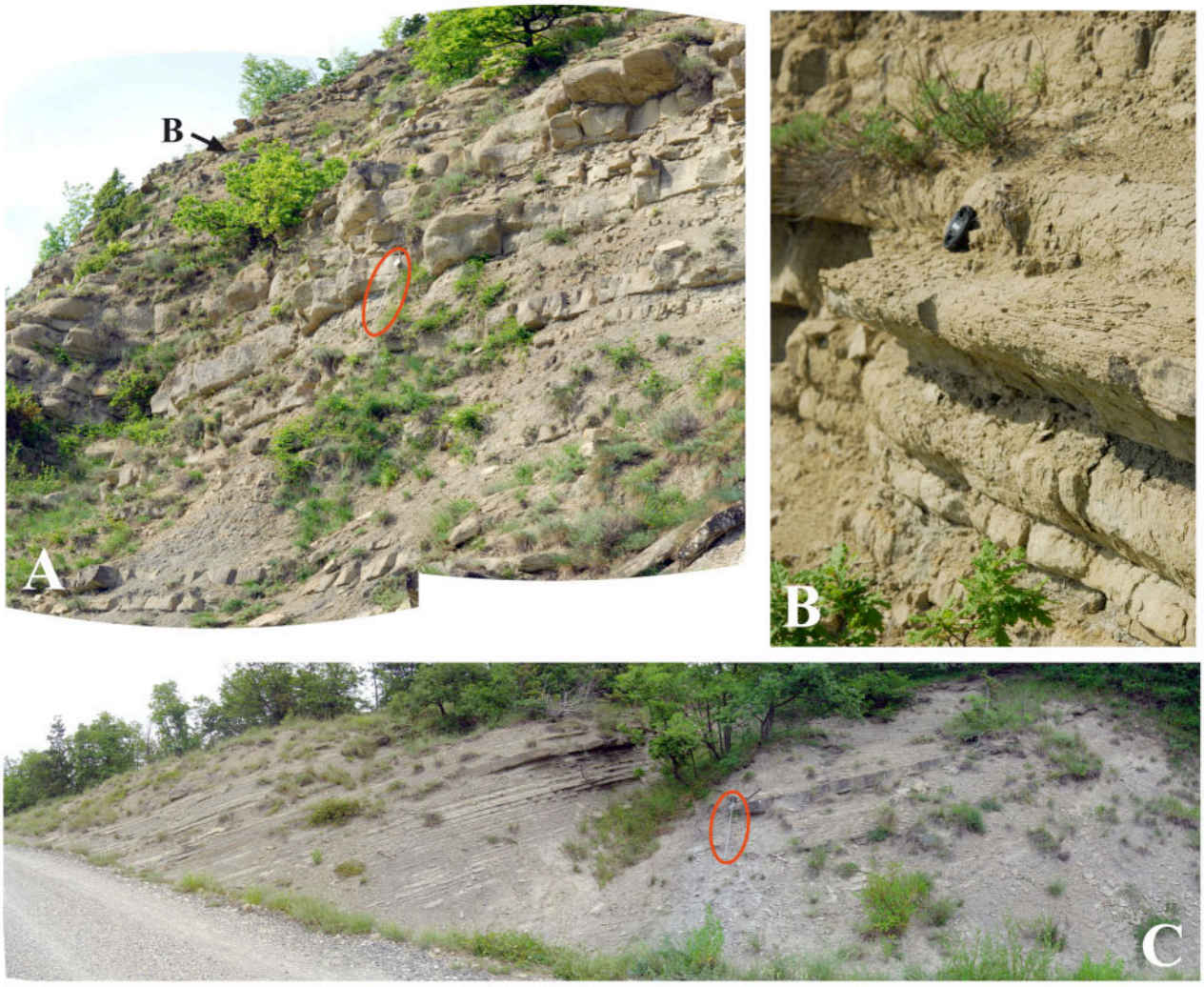

Figure 4.21 - **A**: Outcrop appearance of the R3 unit succession in the western part of the Fosio/Faeto section (see attached Panels n.1 and n. 4). Jacob's staff for scale, 1,5 m long.

B: Amalgamated F7/F8-type bedset characterizing the succession shown in A. Note the faint development of parallel-oblique crude laminations. Camera lens cap for scale, 7 cm in diameter.

C: Outcrop appearance of the R3 unit succession in the eastern part of the Fosio/Faeto section (see attached Panels n.1 and n. 4). Jacob's staff for scale, 1,5 m long.

Figure 4.22 - **A**: General appearance of the middle-upper portion of the R3 unit succession in the eastern sectors of the Fosio/Faeto section (see attached Panels n.1 and n. 4). Note the overall well developed internal cyclicity expressed by high-relief bedsets.

B: Close-up of A showing the well defined erosional profile achieved by F5-F7/F8 bedsets. Dott. Davide Carè for scale.

C
B
A

Figure 4.23 - **A**: Example of F6-type bed characterizing the R3 unit succession (Fosio/Faeto section, see attached Panels n.1 and n. 4). Knife for scale, 9 cm long.

B: Detail of an F6-type bed, with planar base and sharp undulated upper surface. Internal parallel-and oblique-lamination is highlighted by the presence of clearly observable whitish granules. One Euro coin for scale, 2,2 cm in diameter.

C: Overall outcrop appearance of an F6-type-dominated succession with subordinated F7/F8-type bedsets (amalgamated and mud-scoured). Stratification surfaces and mud-draped erosion are labeled. Note the overall lenticular shape and lateral pinch-and-swell trend of F6-type beds. Knife for scale, 9 cm long.

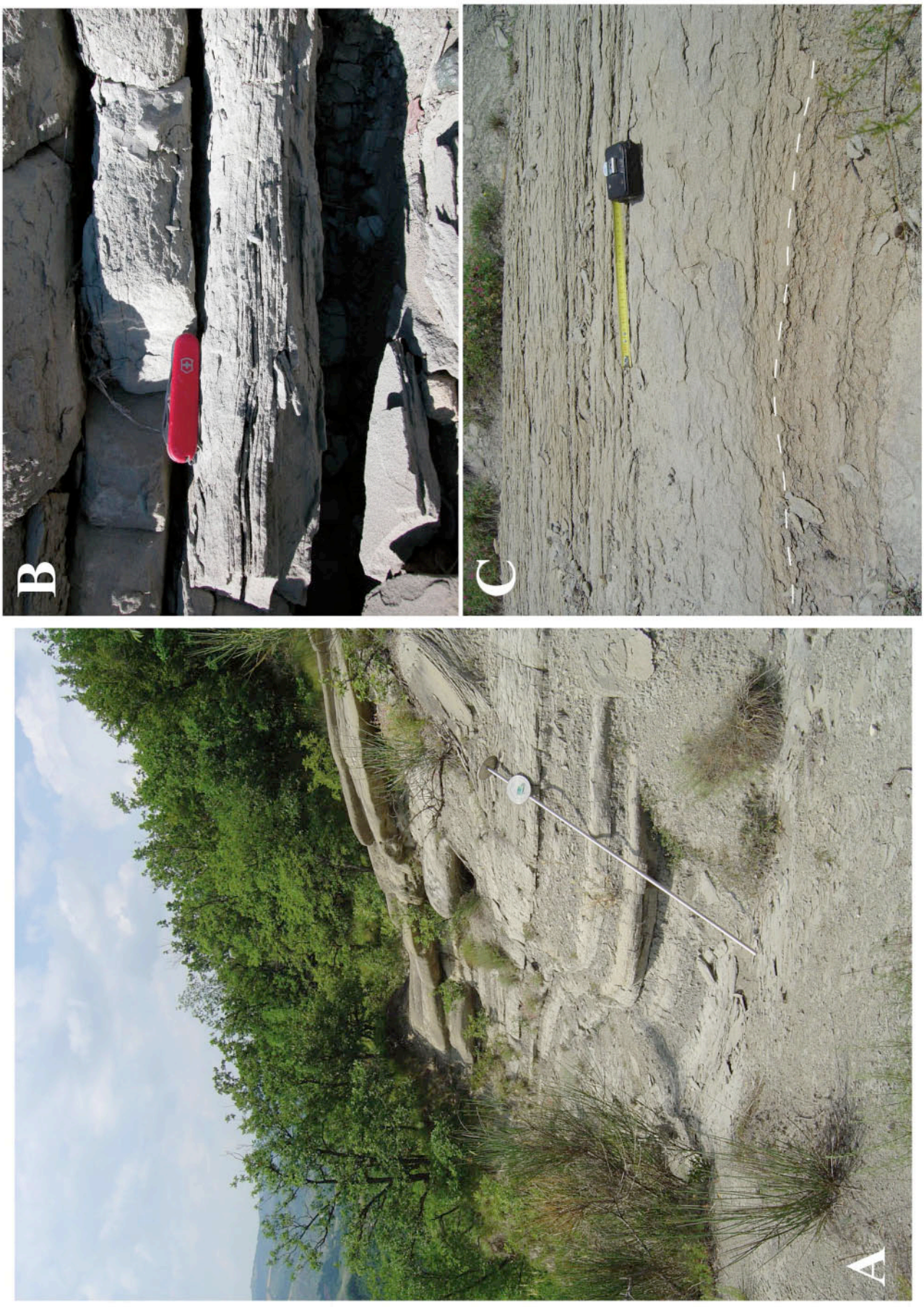
B
C
A

Figure 4.24 - A: General outcrop appearance of an F7/F8-type-dominated succession. Eastern sector of the Fosio/Faeto section (see attached Panels n.1 and n. 4). Jacob's staff for scale, 1,5 m long.

B: Crude laminated (no traction-related whispy laminae) thin-bedded F7/F8-type bed, interpreted as evidence of deceleration-related turbulence suppression. Knife for scale, 9 cm long.

C: Example of two amalgamated F7/F8-type beds. Note the lower massive/liquefied division (sometimes inversely graded) and the upper generally oxidized and crude laminated division characterizing the anatomy of these beds. Sometimes, these amalgamated beds show well-developed lateral continuities, resembling composite or bi-parted strata instead of two separated events. Measuring tape for scale, ~21 cm visible.

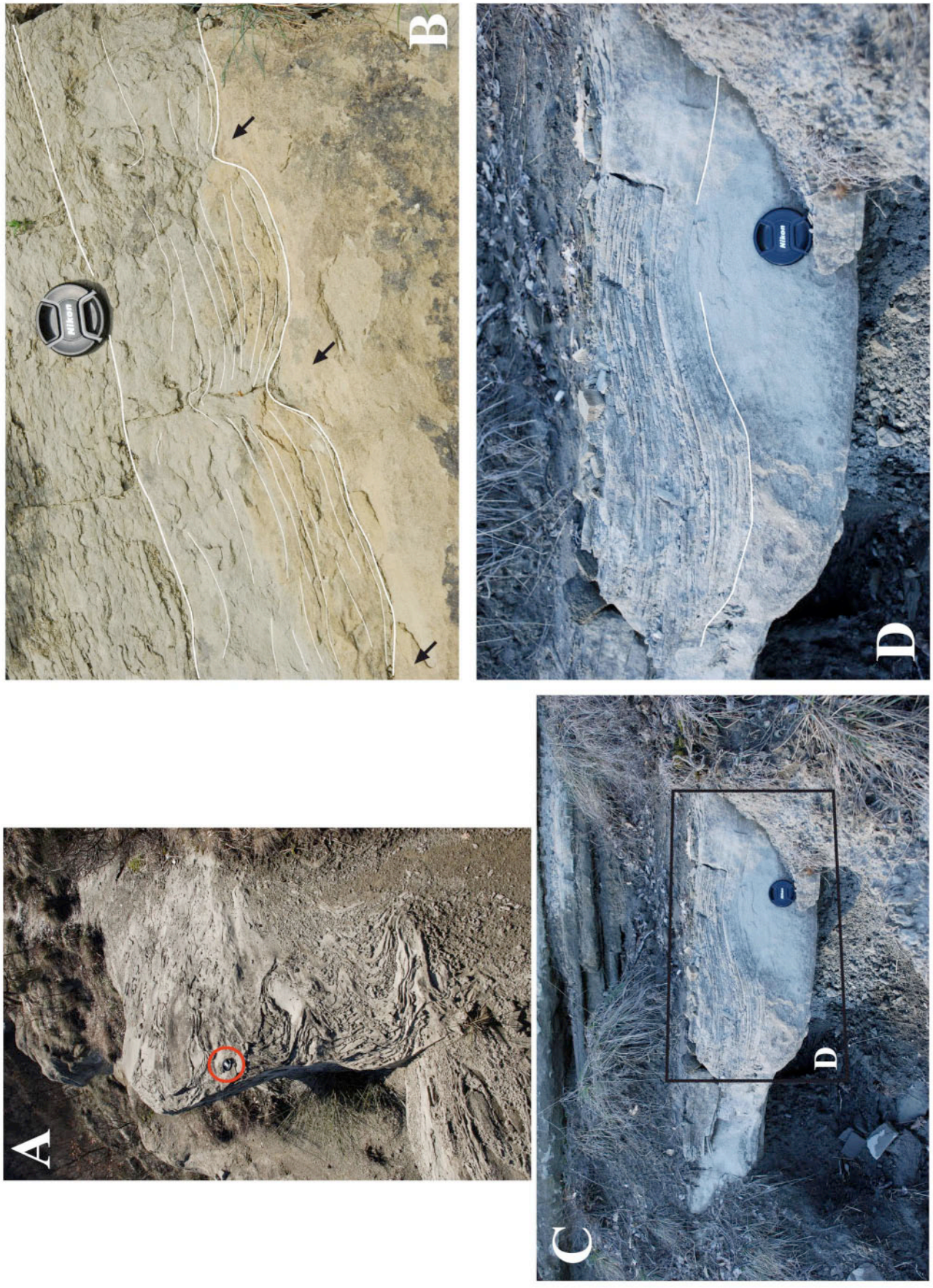
A
B
C
D
D
1

Figure 4.25 - Examples of liquefaction-related evidences and fluid-escape deformations affecting F7/F8-type beds of the R3 unit (Fosio/Faeto section, see attached Panels n.1 and n. 4).

A: Plan view of the upper surface of a F7/F8-type bed, showing the three-dimensional appearance of flame-like structures and upward-convex culminations linked to fluid-escapes deforming crude laminations. Camera lens cap for scale, 7 cm in diameter.

B: Upward fluid-escape structures (flame-like) injecting from the lower liquefied/massive division into the upper laminated divisions of the bed, with bending of the crude laminae (labeled). Camera lens cap for scale, 7 cm in diameter.

C: F7/F8-type bed showing a well-developed bi-partition in a lower liquefied/massive division and an upper laminated divisions. Camera lens cap for scale, 7 cm in diameter.

D: Close-up of C showing the bending of the laminated portion in response to upward fluid-escape from the lower liquefied portion. Separation surface between the two portions is labeled. Camera lens cap for scale, 7 cm in diameter.

A
B
C
D
Nikon
B
D
inverse grading
normal grading
inverse grading
grain-size breacks

Figure 4.26 - Examples of bi-partite/composite appearance sometimes shown by F6- and F7/F8-type beds.

A: Localized grain-size break affecting an F7/F8-type bed, laterally disappearing in short distances. Camera lens cap for scale, 7 cm in diameter.

B: Close-up of C showing a laterally continuous, well-defined grain-size break (amalgamation surface?) affecting a F6-type bed. Camera lens cap for scale, 7 cm in diameter.

C: Overall view of a medium-bedded F6-type bed. Note the pinch-and-swell lateral trend, and the upper and lower sharp contacts. Jacob's staff for scale, 1,5 m long.

D: Detail of bed shown in C, highlighting the presence of two components amalgamated beds (or flow pulses in the same bed) characterized by inverse grading. Grain-size break surfaces are labeled. Camera lens cap for scale, 7 cm in diameter.

C
D
A
B

Figure 4.27 - Examples of isolated clasts and coarse-grained material clusters observable in R3 unit component beds.

A: Isolated well-rounded pebble contained in the upper portion of a massive F7/F8-type bed (northern R3 unit outcrops of the Pessola Valley outlier). Camera lens cap for scale, 7 cm in diameter.

B: Isolated sub-angular carbonatic clast observed in the lower-middle part of F7/F8-type bed (Fosio/Faeto section). Knife for scale, 9 cm long.

C: "Pocket" of sub-angular carbonatic clasts (up to 5 cm across) recognized in the basal amalgamated surface of an F7/F8-type bed (Fosio/Faeto section).

D: Isolated well-rounded pebble contained in the upper portion of a massive F7/F8-type bed (Fosio/Faeto section).

A
B
B
C
D
E
D
E

Figure 4.28 - A: Outcrop appearance of the R3 unit in the lower portion of the eastern Fosio/Faeto section. Stratification surfaces and mud-draped scours are labeled. At the right edge of the photo-mosaic is visible the distinctive thick-bedded sandstone layer marking the R3 unit lower contact with the R2 unit, while at the left edge is observable a minor normal fault displacing the thick F7/F8-type bed visible in the upper side of ~ 3 m. Thoto-mosaic is roughly oriented in a NNW-SSE direction. Dott. Nicola Minelli and Dott. Davide Carè for scale.

B: Close-up of A showing a detail of a mud-draped scour cutting a minor bedset. Note that the internal laminations of the lower bed (labeled) are truncated by the scouring surface. Field notebook for scale, 20 cm long.

C: Example of scour surface cutting a crudely laminated F7/F8-type bed (western Fosio/Faeto section). Note the lateral truncation of the crude laminae (labeled). Camera lens cap for scale, 7 cm in diameter.

D: Close-up of C showing the coarse-grained residual lag deposit draping the scour surface (labeled). One Euro cent coin for scale, 1,1 cm in diameter.

E: Close-up of the coarse-grained pebbly sandstone constituting the lag accumulation. Some scattered *nummulites* and sparse shell debris has been observed. One Euro cent coin for scale, 1,1 cm in diameter.

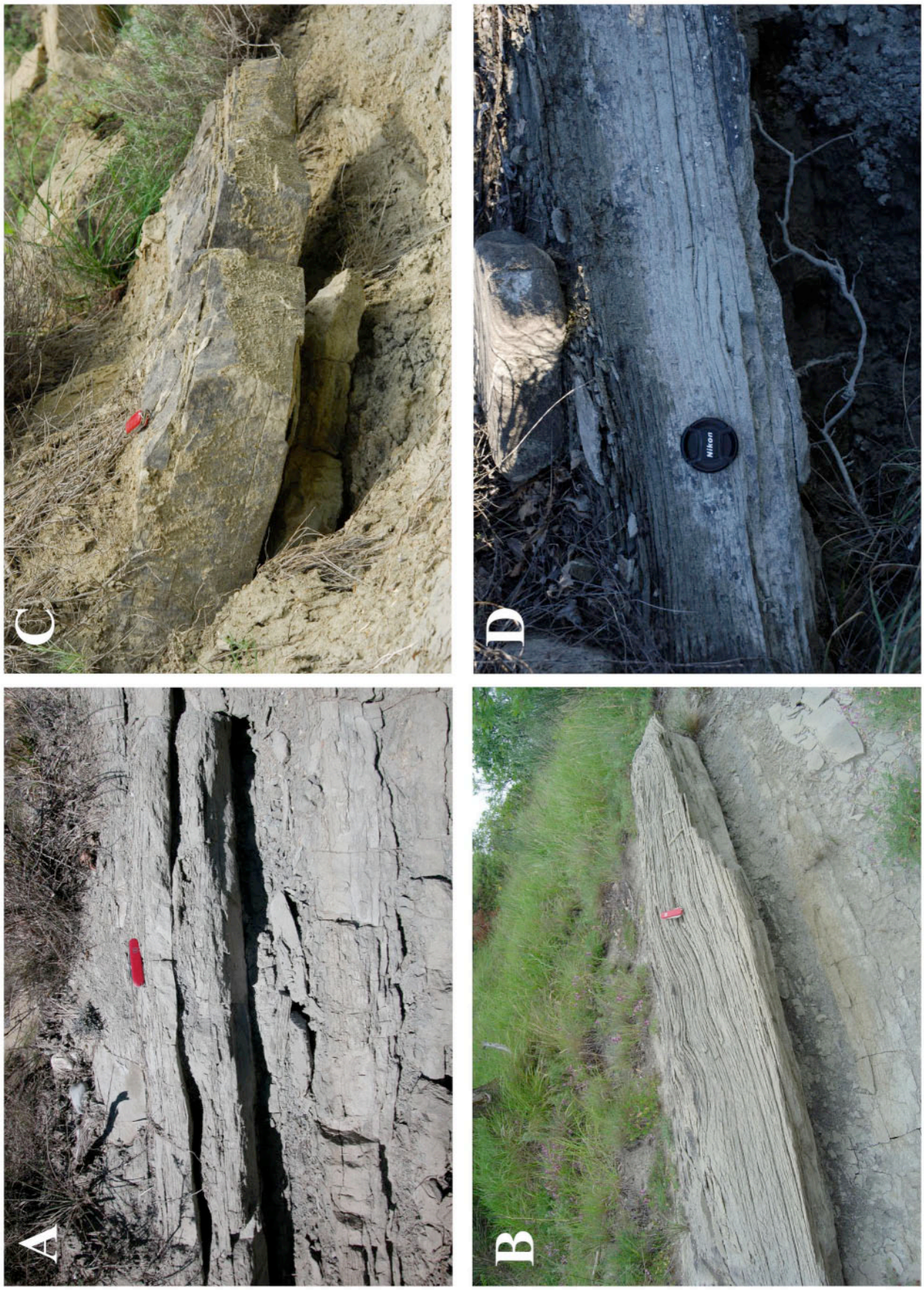
C
D
A
B
Nikon

Figure 4.29 - A: Example of crudely laminated thin- to medium-bedded F7/F8-type beds. These whispy-type laminae are thought to record flow deceleration and consequent enhanced sedimentation-related suppression of the turbulence. Undulated appearance of upper bed surfaces are formed by fluid-expulsion related deformations. Eastern Fosio/Faeto section. Knife for scale, 9 cm long.

B: F7/F8-type bed with well-developed whispy-type lamination (as explained for those shown in A) trough its entire thickness. These laminae are bended by upward fluid-escapes. Eastern Fosio/Faeto section. Knife for scale, 9 cm long.

C: F7/F8-type bed (almost F9-type) with an oblique-laminated upper portion. The oblique laminae represent ripple foresets and thus recording traction plus fallout processes. Parallel crude lamination developed in the lower portion are thought to have the same significance of those described for A and B. Western Fosio/Faeto section. Knife for scale, 9 cm long.

D: Medium-bedded F7/F8-type bed entirely laminated. In this case component laminae seem to show lateral thickness changes and low-angle crossing relationships. In the center of the photo a convex bi-vergent ripple-like structure is observable. In some instances the undulated appearance shown by these beds is referred to as small-scale HCS-like laminations. Eastern Fosio/Faeto section. Camera lens cap for scale, 7 cm in diameter.

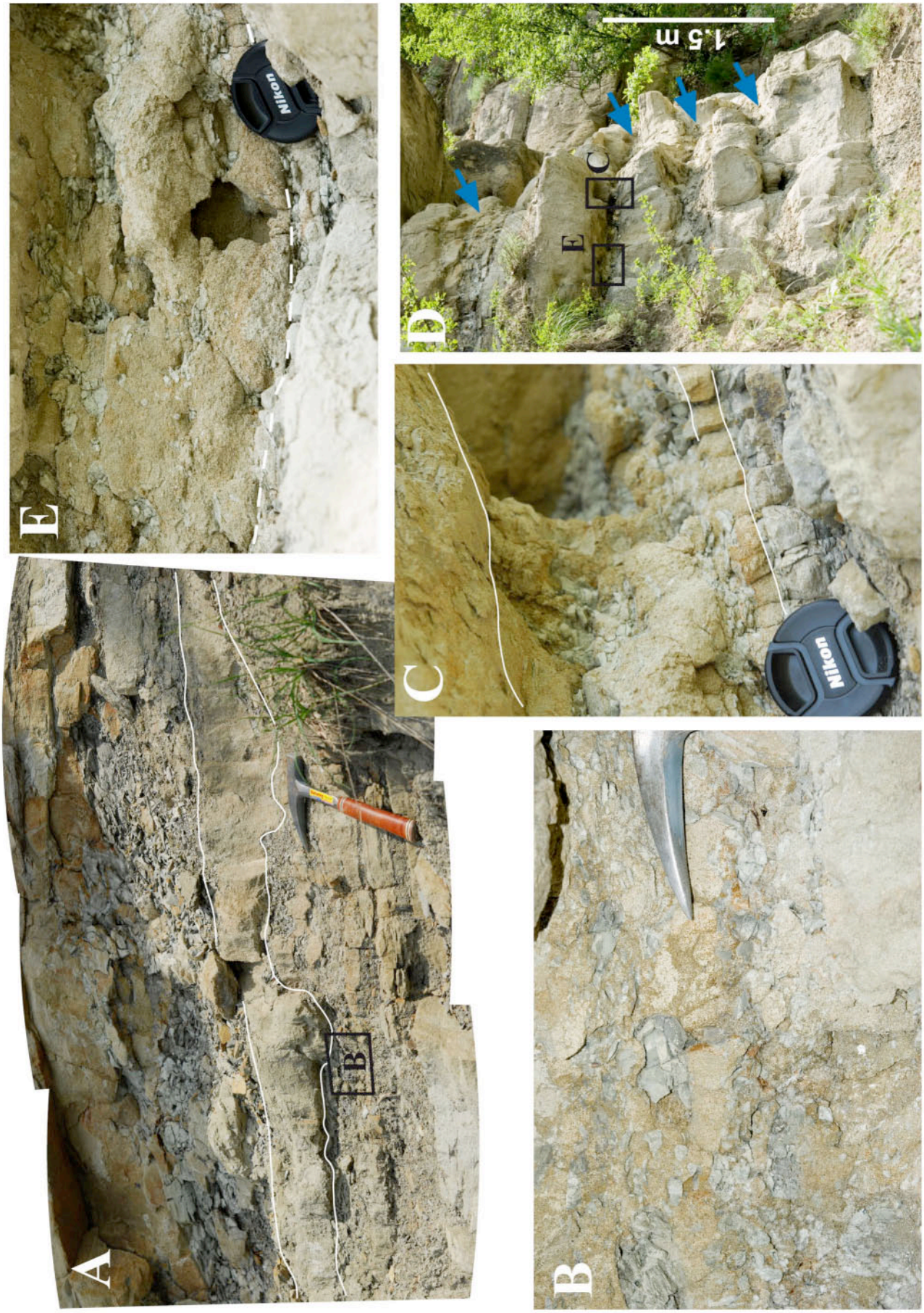
A
B
C
D
E
1.5 m
Nikon

Figure 4.30 - A: Photo-mosaic showing a medium-bedded F7/F8-type bed (labeled), which develops a basal impact breccia-type interval. Ceno-Pessola rivers confluence section (see Panel n.1 and n. 4). Hammer for scale.

B: Close-up of A showing a detail of the impact breccia interval, characterized by significant amount of clay chips and reddish alteration color. Hammer for scale.

C: Close-up of D showing an impact breccia interval. Here it is possible to observe how the impact breccia material comes from the desegregation of thin-bedded sandstone-mudstone inter-layers.

D: Overall appearance of an F5-type bedset characterized by intervals of impact breccias localized along respective amalgamation surfaces (marked by blue arrows). Ceno-Pessola rivers confluence section (see Panel n.1 and n. 4).

E: Close-up of D showing a detail of an impact breccia interval and the upper surface of the underlying bed (labeled). Camera lens cap for scale, 7 cm in diameter.

C
D
A
B

Figure 4.31 - Examples of bioclasts recognized in the R3 unit.

A: Residual coarse-grained lag deposits with scattered *nummulites* and sparse shell debris (labeled with red arrows). One Euro cent coin for scale, 2,2 cm in diameter.

B: Isolated bivalve shell contained in the lower portion of an F7/F8-type bed. Knife for scale, 9 cm long.

C: Isolated transversally cut sponge or echinoid spike contained in the lower portion of a F7/F8-type bed. Note the clay chips alignment in the middle part of the bed. One Euro coin for scale, 2,2 cm in diameter.

D: Isolated shell fragment (ostrachod?) contained in the upper portion of an F7/F8-type bed. Measuring tape for scale.

A

2
EURO
B

Figure 4.32 - Examples of bioturbation recognized in the R3 unit beds.

A: *Ophiomorpha*-like ichnofacies affecting the upper laminated part of an F7/F8-type bed. Knife for scale, 9 cm long.

B: *Planolites*-like ichniofacies observed on the upper bypass surface of an F6-type bed. Two Euro coin, 2,6 cm in diameter.

A
1 m
B
C
D
Nikon

Figure 4.33 - Examples of variously diagenized plant fragments (isolated or clustered along lamination surfaces) recognized in the R3 unit beds.

A: Coalified m-sized plant fragment contained within the basal part of an amalgamated bedset of thick-bedded F5-type beds characterized by faint large-scale oblique laminations (compansation cycle- or prograding bar-like geometries). Ceno-Pessola rivers confluence section (see Panel n.1 and n. 4).

B: Composite-like F7/F8-type bed with a strong enrichment of oxidized plant fragments within the intermediate part. Western Fosio/Faeto section. Camera lens cap for scale, 7 cm in diameter.

C: Coalified cm-sized plant fragments localized within the upper laminated fine-grained portions of F7/F8-type beds. Eastern Fosio/Faeto section. Camera lens cap for scale, 7 cm in diameter.

D: Oxidized plant fragments disposed on surfaces of whispy lamination characterizing F7/F8-type beds. Western Fosio/Faeto section. Camera lens cap for scale, 7 cm in diameter.

A
C
B
D

Figure 4.34 - Examples of particular cylindrical-shaped clay chips observable within the R3 unit beds. These elements, which may resemble bioturbations, where observed in three-dimensional view appear as detached tubular lenses. Their origin should be attributed to flow erosion of early-diagenized, *planolites*-like ichnofacies developed in muddy partings, and preserved within the overlying deposit as "tubular" clay chips. **A**, **B** and **C** are from the eastern Fosio/Faeto section, while **D** is from the northern outcrops of the R3 unit (Dordia section, see attached Panels n.1 and n.4).

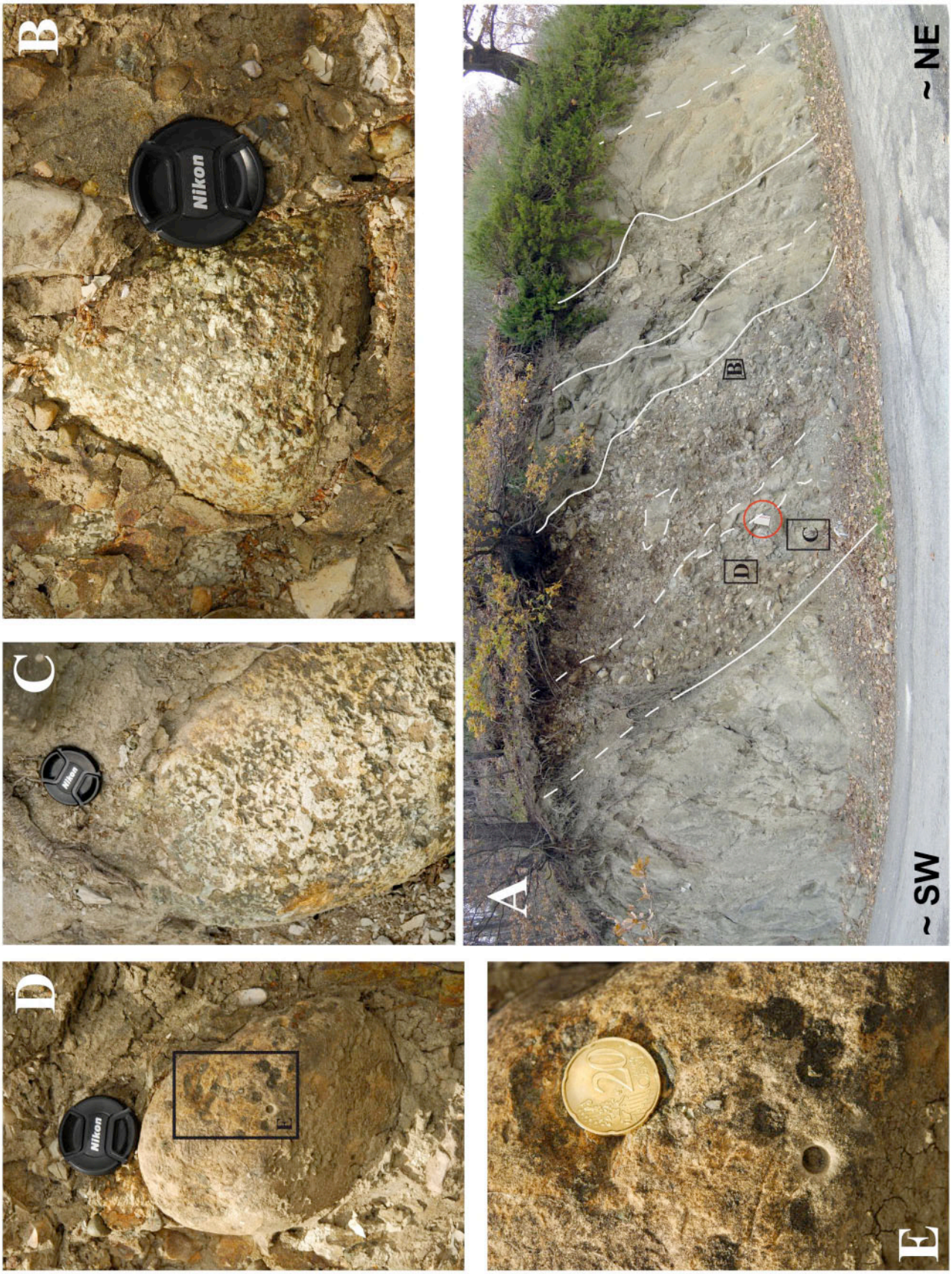
A
~ SW
~ NE
B
C
D
E
Nikon

Figure 4.35 - A: Outcrop appearance of the thick-bedded conglomeratic beds characterizing the northernmost analyzed outcrops of the R3 unit, formerly belonging to the Varano de'M.-Pellegrino P. outlier (Section n. 7, see Panel n. 4). Main stratification surfaces are labeled. Note that the labeled beds are amalgamated, with the overlying one containing rip-up clasts from the upper sandstone parting of the underlying one. Stratigraphic younging to the right. Field notebook for scale, 20 cm long.

B: Close-up of A showing a well-rounded cobble made of gabbro (Internal Ligurian Units?). Note the sparse oxidized patches in the fine-to coarse-grained unsorted sandstone matrix, testifying plant fragments abundance. Camera lens cap for scale, 7 cm in diameter.

C: Close up of A showing another well-rounded cobble of gabbroic lithologies. Camera lens cap for scale, 7 cm in diameter.

D: Close up of A showing a well-rounded sandstone cobble characterized by bioerosional hollows (*i.e.* lithodomes burrows). Camera lens cap for scale, 7 cm in diameter.

E: Close up of D showing a detail of the lithodomes burrows. This evidence indicates reworking in coastal environment. Twenty Euro cent coin for scale, 2,2 cm in diameter.

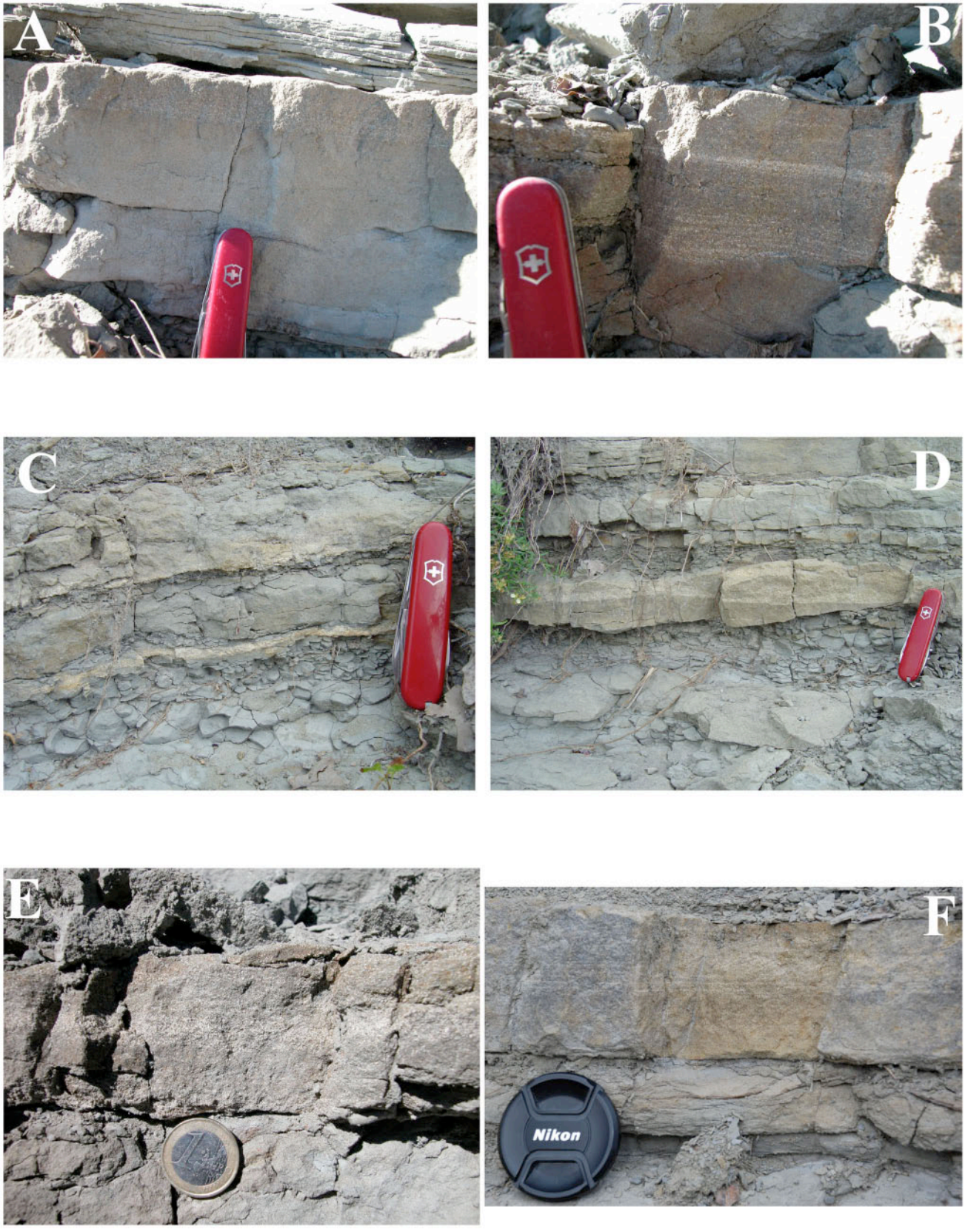
A
B
C
D
E
F
Nikon

Figure 4.36 - Examples of the mixed volcaniclastic layers recognized in the R3 unit succession of the Pessola Valley outlier. These beds show a significant enrichment of a whitish mineral, recognized to be relatively "fresh" calcalkaline volcanism-related plagioclase, localized in clusters or more or less diluted with the other clastic material. Moreover these beds seems to share more cemented conditions and an overall reddish oxidized alteration color. All presented examples are from eastern Fosio/Faeto section.

A: Composite-like F7/F8-type bed characterized by an inverse-grained lower portion separated by a grain-size break surface from an upper coarse-grained crudely laminated portion resembling the F6-type facies. Plagioclase detritus is concentrated in the latter. Knife for scale, 9 cm long.

B: Same type of bed described in A. Note that the plagioclase detritus is concentrated along the parallel and oblique laminae of the upper F6-type portion. Knife for scale, 9 cm long.

C: Very thin-bedded and coarse-grained F6-type layer composed almost entirely of plagiolcase detritus. Knife for scale, 9 cm long.

D: Plagioclase-rich F6-type bed amalgamating with an underlying thin-bedded F7/F8-type bed or composite-like bed (pulses within the same event). In every case it is clearly appreciable the large-scale internal lamination. Knife for scale, 9 cm long.

E: Example of the same type of bed described in A. Note the parallel and oblique laminae. One Euro coin for scale, 2,2 cm in diameter.

F: Another example of the same type of bed described in A. Note the parallel and oblique lamination of the upper portion. Plagioclase detritus is also present in the lower roughly inverse grained portion but more diluted with the other clastic material. Camera lens cap for scale, 7 cm in diameter.

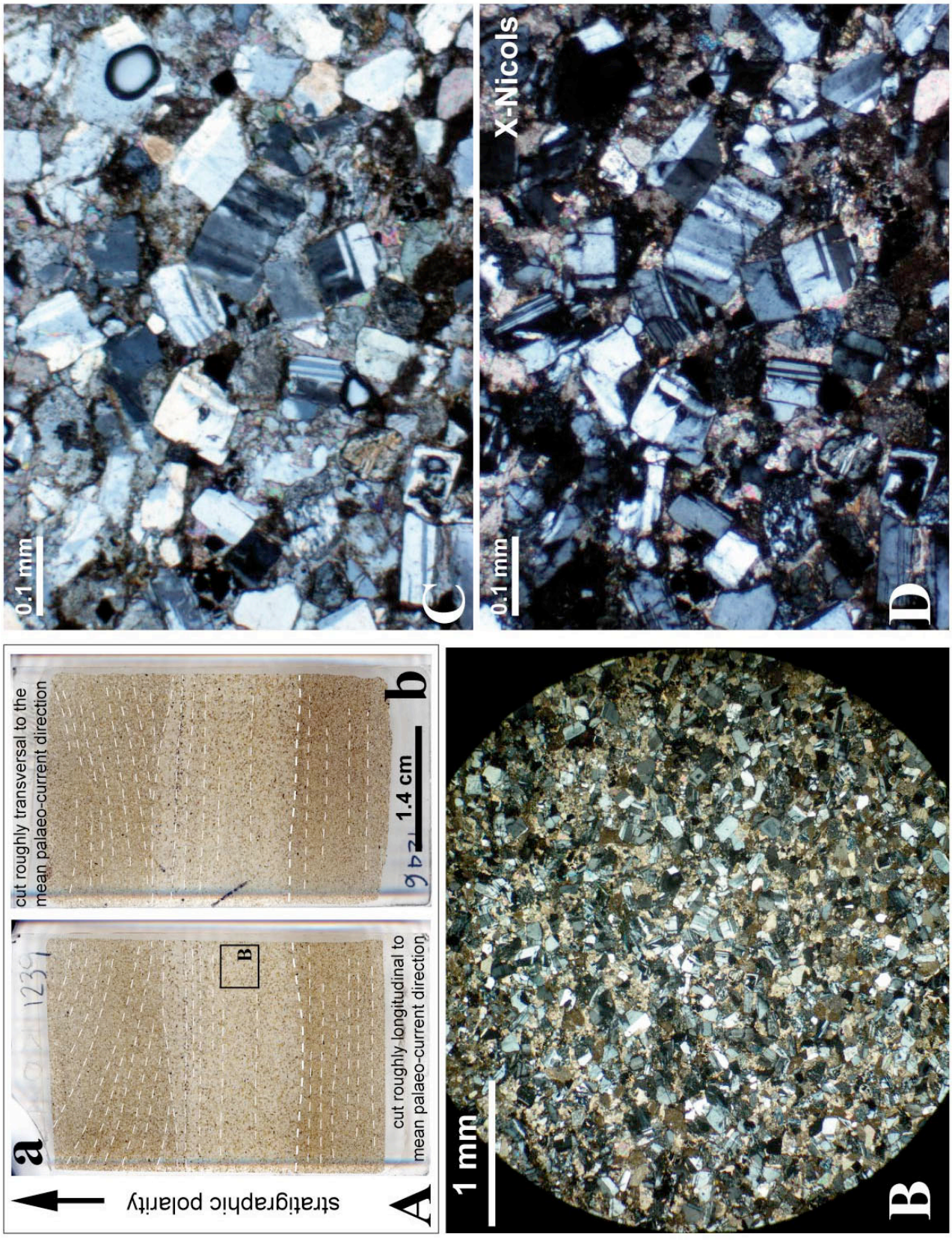
A
stratigraphic polarity
a
B
cut roughly longitudinal to mean palaeo-current direction
cut roughly transversal to the mean palaeo-current direction
1.4 cm
b
B
1 mm
C
0.1 mm
D
X-Nicols
0.1 mm

Figure 4.37 - Examples form the sample R3WCB, taken form a medium-thick mixed volcaniclastic bed with a composite appearance (F7/F8-type lower division and F6-type upper division), located in the middle-upper R3 unit succession (eastern Fosio/Faeto section; for location of the sample see chap. 2).

A: Thin sections of the "white clast banding" lamination, oriented in a parallel and transversal direction respecting to the mean palaeo-current direction ("a" and "b", respectively). Lamination trend is labeled.

B: Optical microscopic general view of the "white clast banding" lamination (crossed Nicols), showing the predominance of well-sorted, angular ("fresh") plagioclase crystals, and characterized by clearly discernible light-dark zonations (*i.e.* Albite-type). Note that the plagioclase clasts share the same overall grain-size shown by the other subordinate elements. Location shown in A.

C: Close-up of the "white clast banding" lamination showing in detail the appearance of the plagioclase clasts.

D: Same close-up represented in C, viewed through crossed Nicols.

C
D
palaeocurrent direction
A
B

Figure 4.38 - Examples of recognized sole structures on the basal surfaces of R3 unit beds. Camera lens cap for scale, 7 cm in diameter.

A: Flute-casts slightly disturbed by bioturbation. Inferred palaeo-flow direction is labeled. Dordia section.

B: Poorly-developed flute- and groove-casts. Inferred palaeo-flow direction is labeled. Dordia section.

C: Example of well-developed groove-casts intersecting each other at high angle. Bounce- and prod-casts evidences are also present, as well as a significant amount of bioturbation. Inferred palaeo-flow direction is labeled. Madonna section.

D: Transversal cut of a down-flow elongated asymmetrical scour filled with pebbly residual lag accumulation. Spiaggio section (see attached Panel n.1).

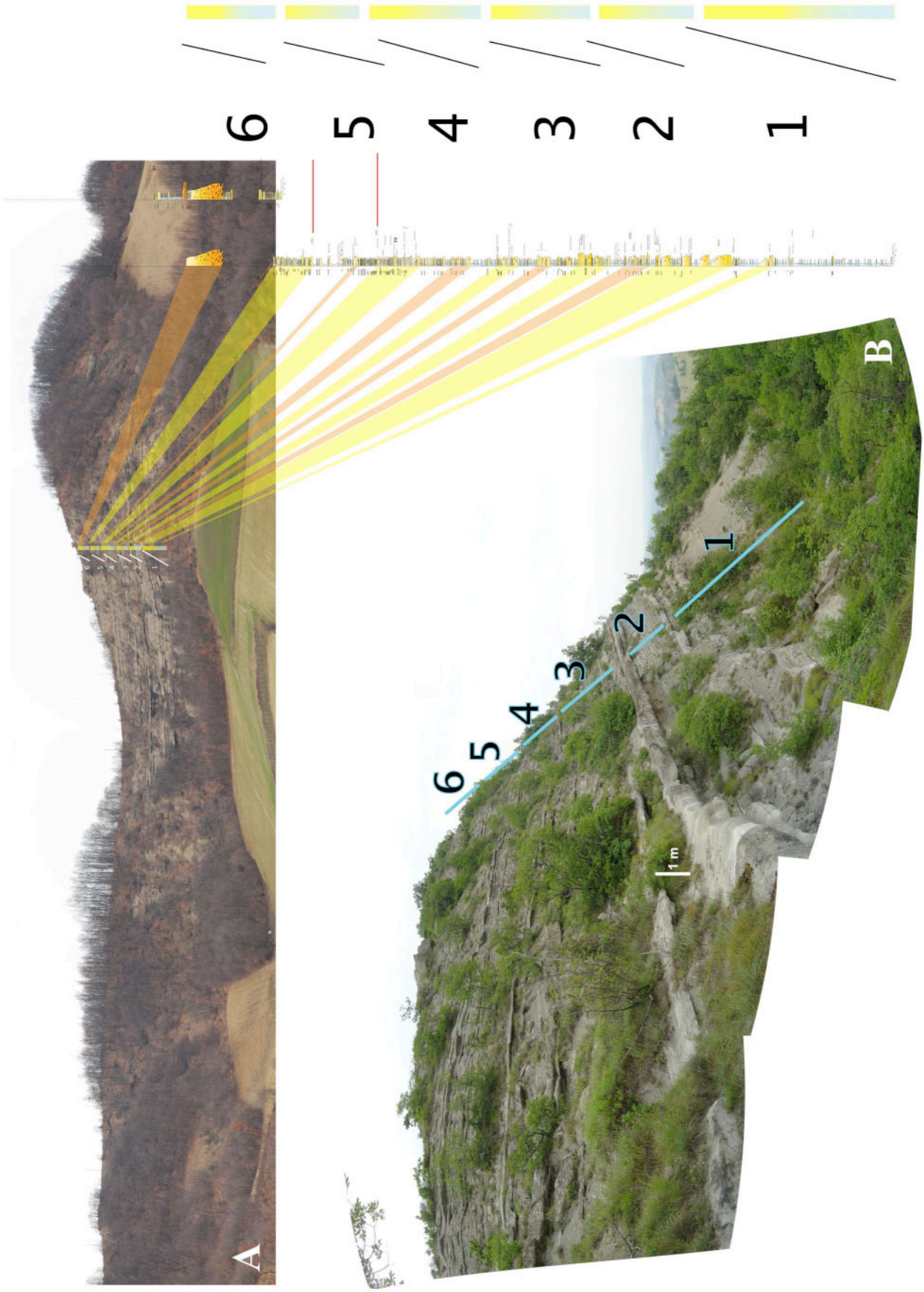
6
5
4
3
2
1
A
B
6
5
4
3
2
1
1 m

Figure 4.39 - A: Panoramic photo-mosaic of the easternmost Fosio/Faeto section showing almost the whole R3 unit succession of the Pessola Valley outlier. The inferred internal stacking pattern of this R3 unit succession is represented at the right side of the stratigraphic column and tentatively correlated with the photo-mosaic (orange label for oxidized, volcaniclastic-rich bedsets; yellow label for F7/F8-type bedsets; F6-type beds and fine-grained, thin-bedded portion represent the background sedimentation). At least 6 meter-scale thickening-upward cycles has been recognized.
B: Detail of the outcrop shown in A, with representation of the recognized inferred cycles. The high erosional relief shared by upper bedsets helps in the visualization of such cycles.

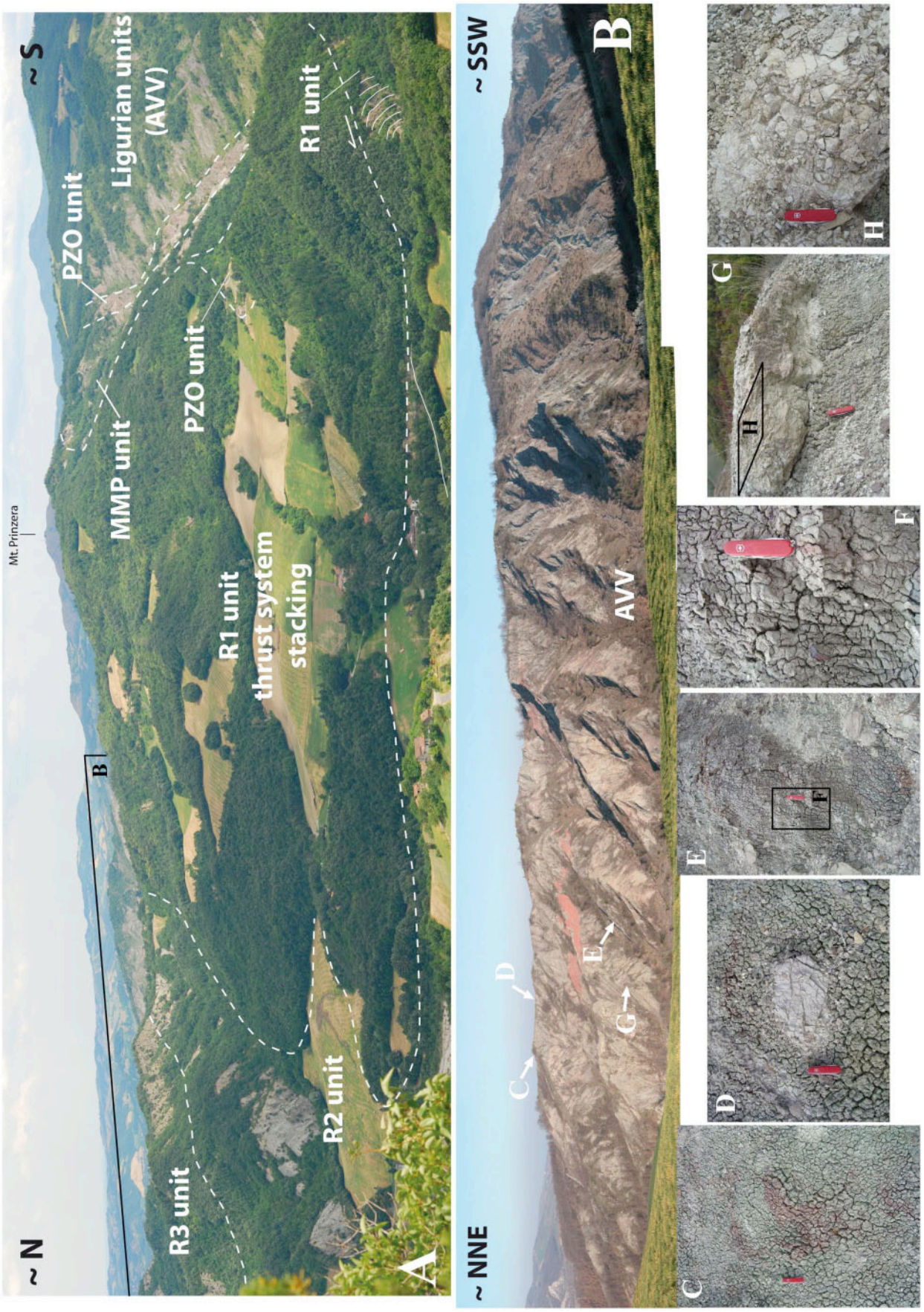
~ N
~ S
Mt. Prinzera
R3 unit
R2 unit
R1 unit
thrust system
stacking
R1 unit
MMP unit
PZO unit
PZO unit
Ligurian units
(AVV)
A
B
~ NNE
~ SSW
AVV
B
C
D
E
G
C
D
E
F
F
G
H
H

Figure 4.40 - A: General panoramic view on the eastern Pessola Valley outlier. Main stratigrahic and structural features has been labeled.

B: Panoramic view of the "badlands" characterizing the E-SE margin of the Pessola Valley outlier. The lithologies belong to the ophiolite-bearing, shale-rich chaotic units of the Ligurian Basal Complexes (*i.e.* geometrical bases of the Helmintoyd Flysch units), herein grouped under the generic name of AVV. These units share complex reciprocal contacts and with the Epiligurian succession, usually resembling high-angle faults. Location is shown in A.

C: Flames-like structures and fluidal-like deformations are observed within these highly deformed shaly units. Such features are usually recognizable thanks to the evident alteration colors of discrete components. Note the strong weathering of these rock exposures. Location shown in B. Knife for scale, 9 cm long.

D: Isolated carbonatic sub-angular clast contained within the varicoloured shaly matrix of AVV units. Location shown in B. Knife for scale, 9 cm long.

E: General appearance of AVV units lithologies. The block-in-matrix fabric seems to be well developed. Isolated clasts are mainly represented by ophiolites, carbonates and sandstones, commonly sharing manganesiferous coatings. Note the strong weathering of these rock exposures. Location shown in B. Knife for scale, 9 cm long.

F: Close-up of E showing some darkish clasts (due to oxide coatings) of sandstone, scattered within the strongly altered fine-grained matrix. Looking a fresh cut, these lithologies appear characterized by a well-developed foliation resembling the typical scaly cleavage. Knife for scale, 9 cm long.

G: Isolated carbonate block contained within the AVV units lithologies. Knife for scale, 9 cm long.

H: Close-up or the carbonate block showed in G. Note the "auto-brecciated" appearance. Part of the angular carbonatic detritus recognizable within these units may be related to the desegregation of such blocks. Knife for scale, 9 cm long.

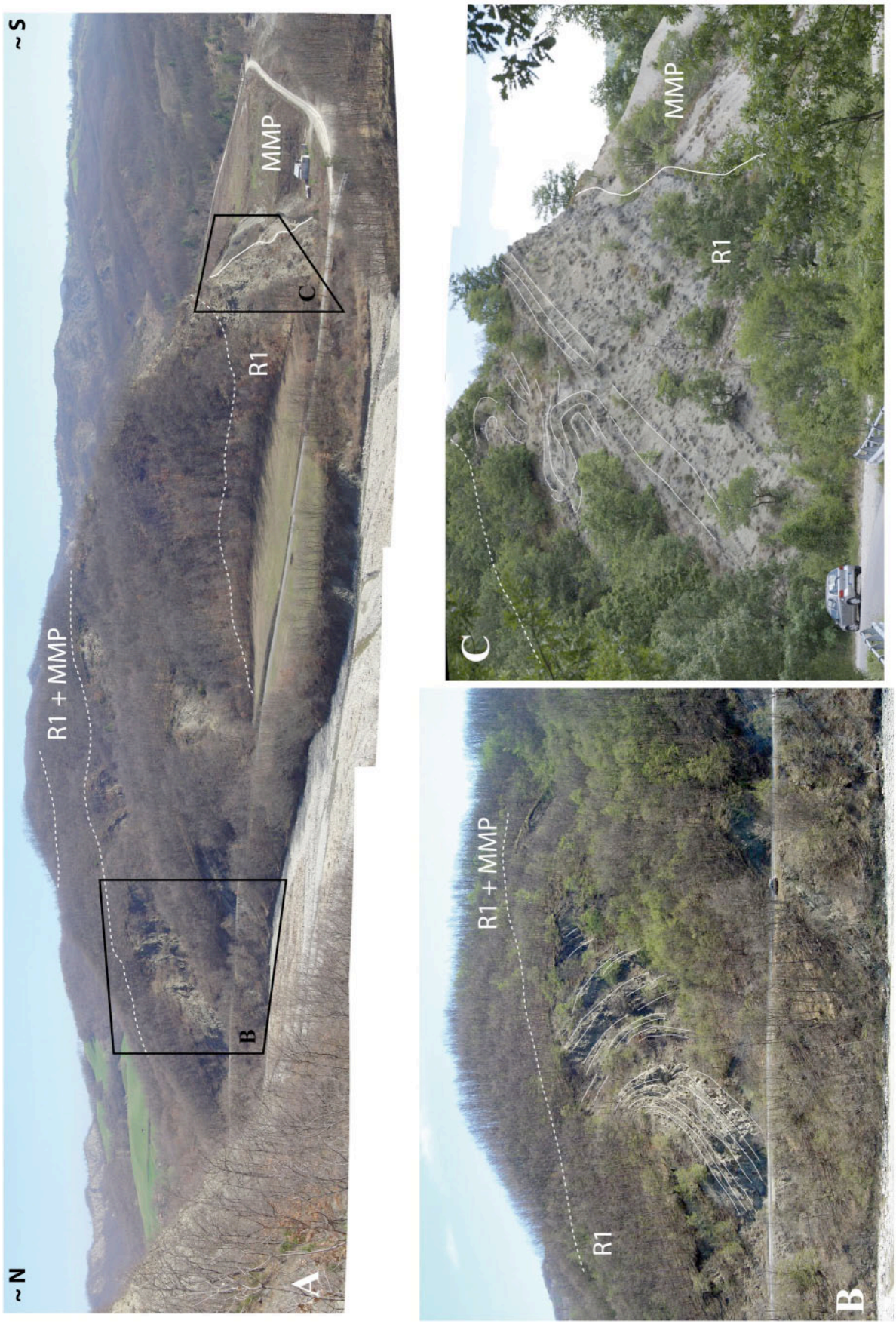
~S
~N
MMP
R1
R1 + MMP
A
B
C
R1 + MMP
R1
B
MMP
R1
C

Figure 4.41 - **A**: General panoramic view of the south-easternmost side of the Pessola Valley outlier, showing the positive structure created by the tectonic stacking of at least three low-angle thrusts, duplicating the MMP-R1 succession, with the partial involvement of the PZO unit (*i.e.* Ricodalle thrust system, see attached Panel n.1). These thrusts seem to be developed at shallow-crustal levels (as confirmed by micro-structural analysis), in response to the tectonic growing of a buried Ligurian-related structure located farther to the S-SE (Mt. S. Antonio-Mt. Pareto-Mt. Dosso structure?). Interpreted thrust surfaces are labeled.

B: N-NW verging recumbent syncline affecting the R1 unit in the right side of the Pessola River. Such structure is thought to develop in response to the dragging force exerted by the overridden thrust. Lateral stratigraphic expansion shared by some of the component beds should be indicative of a growth-like structural evolution of such syncline. Stratification trend and thrust surface are labeled.

C: Soft-sediment folding (slump-like structures) affecting the basal R1 unit, developed in response to the translation of the lower thrust. Folds vergence indicated a N-NW tectonic transport direction. This evidence supports the hypothesis of the shallow-crustal level origin of such structures. Stratification patterns and thrust surfaces are labeled.

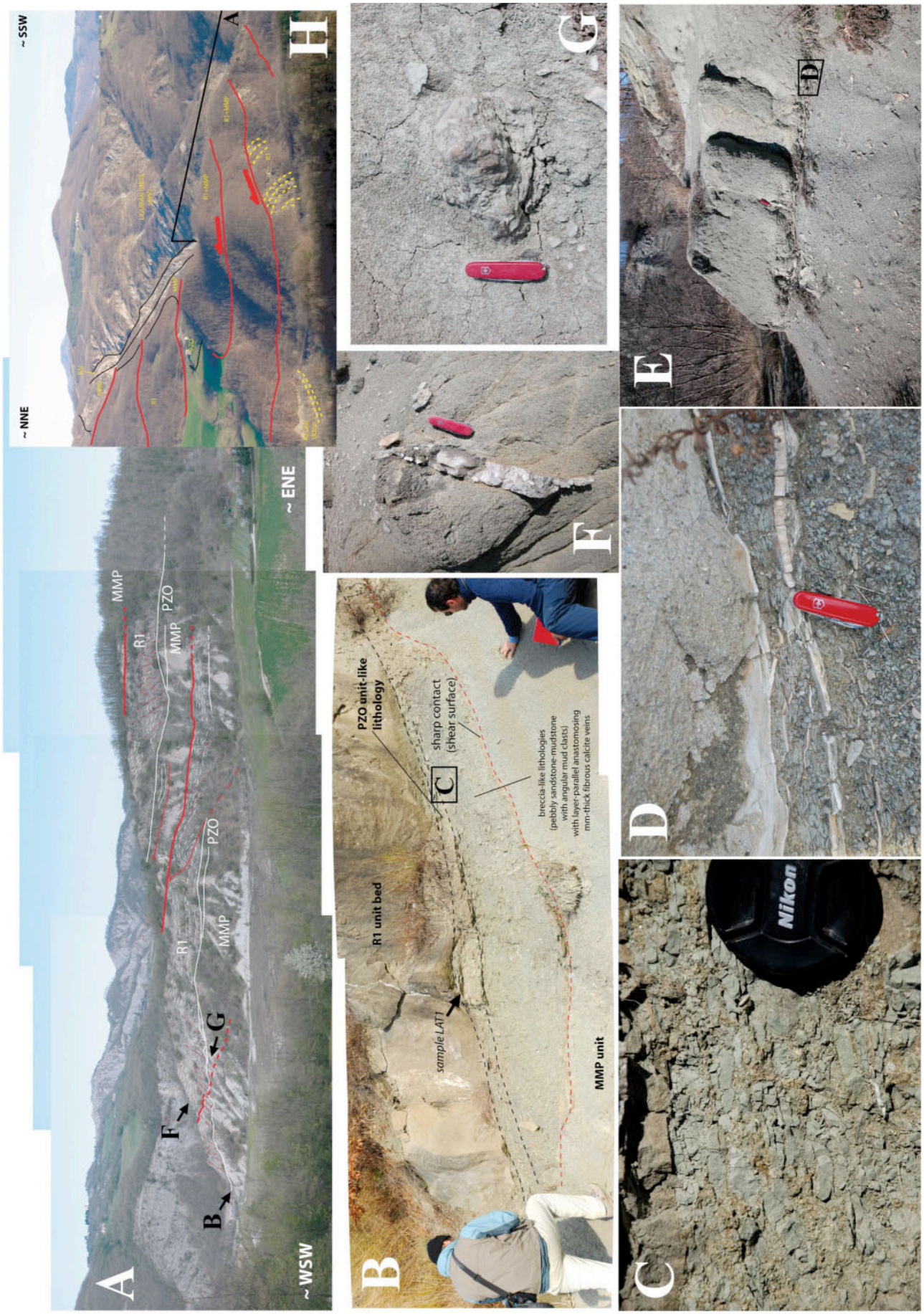
A
~ WSW
~ ENE
MMP
R1
PZO
MMP
R1
MMP
PZO
F
G
B
H
~ NNE
~ SSW
A
B
R1 unit bed
PZO unit-like lithology
C
sharp contact (shear surface)
breccia-like lithologies (pebbly sandstone-mudstone with angular mud clasts) with layer-parallel anastomosing mm-thick fibrous calcite veins
sample LAT1
MMP unit
C
Nikon
D
E
D
F
G

Figure 4.42 - A: The Ricodalle thrust system outcrop viewed from the SE. Note the duplication of the MMP-R1 unit lithologic contact. Recognized thrust surfaces and stratification patterns are labeled.

B: Detail of the MMP-R1 unit lithologic contact. Here this surface seems to be tectonically reactivated as a low-angle thrust. The MMP lithologies are separated from the R1 ones by a small-scale tectonic slice-like body (represented in the photo), "sandwiched" along this thrust surface, and composed of material coming from the MMP, PZO and R1 units. Micro-structural analysis carried on oriented thin section taken from this surface (sample LAT1) unravel lacking of cataclasis, the strong development of layer-parallel fibrous calcite vein seams and the faint arrangement of grains in sigmoidal-like domains. Moreover, the downward transition to MMP lithologies is marked by the presence of a sharp shear surface separating the latter from a mud breccia-like facies composed of angular, consolidated muddy domains, intruded by an anastomosing network of liquefied pebbly-sandstone/mudstone. These evidences are thought to represent proxies of fluid-overpressure conditions. Location shown in A. Dott. Davide Carè and Dott. Nicola Minelli for scale.

C: Close-up of B, showing a detail of the mud breccia-like facies characterizing the lower portion of the MMP-PZO-R1 "tectonic slice". Among other interpretation, this feature should represent an impact breccia linked to the emplacement of the first R1 unit bed. Camera lens cap for scale, 7 cm in diameter.

D: Close-up of E showing the detail of the PZO-like lithologies recognized at the base of the R1 bed shown in B, roughly on the same sampled level. The fine-grained level is thought to represent a minor shear surface. Note the strong development of layer-parallel, lenticular fibrous calcite veins. Knife for scale, 9 cm long.

E: MMP-R1 contact observed in the lowermost portion of the outcrop. The situation is similar to that described in B. Note the mm-sized fibrous calcite veins developed in layer-parallel trend roughly along the base of the sandstone bed. Knife for scale, 9 cm long.

F: Example of tension gash-like joint, filled with massive crystalline calcite. Inferred sense of shear is dextral. Knife for scale, 9 cm long. Location shown in A.

G: Soft sediment deformation-related "sandstone ball", representing an extreme degree of stratal disruption achieved in poorly-consolidated material. Lithologies belonging to the PZO unit. Location shown in A. Knife for scale, 9 cm long.

H: Panoramic view of the Ricodalle thrust system zone, looking toward the SE. Main units and thrust surfaces are labeled. Location of photo-mosaic represented in A is shown.

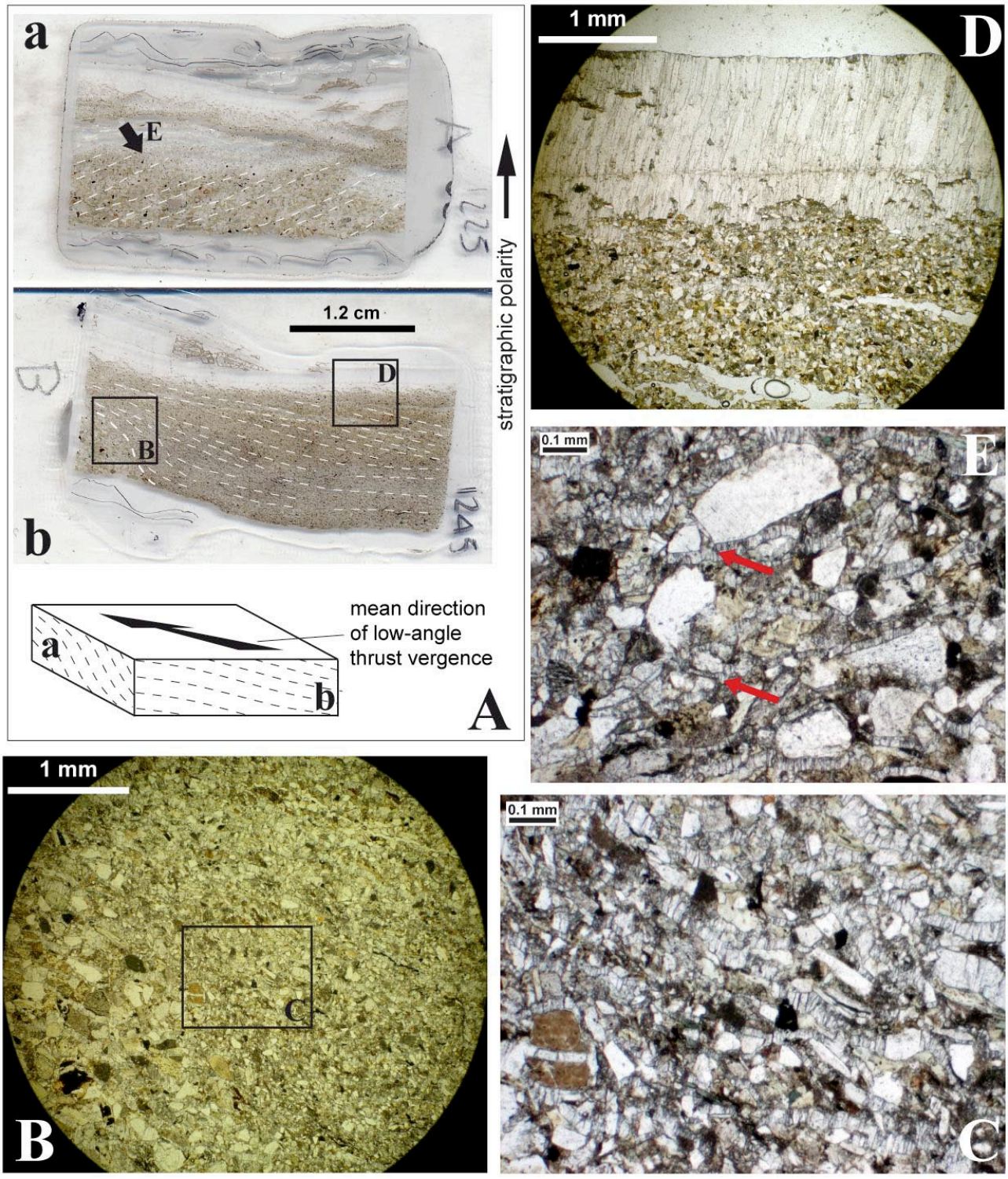
a
E
1.2 cm
D
B
b
stratigraphic polarity
mean direction
of low-angle
thrust vergence
a
b
A
1 mm
D
0.1 mm
E
1 mm
C
B
0.1 mm
C

Figure 4.43 - Examples for the sample LAT1, taken from an inferred shear zone located between the base of an R1-type bed and MMP-type lithologies characterizing a "tectonic slice"-like structure (Ricodalle thrust system; see fig. 4.42 B and chap. 2 for location).

A: Thin sections oriented in a roughly longitudinal- and transversal-way ("a" and "b", respectively) taking into account the mean tectonic transport inferred for the low-angle thrust vergences (see the sketch in the lower part). It is observable a syntaxial fibrous calcite vein developed in a layer-prallel way on the upper side of the thin sections. Note that the sampled layer seems to be normally graded and characterized by oblique lineaments (deformation bands?). These latter linear features are labeled.

B: General microscopic view showing a coarse-grained cluster (down- and left-handed side) separated from a fine-grained domain (up- and right-handed side) by and interval resembling a small-scale shear zone. The trend of this shear zone is highlighted by preferential iso-orientation of the granules' long axis and by the strong development of sub-parallel, anastomosing seams of calcite veining. These structures seem to define some kind of sigmoidal-like lineations. Location shown in A.

C: Close up of B showing the detail of the sub-parallel, anastomosing fibrous calcite seams, which are observed to envelope and separate granules. No evidences of clear shearing-related grain breakage (*i.e.* cataclasis) are observed. Instead, the inferred deformation mechanism is that of a generalized "flow" of grains in contact, developed at low confining pressure.

D: Detail of the syntaxial, mm-thick, layer-parallel fibrous calcite vein. Note the presence of isolated and clustered granules within the vein fibers and its irregular boundary with the clastic material. Some oblique "cusps" of fibrous calcite seems to extend downward and obliquely from the boundary to join the discrete micro-veins characterizing the lower side of the photo, and above-described vein seams. Location in A.

E: Detail of the fibrous calcite seams in which it is possible to observe how these features also seem to inject some granules (red arrows), breaking them in smaller angular elements then enveloped within the calcite material. These evidences are thought to represent fluid-overpressure conditions strong enough to develop hydrofracturing. Location shown in A.

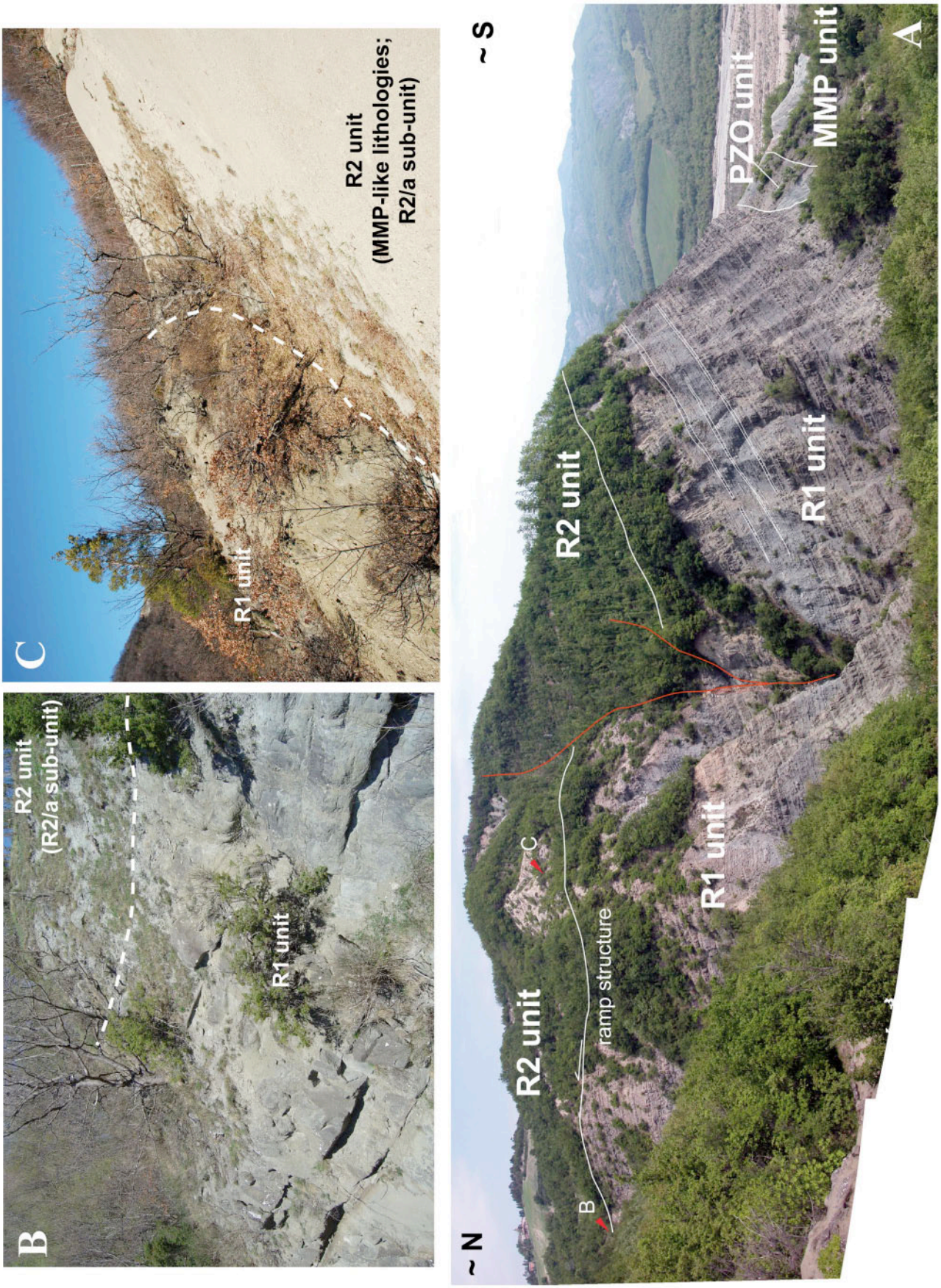
A
MMP unit
PZO unit
R1 unit
R2 unit
R1 unit
R2 unit
ramp structure
B
C
~ N
~ S
B
R2 unit
(R2/a sub-unit)
R1 unit
C
R2 unit
(MMP-like lithologies;
R2/a sub-unit)
R1 unit

Figure 4.44 - A: Panoramic photo-mosaic showing the ramp-like structure developed between the R1 unit and the overlying R2 unit, in the southern sector of the Pessola Valley outlier. Nonetheless the nature of such structure is still debatable (sedimentary *vs* tectonic), this feature should be interpreted as an original sedimentary ramping linked to the emplacement of the lower R2 unit components, successively reactivated in a compressive tectonic regime probably related to the Ricodalle thrust system. Units' names and boundaries, and the main structural features are labeled.

B: Partly covered contact between R1 unit and the overlying R2 unit. Here the ramp structure seems to evolve in a layer-parallel flat. Location is shown in A.

C: Overall appearance of the lower R2 unit lithologies close to the contact with the underlying R1 unit. Here it is possible to observe MMP-like lithologies thrusting above the R1-like lithologies, sometimes expressed by detached but little displaced blocks. The R2 unit lithologies in this case seem more coherent, and the matrix development is subordinated. Location is shown in A.

~ SSW
PZO
MMP
R1
PZO
MMP
BAI
~ NNE

Figure 4.45 - A: Panoramic photo-mosaic of the lower portion of the R1 unit outcrop localized in the northern part of the western sector of the Pessola Valley outlier. Here it is possible to observe the progressive angularly unconformable contacts between the BAI, MMP, PZO and R1 units, achieved in response to a gradual synsedimentary uplift of the northern margin of the Pessola Valley outlier (Vianino structure?). This fact seems to be confirmed also by the southward stratigraphic expansions of the sandstone bodies (*i.e.* growth-like stratal patterns).

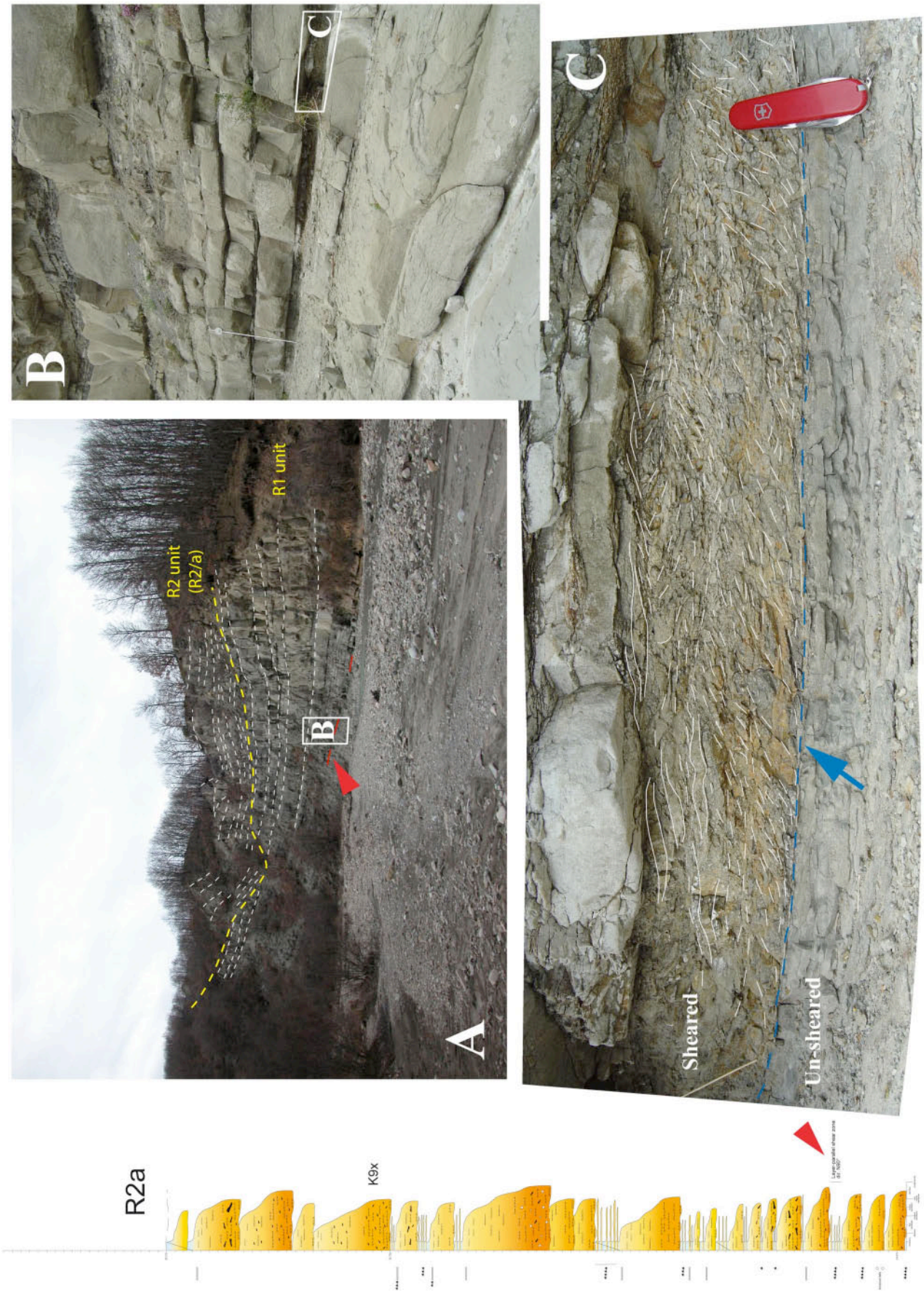
A
R2 unit
(R2/a)
R1 unit
B
B
C
C
Sheared
Un-sheared
R2a
K9x

Figure 4.46 - A: Overall view of the upper contact of the R1 unit with the R2 unit in the Fopla section (see attached Panel n. 1 and n. 4). Main boundary and stratification patterns are labeled. On the left side is represented part of the general R1 unit stratigraphic column (see attached Panel n. 3) concerning the shown interval. Note the faint thinning-upward-like trend expressed by bedsets.

B: Close-up of A showing in detail the overall appearance of the component thinning-upward bedsets. Jacob's staff for scale, 1,5 m long.

C: Photo-mosaic depicting a fine-grained interval characterized by layer-parallel shearing toward the northern sector (as inferred from sigmoidal- and S-C-like structures), recognized few meters below the R1-R2 boundary. Planar structures and foliations are labeled. Note that a layer-parallel fibrous mm-thick calcite vain (blue arrow and blue dashed line) seems to separate an upper strongly sheared portion (oxidized) from a lower undisturbed portion (not oxidized). Location of this layer is shown in A (and in the related stratigraphic column; red arrows) and B. Knife for scale, 9 cm long.

A

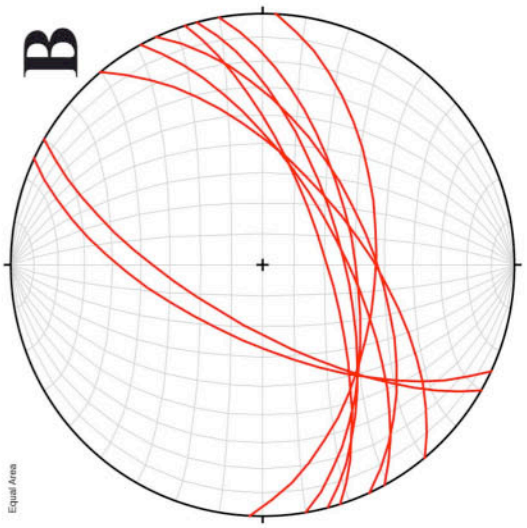
B
Equal Area
Great Circle:
Pattern = solid

B

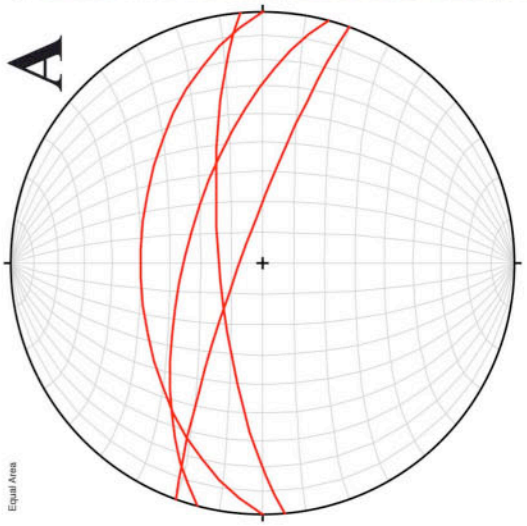
A
Equal Area
Great Circle:
Pattern = solid

Figure 4.47 - Outcrop examples of normal faults (and relative stereograph of plotted fault planes) recognized in the R1 and R2 units, respectively.

A: Minor normal fault system characterized by small offsets (few tens of centimeters) affecting the R1 unit (thin-bedded facies) in the Servazzola section, and relative stereoplot. Camera lens cap for scale, 7 cm in diameter.

B: Minor normal fault with a small offset (~ 50 cm) recognized in the R3 unit, cropping out in the northernmost analyzed sector (formerly belonging to the Varano de'M.-Pellegrino P. outlier), and relative stereoplot. Field notebook for scale, 20 cm long.

5. Mt. ROCCONE OUTLIER

This Epiligurian sedimentary remnant is located in the high sector of the Nure Valley, between the Parma and Piacenza provinces (grid n. 197120 CTR Regione Emilia-Romagna), with an areal extent of about 8 km^2 (fig. 5.1).

Here, the Epiligurian succession unconformably overlies the deformed shale-rich portions of the Helmintoyd Flysch units (*i.e.* Varicoloured Shale and Ostia/Scabiazza Sandstone of the Cassio Unit; Zanzucchi, 1980), and is composed of a relatively thin horizon of MMP at the base, directly surmounted by the R2 Specchio Unit, without the interposition of PZO and R1 units (fig. 5.2).

The succession continues with the relatively well-developed R3 unit, which takes its name from this type locality (*i.e.* Mt. Roccone unit; Mutti *et al.*, 1995).

5.1 Previous studies

The Mt. Roccone Epiligurian outlier was firstly recognized in the ’30 (Sacco, 1933; Anelli, 1938) and then studied since the ’60 from a strictly lithostratigraphic point of view, assuming a continuous sedimentary succession (Boni, 1961; Braga, 1962, 1965; Mutti *et al.*, 1965; Ghelardoni *et al*., 1965).

The last detailed stratigraphic, biostratigraphic and sedimentological studies on these outcrops were made in the ’90 for the general characterization of the Ranzano Unit (Segadelli, 1992; Cibin, 1993; Mutti *et al*., 1995; Catanzariti *et al*., 1997; Martelli *et al*., 1998; Cibin *et al*., 2001, 2003).

These outcrops have been also sampled for diagentic studies on organic matter coalification in the framework of the entire Northern Apennines, highlighting for this area an evidence of abnormally high thermal flux (Reutter *et al.*, 1980).

The Mt. Roccone outlier is represented in the sheet n. 197 “Bobbio” of the 1:50.000 Geological Map of Italy (Italian Geological Survey, 1998).

5.2 Stratigraphy

Here, the Epiligurian sedimentation took place over an undifferentiated chaotic complex of Ligurian-derived lithologies (*i.e.* ophiolites, limestones, cherts, sandstones) with a discontinuous m-thick horizon of MMP (~20 m of maximum thickness) (fig. 5.3).

In this area the BAI unit seems to be missing, even if the upper part of this Ligurian-derived chaotic complex show some similarities with the BAI unit mud breccias. Unfortunately the

lithologic contact is covered and complicated by active and quiescent superficial landslides and slope instabilities, thus excluding the possibility to surely separate them (fig. 5.4).

The **R2** unit unconformably covers the MMP unit, sometimes directly lying on the Ligurian-derived chaotic complex, with an estimated maximum thickness of ~ 120 m. This chaotic unit represents the topic of this work; it is outlined in chap. 7 and further discussed in the text (fig. 5.5).

The **R3** unit succession reaches a maximum thickness of ~ 400 m and can be roughly subdivided in a lower thin-bedded portion and an upper thick-bedded portion, showing an overall thickening-upward trend. The lower portion of this unit overlies the R2 unit through the emplacement of a ~ 2 m thick coarse-grained and graded sandstone bed, characterized by an irregular base and a sharp top. This layer, which has strong similarities with that one cropping out at the base of R3 succession in the Pessola Valley outlier (see chap. 4), is clearly recognizable in the western sector of the outlier, thinning toward SE in short distances and completely disappearing in southern and eastern sectors (Poggiolo sector) (fig. 5.6).

The lower portion of the R3 unit continues for ~ 300 m, with the development of laterally discontinuous thin-bedded (average thickness of ~ 20 cm) fine- to coarse-grained sandstones (sometimes with conglomeratic lenses), vertically stacked without any apparent cyclic organization. Where the above mentioned thick sandstone bed (at the base of this unit) is missing, this facies directly overlies the R2 unit, with an irregular contact (mainly due to the poor lithologic contrast between fine-grained lithologies shared by the two units) (fig. 5.7).

These beds commonly have a sharp erosive base, with abundant clay chips, well-developed sole structures (*i.e.* scours, bounces, grooves and flute casts) and differential loading-related deformations (*i.e.* load casts) (fig. 5.8).

The carbonatic content is commonly abundant in these beds, and sometimes, distinctive layers characterized by oxidized alteration colors and light banding given by clustering of whitish grains are present. These latter beds are similar to those observed in the R3 unit of the Pessola Valley outlier and have been interpreted as mixed terrigenous-volcaniclastic layers (see chap. 4).

The top of the beds is also commonly characterized by bioturbation (*i.e.* mainly *zoophycos*- and subordinately, *ophiomorpha*- and *planolites*-like ichnofacies) (fig. 5.9), and variably coalified plant fragment accumulations, with well preserved elements up to ~ 5 cm in size, disposed with a preferred iso-orientation of the long axis trend according to the palaeo-currents, on the lamina surfaces. Vegetal fragments are also observable within the basal-intermediate parts of the bed, as well as cm-sized clay chips.

Other distinctive beds occurring in this section are thin- to medium-thick, both ortho- (*i.e.* clast-supported) and para-conglomerate (*i.e.* matrix-supported) beds, with the redominance od the

latter, sharing poor lateral continuity (*i.e.* strongly lenticular geometries) and sorting. They are composed of mainly well-rounded carbonatic pebbles up to ~ 10 in size. Usually these beds do not show any internal structures, apart for a poorly developed normal grading, a faint clast imbrication and some large-scale oblique laminations-like geometry. Sometimes they pass upward, usually through a sharp bypass surface, into graded fine- to coarse-grained sandstones (fig. 5.10).

On the basis of these characteristics, the beds of this unit are represented by F6, F7, F8 and F9 facies, and subordinately by rare F2-F3 facies (Mutti, 1992).

It is important to note that a distinctive, depocenter-wide conglomeratic bed with the above mentioned characteristics appears ~ 10 m above the basal contact. This bed shows a laterally variable thickness in short distances (outcrop-scale), from a minimum of ~ 50 cm to a maximum of ~ 3 m, and it is composed of well-rounded pebbles and cobbles (up to ~ 80 cm across) of carbonatic (*i.e.* Ligurian-derived) and sandstone lithologies, characterized by lithodome holes. Subordinately, sub-angular carbonatic elements and intrabasinal (*i.e.* belonging to the R2 unit) deformed bed fragments are also.

Regarding the internal organization of this bed, it shows a relatively thin basal portion characterized by abundant clayey matrix, and an upper one with a matrix composed of coarse sandstone. The overall appearance is clast-supported, with local exceptions, with a relatively flat base and a top sharply passing through an evident grain-size gap (*i.e.* bypass surface) to a very thin (~ 5 cm) medium-grained sandstone bed, sometimes showing poorly developed laminations. Moreover, the uppermost portion of this conglomerate bed seems to show faint large-scale oblique lamination-like alignment of clasts present (fig. 5.11).

The upper portion of the R3 unit is characterized by the presence of amalgamated bedset (up to ~ 20 m thick) constituted by: 1) thick-bedded coarse-grained beds, 2) thin- to medium-bedded, fine- to coarse-grained sandstone and 3) mudstone layers. The thicker beds are observed to be mainly composed of ophiolitic lithologies, while the thinner ones share prevailing carbonatic clasts. Particularly, the sedimentary bodies of this upper portion seem to show a more developed lateral continuity in respect to the lower one present (see fig. 5.6).

In addiction to the facies recognized in the lower portion, here is possible to observe a prevailing development of the F4 and F5 facies (Mutti, 1992).

The uppermost portion of the R3 succession is represented by ~ 20-40 m of roughly stratified and disorganized conglomerates, that are separated from the underlying strata by a markedly erosive surface. These conglomerates are generally clast-supported (*i.e.* ortho-conglomerates) with well-rounded elements up to tens of cm-sized, and characterized by bioerosional hollows (*i.e.*

lithodomes); the prevailing compositions are ophiolitic and sedimentary (*i.e.* limestones, marlstones and sandstones).

These deposits, sharing strong compositional and textural similarities with the Mt. Piattello ones, are poorly exposed in this outlier, being confined in the westernmost, strongly covered and vegetated sector.

5.3 Tectonic setting

As the other Epiligurian sedimentary successions, the Mt. Roccone one is arranged in a synclinalic structure with a roughly WSW-ENE trending axial direction, gently plunging in a converging way to the center of the outlier, giving an overall bowl-shaped (or "saddle"-like) conformation.

There are two main tectonic lineaments affecting this area with almost orthogonal directions, and represented by a SE-NW trending fault system crosscutting a NE-SW one. This tectonic arrangement pervasively dissects the outlier continuity, isolating differentially uplifted and down-pulled sectors, showing however small dislocations.

These tectonic lineaments are expressed by major and associated minor high-angle fault systems, marked by mainly spatic cm-thick calcite veins, sometimes sharing more superimposed translational components (evidenced by several generations of calcite steps and striations), which are observed to put in contact Ligurian-derived lithologies with the Epiligurian ones, especially in the south-eastern sector present (fig. 5.12).

The abundant occurrence of active and quiescent superficial landslides, and recent slope instabilities (also deep-seated) bordering the entire extension of the outlier, significantly complicates the observation and interpretation of such tectonic structures.

5.4 List of figures

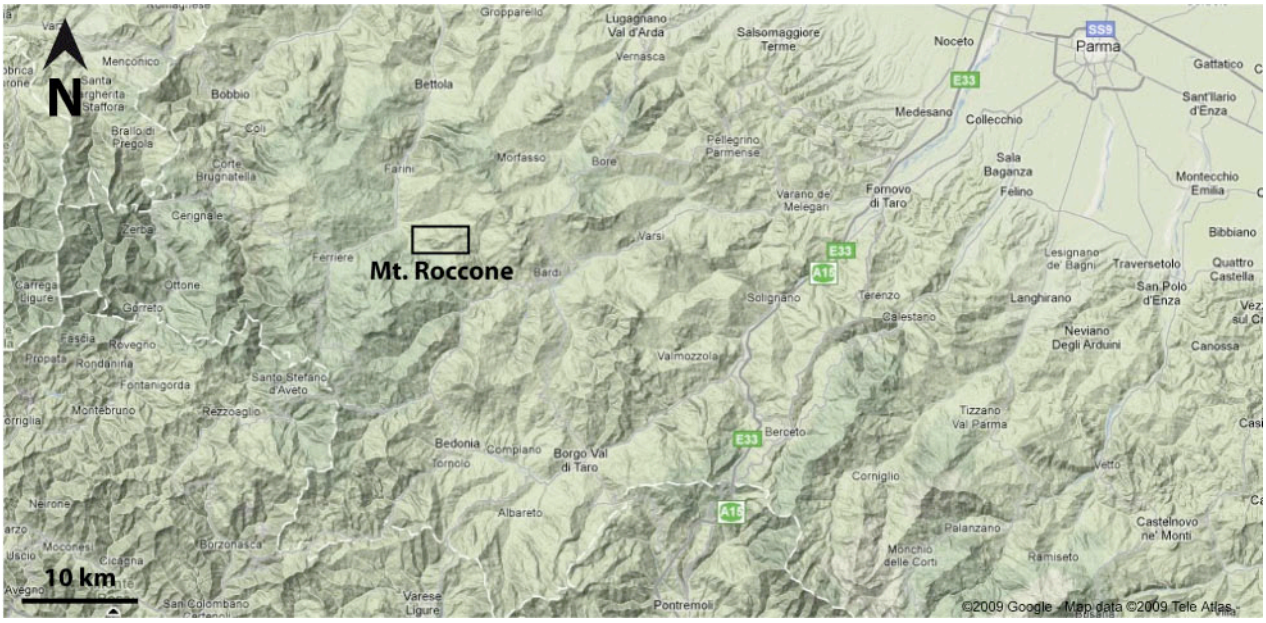

Figure 5.1 - Geographic location of the Mt. Roccone area (from GoogleMaps, 2009).

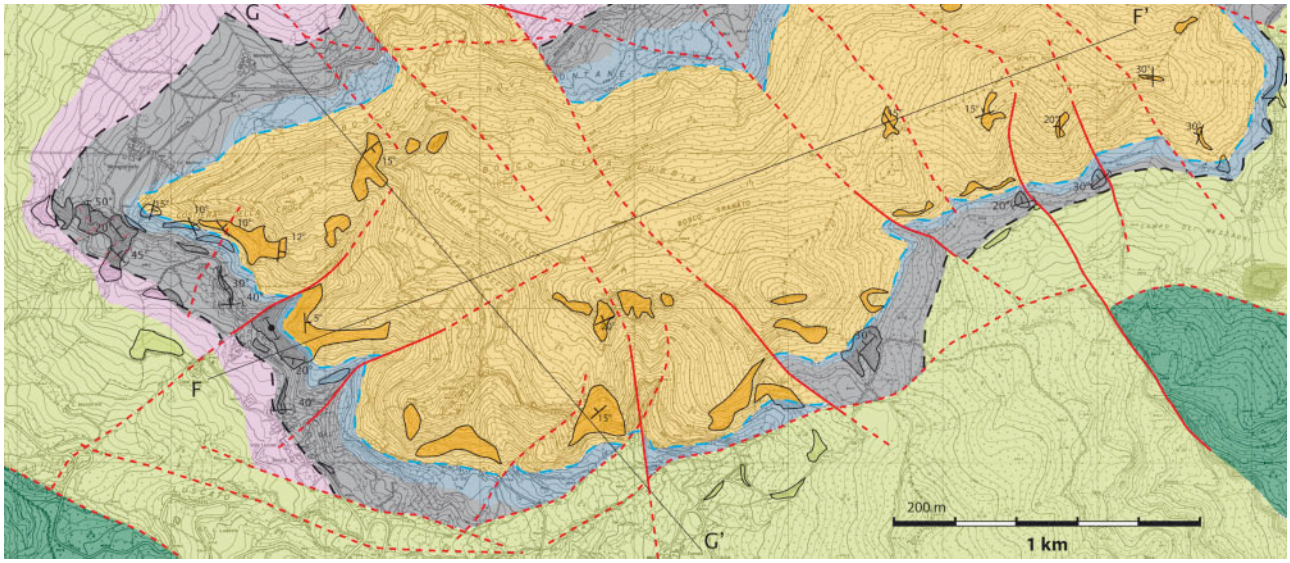

Figure 5.2 - Geologic map of the Mt. Roccone area developed in this work (see attached Panel. n.1). For explanation see fig. 4.3.

Figure 5.3 - **A**: Roughly southeast-looking photo-mosaic of the northwestern side of the Mt. Roccone outlier (Mangiarosto section, see attached Panel n. 1) showing the contact of the Epiligurian succession with the Ligurian substrate. The former is represented by a thin, discontinuous interval of lithologies belonging to the MMP unit, which is in turn overlaid by the Specchio Unit (R2). On the back, in the upper-right side of the photo-mosaic, the topmost R3 unit is cropping out. The Ligurian substrate is mainly represented by shale-rich chaotic complexes belonging to the AVV units. Due to the strong vegetation coverage and the extremely altered outcrop conditions, the contacts between these units are often unclear. Some AVV unit lithologies should be tentatively attributed to the BAI unit (see chap. 4). Contacts and units are labeled.

B: General outcrop appearance of the MMP unit lithologies in the northwestern side of the Mt. Roccone outlier. Location shown in A (few meters in the arrow direction). Hammer for scale.

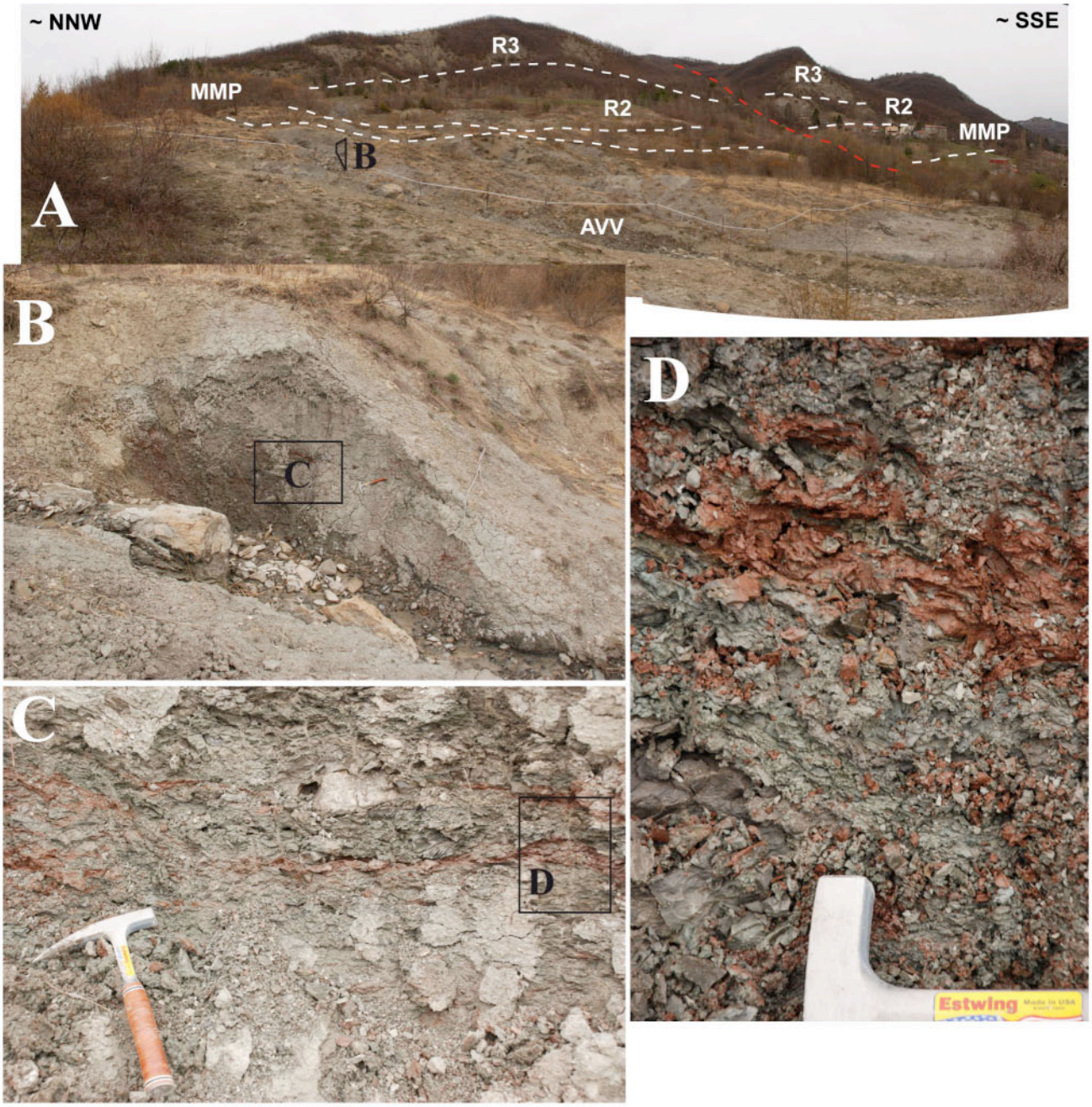

Figure 5.4 - **A**: Photo-mosaic of the western margin of the Mt. Roccone outlier. Here it is possible to observe the

entire Epiligurian stratigraphic succession and the lower contact with the AVV unit lithologies. Note the strongly altered appearance of outcrops, mainly due to the poorly lithified and fine-grained nature of the main stratigraphic units (*i.e.* AVV, MMP, R2 units). Active slope movements commonly complicate this latter contact and the labeled limits are strictly indicative.

B: Close-up of A showing a typical appearance of AVV unit lithologies in outcrop. The rounded sandstone block belongs to the R2 unit, which is almost in contact with the AVV unit substrate in this area. Hammer for scale.

C: Close-up of B. The meso-scale appearance of AVV shale-rich chaotic complexes, in this case is that of a broken-formation (tectonosome *sensu* Pini, 1999). The pseudo-stratification (*i.e.* meso-scale foliation) is defined by reddish bands and scattered sandstone *boudins*, coupled with a diffused scaly fabric. Varicoloured shaly lithologies are typical of the AVV unit lithologies observed in the other contexts, while the sandstone elements should be tentatively attributed to the other classical components of the Ligurian units basal complexes (*i.e.* Ostia/Scabiazza Sandstones *Auctt.*). Hammer for scale.

D: Close-up of C, showing in detail the "fresh" appearance of these shaly lithologies. Note the sandstone element if the lower-left side of the photo (near the hammer's head). Sometimes mud breccia-like patches and bands are present within these lithologies. Hammer for scale.

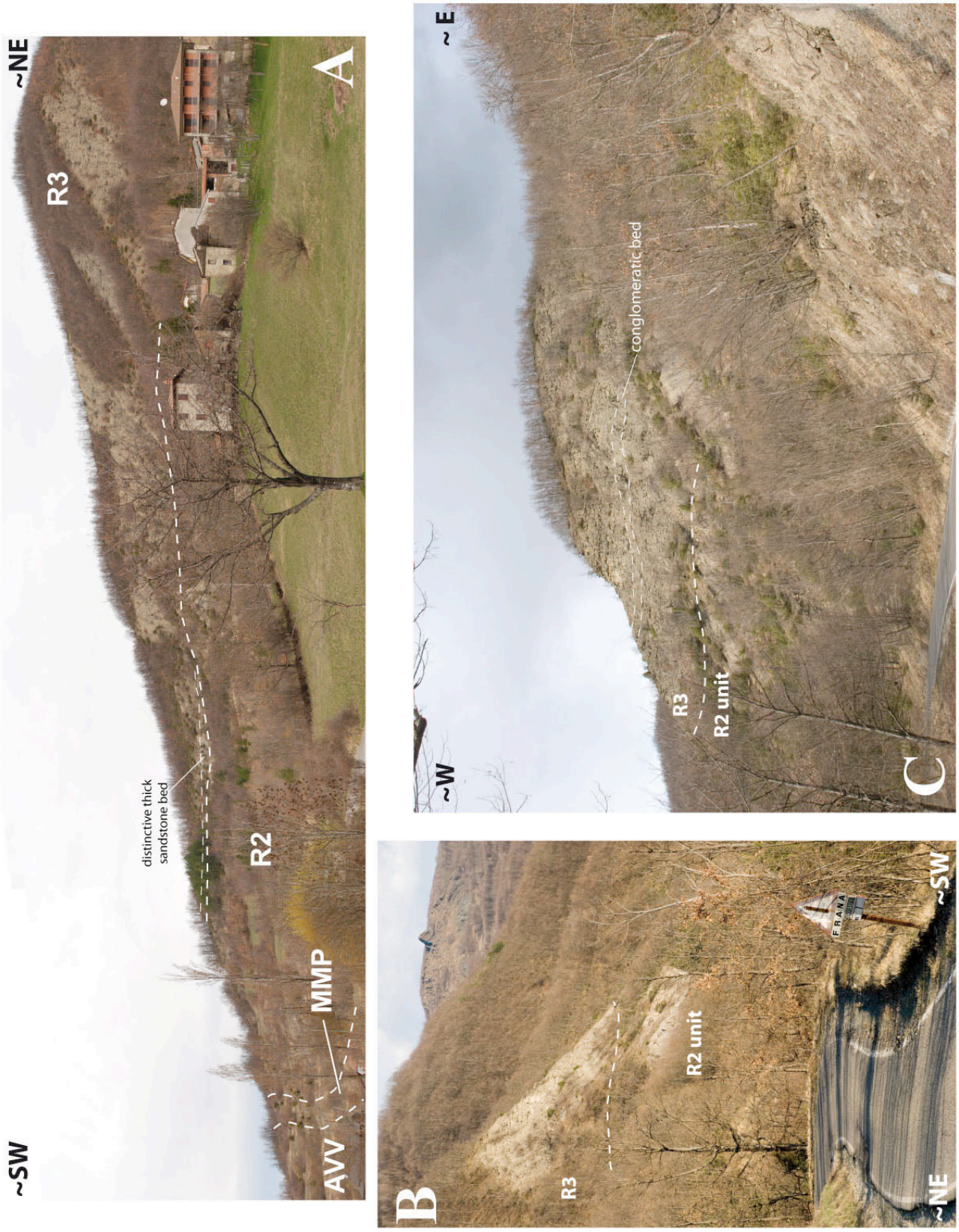
~SW
~NE
R3
A
distinctive thick sandstone bed
R2
MMP
AVV
~W
~E
conglomeratic bed
R3
R2 unit
C
B
R3
R2 unit
~SW
~NE

Figure 5.5 - A: Photo-mosaic of the western margin of the Mt. Roccone outlier (Mangiarosto section, see attached Panel n.1), roughly looking toward the north. Here, a distinctive thick sandstone bed, rapidly disappearing toward the southeastern sectors, marks the limit between Specchio Unit (R2) and the overlying R3 unit (see test for discussion).
B: Photo showing the R2-R3 units boundary in the western sector (to the southeast respecting photo-mosaic shown in A), roughly looking toward the south (Poggiolo section, see attached Panel n. 1). As in the other presented examples, the R3 unit seems to show roughly eastward local onlapping relationships with the underlying R2 unit. Here the distinctive thick sandstone bed shown in A is completely lacking.
C: Photo showing the R2-R3 units limit in the southern part of the Poggiolo section, roughly looking toward the north. A m-thick, discontinuous and irregular conglomerate bed appears in the middle of the stratified succession. The R3 unit beds seem to roughly onlap on the R2 unit; this local feature should be attributable to the uneven nature of the R2 unit upper surface. Units and relative boundaries are labeled.

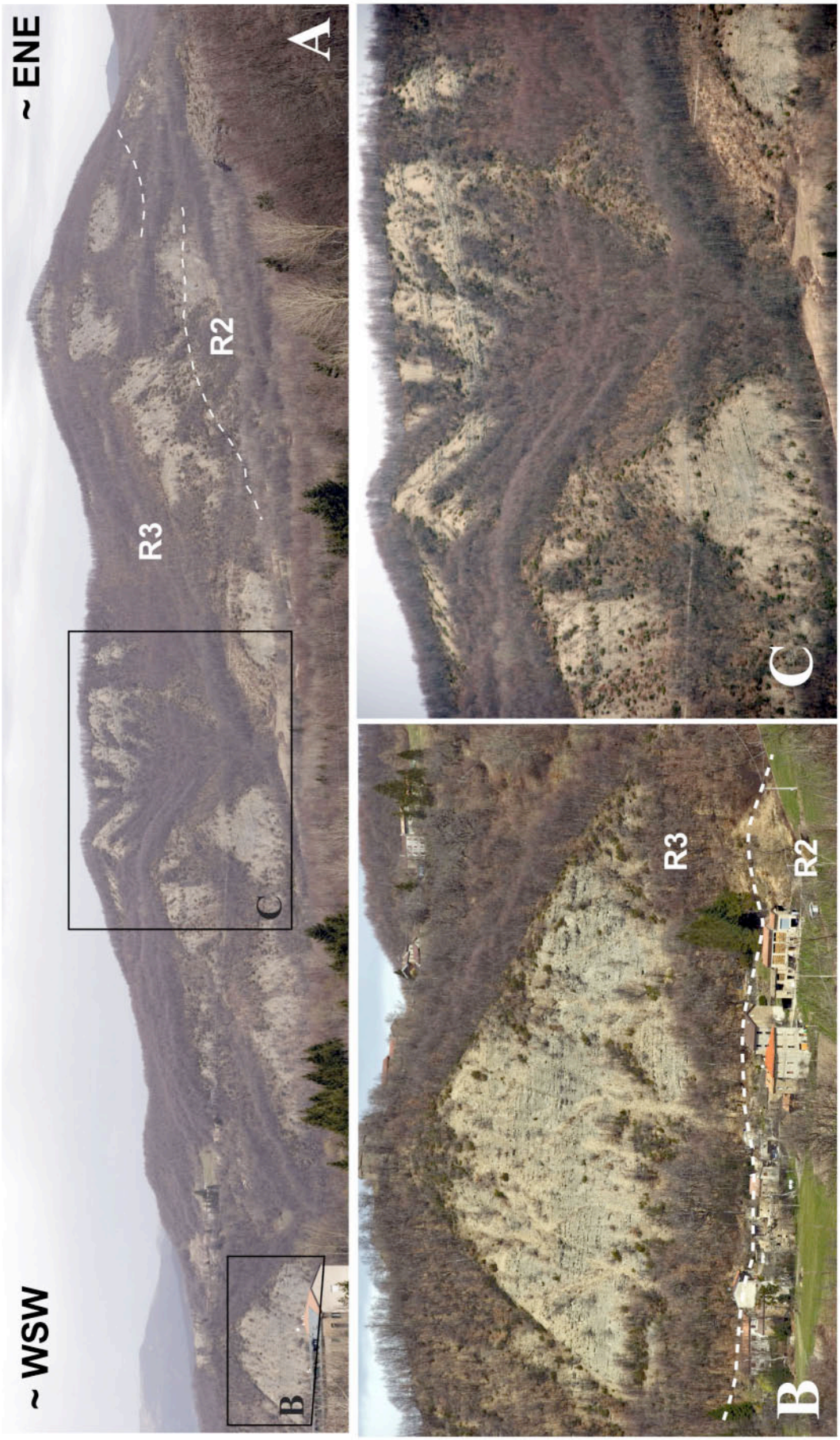
~ WSW
~ ENE
A
R3
R2
C
B
C
R3
R2
B

Figure 5.6 - A: Panoramic photo-mosaic of the southern margin of the Mt. Roccone outlier, roughy looking toward the north. Here it is possible to observe the entire R3 unit succession. The lower contact with the R2 unit is labeled. In this area, R2 unit is relatively thin, reaching the few meters in thickness (toward the E), and locally juxtaposed directly on the Ligurian units.

B: Close-up of A, showing the thin-bedded lower part of the R3 unit sedimentary succession. Although this unit is well stratified, it is possible to note that beds show lenticular geometries, appearing relatively tabular only on short distances.

C: Close-up pf A, showing the middle-upper part of the R3 unit sedimentary succession. Here it is possible to observe that the thin-bedded portions grade upward into a fine-grained portion characterized by the presence of discrete thick-bedded, amalgamated bedsets. In the topmost parts (strongly covered and not represented in photo) some outcrops of conglomerates (mainly ortho-conglomerates) seem to confirm the general thickening- and coarsening-upward trend of the entire R3 succession.

~ NE
~ SW
1 m
A
B
R3 unit
R2 unit
(R2/e)

B
Nikon

Figure 5.7 - A: Outcrop appearance of the lower part of the R3 unit in the Poggiolo section, roughly looking toward the south. The basal boundary with the R2 unit is covered with detritus and its relative position is labeled.
B: Example of roughly graded F7/F8-type bed showing clay-chips clustering and poorly developed traction carpets. In the upper-left side of the bed it is fairly observable a poorly developed vertical bioturbation-related burrowing (*ophiomorpha*-like). Location is shown in A.

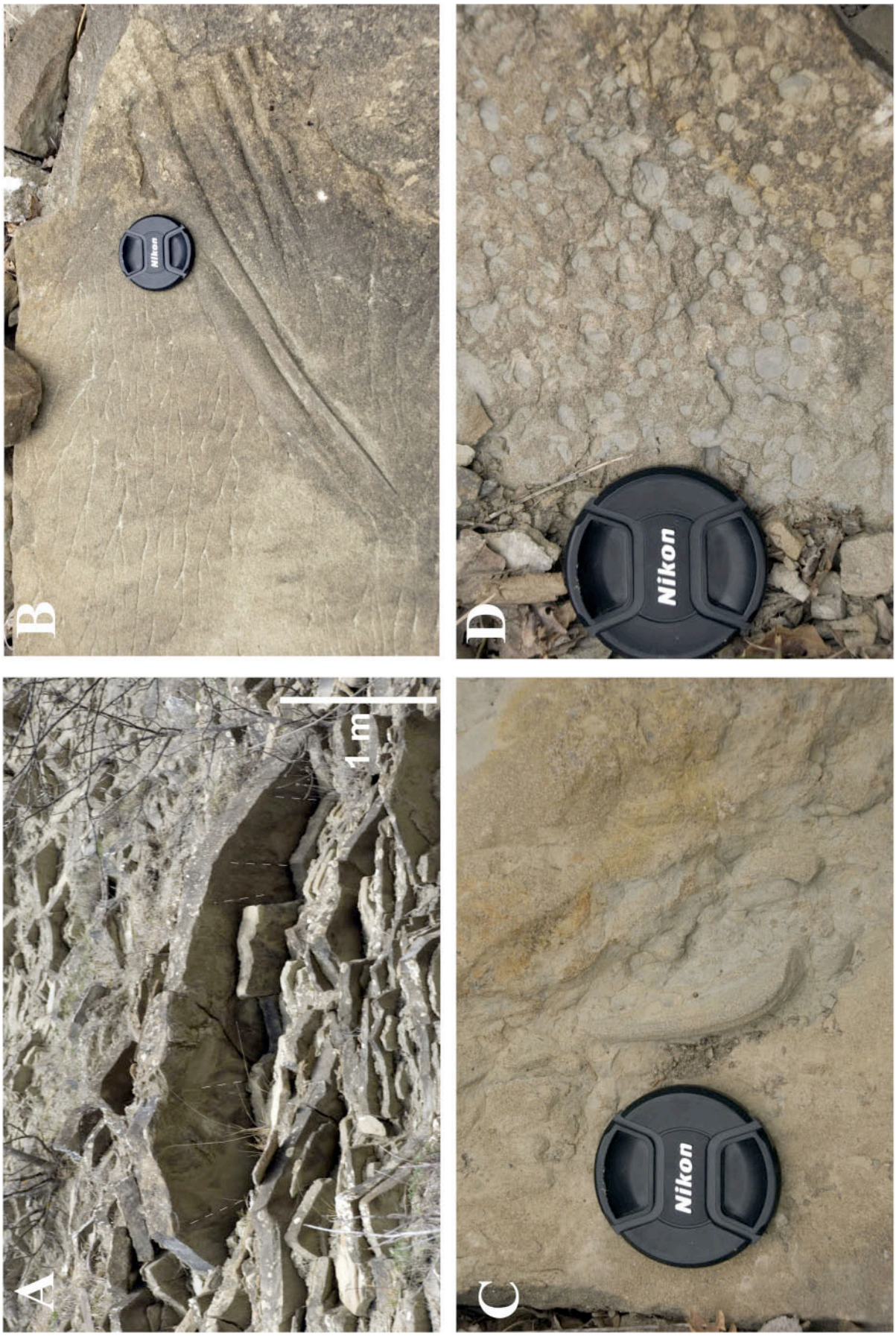
A
1 m
B
Nikon
C
Nikon
D
Nikon

Figure 5.8 - **A**: Basal surface of a medium-bedded F7/F8-type bed showing relatively well developed sole marks (groove- and flute-like). The mean directions are labeled.

B: Example of particular groove-like sole marks (alternatively interpretable as prod- of bounce-casts) developed at the base of a detached F7/F8-type bed. Note the other surrounding linear structures (resembling some kind of frondescent-type structures) affecting the whole basal surface, which origin is debatable. Camera lens cap for scale, 7 cm in diameter.

C: Another example of particular groove-like sole marks (alternatively interpretable as prod- of bounce-casts) developed at the base of a detached F7/F8-type bed.. Relatively abundant bioturbations complicate the geometry of such structures. Camera lens cap for scale, 7 cm in diameter.

D: Cluster of well-rounded clay-chips (bioturbation-related?) observed at the base of a detached F7/F8-type bed. Camera lens cap for scale, 7 cm in diameter.

B

A
Nikon

Figure 5.9 - Examples of *zoophycos*-like ichnofacies observed within detached portions of R3 beds. **A**: Camera lens cap for scale, 7 cm in diameter.
B: Twenty Euro cents coin for scale, 2.2 cm in diameter.

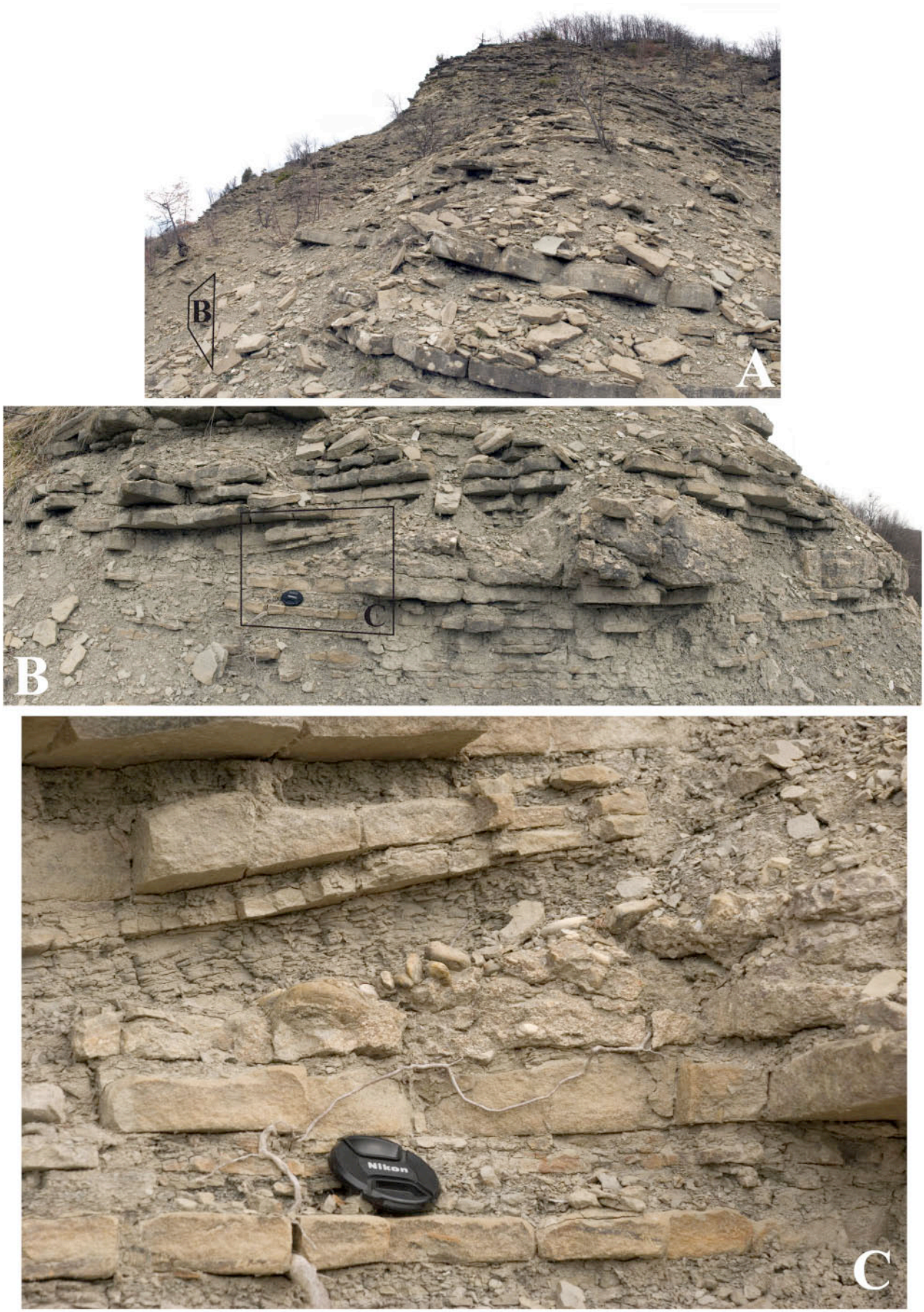
B
A
B
C
Nikon
C

Figure 5.10 - A: General outcrop appearance of the R3 unit in the northern part of the Poggiolo section.

B: Close-up of A, showing the meso-scale appearance of a medium-thick conglomerate bed showing a marked lenticular geometry (pinching out to the left), an overall pinch-and-swell trend, and a crudely developed oblique lamination. This bed should be interpreted as a very-coarse grained F6-type facies bed. Note the wedging-out geometry shown by overlying thin-bedded layers on the thickened portions of the conglomeratic bed. Camera lens cap for scale, 7 cm in diameter.

C: Close-up of B, showing in detail the upper sharp surface of the conglomeratic bed in the point of maximum lateral thinning. Note the mud-draped pebbles aligned along the upper surface, and testifying sediment bypass. Camera lens cap for scale, 7 cm in diameter.

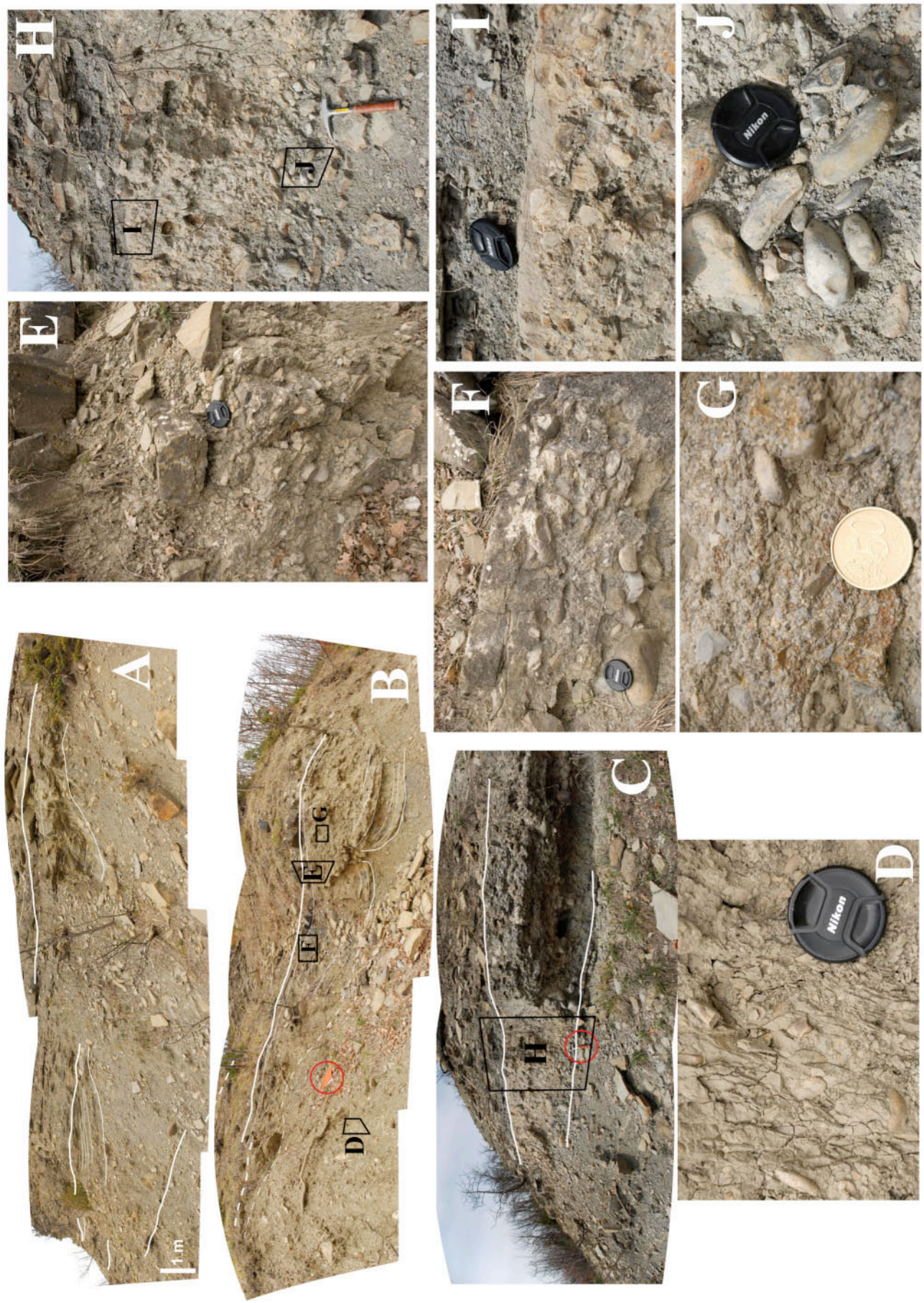
A
B
C
D
E
F
G
H
I
J
1 m
Nikon

Figure 5.11 - Examples coming from the depocenter-wide conglomeratic bed characterizing the lower portion of the R3 unit in the western outcrops of the Mt. Roccone outlier. **A**: Meso-scale appearance of the conglomeratic bed in the northern side of the Poggiolo section. Its thickness in this area is ~ 3 m. Note the lateral wedging-out of the upper crudely oblique lminations and the overall uneven nature of the upper surface of the conglomeratic bed. Main stratification and lamination surfaces are labeled. **B**: Meso-scale appearance of the conglomeratic bed in the southern side of the Poggiolo section. Its thickness in this area is ~ 4 m, and it seems to directly overly the R2 unit, although the contact is completely covered by detritus. Also in this case the conglomentic bed seems to develop a vertical arrangement into a lower massive, para-conglomeratic part and an upper crudely and obliquely laminated, orto-conglomeratic part. In the right side of the photo-mosaic it is possible to observe a fluid-escape structure developed across the limit between the upper and lower part, which bends upward the crude laminae characterizing the upper part. Field notebook for scale, A4 sheet dimensions. Main stratification and lamination surfaces are labeled. **C**: Meso-scale appearance of the conglomeratic bed in the southern side of the Mangiarosto section. Its thickness in this area is ~ 1.5 m. Here the lower clay-rich para-conglomeratic portion is thin or absent, and the vast majority of the bed is sand-rich ortho-conglomeratic. A slight clast imbrication and a crudely developed lamination are appreciable. Hammer for scale. **D**: Close-up of B, showing the detailed appearance of the clay-rich para-conglomeratic lower portion. The overall appearance (texture and composition) resembles that of the R2/e sub-unit (see chap. 7 for discussion). This latter evidence, the unclear lower contacts and the complexity of the local exposure make difficult the sure attribution of such lithologies to the conglomeratic layer or to the underlying (few meters below) R2 unit. Camera lens cap for scale, 7 cm in diameter. **E**: Close-up of B, showing the upper part of the conglomeratic bed. Here it is possible to observe how the sand-rich, ortho-conglomerate interval grades upward into a normally graded coarse- to medium-grained sandstone interval characterized by an upper sharp surface. This evidence is quite well recognizable in almost all the concerning outcrops. Camera lens cap for scale, 7 cm in diameter. **F**: Close-up of B, showing the same feature described in E. Here the uppermost graded sandstone interval is thinner than the preceding example, but maintains the same characteristics. Camera lens cap for scale, 7 cm in diameter. **G**: Close-up of B, showing in detail the coarse-grained sandstone matrix characterizing the upper ortho-conglomeratic division. Fifty Euro cents coin for scale, 2.4 cm in diameter. **H**: Close-up of C, showing the entire thickness of the conglomeratic bed. Here it is possible to observe the thin discontinuous clay-rich para-conglomeratic interval merging upward into the sand-rich, ortho-conglomeratic interval (characterized by un upper coarse-grained sandstone portion), which is in turn overlaid by a very thin (few centimeters), irregular graded sandstone horizon, characterized by an upper sharp surface. Note the dimensions of pebbles. Hammer for scale. **I**: Close-up of H, showing the uppermost part of the bed. Note that the thin graded sandstone interval is separated by a bypass surface from the underlying ortho-conglomerated division. Also its upper sharp surface represents an evidence of sediment bypass. The overall characteristics are the same described for examples represented in E and F. Camera lens cap for scale, 7 cm in diameter. **J**: Close-up of H, showing in detail the lowermost clay-rich para-conglomeratic division, here represented by a discontinuous alignment of thin lenses. The matrix is represented by a variously mixed pebbly mudstone. All the component pebbles are well rounded (reaching dimensions of several decimeters across) and characterized by more or less evident bioerosional holes. Camera lens cap for scale, 7 cm in diameter.

B
Nikon
C
A

Figure 5.12 - A: Example of a cm-thick, striated, mixed fibrous and massive calcite vein localized in the lower R2/d sub-unit (Mangiarosto section). Note the conglomerate block in the left side of the photo. This kind of veins develops at high angle through the matrix-rich portions (*i.e.* fine –grained) and along the block boundaries. Camera lens cap for scale, 7 cm in diameter.

B: Example of striated cm-thick calcite vein developed along the bedding surface of biocalcarenite strata characterizing a still stratified block of the upper R2/d sub-unit (Mangiarosto section). Camera lens cap for scale, 7 cm in diameter.

C: Example of cm-thick, discontinuous calcite veins developed within the fine-grained portions of the R2/d sub-unit in the Poggiolop section. Camera lens cap for scale, 7 cm in diameter.

6. CAFFARACCIA SECTION (Mt. BARIGAZZO OUTLIER)

The Mt. Barigazzo outlier is one of the biggest Epiligurian sedimentary remnants of the eastern side of the Northern Apennines, in the middle-high Taro valley (Parma province; grid n. 216060 CTR Regione Emilia-Romagna) with an areal coverage of about 100 km^2 (fig. 6.1)

The Epiligurian succession of this area unconformably overlies Ligurian-derived shale-rich complexes (*i.e.* S. Siro Shale and Ostia/Scabiazza Sandstone) and locally, isolated and relatively small slabs belonging to the Helmyntoid Flysch units (Zanzucchi, 1980).

It is composed, from the base to the top, by the Lutetian-Priabonian M. Piano Unit (MMP) lithologies, with lenticular chaotic bodies of the Baiso sub-unit (Baiso mud breccia. BAI), locally disposed along the lithologic contact with the Ligurian substrate.

The succession continues with the Priabonian-Rupelian Ranzano Unit for ~ 900 m of thickness; the other upper units have been eroded away. This succession comprises of a relatively well-developed PZO unit interval at the base (~ 250 m thick in the northern sector in localized deposcenters) followed by the R1 unit for the remaining ~ 650 m (~ 250 m of Chiarone unit and ~ 600 m of V. Pessola unit for Mutti *et al.*, 1995).

The herein analyzed outcrops belong to the uppermost portion of the exposed Epiligurian succession (*i.e.* uppermost part of R1 unit), cropping out in the Caffaraccia locality, where the R2 unit has been surely recognized and correlated, according to lithostratigraphic and biostratigraphic data (Mutti *et al*., 1995; Catanzariti *et al*., 1997; Martelli *et al*., 1998).

6.1 Previous studies

Earlier studies on the general stratigraphy of this Epiligurian outlier was made during the middle ‘60 (Radrizzani, 1964; Mutti *et al*., 1965; Zuffa, 1966), and then, more detailed studies on the physical stratigraphy and structural geology have been made between the ‘80 and ’90 (Costa, 1985; Dainelli, 1987; Di Biase, 1994).

As for the other Epiligurian outliers, these outcrops have been intensively utilized to give a regional stratigrahic characterization for the Ranzano Unit through the eastern side of the Northern Apennines (Cibin, 1993; Mutti *et al*., 1995; Catanzariti *et al*., 1997; Martelli *et al*., 1998; Cibin *et al*., 2001; Martelli, 2002; Cibin *et al*., 2003).

The regional tectonic setting and the local structural relationships between Ligurian and Epiligurian Units, has been investigated by Plesi *et alii* (2002), Bernini *et alii* (1997) and Bernini

and Vescovi (2002). Some new structural observations, giving alternative interpretations on the general tectonic arrangement of this zone have been introduced by Artoni *et al.* (2006).

The Mt. Barigazzo outlier is represented in the sheets n. 216 "Borgo Val di Taro" and n.198 "Bardi" of the 1:50.000 Geological Map of Italy (Italian Geological Survey, 2002).

6.2 Stratigraphy

Here I'm going to describe only the topmost part of the R1 unit, where the R2 unit partially crops out, with an areal extent of ~ 0.8 km^2 (fig. 6.2).

The background lithologies belong to the upper **R1** unit, here expressed by a generally thin-bedded lithofacies, similar to those discontinuously cropping out in the western sector of the Pessola Valley outlier, just below the R2 unit (**R1 thin-bedded facies**).

These deposits are composed of fine- to medium-grained, thin- to medium-bedded sandstones and mudstones (S/M ≈ 1), with local intercalations of thick- to medium-bedded coarse-grained graded sandstones (up to 2 m thick), arranged in more or less amalgamated bedsets (fig. 6.3). These deposits are observed to record an overall slight shifting of the mean composition toward more carbonatic lithologies in respect to the other underlying R1 unit deposits.

These layers are essentially represented by F6 and F8 facies (and possibly F9 in some cases), with subordinate bed sets of F5 facies (Mutti, 1992), characterized by a relatively high amount of plant fragments and well-developed developed sole marks (mainly groove casts), indicating a mean direction of the paleo-currents toward the S-SW (fig. 6.4).

Rare distinctive beds characterized by strong occurrence of clay chips in the intermediate parts are also observed, with characteristics resembling "slurry-beds" or "sandwich-beds" (as described by Tinterri and Muzzi Magalhaes, 2009)

The lower part of the R1 succession is characterized by an evident stratigraphic thinning toward a southwestern direction, with the consequent overlapping of the upper part of the R1 unit directly above the MMP unit and, possibly, the Ligurian substratum.

Moreover, the upper and lower parts of the R1 unit can be separated in two different depositional trends, each one recording the gradual evolution from a markedly confined depocenter to a relatively more open one, as observed by Dainelli (1987).

This bipartition of the R1 succession can be attributed to a syn-sedimentary deformational phase (possibly linked to the tectonic structures characterizing the southern sector of the basin; see below), as confirmed by the presence of at least three intrabasinal minor mass transport deposits (m- to ten of m-thick) intercalated in the upper part of the R1 unit (fig. 6.5).

This stratigraphic organization seems to be related to a progressive shifting of the main depocenter toward the E-NE, in response to the syn-sedimentary tectonic-related uplift of the W-SW margin of the outlier, as proposed by Di Biase (1994) and Mutti *et al.* (1995).

The R1-R2 unit contact is almost completely covered by vegetation and detritus in the southern sector, and complicated by recent slope instabilities in the northern sector).

In this section, the **R2** unit reaches a maximum estimated thickness of ~ 150 m, but the actual vertical extent is unknown due to the lacking of the upper R2-R3 contact.

6.3 Tectonic setting

The Mt. Barigazzo Epiligurian outlier is arranged in a large synclinalic structure roughly oriented in a N-S direction.

The entire Mt. Barigazzo area shows evidence of relatively important tectonic signatures, involving both the Epiligurian outlier and the Ligurian substratum. Generally speaking, minor tectonic structures (mainly represented by small-scale thrust and related folds, and small-displacement normal faults) are commonly observable throughout the whole upper part of the R1 unit, as well as its lower part (especially in the southern sectors), with the development of ten of meters-sized fold and duplex-type structures (fig. 6.6).

The sedimentary origin of the lithologic boundary between these units is clearly recognizable in the northern outcrops of the outlier (Di Biase, 1994; Martelli, 2002), while in the southern ones it shows evidence of tectonic reactivation and/or overprinting (Plesi *et al.*, 2002; Bernini and Vescovi, 2002). This aspect is quite well observable also in other Epiligurian outliers, as in the Pessola Valley (Costa *et al.*, 1995) and Enza Valley areas (Papani *et al.*, 1987; Catanzariti *et al.*, 1999).

In the southwestern sector, the Epiligurian succession presents evidence of NE-vergent shearing-related structures (*i.e.* duplexes, recumbent folding and low-angle normal faulting and thrusting; Costa, 1985; Di Biase, 1994; Artoni *et al.*, 2006) within its lower portion, at the basal contact with the MMP unit, and between this last one and the Ligurian units. These deformations, sharing evidence of not completely lithified conditions, have been recently interpreted as low-angle extensional structures developed in response to a northeastward gliding of the entire Mt. Barigazzo succession actuated during the Neogene (Artoni *et al.*, 2006). From a general point of view, some of these shallow-level deformations should be linked to a tectonic activation of the southern margin of the basin, as observed in other Epiligurian outliers (Costa and Frati, 1995; Ottria *et al.*, 2001).

An important NW-SE-directed tectonic lineament, expressed by steep dipping major fault systems, dissects the Mt. Barigazzo outlier, crosscutting preceding structures. This tectonic

lineament is probably linked to the north-westernmost expressions of large-scale structures affecting the Tuscan Units (see chap. 3) of this sector of the Northern Apennines, as expressions of a Neogene-Quaternary extensional phase (Bernini and Papani, 2002).

The analyzed Caffaraccia section outcrops are comprised between at least two NW-SE trending high-angle major faults (Pontolo-Pesche System; Artoni *et al.*, 2006), linked to the above-mentioned later tectonic lineament.

These bounding faults bring down the uppermost portion of the local Ranzano unit (*i.e.* R2 unit) according to a graben-like structure, preserving it from erosion, and thus giving the unique opportunity to study the Specchio Unit in this outlier.

6.4 List of figures

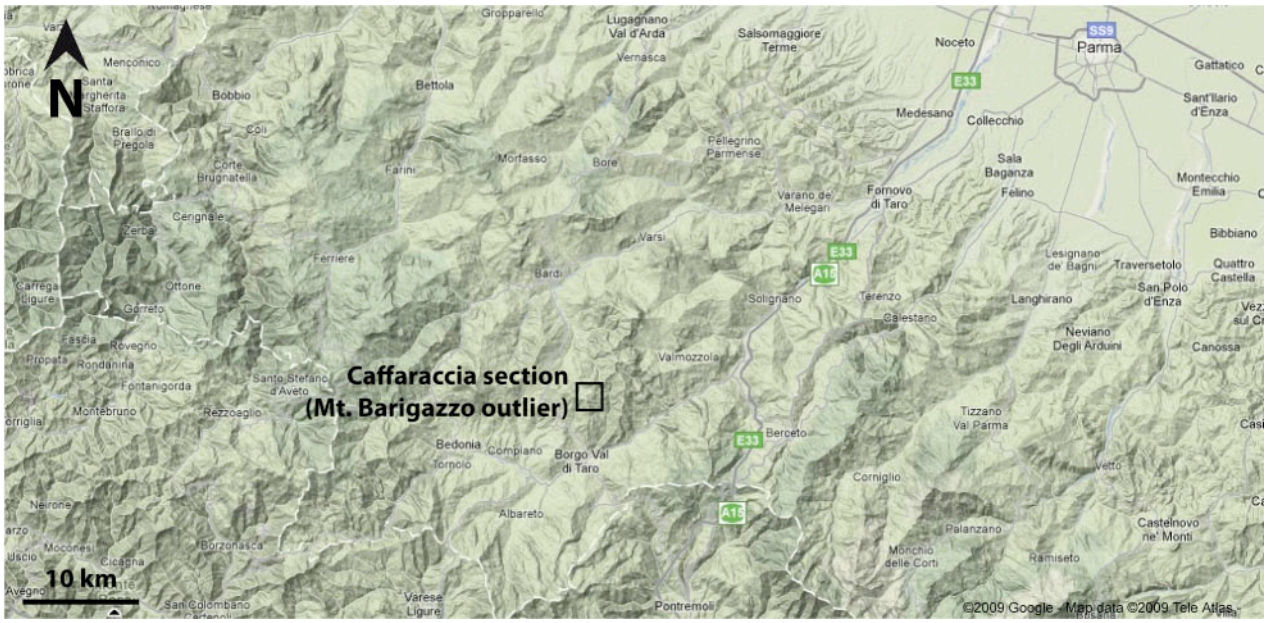

Figure 6.1 - Geographic location of the Caffaraccia section (Mt. Barigazzo area) (from GoogleMaps, 2009).

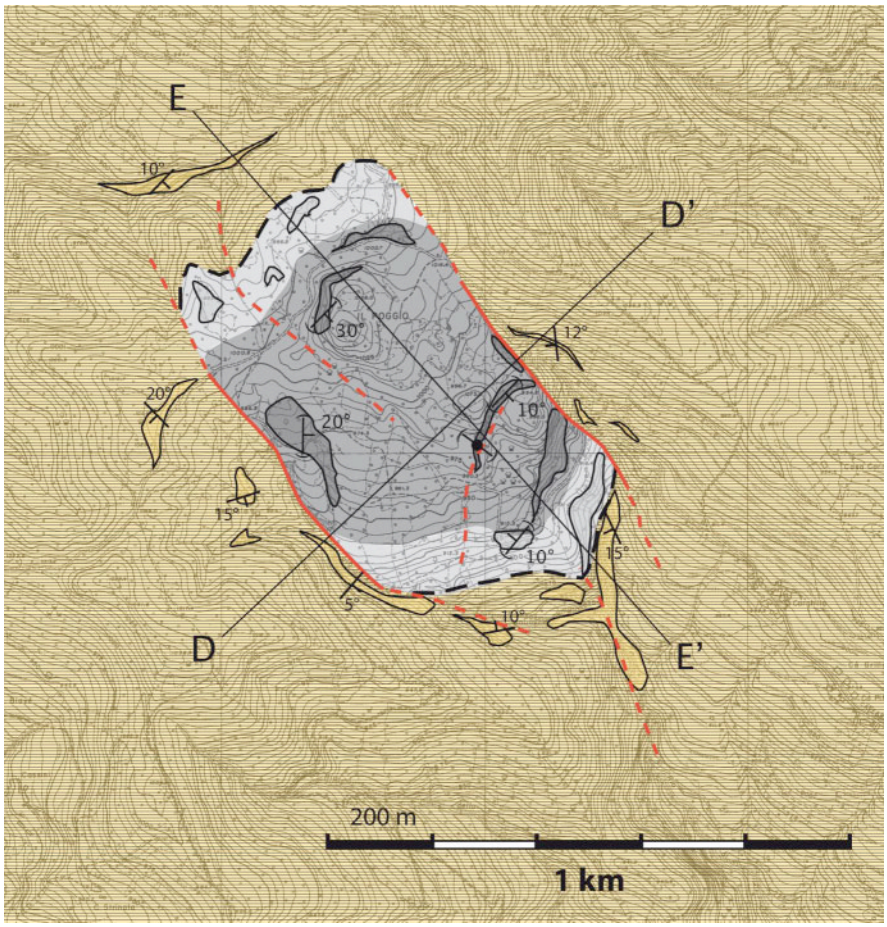

Figure 6.2 - Geologic map of the Caffaraccia section (Mt. Barigazzo area) developed in this work (see attached Panel. n.1). For explanation see fig. 4.3.

Figure 6.3 - Examples representing the outcrop appearance of the R1 unit (thin-bedded facies) cropping out in the upper interval of the sedimentary succession of the Mt. Barigazzo outlier, and representing the substratum of the R2 unit in the Caffaraccia section.

A: Outcrop appearance of the R1 unit just to the south of the Caffaraccia section. Here it is possible to observe that the dominant facies is the thin-bedded one, with the isolated presence of thick-bedded, amalgmanted bedsets.

B: Overall outcrop appearance of the R1 unit thin-bedded facies along the road bound to the Caffaraccia section (few kilometers roughly to the south of the analyzed sector). The rock exposure is slightly complicated by minor high angle fault with short displacements. Hammer for scale.

C: Outcrop of R1 unit thin bedded facies exposed few kilometers to the W of the Caffaraccia section. The component beds are represented by a dominance of F6-type, with intercalated F5- and F7/F8-type facies.

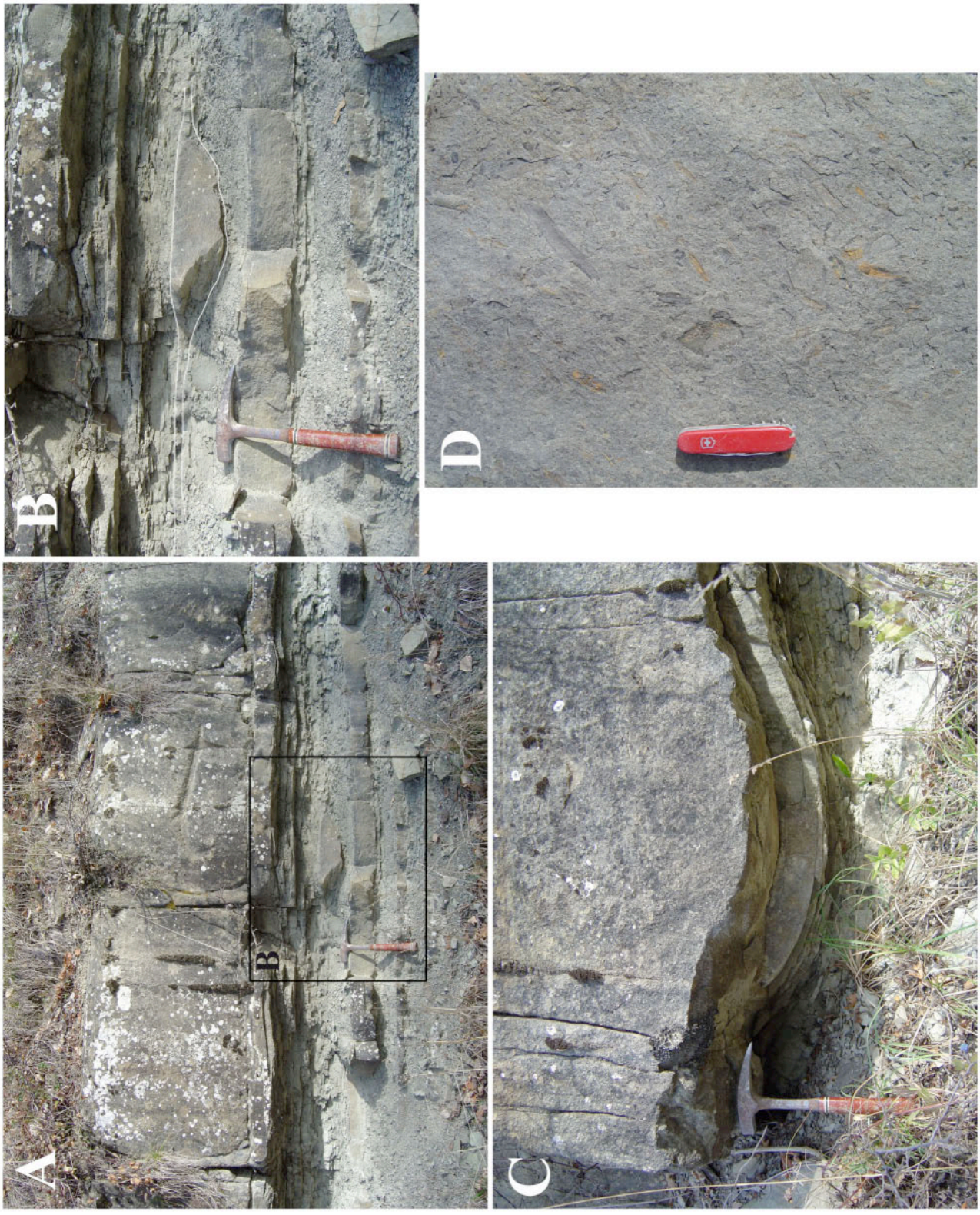
B
D
A
B
C

Figure 6.4 - Examples of meso-scale appearance of R1 unit beds in the Caffaraccia section.

A: An amalgamated medium-bedded bedset of F5-type and F7/F8-type beds, overlying thin-bedded F7/F8-type, and subordinately F6-type beds. Hammer for scale.

B: Close-up of A, showing a scour-like structure (labeled) developed at the base of a thin-bedded F7/F8-type bed. Note the generally massive appearance of these beds. Hammer for scale.

C: Detail of the same thick bed shown in A. Here it is possible to observe a scour-like structure (transversal cut of a large-scale groove-like sole mark?) slightly deformed by loading-related deformation. Hammer for scale.

D: Detail of a lamina surface enriched of plant fragments, recognized within the upper laminated portion of an F7/F8-type bed. Knife for scale, 9 cm long.

~ NW
~ SE
A
B
~ 15 m
B
C
C

Figure 6.5 - A: Panoramic view of an R1 unit outcrop characterizing the western margin of the Mt. Barigazzo outlier (roughly looking to the east). A ten of meter-thick MTD (pebbly sandstone with m- to ten of m-sized stratified blocks) is labeled. At least three of such MTDs have been observed intercalated at various stratigraphic levels within the R1 unit in this sector. Moreover, in this area, strata patterns seem more regular and tabular over relatively long distances.
B: Close-up of A showing the overall appearance of the MTD. Note the development of a relatively thick sandstone bed on top. This feature is shared also by the other observed MTDs characterizing this succession. This recurrence may be indicative of "co-genetic" relationships of this kind of sandstone layer with the underlying MTD.
C: Detail of the pebbly mudstone portion of the MTD (location shown in B). Note the sub-angular carbonatic clast and the enveloping fine-grained, unsorted matrix. Hammer for scale.

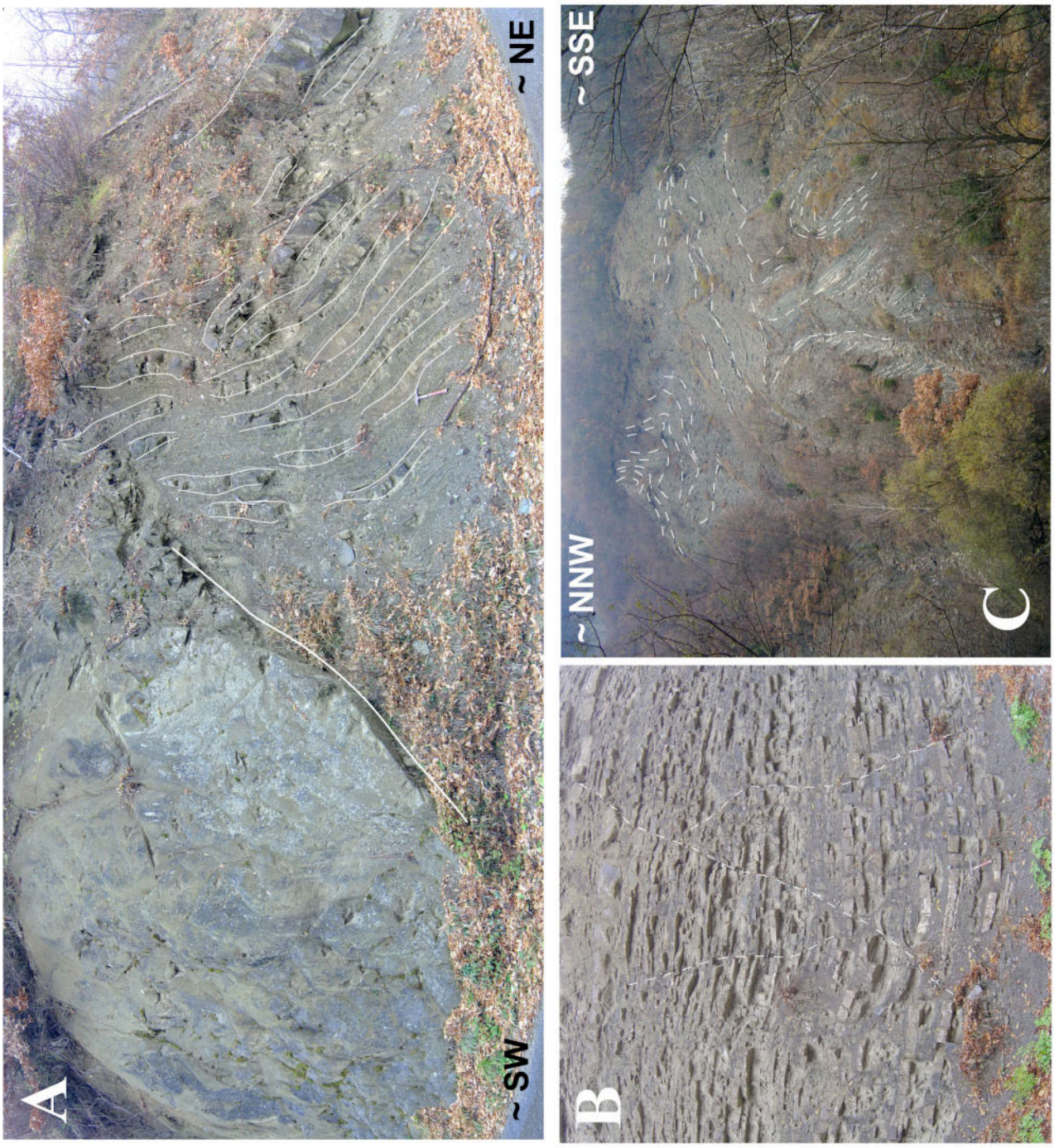
A
~ SW
~ NE
B
C
~ NNW
~ SSE

Figure 6.6 - Examples of tectonic-related features observed in the Mt. Barigazzo outlier.

A: Small-scale thrusting of a thick-bedded F5-type bedset over a thin-bedded portion and related deformation structures (drag folding, *boudinage* and scaly fabric development in the mud partings. Thrust surface and dismembered thin-bedded layers are labeled. Hammer for scale.

B: Detail of the same outcrop presented in fig. 6.3 B. Minor high angle faults, characterized by short displacement ad underlined by mineralized (calcite) veins are labeled. Hammer for scale.

C: General view of the low-angle thrusts and related folds (arranged in some kind of large-scale duplex system) characterizing the lowermost portion of the R1 unit in the southern margin of the Mt. Barigazzo outlier (few kilometers to the south of the Caffaraccia section). Stratification surfaces are labeled.

7. SPECCHIO UNIT (R2) ANATOMY

In all the analyzed outliers, the main features characterizing the R2 unit are: i) strong lateral-vertical variations, with localized extremely thick portions, ii) stratigraphic jumps of the basal contact, iii) incorporation of extra- and intra-basinal elements of various size, iv) large-scale lateral extent, coinciding with a regional unconformity, v) internal organization due to compositional and structural differences, and vi) widespread occurrence of fine-grained unsorted matrix and still stratified blocks associations as fundamental internal component.

The R2 Specchio Unit has a maximum estimated thickness, from base to top, of ~ 450 m in the Pessola Valley area, and ~ 120 m in the Mt. Roccone outlier. In the Caffaraccia section (Mt. Barigazzo outlier) it reaches ~ 150 m, but the roof contact results completely eroded away, and the actual total thickness remains unknown.

The other possible R2 unit-bearing Epiligurian outliers of the Mt. Piattello (Piacenza province) to the NW and the Enza Valley (Reggio Emilia province) to the SE (Mutti *et al.*, 1995) are only partially considered in this work due to biostratigrahic discrepancies (Catanzariti *et al.*, 1997), poorly exposed outcrops (*i.e.* Mt. Piattello) and tectonic disturbance (Enza Valley; Catanzariti *et al.*, 1999; Ottria *et al.*, 2001). Preliminary field observations taken from the these outliers, however, confirm the presence of at least 2 sedimentary chaotic bodies sharing some compositional and structural features, as well as the stratigraphic level, with the R2 unit and the upper mass transport complex (*i.e.* Varano unit, upper mass transport complex) recognized in the Pessola Valley and Varano de'Melegari-Pellegrino Parmense outliers (see attached Panel n. 1).

The R2 Specchio Unit shows an irregular distribution, and its thickness is highly variable also in the same outlier, with rapid variations on short distances. Usually, this unit unconformably overlies the Pessola unit (R1) but sometimes it rests above the M. Piano unit (MMP) and the associated Baiso mud breccias (BAI), or directly upon the Ligurian chaotic complexes, also within the same outlier.

The upper contact with the R3 unit (well recognizable in the Pessola Valley and Mt. Roccone outliers) is commonly underlined by the discontinuous presence of a thick sandstone bed with distinctive characteristics in respect to the overlying "normal" sedimentation, marking the transition between chaotic lithologies of the R2 unit and the well-stratified succession of the R3 unit (see chap. 7).

In the following I will firstly introduce the elements utilized to characterize the R2 unit internal anatomy, briefly discussing their general characteristics and some interpretations about their origin.

These elements are herein simplified in 2 main constituents, matrix and blocks, intended as end-members of a broad spectrum of the soft-sediment deformation process. These 2 elements are arranged within the R2 unit as single elements or associations, and have been investigated through the analysis of the related structures.

The approach used here for the analysis of such features has been tested through the systematic comparison with other sedimentary chaotic units from the Northern Apennines (Italy) and South-central Pyrenees (Spain). Part of the data and interpretations discussed in the following are unpublished, and from ongoing researches. Some results of this work have been presented at the 27th I.A.S. Meeting of Sedimentolgy of Alghero (Sardinia, Italy) (Mutti *et al*., 2009).

7.1 Matrix

The term "matrix" is intended here to define the relatively fine-grained unsorted lithology of a mass transport deposit, which envelopes, injects and in most cases, sustains discrete slide elements ranging from km-scale slabs to mm-scale particles.

The here defined matrix is characterized by evidence of *liquidization* (*sensu* Allen, 1977, 1982, 1984) and it is thought to be the product of saturated sediment remolding and mixing, both failed and eroded from the underlying substrate during the mass transport event, and thus, it can be considered as an extreme example of soft sediment deformation developed in condition of fluid overpressure (fig. 7.1 A, B and C).

Marine geophysical surveys have recently shown that fluid overpressuring is a characteristic feature of shallow-level crustal processes, on both modern convergent and divergent continental margins. These processes are generally represented by:

- sediment gravity sliding;
- thin-skinned thrust tectonics;
- shale and salt diapirism;
- mud volcanism and fluid venting;

Regarding the former, excess pore pressure is retained a common process in the initiation, evolution and emplacement of a submarine landslide, as well as during post-depositional rearrangement, mainly due to its efficiency in decreasing sediment strength (fig. 7.1 D and E).

Evidences of fluid overpressure (mainly in form of fluid escape structures) have been recently documented in seismic and acoustic profiles of submarine landslide deposits (Diviacco *et al.*, 2006; Moernaut *et al.*, 2009), testifying its common occurrence and maintenance even after the deposition (as confirmed by experimental and numerical modeling; Major and Iverson, 1999; Major, 2000).

Apart from the classical Grand Banks event (Piper *et al.*, 1985, 1999; Piper and Aksu, 1987), during the last decade several studies have been carried out to define relationships between submarine landslides and turbidity currents, and to justify the extremely long run-out distances recorded by some huge sediment failures, in particular those from the western African margin (Canary Slide, Saharan Debris Flow; see among the others Gee *et al.*, 1999, 2001; Urgeles *et al.*, 1997, 1999) and North Atlantic European margin (Storegga Slide Complex; see among the others Kenyon, 1987; Bugge *et al.*, 1988, Evans *et al.*, 2005)

Laboratory experiments and numerical modeling suggest that hydroplaning is the most likely moving mechanism for these failed masses (Mohrig *et al.*, 1998; Elverhoi *et al.*, 2000, 2005; Ilstad *et al.*, 2004; Niedoroda *et al.*, 2007) (see chap. 8). This process takes place when significant amount of water is dynamically incorporated during the upward flipping of the slide front, from the surrounding marine environment, developing a basal overpressured horizon capable to reduce the effective friction forces and enhance the slide sheet mobility (fig 7.2).

Scaling problems and resolution limits of the geophysical and laboratory method cannot permit better considerations on the products, especially in terms of internal characteristics and related structures.

Recent acquisition of sedimentological data from cores taken from superficial parts of a selection of modern submarine landslides in the NW Gulf of Mexico and NE American - SE Canadian margin has shown a very high heterogeneity of sedimentary facies at meter scale (McHugh *et al.*, 2002; Tripsanas *et al.*, 2007; Cauchon-Voyer *et al.*, 2008; Jenner *et al.*, 2007): these data also highlight the presence of cm- to m-sized distinct zones of homogeneous fine-grained material with fluidal texture, localized between large relatively undeformed and still stratified sediment packages. No detailed meso-scale interpretations can be done on these cores because of the insufficiency of material sampled and the short length of specimens (~10-20 m) compared to the whole thickness of deposits.

The role of fine-grained material in the evolution of submarine mass transport processes was classically investigated from a rheologic and geotechnical point of view, mainly through laboratory experiments and numerical modeling (Hampton, 1972; Rodine and Johnson, 1976; Lowe, 1982).

From an outcrop perspective, evidences of fluid overpressuring in sediment gravity flow deposits are commonly expressed by soft-sediment deformation structures. The rapid deposition due to flow collapse, traps interstitial fluid in the sediment and results in high and unstable pore pressure. Most of the soft-sediment deformation structures are related to fluid-escape due to squeezing out of excess water from the pores of sediment during compaction.

A general description of soft-sediment deformation has been given by Knipe (1986). The author described deformation type as function of three major parameters: deformation ratio, lithification degree and fluid pressure. Three types of deformation were defined: independent particulate flow, diffusion mass transfer and cataclasis.

Independent particulate flow is retained the most common deformation mechanism in the development of the units described in this study (as confirmed by microscopic analysis; see below). It describes the behaviour of non-cohesive or poorly lithified sediments. Depending on the ratio of excess pore fluid pressure to cohesive strength due to grain weight, three deformational processes are defined:

- hydro-plastic deformation;
- liquefaction;
- fluidization;

Hydro-plastic deformation occurs when fluid pressure is lower than grain weight and preserves, but modifies primary sedimentary structures (*i.e.* bedding and lamination). Many structures created by this kind of deformation usually resemble plastic deformation in metamorphic rocks.

Liquefaction occurs when fluid pressure is equal to grain weight, and then the sediment loses its strength and it may be subject to laminar flow. Most of primary sedimentary features are destroyed, and no volume change occurs due to any phase addiction to the system.

Fluidization occurs when fluid pressure is higher than grain weight, or fluid velocity is high enough to entrain grains in the fluid, and then the sediment loses his strength and is subjected to "turbulent" flow. This process acts when fluid pressure approaches lithostatic pressure, due to conditions that prevents fluid escape: it results in an almost complete destruction of every primary sedimentary feature. In this case volume change is predicted by the addiction of and external phase (*i.e.* water) to the system.

These processes (single and/or combined) are thought to develop most of the sedimentary features observable in the matrix.

Matrix texture presents a scale-invariant appearance resembling an apparent block-in-matrix or brecciated fabric from the microscopic-scale to the outcrop-scale, and possibly up to the seismic- and cartographic-scale (*e.g.* "multi-fractal breccia" of Callot *et al.*, 2008a).

Generally speaking, the matrix is always finer than the sustained element (fig. 7.3).

The meso-scale appearance of this matrix in outcrop differs case by case, and its composition and subordinately, texture and structures, mainly depend on lithology and consolidation degree of the involved sediments, as well as on generating mass transport process.

However, matrix texture shares some common features more or less recognizable in all the analyzed examples:

- Strongly unsorted fashion expressed by various degrees of lithological mixing;
- Evidences of extreme soft sediment deformations (fluidization/liquefaction processes);
- Coexistence of constituting elements characterized by different rheologic behaviours;
- Common occurrence of fluid-escape structures;
- Same preferential localization at the base and along boundaries of discrete slide body parts.

All of these features are in accord with processes involving strong fluid overpressure, developed during movement and deposition of the slide mass.

The matrix production is thus strongly related to mobility and consolidation degree of material involved in the slide process, through internal desegregation (*i.e.* collisions and frictions of constituting elements) and undrained shearing of the seafloor (*i.e.* overloading and dragging force exerted by the overriding slide mass).

In the wide specter of mass transport deposits, as preliminarily defined by Mutti *et al.* (2006), this overpressured matrix play a fundamental role for the characterization of possible flow transformations from submarine landslides to debris flows, and then, to turbidity currents.

Careful analysis carried out mainly on the R2 unit and confirmed by observations taken from other case studies, allow the interpretation of this kind of matrix as a scale-invariant association of 4 main components (fig. 7.4):

A) major rigid elements (*e.g.* completely lithified particle- to boulder-sized clasts);

B) elongated patches and clustering of minor rigid elements in un-lithified fine-grained lithologies;

C) fine-grained poorly- to un-lithified lithology (*i.e.* finer than minor discrete elements) with scattered minor rigid elements, representing some kind of transition from B to D;

D) major soft elements, composed of poorly-lithified but still coherent lithology.

These constituents allow the identification of this kind of matrix as a 4-phase system in which, each phase is thought to behave in a different rheologic manner: solid (A), fluid (B), pseudo-plastic (C) and plastic (D).

Proportions of each phase vary greatly case-by-case, as well as in different points within the same deposit, mostly depending on strain partitioning during the mass transport emplacement.

Sometimes is difficult to recognize such features in outcrop because of the intense weathering, which commonly characterizes fine-grained sediments, and the poor erosional relief shown by slide blocks on surrounding matrix sharing same lithologies.

This matrix is commonly localized within discrete portions of the slide body, as: i) basal shear surface, ii) syn-sedimentary ductile shear zones, iii) hinge zone of rootless/detached slump folds, and iv) surrounding and intruding coherent slide portions and blocks, as separate patches and pseudo-veins.

Moreover, matrix characteristics show significant point-to-point variations, depending on its localization also within the same deposit; for example, an enclosing matrix (*i.e.* matrix sustaining components) show marked compositional and textural differences from a matrix developed inside discrete slide elements (*i.e.* proto-matrix). In fig. 7.5 is tentatively represented the possible evolutionary steps of this kind of matrix developed through progressive stratal disruption of a thin-bedded, poorly lithified siliciclastic succession.

The overall recognized presence of patches of different kind of matrix into another (in terms of texture, fabric and composition) testifies the un-mixing of different matrix generations, thought to be developed in different points within the slide body, involving different materials and possibly through different deformational processes.

7.2 Blocks

With the term "block" here I referred to as meter- to hundreds of meter-sized discrete slide components (possibly up to km-scale), which can be separated from the background lithologies (*i.e.* matrix) because of the maintenance of some kind of internal coherence and primary features.

For reasons of simplicity, this generic term is preferred to other definitions as olistolith, un-dissociated mass, raft, slab, glide blocks, etc. (see Ineson, 1985; Tarquin Teale and Young, 1987; Macdonald *et al.*, 1993; Marroni and Pandolfi, 2001), and for similar discrete elements below the meter-size, here I use the term "clast" or "intra-clast", depending on their "exotic" and intrabasinal origin, respectively, competence and consequent reworking degree.

From a general point of view, blocks can be composed of well- to poorly-lithified lithologies and can range from still stratified or completely deformed sandstone-mudstone elements to single massive carbonate or ophiolitic masses.

Most of the blocks observed in the R2 unit are represented by poorly-consolidated still stratified fragments of sedimentary successions, usually arranged in isolated and rootless slump-like folds, generally isoclinalic, and sharing evidences of various degrees of soft sediment deformations (see below).

These blocks can be completely enveloped by the matrix, as floating isolated elements, or be clustered in close contact, each one separated from the adjacent by matrix-underlined shear surfaces.

Some of these roughly meter-sized rigid blocks are represented by lithified carbonatic elements coming from the Ligurian substratum (*i.e.* Helmintoyd Flysch units). These elements show sub-rounded to sub-angular appearance, and reach the maximum size of ~ 3 m across.

In some cases, within matrix-rich zones, a banded clustering of minor elements (*i.e.* granules and pebbles) surround major rigid elements (*i.e.* well rounded to sub rounded cobbles and boulders), share a common iso-orientation of the major axis oriented according to its boundaries.

From an operative point of view these blocks have been classified taking into account their overall dimensions: discrete slide elements (*i.e.* discernible from the surrounding lithologies) sharing sizes from one to tens of meters across are simply referred to as *blocks*, while those showing dimensions up to (and over) hundred of meters across are defined as *out-size blocks*. All the other elements below the meter are generically termed as *clasts*, and subdivided on the basis of their relative size and consolidation degree in *boulders*, *cobbles* and *pebbles* (in decreasing size order) for well lithified, reworked (*i.e.* generally rounded to subrounded in shape) elements; poorly-consolidated, plastically deformed elements of generally intra-basinal origin are herein simply defined *intra-clasts* (fig 7.6).

7.3 Structures

The meso-scale structures observed within the R2 Unit share the same ductile deformation origin. No evidence of primary brittle deformation has been observed, not even at the micro-scale.

Nonetheless syn-sedimentary tectonics structures have been observed, especially in the southeastern sector of the Pessola Valley outlier, which are thought to cause some local overprinting of the mass transport-related structures of the R2 unit (see chap. 4).

The overall shape of these features mainly depends on the lithology and lithification state of the involved materials, and on the strain partitioning achieved during the emplacement (*e.g.* upper or lower, marginal or axial portions).

Sometimes, meso-scale fluid-escape structures have been recognized and observed to be related to the other described features, especially at the very base of over-sized blocks and, where buckling and interference of structures occur. These structures are underlined by an upward and lateral expulsion of liquidized material (*i.e.* matrix of later generation) along block boundaries and through weak zones and discontinuities affecting their internal integrity.

7.3.1 Folds

The vast majority of the recognized folds are represented by closed to isoclinal, non-cilindrical folds with dimensions ranging from about one meter to tens of meter across, and involving thin- to thick-bedded, single beds or bed sets. These folds generally share axial planes disposed at low-angle in respect to the mean inferred pseudo-stratification (and to the close ductile shear surfaces), and locally they may also be steeply inclined to sub-vertical.

These folds commonly show strong thickening of hinge zones, without evidence of foliation or folding-related cleavage, with an overall soft-sediment deformational style, evidenced by density contrast structures on limbs (*i.e.* mullions-like structures), mud-sand "interfingering" and matrix injections in hinge zones.

Where a continuous three-dimensional view of the outcrop is appreciable, the majority of these folds show a sheath fold-like shape, which complicate fold geometry recognition but at the same time, gives important kinematic information about shearing direction (*i.e.* long axis azimuth and vergence) (fig 7.7).

The observed structures are commonly rootless, isolated as floating elements in the enclosing matrix, and the analysis of stratigraphic polarity highlight their possible complete rotation, giving the common occurrence of antiformal synclines and synformal anticlines, which however maintain their achieved vergence. Anticlines and synclines occur in same amount, with a slight predominance of the latter.

The common occurrence of syn-sedimentary shear zones along the axial plane of these folds and the strong asymmetrical appearance (long back-limb and short "hooked" forelimb) highlight their close genetic relationships.

The inferred mechanism of development for such structures is a progressive fault-related folding of original elements, resulting in a consequent generalized association of shear zones and related drag folds, developed in water-saturated, low-confining pressure conditions.

Other subordinate types of fold recognized are double-vergent box folds, characterized by high-angle axial planes and outward expulsion of hinge zone, sharing common soft-sediment deformation evidences. These kinds of structures, which are commonly enclosed within the matrix occur in discrete zones of the surveyed areas and are commonly associated to interference patterns caused by re-folding of preceding structures (usually as co-planar bending of the fold axe, or co-axial bending of the axial plane; Ramsey, 1967).

The inferred mechanism of generation of such structures is here thought to be a localized buckling, involving already formed folds, developed in water-saturated sediments at shallow-crustal level conditions.

Inside the matrix-rich portions have been documented the presence of fluidal structures (similar to those produced by halo-kinetic processes; *e.g.* Wardlaw, 1972), usually evidenced by the involvement of elongated patches and banded zones characterized by different weathering and alteration colors. These features are commoly recognizable as complex folds, which involve litholologies sharing almost the same rheologic behaviour, and developed in a passive way due to the whole heterogeneous movement of the enclosing matrix.

The above-described folds show complex reciprocal relationships and interference patterns, as well as developing at different scales (fig. 7.8).

7.3.2 Ductile syn-sedimentary shear zones

The other considered structures are ductile syn-sedimentary shear-zones, commonly expressed by low-angle thrust, sometimes and locally with steep-dipping angles, and rarely represented by low-angle normal faults, affecting both matrix and blocks. No clear evidence of tectonic-related brittle deformations has been recognized.

Depending on the consolidation degree of the involved materials, these structures are characterized by a local concentration of matrix (or proto-matrix; see above) and/or a generally banded pattern of the shear plane, sometimes crudely foliated, testifying their overall ductile behaviour.

The kinematic indicators used to define the general shearing mechanism are: drag folds, sigmoidal structures, deformation bands-like features and element imbrication. The general stacking vergence of these thrusts, generally arranged in splays and imbricated sets gives additional kinematic information (fig. 7.9).

The outcrop appearance is not always clear (especially for those contained in matrix-rich zones) due to the general lacking of referring geometrical surfaces and the involvement of easily alterable fine-grained litologies.

Detailed observations on three-dimensional outcrops, integrated with preliminary estimation of palaeo-transport, highlight the common occurrence of low-angle shear zones characterized by opposite shearing directions (pop up- and flower structure-like appearance) in transversal section to the mean transport directions, giving an overall transpressive/buckling-related arrangement of the structures, while in longitudinal section they appear to record an overall preferential direction (see fig. 7.10). These structures develop both at the detailed- and outcrop-scale.

The recognition of such differences in structural style between longitudinal and transversal sections of the slide body permits important considerations about its whole behaviour during the emplacement, first of all giving another significant contribution to the preliminary interpretations of the palaeo-transport (when other structures are not observable) and then, favoring the discrimination of distinctive structure associations.

7.3.3 Structure associations

Developing the above-described observations in working hypothesis, the R2 unit can be thus subdivided into matrix- and blocks-dominated portions (**MDP** and **BDP**, respectively) on the basis of the relative amount of separate elements (*i.e.* clusters of m- to tens of m-sized blocks and detached slump folds) and fine-grained unsorted and clearly mixed lithologies (*i.e.* pebbly- and sandy-mudstones with more or less abundant debris, clasts and hydroplastically-deformed fragments).

Generally speaking, MDPs mesoscopically resemble the block-in-matrix fabric classically ascribed to debris-flow deposits (fig. 7.11), while BDPs seem to share the typical appearance of a slump-like deposit or a megabreccia/olistoliths swarm (fig. 7.12), depending on the nature of the blocks.

The structures occurring inside separate blocks, and generally within BDPs are herein termed as intra-block structures (*e.g.* intra-block thrusts and intra-block folds, **IBT** and **IBF**, respectively), while ones recognizable between separate blocks within the BDPs and distributed through the MDPs, are termed as extra-block structures (*e.g.* extra-block thrusts and extra-block folds, **EBT** and **EBF**, respectively).

7.4 Internal subdivisions of the Specchio Unit (R2)

Detailed 1:5.000 field-mapping survey and careful sedimentologic, stratigraphic and structural analysis carried on selected key-outcrops allow the subdivision of the R2 Specchio Unit in at least 5 sub-units, mainly discriminated on the basis of their lithologic content, meso-scale texture, deformational style of the component structures and geometrical position within the R2 vertical succession.

The boundaries of each subdivision are highly irregular, often transitional and not always clearly recognizable in the outcrop, generally because of the involvement of similar lithologies, often fine-grained and poorly consolidated, and thus particularly susceptible to superficial weathering and active slope instabilities.

However, careful observations on these boundaries exposed in optimal conditions, have shown that in some places there is evidence of structural overprinting (*i.e.* re-folding, thrust bending, buckling) probably achieving the interference caused by the subsequent overlying sub-unit emplacement.

These sub-units, described for each studied outlier in the following, are progressively termed from the base to the top as: i) **R2/a**, ii) **R2/b**, iii) **R2/c**, iv) **R2/d** and v) **R2/e** (fig. 7.13).

7.5 Pessola Valley outlier

In this outlier the R2 unit reach its maximum thickness and it is entirely exposed, from base to top, in quite continuous and sometimes three-dimensional outcrops. Given these characteristics, this area has been selected to define the working hypothesis then exported to the other analyzed outliers (fig. 7.14).

7.5.1 R2/a sub-unit

This sub-unit crops out at the very base of the R2 Unit in the Pessola Valley outlier, and is completely lacking in the Mt. Roccone outlier and in the Caffaraccia section.

In the Pessola Valley area, this sub-unit presents an irregular thickness from few meters (and locally virtually missing) in the SW sector of the up to ~ 80 m on the left side of the Pessola river. In the south-eastern and south-central sectors it shows complex lateral relationships with the low-angle thrust stacking system characterizing the SE portion of the outlier and the ramp structure of the Rio Molinetto section, respectively (see chap. 4). The R2/a sub-unit doesn't crop out in the northern sectors due to the general monoclinalic dipping of the entire Epiligurian succession toward NE, and its overall thinning to NW and NE (fig. 7.15).

The basal contact is strongly erosive, unconformably cutting the R1 unit at different stratigraphic levels (lying on the thin-bedded lithofacies in the south-western sector and on the thick-bedded lithofacies in the central sector), with an overall large- to meso- scale flat-ramp geometry (fig. 7.16).

The R2/a sub-unit is composed of MDP and BDP with lateral-vertical heteropic relationships and is essentially composed of both loose and still stratified sandy-pebbly material coming from the underlying R1 Pessola unit.

Calcareous angular fragments and hydroplastically deformed cm- to m-sized clay-rich blocks of Ligurian origin, and clay-marly heterometric blocks belonging to MMP unit are also present in MDPs characterizing R2/a base. These components sometimes show their original lithologic

relationships (*e.g.* angular fragments of limestone layers contained in foliated shales), thus, virtually not reworked by other preceding subaerial/submarine processes (fig. 7.17).

Matrix characterizing MDPs is highly heterogenous, and it is essentially composed of an enclosing pebbly mudstone/sandstone with marly and clayey hydroplastically deformed clasts, ophiolitic pebbles and carbonatic debris. Blocks are mainly constituted by R1-like facies beds, and subordinately by MMP-, BAI- and AVV-like lithologies (fig. 7.18).

Qualitative microscopic matrix anaylses have been carried on a thin-section and polished counter-cut of a rock sample taken from the enclosing matrix characterizing this sub-unit in western sector (C. Servazzola area; sample R2/aEM).

These observations evidenced the presence of a fine-grained silty-muddy lithology enveloping sub-millimeter- and mm-sized rounded and sub-rounded granules (subordinately angular), arranged in an overall matrix-sustained texture, locally showing preferred orientations of elongated clast major axis. Clast composition is mainly ophiolitic, with subordinate carbonatic lithologies and sparse well-preserved microfossils (probably radiolarians).

The major granules share haloes of a finer grained matrix than the surrounding one, which is characterized by an optically opaque and ferruginous appearance. This matrix is arranged in interconnected and anastomosing pseudo-vein seams, enveloping and sometimes penetrating into the clasts. There is no evidence of mechanically broken grains or brittle deformation, and thus the invoked deformation mechanism is a generalized independent particulate flow (fig. 7.19).

Within BDPs, blocks are composed of m- tens of m-sized faintly stratified and highly deformed medium to coarse-grained and pebbly sandstone rafts, characterized by intense development of IBTs. These blocks share unclear and transitional boundaries, generally grading through an unsorted pebbly sandstone halo to the surrounding pebbly mudstone matrix (see fig. 7.20).

In this sub-unit BDPs seems to be more localized in the lower part while MDPs characterize the upper one, with some local exceptions (*i.e.* C. Servazzola and Fopla sector). Some isolated m- to ten of m-sized sandstone rafts are randomly distributed within upper MDPs.

Meso-structural data from IBT, IBF, EBT and EBF indicate a mass transport direction roughly toward NE (see attached Panel n. 2).

7.5.2 R2/b sub-unit

As the R2/a, this sub-unit is present in the Pessola Valley area and is completely missing in the Mt. Roccone outlier and the Caffaraccia section, sharing also the same lithologic composition.

This sub-unit is well exposed on the left side of the Pessola river cut showing an average thickness of ~ 40 m, while in other sectors of this outlier it is highly variable from a minimum of ~ 20 m to a maximum thickness of ~ 80 m.

The R2/b interval is highlighted in the landscape by clustering of meters- to tens of meter-sized blocks composed of still stratified and plastically deformed coarse-grained sandstone rafts, showing a relatively clear lithologic contrast (*i.e.* high relief erosional profile) with other clay- and marl-rich blocks. The sandstone blocks derive from the R1 unit, while the clay-marly ones are mainly from the MMP unit (fig 7.21).

In this sub-unit BDPs seem to prevail on MDPs, and the matrix content within the BDPs (~ 20% of the outcrop) is mainly localized along ductile syn-sedimentary shear planes dissecting and separating single blocks (IBTs) (fig 7.22).

The qualitative microscopic analyses carried on a matrix sample taken within a localized MDP (sample R2/bEM) evidenced an assemblage of rounded (mm-sized) and subordinately sub-angular (sub-mm-sized) granules, arranged in an overall clast-supported texture, with less evident separated matrix-supported patches. The less abundant finer grained lithology is generally confined in intergranular position.

Thin calcite veneers surround clasts and result interconnect to “vein seams” also separating clast assemblages, without evidence of brittle deformations and grain breakage. The inferred mechanism of deformation is a grain-to-grain particulate flow.

Same analyses have been done on a matrix sample taken from an IBT (sample R2/bIBT), about 30 m over the other one, unraveling similar compositions but slightly different texture. This is due to a better-developed iso-orientation of elongated grains major axis, resulting in a more or less evident banded appearance.

It is important to note that I have sampled only the better lithified pebbly sandstone matrix portions, because of the strongly altered conditions and the weakly-lithified nature of pebbly/sandy mudstone portions, unsuitable for thin-section preparation (fig 7.23).

Ligurian-derived extraformational elements are also present and are expressed by m-sized blocks of massive or brecciated limestones, associated to darkish to reddish mud-breccias and shale-rich blocks (fig 7.24).

In this case meso-structural data from IBT, IBF, EBT, EBF and apparent trend of imbrications of the major components, indicate a general mass transport direction toward northern sectors, with mainly eastern and subordinately western components, roughly according to R2/a sub-unit (see attached Panel n. 2).

In some locations, commonly toward the upper portions, this sub-unit shows a more or less recognizable over-steepening and bending of the planar structures. This fact is particularly evident in the western sector (C. Servazzola section), the upper portion of this subdivision (close to the upper contact with the R2/c sub-unit) is characterized by superimposition of S-verging structures over the N-verging ones, expressed by inverse reactivation of shear zones and re-folding of preceding syn-sedimentary thrusts. This structural interference is interpreted as evidence of reworking of the upper portion of the R2/b subdivision operated by the emplacement of the overlying R2/c sub-unit (fig 7.25).

7.5.3 R2/c sub-unit

The following R2/c sub-unit represents the more extended among the recognized subdivision with a thickness ranging from a minimum of ~ 80 m to a maximum of ~ 230 m, in the central sector of the area, and it records a significant changing in lithologic composition and structural style.

Here BDPs are dominant in the upper half and the associated matrix is generally concentrated within IBT and EBT, while a relatively continuous m-thick interval of MDPs occurs in the lower part (fig. 7.26).

The major components are meters- to ten of meters-sized blocks, and sometimes also reaching hundreds meters across (out-size block shown in fig. 7.6 C), of still recognizable thin-bedded (locally thick-bedded) sandstones and mudstones belonging to the Pizzo d'Oca unit (PZO), and partly from some kind of intermediate facies between the latter and the R1 unit (V. Chiarone unit?).

Other meters- to ten of meters-sized blocks composed of very thin inter-bedded siltstones/fine-grained sandstones and mudstones share a common "streaky" appearance, typical of pro-delta deposits, and probably belonging to basin margin equivalents of R1 coarse-grained turbidites. Within these thin-bedded portions several evidences of bioturbation have been found (fig. 7.27).

Generally, angular clasts and more or less reworked m-sized blocks of Ligurian-derived carbonates represent the minor components; the clasts are randomly scattered across the entire thickness of this sub-unit, while the blocks are commonly localized along the basal contact (fig. 7.28).

This sub-unit is characterized by the presence of mainly carbonatic rounded and sub-rounded pebbles and cobbles generally scattered within MDPs and localized within EBT separating blocks, which relative amount seems to increase upwards. These pebbles and cobbles show evidence of bioerosional hollows, and rarely, traces of encrusting oysters, confirming their provenance from shallow-marine environments, possibly close to the coast line (fig. 7.29).

Moreover, some m-sized, medium- to coarse-grained sandstone lens-like blocks appear to be roughly aligned within the upper part of this sub-unit; these elements, which share a pseudo-boudinated shape and are usually arranged in rootless, locally double-vergent folds, seems to be developed by the involvement of a single thick sandstone layer (fig. 7.30).

Rare m-sized conglomeratic blocks are locally present within the basal MDP.

The general deformational style is characterized by the presence of sheath fold-like structures, affecting both single detached beds and stratified blocks, and more or less recognizable also as fold trains (*i.e.* series) affecting the pseudo-stratification within MDPs.

The qualitative microscopic analyses carried on a matrix sample taken from the basal MTDs of this sub-unit (sample R2/cEM) highlight the presence of well rounded, and subordinately, sub-rounded and angular, grains, contained in a fine grained marly lithology with an overall matrix-sustained texture. Some still preserved and fragmented microfossils are also present.

As observed for the R2/a sub-unit, major granules show a marked concentration of very fine-grained matrix around borders, which is sometimes injected inside through discontinuities affecting clast integrity (*i.e.* primary veins). This kind of finer matrix seems to constitute thin bands, which suddenly merge into the surrounding matrix; it doesn't show optically opaque and ferruginous appearance, without developing discrete pseudo-veining systems.

Moreover it is possible to observe elongated clusters of grain- and matrix-dominated portions, organized in almost parallel and slightly anastomosing seams, sharing granular reorientation without brittle fracturing and an overall ductile behaviour.

Also in this case the most likely deformation mechanism is supposed to be an independent particulate flow (fig. 7.31).

The lithologic homogeneity and consequent weak erosional relief of the components, except for the thicker sandstone elements, complicate the observation of such structures.

Data from meso-structural analysis carried on these folds and syn-sedimentary thrusts (both intra- and extra-block) present a significant areal dispersion, but however suggest an inferred mass transport direction toward the southern sectors (see attached Panel n. 2).

It is important to stress the presence of huge stratified blocks of sedimentary succession belonging to the PZO (up to ~ 500 m across) in the south-central sectors of the outlier (*i.e.* C. Servazzola, R. Molinetto and C. Borbetti sectors; see attached Panel n. 2). Some possible matrix-related fluid-escape structures have been documented injecting the basal contact of such out-sized blocks (see fig. 7.6 C).

Evidence of structural overprinting, mainly expressed by re-folded folds and generalized buckling, can be observed along an elongated band roughly trending W-E (almost coinciding with

the Rio Pratorotondo and Rio dei Corvi waterways), which separates the two main opposite-directed portions of the R2 unit (*i.e.* R2/a, R2/b from R2/c, R2/d) (fig. 7.32). Particularly, in the eastern sector, this elongated zone of structural overprinting seems to boarder the northern flank of the low-angle thrust stacking of the Ricodalle section (see chap. 4).

Here, the structures (linear and planar) seem to be verticalized, with the general arrangement in a parallel way to the lithologic contacts between the concerning subdivisions; this situation is observable in the right side of the Pessola river incision (see Panel n. 2) (fig. 7.33).

7.5.4 R2/d sub-unit

This sub-unit shows a remarkable areal extent with a thickness ranging from a minimum of ~ 80 m in the southern sectors to a maximum of ~ 140 m in the northern sectors, and it is characterized by the evident predominance of intraformational elements belonging to the R1 unit (rarely PZO and intermediate terms) coming from basin margins.

These elements are blocks composed by still stratified portions of conglomerates, microconglomerates, medium- to coarse-sandstones and thin-bedded sandstone-mudstones, structurally arranged in m-sized, usually rootless, recumbent and isoclinalic folds, and locally with a staked appearance roughly resembling S-vergent imbrications (fig 7.34).

The most part of the IBTs and EBTs trends present a significant coincidence with axial planes of IBFs and EBFs, thus evidencing the possible evolutionary relationships between these elements (see attached Panel n. 2).

In this case, MDPs seems to be more continuous and abundant than the BDP; the matrix locally represents ~ 40-50% of the rock exposure and it is preferentially localized around blocks (sometimes showing transitional boundaries) and along the ductile shear surfaces characterizing folds axial planes (fig 7.35).

Qualitative microscopic analyses carried on a matrix sample coming from the enclosing matrix of the R2/d sub-unit (sample R2/dEM) show more or less similar compositions and structures observed in the other examples.

The overall appearance resembles a matrix-sustained texture with major rounded granules surrounded by haloes of fine-grained lithologies (finer than enclosing matrix) and thin enveloping calcite veneers.

Moreover here it is possible to observe the presence of unconsolidated fine-grained sandstone fragments sharing irregular shapes and transitional contacts, sometimes forming an intergranular pseudo-matrix. The deformation mechanism is attributed an overall independent particulate flow (fig 7.36).

The diagnostic feature of this sub-unit is the presence of m- to ten of m-sized blocks of still slightly stratified graded orthoconglomerates, with carbonatic and sedimentary clasts, and generally m-sized fragments of sandy-marly successions, containing shell debris, nummulites and glauconitic grains, and thus belonging to shelfal environments.

The carbonatic component (both rounded pebbles with bioerosional holes and sub-angular debris) seems to increase upwards, as well as the plant fragment content (*i.e.* cm-sized wood coal clasts), discovered also within the sandstone blocks (fig 7.37).

The meso-structural analysis of this sub-unit allows the interpretation of a mass transport direction toward southern sectors (see attached Panel n. 2).

As observed for the underlying R2/c sub-unit, it is possible to recognize some localized structural overprinting roughly occurring in the same area (Rio Pratorotondo and Rio dei Corvi W-E alignment; see above). Here, re-folded, double vergent and box-folds with sub-vertical axial planes are quite well represented, sharing a more or less structural parallelism with the elongated hosting band (fig 7.38).

7.5.5 R2/e sub-unit

The top of the R2/d sub-unit is characterized by the presence of a discontinuous m- to tens of m-thick interval (up to 30 m) composed of a para-conglomerate (*i.e.* matrix-supported) with prevailing carbonatic elements (subordinately sedimentary and ophiolitic), and "floating" m-sized fragments of thin-bedded sandstone packages, arranged in particular lenticular shapes (fig 7.39).

The component cobbles and pebbles are sometimes characterized by lithodome burrowings, and the enclosing matrix commonly contains cm-sized and variously oxidized plant fragments (fig 7.40).

Apart this isolated m-sized blocks, the R2/e sub-unit results almost completely composed of MDPs, with an enclosing matrix showing an overall pebbly mudstone appearance.

The qualitative microscopic analyses carried on a matrix sample characterizing this sub-unit (sample R2/eEM), has evidenced similar textures and composition of that found in the R2/d matrix: the general texture is matrix-dominated with calcite and fine-grained haloes bordering major granules. Also in this case matrix injections are recognizable along grain boundaries. Some scattered microfossils are present (radiolarians?).

As hypothesized for the majority of the other examples, the inferred deformation mechanism is a generalized independent particulate flow (fig 7.41).

The R2/e sub-unit shows highly variable thickness over short distances, and locally is almost completely missing.

The mesoscopic features of this interval are comparable with those presented by para-conglomeratic layers cropping out in the basal portions of the R3 unit, particularly well observable in the M. Roccone outlier.

The upper boundary to the overlying stratified R3 unit is underlined by the presence of a medium- to thick-bedded, graded, coarse- to fine-grained sandstone layer with irregular base and a usually sharp top, which drapes the R2/e sub-unit smoothing its upper surface asperities (fig 7.42).

This bed is quite well recognizable at the top of the R2/e sub-unit in the whole Pessola Valley outlier, varying in thickness from ~ 80 cm to ~ 2 m also within the same outcrop.

The lithologic composition is similar to that shared by F5 strata of the R3 unit, with mainly carbonatic and subordinately ophiolitic clastic detritus. The lower portion of this layer is characterized by the presence of abundant rip-up clasts (up to ~ 40 cm across) coming from the underlying R2/e subdivision.

The base is usually irregular, with load-casts and clay-chip clustering, showing downward cutting cusps (up to 2-3 m long) filled of coarse-grained sand coming from the bed, which found into the fine-grained lithologies of the underlying R2/e sub-unit, sometimes also recognizable as completely detached elongated "pseudo-nodules" (fig. 7.43). These features are similar to those observed by Van der Merwe *et al.* (2009) on top of some thick-bedded (~ 50 m) debris flow-like deposits (blocky-flow-deposits?) from the Karoo Basin, in South Africa.

This bed commonly rests upon a discontinuous interval (from 0 to 3-4 thick) of very oxidized, mixed and un-mixed pebbly-cobbly sandstone-mudstone, resembling the classical appearance of an intraclast-rich "impact breccia", which represents some kind of transitional zone between the overlying coarse-grained bed and the underlying matrix-sustained conglomerate of the R2/e sub-unit (fig. 7.44). Sometimes, the elements constituting this horizon seem to show a weak imbrication pattern toward southern directions. This association is locally represented also in the Mt. Roccone outlier (see below).

The top of this bed is usually laminated, locally sharp, amalgamated to the overlying layer, or showing a faint grading to the upper mud partings. The laminated portion has an average thickness of ~ 40-50 cm and is mainly composed of oblique, and subordinately in lower part, parallel laminations complicated by fluid-escape structures. Where the conditions are favorable, ripple trains (wave-length ~ 5-10 cm) with opposite facing fore-sets and in-phase ripples (*i.e.* climbing ripples) are observable (fig. 7.45).

These features allow the interpretation of this bed as the deposit of a ponded, high-density bipartite flow, strongly associated with the R2/e sub-division.

7.6 Mt. Roccone outlier

In this outlier the R2 unit is represented by the R2/d and R2/e subdivisions and it is almost completely exposed, from base to top, only in the western sector (fig. 7.46).

Here the R1 unit is completely missing and the R2 unit directly overlies a thin and discontinuous horizon of MMP and, locally, the Ligurian substratum.

In the eastern sector, the R2 unit punctually crops out in few isolated places, and the upper, lower and internal contacts are completely covered.

7.6.1 R2/d sub-unit

Here, this sub-unit is relatively well organized in a basal MDP and an upper BDP, with an intermediate interval characterized by isolated blocks, representing the transition between these two portions, for an estimated minimum and maximum thickness of ~ 50 m and ~ 100 m, respectively (fig. 7.47).

The basal MDP is composed of a pebbly/sandy mudstone containing well-rounded mainly carbonatic pebbles and sub-rounded cobbles (up to ~ 40 cm), with discrete portions of marly lithologies probably belonging to the underlying MMP unit. The lower contact is quite unclear, due to the poor lihologic contrast between these units, but however identifiable by the sudden appearing and upward increasing of pebbles and blocks.

The intermediate part is composed of isolated blocks (up to ~ 8 m across) of ortho-conglomeratic lenses and deformed biocalcarenite-rich sandstone-mudstone blocks, floating within the above-mentioned matrix. Here the matrix shows an overall increasing in the sedimentary pebbles content, probably deriving from the ortho-conglomeratic lenses.

Few EBT and EBF are recognizable within these two subdivisions, mainly represented by intrafolial folds affecting matrix pseudo-stratification. Notably, in the intermediate portion, ortho-conglomeratic and sandstone blocks seem to share an apparent S-verging imbrication.

The upper BDP is essentially composed of shelfal-derived well-stratified blocks (up to ~ 40 m across), sharing well developed IBT and IBF.

Examples of such elements and structures are presented in fig. 7.48.

These generally thin-bedded sandstone-mudstones are sometimes characterized by preserved bioturbation evidences (*i.e. ophiomorpha*- and *planolites*-like). Component sandstone beds share abundant *nummulites*, shell debris and glauconite nodules. These elements are observable as scattered grains dispersed within the matrix (fig. 7.49).

In the eastern sector, nonetheless the diffuse tectonic disturbance and the poor exposures, this sub-unit seems to rest directly upon the AVV lithologies.

In the central-western sector (*i.e.* Poggiolo section), the internal structures, both folds and shear surface, appear sub-verticalized even maintaining their planar relationships. This structural arrangement, similar to that observed in the central-eastern sector of the Pessola Valley (*i.e.* Pratorotondo section), seems to be produced by a roughly WSW-directed generalized buckling (fig. 7.50).

7.6.2 R2/e sub-unit

This sub-unit is particularly well developed in this outlier, continuously marking the R2 unit top across the whole investigated area with an estimated thickness varying from ~ 5 m to ~ 30 m.

The overall appearance is that of a hyper-concentrated flow deposit (*i.e.* debris flow facies; F2 facies of Mutti, 1992), locally resembling a muddy para-conglomerate, characterized by well-rounded cobbles and pebbles (mainly of carbonatic and sedimentary origin) and cm- to m-sized, poorly consolidated bed or bedset fragments and blocks (generally smaller than those observable in the underlying R2/d sub-unit) enclosed within a pebbly mudstone matrix. The uppermost portion is characterized by the discontinuous presence of a coarse sand-sustained para-conglomerate, which seems to grade upwards to the basal "impact breccia" of the overlying distinctive sandstone layer (see below). Sometimes ten of m-sized blocks of fine-grained, thin-bedded lithologies have been observed, especially in the southern sectors (fig. 7.51).

These blocks are usually arranged as rootless isoclinal and sheath-like folds, with roughly phacoidal and lenticular shapes. As observed for the underlying R2/d sub-unit, the well-rounded elements sometimes show evidence of lithodome holes, and abundant variously coalified plant fragments (with dimensions up to ten of centimeters) are scattered within the matrix (fig. 7.52).

This sub-unit shows only little appreciable evidence of syn-sedimentary structures as EBTs, roughly indicating an overall movement direction toward the southern sectors. A weakly recognizable element imbrication seems to be present in the upper clast-supported portion, resembling an overall palaeo-transport direction toward southern sectors.

The overall characteristics of this sub-unit, as well as its composition, are quite similar to that observable in the Pessola Valley outlier, sharing also some features (mainly compositional) with the conglomeratic beds present within the R3 unit succession.

As observed in the Pessola Valley outlier, the top of this sub-unit is locally characterized by the presence of a thick (~ 1-2 m) coarse- to medium-grained and graded sandstone bed, smoothing and leveling the R2 unit upper surface (fig. 7.53).

This layer crops out only in the northwestern part of the outlier (*i.e.* Mangiarosto section), pinching out in short distance toward the S and E, and completely disappearing in some places, nonetheless a possible thin-bedded equivalent seems to be observable (Poggiolo section). Regarding this latter area, it is worth to note that the disappearing of this layer coincides with the localized buckling-related verticalization of the underlying R2/d structures (see above).

In the outcrop area, this bed shows an irregular massive basal portion, characterized by fluid escape structures, differential loading-related structures and concentrations of clayey rip-up clasts (sometimes composed of pebbly mudstone) coming from the underlying R2/e sub-division.

In this case the top surface is represented by a sharp amalgamation formed by an overlying F5-like bed, which truncate its upper fine-grained and laminated portion. Laterally, this laminated portion (about 40-60 cm thick) shows oblique and subordinately, parallel lamination, commonly affected by fluid escaping-related convolutions, and characterized by the diffused presence of still recognizable ripple trains sharing vertical alternating opposite verging directions (fig. 7.54).

As observed in the Pessola Valley outlier, this bed overlies a discontinuous (from 0 to 2-3 m thick) interval composed of mixed and unmixed coarse- to fine-grained lithologies (mainly pebbly-cobbly mudstones and sandstones), characterized by a strongly oxidized appearance (*i.e.* "impact breccia" facies; see chap. 4). This horizon passes downward into the para-conglomeratic and clay-rich lithologies of the R2/e subdivision with a generally transitional contact, sometimes relatively sharp (marked by evident lithologic contrast) with evidence of upward fluid-escape structures rooted in the underlying R2/e sub-unit lithologies.

7.7 Caffaraccia section (Mt. Barigazzo outlier)

In this area, the R2 unit represents the uppermost member of the Ranzano Unit. Here the quality and quantity of outcrops is quite poor, but anyway still enough to allow the recognition of R2/c and R2/d subdivisions.

The former seems to be directly juxtaposed upon the R1 unit, but the basal contact is entirely covered, as well as the upper transition to the R2/d sub-unit. The roof contact of the R2/d sub-unit is no more visible being completely eroded away (fig. 7.55).

7.7.1 R2/c sub-unit

The upper and lower boundaries of this sub-unit are covered, avoiding the correct estimation of its thickness, however tentatively calculated on the basis of cropping out points and inferred stratigraphic level in ~ 10-40 m.

Nevertheless, some well-exposed sections in the southern sector have permitted the recognition of a lower part characterized by MDPs and an upper one essentially composed of BDPs, locally showing lateral heteropic relationships.

The MDPs are represented by an almost homogeneous pebbly mudstone with hydroplastically-deformed mudstone and fine sandstone intra-clasts, and scattered well-rounded pebbles (rarely reaching cobble dimensions), sometimes showing lithodome holes. These lithologies seem to belong to the underlying thin-bedded lithofacies of the R1 unit and subordinately to the PZO unit. EBF are scarce and EBT are virtually absent.

The BDPs are instead characterized by the presence of ten of m-sized soft-sediment deformed blocks of thin-bedded, fine- to medium-grained sandstone and mudstones, belonging to the R1 and PZO units (and intermediate terms?; V. Chiarone Unit of Mutti *et al.*, 1995). These blocks share evidence of IBT, mainly developed along or at low-angle in respect to the stratification, and associated IBF; the structural analysis of such structures suggests mass transport directions roughly toward SSE (fig. 7.56).

As pointed out before, the upper contact is not exposed, but some evidence of MDPs bearing lithologies belonging to the R2/d sub-unit has been recognized at the very top of R2/c outcrops in the southern sector, probably indicating the transition to the upper unit.

7.7.2 R2/d sub-unit

This sub-unit has an estimated thickness varying from ~ 30 m to ~ 120 m, and it is mainly represented by BDPs, while few scattered evidence of MDPs are present at the very base of the concerning outcrops, probably close to the supposed basal boundary.

This configuration is also visible in the irregular mounded morphology of the area, where differential erosion marks topographic highs roughly corresponding to culminations of the blocks.

The BDPs are composed of tens of m-sized (up to hundred of meters across) internally soft sediment deformed blocks of still stratified and generally massive (or poorly graded), medium-to thick-bedded, fine- to coarse-grained sandstones, with relatively high carbonatic content (fig. 7.57).

These blocks are characterized by abundant *nummulites* and shell debris, and generally lacking of marly partings; sometimes, isolated well-rounded pebbles have been observed, generally within the lower portions of beds. Within well-stratified portions it is also possible to observe several evidences of vertical- (*i.e. ophiomorpha*-like) and horizontal trending (*i.e. planolites*-like) bioturbation traces (fig. 7.58).

These blocks are internally affected and separated by syn-sedimentary shear zones marked by tens-of cm-thick matrix-rich bands, represented by a pebbly sandstone with scattered *nummulites*,

composed of material coming from adjacent blocks. Here, the discrimination of IBT from EBT is quite difficult because of the involvement of same lithologies and the limited lateral-vertical extent of the outcrop, generally exposing only the relatively less deformed central part of the block, leaving covered its boundaries.

The EBF are poorly represented, while the IBF are quite commonly distributed inside and at the edge of blocks, probably related to the IBT an EBT development.

The most prominent structures observed in this sub-unit are some meso-scale fluid escape structures, which inject the pebbly sandstone matrix upwards and laterally along internal weak zones and boundaries of these blocks, bending the stratification, where still present (fig. 7.59).

7.8 List of figures

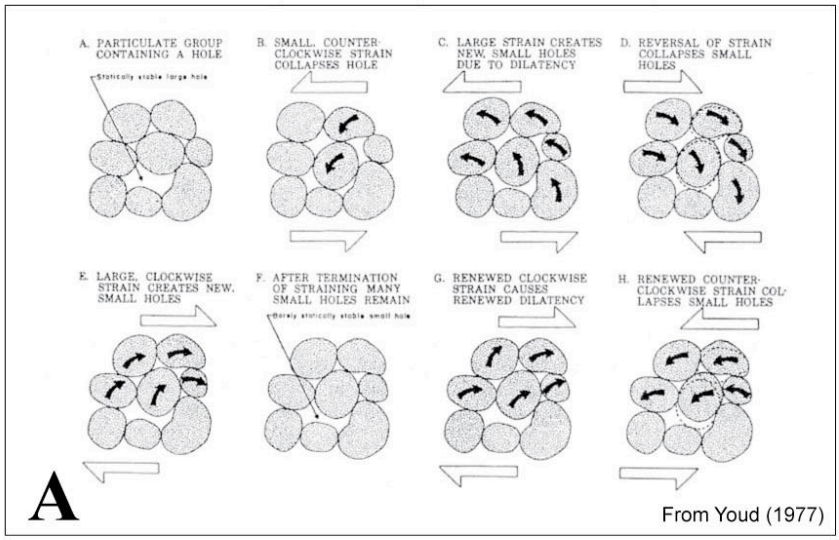

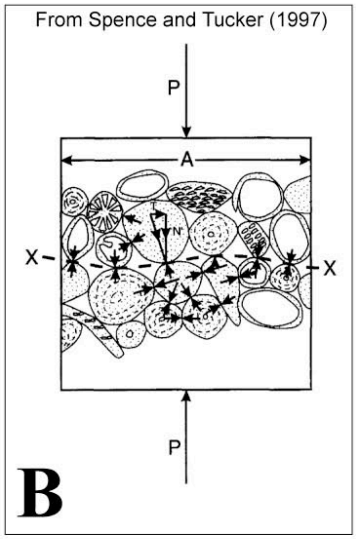

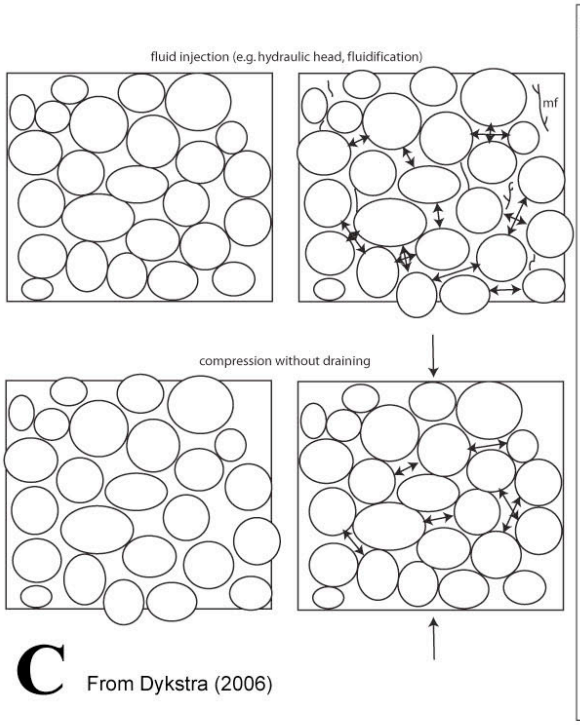

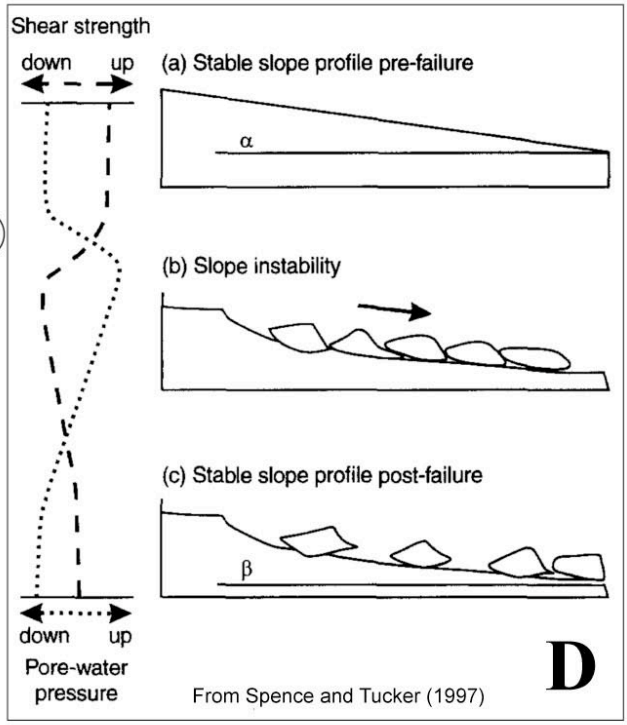

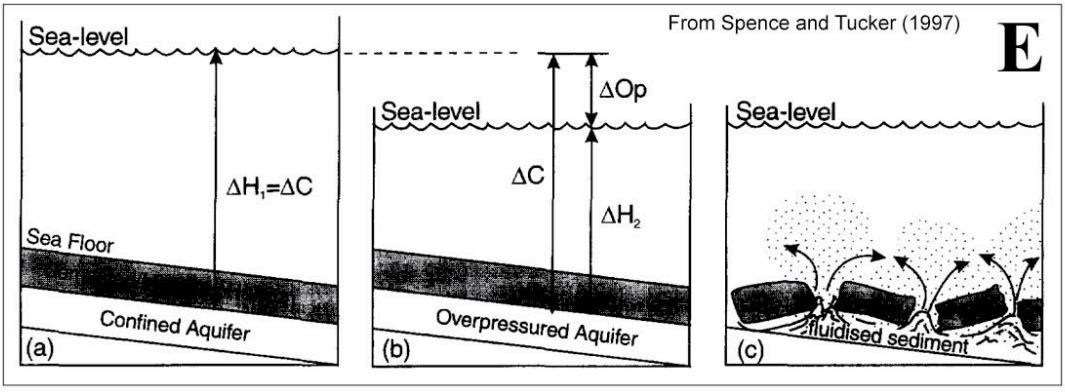

Figure 7.1 - **A**: Cross section of particulate group showing packing changes that occur during cyclic loading (from Youd, 1977). Excess pore pressure generates during the collapse of grain packing in undrained conditions.

B: Relationship between total stress (σ), effective stress (σ') and pore-water pressure (u) illustrated for a plane x-x (after Craig, 1974) in a submarine grainstone in which interstitial pore-space between grains is filled with water. The apparent wavy plane x-x approximates to a flat surface on a large scale. Resistance to a normal load P, produced by a hydrostatic head and sediment weight over an elemental area A, is divided between the sediment skeleton through intergranular forces at grain-grain contacts and pressure in the pore-water. Intergranular forces are randomly oriented and variable in magnitude, reflecting grain arrangement along the plane x-x. They may be resolved into normal (N') and tangential (T) vectors. Effective normal stress is the sum of all N' components which impinge on the plane x-x within the area A, divided by the area:

$\sigma' = \Sigma N'/A$

Total stress is given by the total load divided by the total area:

$\sigma = P/A$

Assuming point contact between grains, pore-water acting on the plane over the entire area A:

$P = \Sigma N' + uA \qquad i.e. \quad \sigma = \sigma' - u$

From Spence and Tucker (1997).

C: Cartoon exhibiting two different ways to generate elevated pore fluid pressures: fluidization *s.s.* and liquefaction *s.s.* (slightly modified from Dykstra, 2005b).

D: Effects of overpressure in triggering low-angle slope instability. (a) Kinematically stable slope. (b) Preferential increase in pore-water pressure (dotted line) at a discrete horizon beneath the seafloor (for causal mechanisms see text) results in local decrease or total loss in shear strength (dashed line). Overlying more-lithified sediment above this *décollement* horizon undergoes sliding as coherent slide blocks if the existing slope-parallel shear stress exceeds this decreased shear strength. Overpressure at the *décollement* plane helps propagate downslope transport by increasing debris buoyancy. (c) During transport, overpressure is dissipated and there is a corresponding recovery in shear strength and increase in basal friction at the drcollement plane. If this occurs rapidly the slope may return to a stable condition with there being no modification in slope angle post-failure (*i.e.*, $\alpha = \beta$). From Spence and Tucker (1997).

E: Preservation of original pore-water pressure in a confined aquifer trapped beneath a micritic or preferentially cemented impermeable cap may become overpressured during a relative sea-level fall. (a) Confined aquifer with pore-water pressure ΔC preserves the hydrostatic head ΔH_1 at the time of its initial hydrostatic isolation. (b) Relative sea-level reduces hydrostatic head confining pressure ΔH_2, causing the confined aquifer to become overpressured by an amount ΔO_P (c) Overpressure may re-equilibrate by fluid violently migrating upwards, fracturing the confining cap rock and resulting in catastrophic seafloor instability and potential megabreccia formation during relative sea-level falls and lowstands. From Spence and Tucker (1997).

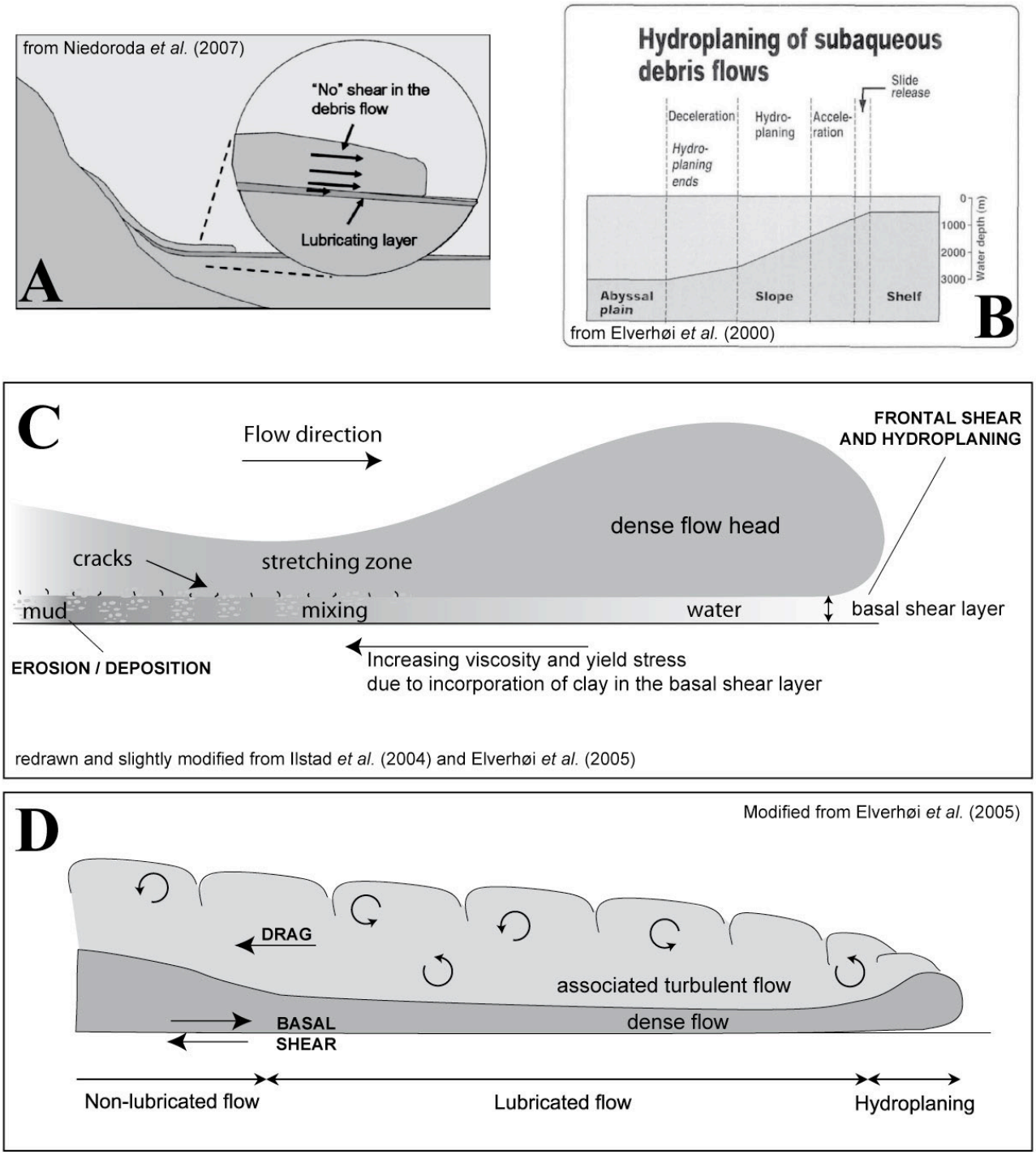

Figure 7.2 - **A**: Schematic cartoon showing a possible example of debris flow, lubricated by the high-water-content sediment zone (from Niedoroda *et al.*, 2007). Hydroplaning may occur throughout the frontal incorporation of water from both surrounding environment and form the loose sediment characterizing the water-sediment interface.

B: Sketch of a conceptual slope profile showing the inferred bathymetric domains possibly characterized by hydroplaning development in the slide evolution from (Elverhøi *et al.,* 2005).

C: Schematic representation of head–neck–body structure of clay rich debris flow with hydroplaning head, slow body and stretching neck. Redrawn and slightly modified from Ilstad *et al.* (2004) and Elverhøi *et al.* (2005).

D: Schematic representation showing a dense flow with an associated turbulent flow on top, mainly generated by the dragging effect with the ambient water. Hydroplaning, lubricating and non-lubricating basal domains are indicated. Modified from Elverhøi *et al.* (2005).

Scale-independent (fractal) appearance of matrix
~ W
~ E
R2/d
R2/e
b = block
R2/d-e sub-unit
Mt. Roccone outlier
South-central sector
(Confine section)
A
B
C
D

Figure 7.3 - Photos showing the scale-independent appearance of the matrix, from the whole outcrop-scale (**A**) to the hand specimen-scale (**D**). This fractal appearance is also appreciable up to the cartographic-scale and down to the microscopic-scale. All examples are from the R2/d sub-unit (upper part Specchio R2 unit) cropping out in the Mt. Roccone outlier (see text for discussion). Hammer and one Euro coin for scale (2,2 cm in diameter).

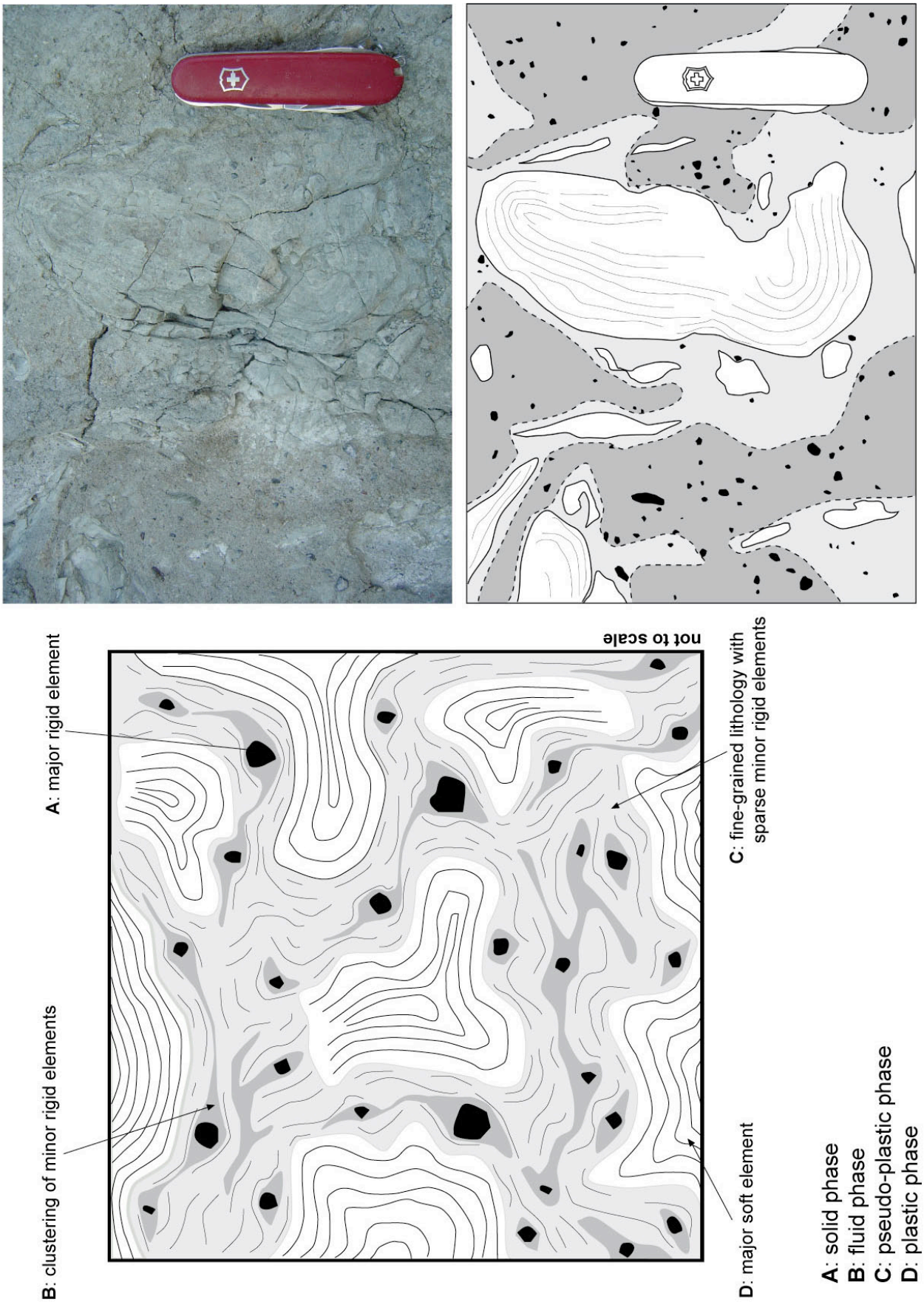
not to scale
A: major rigid element
B: clustering of minor rigid elements
C: fine-grained lithology with sparse minor rigid elements
D: major soft element
A: solid phase
B: fluid phase
C: pseudo-plastic phase
D: plastic phase

Figure 7.4 - Conceptual scheme showing the main components (*i.e.* phases) of the herein described matrix (left), and a photo (with relative interpretation) representing the matrix appearance on outcrop (right). The photo is taken within a ductile shear zone characterizing a block-dominated portion (BDP proto-matrix; see text for discussion) of the R2/a sub-unit, in the Pessola Valley outlier (knife for scale, 9 cm long). This interpretation is allowed by many other careful observations carried on several ancient MTDs on outcrop (mainly form Northern Apennines and South-central Pyrenees). This figure was presented at the 27th I.A.S. Meeting of Sedimentolgy of Alghero (Sardinia, Italy) (Mutti *et al*., 2009).

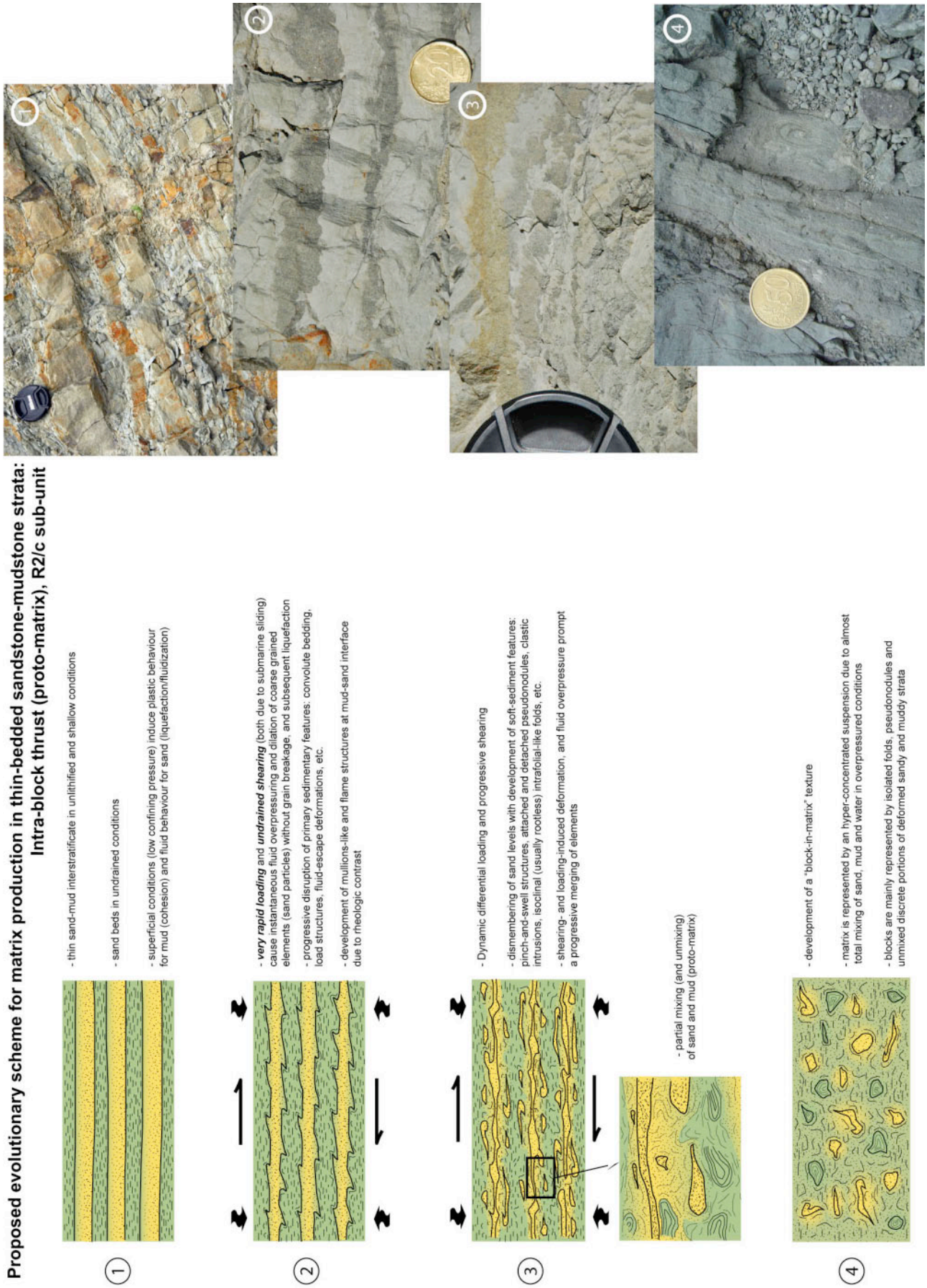
Proposed evolutionary scheme for matrix production in thin-bedded sandstone-mudstone strata:
Intra-block thrust (proto-matrix), R2/c sub-unit
- thin sand-mud interstratificate in unlithified and shallow conditions
- sand beds in undrained conditions
- superficial conditions (low confining pressure) induce plastic behaviour for mud (cohesion) and fluid behaviour for sand (liquefaction/fluidization)
- very rapid loading and undrained shearing (both due to submarine sliding) cause instantaneous fluid overpressuring and dilation of coarse grained elements (sand particles) without grain breakage, and subsequent liquefaction
- progressive disruption of primary sedimentary features: convolute bedding, load structures, fluid-escape deformations, etc.
- development of mullions-like and flame structures at mud-sand interface due to rheologic contrast
- Dynamic differential loading and progressive shearing
- dismembering of sand levels with development of soft-sediment features: pinch-and-swell structures, attached and detached pseudonodules, clastic intrusions, isoclinal (usually rootless) intrafolial-like folds, etc.
- shearing- and loading-induced deformation, and fluid overpressure prompt a progressive merging of elements
- partial mixing (and unmixing) of sand and mud (proto-matrix)
- development of a "block-in-matrix" texture
- matrix is represented by an hyper-concentrated suspension due to almost total mixing of sand, mud and water in overpressured conditions
- blocks are mainly represented by isolated folds, pseudonodules and unmixed discrete portions of deformed sandy and muddy strata
1
2
3
4

Figure 7.5 - Conceptual cartoon representing an attempt to define evolutionary stages of matrix development through progressive stratal disruption of a thin-layered sequence, as it is thought to occur within IBTs and in overall BDPs (intra-block thrusts and block-dominated portions, respectively) of the Specchio Unit component MTDs. This kind of matrix is herein identified as proto-matrix, due to its "intrabasinal" character. Photos are taken form the R2/c sub-unit in the Pessola Valley outlier (Specchio and Pessola sections). See text for discussion.

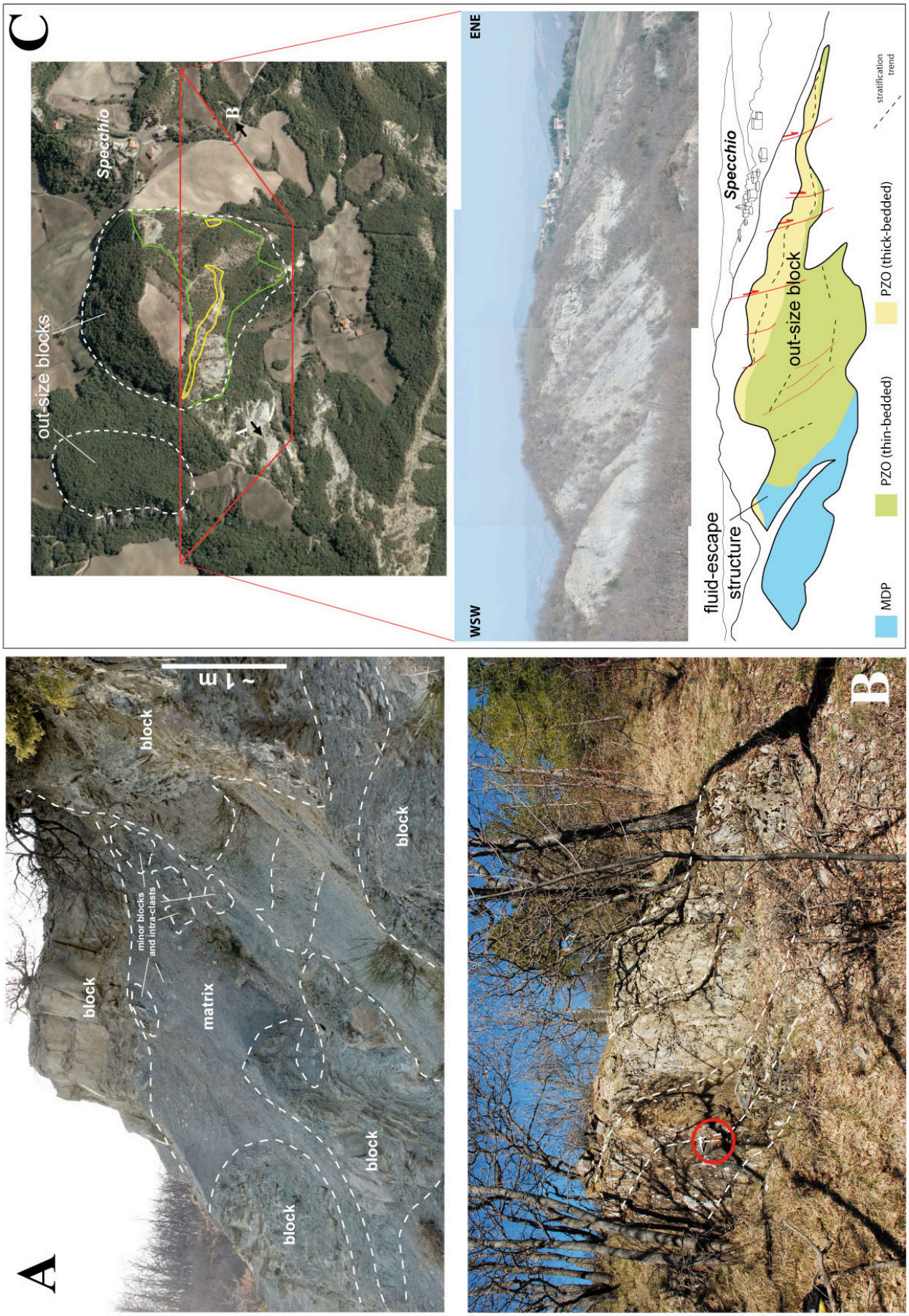
C
Specchio
out-size blocks
B
A
ENE
WSW
Specchio
out-size block
fluid-escape
structure
stratification
trend
PZO (thick-bedded)
PZO (thin-bedded)
MDP
A
~ 1 m
block
block
block
block
block
block
minor blocks
and intra-clasts
matrix
B

Figure 7.6 - **A**: Examples of hydroplastically deformed blocks and intraclasts of thin-bedded sandstone-mudstone beds, contained within a fine-grained matrix. Elements' boarders are labeled. Basal MDP of the R2/c sub-unit (Servazzola section, Pessola Valley outlier; see attached Panels n. 1 and 2). See satellite map slice in C for location.
B: Well-lithified, sub-angular, marlstone-limestone block of Ligurian origin (*i.e.* Helmintoyd Flysch units) characterizing the lowermost portions of the R2/c sub-unit (Specchio section, Pessola Vally outlier; see attached Panels n. 1 and 2). Stratification surfaces are labeled. Hammer for scale (circled). See satellite map slice in C for location.
C: Satellite map slice of the area nearby the Specchio settlement (from www.viawindowslive.com/VirtualEarth.aspx) and panoramic photo-mosaic (and interpretation) of the outcrop exposing the southern margin of the largest out-size block recognized in the Pessola Valley area (for location see attached Panel n. 1). Out-sized blocks emerge from the local topography as local hill culminations (boarders are roughly labeled). The block is composed of thick- and thin-bedded strata belonging to the PZO unit; note the large-scale dome-like fluid injection affecting the block's margin to the left of the photo-mosaic. This fluid expulsion-related structure bends the local stratification trend. The syn-sedimentary normal faults observable in the right side of the photo-mosaic are probably related to early post-depositional re-arrangement of the block, as well as the fluid escape structure.

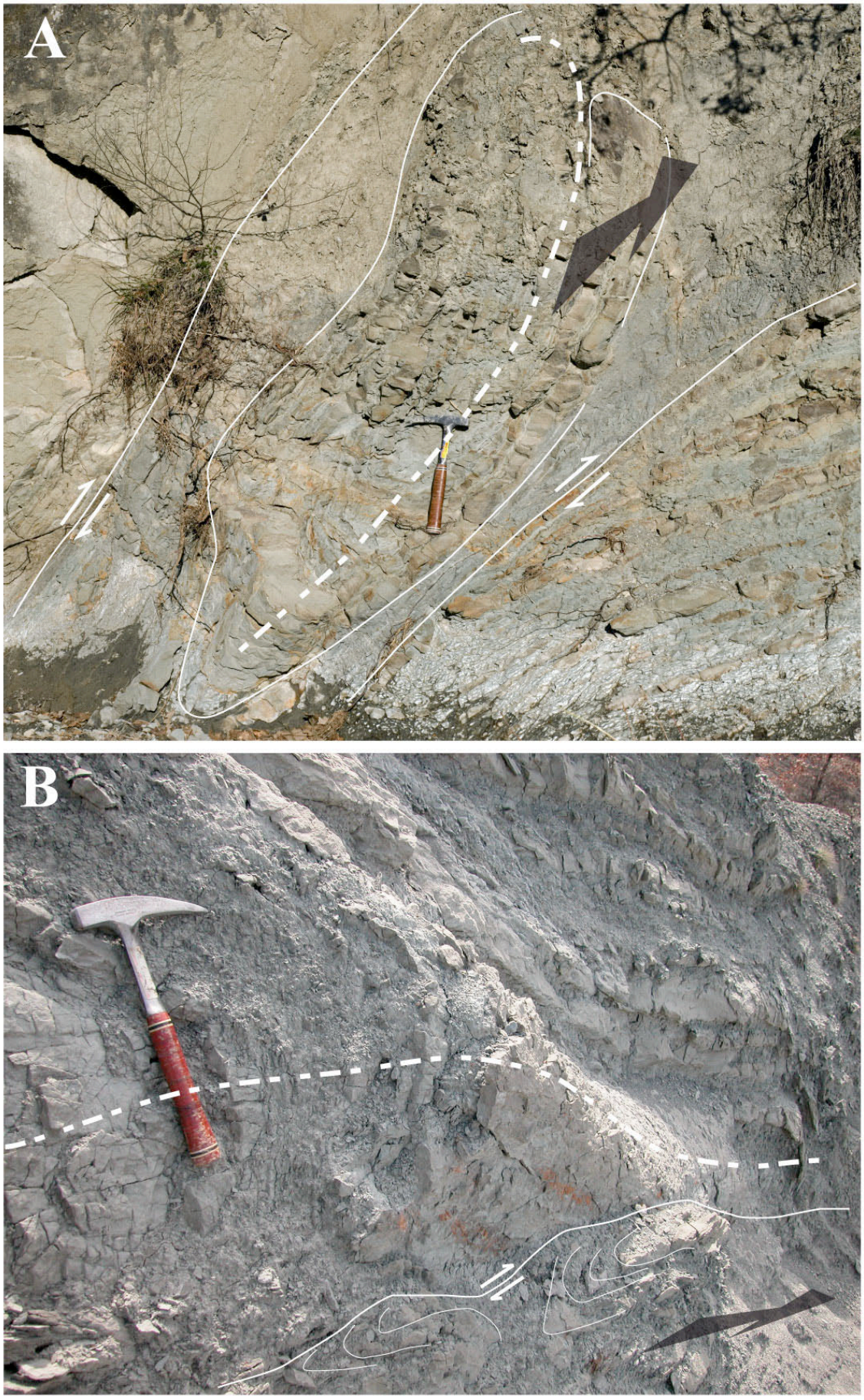
A
B

Figure 7.7 - Examples of meso-scale folds showing complex sheath fold-like geometry. Elements' boarders, shear surfaces (and shear sense) and traces of sheath fold axial planes (dotted lines) are labeled. Transparent black arrows roughly indicate the inferred local transport direction. Hammer for scale.

A: Sheath fold developed in a matrix-dominated portion, and comprised within a ductile shear zone separating two m-sized blocks. The cut is roughly oblique, at high-angle with the sheath fold long axis (note the curving axis and the "concentric" appearance of internal deformed stratification). Sub-unit R2/c (Dx Pessola section, Pessola Vally outlier; see attached Panels n. 1 and 2).

B: Sheath fold developed within a thin stratified block. Note the gently curving appearance of the fold axis. This fault is thought to develop in response to the dragging force exerted on the underlying shear surface. Sub-unit R2/d (Pratorotondo section, Pessola Vally outlier; see attached Panels n. 1 and 2).

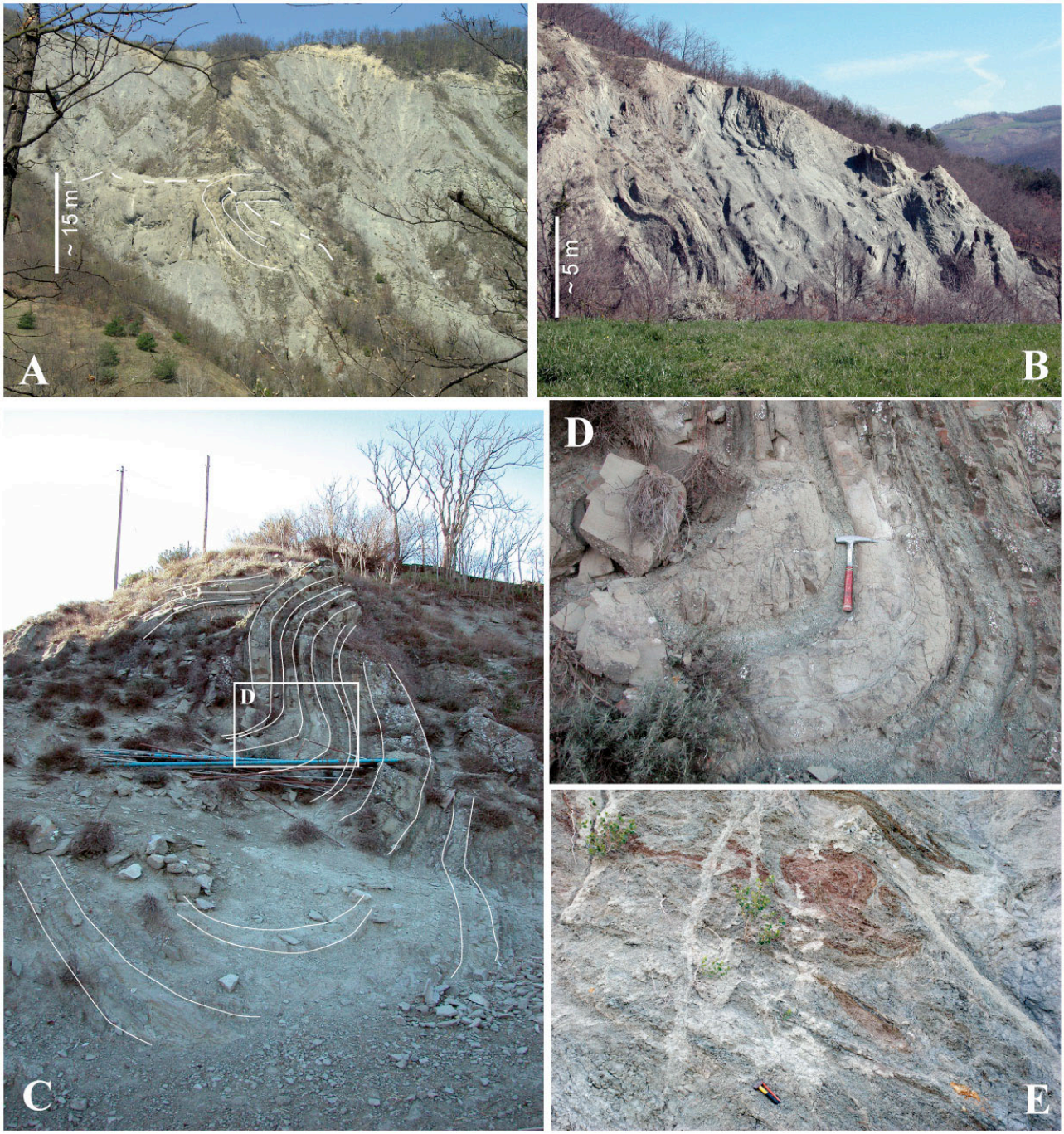
~ 15 m
A
~ 5 m
B
D
C
D
E

Figure 7.8 - Outcrop examples of fold types recognized.

A: Tens of meters-sized, rootless and roughly isoclinalic fold composed of thick-bedded, coarse-grained sandstones; its vergence is roughly toward the S. Stratification surfaces and axial plane trace (dotted line) are labeled. Sub-unit R2/d (Sx Pessola section, Pessola Vally outlier; see attached Panels n. 1 and 2).

B: Complex association of folds comprised within a fine-grained matrix affected by interference patterns. The poor erosional relief is due to the fine-grained and thin-bedded lithologies of blocks, similar to those composing the enclosing matrix. These folds are characterized by a SE-vergent appearance, complicated by a generalized verticalization of axial planes. Sub-unit R2/c (Pettenati section, Pessola Vally outlier; see attached Panels n. 1 and 2).

C: Sinistral, roughly S-vergent meso-scale fold developed in medium-bedded sandstone strata, comprised within a block-dominated portion of the sub-unit R2/c (Specchio section, Pessola Vally outlier; see attached Panels n. 1 and 2). Stratification surfaces are labeled.

D: Close-up of C, showing in detail the hinge zone of the meso-scale fold. Note the overall thickening of the core zone and the development of folding-related cm-spaced joint system affecting the outer convex limb. Hammer for scale. Sub-unit R2/c (Specchio section, Pessola Vally outlier; see attached Panels n. 1 and 2).

E: Fluidal-like complex intra-folial folds developed within a matrix-dominated portion of the R2/b unit (Sx Pessola section, Pessola Vally outlier; see attached Panels n. 1 and 2). These folds are underlined by elongated bands of Ligurian-related fine-grained lithologies (AVV units), un-mixed with the enclosing matrix. Hammer for scale.

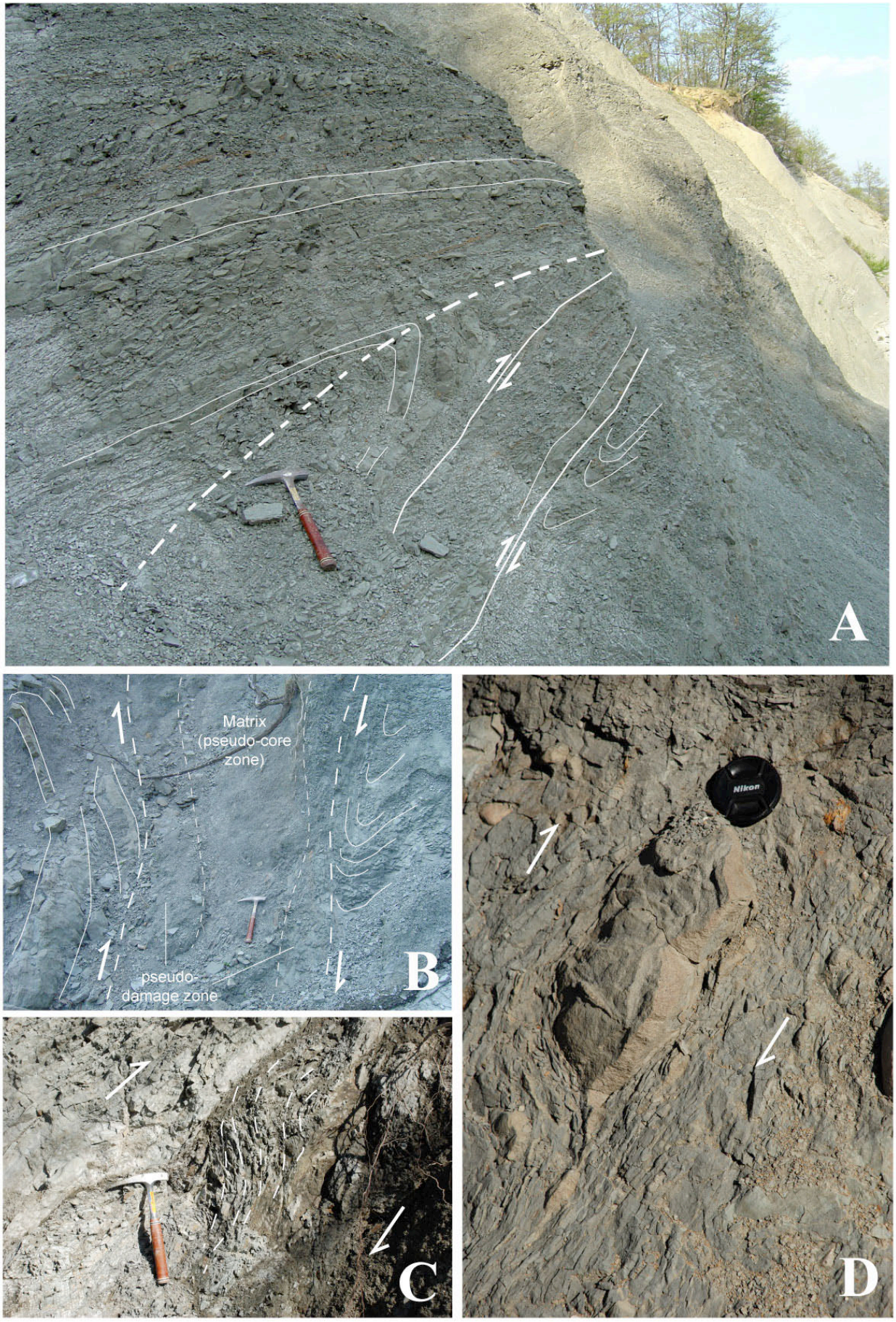
A
Matrix
(pseudo-core
zone)
pseudo-
damage zone
B
C
Nikon
D

Figure 7.9 - A: Intra-block thrust and related intra-block fold developed within a block-dominated portion made up of fine-grained and thin-bedded strata. Note the gently curving axis of the fold, unraveling its sheath-like nature, and the drag folds, indicative of the shear sense. The light grey bands developed along shear surfaces are composed of pebbly mudstone matrix. Beds, shear surfaces (and shear sense) and fold axis (dotted line) are labeled. Hammer for scale. Sub-unit R2/c (Tintori section, Pessola Vally outlier; see attached Panels n. 1 and 2).

B: Shear zone marked by abundant pebbly mudstone matrix. Drag folds developed along boarders give shear sense. Here it is possible to observe the apparent internal organization of the shear zone, resembling that of classical fault zones, with a pseudo-core region bounded by pseudo-damage zones (herein identified by block-matrix transition). Locally a closely spaced and pervasive foliation has been observed. Stratification and bounding surfaces of the shear zone (dotted lines) are labeled. Hammer for scale. Sub-unit R2/c (Tintori section, Pessola Vally outlier; see attached Panels n. 1 and 2).

C: Example of SC-like structure used as kinematic indicator within shear zones. Structural trend and shearing sense are labeled. Hammer for scale. Sub-unit R2/c (Dx Pessola section, Pessola Vally outlier; see attached Panels n. 1 and 2).

D: Example of sigmoidal-like structure used as kinematic indicator within shear zones. Shearing sense is indicated. Camera lens cap for scale, 7 cm in diameter. Sub-unit R2/c (Dx Pessola section, Pessola Vally outlier; see attached Panels n. 1 and 2).

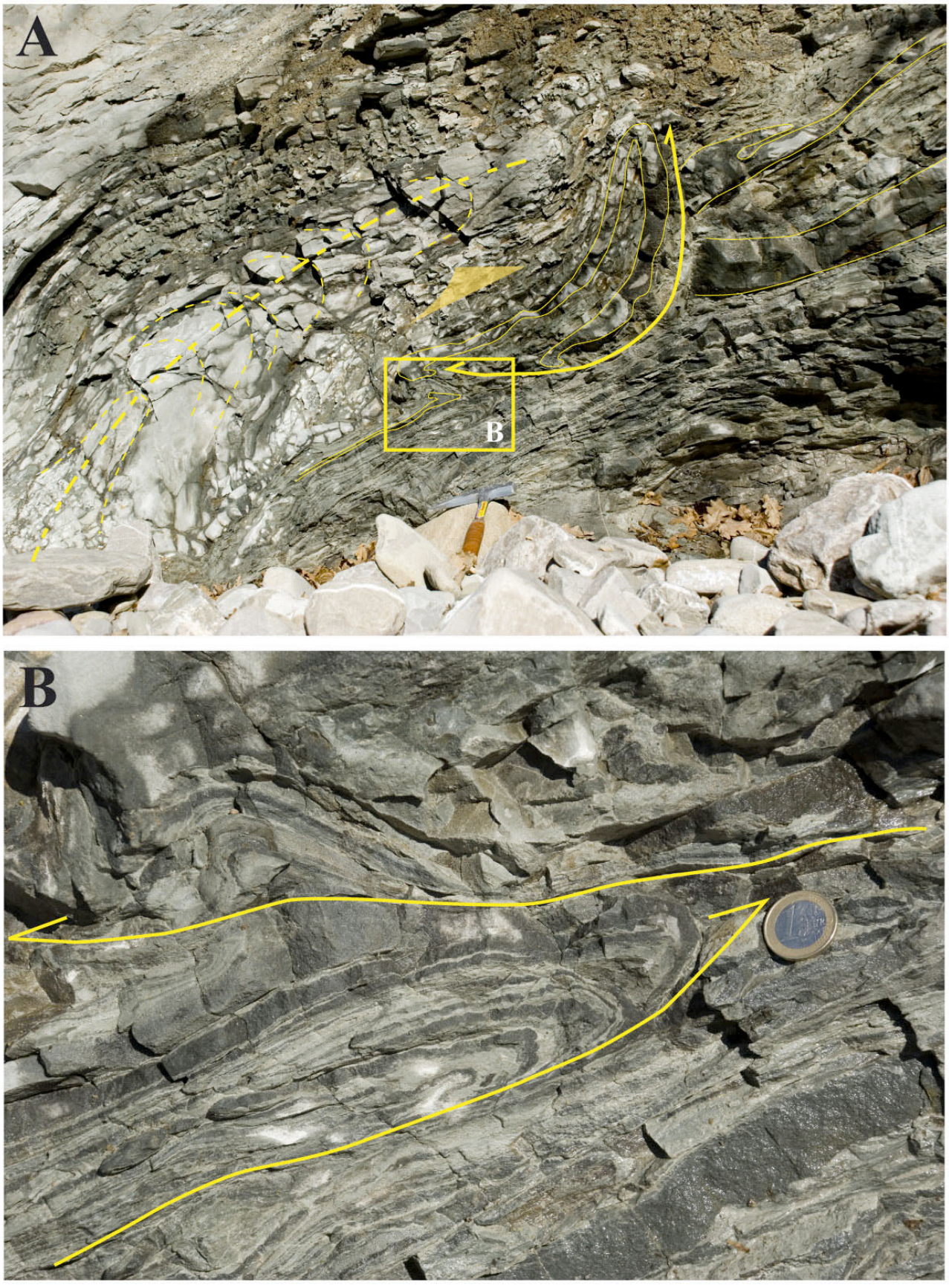
A
B
B

Figure 7.10 - A: Shear zone characterized by complex structural arrangement. Here it is possible to observe a sheath-like fold (axis indicated by dotted yellow line) comprised within the matrix characterizing the shear zone. The transparent yellow arrow indicates the overall inferred transport direction. The bounding blocks shear surfaces are complicated by some opposite verging shear surfaces (backthust-like geometries), forming "pop up"-like structures and box-like folding. Main stratification surfaces and structural lineaments are labeled. Hammer for scale. Sub-unit R2/c (Dx Pessola section, Pessola Vally outlier; see attached Panels n. 1 and 2).

B: Close-up of A, showing in detail two minor shear surfaces characterized by opposite directions. Note the unconsolidated style shared by drag folds. One Euro coin for scale, 2,2 cm in diameter.

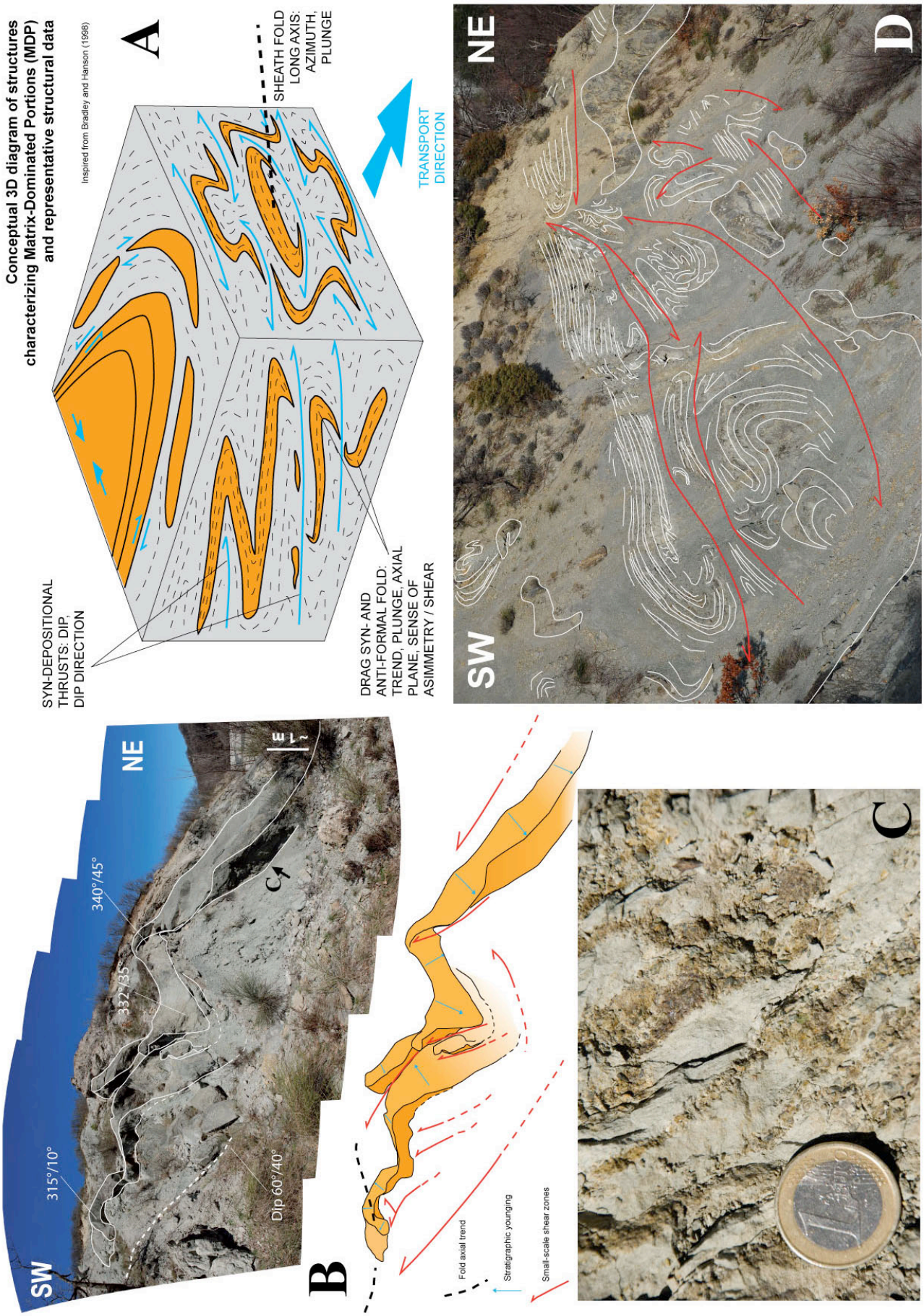
Conceptual 3D diagram of structures characterizing Matrix-Dominated Portions (MDP) and representative structural data
Inspired from Bradley and Hanson (1998)
A
SHEATH FOLD LONG AXIS: AZIMUTH, PLUNGE
TRANSPORT DIRECTION
SYN-DEPOSITIONAL THRUSTS: DIP, DIP DIRECTION
DRAG SYN- AND ANTI-FORMAL FOLD: TREND, PLUNGE, AXIAL PLANE, SENSE OF ASIMMETRY / SHEAR
SW
NE
D
B
315°/10°
340°/45°
332°/35°
Dip 60°/40°
C1
Fold axial trend
Stratigraphic younging
Small-scale shear zones
C

Figure 7.11 - A: Conceptual block diagram representing structural associations (inspired from Bradley and Hanson, 1998), which characterize matrix-dominated portions (MDP). Representative features and relative structural data used for kinematic analysis are indicated.

B: Photo-mosaic and relative interpretation of a meso-scale folding system involving a single thick, coarse-grained sandstone bed, comprised within a MDP (structural data are labeled). Asymmetries and relative vergences are roughly uniform (apart from few minor backthrusts). Note the sheath-like geometry shown by the main fold apex (left side). This structural association represents the longitudinal side of the block diagram shown in A. Sub-unit R2/d (Sx Pessola section, Pessola Vally outlier; see attached Panels n. 1 and 2).

C: Close-up of B, showing the incipient admixing of coarse- and fine-grained lithologies close to the folded bed boundaries (progressive matrix development). One Euro coin for scale, 2,2 cm in diameter.

D: Photo and line drawing of a MDP characterized by complex folding due to the occurrence of several opposite verging shear zones, causing a generalized buckling of structures. This structural association represents the transversal side of the block diagram shown in A. Sub-unit R2/c (Servazzola section, Pessola Vally outlier; see attached Panels n. 1 and 2).

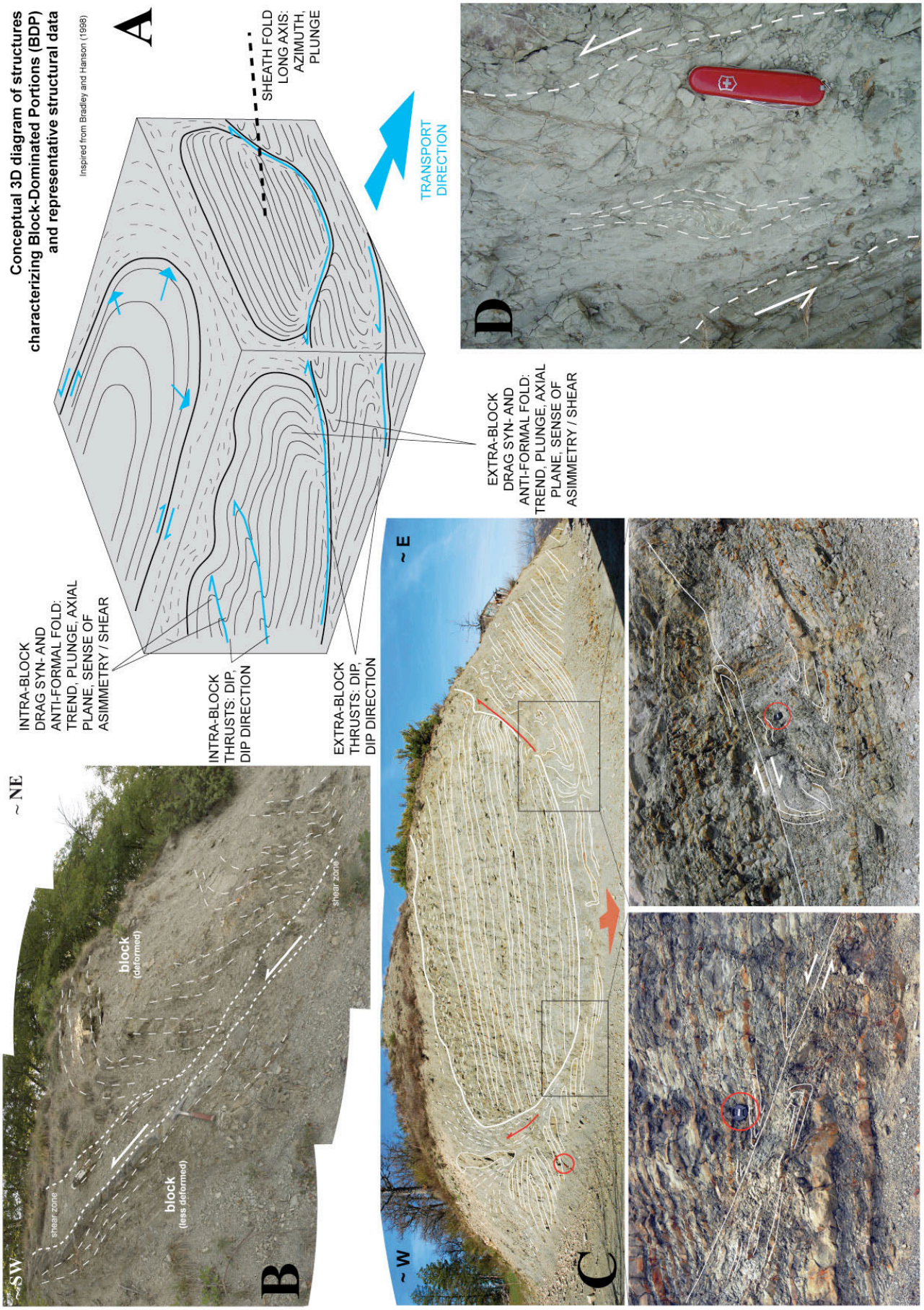
A
Conceptual 3D diagram of structures characterizing Block-Dominated Portions (BDP) and representative structural data
Inspired from Bradley and Hanson (1998)
SHEATH FOLD LONG AXIS: AZIMUTH, PLUNGE
TRANSPORT DIRECTION
INTRA-BLOCK DRAG SYN- AND ANTI-FORMAL FOLD: TREND, PLUNGE, AXIAL PLANE, SENSE OF ASIMMETRY / SHEAR
INTRA-BLOCK THRUSTS: DIP, DIP DIRECTION
EXTRA-BLOCK THRUSTS: DIP, DIP DIRECTION
EXTRA-BLOCK DRAG SYN- AND ANTI-FORMAL FOLD: TREND, PLUNGE, AXIAL PLANE, SENSE OF ASIMMETRY / SHEAR
D
~ NE
~SW
shear zone
block (less deformed)
block (deformed)
shear zone
B
~ E
~ W
C

Figure 7.12 - A: Conceptual block diagram representing structural associations (inspired from Bradley and Hanson, 1998), which characterize block-dominated portions (BDP). Representative features and relative structural data used for kinematic analysis are indicated.

B: Photo-mosaic and line drawing representing a shear zone underlined by a matrix horizon, which separates two block portions (intra-block thrust). This structural association represents the longitudinal side of the block diagram shown in A. Hammer for scale. Sub-unit R2/c (Servazzola section, Pessola Vally outlier; see attached Panels n. 1 and 2).

C: Photo-mosaic and line drawing showing a block overriding another through an intra-block shear zone. The cut is roughly perpendicular to the main inferred transport direction (transparent red arrow). Close-ups show in detail the same shear surface characterized by two apparent opposite shear senses. This structural association represents the transversal side of the block diagram shown in A. Hammer and Camera lens cap (circled) for scale, 7 cm in diameter. Sub-unit R2/c (Specchio section, Pessola Vally outlier; see attached Panels n. 1 and 2).

D: Detail of an intra-block shear zone. Note the matrix development and the occurrence of sigmoidal-like structures, used as kinematic indicators. Knife for scale, 9 cm long. Sub-unit R2/d (Fosio section, Pessola Vally outlier; see attached Panels n. 1 and 2).

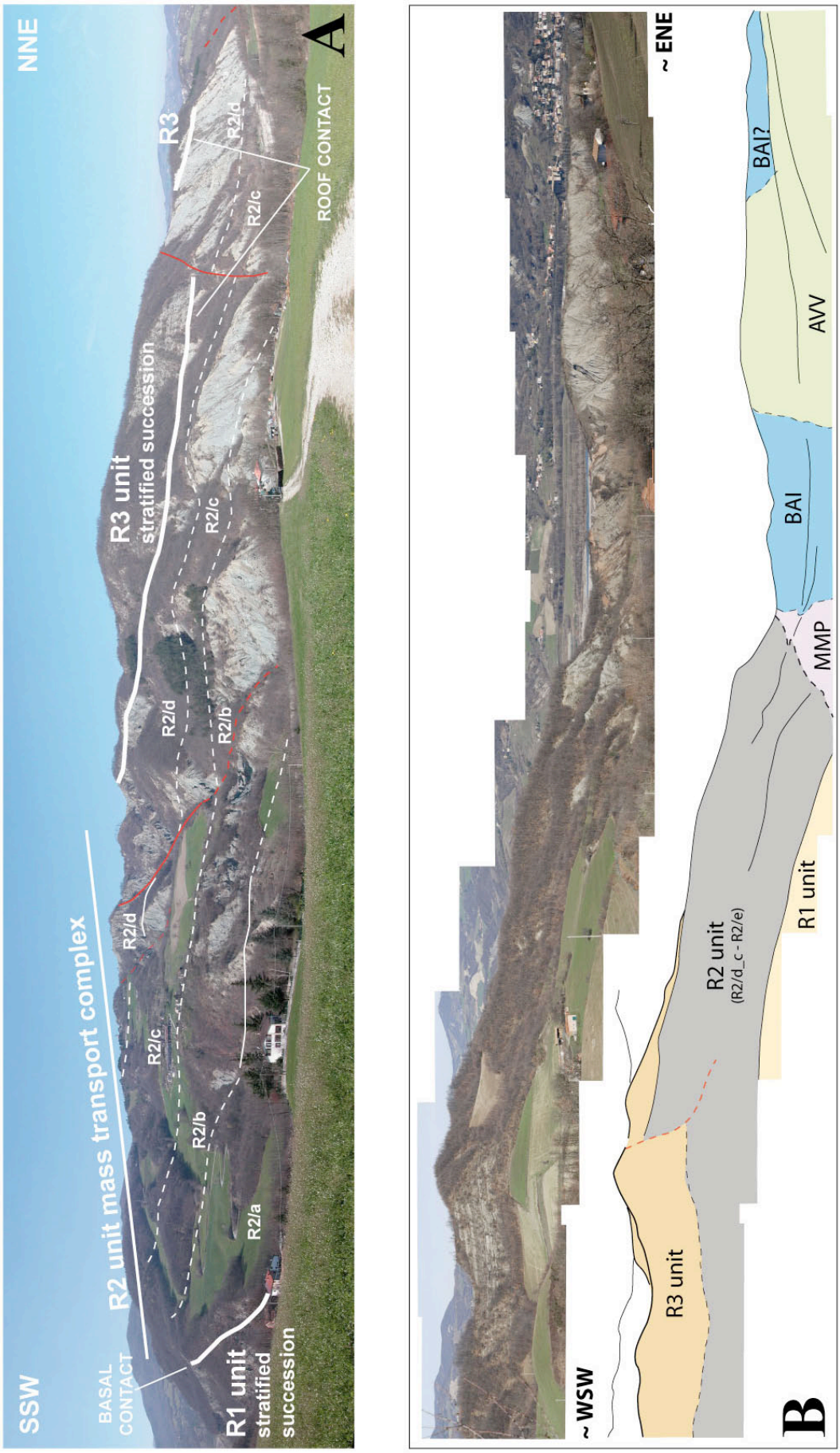
A
SSW
NNE
BASAL CONTACT
R2 unit mass transport complex
R1 unit
stratified succession
R3 unit
stratified succession
R3
ROOF CONTACT
R2/a
R2/b
R2/c
R2/d
B
~ WSW
~ ENE
R3 unit
R2 unit
(R2/d_c - R2/e)
R1 unit
MMP
BAI
BAI?
AVV

Figure 7.13 - A: Panoramic photo-mosaic showing the western side of the Pessola Valley outlier, with line drawing of the internal subdivisions from base to top.

B: Panoramic photo-mosaic and relative interpretation of the northeastern margin of the Pessola Valley outlier. Note the lacking of the lower subdivisions of the Specchio Unit R2 (*i.e.* R2/a and R2/b) and of the R1 unit (*i.e.* wedging out toward NE), causing the juxtaposition of the R2 unit directly over the Ligurian units (*i.e.* AVV units), with the local discontinuous occurrence of MMP and BAI units. Note that the AVV unit seems to show an overall large-scale, dome-like structure, bordered by BAI unit lithologies; this kind of configuration is thought to be produced by shale diapirism, affecting the outlier margins, and probably concurring to the local confinement conditions.

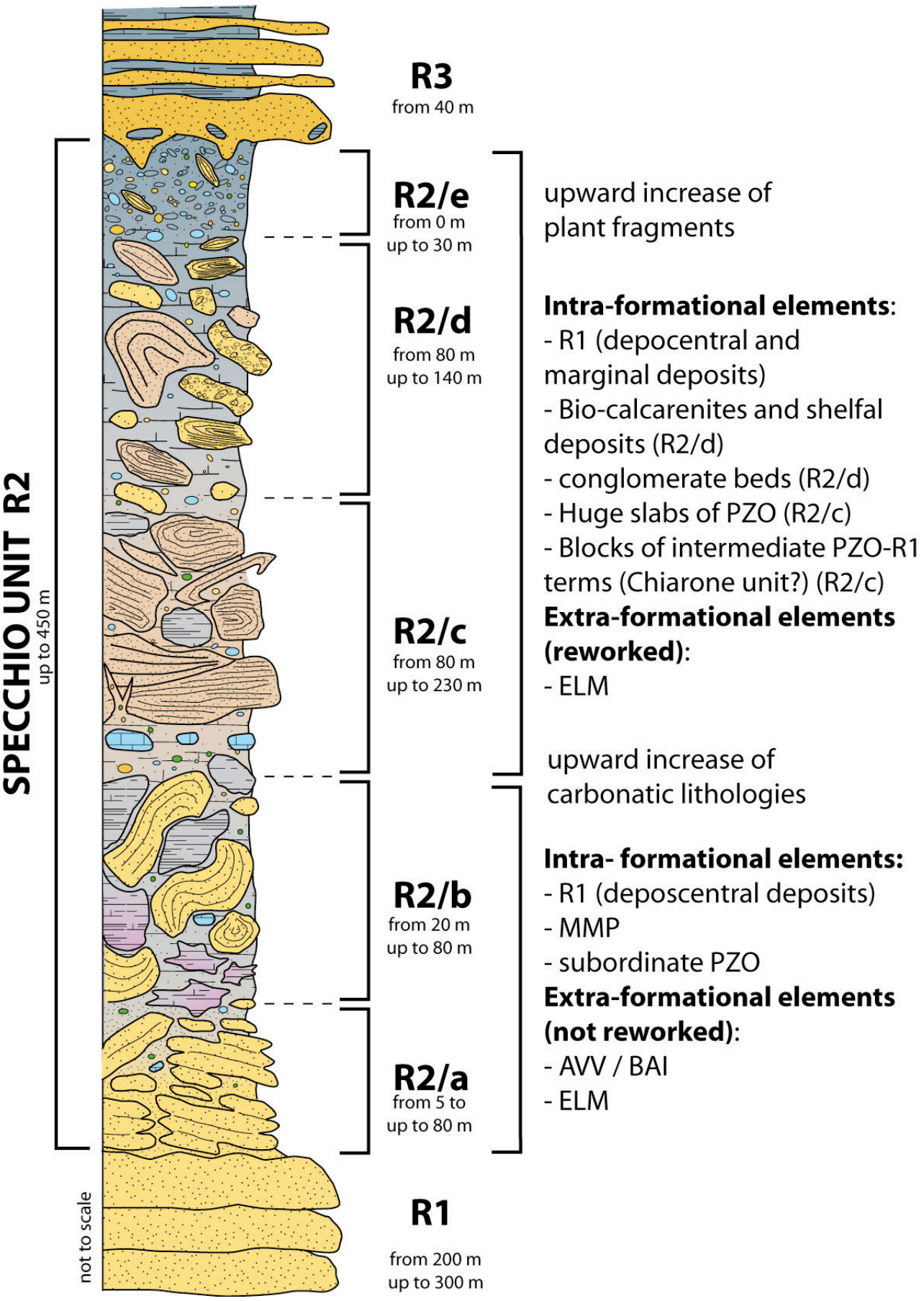
SPECCHIO UNIT R2
up to 450 m
not to scale
R3
from 40 m
R2/e
from 0 m
up to 30 m
R2/d
from 80 m
up to 140 m
R2/c
from 80 m
up to 230 m
R2/b
from 20 m
up to 80 m
R2/a
from 5 to
up to 80 m
R1
from 200 m
up to 300 m
upward increase of
plant fragments
Intra-formational elements:
- R1 (depocentral and
marginal deposits)
- Bio-calcarenites and shelfal
deposits (R2/d)
- conglomerate beds (R2/d)
- Huge slabs of PZO (R2/c)
- Blocks of intermediate PZO-R1
terms (Chiarone unit?) (R2/c)
Extra-formational elements
(reworked):
- ELM
upward increase of
carbonatic lithologies
Intra- formational elements:
- R1 (deposcentral deposits)
- MMP
- subordinate PZO
Extra-formational elements
(not reworked):
- AVV / BAI
- ELM

Figure 7.14 - Simplified stratigraphic scheme of the Pessola Valley outlier focusing on the internal subdivisions of the Specchio Unit R2. Main features and characteristics, as well as inferred thickness, are described.

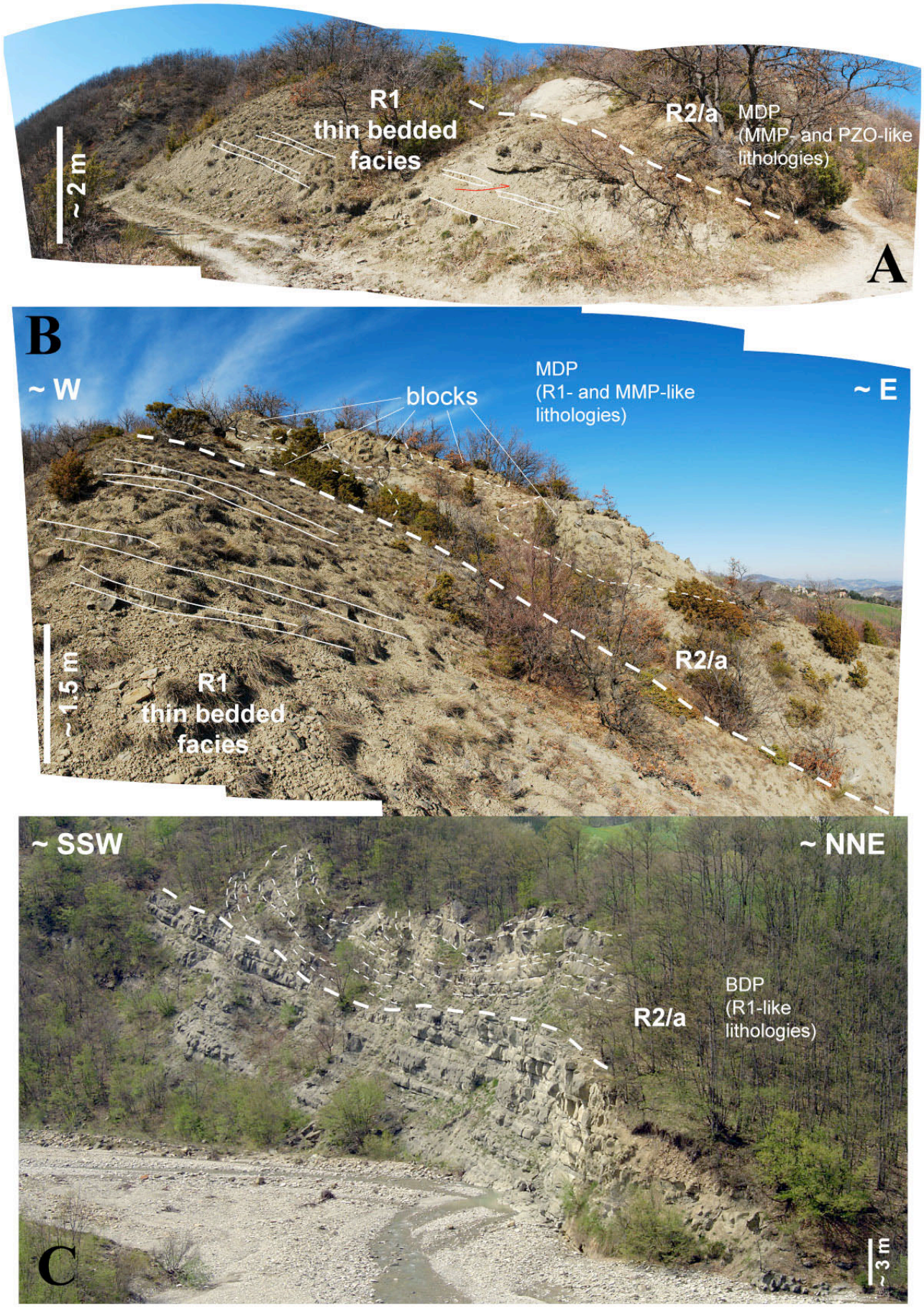
R1
thin bedded
facies
R2/a
MDP
(MMP- and PZO-like
lithologies)
~ 2 m
A
B
~ W
blocks
MDP
(R1- and MMP-like
lithologies)
~ E
R2/a
~ 1.5 m
R1
thin bedded
facies
~ SSW
~ NNE
R2/a
BDP
(R1-like
lithologies)
C
~ 3 m

Figure 7.15 - Outcrop examples of the lower boundary of the Specchio Unit R2 with the underlying R1 unit in the southern margin of the Pessola Valley outlier.

A: Lower boundary in the western sector of the Servazzola section (see attached Panels n. 1 and 2). Here the R2 unit (*i.e.* R2/a sub-unit) overlies the thin-bedded facies of the R1 unit. Note that the R1 unit beds show evidence of low angle minor thrusting, few meters below the contact. Main contact and some stratification surfaces are labeled.

B: Lower boundary in the eastern sector of the Servazzola section (see attached Panels n. 1 and 2). Also in this case the R2/a sub-unit is mainly represented by MDPs and overlies the thin-bedded facies of the R1 unit (wedging out toward the E because of the erosion operated by R2/a sub-unit emplacement. Main contact, blocks' boundaries and some stratification surfaces are labeled.

C: Lower boundary in the Fopla section (see attached Panels n. 1 and 2). In this case, the R2/a unit is in contact with the typical thick-bedded facies of the R1 unit, and it is almost entirely composed of BDPs, with stratified blocks coming from the underlying unit. Note the irregular trending of the basal surface, testifying significant erosion and involvement of the substrate. Main contact and still recognizable stratification surfaces within the blocks are labeled.

WSW
ENE
R2/a
~ 2 m
R1 unit
A

~ S
~ N
R2 unit
(R2/a)
R1 unit
B
~ 3 m

Figure 7.16 - A: Another view of the outcrop shown in fig 7.15 C. Here it is possible to observe how the basal surface of the R2/a sub-unit seems to ramp roughly toward the W, cutting the underlying strata. Main contact and still recognizable stratification surfaces are labeled.

B: Detail of the basal surface in the southern Sx Pessola section (see attached Panels n. 1 and 2), roughly ramping toward the N. Here it is possible to observe dragging-related recumbent synclines, caused by the roughly N-ward R2/a sub-unit emplacement. Main contact and stratification surfaces are labeled.

Figure 7.17 - An example of angular calcareous (limestone) block, and associated primary enveloping fissile shale, enclosed within a MDP of the R2/a sub-unit (Fopla section, Pessola Vally outlier; see attached Panels n. 1 and 2). Due to this lithologic association, these kinds of elements are thought to come from shale-rich Ligurian chaotic complexes, without significant sedimentary reworking. Other Ligurian-related elements recognized in this subdivision are mainly varicolored shales (reddish and greenish) belonging to the AVV unit, and usually observable on outcrop as passively folded and deformed elongated bands dispersed within the matrix. Hammer for scale.

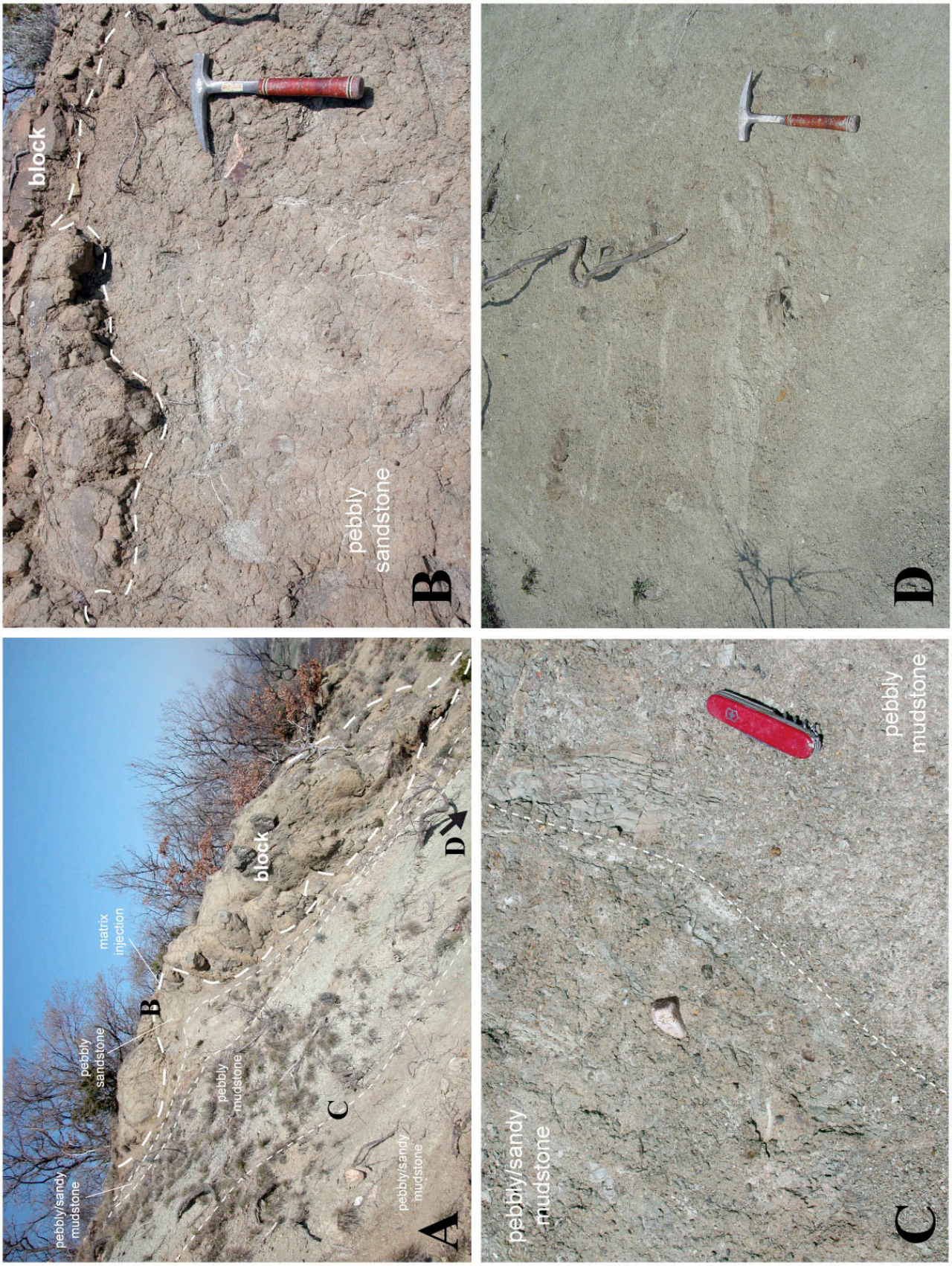
block
pebbly sandstone
B
D
pebbly/sandy mudstone
pebbly mudstone
C
pebbly/sandy mudstone
pebbly sandstone
matrix injection
B
pebbly mudstone
block
C
D
pebbly/sandy mudstone
A

Figure 7.18 - Outcrop examples of R2/a sub-unit main components.

A: Overall appearance of a MDP of the R2/a sub-unit in the Servazzola section. Here it is possible to observe a highly deformed sandstone block enclosed within a fine-grained matrix, showing compositional difference point to point. The matrix closely surrounding the block is enriched in sandy component (pebbly sandstone), becoming more and more fine-grained (pebbly mudstone) to the outer portions. This fact is probably related to the progressive dismembering of blocks in favor of matrix production. Note the injection-structure affecting the block. Block boundaries and different matrix domains are labeled.

B: Close-up of A, showing in detail the pebbly sandstone appearance of the matrix close to the block (within the injection). Note the presence of angular carbonatic clasts and mudstone intra-clasts, as well as the irregular boundaries of the block, showing detaching pseudo-nodules prone to be enclosed within the matrix. Hammer for scale.

C: Close-up of A, showing the contact between the pebbly/sandy mudstone matrix and the pebbly mudstone one. The pebbly/sandy mudstone it is herein thought to represent the transition between the enclosing matrix *s.s.* and the block-surrounding matrix. Knife for scale, 9 cm long.

D: Close-up of A, showing in detail the enclosing matrix *s.s.* (pebbly mudstone). Note the "fluidal" appearance given by the passive folding of poorly consolidated mudstone elements (in this case belonging to the MMP unit). The preferred elongation of these elements, coupled with the overall trend of the different matrix domains, seem to develop more or less evident pseudo-stratification. Hammer for scale.

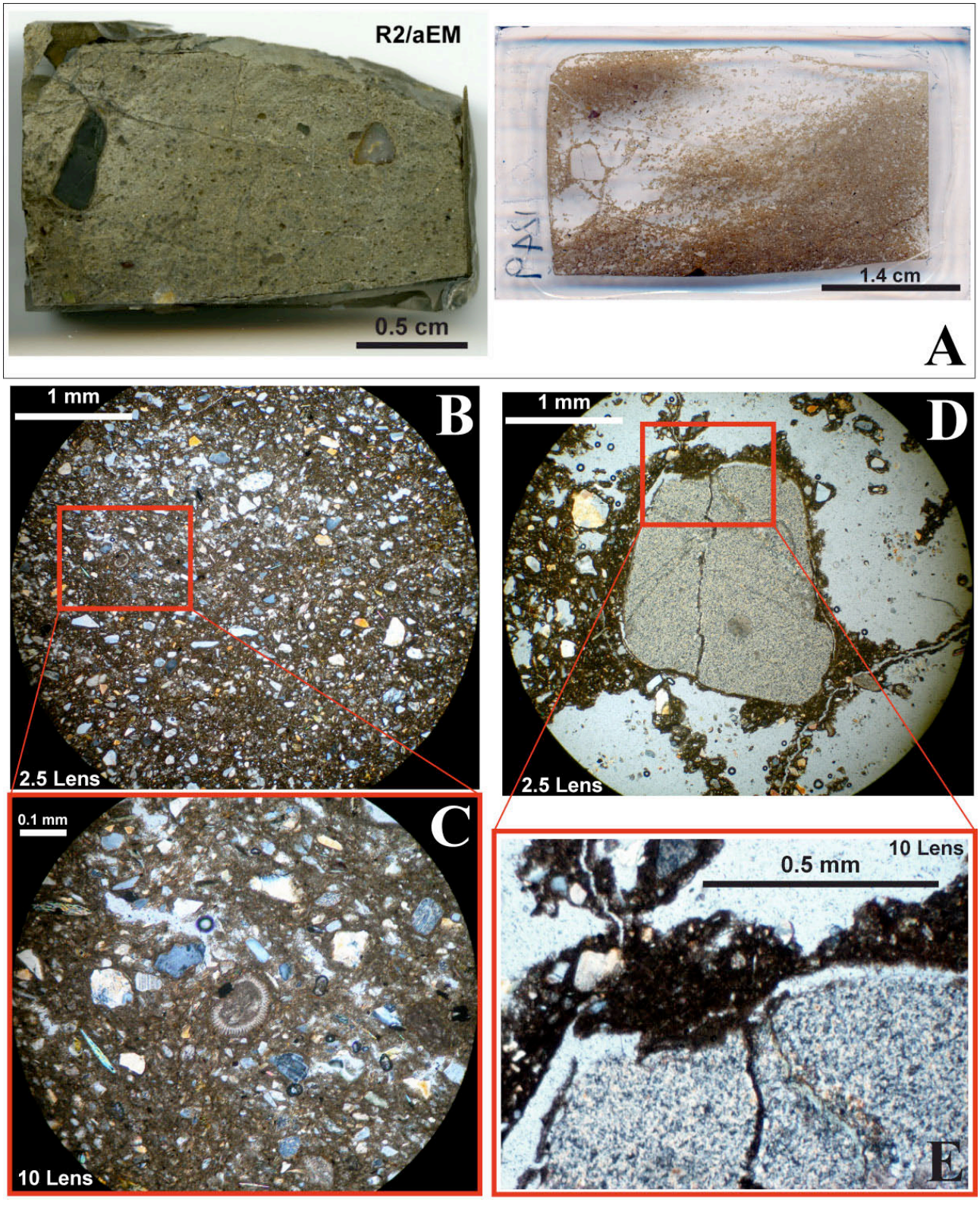
R2/aEM
0.5 cm
1.4 cm
A
1 mm
B
2.5 Lens
1 mm
D
2.5 Lens
0.1 mm
C
10 Lens
0.5 mm
10 Lens
E

Figure 7.19 - A: Thin section and polished counter-cut of the sample R2/aEM, taken form the enclosing matrix of a MDP of the R2/a sub-unit in the Servazzola section. Due to the generally unconsolidated nature and the fine-grained lithologies, some material (not consolidated by the resin) has been taken away, leaving blanket regions as observable in the thin section (to the right). Where not specified, the photos have been taken with an optical microscope, through polarized light. For location see chap. 3.

B: Overall microscopic appearance of the fine-grained portions of the matrix. Note the general "block-in-matrix" appearance and the occurrence of both rounded and angular grains, sustained by a finer lithology.

C: Close-up of B, showing in detail the appearance of the finer granulometric population of the matrix. Note the occurrence of well-preserved microfossils (radiolarians?) and the "fluidal" appearance of the finer matrix, enveloping grains and filling voids between elements.

D: Example of a sub-rounded lithic grain showing a fracture filled with finer material. These elements commonly share thin haloes of calcite along the borders.

E: Close-up of D, showing in detail the injection of fine-grained matrix within the fracture. This evidence may indicate fluid overpressure conditions of the matrix, possibly up to hydrofracturing. Note the thin calcite halo (transparent) enveloping the grain.

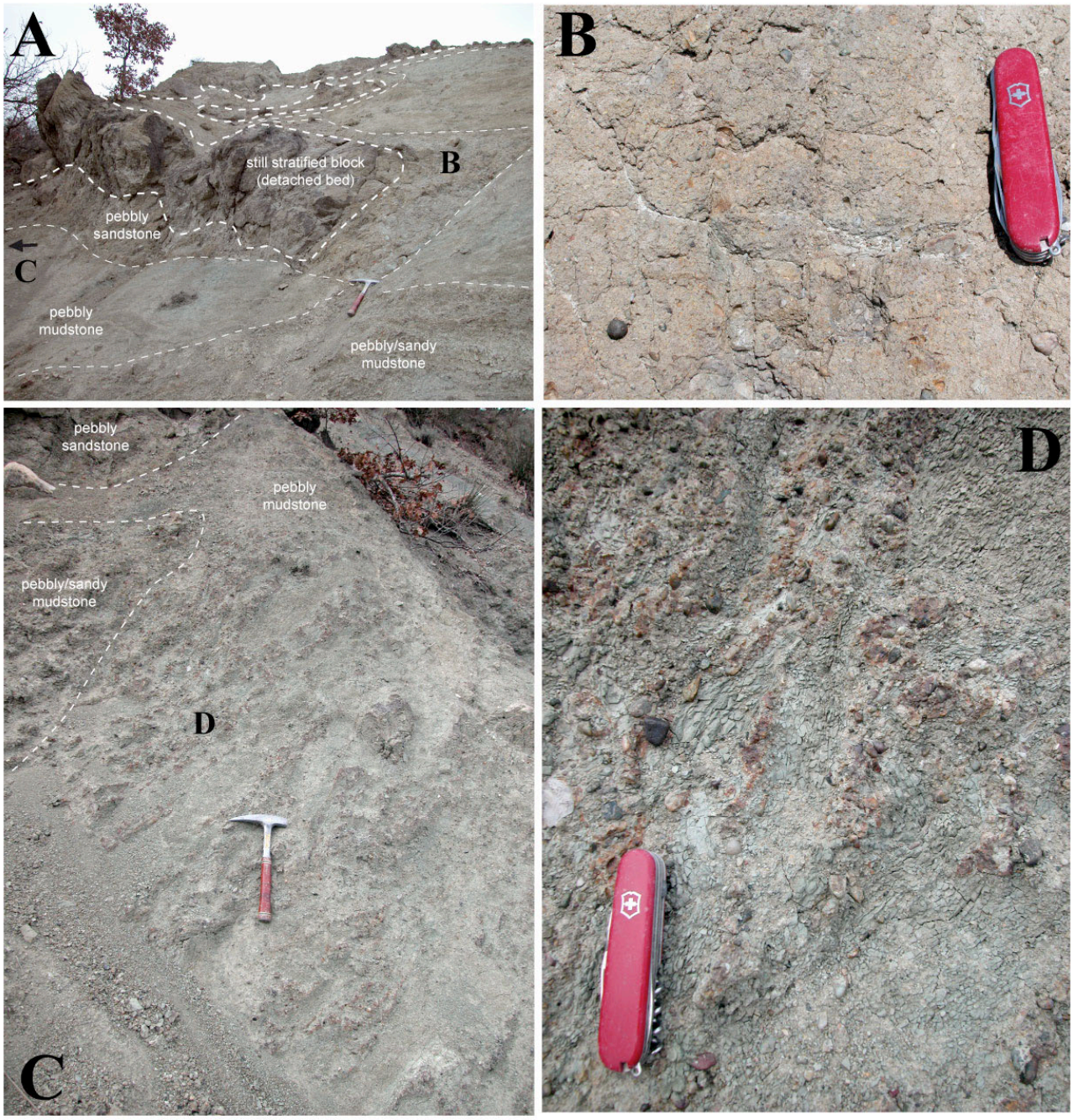
A
still stratified block
(detached bed)
B
pebbly
sandstone
C
pebbly
mudstone
pebbly/sandy
mudstone
B
pebbly
sandstone
pebbly
mudstone
pebbly/sandy
mudstone
D
C
D

Figure 7.20 - Other examples coming from MDPs of the R2/a sub-unit (Fopla section, Pessola Vally outlier).

A: Outcrop example of a sandstone block (single detached bed) enclosed within a pebbly mudstone matrix, with the interposition of a pebbly sandstone matrix closely surrounding the block. Blocks' boundaries and matrix domains are labeled. Hammer for scale.

B: Close-up of A, showing in detail the appearance of pebbly sandstone matrix closely surrounding the block. Knife for scale, 9 cm long.

C: Overview of the enclosing pebbly mudstone matrix. Note the diffused presence of small patches formed by clusters of coarse-grained material. These elements are thought to be produced by the progressive disintegration of the poorly consolidate coarse-grained sandstone blocks. Location is roughly shown in A. Matrix domains are labeled. Hammer for scale.

D: Close-up of C, showing in detail the coarse-grained patches characterizing the enclosing matrix. Note the overall arrangement of these elements in "seams"-like patterns. Knife for scale, 9 cm long.

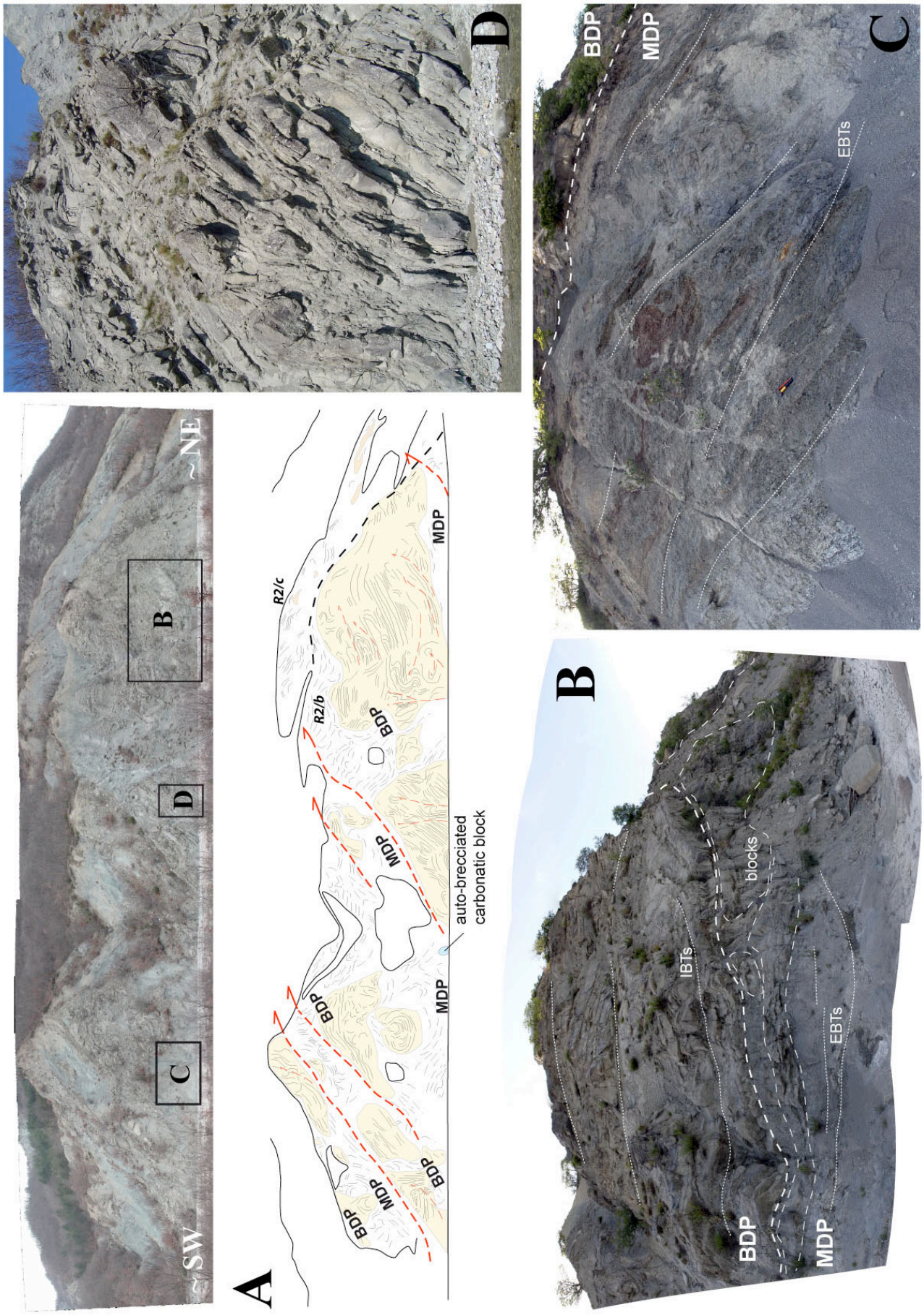
D
C
B
~NE
~SW
A
R2/c
R2/b
BDP
MDP
auto-brecciated carbonatic block
B
IBTs
blocks
EBTs
BDP
MDP
C
BDP
MDP
EBTs

Figure 7.21 - A: Panoramic photo-mosaic and interpretation of the R2/b sub-unit outcrop of the Sx Pessola Section. Generally speaking this outcrop is mainly composed of BDPs, with some localized evidences of MDPs. The labeled shear surfaces, marked by the localized MDPs, seem to bind BDPs composed of R1 and MMP units' lithologies. The overall curved appearance of shear surfaces (and the general complex deformation of the internal elements) is thought to be related to later deformations induced by the emplacement of the overlying R2/c sub-division, which basal boundary is observable in the right side of the photo-mosaic.

B: Close-up of A, showing the contact between an upper BDP and lower MDP. Main contacts, structural features (IBTs and EBTs) and still recognizable blocks' boundaries are labeled.

C: Close-up of A, showing the overall appearance of a localized MDP, characterized by relatively well developed EBTs. Here the matrix is highly heterogeneous, mainly represented by a pebbly mudstone. Note the significant occurrence of Ligurian shaly lithologies within the matrix, arranged in "flames" and complex folds, and sharing an overall "fluidal" appearance. Main contact and structural features are labeled. Hammer for scale.

D: Close-up of A, showing a plastically deformed sandstone block comprised within a BDP. Note the presence of IBTs and related IBFs, marked by incipient matrix intervals. Some beds seem to show some kind of *boudinage*-related structures, reactivated in compressive regime.

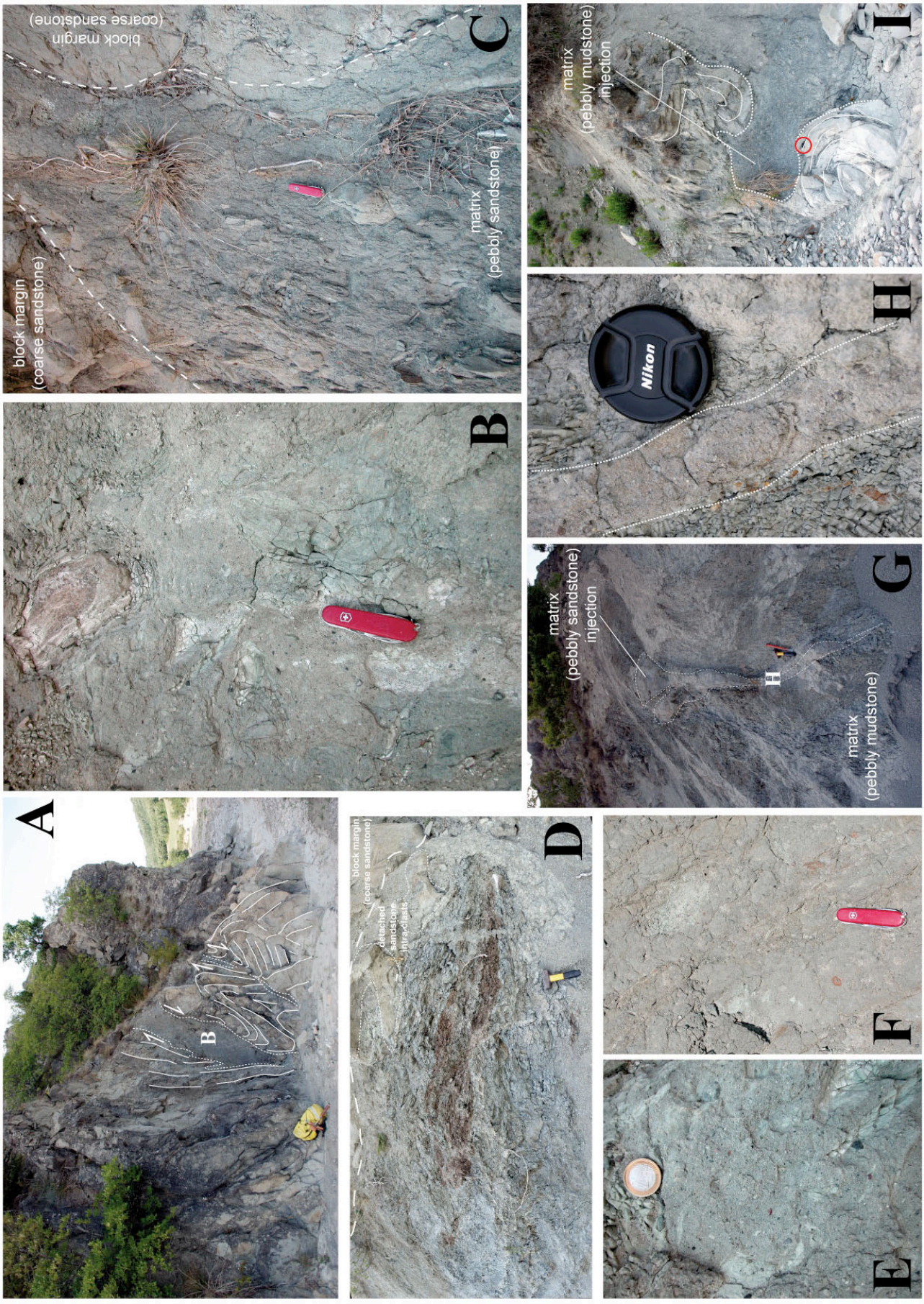
A
B
C
block margin
(coarse sandstone)
matrix
(pebbly sandstone)
D
block margin
(coarse sandstone)
detached
sandstone
intra-clasts
E
F
G
matrix
(pebbly sandstone)
injection
matrix
(pebbly mudstone)
H
Nikon
I
matrix
(pebbly mudstone)
injection

Figure 7.22 - **A**: Outcrop example of a plastically deformed sandstone block, affected by a well-developed intra-block thrust (IBT), characterized by abundant matrix, probably developed by the shearing-related soft sediment stratal disruption (*i.e.* proto-matrix; see text for discussion). The sample R2bIBT come from this shear zone (see below). Still recognizable beds and inferred sense of shearing are labeled. The presented block is contained within a BDP belonging to the R2/b sub-unit in the Sx Pessola section. Backpack for scale.

B: Close-up of A, showing in detail the matrix (mainly pebbly sandstone) characterizing the core shear zone. Note the sparse occurrence of hydroplastically folded mudstone and sandstone intra-clasts. Knife for scale, 9 cm long.

C: Another example of IBT observed few tens of meters to the N from the location shown in A. Here the matrix seems to show a more "sheared" appearance, with the development of a faint (but still observable) foliation running parallely with the shear zone margins. Note the presence of plastically deformed of mudstone and sandstone intra-clasts, and scattered rounded pebbles. In this case no evident kinematic indicators have been found. Shear zone margins are labeled. Knife for scale, 9 cm long.

D: Outcrop appearance of the enclosing matrix that characterizes a lower BDP. This photo has been taken few ten of meters to the S respect to the location shown in A. Here it is possible to observe an elongated, plastically deformed shaly intra-clast of Ligurian origin (*i.e.* AVV unit), contained within a pebbly sandstone portion (locally pebbly/sandy mudstone). Note the detached sandstone intra-clasts (close to the border of a sandstone block) and the well-rounded dm-sized carbonatic pebble in the upper and right side of the photo, respectively. Block and intra-clasts margins are labeled. Hammer for scale.

E and **F**: Two different aspects of the enclosing matrix of the R2/b sub-unit (essentially an unsorted pebbly/muddy sandstone). Note the significant occurrence of rounded ophiolitic pebbles, disrupted and plastically deformed mudstone intra-clasts, and sparse cm-sized plant fragments. Sometimes mm-sized pyrite nodules characterized by oxidized haloes have been observed. Sample R2bEM come from the matrix shown in F. Knife (9 cm long) and one Euro coin (2,2 cm in diameter) for scale.

G: Example of an injection-like structure composed of pebbly sandstone matrix intruding a coherent portion made up of pebbly mudstone matrix. This structure seems to be developed following the overall pseudo-foliation foliation of the enclosing material, and it is thought to be related to later phases of overpressure dissipation (*i.e.* mass transport post-depositional processes; see chap. 9 for discussion). Under low confining pressure conditions, the clayey material is thought to behave in a more rigid manner than the sandy material, which is prone to be liquefied. Nonetheless it is possible that this element actually represents a strongly liquefied and deformed isolated, detached sandstone bed. Element boarders are labeled. Hammer for scale.

H: Close-up of G, showing in detail the pebbly sandstone matrix composing the injection-like structure. The coarse-grained material seems to be concentrated within the core of the structure and faintly aligned. This evidence seems to support the inferred intrusive nature of this element. Element margins are labeled. Camera lens cap for scale, 7 cm in diameter.

I: Outcrop example of matrix injection into a sandstone block. The enclosing pebbly mudstone matrix intrudes the sandstone block, bending inward the composing strata. This photo is taken few meters to the N from the location of C. Injection margins and related deformed beds are labeled. Camera lens cap (encircled) for scale, 7 cm in diameter.

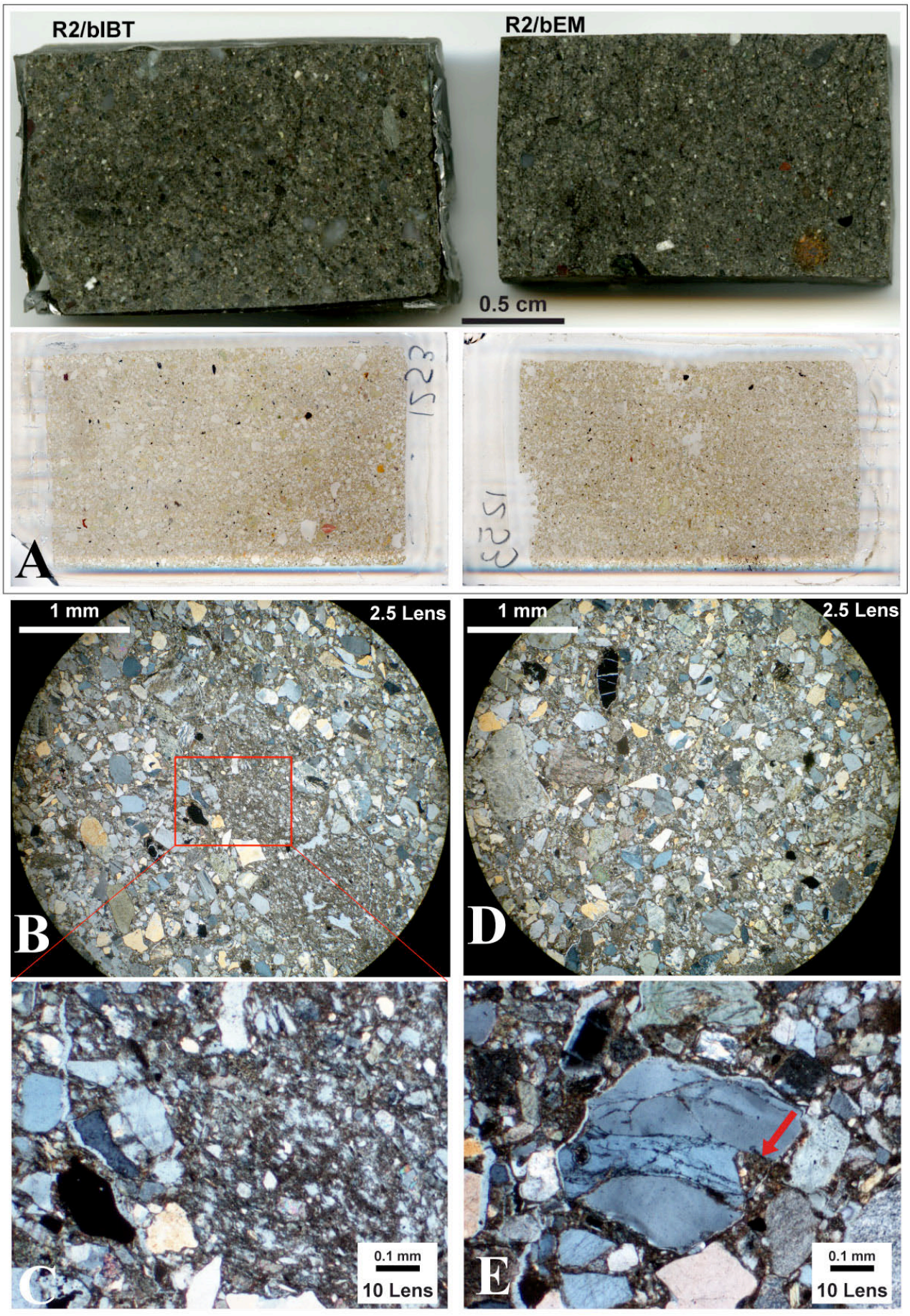
R2/bIBT
R2/bEM
0.5 cm
A
1 mm
2.5 Lens
B
1 mm
2.5 Lens
D
0.1 mm
10 Lens
C
0.1 mm
10 Lens
E

Figure 7.23 - A: Thin sections and polished counter-cuts of samples R2bIBT and R2bEM (left and right side, respectively). The minor presence of void spaces in thin sections is indicative of more consolidated nature and the less mud content of the matrix. For location see fig. 7.23 and chap. 2.

B: Microscopic overview of the sample R2bIBT. The matrix is mainly composed of medium- to coarse-grained sand particles and mud filling inter-granular spaces, and sometimes sustaining grains. In this case it is possible to observe an elongate patch of fine-grained material, sharing the same characteristics of the muddy component. Rounded and angular quartz and lithic grains are abundant. Note that this elongated patch is disposed in a parallel way to an overall oblique banding (from the upper-left to the lower-right), essentially expressed by alignment of grains' long axis and by elongated clustering of particles sharing similar dimensions.

C: Close-up of B, showing in detail the transitional boarder of the fine-grained elongated patch to the surrounding matrix material. The fine-grained lithology is the same of that observable filling inter-granular spaces and sustaining sandy particles. Note the "fluidal" appearance of the fine-grained material and the development of faint lineations marked by the preferential alignment of elongated grains. Note also the same fine-grained material disposed within grains and enveloping them.

D: General view of the sample R2bEM. The overall composition is similar to that shown in B. In this case, the fine-grained material seems more diffused and diluted within the sandy grains, and lineations and banding are less evident. Locally, the overall appearance is more "matrix-sustained" than that shown in sample R2bIBT. Also in this case clusters of coarser grain-size particles have been observed. Note the presence of mm-sized particles of coalified organic matter (*i.e.* plant fragment).

E: Detail of a fractured sub-angular quartz grain characterized by a thin calcite halo, and surrounded by fine-grained material. This material seems to intrude into internal voids of the grain (red arrow); other minor injections along fractures are present. Note how the fine-grained material envelops particles (even where grains are almost in contact), adapting along the borders, and testifying its plastic/fluidal nature. Note also that calcite seams-like micro-veins, cutting the fine-grained material, reciprocally connect thin, fibrous calcite haloes surrounding grains.

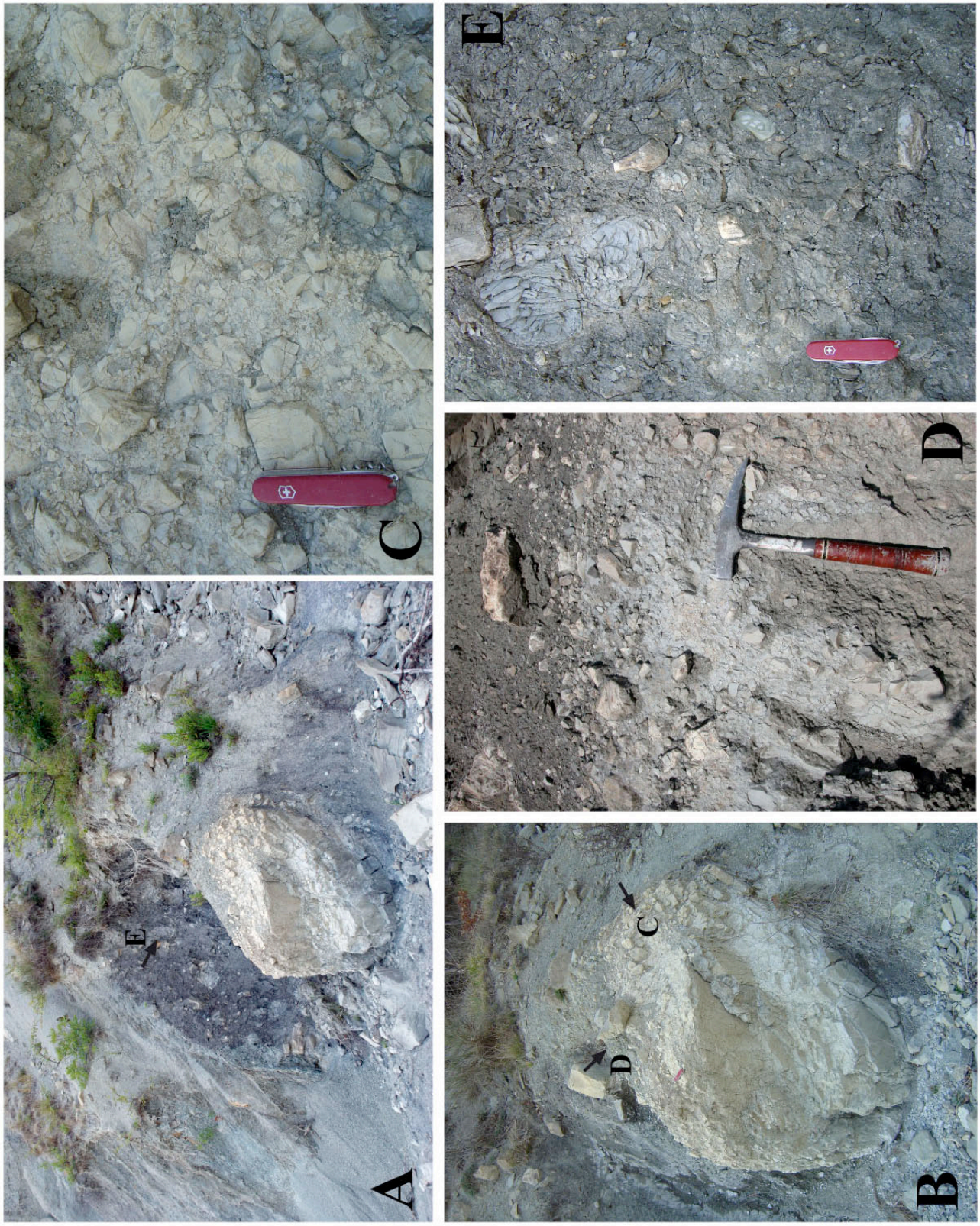
A
E
B
C
D
C
D

Figure 7.24 - **A**: Outcrop appearance of a carbonate block contained within a matrix characterized by the diffused presence of Ligurian-related shales and carbonate clasts. This kind of matrix is concentrated close to the block (probably produced by the progressive dismembering of the block and the associated fine-grained lithologies), while the above-described pebbly/sandy mudstone matrix represents the overall enclosing matrix. This block crops out in a MDP characterizing the lower portions of the R2/b sub-unit in the Sx Pessola section.

B: Close-up of the block shown in A. Here it is possible to observe the overall auto-brecciated appearance of the composing calcareous material, and some remnants of the original stratification (nonetheless bended and deformed) are still recognizable. Knife for scale, 9 cm long.

C: Close-up of B, showing in detail the auto-brecciation shared by calcareous material forming the block. Similar feature has been classically observed within shale-rich chaotic complexes belonging to the Ligurian Units. The origin if such brecciation is doubtful, and in some instances it should be related to some kind of differential pressure-related "implosion" of fine-grained lithologies due to diapiric uplift (*i.e.* "pop corn"-like structures). Knife for scale, 9 cm long.

D: Close-up of B, showing the upper margin of the block. Here it is possible to observe the quite transitional appearance of the contact and how the surrounding matrix is composed of calcareous elements detahced from the already brecciated block. Hammer for scale.

E: Close-up of A, showing the overall appearance of the dark matrix closely enveloping the block. In this case a strong contribution to the matrix development is due to the progressive disintegration of black, foliated shales probably associated in origin with the calcareous block. Mudstone intra-clasts and angular calcareous fragments coming from the block are present. Knife for scale, 9 cm long.

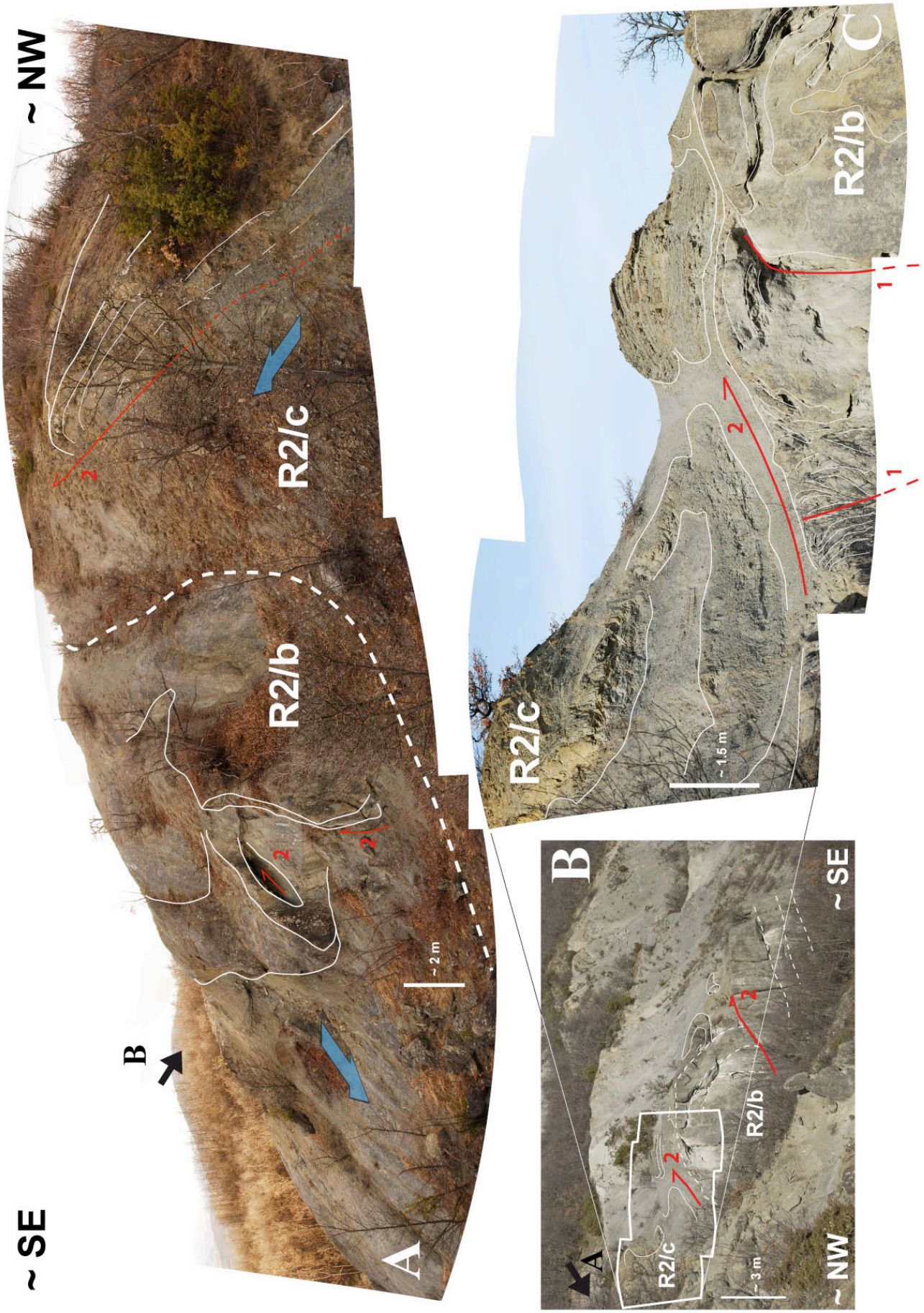
~ NW
~ SE
R2/c
R2/b
R2/c
R2/b
R2/c
R2/b
A
B
C
B
A
~ 2 m
~ 1.5 m
~ 3 m
~ SE
~ NW
1
2

Figure 7.25 - Example of interference deformations observed close to the R2/b-R2/c sub-units contact.

A: Photo-mosaic of the R2/b-R2/c sub-units contact in the Servazzola section. Mean inferred transport direction for the two subdivisions are indicated by blue arrows. The shear zones identified with red lines and labeled with the "2" are thought to be related to the R2/c sub-unit emplacement. The deposition of this latter sub-unit is thought to have produced interference deformations on the upper part of the sub-unit R2/b, close to the contact, with refolding of preceding structures and reactivation with roughly opposite shearing sense of shear zones. Indicative location shown in B. Main contact (dashed line) and still recognizable stratification surfaces are labeled.

B: Photo-mosaic of the same situation shown in A, view from another perspective (indicative location is shown in A). Shear surface (underlined by red lines and labeled with "2") affecting the upper portion of the R2/b sub-unit are thought to be related to the emplacement of the R2/c sub-unit. Main contact and still recognizable stratification surfaces are labeled.

C: Close-up of B, showing in detail the R2/b-R2/c sub-units contact. The R2/b-related structures (*i.e.* IBTs; labeled with "1") are verticalized and truncated by R2 (labeled with"2"). Main element and recognizable linear features are labeled.

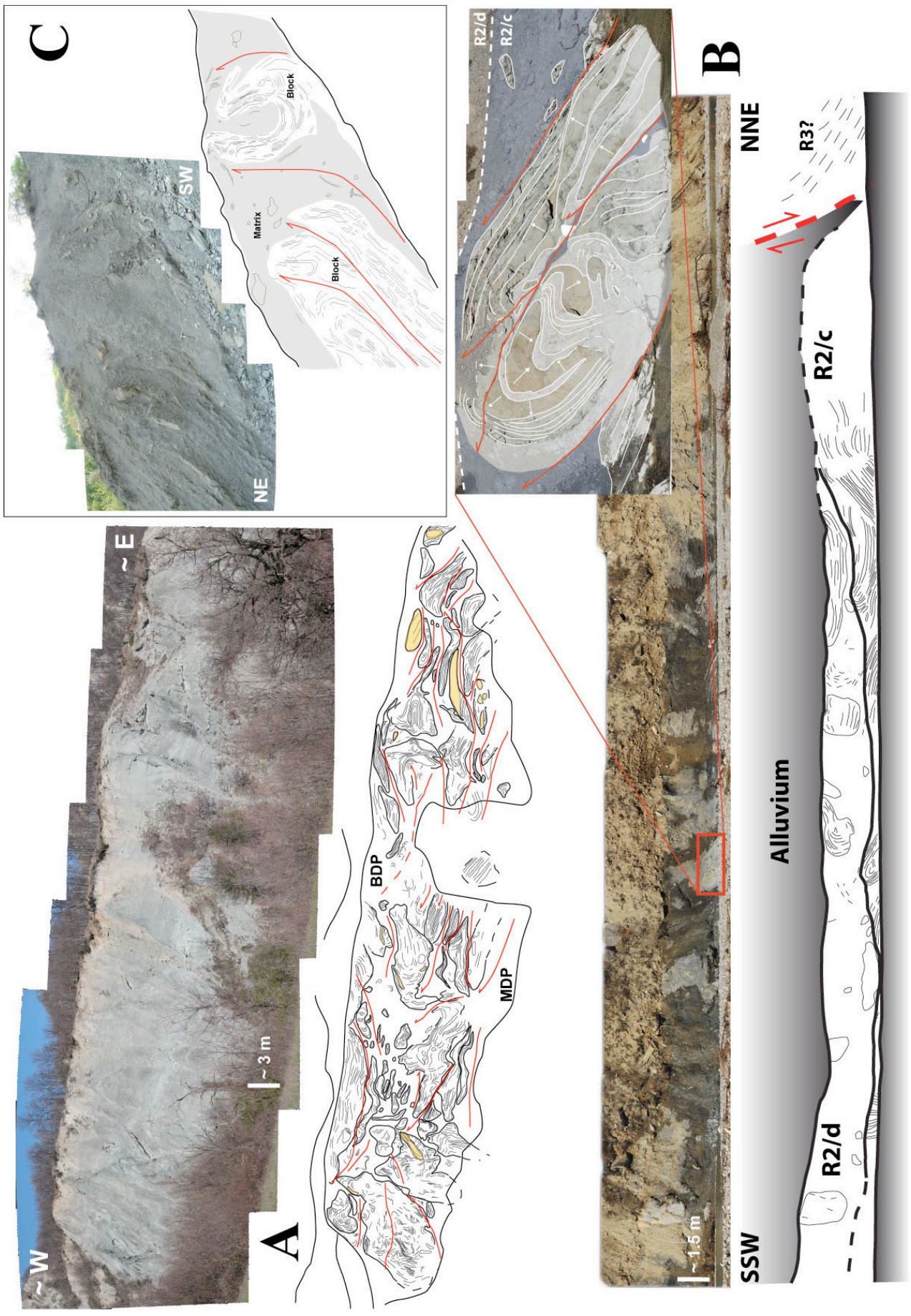
C
SW
NE
Matrix
Block
Block
B
R2/d
R2/c
NNE
R3?
R2/c
Alluvium
R2/d
SSW
~ 1.5 m
A
~ W
~ E
~ 3 m
BDP
MDP

Figure 7.26 - General outcrop appearance of the R2/c sub-unit in the Pessola Valley outlier.

A: Photo-mosaic and interpretative line drawing of the middle-lower R2/c sub-unit in the Tintori section. Here it is possible to observe an upper BDP, characterized by blocks arranged as complex sheath-like folds and opposite-verging shear zones, overlying a lower MDP, poorly exposed and covered by vegetation (mainly due to the more alterable nature of matrix). Note the sparse occurrence of sandstone blocks developed by the disruption of a single thick bed. The rock exposure cut is roughly transversal to the inferred palaeo-transport direction (toward the viewer).

B: Photo-mosaic and interpretative line drawing of the upper R2/c sub-unit, and its contact with the overlying R2/d sub-unit, in the Sx Pessola section. The upper portion of the R2/c sub-unit is represented by a BDP, while the lower portion of the R2/d sub-unit shows the characteristics of a MDP. In the close-up is shown a meso-scale example of co-axial refolding of an isoclinalic fold just below the main inferred contact with the R2/d sub-unit. Note the significant development of ductile shear surfaces. This kind of interference pattern is thought to be caused by the dragging force exerted by the R2/d sub-unit emplacement. Main structures and stratigraphic polarity (white arrows) are labeled. Incipient matrix (*i.e.* proto-matrix) portions are labeled in transparent white, while enclosing matrix portions are identified by transparent grey areas.

C: Photo-mosaic and interpretative line drawing of the MTD characterizing the lower R2/c sub-unit in the Tintori section (few tens of meter to the NW from the location shown in A). In this case the outcrop cut is roughly longitudinal to the inferred palaeo-transport direction. Here it is possible to observe thin-bedded sandstone-mudstone blocks (arranged as rootless folds), IBTs and EBTs, coherently-verging in the same direction (roughly toward the SW). Enclosing matriz ir represented by a pebbly/sandy mudstone. Hammer for scale.

A
B
I
C
E
D
E
F
G
H
I

Figure 7.27 - A: Very thin-bedded ("streacky" appearance) mud-fine sand couplets observed within a block characterizing the upper portion of the R2/c sub-unit in the Sx Pessola section. Lithologies seem to belong to PZO unit or intermediate terms with the R1 unit (Chiarone unit?). This facies strongly resemble that ascribed to pro-deltaic plume deposits. Fifty Euro cent for scale, 2,4 cm in diameter.

B: Common outcrop appearance of PZO unit-type beds observable within blocks characterizing the middle-upper part of the R2/c sub-unit in the Specchio section. Hammer for scale.

C: Common outcrop appearance of PZO-R1 intermediate-type beds (Chiarone unit?) observable within blocks characterizing the middle part of the R2/c sub-unit in the Specchio section. Encircled Camera lens cap for scale, 7 cm in diameter.

D: *Planolites*-like ichnofacies observed at the base of some beds characterizing the thin-bedded portions of the out-size block of PZO-unit type lithologies cropping out in the Specchio section. One Euro coin for scale, 2,2 cm in diameter.

E: Well preserved worm-form bioturbations (reptation-like traces) characterizing the PZO-R1 intermediate-type beds (Chiarone unit?). Location shown in C. Camera lens cap for scale, 7 cm in diameter.

F: *Zoophycos*-like ichnofacies observed within a m-sized PZO-unit type block within the upper portion of the R2/c unit in the Sx Pessola section. Knife for scale, 9 cm long.

G: *Ophiomorpha*-like ichnofacies recognized in a medium-thick, coarse- to fine-grained, graded bed intercalated within the thin-bedded portions of the out-size block of PZO-unit type lithologies cropping out in the Specchio section. Knife for scale, 9 cm long.

H: *Zoophycos*-like ichnofacies observed within a m-sized thin-bedded sandstone block (Chiarone unit lithlogies?) characterizing the basal MDP of the R2/c sub-unit and cropping out in the Servazzola section. Knife for scale, 9 cm long.

I: *Zoophycos*-like ichnofacies recognized within the thin-bedded portions of the PZO-unit type out-size block characterizing the middle R2/c sub-unit in the Specchio section. Location shown in B. Knife for scale, 9 cm long.

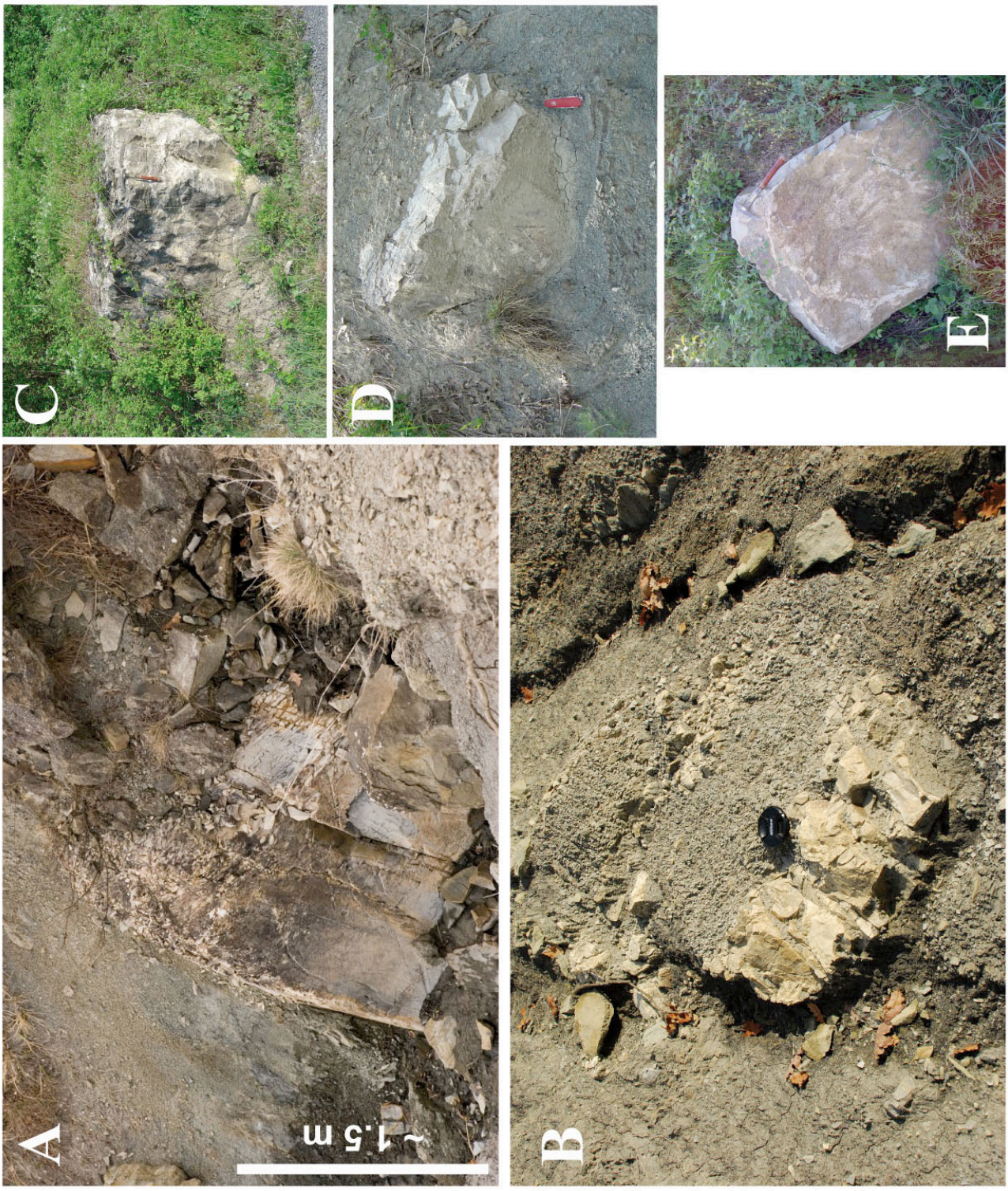
C
D
E
A
~1.5 m
B

Figure 7.28 - Examples of sub-angular to sub-rounded, generally m-sized, lithified carbonatic blocks (mainly laminated marl- and limestones) characterizing the R2/c sub-unit (especially its lower MDP). Vast majority of these blocks belong to the Ligurian Helminthoyd Flysch units, and share evidence of sedimentary reworking and lack of associated shaly portions. For locations see Panels n. 1 and n. 2.

A: Servazzola section; marking the contact between the R2/c sub-unit and the underlying R2/b sub-unit.

B: Pratorotondo section; upper localized MDP of the R2/c sub-unit. Camera lens cap for scale, 7 cm in diameter.

C: Fopla section; roughly across the contact between the R2/c sub-unit and the underlying R2/b sub-unit. Hammer for scale.

D: Tintori section; few meters above the contact between the R2/c sub-unit and the underlying R2/b sub-unit. Knife for scale, 9 cm long.

E: Pettenati section; roughly in the lower-middle portions of the R2/c sub-unit. Hammer for scale.

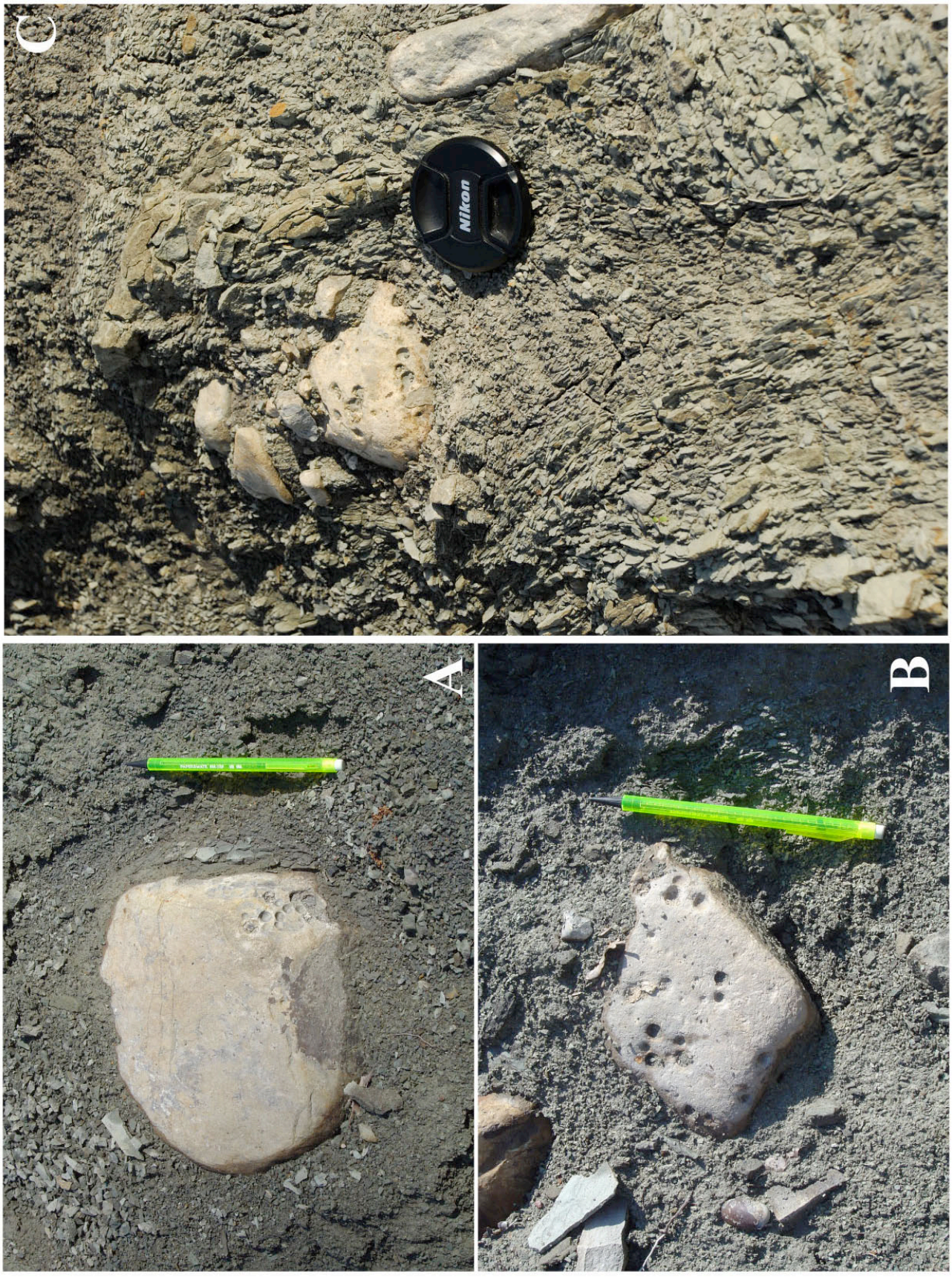
C
Nikon
A
B

Figure 7.29 - Examples of calcareous pebbles showing evidences of lithodome holes recognized within the R2/c sub-unit. For locations see Panels n. 1 and n. 2.

A: Pratorotondo section; lower MDP of the R2/c sub-unit. Pencil for scale, 15, 2 cm long.

B: Dx Pessola section; upper localized MDP of the R2/c sub-unit. Pencil for scale, 15, 2 cm long.

C: Pratorotondo section; lower MDP of the R2/c sub-unit. Pencil for scale, 15, 2 cm long.

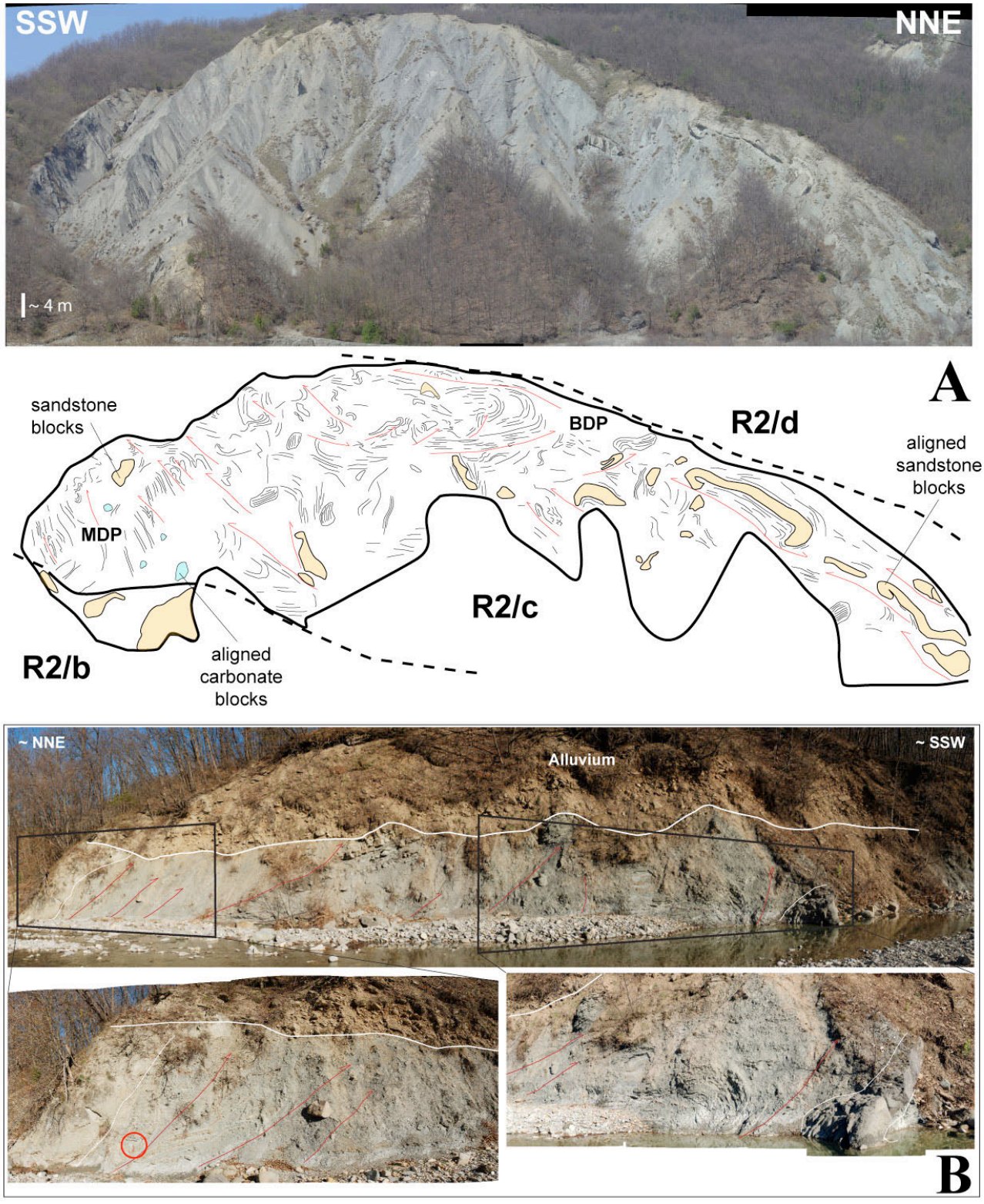
SSW
NNE
~ 4 m
A
sandstone blocks
BDP
R2/d
aligned sandstone blocks
MDP
R2/c
R2/b
aligned carbonate blocks
~ NNE
Alluvium
~ SSW
B

Figure 7.30 - **A**: Panoramic photo-mosaic and interpretative line drawing of the R2/c sub-unit in the Sx Pessola section. Note the carbonatic blocks characterizing the lower MDP and the folded sandstone blocks (representing fragments of a single dismembered thick bed) characterizing the upper BDP, particularly the double-vergent fold shape shown by the largest sandstone block.

B: Photo-mosaic representing the middle-upper portion of the R2/c sub-unit in the Dx Pessola section. The outcrop represents a BDP with a localized MDP. In the close-up to the left side the localized MDP is shown (note the sub-angular carbonatic block in relief). In the close-up to the right side it is shown in detail m-scale drag folds (both antiformal and synformal; IBFs) linked to the development of associated shear zones (IBTs). Note the reciprocally coherent verging direction of the structures. Still recognizable stratification, blocks' boundaries and shear surfaces are labeled. Encircled hammer for scale.

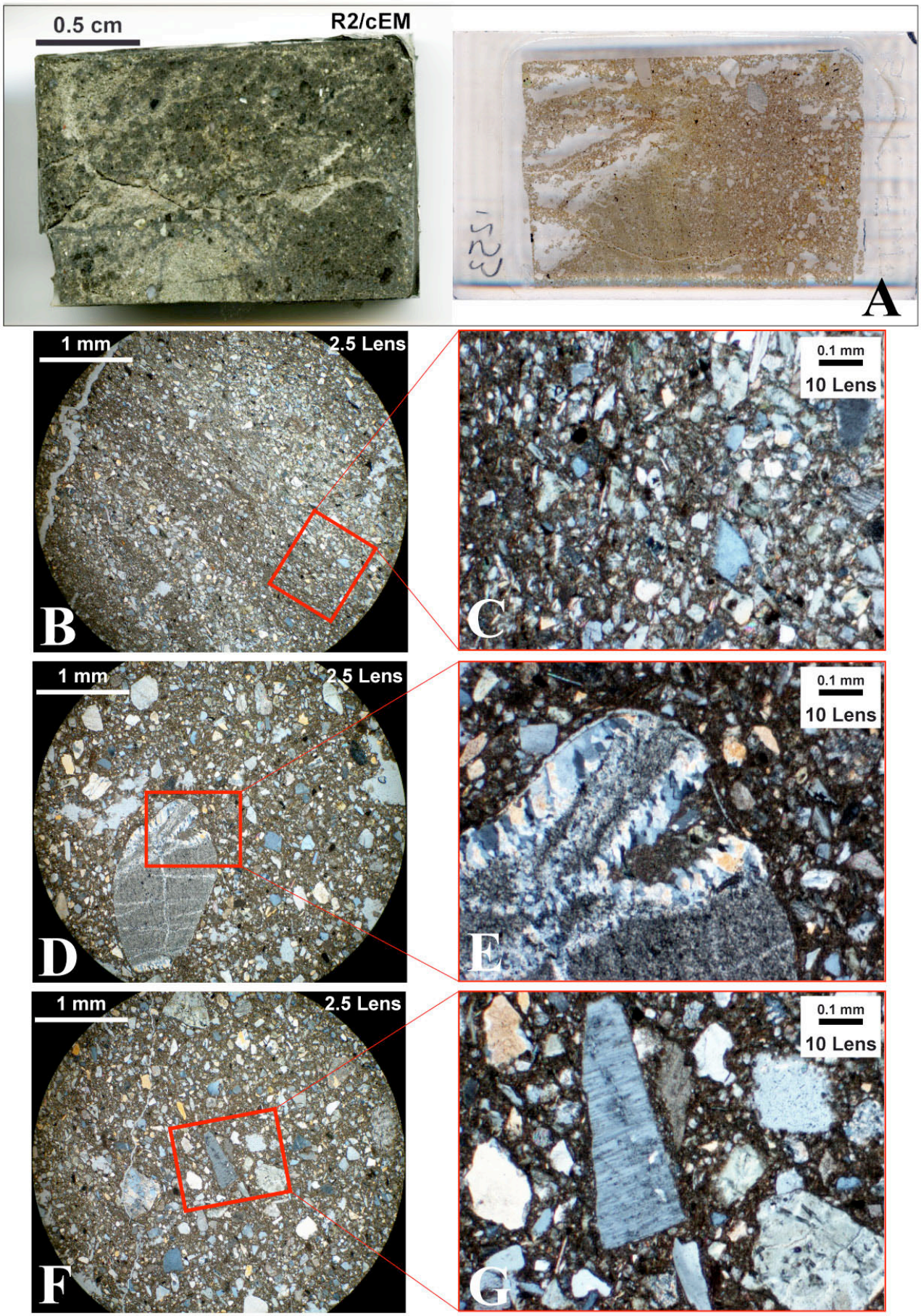
0.5 cm
R2/cEM
A
1 mm
2.5 Lens
B
0.1 mm
10 Lens
C
1 mm
2.5 Lens
D
0.1 mm
10 Lens
E
1 mm
2.5 Lens
F
0.1 mm
10 Lens
G

Figure 7.31 - A: Thin section and polished counter-cut of sample R2cEM. For location see chap. 2. Note the vertically banded appearance of the thin section (with elongated clusters of fine- and coarse-grained material, to the left and right sides, respectively).

B: Microscopic overview of the banded fine-grained portion. Note the fine-grained material arranged in "ribbon"-like patches. Lineations are also highlighted by the preferential alignment of particles, along their long axis.

C: Close-up of B, showing the boundary between two relatively fine- and coarse-grained elongated clusters. A faintly recognizable transitional interval seems to separate finer material from coarser particle cluster. The overall appearance of the contact is quite gradational (merging and interconnection of finer enveloping material), nonetheless a distinct separation plane between coarser and finer particles seems to exist. These lineations are interpreted plastic deformation bands, in which the overall movement is achieved by an independent particulate flow (no evidences of grain breakage).

D: Overall view of the sustained "block-in-matrix"-like appearance characterizing the coarse-grained portion of the matrix. The well-rounded, mm-sized, lithic pebble (metamorphic?) observable in the lower-left side of the photo is internally characterized by at least two systems of preexisting mineralized (quartz?) veins; note the intrusion of the finer material into the voids left by these mineralized veins (upper and lower margins). Particles dispersed within the finer material seem to envelope the major elements. Note also the faintly recognizable shear-like band passing tangentially to the upper-right margin of largest pebble, and trending obliquely the photo, from the upper-left side to the lower-right side.

E: Close-up of D, showing in detail the primary mineralized vein and the injected fine-grained material. This evidence supports the fluid-like state of the matrix. Note the thin calcite veneer developed along the upper margin of the pebble, and the fluidal-like appearance of the surrounding matrix, simulating pebble boundaries.

F: Another general view of the coarse-grained portion of the matrix, showing a more iso-oriented arrangement of particles. Note how the finer material envelopes major grains.

G: Close-up of F, showing an angular fragment of a fibrous mineral (quartz vein fragment?). Note the fluidal-like appearance of the enveloping finer material.

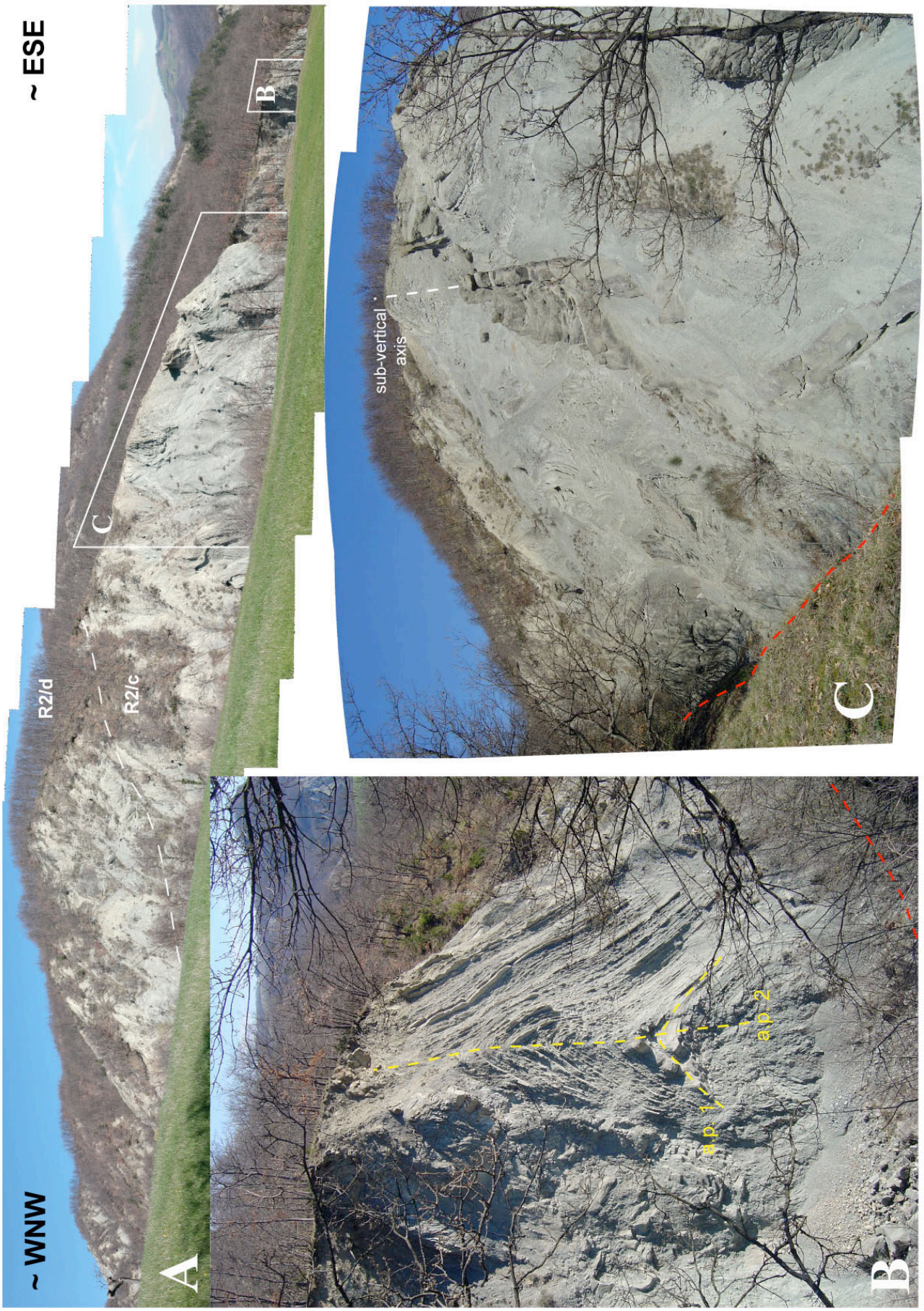
~ WNW
~ ESE
R2/d
R2/c
A
B
C
sub-vertical axis
ap 1
ap 2
B
C

Figure 7.32 - A: Panoramic photo-mosaic showing the contact between the R2/c and R2/d units, in the the Pettenati section; between these outcrops and the Pratorotondo sections (in a roughly WSW-ENE direction), the internal structural elements of both the sub-units seem to be characterized by a generalized buckling, in longitudinal sense to the inferred transport direction. Structures appear verticalized, with development of opposite verging features and refolding phenomena. A fault runs roughly parallel to the rock exposure cuts. Main contact is labeled.

B: Close-up of A, showing a co-axially refolded isoclinal fold developed within a tens of meters-sized, thin-bedded, mudstone-sandstone block (IBF). Axial plane traces of first and second generation are labeled. Red dashed line roughly indicates the position of the fault described in A.

C: Close-up of A, showing a localized MDP characterized by m- to ten of meters-sized EBFs sharing verticalized axes. These folds appear highly deformed and, where the erosional relief allows the observation, seem to show sheath-like geometries. The trend of a sub-verticalized fold axis is labeled. Red dashed line roughly indicates the position of the fault described in A.

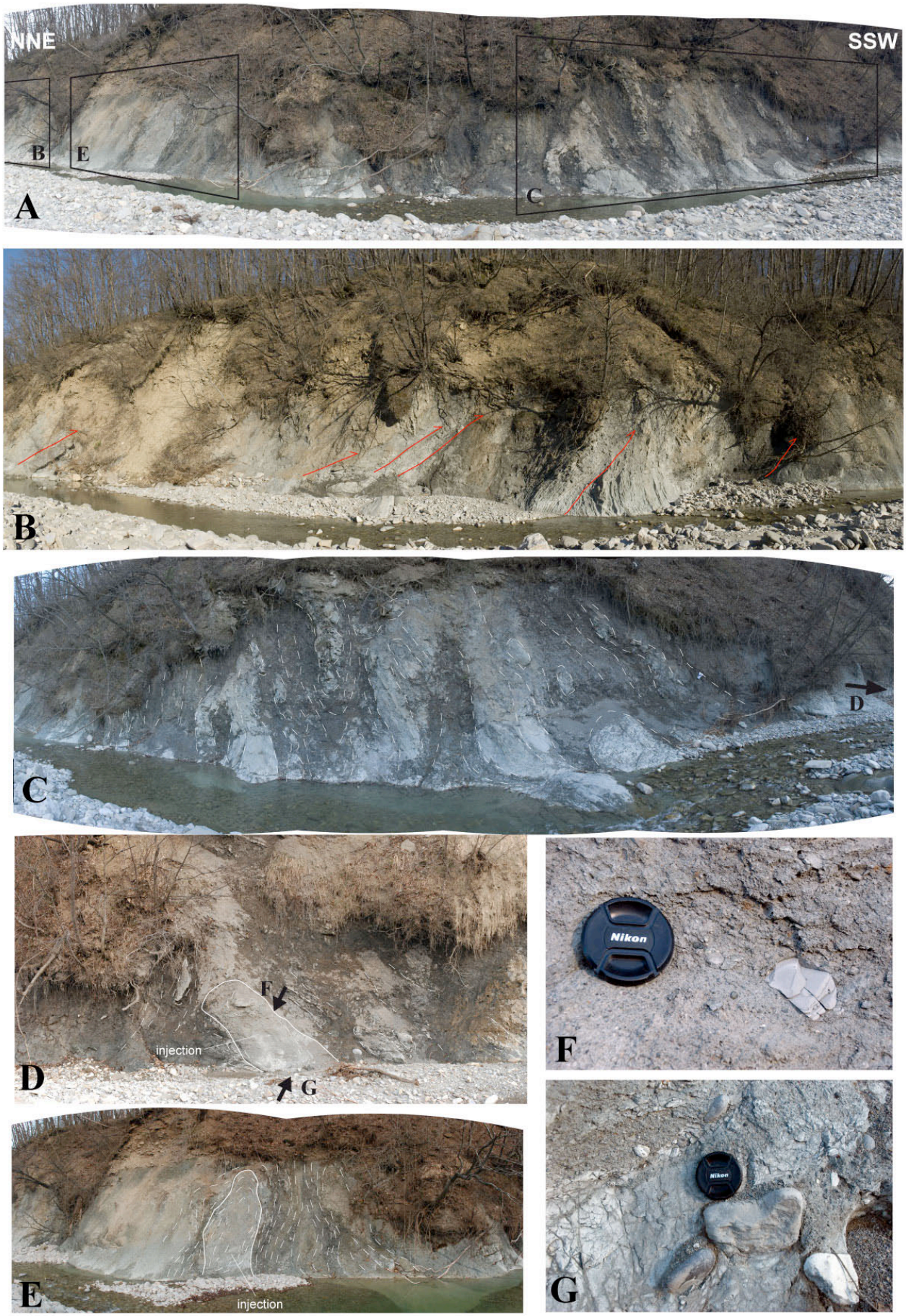
NNE
SSW
B
E
C
A
B
C
D
F
injection
G
D
Nikon
F
E
injection
Nikon
G

Figure 7.33 - A: Panoramic photo-mosaic representing the middle part of the R2/c sub-unit in the southern sector of the Dx Pessola section. These outcrops are roughly located within the zone of structural disturbance (between the Pettenati and Pratorotondo sections).

B: Close-up of the northeastern portion of the rock exposure shown in A. In this portion (essentially a BDP), internal structures (IBTs and IBFs) seem to share the same shearing direction (roughly t the S). Main recognized shear surfaces are labeled.

C: Close-up of the southwestern portion of the rock exposure shown in A. In this case, it is observable a MDP characterized by a sub-vertical structural trending. Sandstone elements are strongly deformed, and injection-like structures filled of pebbly sandstones seem to intrude within the enclosing pebbly mudstone strata. The distinction between deformed sandstone bed fragments and injection-like structures is usually difficult due to the outcrop conditions and the fine-grained, poorly lithified lithologies. Elements' boundaries and main structural trends are labeled.

D: Example of an oblique trending injection-like structure within a MDP, recognized few meters to the SW of the location shown in A. The overall structural trending is oblique, coherently to the injection-like structure. Taking into account the structural trending observed in the other analyzed outcrops, the overall arrangement of this area seems to resemble a dome-like, antiformal configuration, which axis roughly trends in a WSW-ENE direction. The internal deformation and structural verticalization seem to become stronger going from the N to the S. Elements' boundaries and overall structural trending are labeled.

E: Close-up of A, showing an example of a sub-vertical trending injection-like structure within a MDP. General characteristics are quite similar to those of the example shown in D. Elements' boundaries and overall structural trending are labeled.

F and **G**: Close-ups of D, showing in detail the characteristics of the infilling matrix of the injection-like structures. It is essentially represented by pebbly sandstone with variable muddy content. Note the presence of both angular (mainly carbonatic) and rounded cm- to dm-sized pebbles.

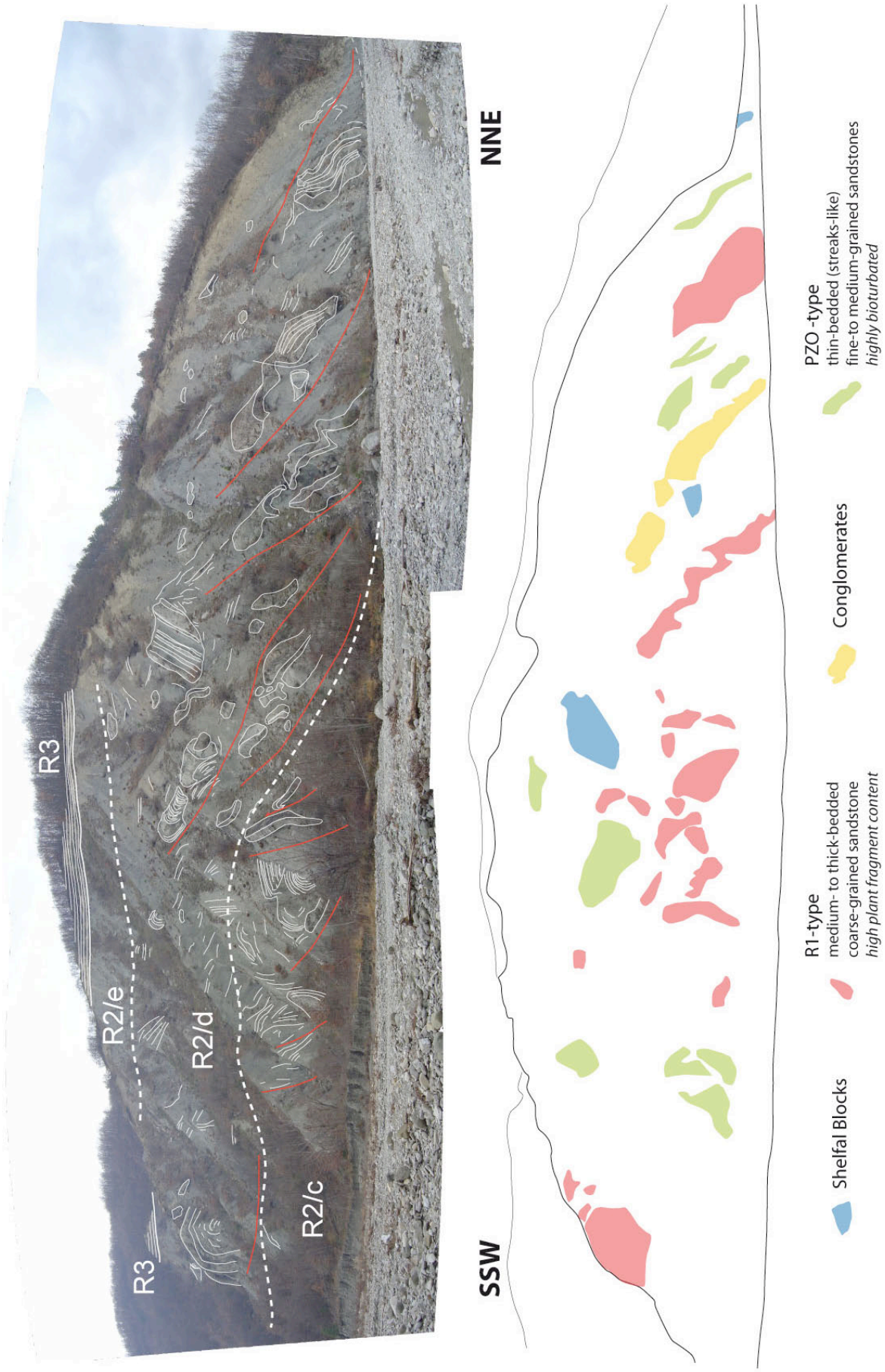
R3
R2/e
R2/d
R2/c
R3
NNE
SSW
R1-type
medium- to thick-bedded
coarse-grained sandstone
high plant fragment content
Conglomerates
PZO -type
thin-bedded (streaks-like)
fine-to medium-grained sandstones
highly bioturbated
Shelfal Blocks

Figure 7.34 - Panoramic photo-mosaic, line drawing and relative interpretation of a key-outcrop (Sx Pessola section) showing the vertical depositional stacking of the upper subdivisions of the Specchio Unit R2 (focusing on the R2/d sub-unit), and the contact with the overlying R3 unit. In the drawing on the lower side, lithologies, overall features and inferred provenances of the recognizable blocks are labeled. The R2/d sub-unit is essentially represented by MDPs. Note the overall concordance of the structural trending, and particularly the imbricated appearance of the R2/d elements, just backward of a mounded-like structure that seems to chracterize R2/c sub-unit. These observations may support the possible interpretation of such structures as developed through an obstacle-related localized compression.

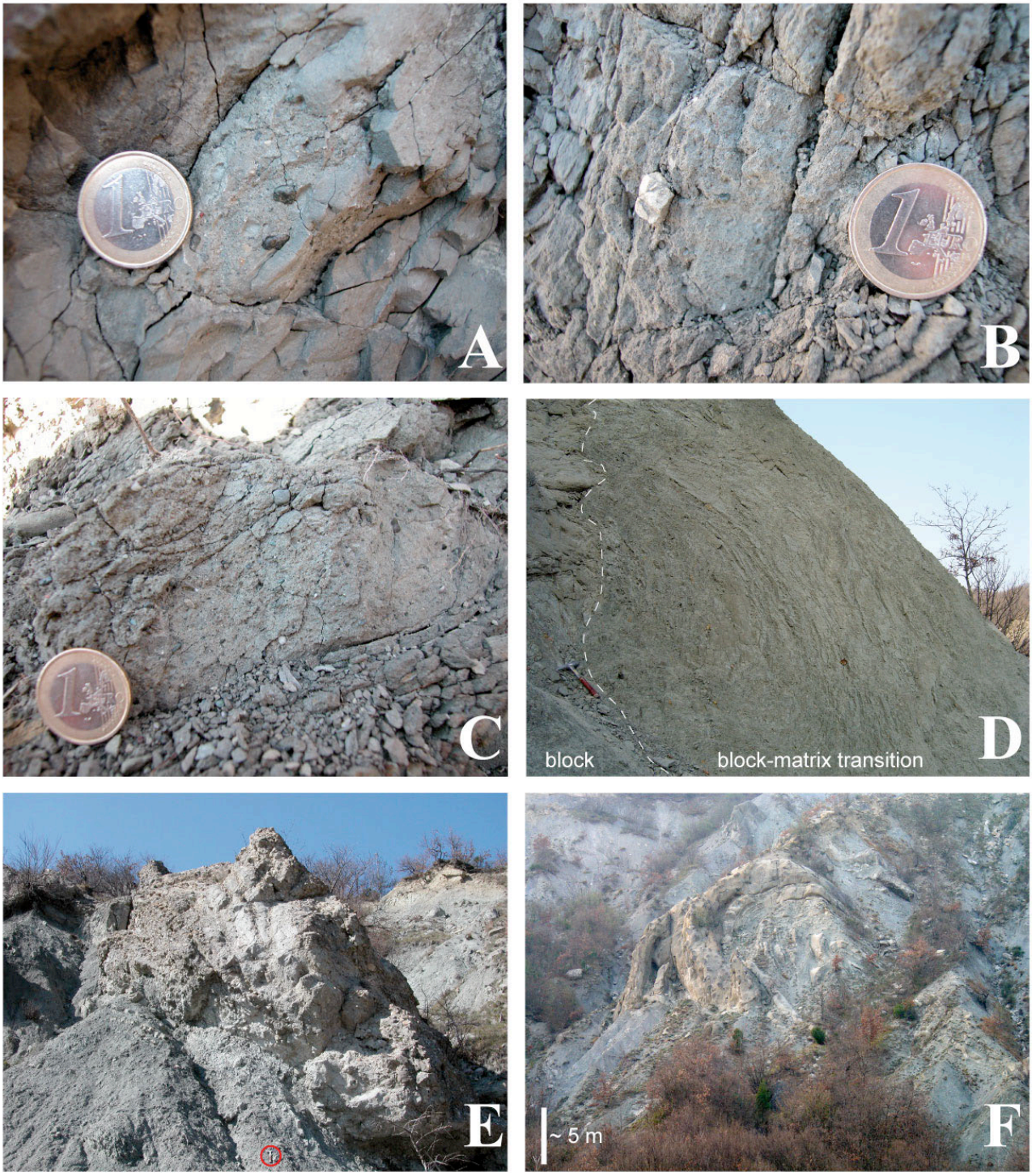
A
B
C
block
block-matrix transition
D
E
~ 5 m
F

Figure 7.35 - A: Example of well-rounded ophiolitic pebbles cluster observable within the enclosing matrix (pebbly mudstone) of the R2/d unit in the Specchio section. One Euro coin for scale, 2,2 cm in diameter.

B: Example of angular carbonatic clast observable within the enclosing matrix (pebbly/sandy mudstone) of the R2/d unit in the Pratorotondo section. One Euro coin for scale, 2,2 cm in diameter.

C: Overall appearance of the pebbly/sandy mudstone representing the enclosing matrix of the R2/d unit in the Specchio section. One Euro coin for scale, 2,2 cm in diameter.

D: Photo showing an highly deformed block margin representing the transition between still coherent lithologies and the matrix (Sx Pessola section). Similar features are localized where significant shearing between block and matrix occur. Hammer for scale.

E: An example of a still stratified conglomeratic-coarse sandstone block, observable in the Sx Pessola section. Encircled hammer for scale.

F: An example of tens of meters-sized, thick-bedded sandstone block deformed in a rootless, tight fold, characterized by strong stratal disruption in the core zone.

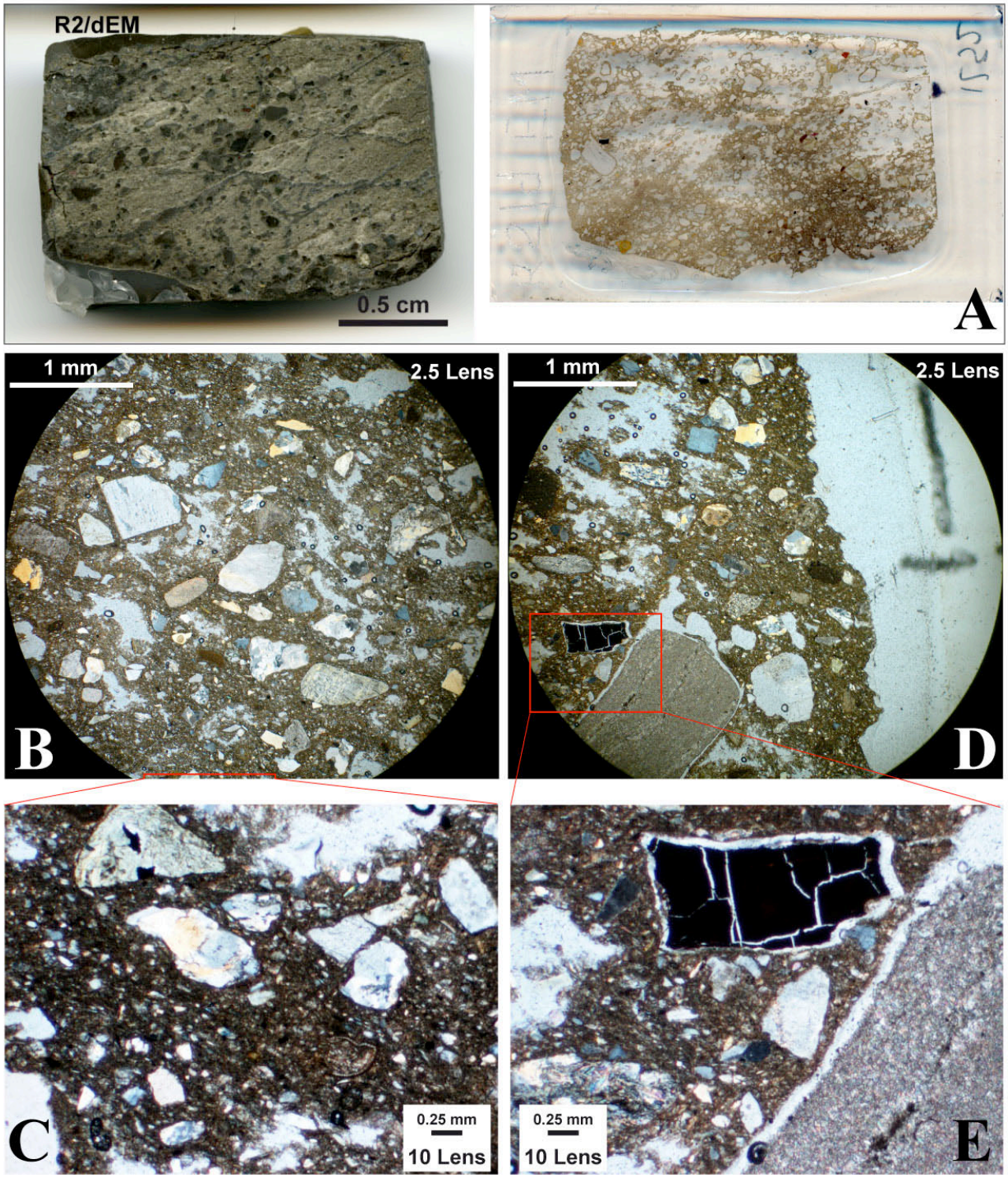
R2/dEM
0.5 cm
A
1 mm
2.5 Lens
B
1 mm
2.5 Lens
D
0.25 mm
10 Lens
C
0.25 mm
10 Lens
E

Figure 7.36 - A: Thin section and polished counter-cut of sample R2dEM. For location see chap. 2. Note the faint oblique lineations and the diffused presence of void areas, indicating the significant amount of unconsolidated finer material.

B: General view of the matrix. The overall appearance is that of a "block-in-matrix"-like texture, with rigid particles dispersed and sustained within a fine-grained, unconsolidated lithology.

C: Partial close-up of B, showing the relationships between particles and the finer material, which envelopes grains and seems to be structurally arranged in a crude oblique lineation (deformation bands-like structures), as underlined by particles alignment. Note the presence of a well-preserved micro-fossil (radiolarian?).

D: Overview of the matrix close to a major, mm-sized, well-rounded pebble of sedimentary origin.

Also in this case, the pebble shows a thin calcite halo along the margins.

E: Close-up of D, showing in detail the finer matrix surrounding the pebble. Note the presence of a coal fragment (vegetal organic matter) enveloped by a thin calcite halo, as observed for the other rigid elements.

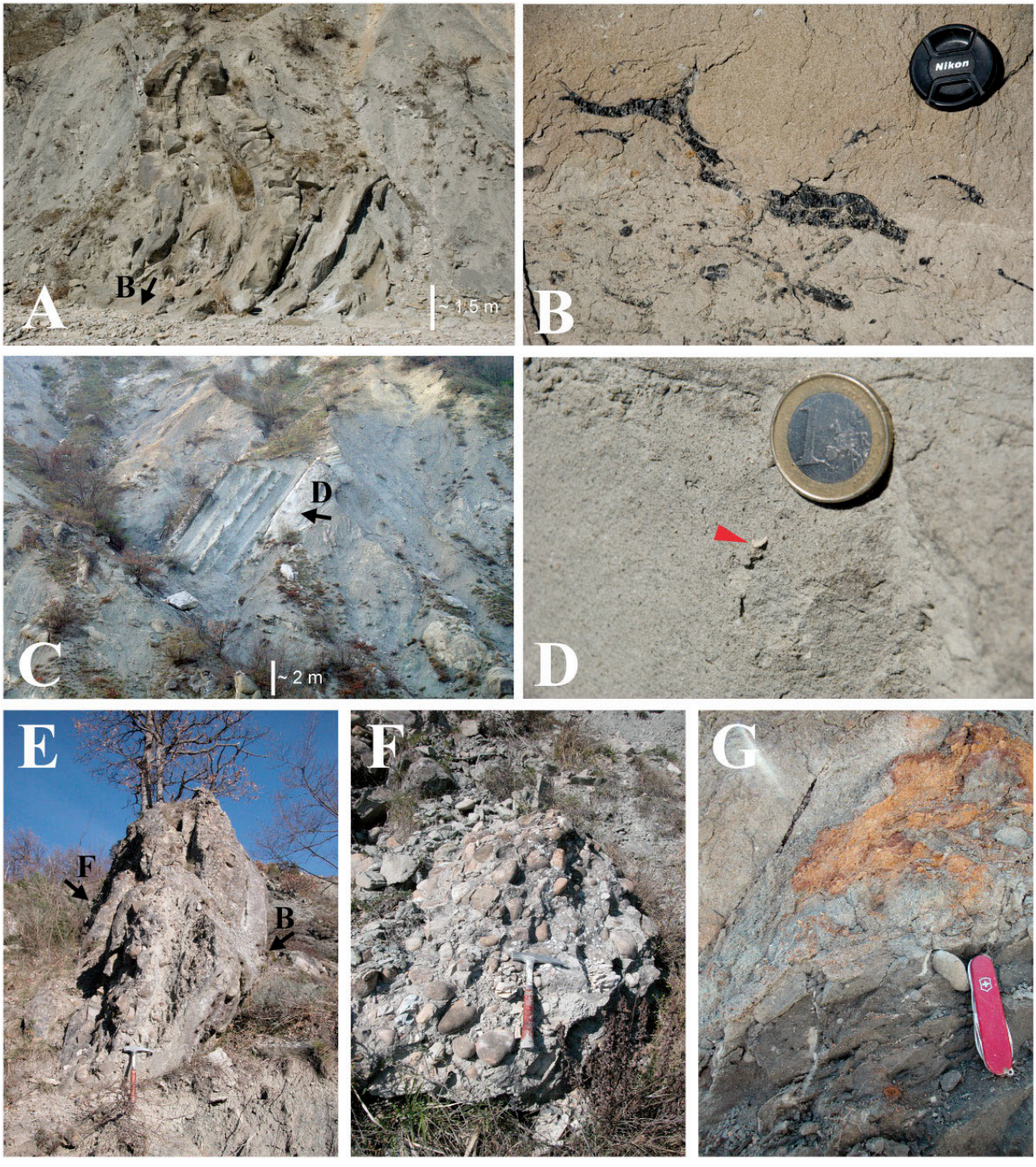
A
B
~ 1.5 m
B
Nikon
C
D
~ 2 m
D
E
F
B
F
G

Figure 7.37 - **A**: Example of still stratified, coarse-grained and thick-bedded sandstone block, arranged in a S-like detached fold, contained within the R2/d sub-unit in the Sx Pessola section.

B: Close-up of A, showing coalified plant fragments (up to tens of dm-sized), which characterize upper portions of component sandstone beds. Camera lens cap for scale, 7 cm in diameter.

C: Relatively well-cemented and stratified sandstone block contained within the R2/d sub-unit in the Sx Pessola section. These sandstone beds are characterized by a more abundant carbonatic content (favoring incipient cementation), and the diffused presence of *nummulites* and shell debris, as well as glauconitic grains (resulting in a faintly greenish alteration color).

D: Close-up of C, showing a *nummulite* fossil (labeled with a red arrow) scattered within the medium-to fine-grained sandy material; darker particles are represented by glauconitic aggregates. One Euro coin for scale, 2,2 cm in diameter.

E: Example of a stratified, m-sized, conglomerate-coarse sandstone block (sub-verticalized) recognizable in the Specchio section. These kinds of blocks are diagnostic of the R2/d sub-unit. Hammer for scale.

F: Close-up of E, showing the common appearance of the component conglomerates. Well-rounded carbonatic and sedimentary (mainly sandstone) pebbles show both local clast- (ortho-conglomerates) and matrix-supported (para-conglomerates) textures; the finer material is represented by a coarse- to medium-grained sandstone. Hammer for scale.

G: Close-up of E, showing block margins and the enclosing pebbly mudstone matrix. Note the significant occurrence of variously oxidized plant fragments (up to tens of dm-sized), characterizing marginal component beds of the block and dispersed within the matrix. Knife for scale, 9 cm long.

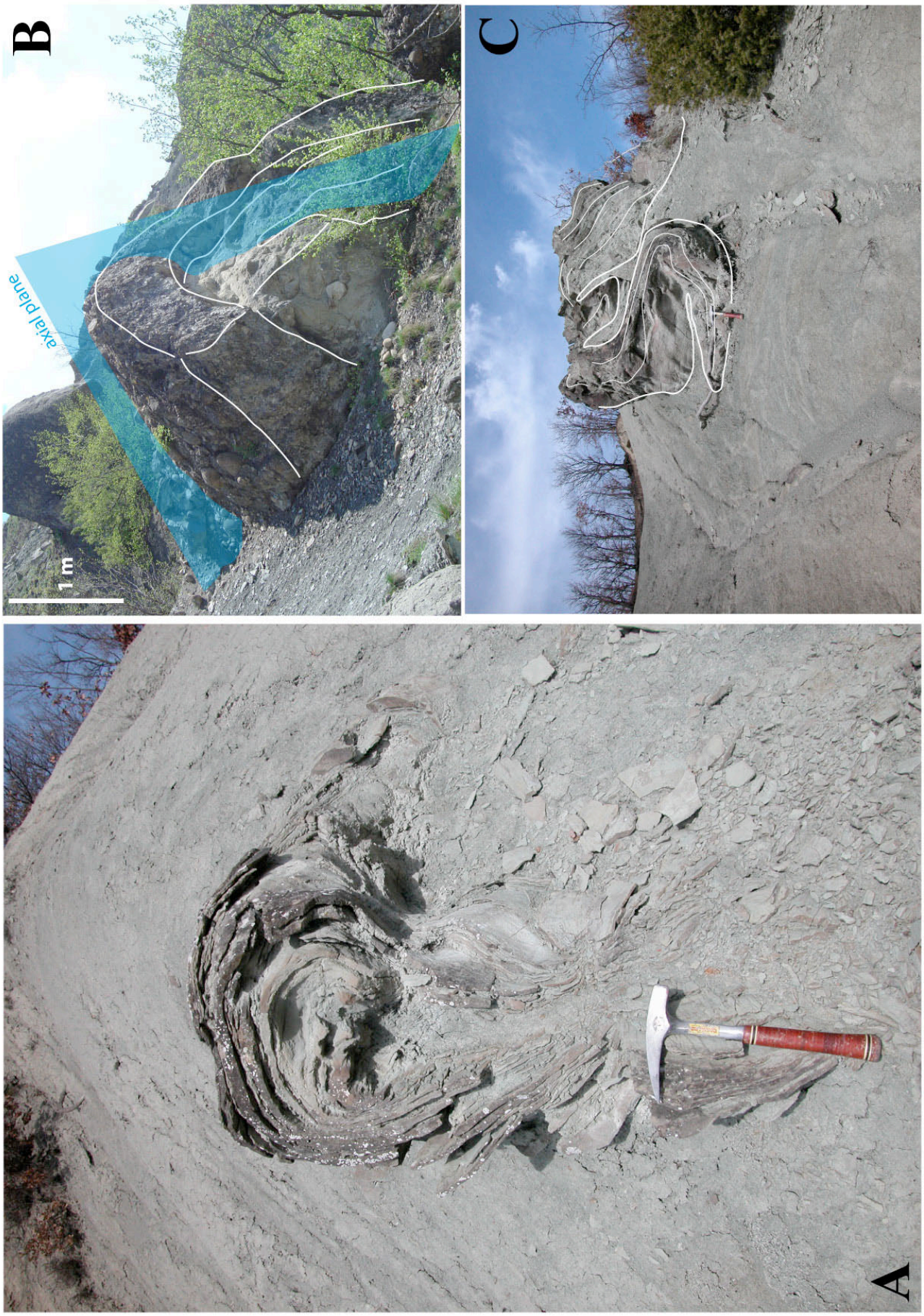
B
axial plane
1 m
C
A

Figure 7.38 - Meso-scale appearance of folds characterizing R2/d sub-unit in the Pratorotondo section.

A: Example of box-like fold (EBF) developed in thin-bedded sandstones, characterized by vertical axial plane, slightly curving axis, limbs parallelization, and expulsion of the core zone (overpressured conditions into the hinge zone). Hammer for scale.

B: Example of symmetric antiformal synline (EBF) developed in conglomeratic lithologies (coarse-grained sandstone in the core) and characterized by a vertical axial plane (labeled in transparent blue). Fold contours are labeled.

C: Example of a deformed thin-bedded sandstone block showing complex folding (and probable refolding) and enclosing matrix injections into the core zones. These structures are likely to develop in a passive way due to the generalized enclosing matrix movement. Hammer for scale.

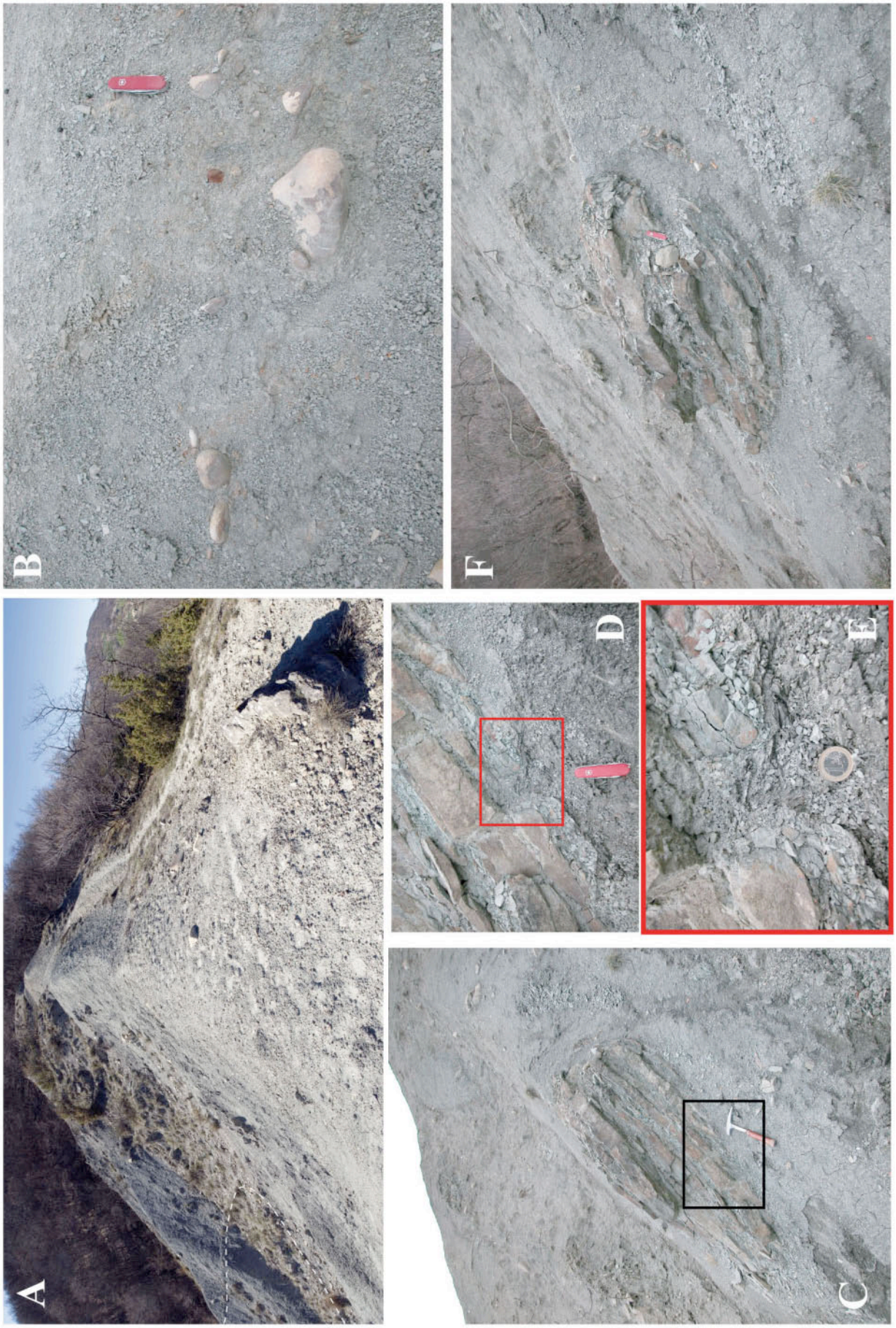
B
F
A
D
E
C

Figure 7.39 - Outcrop examples of the R2/e sub-units in the Sx Pessola section.

A: General view of the outcrop appearance of the R2/e sub-unit. Note the overall homogeneous aspect, with sparse presence of isolated, generally m-sized sandstone blocks, and carbonatic pebbles and cobbles. The contact with the underlying R2/d sub-unit is roughly indicated by the white dashed line.

B: Detail of the pebbly/sandy mudstone matrix and the enclosed well-rounded carbonatic pebbles. Knife for scale, 9 cm long.

C: Example of lenticular-shaped (phacoidal), m-sized, still stratified thin-bedded sandstone block, commonly occurring within the R2/e sub-unit. Hammer for scale.

D: Close-up of C, showing the lower block margin and the surrounding pebbly mudstone matrix. Note the matrix injection cutting the block margin. Knife for scale, 9 cm long.

E: Close-up of D, showing in detail the matrix injection. Note the pseudo-foliation trend of the matrix and the inward bending of the block margin. One Euro coin for scale, 2,2 cm in diameter.

F: The same block shown in C, viewed from a different perspective to highlight the evident lenticular appearance. Note matrix intrusions roughly along the stratification. Knife for scale, 9 cm long.

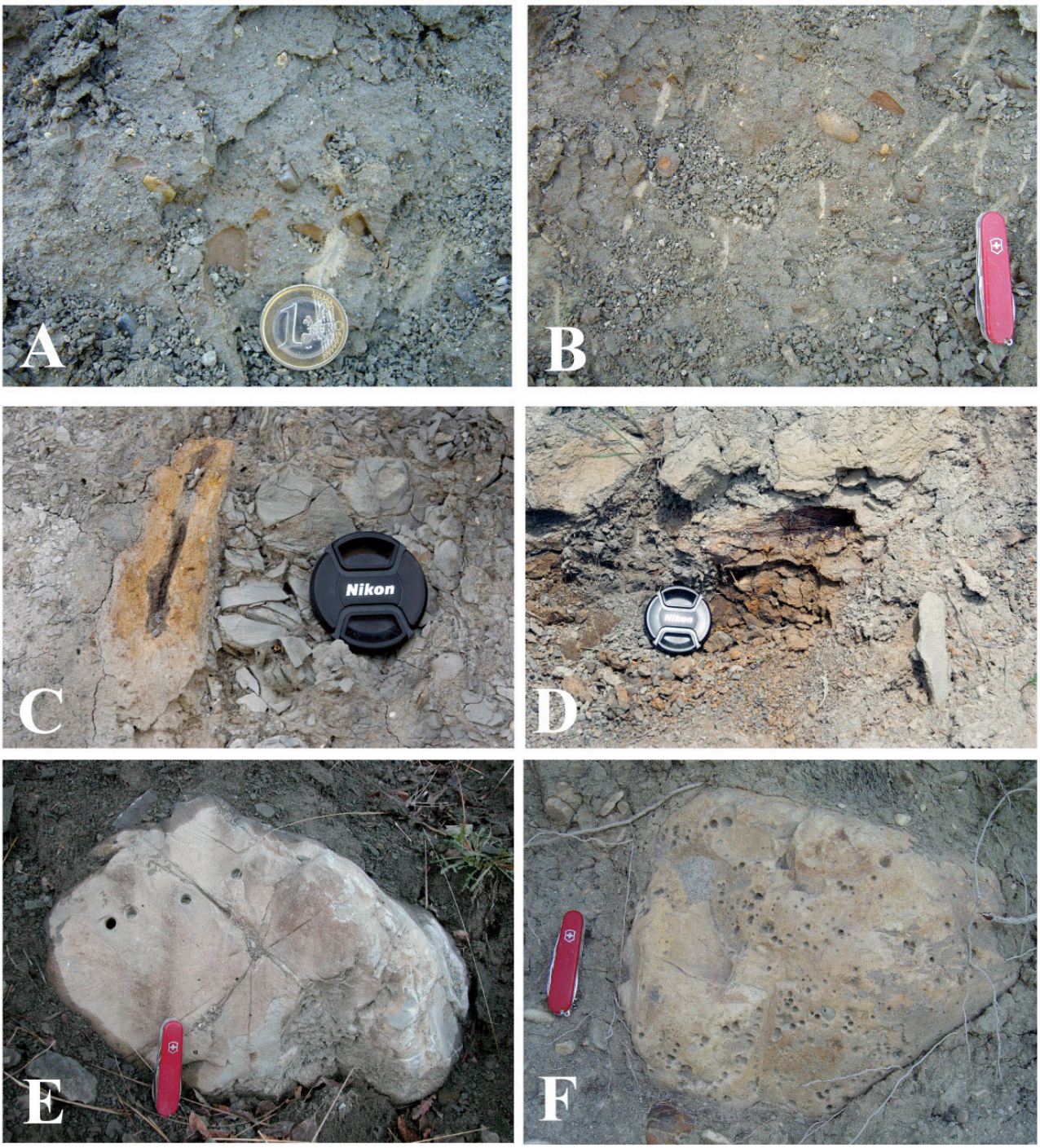
A
B
Nikon
C
D
E
F

Figure 7.40 - **A**: R2/e sub-unit matrix appearance (pebbly mudstone) in the northernmost outcrops of the Pessola valley outlier. One Euro coin for scale, 2,2 cm in diameter.

B: R2/e sub-unit matrix appearance (pebbly/sandy mudstone) in the Fosio section. Knife for scale, 9 cm long.

C: Ten of cm-sized coalified plant fragments (and related oxidation halo) recognized within the enclosing matrix in the Sx Pessola section. Camera lens cap for scale, 7 cm in diameter.

D: Cm-sized oxidized plant fragments observed in the Camera lens cap for scale, 7 cm in diameter.

Dordia section (see attached Panels n. 1 and n. 2). Camera lens cap for scale, 7 cm in diameter.

E: Sub-rounded carbonatic cobble showing evidences of bioerosional burrowings (lithodome holes), observed within the uppermost portion of the R2/e sub-unit in the Dx Pessola section. Knife for scale, 9 cm long.

F: Sub-rounded carbonatic cobble strongly affected by lithodome holes, recognized within the uppermost portion of the R2/e sub-unit, in the northern outcrops of the Pessola Valley outlier. Knife for scale, 9 cm long.

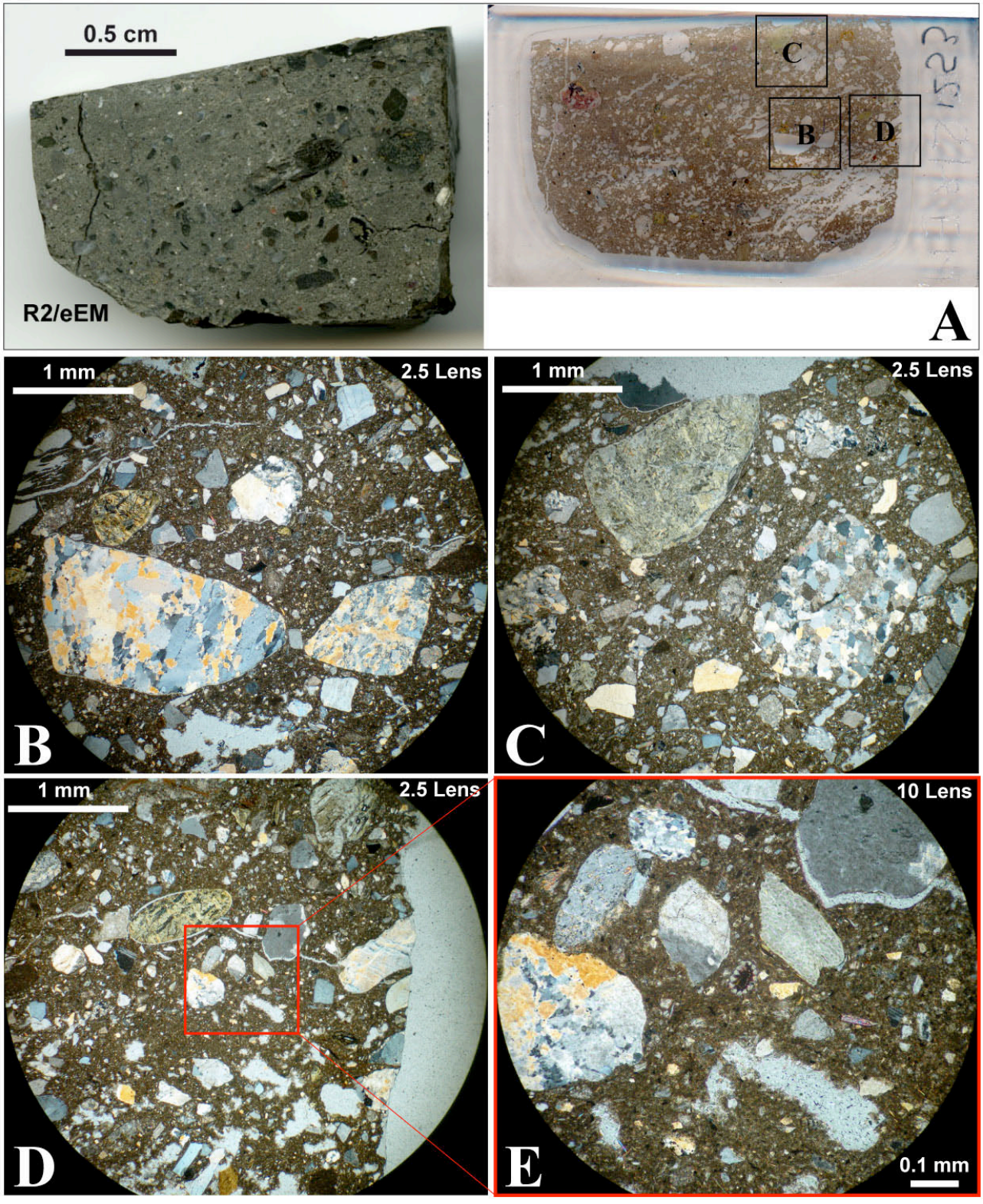
0.5 cm
R2/eEM
C
B
D
A
1 mm
2.5 Lens
B
1 mm
2.5 Lens
C
1 mm
2.5 Lens
D
10 Lens
0.1 mm
E

Figure 7.41 - **A**: Thin section and polished counter-cut of sample R2eEM. For location see chap. 2. In this case, nonetheless the fine-grained material dominance, the lithologies seem relatively well cemented.

B: General appearance of the matrix. The overall characteristics are similar to those observed for the other samples (apart for R2bIBT and R2bEM), with the typical "block-in-matrix" texture. Larger particles are well rounded while smaller ones share angular shapes. Note the enveloping pattern of the matrix around rigid elements and the sparse occurrence of mm-thick calcite veins.

C: Another general view of the matrix. Note calcite haloes and enveloping pattern of the matrix around the larger rigid particles.

D: Overview of a slightly more fine-grained portion of the matrix. Note the mm-calcite vein cutting the matrix and joining thin haloes characterizing grain margins. Also these features seem to show fractal (scale-independent) potential of development.

E: Close-up of D, showing in detail relationships between rigid particles and the sustaining plastic matrix. Here the enveloping and "fluidal" character of the finer material is fairly clear. Note the appearance of the mm-thick calcite vein described in D, and the occurrence of well preserved, isolated micro-fossil (radiolarian?).

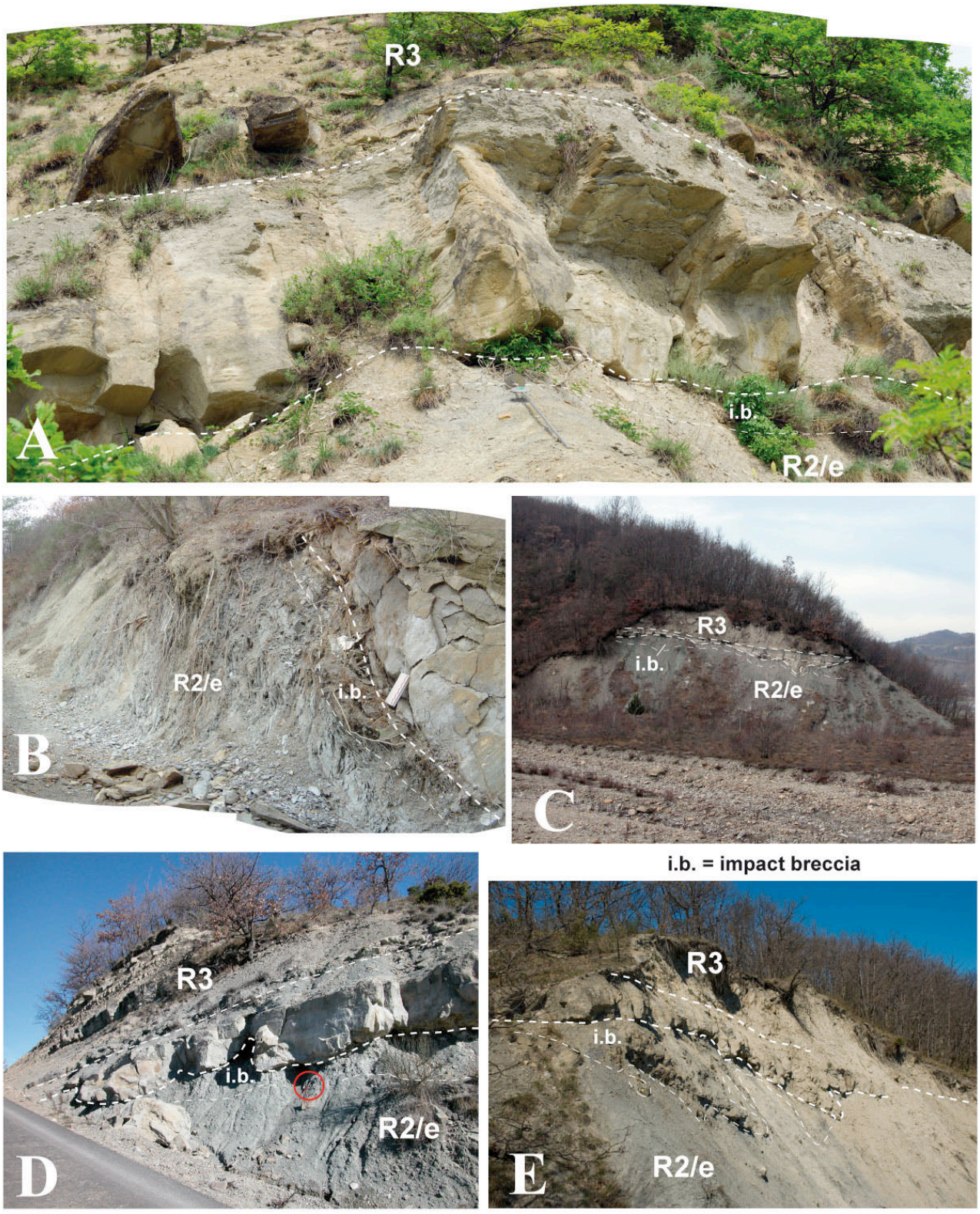
R3
i.b.
R2/e
A
R2/e
i.b.
B
R3
i.b.
R2/e
C
i.b. = impact breccia
R3
i.b.
R2/e
D
R3
i.b.
R2/e
E

Figure 7.42 - Examples showing the general outcrop appearance of the distinctive sandstone bed, representing the first depositional event of the "restored" sedimentation above the Specchio Unit R2, and the upper R2 unit contact. This latter contact is commonly underlined by an "impact breccia"-type interval, developed at the base of the distinctive sandstone bed. Upper and lower bed contacts, and basal "impact-breccia" interval are labeled.

A: Faeto section. Jacob's staff for scale, 1,5 m long.

B: Northernmost outcrops of the Pessola Valley outlier (formally belonging to the Varano de' M.- Pellegrino P. outlier; Madonna section). Field notebook for scale, 20 cm long.

C: Northernmost Sx Pessola section (confluence zone of Pessola and Ceno rivers). Note the irregular base of distinctive sandstone bed and the amalgamation relationships with the overlying thick-bedded R3 unit layer.

D: Fosio section. Note the irregularly trending basal surface of the distinctive sandstone bed on the "impact breccia"-type interval. Encircled hammer for scale.

E: Upper Sx Pessola section. Note the irregular base of the distinctive sandstone bed (deformed) and the discontinuous "impact breccia"-type interval (with some incipient and detached pseudo-nodules foundering into the underlying R2/e sub-unit fine-grained lithologies).

A
i.b.
C
Nikon
B
i.b.
~ 2 m
i.b. = impact breccia

Figure 7.43 - **A**: Photo-mosaic of the distinctive sandstone bed in the northernmost Dx Pessola section. Note the occurrence of a downward-injecting cuspidate structure (with a core of pebbly coarse-grained sandstone material) rooted in the "impact breccia"-type interval and intruding into the underlying R2/e sub-unit lithologies. The "impact-breccia" interval is labeled. Hammer for scale.

B: Photo-mosaic showing a detail of the rock exposure presented in fig. 7.42 C. Here, the distinctive sandstone bed seems to deeply cut into the underlying R2/e sub-unit fine-grained lithologies, forming a downward cuspidate basal structure. The smooth and roughly planar trending of the upper surface of the distinctive bed confirm the sedimentary origin of such structures, instead of a post-depositional nature (*i.e.* differential loading-related structures). The "impact-breccia" interval is labeled.

C: Detail of the lower apex of a cuspidate structure (location is roughy indicated in A). The observed characteristics support the interpretation of such structures as downward injections of coarse-grained material into the pebbly mudstone matrix of the R2/e sub-unit. Sometimes these structures (and particularly their lower apical portions) are detached from the overlying distinctive sandstone bed (and the associated "impact breccia"-type interval), resulting completely enveloped by the enclosing matrix (as pseudo-nodules). This evidence is thought to be related to later (*i.e.* post-depositional) differential movements, mainly due to the structural rearrangement of chaotic lithologies of the underlying R2 unit during and/or immediately after the deposition of the distinctive sandstone bed. Camera lens cap for scale, 7 cm in diameter.

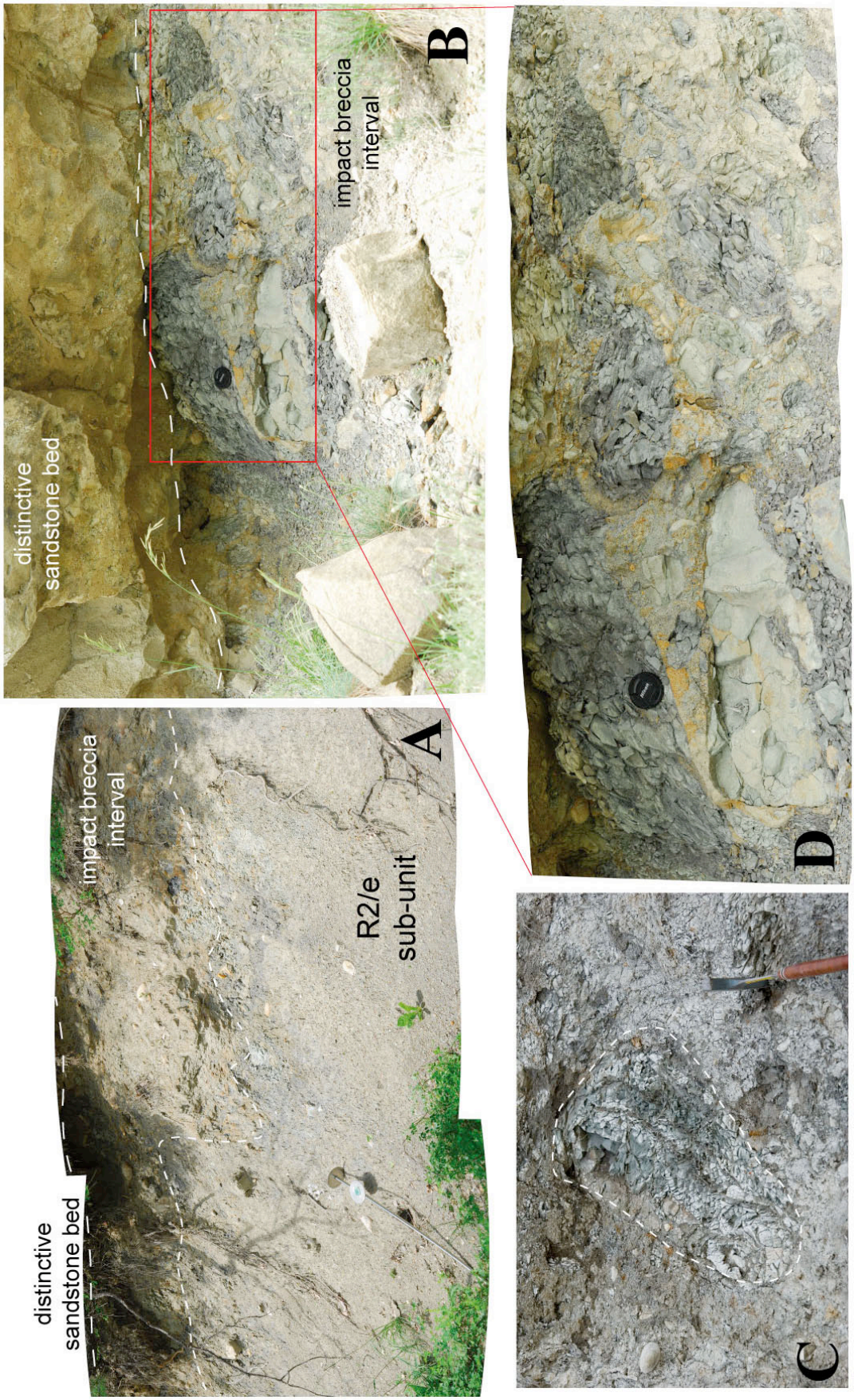
distinctive
sandstone bed
impact breccia
interval
R2/e
sub-unit
A
B
C
D

Figure 7.44 - A: Distinctive sandstone bed "impact breccia"-type interval observed in the Dordia section. The oxidized appearance and coarse-grained nature of this interval is usually well discernible form muddier lithologies of the underlying R2/e sub-unit. Basal surface of the distinctive bed and the "impact breccia"-type interval are labeled. Jacob's staff for scale, 1,5 m long.

B: Detail of the "impact breccia"-type interval in the Faeto section. Camera lens cap for scale, 7 cm in diameter.

C: Example of a pebbly mudstone element (rip-up intra-clast coming form the R2/e sub-unit) characterizing the "impact breccia"-type interval in the Sx Pessola section. Hammer for scale.

D: Close-up of B, showing the typical appearance of the "impact breccia"-type interval. Note the "rounded" mudstone elements (sometimes composed of pebbly mudstone), separated and sustained by oxidized pebbly and coarse-grained sandy material. Fine-grained sandstone elements are also present. The oxidized appearance is mainly due to the significant content of plant fragments. Camera lens cap for scale, 7 cm in diameter.

B
D
A
C
Nikon
Nikon
Nikon
Nikon

Figure 7.45 - Examples of ponding-related opposite facing ripples characterizing the upper laminated part of the distinctive sandstone bed. Some recognizable ripples foresets are labeled. For locations see attached Panel n. 1.

A: Faeto section. Camera lens cap for scale, 7 cm in diameter.

B: Fosio section. Camera lens cap for scale, 7 cm in diameter.

C: Faeto section. Camera lens cap for scale, 7 cm in diameter.

D: Fosio section. Knife for scale, 9 cm long.

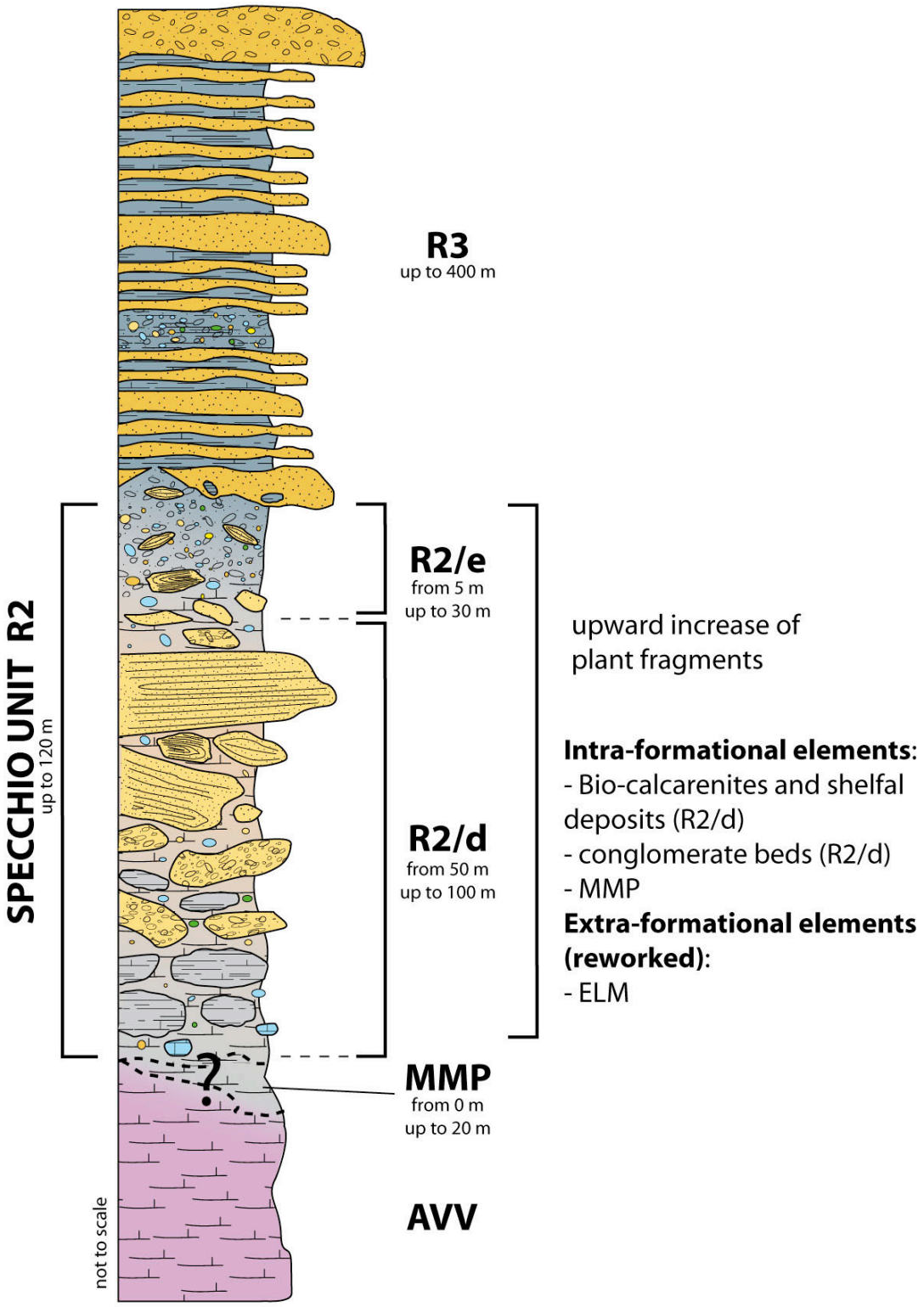

Figure 7.46 - Simplified stratigraphic scheme of the Mt. Roccone outlier focusing on the internal subdivisions of the Specchio Unit R2. Main features and characteristics, as well as inferred thickness are described.

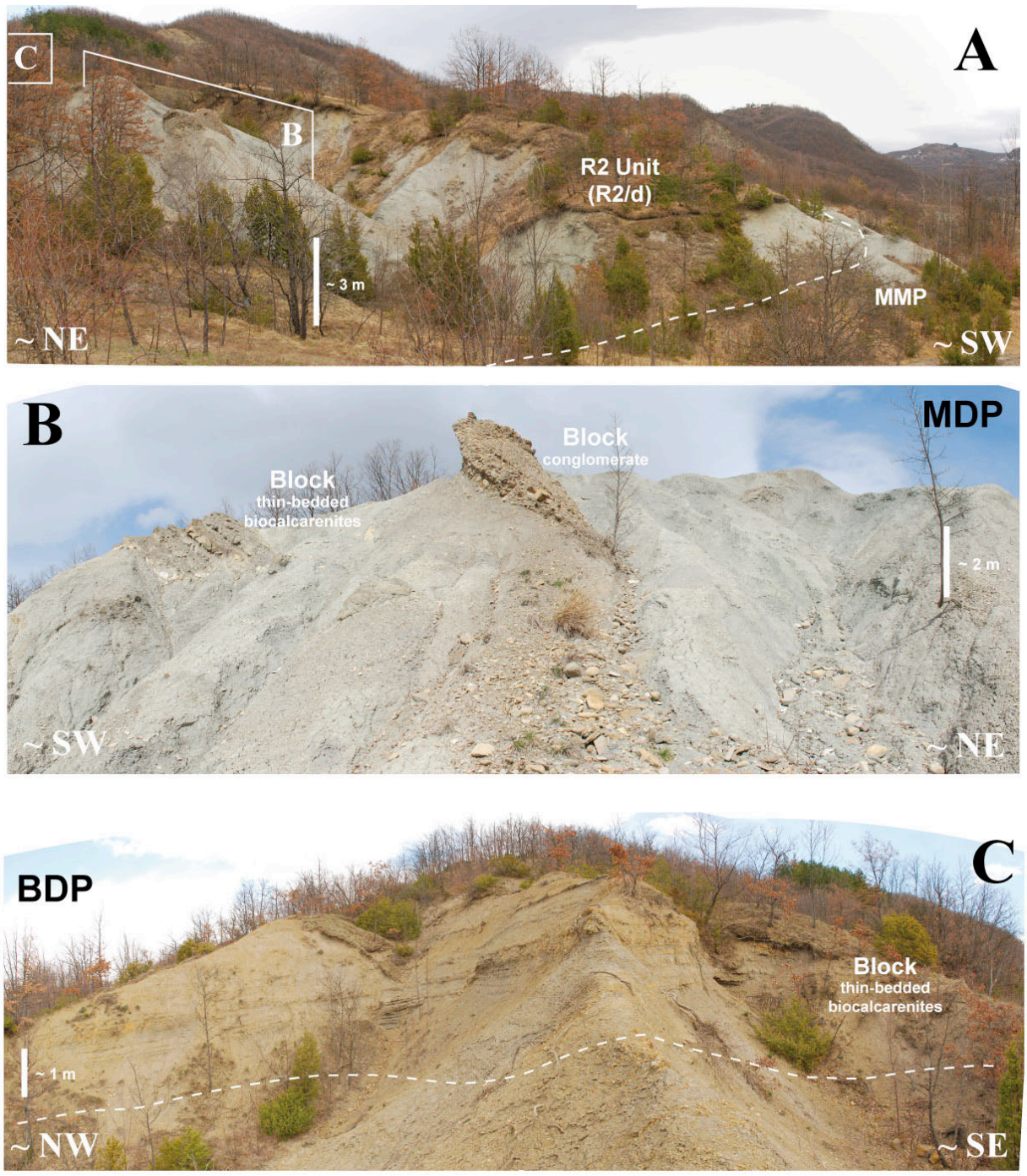

Figure 7.47 - **A**: Panoramic view of the lower Mangiarosto section (for location see attached Panel n. 1 and n. 2). The main contact between MMP unit and the overlying Specchio Unit R2 (here represented by the R2/d sub-unit) is labeled.

B: Close-up of A, showing the common appearance of the lower MDP of the R2/d sub-unit. Two m-sized, folded blocks, made up of conglomerate (to the right) and thin-bedded biocalcarenite (to the left), are sustained by the enclosing pebbly mudstone matrix. The conglomeratic block seems to be arranged as a rootless isoclinalic fold. These blocks show a faintly recognizable "imbricated"-like appearance, roughly verging to the SW (toward the left).

C: Close-up of A, showing the common appearance upper BDP characterizing the R2/d sub-unit in this outlier. Particularly in this photo-mosaic is shown a roughly tabular, tens-of-m-sized block, made up of well-stratified, thin-bedded sandstones characterized by high fossiliferous and carbonatic content.

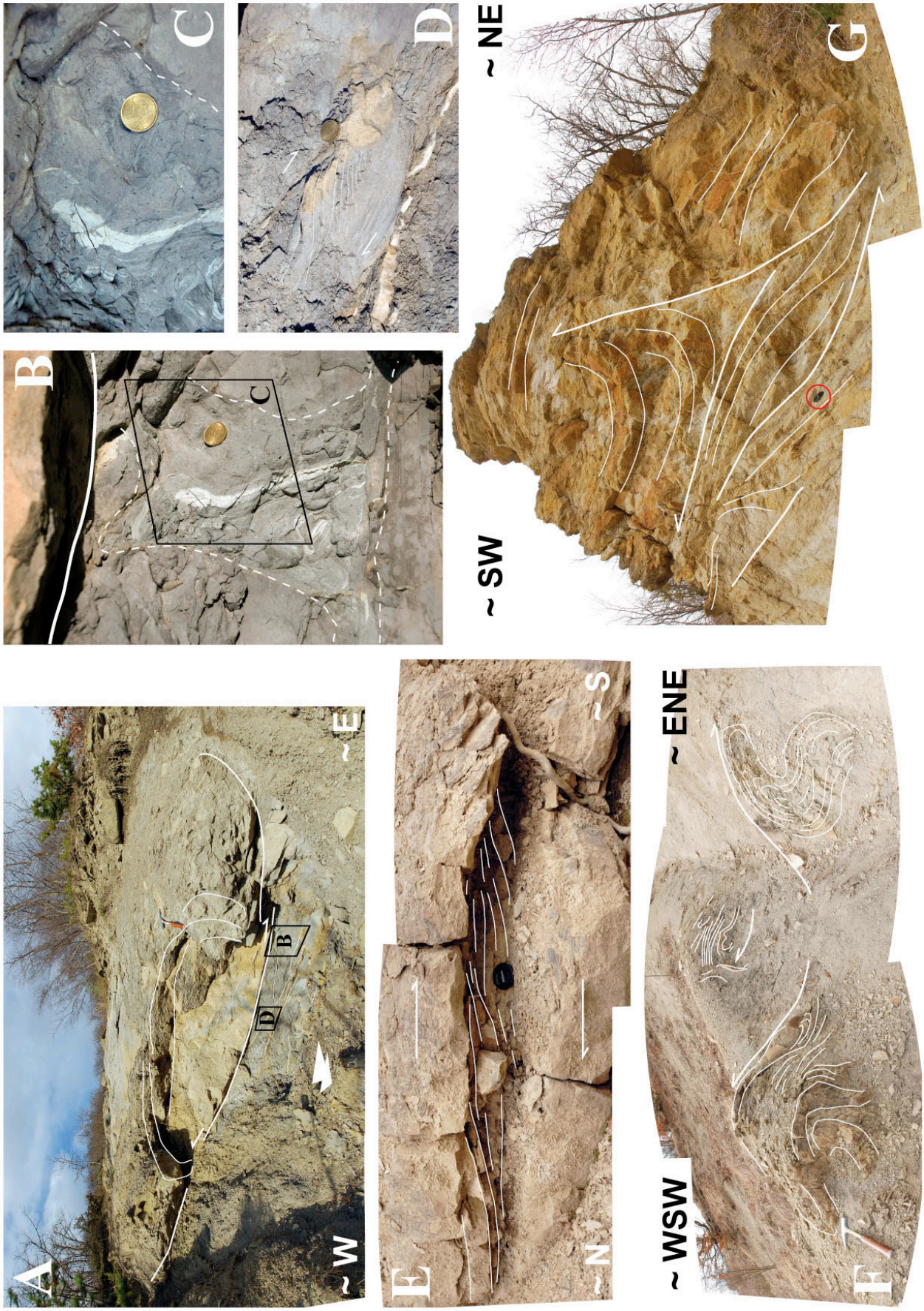
C
D
B
C
~ NE
G
~ SW
A
~ E
B
D
~ W
E
~ S
~ N
~ ENE
~ WSW
F

Figure 7.48 - Some outcrop examples of component elements and structures observed in the R2/d sub-unit in the Mt. Roccone outlier.

A: Example of a roughly tabular, folded, ten-of-m-sized block of thin-bedded biocalcarentites. Particularly, it is presented the base of the block (the rest has been probably eroded away) and the related basal shear zone separating coherent lithologies of the block from the underlying matrix. Note the overall arrangement of the block in a dragging-related, sheath-like fold (white arrow indicates the inferred transport direction). Block basal boundary, representative folded strata and minor shear surfaces are labeled. Southernmost Poggiolo section (for location see attached Panels n.1 and n. 2). Hammer for scale.

B: Close-up of A, showing an upward fluid escape-like structure developed at the base of the block. This structure is rooted in the "liquefied" matrix characterizing a shear surface (EBT) and injects into more coherent matrix portions and/or between discrete muddy components). Structure margins are labeled. Fifty Euro cent coin for scale, 2,4 cm in diameter.

C: Close-up of B, showing in detail the matrix composing the injection-like structure. It is mainly pebbly sandstone, with some sandy content. Particularly, this kind of matrix differs from the hosting one for the presence of strongly deformed and partially mixed marly intra-clasts (MMP unit?), arranged in complex fluidal-like folds. Structure margins are labeled. Fifty Euro cent coin for scale, 2,4 cm in diameter.

D: Close-up of A, showing an example of SC-type structures involving both matrix and an enclosed softly deformed biocalcarenite fragment, developed within a minor EBT. Note the cm-thick fibrous calcite vein in the lower side of the photo; this vein is thought to be of later origin, developing along the preexisting planar discontinuity represented by the margin of the minor EBT. Structural features and inferred shear sense are labeled. Fifty Euro cent coin for scale, 2,4 cm in diameter.

E: Example of a shear zone developed in a layer-parallel way, within a tens-of-m-sized, stratified block. The overall shearing sense is given by relatively well-developed sigmoidal-like pattern (labeled) of this IBT, probably developed through progressive deformation of a thin-bedded interlayer. Lower Poggiolo section (for location see attached Panels n.1 and n. 2). Camera lens cap for scale, 7 cm in diameter.

F: Example of opposite-verging shear zones and related folded blocks within a localized MDP. The inferred palaeo-transport direction is roughly directed toward the viewer. These kind of structure associations is thought to commonly represent transversal cuts (in the sense of transport) of MDPs, as described in fig. 7.11. Blocks' features and inferred shear surfaces are labeled. Confine section (for location see attached Panels n.1 and n. 2). Hammer for scale.

G: Example showing a system of shear surfaces (IBTs) and related folds (IBF), affecting the exposed margin of a ten-of-m-sized biocalcarenite block in the Mangiarosto section. Beds are softly deformed, up to complete disruption (*i.e.* proto-matrix) within and close to IBTs. Inferred palaeo-transport direction is roughly toward the SW. Encircled camera lens cap for scale, 7 cm in diameter.

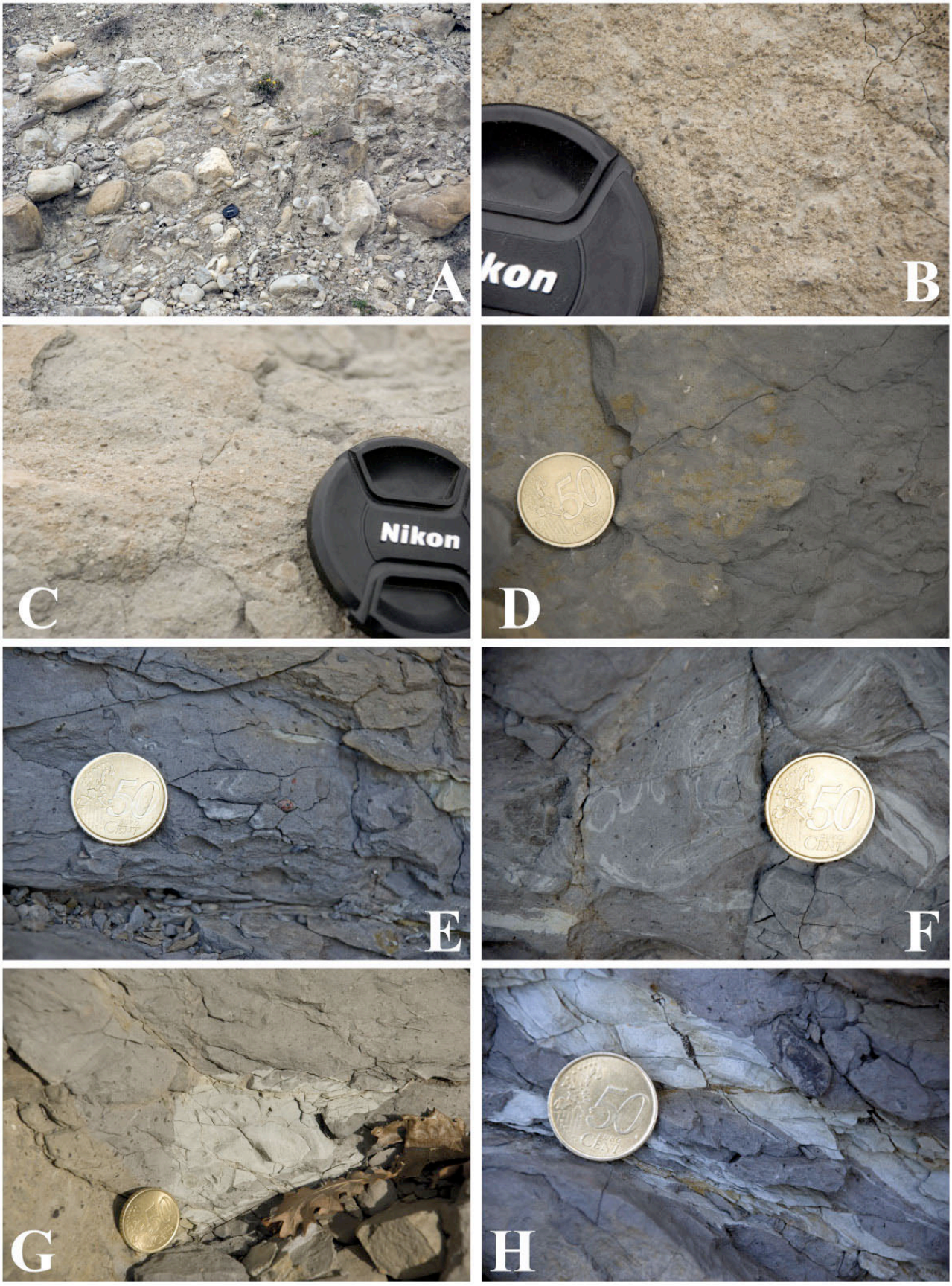
A
B
C
Nikon
D
E
F
G
H

Figure 7.49 - Some examples illustrating lithologic characteristics of the component block and matrix of the R2/d sub-unit in the Mt. Roccone outlier.

A: Photo showing the overall appearance of conglomeratic lithologies composing R2/d sub-unit blocks in the Mangiarosto section. Composing elements are well-rounded cobbles and pebbles, mainly of carbonatic and siliciclastic origin, with a variable amount of coarse sand representing the finer fraction. Camera lens cap for scale, 7 cm in diameter.

B: Detail of the base of a thin, bioclast-rich sandstone bed, composing m- to tens-of-meter-sized blocks in the Mangiarosto section. Abundant darkish grains are mainly *nummulites*. Camera lens cap for scale, 7 cm in diameter.

C: Detail of a medium-thick, bioclast-rich sandstone bed, composing generally m-sized blocks (single detached beds) in the lower Poggiolo section. Note the more "diluted" arrangement of *nummulites* respecting to that observable within thin-bedded example shown in B. Camera lens cap for scale, 7 cm in diameter.

D: Example of enclosing matrix (pebbly mudstone) with scattered bioclasts (*nummulites*), observed in the Poggiolo section. Fifty Euro cent coin for scale, 2,4 cm in diameter.

E: Example of an enclosing matrix developed near the margin of a m-sized block. The sandy content of this pebbly mudstone increases toward the block margin (upwards). Note the presence of well-rounded ophiolitic pebbles and muddy intra-clasts. Poggiolo section. Fifty Euro cent coin for scale, 2,4 cm in diameter.

F: Detail of the enclosing pebbly mudstone matrix, showing the occurrence of hydroplastically deformed (and almost fully mixed), marly intra-clasts, giving an overall fluidal-like appearance. Poggiolo section. Fifty Euro cent coin for scale, 2,4 cm in diameter.

G: Example of cm-sized marly intra-clast contained within a pebbly/sandy mudstone matrix. Note the scattered occurrence of bioclasts, and the intra-clast margins incipiently merging into the surrounding matrix. Confine section. Fifty Euro cent coin for scale, 2,4 cm in diameter.

H: Detail of the pebbly/sandy mudstone characterizing an EBT in the Poggiolo section. Note the plastically stretched appearance marly intra-clasts (disposed parallely to the shear zone margins). Poggiolo section. Fifty Euro cent coin for scale, 2,4 cm in diameter.

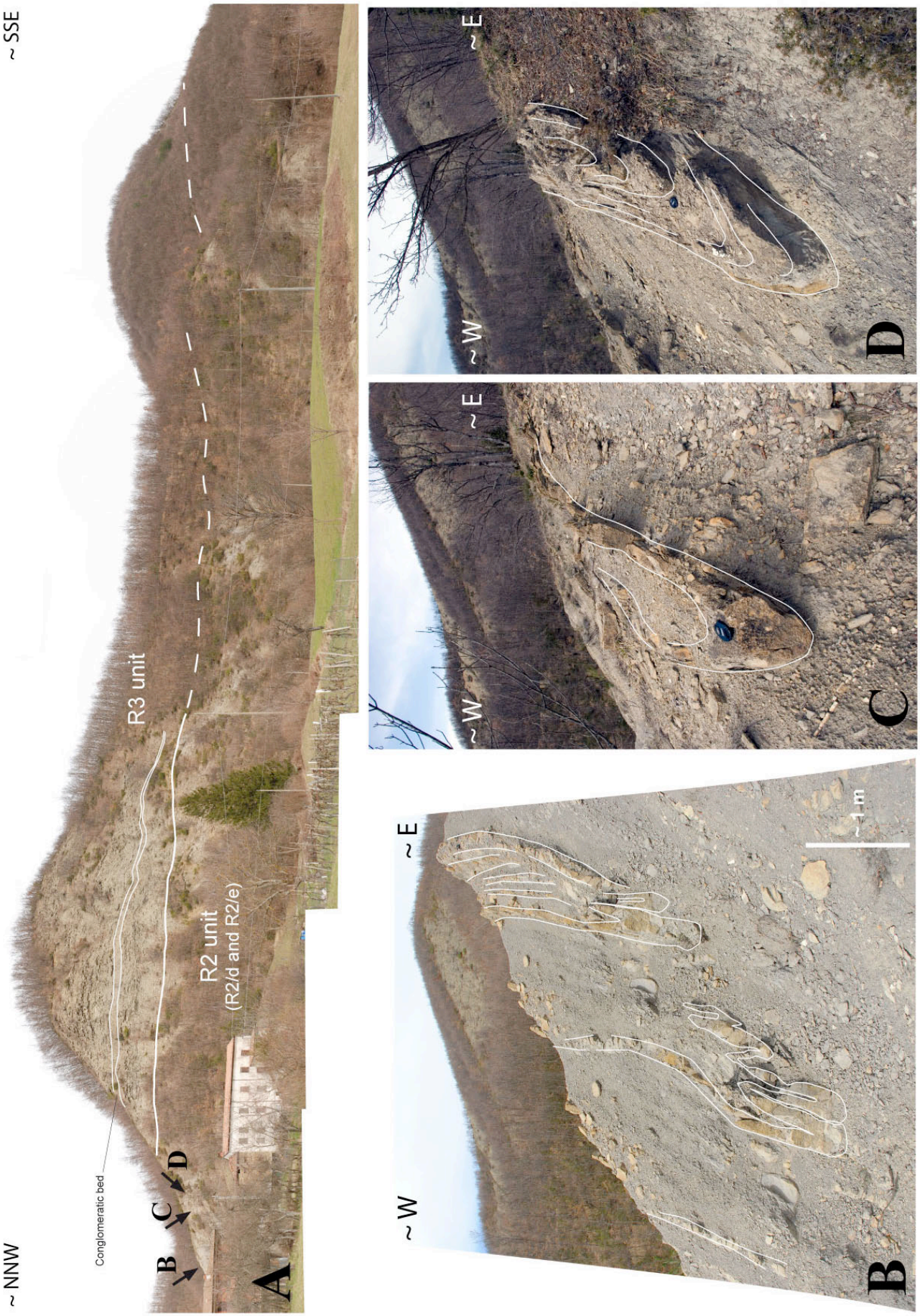
~ NNW
~ SSE
A
B
C
D
R3 unit
R2 unit
(R2/d and R2/e)
Conglomeratic bed
~ W
~ E
~ 1 m

Figure 7.50 - A: Panoramic photo-mosaic of the Poggiolo section (for location see attached Panes n. 1 and n. 2). The solid-dashed white line indicates the boundary between R2 and R3 units. The distinctive conglomeratic bed characterizing the lower portion of the R3 unit is also labeled (see chap. 5 for discussion).

B: Meso-scale tight- to isoclinal folds system (with roughly sheath-like geometries) characterized by sub-vertical axial planes. Folds geometries are labeled. Location is roughly indicated in A.

C: Isoclinal synformal fold with a sub-verticalized axial plane. Note the hinge zone thickening. Fold geometry is labeled. Camera lens cap for scale, 7 cm in diameter. Location is roughly indicated in A.

D: Example of a vertical trending, meso-scale sheath-like fold, showing an exposed cut roughly perpendicular to the main long axis. Fold geometry is labeled. Camera lens cap for scale, 7 cm in diameter. Location is roughly indicated in A.

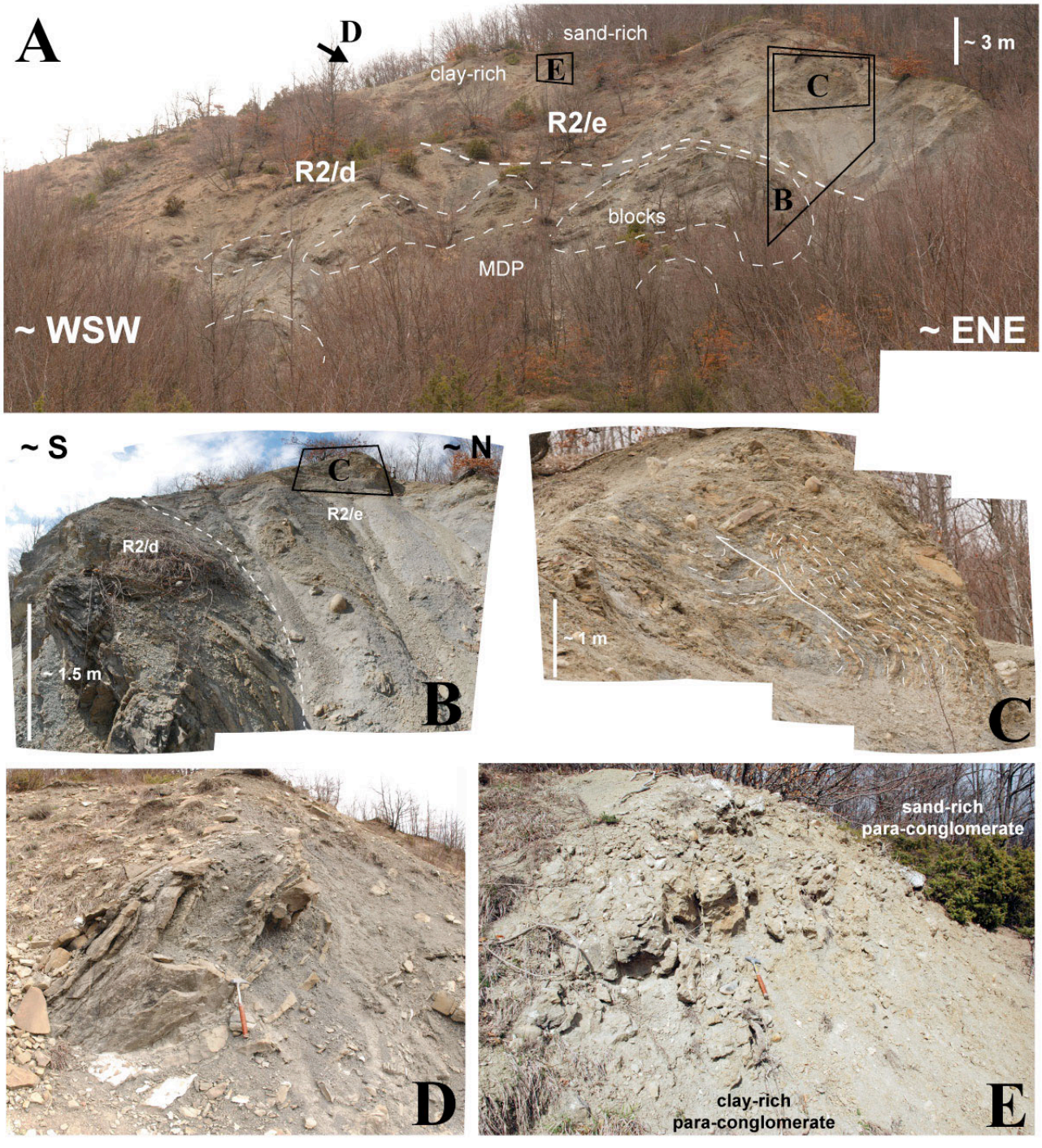
A
D
sand-rich
clay-rich
E
C
~ 3 m
R2/e
R2/d
B
blocks
MDP
~ WSW
~ ENE
~ S
~ N
C
R2/e
R2/d
~ 1.5 m
B
~ 1 m
C
D
sand-rich
para-conglomerate
clay-rich
para-conglomerate
E

Figure 7.51 - A: Panoramic photo-mosaic of the Confine section (for location see attached Panes n. 1 and n. 2). Here it is possible to observe the R2/e sub-unit overlying the R2/d sub-units. Main blocks' boundaries, internal structural-compositional portions and the main separation surface are labeled.

B: Close-up of A, showing in detail the boundary between R2/d and R2/e sub-units. Main contact surface is labeled.

C: Example of a highly disrupted thin-bedded sandstone block (almost completely merged into the enclosing matrix) localized within the middle-upper portion of the R2/e sub-unit. Note the occurrence of a shear zone (EBT) and related fold (EBF). These kinds of blocks seem to be associated in isolated clusters within the MDPs. Fold geometry and shear surface are labeled. Location is indicated in A and B.

D: An example of a lens-shaped (phacoidal), thin-bedded bioclastic sandstone block contained within the matrix. Where a three-dimensional view is allowed, these blocks seem to show sheath-like geometries. These kinds of elements are commonly observed within the R2/e sub-unit. Note the enclosing matrix (pebbly mudstone) injection into the core of the structure. Hammer for scale. Indicative location is shown in A.

E: Example of the local appearance of the uppermost R2/e sub-unit; with a lower clay-rich para-conglomerate portion, grading downward into the typical enclosing matrix, and an upper sand-rich conglomerate portion, which seems to grade upward (and laterally?) into the "impact breccia"-like interval characterizing the upper limit of the R2 unit (distinctive sandstone bed; see text for discussion). No clear separation seems to exist between these two portions. Hammer for scale. Location is indicated in A.

G
H
D
E
F
A
B
C

Figure 7.52 - A: Overall appearance of the R2/e sub-unit in the Confine section (for location see attached Panes n. 1 and n. 2). Note the classic block-in-matrix fabric (MDPs). Hammer for scale.

B: Detail of a typical lens-shaped, folded, thin-bedded bioclastic sandstone block. Same element shown in fig. 7.51 D, viewed from another perspective. Note the complex soft sediment deformation-related internal folding (rough sheath-fold like geometry?). Hammer for scale.

C: Detail of a rootless, matrix-sustained sheath-like fold developed in thin-bedded bioclastic sandstone strata. Taverna section (easternmost outcrops of the Mt. Roccone outlier; for location see attached Panels n. 1 and n. 2). Hammer for scale.

D: Detail of the enclosing matrix typical of the R2/e sub-unit in the Confine section. It resembles a pebbly mudstone (locally with significant sandy fraction), characterized by sparse mainly carbonatic pebbles and cobbles, and soft mudstone/fine-sandstone intra-clasts. Hammer for scale.

E: Example of a dm-sized coalified plant fragment recognized within the matrix in the Confine section. Such elements are relatively abundant in this sub-unit. Camera lens cap for scale, 7 cm in diameter.

F: Detail of a bioclastic (*nummulites*), thin-bedded sandstone bed composing the lens-shaped block shown in B. Camera lens cap for scale, 7 cm in diameter.

G: Well-rounded, fine-grained sandstone cobble characterized by evidence of lithodome hole. Confine section. Camera lens cap for scale, 7 cm in diameter.

H: Outcrop appearance of the sand-rich para-conglomerate portion characterizing the uppermost part of the R2/e sub-unit in the Confine section (see fig. 7.51 E). Hammer for scale.

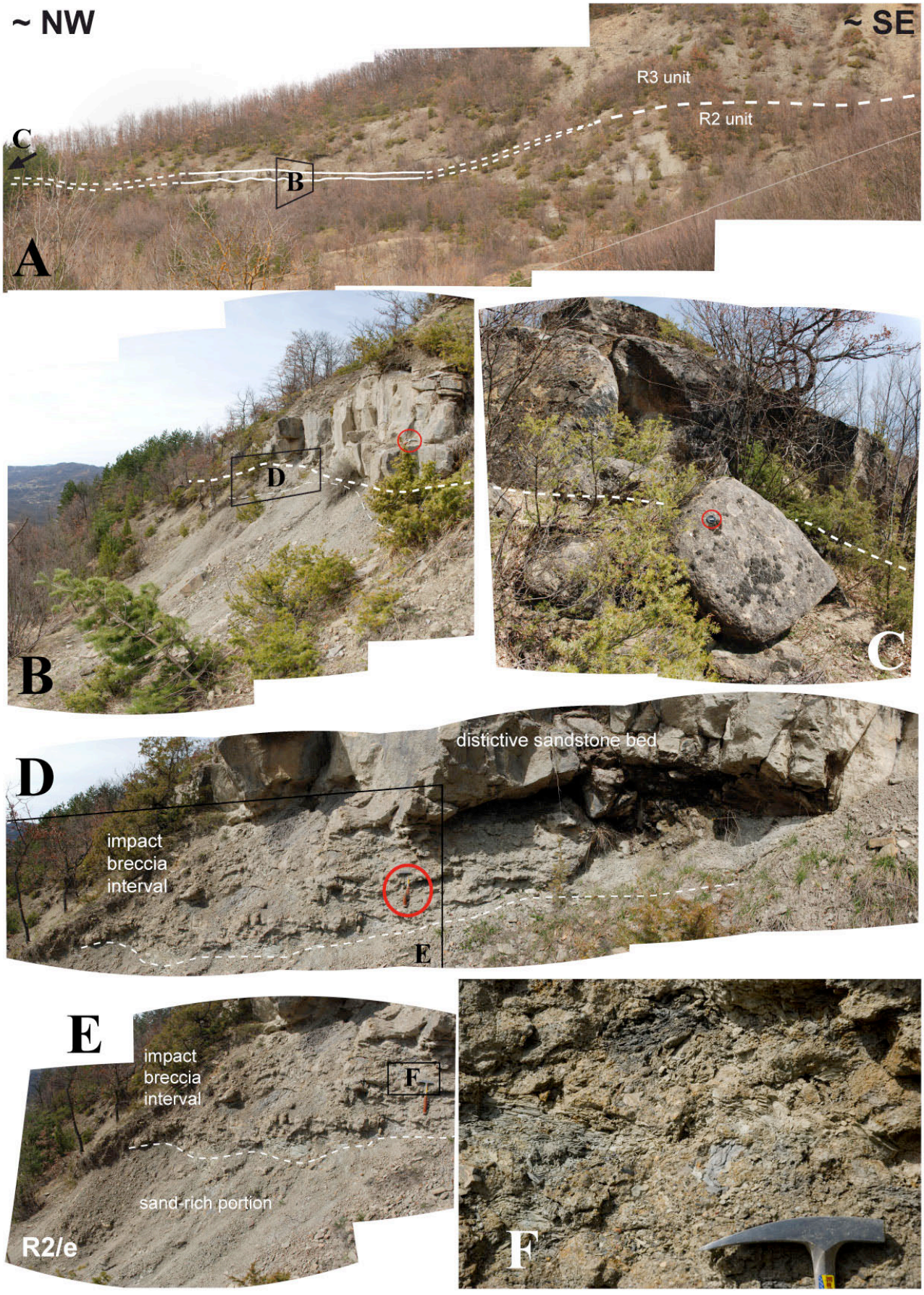
~ NW
~ SE
R3 unit
R2 unit
C
B
A
D
B
C
distictive sandstone bed
D
impact
breccia
interval
E
E
impact
breccia
interval
F
sand-rich portion
R2/e
F

Figure 7.53 - **A**: Panoramic photo-mosaic of the southeastern side of the Mangiarosto section (for location see attached Panes n. 1 and n. 2). The distinctive sandstone bed (labeled), representing the conceptual upper contact of the R2 unit, crops out in this section, apparently wedging out to the SE and disappearing in the other sections.

B: Outcrop appearance of the distinctive sandstone bed. In this case, this bed seems amalgamated with an overlying one, sharing the same characteristics. Underlying fine-grained lithologies belong to the R2/e sub-unit. Encircled hammer for scale. Location is shown in A.

C: Appearance of the distinctive sandstone bed in the north-westernmost side of the Mangiarosto section. Encircled camera lens cap for scale, 7 cm in diameter. Indicative location is shown in A.

D: Close-up of B, showing the basal "impact breccia"-like interval commonly underlying the distinctive sandstone bed. Note their irregular contact. The boundary with the underlying R2/e sub-unit lithologies is labeled. Encircled hammer for scale.

E: Detail of D, showing the passage between the sand-rich portions locally characterizing the uppermost R2/e sub-unit, and the overlying "impact breccia"-like interval. Apparent limit between the two is roughly labeled. Hammer for scale.

F: Close-up of E, showing the typical appearance of the "impact breccia"-like interval. Hammer for scale.

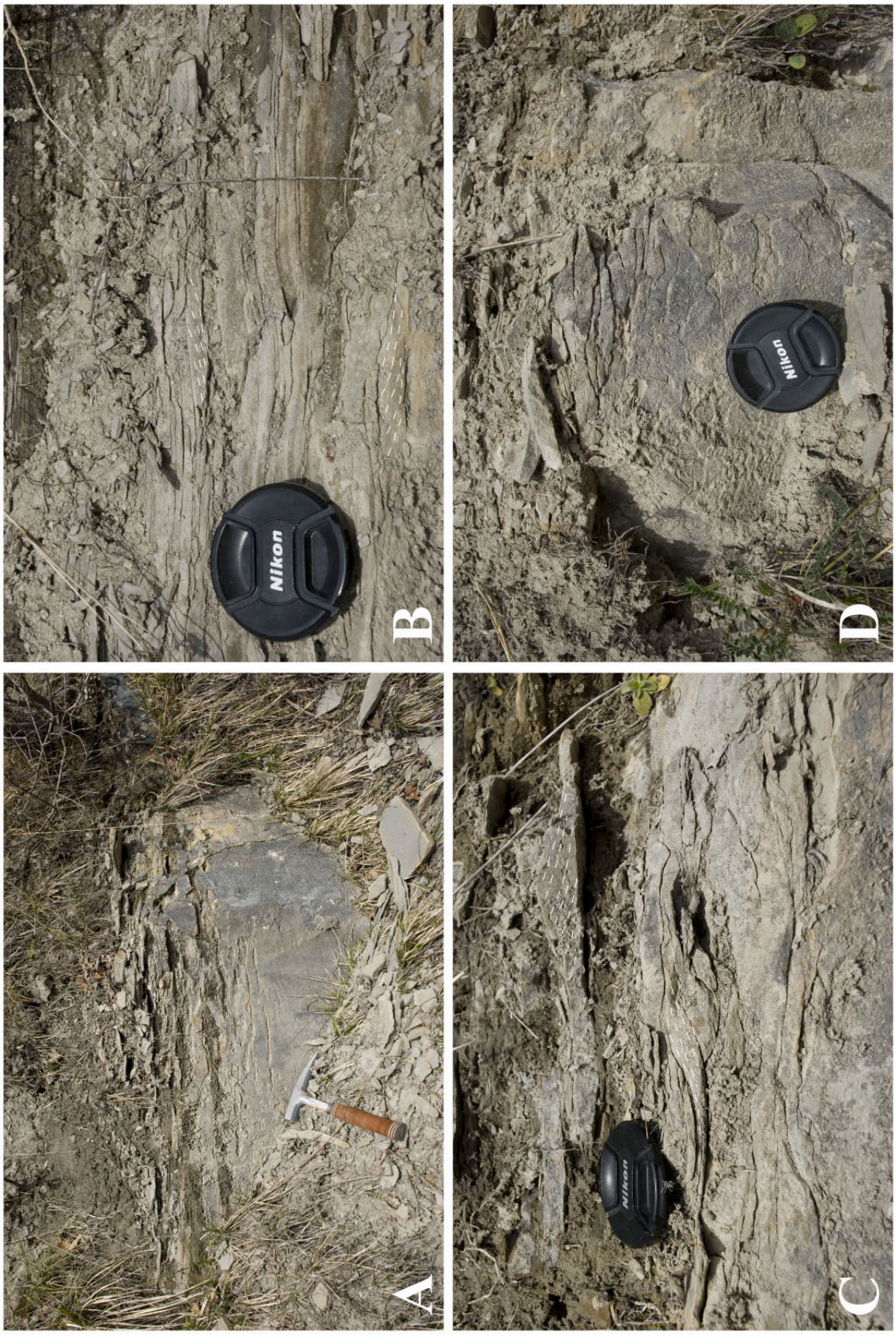
B
D
A
C

Figure 7.54 - Outcrop examples of the upper laminated part of the distinctive sandstone bed. The poor outcrop conditions avoid detailed characterization, nonetheless some evidence of apparent opposite-verging ripples have been recognized.

A: Overall appearance of the upper part of the distinctive sandstone bed in the southern side of the Mangiarosto section. Hammer for scale.

B: Detail of the laminated portion of the distinctive sandstone bed in the southern side of the Mangiarosto section (few meters to the E from the location shown in A). Still recognizable, opposite-verging ripples' foresets are labeled. Camera lens cap for scale, 7 cm in diameter.

C: Detail of the laminated portion of the distinctive sandstone bed in the southern side of the Mangiarosto section (few meters to the E from the location shown in B). Still recognizable, opposite-verging ripples' foresets are labeled. Camera lens cap for scale, 7 cm in diameter.

D: Detail of the laminated portion of the distinctive sandstone bed in the southernmost side of the Mangiarosto section (roughly a ten of meters to the E from the location shown in C). Here the distinctive sandstone bed seem to be strongly thinned, nonetheless it is almost completely covered. Camera lens cap for scale, 7 cm in diameter.

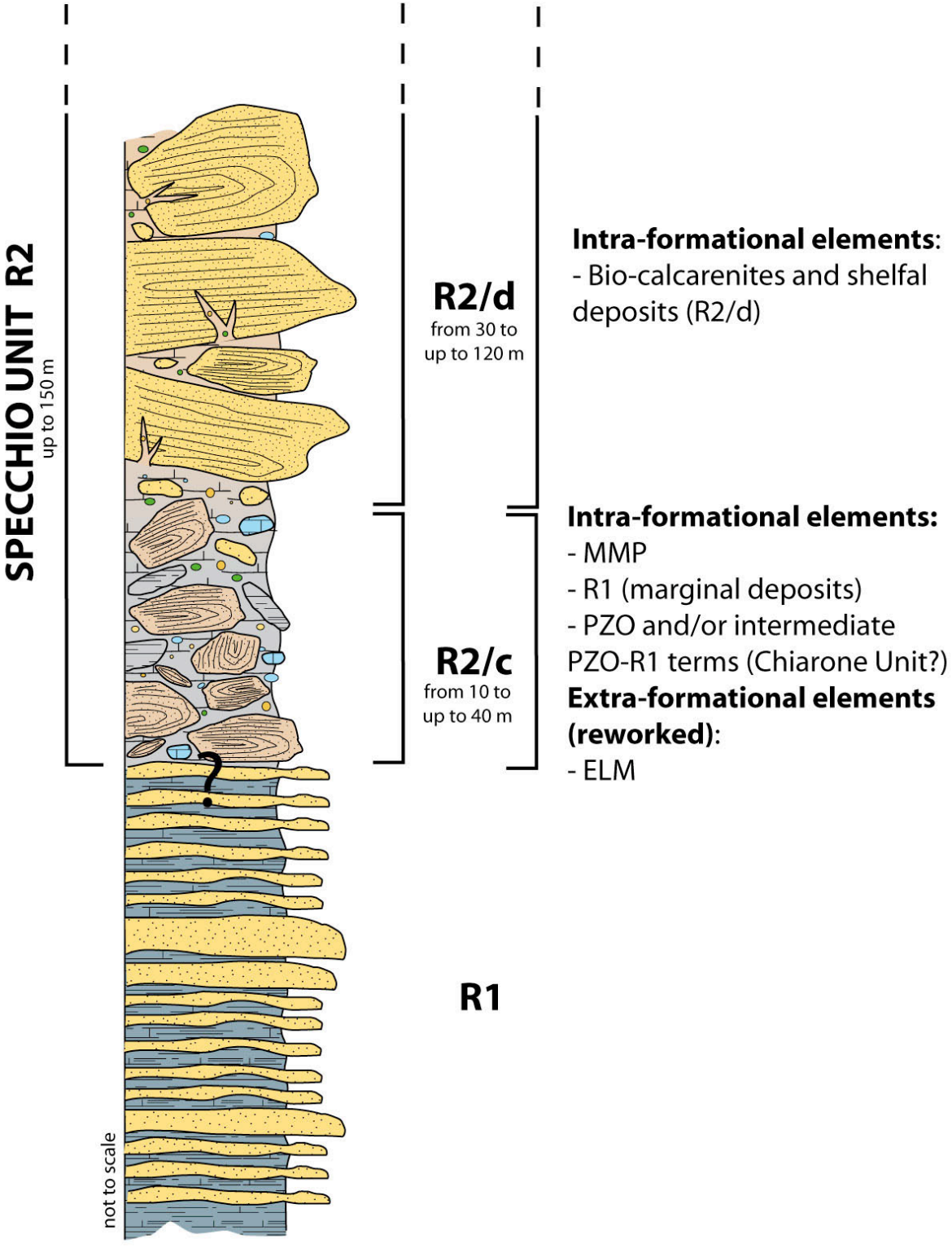
SPECCHIO UNIT R2
up to 150 m
R2/d
from 30 to
up to 120 m
R2/c
from 10 to
up to 40 m
R1
?
not to scale
Intra-formational elements:
- Bio-calcarenites and shelfal deposits (R2/d)
Intra-formational elements:
- MMP
- R1 (marginal deposits)
- PZO and/or intermediate PZO-R1 terms (Chiarone Unit?)
Extra-formational elements (reworked):
- ELM

Figure 7.55 - Simplified stratigraphic scheme of the Caffaraccia section (uppermost part of the Mt. Barigazzo outlier) focusing on the internal subdivisions of the Specchio Unit R2. Main features and characteristics, as well as inferred thickness are described.

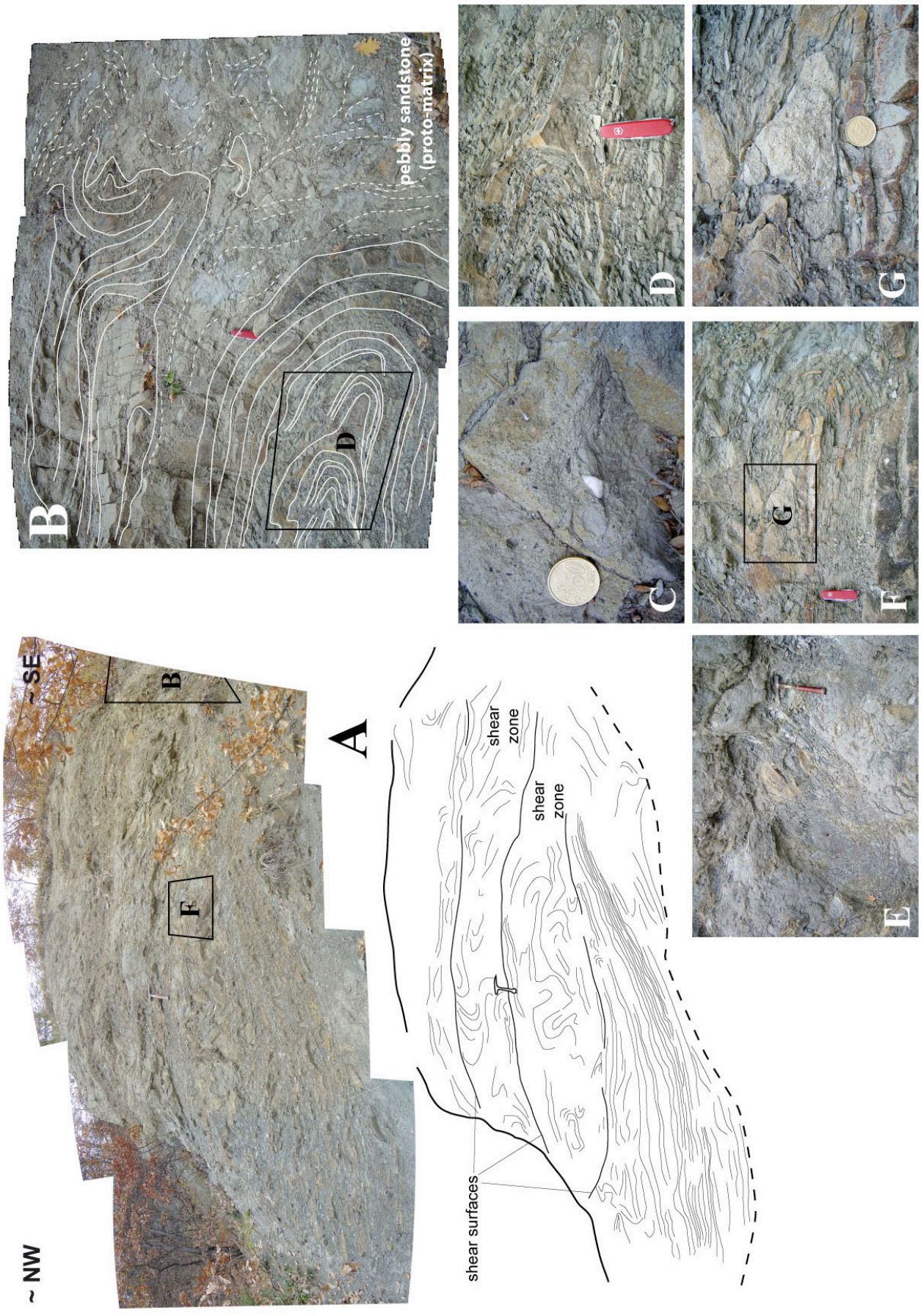

Figure 7.56 - **A**: Photo-mosaic and interpretative line drawing of the upper BDP characterizing the R2/c sub-unit

outcrop in the Caffaraccia section (dashed line roughly indicates the basal contact of the upper BDP with the lower MDP (almost completely covered in this area). The observed IBTs seem to share opposite shearing senses. The inferred transport direction is roughly toward the viewer. Hammer for scale.

B: Close-up of A, showing the significant occurrence of proto-matrix, enveloping folded discrete elements, and testifying a strong localized stratal disruption. Main geometric features of folded elements and matrix are labeled. Knife for scale, 9 cm long.

C: Detail of the pebbly/sandy mudstone representing the enclosing matrix of lower MDP. Fifty Euro cent coin for scale, 2,4 cm in diameter.

D: Close-up of B, showing in detail the evident, strong thickening of the hinge zone, characterizing thin-bedded folded elements, and testifying soft sediment nature of the deformation. Knife for scale, 9 cm long.

E: Example of m-sized, folded mudstone block contained within the enclosing matrix of the lower MDP. Note the carbonate cobble-bearing intrusion of the enclosing matrix into the core zone of the rootless fold. Hammer for scale.

F: Close-up of A, showing a dragging-related synformal fold (IBF) developed just below to a shear surface (IBT). Knife for scale, 9 cm long.

G: Close-up of F, showing in detail a proto-matrix intrusion into the core of the fold. The proto-matrix comes from the upper shear zone. Fifty Euro cent coin for scale, 2,4 cm in diameter.

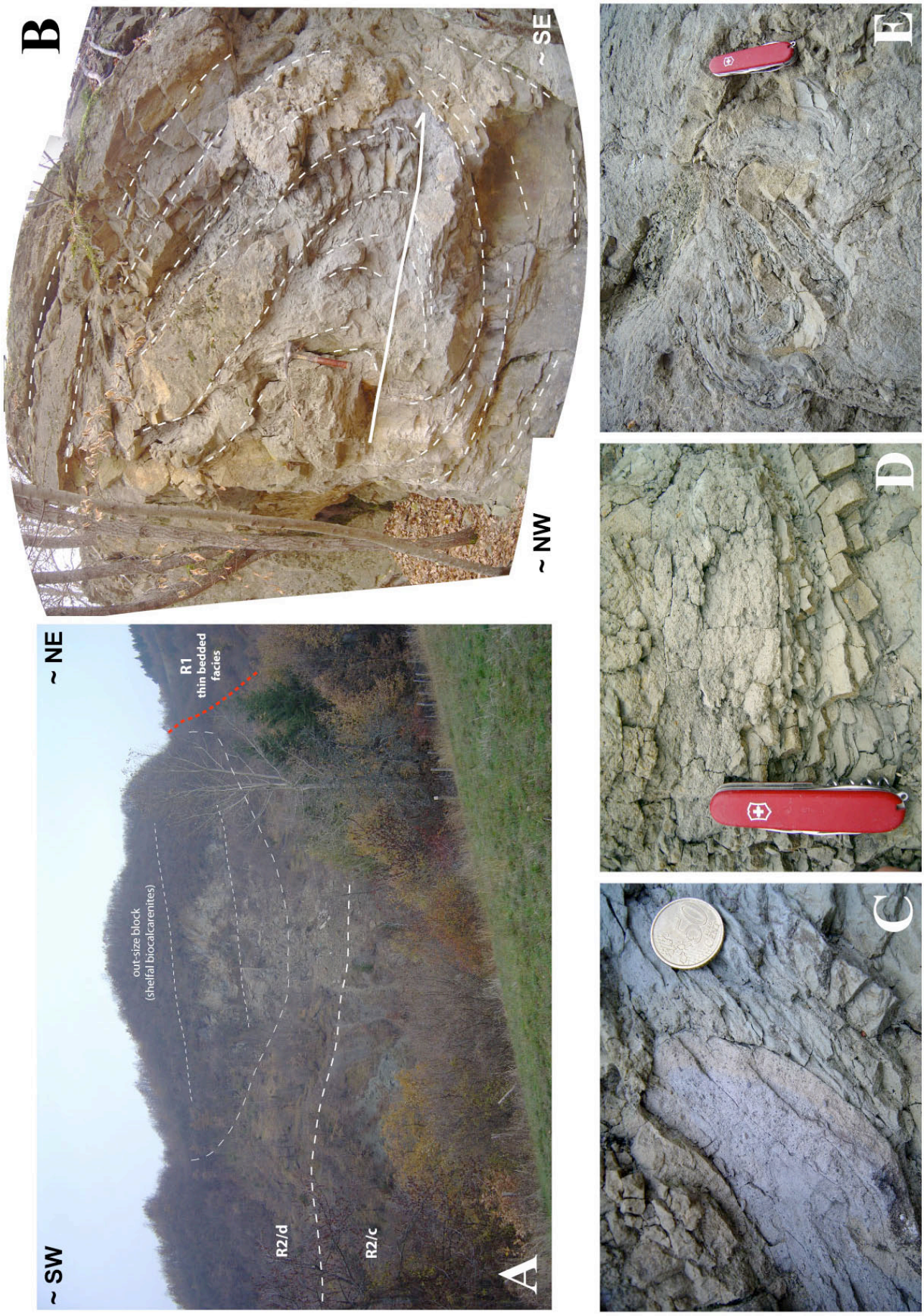
A
~ SW
~ NE
R2/d
R2/c
out-size block
(shelfal biocalcarenites)
R1
thin bedded
facies
B
~ NW
~ SE
C
D
E

Figure 7.57 - **A**: Panoramic view of the southern Caffaraccia section outcrops. Note the occurrence of out-sized blocks characterizing the R2/d sub-unit, which give a mounded appearance to the local topography. Internal apparent stratification pattern of the out-sized block is tentatively labeled. In the right side of the photo it is possible to observe a high-angle normal fault (red dashed line), putting in lateral contact R1 and R2 units' lihologies. The contact between the two sub-units and the recognizable out-sized block boundaries are roughly labeled.

B: Example of a thrusting-related, tight meso-scale fold, developed within the bioclastic sandstone characterizing out-size blocks (IBF). Folded beds and axial shear surface are labeled. Hammer for scale.

C: Example of enclosing pebbly/sandy mudstone matrix characterizing R2/d sub-units MDPs in this area. Note the abundant bioclastic fraction (darker lenticular grains; *nummulites*), and the downward transition to muddier portions (highly disrupted mudstone intra-clast). Fifty Euro cent coin for scale, 2,4 cm in diameter.

D: Example of pebbly/muddy sandstone characterizing shear zones within BDPs. Note the sharp contact with the underlying layered discrete block portion. Knife for scale, 9 cm long.

E: Example of folded, fine-sandstone/mudstone intra-clast (thin-bedded detached bedset) recognized within the matrix of the lower MDP of the R2/d sub-unit. The matrix appearance is shown in C. Knife for scale, 9 cm long.

B
C
A
50
EURO
CENT

Figure 7.58 - A: Detail of the base of a thick sandstone bed observable within an out-sized block. Note the occurrence of isolated or clustered well-rounded pebbles and the sparse presence of shell debris. Fifty Euro cent coin for scale, 2,4 cm in diameter.

B: Overall outcrop appearance of bioclastic-rich layered sandstones, as observable within less deformed portions of out-sized blocks. Hammer for scale.

C: Close-up of B, showing an example of the typical "worm-like burrowing" bioturbation, which characterizes biolcastic-rich sandstone beds, especially within the thin- and medium-bedded ones. Knife for scale, 9 cm long.

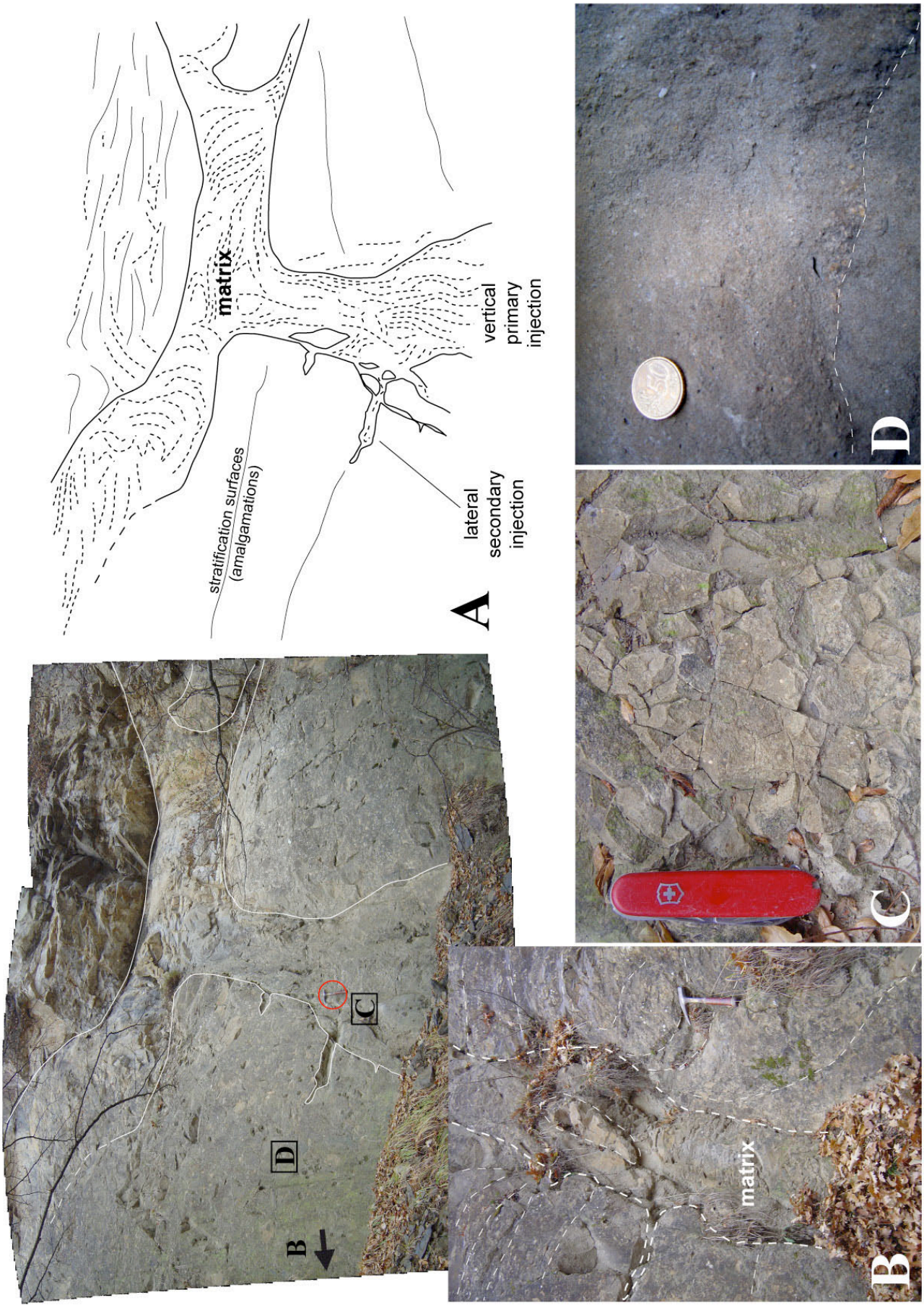
matrix
vertical primary injection
lateral secondary injection
stratification surfaces (amalgamations)
A
B
C
D
matrix

Figure 7.59 - A: Photo-mosaic and interpretation of a meso-scale injection-like structure observed within the upper BDP of the R2/d sub-unit in the Caffaraccia section. These kinds of structures dissect the block integrity; probably joining different matrix-rich shear zones through vertical and oblique pathways. The infilling matrix intrudes along weak zones (*e.g.* stratification surfaces), as observable along the margins (secondary lateral injections). Note also the occurrence of sandstone intra-clasts within the infilling matrix, ripped up from structure margins Encircled hammer for scale.

B: Another vertical-trending, meso-scale injection-like structure, showing the same characteristics described for A. Note in this case the faint upward flipping of stratification surfaces in the right side margin. Main features are labeled. Indicative location is shown in A. Hammer for scale.

C: Close-up of A, focusing on the infilling matrix of the injection-like structure. The overall appearance is that of a bioclasts-rich (whitish lenticular particles; *nummulites*) pebbly sandstone (resembling the typical IBT-related proto-matrix). Knife for scale, 9 cm long.

D: Close-up of A, showing in detail one of the amalgamation surfaces, which characterize the thick sandstone bedsets composing these blocks; these surfaces represent possible preferential pathways for lateral matrix injections. Note the overall normally graded appearance, and the strong occurrence of *nummulites* and scattered shell debris. Fifty Euro cent coin for scale, 2,4 cm in diameter.

8. INTEGRATION WITH MODERN GEOPHYSICAL EXAMPLES

During the last 3 decades, the marine geological exploration highlighted the presence of sediment mass transport deposits in almost every continental margin surveyed (especially "passive" margin settings), even on very low slope gradient (< 1°). These observations enhanced inherent socio-economic (*i.e.* geohazard mitigation and hydrocarbon exploration) and academic interests (see chap. 1).

The seismo-stratigraphic definition of *Mass Transport Deposit* was firstly introduced by Weimer (1989, 1990) to identify seismically chaotic deposits (*i.e.* transparent and laterally discontinuous zone with hyperbolic reflectors) generated by large-scale sediment failures, representing fundamental elements in the stratigraphic architectures of divergent/passive continental margin contexts, especially those associated to high sedimentation rates (*e.g.* Gulf of Mexico) (fig 8.1).

Since then, evidence of small- and large-scale MTCs and MTDs have been discovered in almost every modern seafloor (and sub-seafloor), highlighting mass wasting processes as fundamental features characterizing shallow- to deep-water dynamics, spanning from epicontinental contexts as the Mediterranean Sea (*e.g.* Trincardi and Normark, 1989; Frey-Martinez *et al.*, 2005, 2006; Gazioglu *et al.*, 2005; Minisini, 2008; Loncke *et al.*, 2009) to the oceanic continental margins of the North Europe, Western Africa and North America Atlantic Coast (*e.g.* Embley, 1976; Coleman and Prior, 1988; Booth *et al.*, 1993; Hampton *et al.*, 1996; Huhnerbach and Masson, 2004; Evans *et al.*, 2005; Lamberg *et al.*, 2006; Twitchell *et al.*, 2009), and the central- and circum-Pacific regions (*e.g.* McMurtry *et al.*, 1999; Normark *et al.*, 2004; Fisher *et al.,* 2005; Guanghai *et al.*, 2009; Hu *et al.,* 2009).

In recent years the increasing development of scientific drilling and seimic/acoustic imagery technology in marine geology surveys of continental margins allows important consideration on general internal and external morphology and areal extent of recent to modern giant submarine landslides (Canals *et al*., 2004; Frey-Martinez *et al*., 2005, 2006; Bull *et al.*, 2008; Gee *et al*., 1999, 2001, 2005, 2006, 2007).

After these continued discoveries and descriptions of new submarine landslide deposits, the scientific community is now focusing its attention to the systematic database compilation and mapping of these units (*e.g.* Hance, 2005; Ten Brick *et al.*, 2009; Twitchell *et al.*, 2009; Chaytor *et al.,* 2009; Lee, 2009; Camerlenghi *et al.*, 2009), and to the development of updated models and interpretations, mainly for geotechnical purposes (see Mosher *et al.*, 2009) (fig 8.2).

In this chapter I will firstly discuss the state-of-the-art of marine geology investigations on submarine landslides, and then I will briefly describe the overall physiographic setting of some selected examples of "active" continental margins, thought to represent modern analogs of the inferred depositional setting of the R2 unit, focusing on structural and depositional domains, and MTDs typology and occurrence.

8.1 Physical characteristics of a submarine landslide deposit

Subaerial and subaqueous mass gravity failures share almost the same features and related deposits have similar anatomy. The subaerial landslides classification originally proposed by Varnes (1978), updated by Cruden and Varnes (1996), is therefore relatively applicable to subaqueous ones (fig. 8.3). Obviously, the different hosting fluid puts strong limitations in this comparison.

The first tentative of integrated approach taking in account analogies and differences between subaerial and subaqueous landslides has been developed by Hampton *et al.* (1996), while an attempt of static classification for submarine mass movements has been proposed by Mulder and Cochonat (1996), mainly based on general morphology of several modern and recent examples collected from different environmental contexts. Another classification based on geophysical data collected in an active mud-dominated accretionary context has recently proposed by Moscardelli and Wood (2007) for mass wasting bodies in offshore Trinidad (fig. 8.4).

Some attempts to integrate 2D/3D seismic stratigraphy to micro- and meso-scale sedimentologic observations on cores have been made by McHugh *et al.* (2002), Tripsanas *et al.* (2007), Cauchon-Voyer *et al.* (2008) and Jenner *et al.* (2007), for examples coming from divergent margin settings (*i.e.* Gulf of Mexico, offshore New Jersey, and from the Scotian Slope offshore Canada) (fig 8.5). However these studies have strong limitations due to the limited penetration of piston corers (*i.e.* ~ 10-20 m) and the lacking of lateral continuity of cores.

One of the clearest differences observed between subaerial and subaqueous landslides is the volume of material involved in the generating event: for example, the biggest subaerial landslide ever documented in the literature is that of Mt. Shasta (California) with about 26 km^3 of involved material (Crandell *et al*., 1984), while the largest submarine one is the Agulhas slide (Dingle, 1977), localized in the South Africa offshore, which is interpreted having remobilized about 20.000 km^3 of sediments during a single event.

Among the notable examples of large-scale/long-runout submarine landslides there are the well-studied volcanic processes-related Hawaiian slides (Lipman *et al.*, 1988; Normark *et al.*, 1993;

Moore *et al.*, 1989; 1994, 1995; McMurtry *et al.*, 2004; Yokose and Lipman, 2004; Garcia *et al.*, 2006), and the generally glacial processes-related MTDs of the Storegga slide complex (Bugge *et al*., 1988; Bryn *et al*., 2003; Kvalstad *et al*., 2003), localized in the Norway offshore, and those characterizing the western African margin (*e.g.* the Saharan debris flow; Gee *et al.*, 1999; 2001; Wynn *et al.*, 1999; Talling *et al.*, 2007), and the Atlantic margin of North America (*e.g.* the Grand Banks slide; Heezen and Ewing, 1952; Piper *et al*., 1985;) (fig. 8.6).

Generating processes of some huge chaotic bodies (*e.g.* the Gela slide, the "Olistostome" complex of the Gibraltar Arc; Trincardi and Argnani, 1990; Medialdea *et al.*, 2004) have particular analogies with those classically ascribed to gravity tectonics (*sensu* De Jong and Scholten, 1973).

However it is important to note that most of such sedimentary units record almost instantaneous events in the geologic time scale, while tectonic ones are characterized by a relatively slower progressive mechanisms.

Given these features (*e.g.* huge volume and fast motion), submarine landsliding are likely to represent a possible major concurrent factor in generating tsunamis, more than the classically inferred earthquakes (*e.g.* Fryer *et al.*, 2004; McMurtry *et al.*, 2004; McAdoo and Watts, 2004; Locat *et al.*, 2004; Fisher *et al*., 2005).

Physical characteristics achieved by these deposits are the result of processes acting in different phases of the sliding mass evolution. These evolutionary phases take place between a failure and an accumulation zone, and can be summarized in 3 main steps: i) triggering, ii) transport and iii) accumulation. These phases respectively identify 3 different domains characterized by different structural styles, and classically referred to, from up-slope to downslope regions, as i) headwall, ii) translational and iii) toe regions (fig. 8.7).

As defined in the dislocation model by Farrel (1984), the accumulation zone is generally characterized by compressive regime while the failure zone is instead dominated by a distensive regime.

In the following I will describe in detail the mechanisms acting during each phase, as defined in the concerning literature.

8.1.1 Triggering mechanisms

The modern definition of triggering mechanism is: "the external impulse initiating a slope instability process" (Sultan *et al.*, 2004). According to Locat and Lee (2002) and Leynaud *et al.* (2009), the possible triggering mechanisms interpreted for modern and recent submarine slope failures are: 1) slope over-steepening, 2) cyclic wave loading-unloading, 3) seismic shock, 4) high sedimentation rates, 5) sediment under-consolidation, 6) gas releasing, 7) sea-level falls, 8) fluid

infiltrations, 9) glacial overloading and 10) volcanic processes.

Following what proposed by Sultan *et al.* (2004), these mechanisms could be defined as short-term triggers, while those ones strictly acting on slope stability (*e.g.* slope angle and rate of lithostatic unloading) and the preconditioning factors (*e.g.* weak layers) could be termed as long-term triggers. Each one of these factors directly or indirectly influence slope stability, perhaps increasing down-slope shear forces and/or decreasing shear resistance of sediments (Martel, 2002). These processes, coupled with the general substrate stratigraphy, are responsible for the localization and development of the landslide main rupture surface (*i.e.* basal *décollement*/detachment), which may evolve downslope (cutting upward to the seafloor) in the basal shear surface of the translating slide body.

Recently Camerlenghi and Pini (2009) tentatively proposed a systematic comparison of mass wasting deposits characterizing both divergent and convergent margin settings (fig. 8.8). Triggering mechanisms in convergent margin settings are strongly influenced by active tectonics (*i.e.* seismic shocks, tectonic slope over-steepening, shallow-level thrusting) and overpressured fluid extrusions (*i.e.* mud volcanism). All of these phenomena are related to tectonic thickening and sediment over-consolidation. In divergent margin settings instead, triggering mechanisms are influenced by "passive" tectonics (*i.e.* salt-mud diapirism, gravity-induced faulting) and sediment under-consolidation.

On fossil examples, the recognition of triggering mechanisms should be very difficult. Some considerations in this sense could be proposed only through a detailed characterization of hosting basin morphology, as well as the tectonic and stratigraphic setting.

8.1.2 Transport mechanisms

These mechanisms act during the basinward slide mass movement, in a segment of the landslide translation path comprised between the failure zone upslope and the accumulation zone downslope, and herein referred as transport zone (*i.e.* depletion zone of Frey-Martinez *et al.*, 2005). During this phase, major transformations of the sliding body may occur.

The distance measured from the upper failure zone (*i.e.* crown/head) to the lower accumulation zone (*i.e.* toe) is termed run-out distance (Hampton *et al.*, 1996), and roughly coincides with the transport zone length. The run-out distance, defined by the H/L ratio, is function of the mobility degree achieved by the sliding body, and thus depending on mass transport type (fig. 8.9).

In both subaerial and subaqueous contexts, the transport dynamics and related processes are strongly influenced by: 1) lithology, composition and consolidation degree of sediments involved,

2) degree of desegregation achieved, 3) geometry and depth of basal rupture surface and 4) morphology of the depositional context.

Some processes as slumps, creeps/topples and some kind of rotational slides, generally share slow kinematics (low strain rates) and short transfer distances. Other ones like debris/rock avalanches, debris flows and most part of rotational and translational slides are instead characterized by fast kinematics, with long run-out distances, sometimes exceeding hundreds of kilometers (see Hampton *et al.*, 1996; Canals *et al.*, 2004). Numerical simulations on a debris avalanche developed offshore Sumatra have highlighted possible maximum acceleration values ranging from 0.35 to 0.47 m/s^2, and maximum velocities ranging from 40 to 47 m/s (Bradshaw *et al.*, 2009).

The observed long run-out distances and huge amount of involved material of some large-scale seismic examples of MTC put in light the needed of a sediment/block supporting mechanism capable to significantly reduce friction, enhancing sliding mass mobility.

According to several numerical and experimental simulations, the more plausible process that can be invoked is the hydro-planing (Morhrig *et al.*, 1998; Elvheroi *et al.*, 2000; Harbitz *et al.*, 2003; Ilstad *et al.*, 2004a, 2004b; De Blasio *et al.*, 2006). Such process develops through the entrainment of water in the basal shear layer of a sliding mass, with the consequent rising of excess pore water conditions over the lithostatic pressure exerted by the overriding material. If the overpressured conditions of this relatively thin layer are maintained, the sliding mass can virtually move without any resistance (apart from that exerted by surrounding seawater) (fig. 8.10).

It's worth to note that some documented huge subaerial rock avalanches show longer run-out distances than those expectable utilizing conventional slope stability criteria, with extremely low friction coefficients similar to those of subaqueous ones. Recognition of similar bodies in extra-terrestrial settings like Moon and Mars, where there are no liquid water conditions, induced the introduction of another process defined as "acoustic fluidization" (Melosh, 1987). As defined by the author, this process invokes no gaseous and/or liquid phase, and is conceptually similar to the "dispersive grain stress" proposed by Bagnold (1954) for dry granular flows. The high mobility of these large dry rock avalanches is thus explained through a bulk weight decreasing caused by random movements of the constituents, organized in self-moving domains that act together transmitting kinematic energy under form of elastic waves. Hypothetically, with necessary considerations, and expectable minor effects, this kind of process may occur also in submarine systems, in synergy with other mentioned mechanisms.

Transport mechanisms are generally influenced by geodynamic setting: in convergent margins submarine mass transport events seem to be concentrated at the slope base, with shorter run-out

distances and less evolved processes, while in divergent margins these phenomena seem to be common at the shelf-break/upper continental slope, and are characterized by longer run-out distances and by various degree of transformation and evolution of processes (Camerlenghi and Pini, 2009).

In this phase both extensional and compressive regimes may take place, due to differential moving of slide component and the margin-induced velocity gradient. At the outcrop scale, this may results in the superposition and coexistence of extensional and compressive structures affecting slide components.

It's important to note that sedimentary products developed during this phase have a relatively low preservation potential, because of the syn-depositional deformations achieved during the subsequent accumulation phase. Anyway, the basal shear surfaces are possibly recognizable as erosional gaps in the sedimentary successions.

8.1.3 Accumulation mechanisms

These mechanisms characterize the accumulation zone, localized some distance away from the failure zone, and represent the point where the moving slide mass came to arrest. During this phase several deformational structures may develop both inside, laterally and below slide body. These deformations are mainly caused by dynamic/static overloading and rear push of the sliding mass.

Compressive stresses are mainly located at the front of the slide mass and in the surrounding sediments. Folding and thrusting at various scales are the most common structural expressions of these processes.

These structures generally develop over the basal shear plane and, depending on the decoupling degree between slide mass and substrate, also in the underlying sediments. Evidence of this kind of mass transport-induced substrate deformation (and possibly erosion) is provided by observations made by Schnellmann *et al.* (2005) on some high-resolution 2D seismic profile taken fom some small-scale (nonetheless "basin-wide" for the depositional setting) MTDs, affecting margins of the Lake Lucerne (Switzerland) (fig. 8.11).

Accumulation zone is therefore characterized by low- to high-angle thrusts, rooted in the basal shear plane and that cut upward through the slide mass, sometimes forming meso- to mega-scale folds (*i.e.* blind thrusts).

At the entire slide body scale, these shear zones develop in some kind of backstepping way, following the upslope migration of the deformation due progressive stopping of slide mass front and margins. Similar structures may develop both inside and outside slide body (*i.e.* surrounding

sediments) and their surface expression are the so-called pressure ridges, elongated arcuate lineaments commonly observed in marine geomorphology. During the emplacement, the distensive structures achieved during the failure and transport phases are likely overprinted and/or re-utilized in a generally compressive regime.

Recent observation taken from the Levantine Sea in the offshore of Israel (*i.e.* Eastern Mediterranean continental margin) allow the discrimination of two main types of submarine landslides, according to their frontal morphology, and thus subdivided into frontally-confined and frontally-emergent submarine landslides, representing two end-members of a slope failure process continuum (Frey-Martinez *et al.*, 2005, 2006). The authors separate landslides characterized by restricted basinward transport, without overrunning the undeformed downslope strata, from those able to ramp up from the original basal shear surface, translating in unconfined manner over the seafloor with much larger downslope transport, respectively (fig 8.12).

The emplacement of such deposits strongly influence the physiography of the depositional context; the short time (*i.e.* geologically instantaneous) accumulation of huge amount of remolded material causes a strong reduction of the basinal volumetric potential (*i.e.* accommodation space), generating punctual and localized minor depocenters around and/or above the MTC, due to its irregular surface perhaps.

The un-loading of the failure zone and the subsequent over-loading in the accumulation zone may also result in an isostatic rearrangement of the slope profile, with a relative upslope uplift and a downslope subsidence (Dykstra, 2005a, 2005b) and gas emissions (*e,g,* Mienert *et al.*, 2006) (fig 8.13).

It's important to note that post-depositional processes seem to play a major role in the final anatomy of a slide body, as observed on ancient (Strachan, 2002, 2008) modern examples (Diviacco *et al.,* 2006; Rebesco *et al.*, 2009; Moernaut *et al.*, 2009) and inferred from experimental and numerical modeling (Major and Iverson, 1999; Major, 2000). During the deposit compaction, perhaps, the internal fluid overpressure may be dissipated through developing of fluid-escape structures, sometimes reaching the slide surface as mud volcanoes, or can be retained for a relative time interval, favoring slow differential movements of the entire mass. All of these features can strongly influence the subsequent deposition of the overlying sediments.

In convergent geodynamic settings, classic and updated models, forecast MTC accumulation zones as generally concentrated at the deformation front of tectonic nappes (*i.e.* base-of-slope), where they are progressively incorporated within the advancing thrust systems (Elter and Trevisan, 1973; Vollmer and Bosworth, 1984; Labaume, 1992; Labaume and Rio, 1994; Yamada *et al.*, 2009) (fig 8.14).

In divergent settings instead, the generally graded slope profile (*sensu* Prather *et al.*, 1998) allow transportation and acceleration of sliding masses, thus possibly favoring slide evolution and transformation in hyperconcentrated flows, responsible for megabed deposition in the basin plain (Rothwell *et al.*, 1998, 2000; Camerlenghi and Pini, 2009).

A general and useful review of seismic-scale internal and external structures of a MTD, focusing on possible kinematic indicators, is provided by Bull *et al.* (2008) (fig. 8.15), while a preliminary (and generally conceptual) attempt of comparison between seismic and outcrop structural data has been recently proposed by Bull and Cartwright (2010).

8.2 MTDs in modern convergent/collisional margin settings

Convergent and collisional margin settings are commonly retained as typically "active" contexts, where tectonics plays the major role in the environmental evolution.

The subduction zones, which are the main causes of seismicity in "active" margins, produce roughly the 60% of Earth's shallow earthquakes, large enough to be detected by distant seismic stations. The seismic moment release in most subduction zones is typically heterogeneous, depending on:

- existence and rate of backarc spreading;
- thickness of incoming sediment layer;
- convergence rate;
- dip direction and steepness of the subducting plate;
- width of the seismogenic zone;
- nature of interplate stresses;
- physical, chemical and hydrogeological properties;
- pore fluid pressures and permeabilities.

The type and the magnitude of such earthquakes are variable, depending on the crustal level of development (sometimes very deep), commonly sharing relatively short recurrence time.

On the other hand, significant intraplate seismicity exists on "passive" margins that usually correspond to the transition between continental and ocean lithospheres.Among the various processes proposed to explain long-term crustal deformations affecting these contexts there are:

- the isostatic response due a loading/unloading (*i.e.* ice/sediment accumulation or removal);
- tregional thermal adjustments;
- regional compression;
- ridge-push;

Also in this case, the type and magnitude of these earthquakes mainly depends on the crustal level of development (sometimes relatively shallow), with the most evident difference expressed by longer recurrence time (Morgan *et al.*, 2008).

At the same time, the vast majority of current interpretations, both from ancient and modern examples, consider the earthquake pulse as the more likely the triggering of MTDs (Canals *et al.*, 2004; Masson *et al.*, 2006). The seismic-shock is commonly retained as the best candidate in generating a process of slope failure among the currently inferred short-term triggers (Sultan *et al.*, 2004; see above).

During earthquakes, soil layers are subjected to multi-directional cyclic stresses with different amplitudes and frequencies, that lead to cyclic deformations and to changes in stress-strain field, and strength properties of soil layers. Thus, the response of soil layers and the earthquake characteristics on the ground surface are mainly influenced by the properties of soil layers.

The marine sediments behavior in response to an earthquake-induced cyclic loading generally results in a generalized decreasing of material strength, with some exceptions.

Normally consolidated clays share soft appearance and cohesive rheology, and their further weakening occurs through: i) degradation of the sediment stiffness (*i.e.* elasticity), ii) degradation of the shear strength (*i.e.* accumulation of plastic strain) and iii) increasing in shear-induced pore pressure (*i.e.* un-drained conditions) (Pestana *et al.*, 2000; Biscontin *et al.*, 2004). In the case of involvement of sensitive clays (*i.e.* high ratio between undisturbed and remoulded shear strength) the shear strength may be loose nearly entirely after the cycling loading and behave as liquefied soil (typically observed in terrestrial quick clays).

These mechanisms concur also in the effective stress reduction and liquefaction of loose, saturated granular sediment (*i.e.* coarse silts and sands): in fact, ground shaking produces sudden granular rearrangement. Because the duration of the cyclic loading is too short to ensure the drainage of water, an increase in pore water pressure produces an equal magnitude decrease in the effective confining stress. If the vertical effective stress drops to zero then liquefaction occurs.

In spite of the above-discussed considerations, “active” margins settings are generally characterized by an overall increasing of the sediment strength, interpreted as a “seismically-related strengthening”. Repeated, non-failure seismic events can actually strengthen the sediment column through the development of excess pore-water pressure during seismic-shocks, and subsequent drainage, resulting in a densification of the sedimentary packing during intervening periods (Locat and Lee, 2002).

The MTD observed in these settings are generally characterized by relatively small-scale extensions, mainly developed at the principal deformation front, and attached to thrust-related uplifts.

Leaving aside the herein analyzed examples (see below), the other few examples of modern large-scale submarine landslide developed in subduction-related contexts (perhaps still recognizable) have been observed in the Pacific margin of the Middle-Southern America (*i.e.* offshore Perù, Equador, Nicaragua, Costa Rica; Duperret *et al.*, 1995; Von Huene *et al.*, 2004; Ratzov *et al.*, 2008; Talukder *et al.*, 2008), from the northeastern margin of the New Zealand (*i.e.* Matakaoa and Ruatoria Submarine Instability Complexes; Collot *et al.*, 2001; Lewis *et al.*, 2004; Lamarche *et al.*, 2008), and from the North Pacific Aleutinian accretionary complex (*i.e.* Ugamak Slide; Fryer *et al.*, 2004) (fig. 8.16).

It is worth to note that this latter submarine landslide is developed in the upper forearc region of the Aleutian accretionary wedge, falling in the category of the large-scale MTDs, with a length of ~ 65 km, ~ 25 km in width, localized thickness (at the toe of the slide) up to 400 m, and an estimated volume of ~ 200-300 km^3. The Ugamak slide is interpreted having been generated by the failure of the Aleutian shelf margin (at water depths of ~ 120 m) in response to an earthquake. This event produced an highly directional tsunami which crossed the entire Pacific Ocean, from the Aleutian Arc to Antarctica, with near- and far-field run-ups of ~ 42 m and ~ 4 m, respectively (Fryer *et al.*, 2004). Apart from the oceanic subduction-related context, by size, mode of development and emplacement setting, this slide represents a possible good analog for the Specchio unit (R2), analyzed in this work.

Generally speaking, slides developed in these settings share their overall occurrence in the proximity of the main tectonic front, and are commonly thought to develop through processes related to tectonic erosion of oceanic crust or accretionary prism dynamics (*e.g.* oblique subduction of a seamount and polyphasic oversteepening of the toe of the margin, respectively; Von Huene *et al.*, 2004; Bangs *et al.*, 2006). It is interesting to note that the tectonic erosion-related slides seem to be characterized by larger dimensions than ones developed in internal portions of accretionary complexes. The typical characteristics of submarine landslides so far recognized in modern "active" margin setting are the following:

- development as cohesive/coherent failures (*i.e.* blocky landslides and slumps), suggesting involvement of over-consolidated materials;
- localization at the base of the slope;
- development of higher topographic elevations of the slide scars, due to stronger nature of the involved sediments;

- occurrence on steeply inclined slopes (over 15°).

One of the most striking observations emerging from the present-day investigations of modern "active" continental margins is that, surprisingly, only few large-scale failures have been recognized, with respect to those observed in "passive" counterparts. Perhaps active margins are so complex structurally and morphologically, that modern submarine landslides are less easily recognizable in the geophysical record.

Regarding mass wasting processes development in convergent-collisional margin settings, there is a general agreement on the common occurrence of several recurrent small-scale mass transport deposits, mainly developed close to the main deformational front (*i.e.* at the toe of the accretionary prism) and, subordinately, from other topographic highs characterizing more nternal depositional domains.

These latter depositional settings are characterized by intra-slope ponded accommodations (*i.e.* structurally-confined depocenters), similar to those commonly recognizable on divergent ("passive"), highly fed siliciclastic continental margins, especially those sharing shale- or salt-based sedimentary contexts (*e.g.* Gulf of Mexico, offshore coast of Nigeria and Angola; Prather *et al*., 1998; Winker and Booth, 2000; Steffens *et al.*, 2003; Adeogba *et al.*, 2005; Owoyemi and Willis, 2006; Behrmann *et al.*, 2006; Hutchinson *et al.*, 2008; Madof *et al*., 2009).

In these situations, the extended above-grade profile of the slope and the structural control on the sub-basin morphologies, are largely influenced by gravity-driven slope tectonics, and shale- and halo-kinetic mechanisms (*e.g.* salt withdrawal, disequilibrium compaction, salt-shale diapirism).

By the way, very similar physiographic settings may be observed on top of accretionary belts characterizing some convergent margin settings, particularly those involving continental crust subduction (fig. 8.17). In these accretionary convergent settings, characterized by compressive and transpressive regimes, the tectonic-related subsurface mud remobilization and fluid expulsion (fig. 8.18) seems to play a major role in the genesis and evolution of such mini-basins (*e.g.* Barbados-Trinidad, Mediterranean Ridge, Calabrian accretionary prisms; Brown, 1990; Camerlenghi *et al.*, 1995; Maltman *et al.*, 1997; Kopf, 1999; Huguen *et al.*, 2001; Bohrmann *et al.*, 2002; Deville *et al.*, 2003, 2006; Praeg *et al.*, 2009; Rebesco *et al.*, 2009).

In such mud-rich contexts, mass wasting processes are thought to significantly contribute in the morphologic shaping of the depositional environment (*e.g.* offshore Trinidad; Moscardelli *et al.*, 2005; Moscardelli and Wood, 2007)

Summarizing the present-day accepted hypothesis on slope failure influencing factors, the main differences with divergent margin contexts are the following:

- sediment over-consolidation, mainly due to tectonic compaction (due to both overloading, early diagenesis and high-frequency small-magnitude earthquakes);
- progressive tectonic oversteepening of slopes;
- small potential energy gradients from failure to accumulation zones.

8.3 General physiographic setting of an "active" margin

In this section I will briefly discuss some considerations regarding the general morphology of those convergent systems, mainly in terms of slope profiles and depositional domains (fig. 8.19), underlining the mode and style of development of structurally-confined basin systems, and analyzing the so far, surely identified, few examples of related large-scale MTDs.

The selected examples for the general morphologic and physiographic overview are from classical and well-studied subduction-related convergent margin situations, as: the Nankai subduction zone (SW Japan), the Cascadia subduction zone (NW North America), and the Sunda Arc (SW Indonesia) (fig. 8.20).

The other analyzed examples (discussed in the section 8.4) are the nowadays-active incipient, or more or less evolved continental collisions, developed in offshore areas of the SW Taiwan, NW Borneo, SW New Zealand and SE Indonesia (fig. 8.21).

These observations are based on careful updated reviews of inherent literature and recently published data.

8.3.1 Nankai (SW Japan)

The Nankai Trough is a subducting plate boundary, where the Philippine Sea plate underthrusts the southwestern Japan margin at a rate of ~4.1–6.5 cm/yr, along an azimuth of 300°–315°N (DeMetz *et al*., 1990; Seno *et al.*, 1993; Miyazaki and Heki, 2001) down an interface dipping 3°–7° (Kodaira *et al.*, 2000). The Nankai subduction zone is characterized by an "end-member" of sediment-dominated accretionary prism. In the toe region off the Muroto peninsula, a sedimentary succession ~1 km thick is accreted to or underthrust below the margin (Taira *et al.*, 1989; Moore *et al.*, 2001).

In the Nankai subduction zone, apart from the attached, small-scale sediment failures occurring along the main thrust front (*i.e.* toe of the accretionary prism; Kawamura *et al*., 2009) and the internal surface expression of buried mega-splay structures (Moore *et al.*, 2007), some other small-scale MTDs (tens of km^2 of areal extension) are observed to border the Kumano forearc basin margins (Camerlenghi, 2009, pers. comm.). By the way, some other mass transport deposits

identified from cores collected in the slope basin system off the Muroto Peninsula has been interpreted as relatively small-scale slumps and debris flow involving fine-granined sediments, and developed in more internal position in respect to the main thrust front (~ 40 km). These events are thought to come from the backlimb of an intrabasinal structural high related to out-of-sequence thrust splays, with an inferred movement apparently trending up-slope (Underwood *et al.*, 2003) (fig. 8.22).

8.3.2 Cascadia (NW North America)

Another sediment-dominated accretionary prism develops in the Cascadia suduction zone, where the relatively young oceanic crust of Juan de Fuca plate underthrust the North American plate toward E, with velocities of ~ 4,2 cm/yr along an azimuth of 69°N (DeMets *et al.*, 1990). The thick siliciclastic sedimentary cover of the Juan de Fuca plates (*i.e.* terrigenous material coming from the Astoria fan; McAdoo *et al.*, 1997; 2004) results offscraped and accreted onto the North American plate margin.

Some relatively large MTCs have been recognized in the southern margin of the accretionary wedge of the Cascadia subduction zone, thought to being developed in response to tectonic accretion/erosion processes (Goldfinger *et al.*, 2000; McAdoo *et al.*, 2000; McAdoo and Watts, 2004).

It is interesting to note that in the seismically active northern margin, MTDs are quite poorly represented in respect to turbidite deposits; this fact has commonly explained invoking the frequent earthquake-related strengthening of sediment pile (see above), that should favor the synchronous development of relatively small-scale dense and turbulent gravity flows instead of large-scale slope failures (Nelson *et al.*, 2008) (fig. 8.23).

8.3.3 Sunda Arc (SW Indonesia)

The Sunda-Banda subduction-related accretionary complexs are composed of a western arc-ocean and an eastern arc-continent collision zones, respectively, localized at the junction of at least three major plates: Eurasian (South-East Asia), Pacific and Indo-Australian (Van der Werff, 1995). In the Sunda Arc subduction zone, the oceanic crust of the Indo-Australian plate underthrust the Eurasian plate, while, further to the E, in the Banda Arc subduction zone, it is the continental crust belonging to the same plate to be subducted. The Indo-Australian plate motion is ~ 7 cm/yr toward the N, along an azimuth of ~ 30°N. The eastern bending (*i.e.* oroclinal appearance) of the Banda Arc is interpreted to be associated to the westward motion of the Pacific plate, showing velocities of ~ 7 cm/yr along an azimuth of ~ 290°N, giving an overall apparent anti-clockwise rotation of the

entire system (Van der Borch, 1978; McCaffrey *et al.*, 1985; Spence, 1986; Eva *et al.*, 1988; Charlton, 2000; Milsom, 2000; Hinschberger *et al.*, 2001, 2005; Hanson, 2004; and reference therein) (fig. 8.24).

The general physiography of the Sunda Arc subduction system is characterized by the typical bathymetric domains of a convergent-related accretionary complex profile (Busby and Ingersoll, 1995), with relatively well-developed trench-slope-forearc depositional settings (fig. 8.25), strongly dissected by active faulting and with the relatively limited development of small-scale MTDs, locally over-thickened by the confined conditions of the accommodation (Karig *et al.* 1980; Fortuin *et al.*, 1992; Dickinson, 1995; Van der Werff, 1996; Susilohadi *et al.*, 2005; Moran and Tappin, 2006; Seeber *et al.*, 2007; Mosher *et al.*, 2008). Particularly the complex lateral evolution of the Java subduction zone caused a further segmentation of the forearc domain, resulting in the formation of an inner- and outer-forearc depositional domains (Beaudry and Moore, 1981; Van der Werff, 1996). These forearc sectors are the main *loci* of gas hydrate concentrations, which seem to be absent in other part of the accretionary prism (Kopp, 2002; Wiedicke *et al.*, 2002).

An evidence of large-scale MTD from the northwesternmost Sunda Arc is provided by Moore *et al.* (1976), but its position within the base of continental slope off Burma should be interpreted as related to processes typical of the Bengal Fan, nonetheless the Sunda subduction zone dynamics should have contributed to its development.

In the Sunda subduction complex, several minor slope instabilities and low-rated movements have been observed, and particularly, a relatively large debris avalanche (~ 50 km^2 of areal extension) has been recently observed in the offshore area off the northwest coast of Sumatra, originating from a thrust ridge developed in a sea-ward position with respect to the main trench zone (Moran and Tappin, 2006; Bradshaw *et al.*, 2009). These examples are mainly developed in the outer trench/trough regions and only minor evidence of small-scale, short-runout MTDs have been recognized along the main accretionary wedge slope (Seeber *et al.*, 2007; Mosher *et al.*, 2008) (fig. 8.26).

8.4 Possible analogs for comparison purposes

However, leave aside the general morphology, the anatomy of present day accretionary margins, and particularly those involving a continental collision, are relatively poorly represented in modern geophysical dataset, mainly due to their occurrence in restricted portions of plate boundaries, sharing complicated geodynamic contexts (*e.g.* oroclinal, arcuate, double-vergent and oblique subductions; Milsom, 2000) and extremely complex structural architectures (Cowan, 1985;

Scholl *et al.*, 1980). Apart from some few fortunate examples, the seismic identification of mass transport-related "chaotic" features from those of tectonic origin is commonly difficult in these settings, especially without the support of extensive (and expensive) 3D coverage.

8.4.1 NW Borneo

Among the published data analyzed in this work, the best example of large-scale MTD so far recognized in a collisional margin setting is that of the Brunei Slide, offshore the coast of NW Borneo (McGilvery *et al.*, 2004; Gee *et al.*, 2007; Morley, 2007).

The NW Borneo continental slope is represented by fold-and-thrust belt (*i.e.* Crocker thrust belt) is interpreted as developed in response to the SE-subduction of continental crust fragment (*i.e.* Dangerous Ground block) under thinned continental-oceanic (?) crust and related accreted sediments of the northwestern margin of the Borneo accretionary complex, which toe is represented by the inner slope of the Borneo Trough (Curiale *et al.*, 2000; Morley *et al.*, 2003 and reference therein). This irregular slope, from shallow- to deep-water settings, is characterized by development of elongated intra-slope mini-basins, confined by local to regional roughly linear, slope-parallel structures (*i.e.* anticline crests), associated to the general regional compressive regime coupled with mud diapirism, gravity-driven slope tectonics and large sedimentary accumulations (*i.e.* Champion and Baram Delta) (fig. 8.27) (Van Rensbergen and Morley, 2000; Lambiase *et al.*, 2002; Morley *et al.*, 2003; Tingay *et al.*, 2007; Morley, 2007, 2009a, 2009b; Morley and Leong, 2008). Apart for the larger size (about 5 times greater), mode of development and depositional context of this MTD seem tentatively well comparable with those inferred for the Specchio R2 unit.

The Brunei Slide covers part of the inner slope and the basin floor of the NW Borneo Trough for an area of ~ 5.300 km^2, showing an average thickness of ~ 240 m, locally reaching more than 400 m. It is inferred to be originated from an single catastrophic failure of a localized part of the upper slope-shelf edge region, in response to a combination of fluid seepage, high sedimentation, and tectonic- and mud diapiric-related growing structures affecting the Baram Delta-Canyon system. The depositional environment strongly influences the slide development, which is characterized by a transport pattern curving from the failure zone to the accumulation zone (up to 60-80° divergence angle), showing a "fingered" appearance where slide lobes are forced to infill elongated mini-basins in sub-parallel direction to the anticlinal ridges trend (fig. 8.28) (Gee *et al.*, 2007).

This large-scale MTD emplacement is interpreted to develop strong seafloor erosion, as confirmed by: 1) truncation of the seismic reflectors along the basal shear plane (especially on the anticline crests), 2) presence of giant striations (~ 30–120 km long, ~ 100–600 m wide and 10–30 m

deep) along the basal surface, and 3) inferred excess mass balancing in respect to the failed mass (Gee *et al.*, 2007). Moreover, evidence of subsurface sediment remobilizations and overpressured zones, have been recognized close to the basal surface of the slide, both in proximity to the failure and accumulation zones. The mode of emplacement suggested for this slide forecast a progressive down-slope evolution involving the forced confinement (*i.e.* damming) of the failed mass operated by the slope parallel trending anticlinal ridges and their subsequent collapse (*i.e.* dam breaking) caused by the rear push of the accumulating slide mass, possibly favored by the presence of gas hydrates levels on anticline apexes (*i.e.* BSR as preferential rupture layer; Gee *et al.*, 2007) (fig. 8.29).

This slide is interpreted on the basis of seismic facies as a debris-flow, nonetheless the widespread presence of outsize blocks of deformed strata may support its identification as a debris avalanche or blocky-flow (*sensu* Mutti *et al.*, 2006).

Subsurface data also show the presence of other episodic and relatively large-scale MTDs buried on the basin-floor (Gee *et al.*, 2007), and the widespread occurrence of small-scale MTCs on the slope, mainly developed on the basin-ward forelimb of growing anticlines (*i.e.* degradation complexes; Morley and Leong, 2008; Morley, 2009a, 2009b), and represented by limited runout MTDs (*e.g.* slump bodies) which are progressively involved in the anticline-related thrust system (fig. 8.30). Similar degradation features have been also observed in other deep-water compressional belts, developed through gravity-driven slope tectonics (*e.g.* Niger Delta; Heiniö and Davies, 2006).

Summarizing observations and interpretations for the Brunei Slide and its depositional environment, the most prominent features arising are: 1) widespread occurrence of degradation complex, 2) evidence of seafloor erosion, especially on the anticline crests, 3) localized over-thickening of the slide mass within the structurally-controlled depocenters, 4) evidence of fluid overpressuring and escape structures, 5) presence of tens to hundred of m-sized stratified deformed blocks, 5) and general down-slope sliding movement in the failure zone and along-slope transport in accumulation zone, sub-parallel to the overall trending of elongated structural highs (Gee *et al.*, 2007; Morley, 2009a, 2009b).

8.4.2 SW Taiwan

The best analog recognized for the physiographic and depositional setting is thought to be the Kaoping Slope, developed on the accretionary complex (*i.e.* Hengchun Ridge/Manila accretionary wedge) of the SW offshore of Taiwan (Yu and Song, 1993; Huang *et al.*, 2000; Chang *et al.*, 2000; Yu and Huang, 2006; ChunFeng *et al.*, 2007; Malavieille and Trullenque, 2007; Chiu and Liu, 2008) (fig. 8.31). Here the foreland sediments of the SE China continental margin are accreted on

the submerged southernmost Taiwan orogen (formed at the junction between the Luzon and the Ryukyu Arcs) in response to the oblique collision caused by the NW translation of the Philippine plate (7-8.2 cm/yr) against the Eurasian plate (Suppe, 1981; Yu and Song, 1993; Biq, 1997).

The wide Kaoping Slope (~ 100 km of maximum width) is comprised between a narrow shelf (~ 20 km of maximum width; Kaoping Shelf) and a trench zone marking the toe of the accretionary wedge (Penghu Canyon/Manila trench). This slope shows a well-developed above-grade profile in which mini-basins are separated by roughly arcuate positive structures, interpreted as contraction tectonics-related mud diapiric ridges, and some canyons (*e.g.* Kaoping and Penghu canyons), partly influenced and roughly cutting down-slope these structures (fig. 8.32). These canyons are partly filled by channelized sedimentary bodies (in some case with meandering appearance), associated to the main sediment discharge systems (*e.g.* Kaoping river system) (Chiu and Liu, 2008).

This basin system is mainly fed by syn-orogenic sediments coming from the south-central Taiwan Muntain Range, directly delivered and "trapped" into the Kaoping Slope (in most part bypassing the Kaoping Shelf) by hyperpicnal flows associated to the main Kaoping alluvial system and other relatively small, high-gradient river systems (*i.e.* small mountainous rivers *sensu* Milliman and Syvitski, 1992), leaving the deep-water foreland in relatively under-filled conditions (*i.e.* South China Sea base of slope and basin floor) (Chiang and Yu, 2006; Yu *et al.*, 2008). The high sediment discharge of these systems is thought to be controlled by high-magnitude mass wasting events (tectonic and climatic) influenced by the on land geomorphology, which favor their direct input into the main drainage system and then to the sea (Hovius *et al.*, 2000).

The maximum size reached by these mini-basins is ~ 40 km in length and ~ 12 km in width, and their common sedimentary infilling show an overall tripartition in the vertical stacking of the seismic facies: 1) a basal convergent-baselapping facies, 2) an intermediate chaotic facies, and 3) an upper parallel-draping facies. This upward change in the seimic character of the deposits is interpreted to reflect a "fill-and-spill"-type evolution (see Sinclair and Tomasso, 2002; Lomas and Joseph, 2004) for these intra-slope basins, which forecasts an early confined basin-fill stage, followed by a mass wasting from flanking structural highs and a later progradation and spill over deposition (Yu and Huang, 2006) (fig. 8.33).

8.4.3 SW New Zealand

The New Zealand is formed by the complex double-vergent and oblique subduction between the Australian and Pacific plates. In the eastern side of the Northen Island (*i.e.* Hikurangi Margin), the oceanic crust of the Pacific plate obliquely subducts under the Australian plate, with an average convergence rate of ~ 4.5 cm/yr, while in the south-westernmost part of the Southern Island

continental margin the geodynamic situation is almost inverse, with the high-angle oblique subduction of the Australian plate under the Pacific plate, roughly at the, with averange convergence rates of 2-3 cm/yr (*i.e.* Puysegur Trench), and the inferred involvement of Australian plate-related thinned continental crust (Davey *et al.*, 1998; Beavan *et al.*, 2002; Furlong and Kamp, 2009).

These two quite opposite subductions are linked by a transpressive zone (*i.e.* Alpine Fault), roughly coinciding with the axial trend of the Southern Alps mountain range for ~ 800 km long, which accommodates ~ 70% of the plate motion, giving an overall anti-clockwise rotation sense to the entire geodynamic system. It is along this transpressional zone where the bulk of continental collision occurs (Sutherland *et al.*, 2000) (fig. 8.34).

The eastern part of the Southern Island represents therefore an example of transpressive-transtensive incipient continental collision, developing an accretionary complex with physiographic characteristics quite different from the Hikurangi Margin of the Northern Island (Davey *et al.*, 1986; Wood *et al.*, 2000; Barnes *et al.*, 2005; Bailleul *et al.*, 2007), where the vast majority of MTDs is observed to occur, either as slow moving, small-scale ones, (*e.g.* Tuaheni landslide complex; Mountjoy *et al.*, 2009), and fast-moving, large-scale ones, characterizing both internal depositional zones and the main deformational front (see above; section 8.2) (fig. 8.35).

The eastern collision-related foreland region of the Southern Alps is represented by the South Westland Basin, which shows the typical stratigraphic architecture of an under-filled peripheral foreland basins, developed in response to the lithospheric flexure-related subsidence operated by the orogenic growth (Sircombe and Kamp, 1998). The internal (in the sense of the chain) accretionary complex is essentially formed by the dextral transpressive-transtensive regime linked to the Alpine Fault tectonic system, and is superficially represented by a ~ 50 km-wide slope and a very narrow shelf, directly attached to the mountain belt.

The Alpine Fault represent the back-stop zone of the accretionary wedge, roughly separating an internal sector characterized by the development of a pull-apart and releasing basin system (related to the general dextral strike-slip regime) from an external one presenting a compression-related intra-slope depositional setting. This situation is commonly observable in the southwestern most part of the Southern Island (Barnes *et al.* 2005).

The sediment discharge to those depositional settings thought to be achieved by high-gradient small drainage river systems controlled by both periodic and episodic factors, and by the general significant uplift of the mountain belt (Korup *et al.*, 2004). The fast-eroded, coarse-grained material delivered by these systems is thought to largely bypass the narrow shelfal environments, with the maximum sediment entrainment in the wedge-top intra-mountain and intra-slope depositional

domains, on- and offshore respectively (McConnico and Bassett, 2007).

8.4.3 Banda Arc (SE Indonesia)

The Banda Arc is the eastern expression of the Sunda-Java trench oceanic subduction zone (*i.e.* Sunda-Sumatra Arc; Hall and Wilson, 2000; Barber and Crow, 2003) and represent one of the few classical example of an orogenic system related to an arc-continent collision, characterized by a significant strike-slip tectonic component (McCaffrey and Abers, 1991; Hamson, 2004). The eastern Banda Arc represents an incipient evolving continental collision, characterized by strong tectonism expressed by high relief of structural highs, volcanism, seismicity, rapid uplift and exhumation (Hanson, 2004 and reference therein). The overall physiography is represented by a well-defined trench zone (*i.e.* Timor-Weber-Seram Trough), uneven and relatively steep outer trench-slope and foreland sectors (with a relatively smooth and wide continental shelf), and an inner accretionary wedge with a steep-graded profile, characterized by trench-slope basins confined by thrust- and backthrust-related, steep-sided structural highs; the overall high-angle inclined slopes of both inner and outer margin, favor the development of short-runout, small-scale MTDs (Nitzsche, 1989; Situmorang, 1989; Van der Werff, 1995). The influence of tectonic-related mud-diapirism seems to play a significant role in the development of such positive structures (Williams *et al.*, 1984), especially in the outer forearc and trench-slope areas (Harris, 2000).

Moreover, the oblique convergence-related continued accretion of the Australian continental margin rocks against the Banda Arc caused a high-rated uplift with the local emergence of the accretionary wedge (particularly its outer forearc region), expressed by the Timor, Rote, Sumba and Savu Islands, (Roosmawati and Harris, 2009). A similar situation is observable in the Nias and Simeulue Islands of the Sunda Arc (Harbury and Kallagher, 1991). In these cases the forearc region remains isolated between an inactive, inner volcanic arc and an outer arc, represented by the rising trench-slope break of the accretionary prism above the sea level.

Most of the coarse-grained population of sediment coming from the fast-rated erosion of the uplifting relieves is thought to be "trapped" within the accretionary wedge confined depozones (*i.e.* forearc and trench-slope domains), while the trench infilling is interpreted to be mainly fed by fine-grained sediments coming from the outer regions (*i.e.* foreland-continental shelf) (Situmorang, 1989).

Apart form the evident physiographic differences between the adjacent oceanic- and continental-related subduction settings, the striking characteristic emerging from the summary of the above mentioned observations is that the characterizing MTDs, nonetheless relatively scarce,

present limited sizes and runouts, and are equally distributed from the outer trench to the inner forearc areas (fig. 8.37).

8.5 List of figures

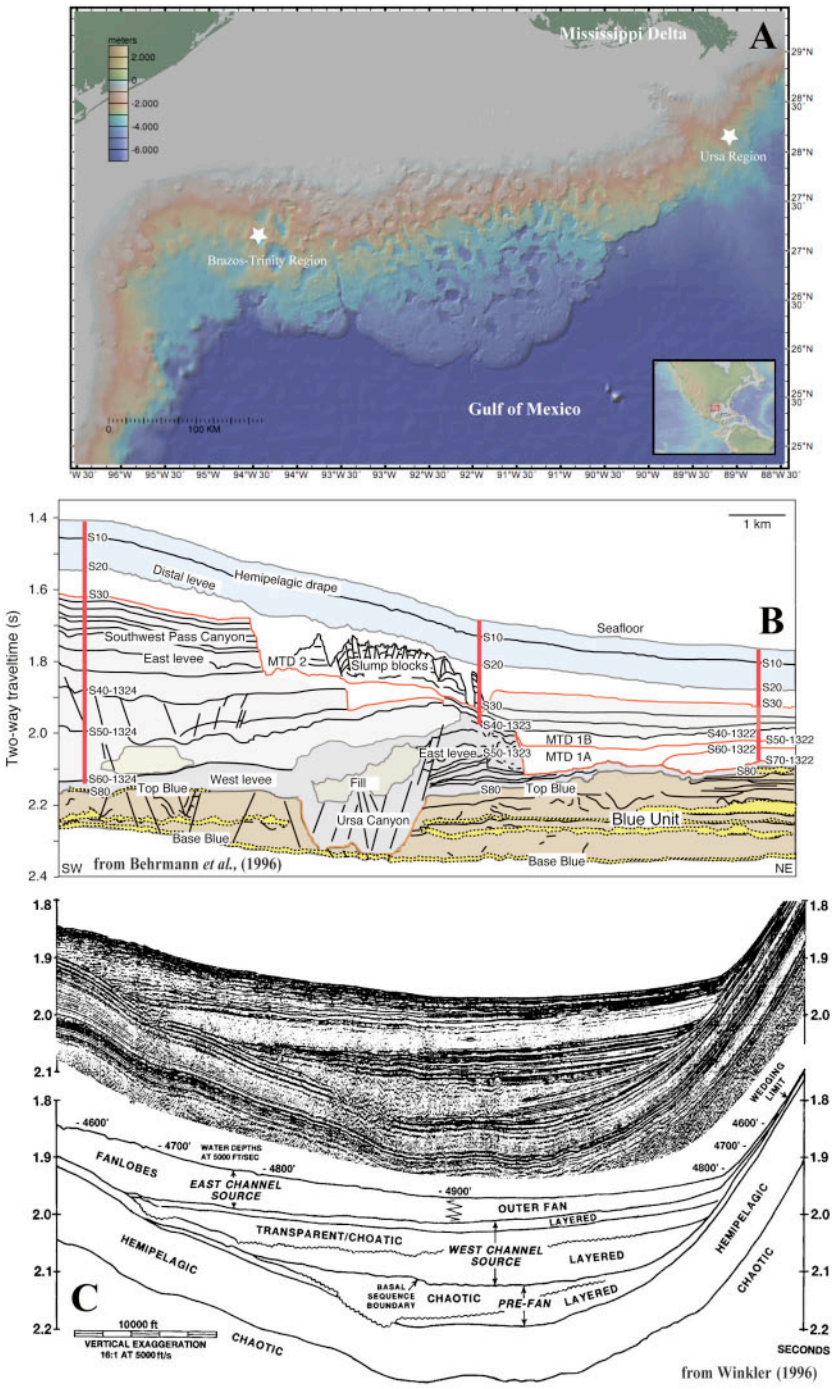

Figure 8.1 - **A**: Morpho-bathymetric map of the salt-based shelf-slope-basin plain system of the Gulf of Mexico, with localization of transects shown in B and C. Compiled with GeoMapApp (2009).

B: interpreted cross-section from Ursa Basin. Sand-prone Blue Unit has been incised by channel-levee complex and then overlain by thick and heavily slumped (*i.e.* MTD) hemipelagic mudstone wedge that thickens westward (left). Blue Unit sands correlate to distinct seismic facies. Thickness of hemipelagic mudstone above Blue Unit does not change significantly in north-south direction. From Behrmann *et al*. (2006).

C: High-resolution seismic dip profile of a salt-withdrawal mini-basin on the northern continental slope of the Gulf of Mexico (*i.e.* Trinity-Brazos, showing differentiation of major seismic facies. From Winkler (1996).

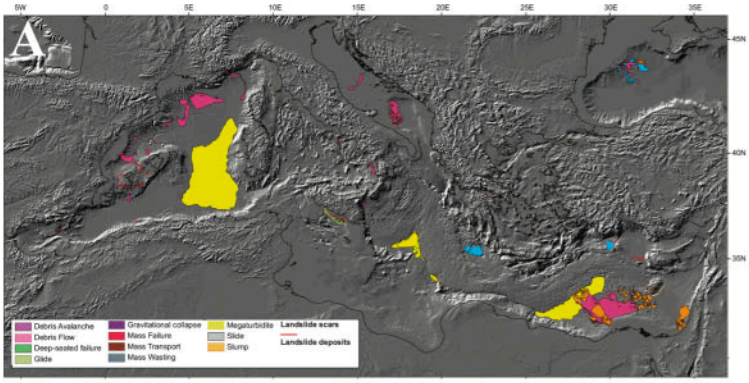

from Camerlenghi *et al.* (2010)

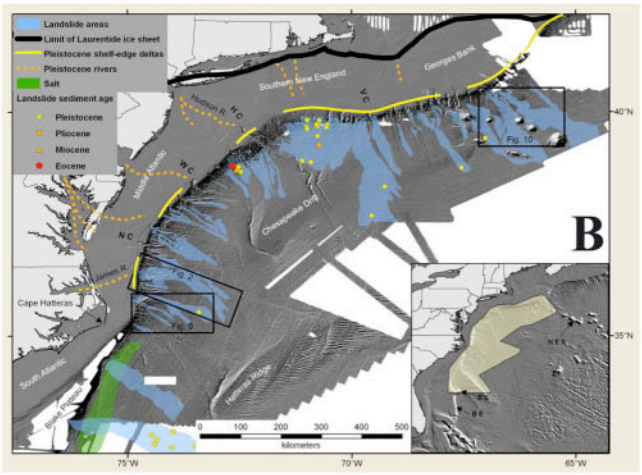

from Twitchell *et al.* (2009)

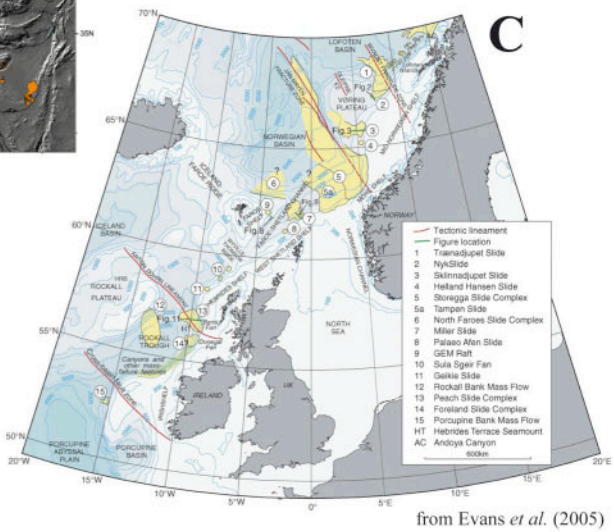

from Evans *et al.* (2005)

Figure 8.2 - **A**: shaded relief map of Mediterranean bathymetry displaying location and typology of the so far recognized submarine landslides. From Camerelenghi *et al.* (2010).

B: regional morphology and landslide distribution on the U.S. Atlantic margin revealed by available multi-beam bathymetry. The names of areas referenced in the text and geologic features that may influence landslide distribution are shown as well. The abbreviations NES, BOR, BS, and BE in the inset map refer to the New England Seamounts, Blake Outer Ridge, Blake Spur, and Blake Escarpment respectively, and VC, HC, WC, NC on the main part of the figure refer to Veatch, Hudson, Wilmington, and Norfolk Canyons, respectively. From Twitchell *et al.* (2009).

C: The latitudinal extent of the Atlantic margin of the NW Europe, together with the locations of the slides and palaeoslides discussed, and selected tectonic features. Bathymetry after GEBCO. From Evans *et al*. (2005).

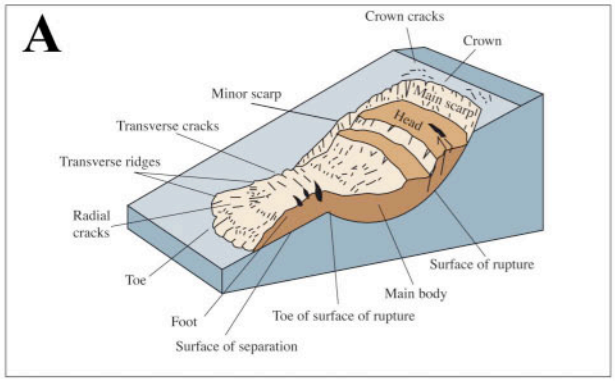

from Highland and Johnson (2004) after Varnes (1978)

B

TYPE OF MOVEMENT		TYPE OF MATERIAL		
		BEDROCK	ENGINEERING SOILS	
			Predominantly coarse	Predominantly fine
FALLS		Rock fall	Debris fall	Earth fall
TOPPLES		Rock topple	Debris topple	Earth topple
SLIDES	ROTATIONAL	Rock slide	Debris slide	Earth slide
	TRANSLATIONAL			
LATERAL SPREADS		Rock spread	Debris spread	Earth spread
FLOWS		Rock flow (deep creep)	Debris flow (soil creep)	Earth flow
COMPLEX		Combination of two or more principal types of movement		

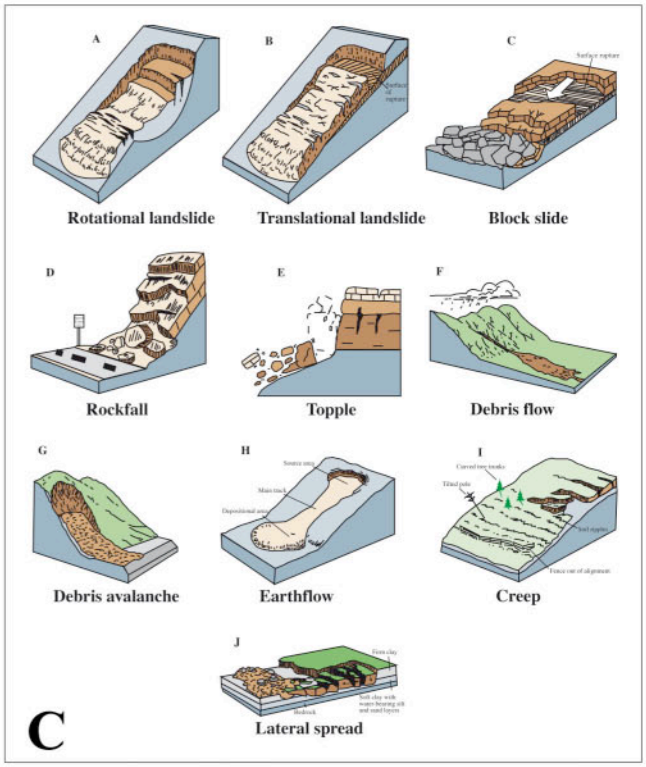

Figure 8.3 - **A**: An idealized sketch for subaerial slump-earth flow, showing commonly used nomenclature for labeling the parts of a landslide.

B: Types of landslides. Abbreviated version of Varnes' classification of slope movements.

C: Schematic cartoons illustrating the major types of subaerial landslide movement. All figures are from Highland and Johnson (2004), after Varnes (1978).

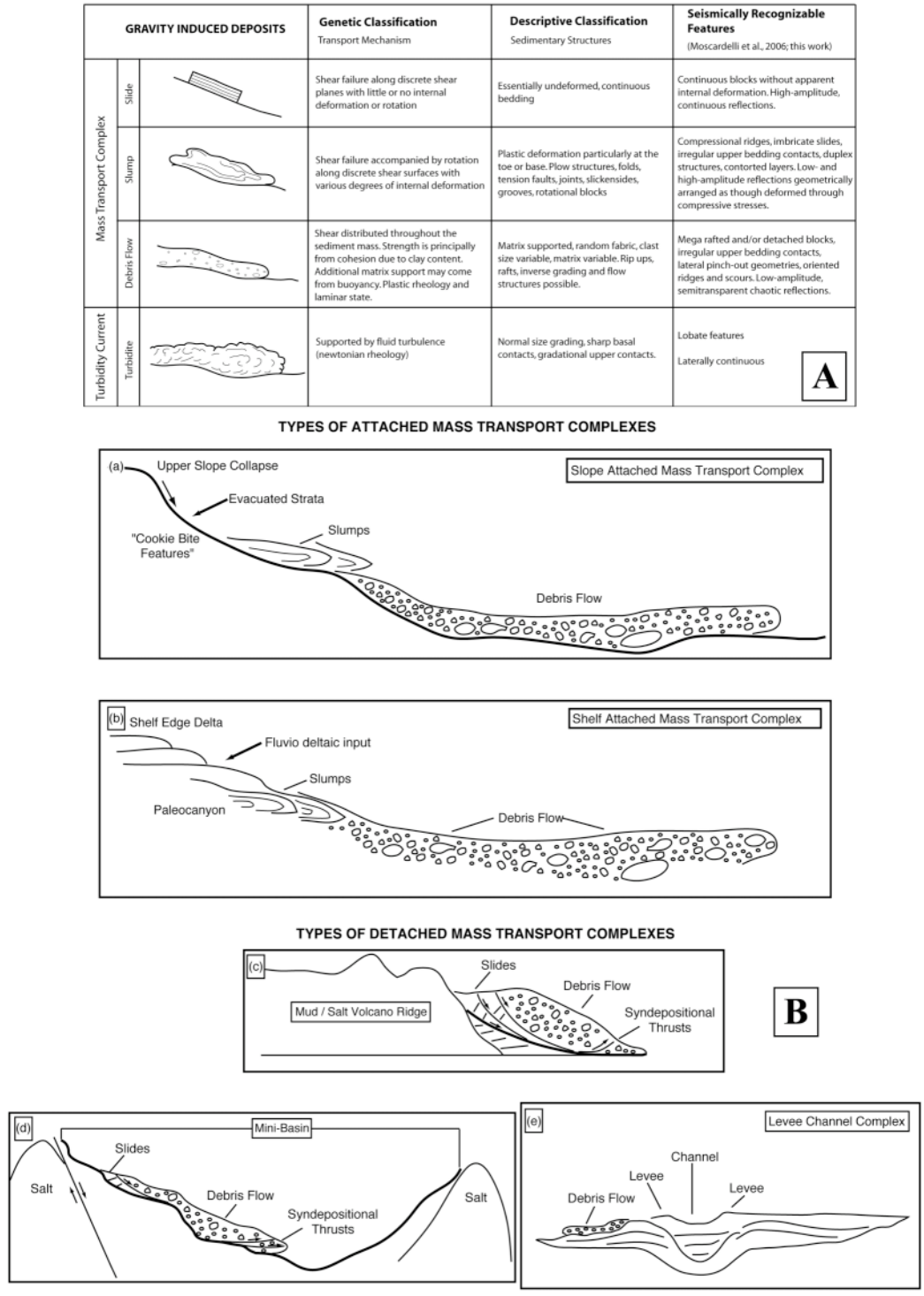

Figure 8.4 - **A**: Classification of sediment gravity-induced deposits from Moscardelli and Wood (2007). Compiled after Dott (1963), Nardin *et al*. (1979) and Moscardelli *et al*. (2005).

B: Schematic depiction of the different kinds of MTCs and the processes associated with their genesis. (a) Slope-attached mass transport complex: sediments are derived from the catastrophic collapse of the upper slope area. (b) Shelf-attached mass transport complex: sediments are provided by shelf-edge deltas and are dumped into the deep-marine basin. (c) Detached mass transport complex: whose genesis is associated with the collapsing flank of a mud-volcano ridge. (d) Detached mass transport complex: whose genesis is associated with oversteepening of one of the margins of a deep-water mini basin. (e) Detached mass transport complex: whose genesis is associated with a levee-channel complex. From Moscardelli and Wood (2007).

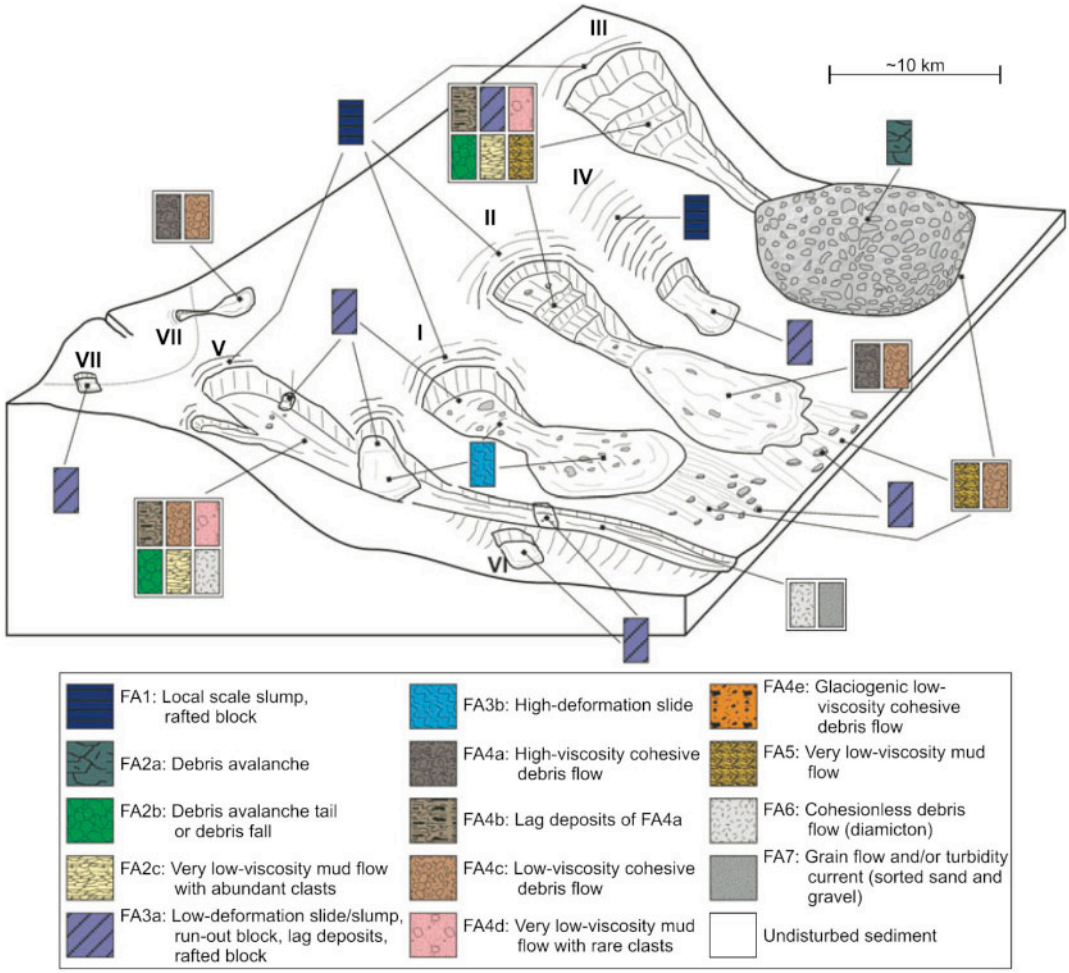

Figure 8.5 - Cartoon displaying several different types of sediment failures and the spatial distribution of the mass-transport deposit (MTD) facies associations, mainly determined through core analysis. Roman numerals indicate examples of the types of failures as recognized so far in modern seafloor worldwide. **I**: High-deformation landslide – failure A in the Atlantis Prospect (Tripsanas *et al.*, 2007), T20 Slide (Frey-Martinez *et al.*, 2006). **II**: Landslide transformed into cohesive debris flow – Sheridan and Bonanza Canyon systems and failures D and H–L (Tripsanas *et al.*, 2007), Afen Slide (Wilson *et al.*, 2004) **III**: Debris avalanche – Blocky MTD sampled in core JPC-07 (Tripsanas *et al.*, 2007), San Pedro Escarpment (Bohannon & Gardner, 2004; Normark *et al.*, 2004), El Hierro (Gee *et al.*, 2001), northern Hikurangi margin (Collot *et al.*, 2001). **IV**: Low-deformation slides/slumps –MTDs sampled in cores EG-1, EG-3 and NWF-56 (Tripsanas *et al.*, 2007), South Korea Plateau (Lee & Chough, 2001), southwest Gulf of Corinth (Papatheodorou & Ferentinos, 1997), ISC slide (Frey-Martinez *et al.*, 2006). **V**: failures in canyons –canyoned central Scotian slope and Sheridan and Bonanza Canyon systems (Tripsanas *et al.*, 2007), mass-transport complexes offshore of Trinidad and Venezuela (Moscardelli *et al.*, 2005), Aoga Shima Canyon (Klaus & Taylor, 1991). **VI**: Local-scale slides and slumps in channels and levees – MTDs sampled in cores 33-23 and 24-31 (Tripsanas *et al.*, 2007), Mississippi Fan (Turner, 1983). **VII**: Slumps/slides and debris flows on river deltas – Kitimat fjord river delta (Prior *et al.*, 1984), Mississippi River Delta (Coleman *et al.*, 1988), river deltas in the south- west Gulf of Corinth, Greece (Hasiotis *et al.*, 2002). From Tripsanas *et al.* (2007).

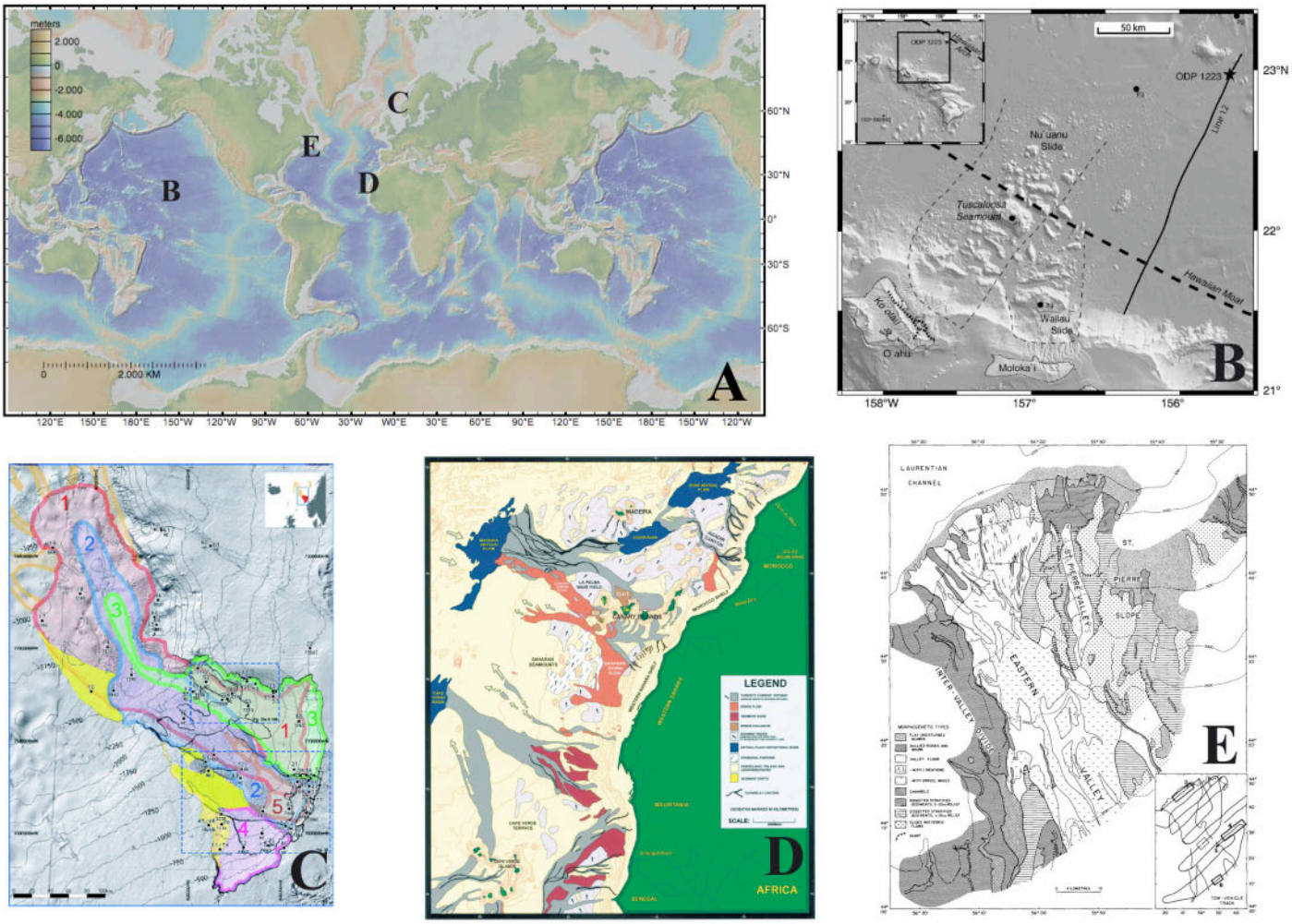

Figure 8.6 - **A**: Morpho-bathymetric map of the worldwide oceans displaying locations of classical giant submarine landslides shown in fig B, C, D and E. Elaborated with GeoMapApp (2009).

B: Shaded relief map showing the location of ODP Site 1223 (Hawaii), the islands of O'ahu and Moloka'i (outlined by thin black line), and the debris fields for the giant Nu'uanu and Wailau landslides from Ko'olau and East Moloka'i volcanoes (thin dashed lines show slide boundaries). From Garcia *et al.* (2006).

C: General bathymetric map of the Storegga mass transport complex, offshore Norway. Main mass transport events are labeled 1–5. Different colors represent consecutive phases. The yellow color shows the compression zones created by the impact. From De Blasio *et al.* (2005).

D: Sidescan sonar- and 3.5 kHz-based map showing sediment process of the Northwest African margin. This map also shows the complex interplay between pelagic, hemipelagic sedimentation, alongslope bottom currents and downslope gravity flows. Bathymetric contours in kilometres. Abbreviations for giant submarine landslides: Te – Tenerife; L - La Palma; H - El Hierro; O-I-T – Oratava-Icod-Tino Debris Avalanche; EG - El Golfo Debris Avalanche. From Wynn *et al.* (1999).

E: Sidescan sonograph- and subbottom profile-based map of the surface morphology of the southern Newfoundland continental slope, showing the upperslope part of the 1929 earthquacke-triggered Grand Banks slide. From Piper *et al.* (1985).

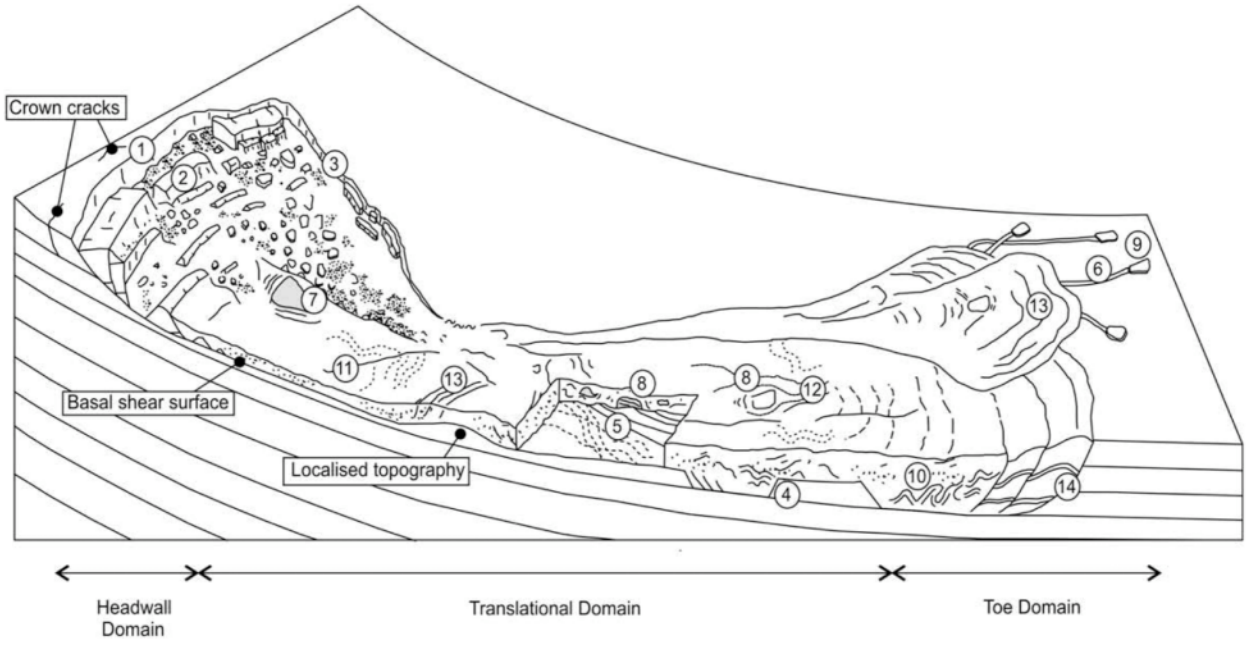

Figure 8.7 - Schematic representation of a MTC and the likely occurrence and associations of kinematic indicators relative to the headwall, translational and toe domains: (1) Headwall scarp, (2) Extensional ridges and blocks, (3) Lateral margins, (4) Basal shear surface ramps and flats, (5) Basal shear surface grooves. (6) Basal shear surface striations, (7) Remnant blocks, (8) Translated blocks, (9) Outrunner blocks. (10) Folds, (11) Longitudinal shears/ first order flow fabric, (12) Second order flow fabric, (13) Pressure ridges, (14) Fold and thrust systems. From Bull *et al.* (2008) after Prior *et al.* (1984).

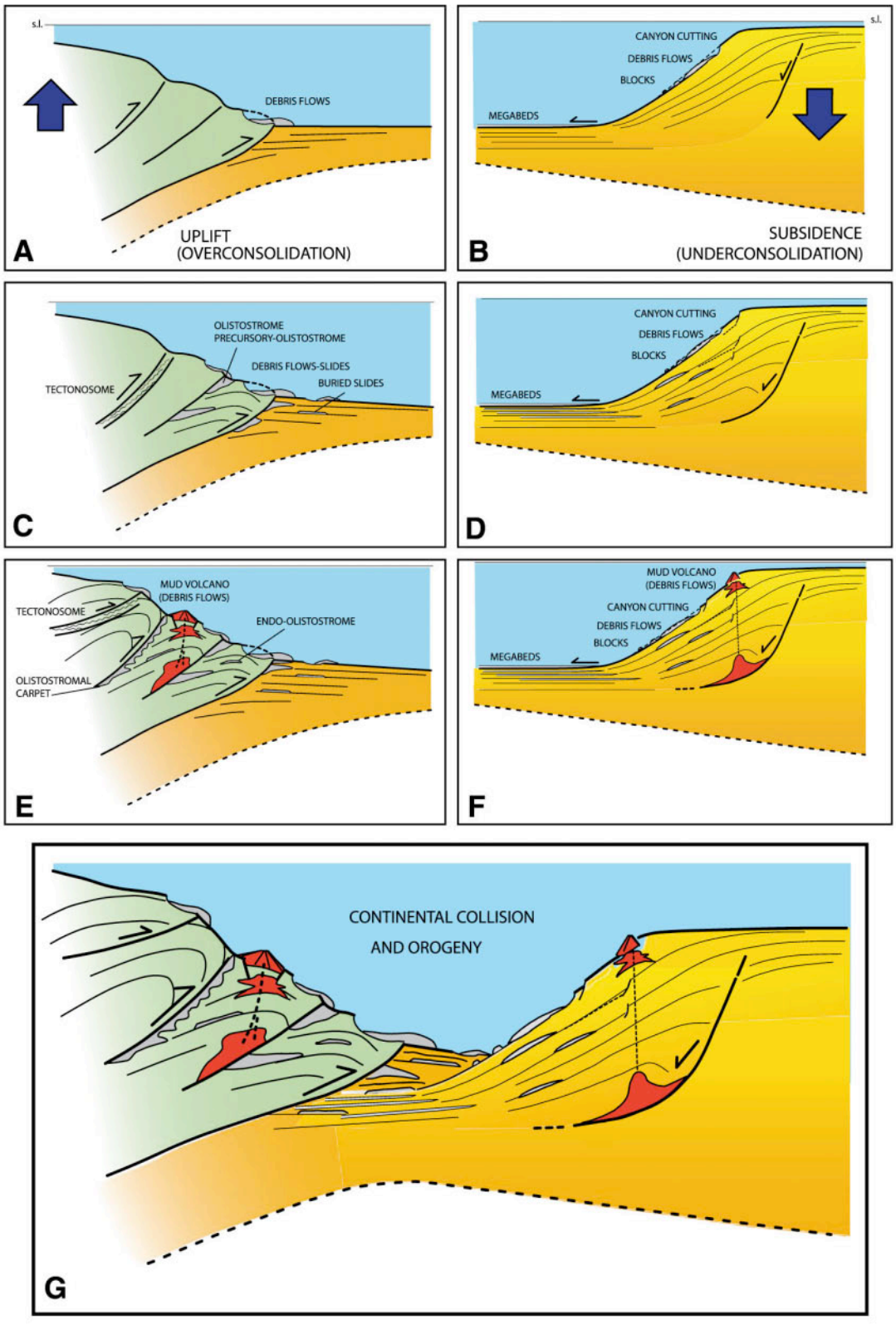
s.l.
DEBRIS FLOWS
A
UPLIFT
(OVERCONSOLIDATION)
s.l.
CANYON CUTTING
DEBRIS FLOWS
BLOCKS
MEGABEDS
B
SUBSIDENCE
(UNDERCONSOLIDATION)
OLISTOSTROME
PRECURSORY-OLISTOSTROME
DEBRIS FLOWS-SLIDES
BURIED SLIDES
TECTONOSOME
C
CANYON CUTTING
DEBRIS FLOWS
BLOCKS
MEGABEDS
D
MUD VOLCANO
(DEBRIS FLOWS)
TECTONOSOME
ENDO-OLISTOSTROME
OLISTOSTROMAL
CARPET
E
MUD VOLCANO
(DEBRIS FLOWS)
CANYON CUTTING
DEBRIS FLOWS
BLOCKS
MEGABEDS
F
CONTINENTAL COLLISION
AND OROGENY
G

Figure 8.8 - Conceptual model displaying the genetic phylum relating a large number of olistostromes (*i.e.* MTDs and MTCs), tectonosomes (*i.e.* tectonic *mélanges*), mud volcanoes and diapirs to the geological history of an hypothetical sedimentary basin (*e.g.* the Mediterranean Basin) ending with collisional orogeny (not to scale). From Camerlenghi and Pini (2009).

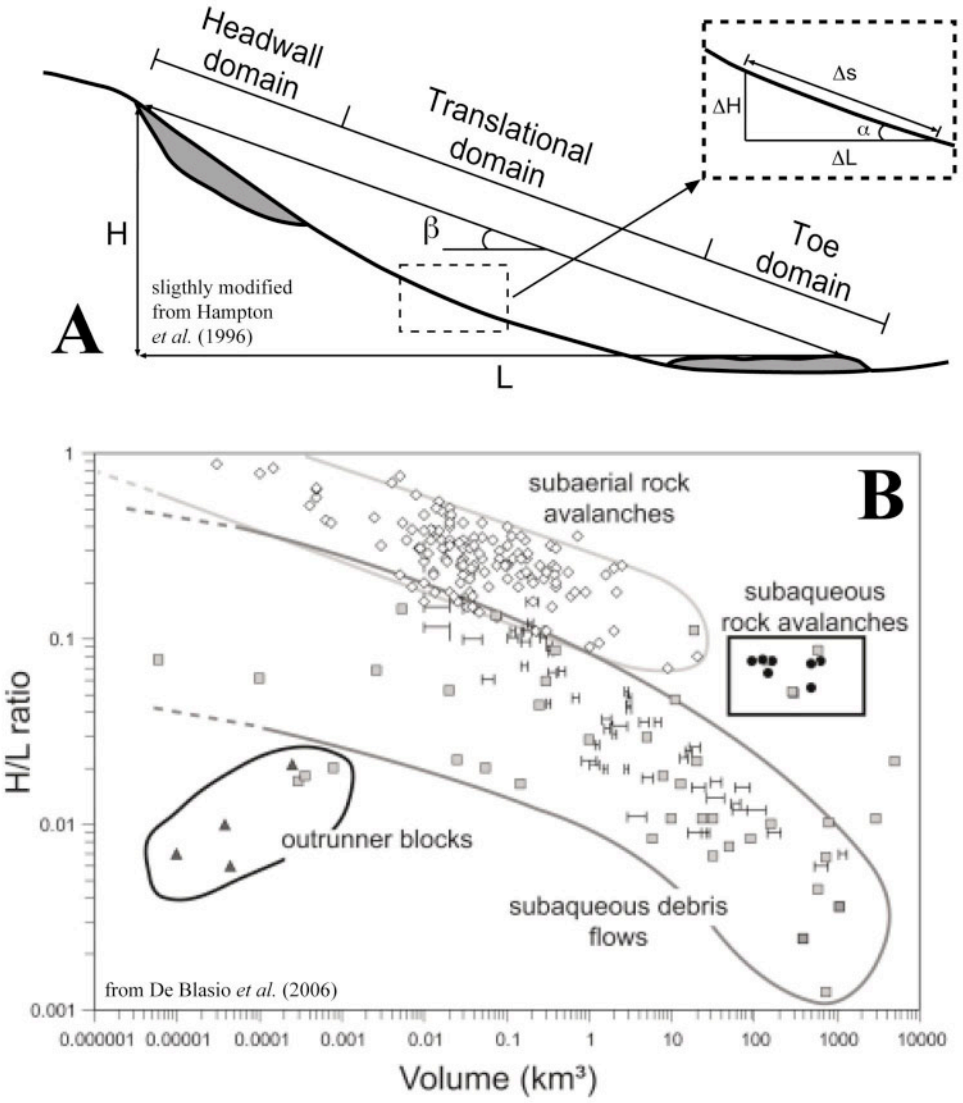

Figure 8.9 - **A**: Conceptual scheme on landslide runout. Represented parameters are: H – topographic elevation difference from failure (headwall) to accumulation zone (toe); β – angle between the horizontal and the line connecting headwall and toe zones; α – slope angle in the translational domain; s – travel distance of the slide mass; L – amount of the horizontal displacement. Slightly modified from Hampton *et al.* (1996).

B: Diagram showing the distribution ofsubaqueous and subaerial landslide deposits, where the abscissa reports the volume of the landslide, and the ordinate scale is the ratio H/L between the height fall of the landslide, H, and the horizontal runout, L (see A). Data for subaqueous debris flows (grey squares) are mainly from Edgers and Karlsrud (1982), Elverhøi *et al.* (2002) and Masson *et al.* (1998). Outrunner block data (black triangles) are from Nissen *et al.* (1999), Prior *et al.* (1982a; 1982b), Kuijpers *et al.* (2001), and Longva *et al.* (2003). Data for subaerial rock avalanches (empty squares) derive from various sources. Subaqueous rock avalanches (black dots) are taken from Masson *et al.* (1998). The segments (with length indicating the uncertainty in the volume) are the debris flow lobes of the Storegga slide (Haflidason *et al.,* 2005). For very small volumes (0.01 to 0.2 km) the Storegga data are in reality more numerous than suggested by figure 1, as greater uncertainty make many data fall on the same segment (Haflidason *et al.,* 2005). The data from the Storegga landslide area indicates a distribution $f \propto 1/V$ of landslide frequency distribution f as a function of the volume (Issler *et al.,* 2005).

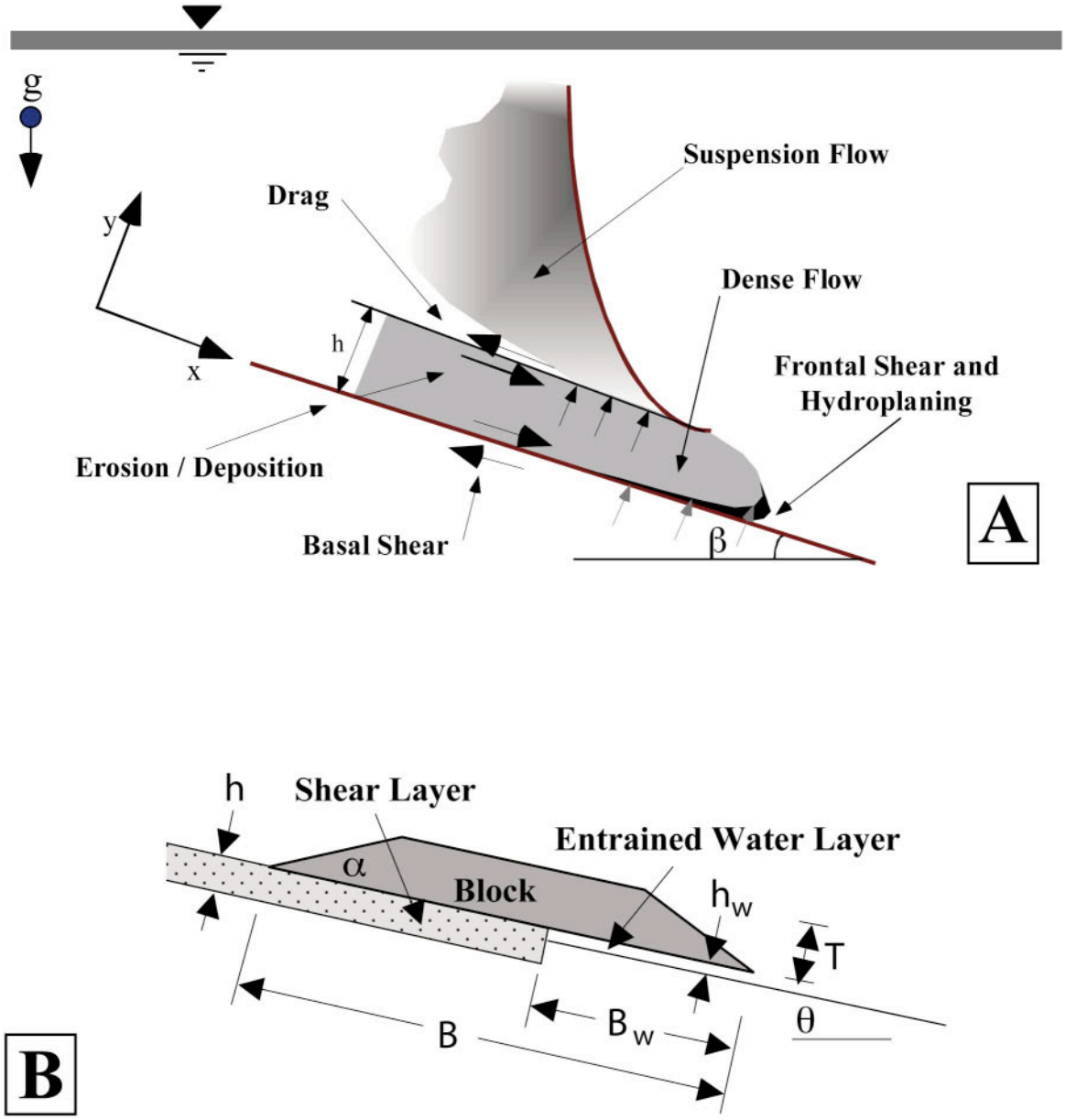

Figure 8.10 - A: Schematic diagram showing the potential lifting of frontal lobe of a sliding mass (Bingham fluid) leading to the process of hydroplaning, the basal shear stress causing erosion and deposition, and possible generation of a turbidity current (suspension flow) for drag forces on the surface. Described parameters are: h = thickness of the slide mass; g = gravitational acceleration; β = slope angle. From Locat and Lee (2002).

B: kinematic model of hydroplaning for a slide block (assumed to be trapezoidal from geophysical observations). Described parameters are: h = thickness of the shear layer; h_w = thickness of the entrained water layer; α = angle of the trapezoid; T = slide block thickness; $\emptyset$ = slope angle; B_w = length of entrained water layer; B = slide block length. From Bradshaw *et al*. (2009).

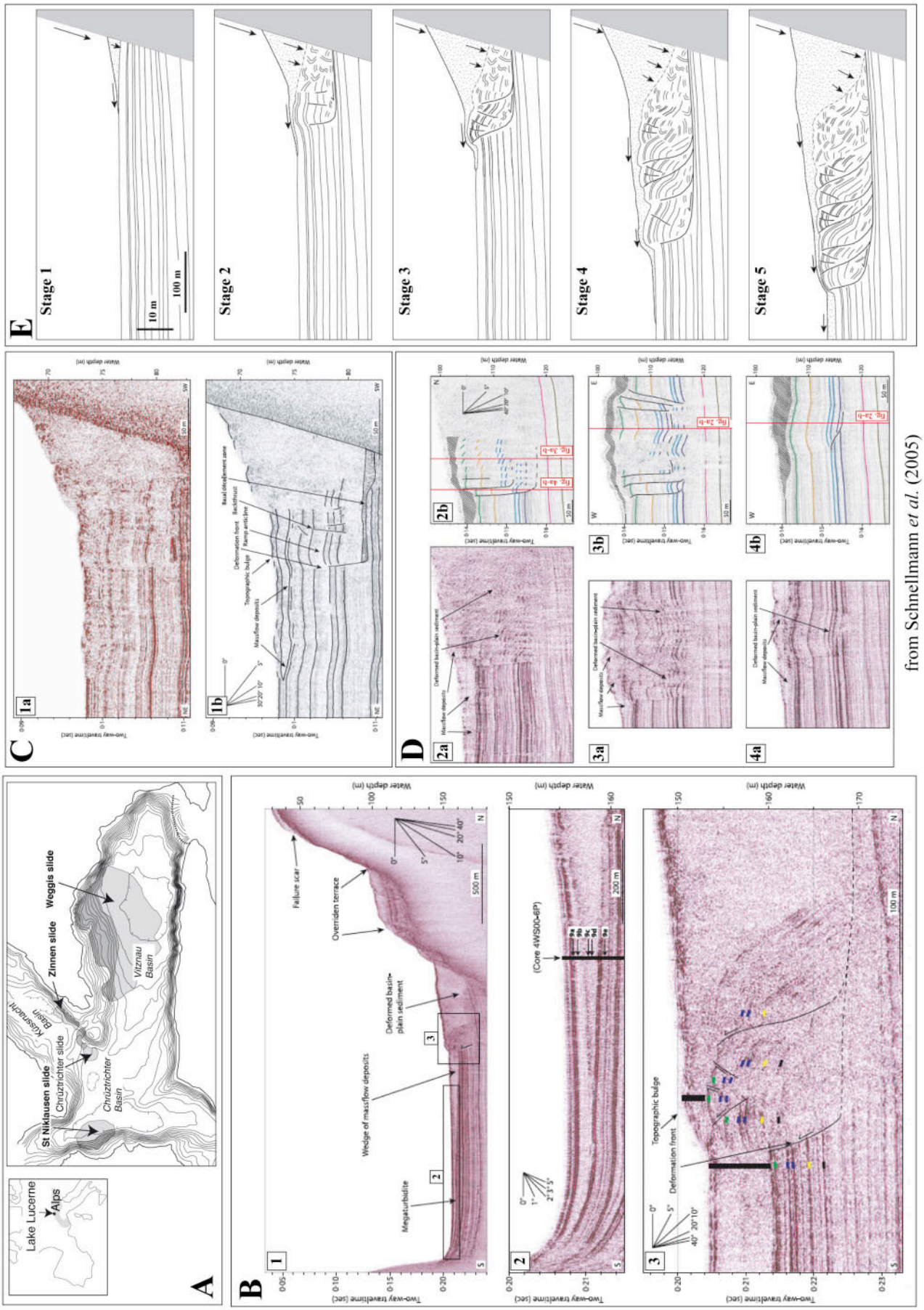

from Schnellmann *et al.* (2005)

Figure 8.11 - A: Location and bathymetry map of the Lake Lucerne (Switzerland) as derived from the seismic data. Contour interval is 10 and 5m for solid and dotted lines respectively. The bold dotted line indicates a major subaqueous sill. Slide complexes are named and marked with grey shadings, whereby dark and light grey indicate dominant erosional and depositional zones, respectively.

B: High-resolution 3.5 kHz seismic line illustrating the structure of the Weggis Slide. (1) Seismic profile showing the morphology of the entire basin (*i.e.* Vitznau Basin) and the acoustic signature of its sedimentary infill. (2) Enlargement of seismic line (1) showing distal massflow wedge and overlying contained megaturbidite. (3) Enlargement of line (1) showing the boundary between deformed and almost undeformed basin-plain sediment. Black lines denote faults, coloured bars mark specific seismic stratigraphic horizons. Note the major frontal thrust with a vertical offset of about 5 m and the overlying slight bulge in topography. The deposits overlying the green seismic stratigraphic horizon (indicated by a vertical black bar) are thicker in the footwall than in the hangingwall, indicating syndepositional thrust emplacement.

C: High-resolution 3.5 kHz seismic line (1a) and interpretation (1b) across the deposits of the Zinnen Slide. Note the slight bulge in the lake floor directly above the blind thrust. It indicates thrust emplacement during and/or just after massflow deposition.

D: Three 3.5 kHz seismic lines and interpretations of the depositional zone of the Chruztrichter Slide. Whereas the line displayed in (2a-b) is approximately parallel to the movement direction of the slide, the profiles shown in (3a-b) and (4a-b) represent slightly oblique cross-sections. Interpretations are given on separate panels on the right-hand side. Coloured lines mark seismic stratigraphic horizons, whereas black lines denote faults. Hatched surfaces are interpreted as massflow deposits. Vertical red lines indicate intersections between the individual seismic sections.

E: Schematic kinematic model proposed for the evolution of basin-plain deformation as deduced from the slides of the Lake Lucerne. Dotted surfaces represent massflow deposits. Loading of the marginal basin floor during a massflow event is regarded as the driving mechanism for the development of basinward propagating fold-and-thrust deformation. Note that, in the very slope-prone area, the boundary (dashed line) between massflow deposits and deformed basin-plain sediments can generally not be identified on seismic sections as a result of their similar chaotic-to-transparent seismic facies. All figures are from Schnellmann *et al.* (2005).

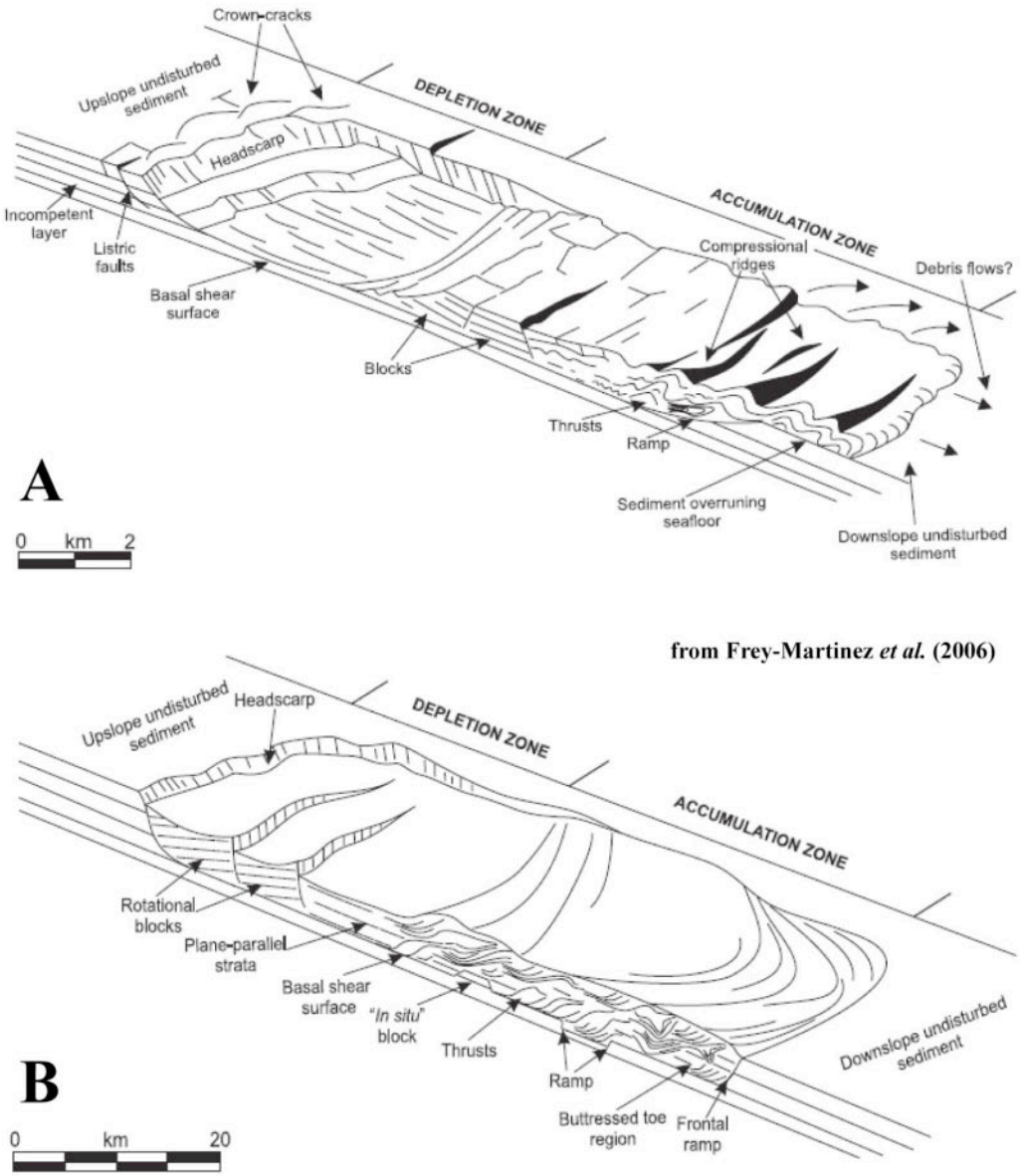

Figure 8.12 - **A**: Schematic depiction of a frontally-emergent slide (part of the Gaza Slump Complex). The slump body is divided into two main parts: the depletion zone and the accumulation zone. The depletion zone shows a spoon-shaped depression suggesting reduction of the sediment column. Note the presence of a clear headscarp and evidences of retrogressive failure in the upslope parts. The accumulation zone is characterised by compressional structures and gain of material. In the toe region, the slumped material over runs the previous seabed.

B: Schematic depiction of a frontally-confined slide (part of the Israel Slump Complex). The upslope parts of the slump mass correspond to the depletion zone. This is characterised by extensional deformational structures and thinning of the slump mass. Note the presence of listric faults forming a series of rotational blocks that are tilted downslope. The downslope part of the slump body corresponds to the accumulation zone. This is characterised by compressional structures and thickening of the slump mass. The slump mass is buttressed against thedownslope strata in the toe region. Note the presence of individual in situ blocks, which have been interpreted as indicators of a limited downslope displacement. All figures are from Frey-Martinez *et al*. (2006).

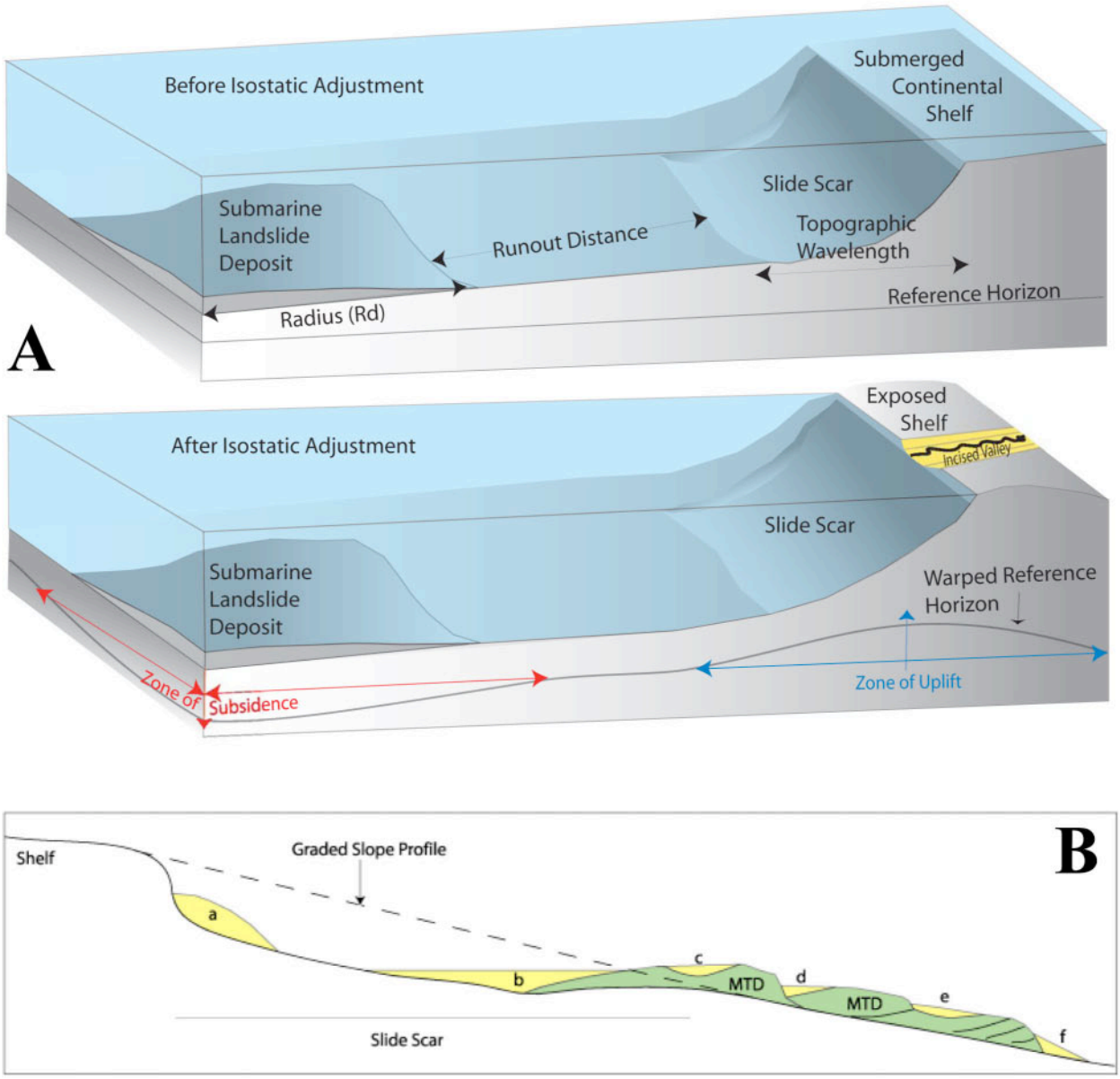

Figure 8.13 - A: Cartoon exhibiting some of the factors and potential effects of the isostatic rebound after large-scale mass-transport events. A zone of subsidence forms under and surrounding the mass-transport deposit, and a zone of uplift surrounds the slide-scar. If the uplift is great enough in amplitude it could potentially cause the shelf or shelf-edge to become emergent.

B: Schematic profile across a failed slope with depiction of the possible sedimentary accommodations (*i.e.* depocenters) directly or undirectly produced by the mass transport development. All figures are from Dykstra (2005b).

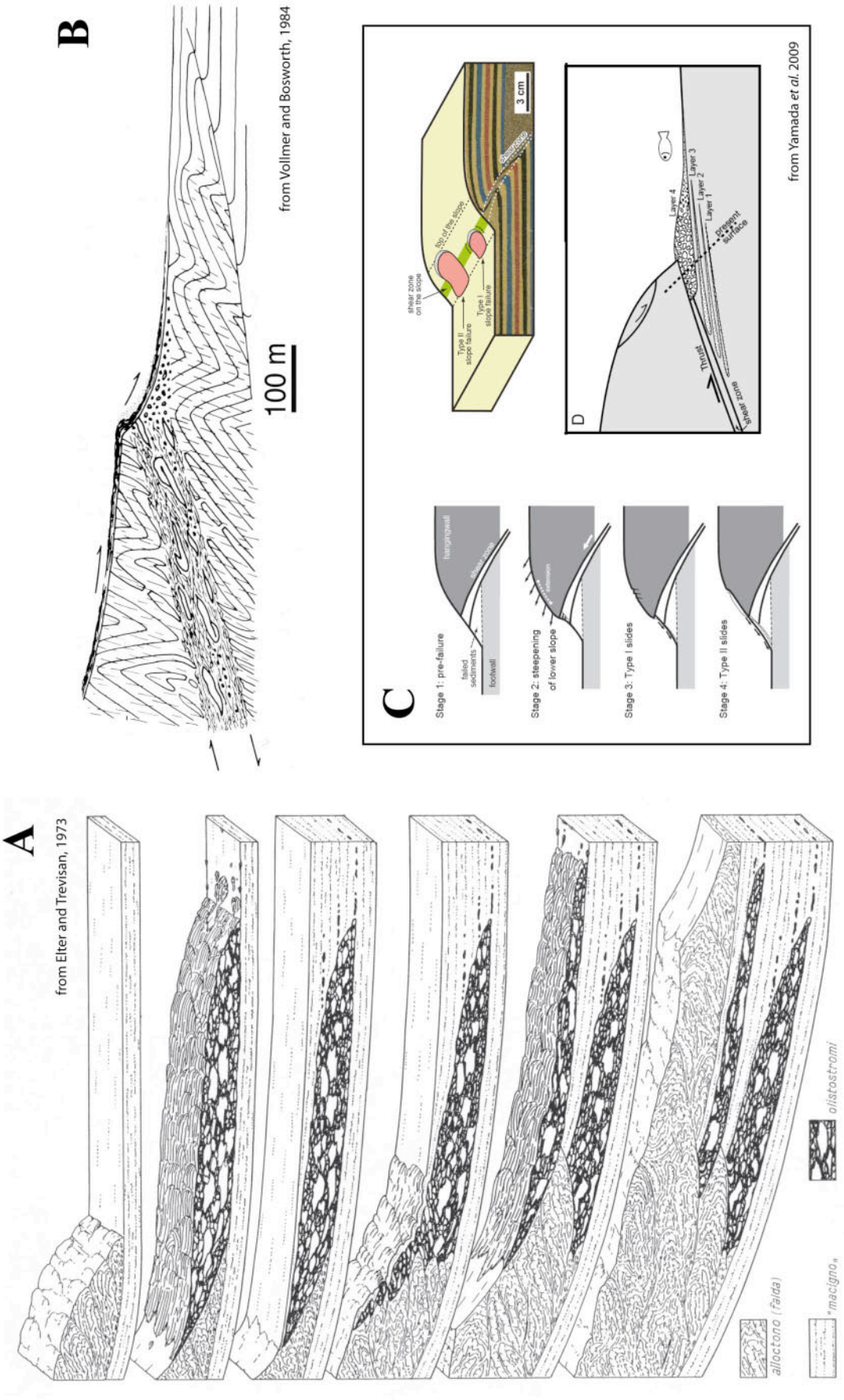
A
from Elter and Trevisan, 1973
allocotono (falda)
"macigno"
olistostromi
B
from Vollmer and Bosworth, 1984
100 m
C
from Yamada et al. 2009
Stage 1: pre-failure
hangingwall
shear zone
failed sediments
footwall
Stage 2: steepening of lower slope
Stage 3: Type I slides
Stage 4: Type II slides
3 cm
Type II slope failure
Type I slope failure
shear zone on the slope
top of the slope
D
Layer 4
Layer 3
Layer 2
Layer 1
present surface
Thrust
shear zone

Figure 8.14 - A: Conceptual model showing how, in a continent-continent collision zone, submarine mass flows may be deposited in front of the advancing thrust sheets with the subsequent incorporation into evolving, tectonically controlled *mélange* zones characterized by a stack of thrust sheets. Note that the so-called 'precursory' olistostromes are clearly interpreted by the authors as submarine slides detached from the frontal part of the thrust sheet along low-angle rupture surfaces. This model derived from field-based studies carried on the Northern Apennines. From Elter and Trevisan (1973).

B: Schematic drawing for the origin of a *mélange* complex in a foreland basin. Turbidity currents and MTDs (single arrows) deliver sediments to the foreland basin. Coarse material (pebbly and bouldery mudstones–stipple pattern) is deposited near active fault scarps, where it is progressively incorporated into an evolving *mélange* zone. Shearing across the *mélange* zones (paired arrows) results in progressive *boudinage* and eventual disruption of the bedded *flysch* sequence, producing the bulk of the *mélange* blocks and clasts. This model derived from field-based studies carried on the Taconic Orogen (North U.S.). From Vollmer and Bosworth (1984).

C: 3D synoptic models derived from the experimental results, showing two types of slope failure due to thrusting (right-hand side), and a four-stage synoptic model showing the process of slope formation and failure (left-hand side). The slope and failed deposist have been formed before a slide event (Stage 1). Then the thrust displacement along a convex-upwards geometry steepens the lower part of the slope and produces local extension in the hangingwall (Stage 2). The steepened part of the slope collapses to form small and frequent Type I failures (Stage 3). The slope instability produced by Type I failures triggers larger Type II failures (Stage 4). The minor extension faults generated during Stage 2 may become the fault scarps of failures. From Yamada *et al.* (2009).

<table>
<tr><td>Headwall domain</td><td></td><td>Headwall scarps
 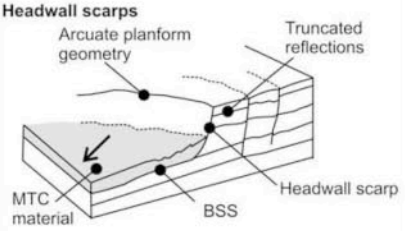

KI: Direction of initial movement roughly perpendicular to headwall propagation</td><td>Extensional ridges and blocks
 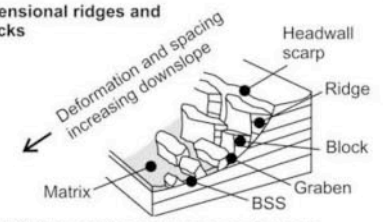

KI: Initial translation occurs perpendicular to headwall scarp. Blocks may re-align to be parallel to transport direction.</td></tr>
<tr><td rowspan="4">Translational domain</td><td>Lateral margins</td><td>Scarps
 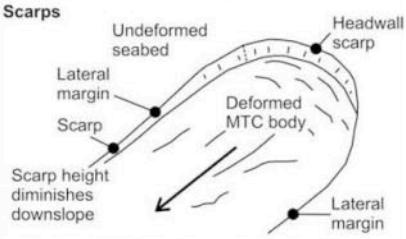

KI: Delimits strike-parallel extent of MTC and constrains gross general transport direction.</td><td>Strike slip deformation
 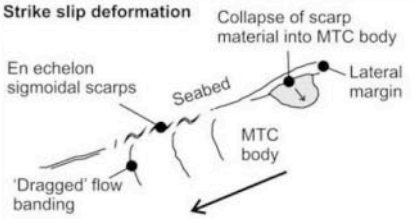

KI: Presence of sigmoidal scarps or strike-slip affected MTC material differentiates lateral margin from headwall scarp.</td></tr>
<tr><td>Basal shear surface</td><td>Ramps and flats
 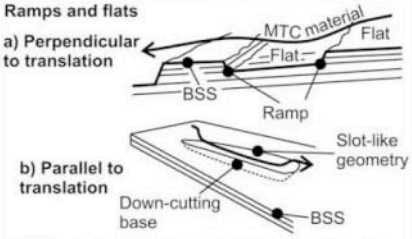

KI: Trend of ramps relative to translation direction must be confirmed by evaluation of other indicators</td><td>Grooves and striations
 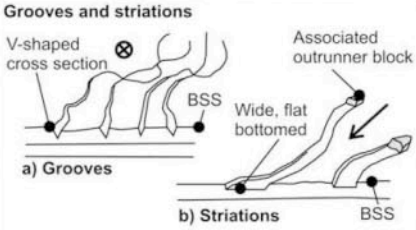

KI: Grooves imply debris flow processes. Translation direction is parallel to trend of grooves and striations</td></tr>
<tr><td>Internal MTC body</td><td>Translated and outrunner blocks
 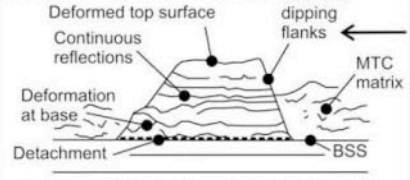

N.B.Outrunner blocks deposited downslope of toe
KI: General translation direction provided by path of blocks. Blocks often align long-axis downslope.</td><td>Slump folds
 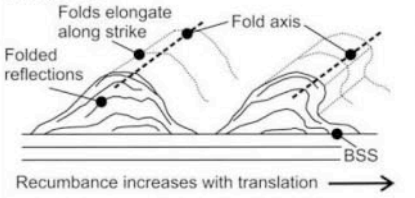

KI: Translation direction perpendicular to fold axis. Indicates plastic deformation. Fold attitude can assist in constraignt of translation.</td></tr>
<tr><td>Top slide surface</td><td>Longitudinal shears
 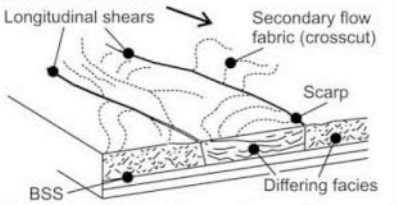

KI: Indicates different phases or types of movement within one MTC event. Translation direction of material within shears constrained by their trend</td><td>Secondary flow fabrics
 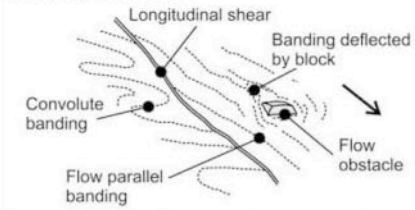

KI: Translation direction indicated by trend of flow parallel banding</td></tr>
<tr><td>Toe domain</td><td>Pressure ridges
 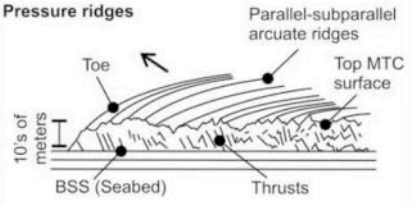

KI: Translation perpendicular to alignment of ridges.</td><td>Fold and thrust systems b) Pop-up blocks
 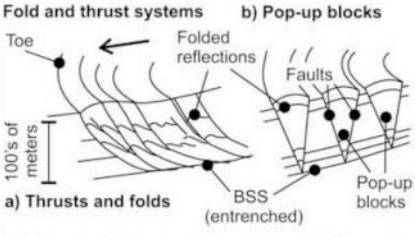

KI: Translation perpendicular to strike of thrust faults or faults defining pop-up blocks.</td></tr>
</table>

Figure 8.15 - Summary diagram showing key geometrical and geological criteria for the recognition of kinematic indicator types within a MTD. BSS – basal shear surface; KI – kinematic information. Bold arrow indicate direction of translation. From Bull *et al.* (2008).

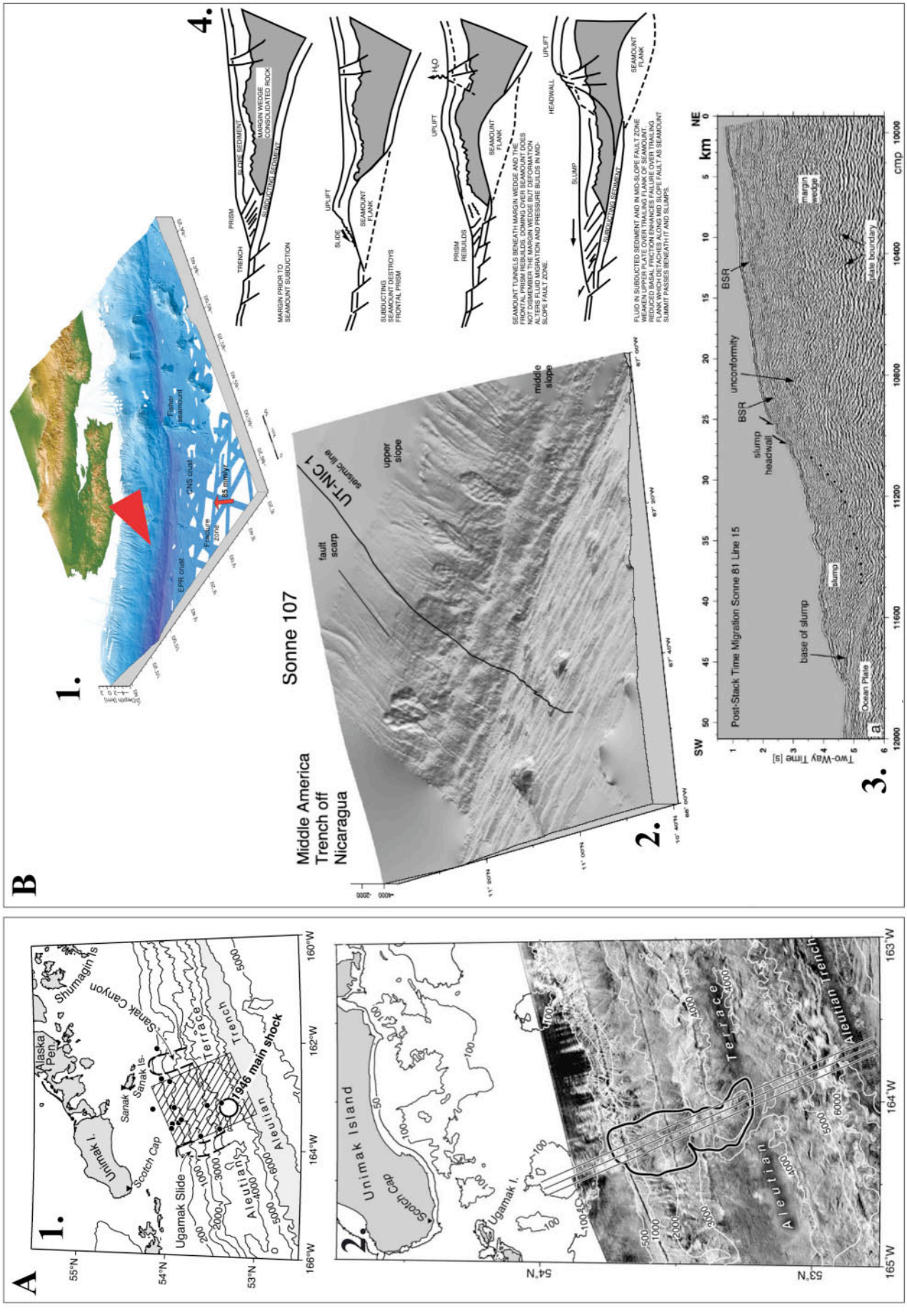
A
1.
Alaska Pen.
Shumagin Is
Sanak Canyon
Sanak
Sanak Is.
Unimak I.
Scotch Cap
Ugamak Slide
Terrace
Trench
Aleutian
1946 main shock
55°N
54°N
53°N
166°W
164°W
162°W
160°W
2.
Unimak Island
Scotch Cap
Ugamak I.
Terrace
Aleutian Trench
54°N
53°N
165°W
164°W
163°W
B
1.
Fraher seamount
EPR crust
Fracture zone
85 mm/yr
NS crust
Middle America Trench off Nicaragua
Sonne 107
UT-NIC 1
seismic line
fault scarp
upper slope
middle slope
2.
3.
Post-Stack Time Migration Sonne 81 Line 15
unconformity
BSR
slump headwall
base of slump
slump
Ocean Plate
margin wedge
plate boundary
Two-Way Time [s]
SW
NE
km
cmp
4.
TRENCH
PRISM
SLOPE SEDIMENT
MARGIN WEDGE
CONSOLIDATED ROCK
SUBDUCTED SEDIMENT
MARGIN PRIOR TO SEAMOUNT SUBDUCTION
SLIDE
UPLIFT
SEAMOUNT FLANK
SUBDUCTING SEAMOUNT DESTROYS FRONTAL PRISM
PRISM REBUILDS
SEAMOUNT TUNNELS BENEATH MARGIN WEDGE AND THE FRONTAL PRISM REBUILDS, DOMING OVER SEAMOUNT DOES NOT DISMEMBER THE MARGIN WEDGE BUT DEFORMATION ALTERS FLUID MIGRATION AND PRESSURE BUILDS IN MID-SLOPE FAULT ZONE.
HEADWALL
SLUMP
SUBDUCTING SEDIMENT
FLUID IN SUBDUCTED SEDIMENT AND IN MID-SLOPE FAULT ZONE WEAKEN SUBDUCTING PLATE INTERFACE. SEAMOUNT FLANK REDUCED BASAL FRICTION ENHANCES FAILURE OVER TRAILING FLANK WHICH DETACHES ALONG MID SLOPE FAULT AS SEAMOUNT SUMMIT PASSES BENEATH IT AND SLUMPS.

Figure 8.16 - A: (**1**) Bathymetry of the rupture area of the Unimak earthquake. The open circle is the epicenter of the main shock; closed circles are aftershocks. The shaded area is the preferred rupture plane. The patterns of bathymetric contours allow the recognition of the Sanak Canyon and Ugamak Slide. Tsunami runup was 42 m at Scotch Cap, 6 m at Sanak (Village). (**2**) Setting of the Ugamak Slide (outlined in black). Notice how the slide points upslope directly at Scotch Cap. From Fryer *et al.* (2004).

B: (**1)** Perspective view of the subduction zone offshore Middle America. The red triangle roughly indicates the position of (**2**). From Petersen *et al*. (2009). (**2**) Perspective view of the central Nicaragua margin showing a segment where multiple slide scars across the steep middle slope were swath-mapped. Because of a thin slope sediment cover in the seismic image, the diagonal grain across the mid-slope is inferred to show basement structure. Note low fault scarps at the mid- to upper-slope break. (**3**) Seismic line across the Nicoya Slump. This time section crosses the southeast extremity where the slump advanced ~ 3.5 km over the trench axis. Doted line is just below the slump detachment reflections. (**4**) Diagrammatic sections across the Nicoya Slump showing a sequence of slide development in response to a seamount subduction. From Von Huene *et al*. (2004).

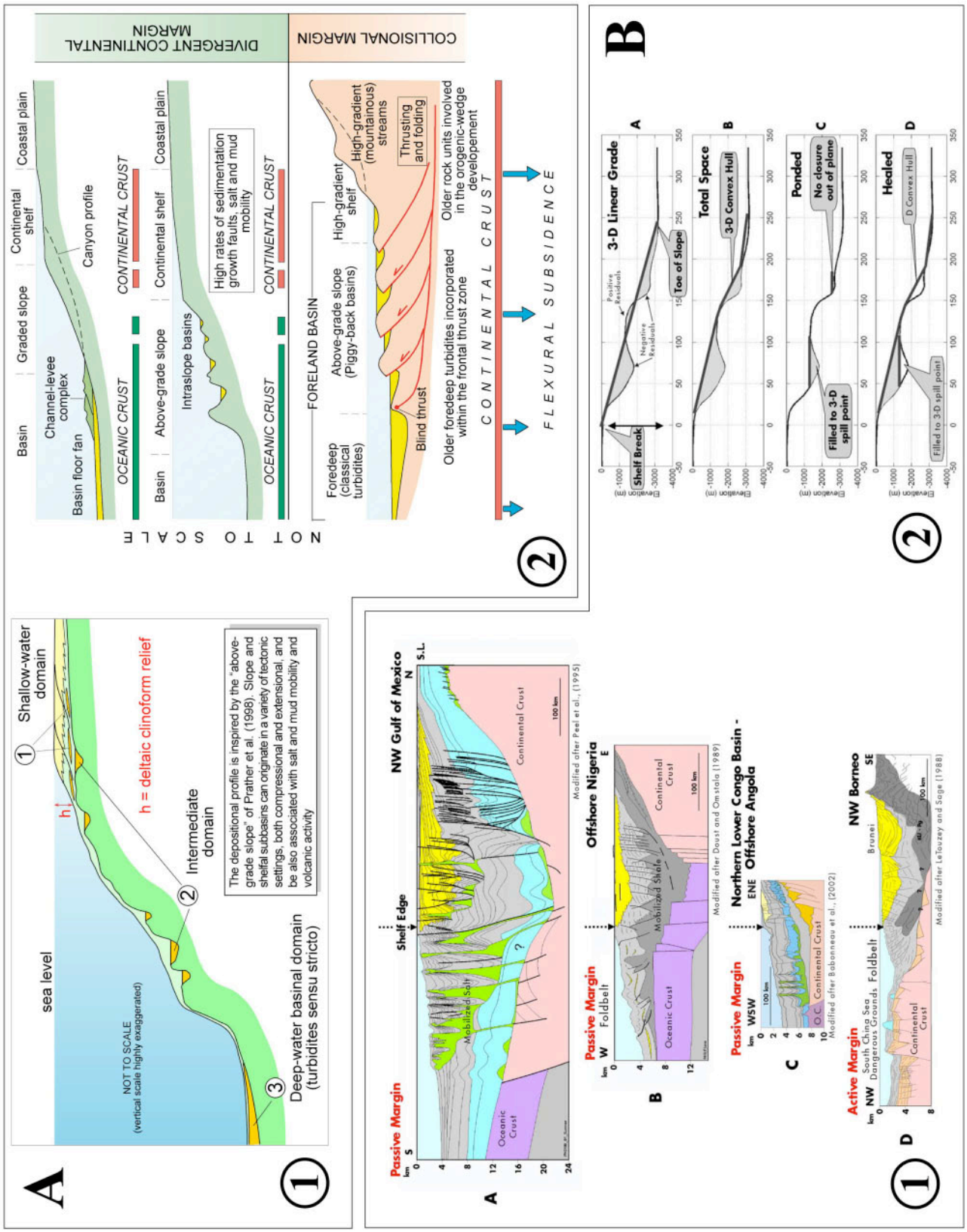
A
1 Shallow-water domain
sea level
h
h = deltaic clinoform relief
2 Intermediate domain
NOT TO SCALE
(vertical scale highly exaggerated)
3 Deep-water basinal domain
(turbidites sensu stricto)
The depositional profile is inspired by the "above-grade slope" of Prather et al. (1998). Slope and shelfal subbasins can originate in a variety of tectonic settings, both compressional and extensional, and be also associated with salt and mud mobility and volcanic activity
1
NOT TO SCALE
DIVERGENT CONTINENTAL MARGIN
COLLISIONAL MARGIN
Basin
Graded slope
Continental shelf
Coastal plain
Channel-levee complex
Canyon profile
Basin floor fan
OCEANIC CRUST
CONTINENTAL CRUST
Basin
Above-grade slope
Continental shelf
Coastal plain
Intraslope basins
High rates of sedimentation growth faults, salt and mud mobility
OCEANIC CRUST
CONTINENTAL CRUST
FORELAND BASIN
Foredeep (classical turbidites)
Above-grade slope (Piggy-back basins)
High-gradient shelf
High-gradient (mountainous) streams
Thrusting and folding
Blind thrust
Older foredeep turbidites incorporated within the frontal thrust zone
Older rock units involved in the orogenic-wedge developement
CONTINENTAL CRUST
FLEXURAL SUBSIDENCE
2
B
3-D Linear Grade
Positive Residuals
Negative Residuals
Shelf Break
Toe of Slope
Total Space
3-D Convex Hull
Ponded
No closure out of plane
Filled to 3-D spill point
Healed
D Convex Hull
Filled to 3-D spill point
Elevation (m)
2
Passive Margin
NW Gulf of Mexico
Shelf Edge
Mobilized Salt
Oceanic Crust
Continental Crust
Modified after Peel et al., (1995)
A
Passive Margin
Offshore Nigeria
Foldbelt
Mobilized Shale
Oceanic Crust
Continental Crust
Modified after Doust and Omatola (1989)
B
Passive Margin
Northern Lower Congo Basin - Offshore Angola
Foldbelt
O.C.
Continental Crust
Modified after Babonneau et al., (2002)
C
Active Margin
NW Borneo
South China Sea
Dangerous Grounds
Foldbelt
Brunei
Continental Crust
Modified after LeTouzey and Sage (1988)
D
1

Figure 8.17 - A: (**1**) Diagram showing the three main depositional domains of the marine environment where graded sandstone beds can produce substantial accumulations of turbidites and turbidite-like deposits. (**2**) Synoptic diagram showing the development and main characteristics of graded and above-grade slope profiles in a divergent margin settings, in respect to the above-grade slope profile achieved by a convergent/collisional margin. From Mutti *et al*. (2007).

B: (**1**) Regional cross-sections of the Northwest Gulf of Mexico, Nigeria, Angola, and Northwest Borneo continental margins are displayed at the same scale for direct comparison. Gulf of Mexico and offshore Angola are salt-based systems while offshore Nigeria and Northwest Borneo are shale-based systems. Gulf of Mexico, Angola, and Nigeria are passive margin settings, dominated by gravitationally driven linked extensional–contractional tectonics systems detaching on mobile substrates (thin-skinned). In contrast, Northwest Borneo is an active margin setting underlain by the Crocker thrust belt and mobilized shale; much of the compressional deformation is basement related (thick-skinned) and is pervasive throughout the margin(slope, shelf, and hinterland). (**2**) Accommodation definitions. (A) linear grade trend surface is computed by fitting a slowly varying surface to the shelf break and toe-of-slope surfaces. In an arbitrary dip profile down the slope, this surface is approximately linear. Where the local bathymetry is shallower than this linear grade, the residual is termed positive; where the bathymetry is deeper than this linear grade, the residual is termed negative. (B) Total accommodation is determined by first locating the points of maximum positive curvature (the‘ hills’) on the slope and then by creating a convex hull passing through those points. Because this surface essentially ‘drapes’ across the local bathymetry maxima, the total accommodation space will generally be greater than the linear grade accommodation. (C) Ponded accommodation is an area of negative curvature with closure (the ‘bowls’ or ‘sinks’ related to intra-slope basins). This closure is filled to the lowest spill point. (D) Healed slope accommodation is simply the difference between the total and ponded accommodation. Note that by construction, the total accommodation will always be greater than or equal to the healed slope accommodation. From Steffens *et al*. (2003).

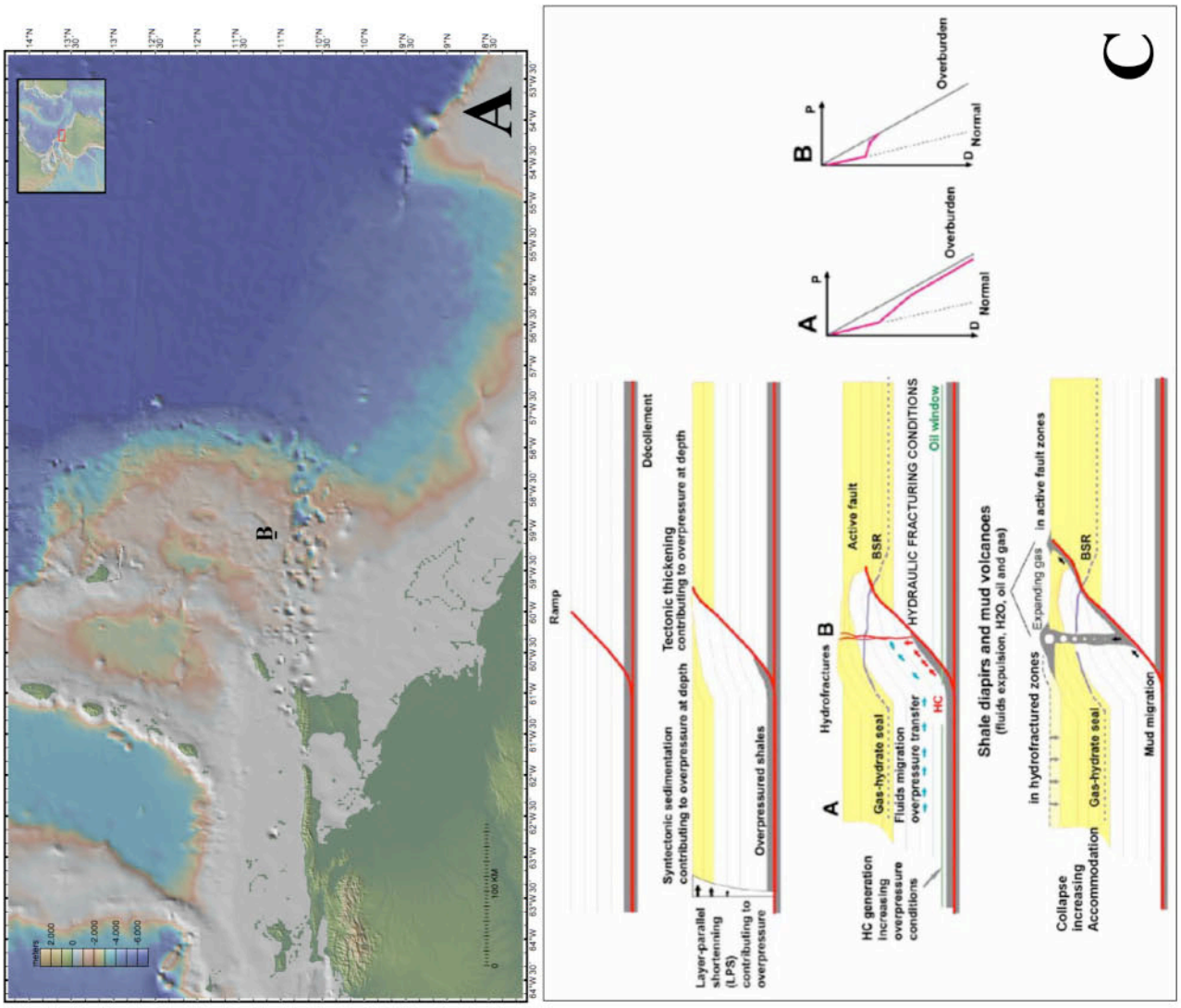
A
B
Depth-migrated
3.5 kHz
Piggy-back basin
Mud volcano
Fold
caram#3
10 km
Seismic line #39
'blister'
BSR
W
E
D
Mud volcano expelling shallow fluids
Uplift
Collapse
Mud volcano expelling deep fluids
Deep fluid migration
Mobile shale
Caldera
Intrusion
Mud chamber
Deep conduit
Hydraulic fracturing
C
Ramp
Décollement
Syntectonic sedimentation contributing to overpressure at depth
Tectonic thickening contributing to overpressure at depth
Layer-parallel shortening (LPS) contributing to overpressure
Overpressured shales
Hydrofractures
Active fault
Gas-hydrate seal
Fluids migration
overpressure transfer
HC
HYDRAULIC FRACTURING CONDITIONS
Oil window
HC generation increasing overpressure conditions
Overburden
Normal
Shale diapirs and mud volcanoes
(fluids expulsion, H2O, oil and gas)
Expanding gas
in active fault zones
in hydrofractured zones
Collapse increasing Accommodation
Mud migration

Figure 8.18 - A: Morpho-bathymetric map slice of the Barbados-Trinidad accretionary complex (SE Caribbean) at the junction between the South American and Caribbean plates. Note the strong development of mud diapirism-related mini-basin systems roughly located along the northern Venezuela transform system. Elaborated with GeoMapApp (2009).

B: Seismic profile across mini-basins bounded by massive sedimentary extrusion (*i.e.* mud diapiric ridges). Location in A. From Deville *et al.* (2006).

C: Cartoon showing evolutionary steps of the possible pressure distribution leading to the occurrence of mud diapirs/volcanoes in a tectonic-related compressive regime. From Deville *et al.* (2003).

D: (**1**) Interpretative scheme for the massive sedimentary uplifts as shale mobilization at depth (solid hypothesis); (**2**) Interpretation of the massive sedimentary uplifts as related to mud intrusion at depth (liquid hypothesis). From Deville *et al.* (2006).

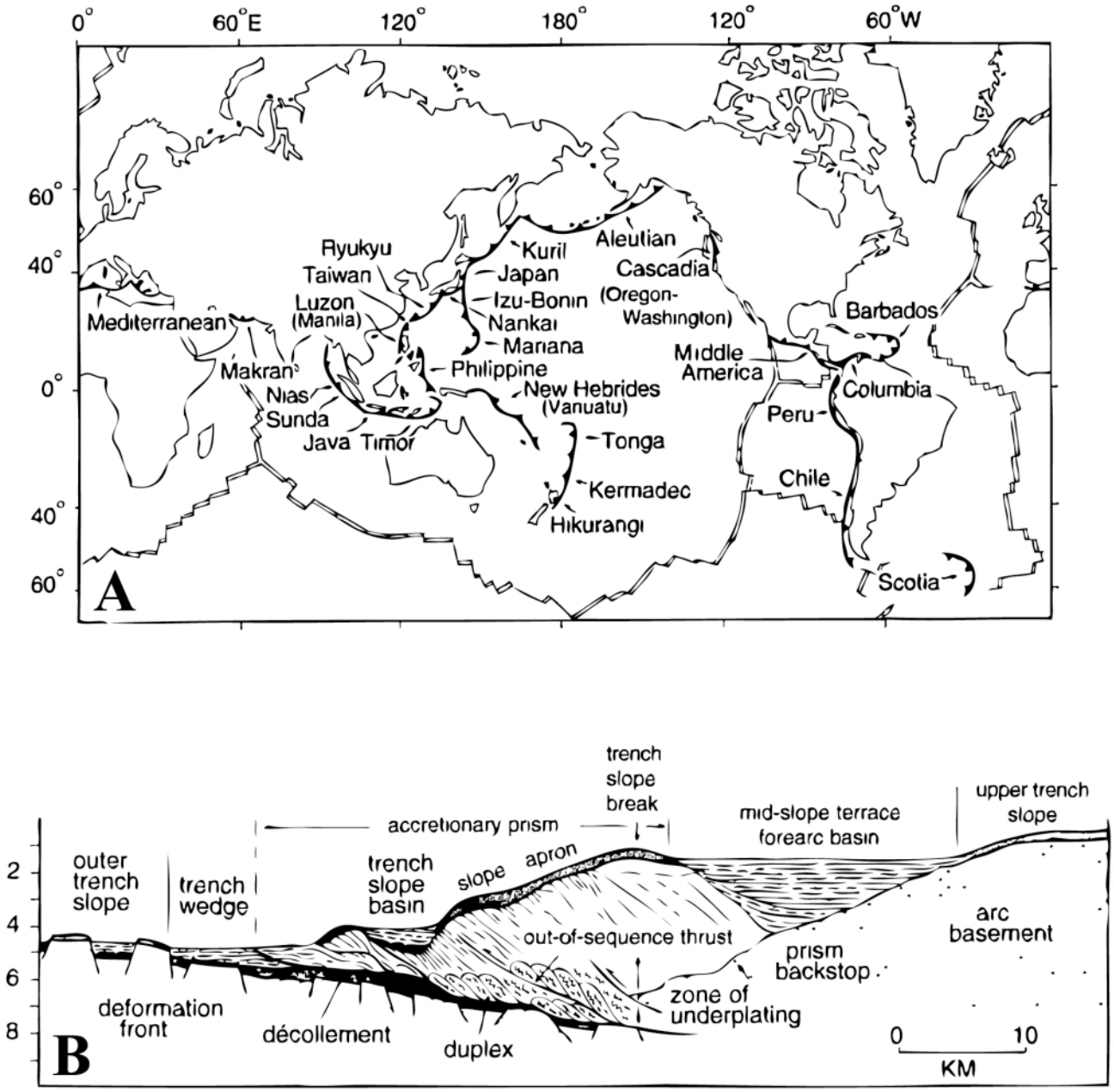

Figure 8.19 - A: Global distribution of active oceanic subduction zones.

B: Schematic illustration of major bathymetric domains, regional-scale features, and sites of deposition within subduction zones. From Underwood and Moore (1995).

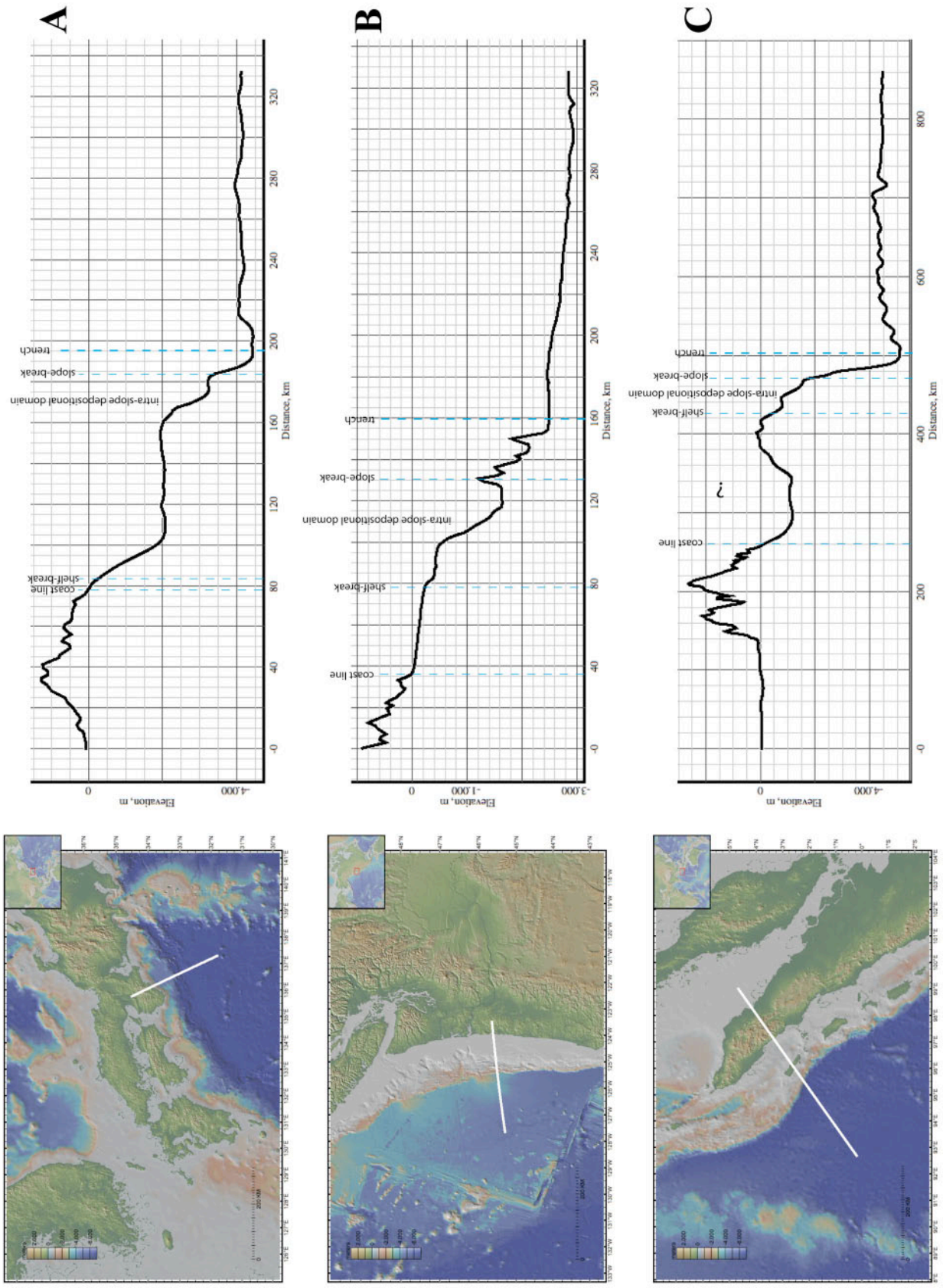

Figure 8.20 - Morpho-bathymetric maps and topographic profiles of the selected active oceanic subduction zones, with location of the superficial structural features and major bathymetric domains. Elaborated with GeoMapApp (2009). **A**: Nankai subduction zone (SW Japan). **B**: Cascadia subduction zone (NW North America). **C**: Sunda subduction zone (SW Indonesia).

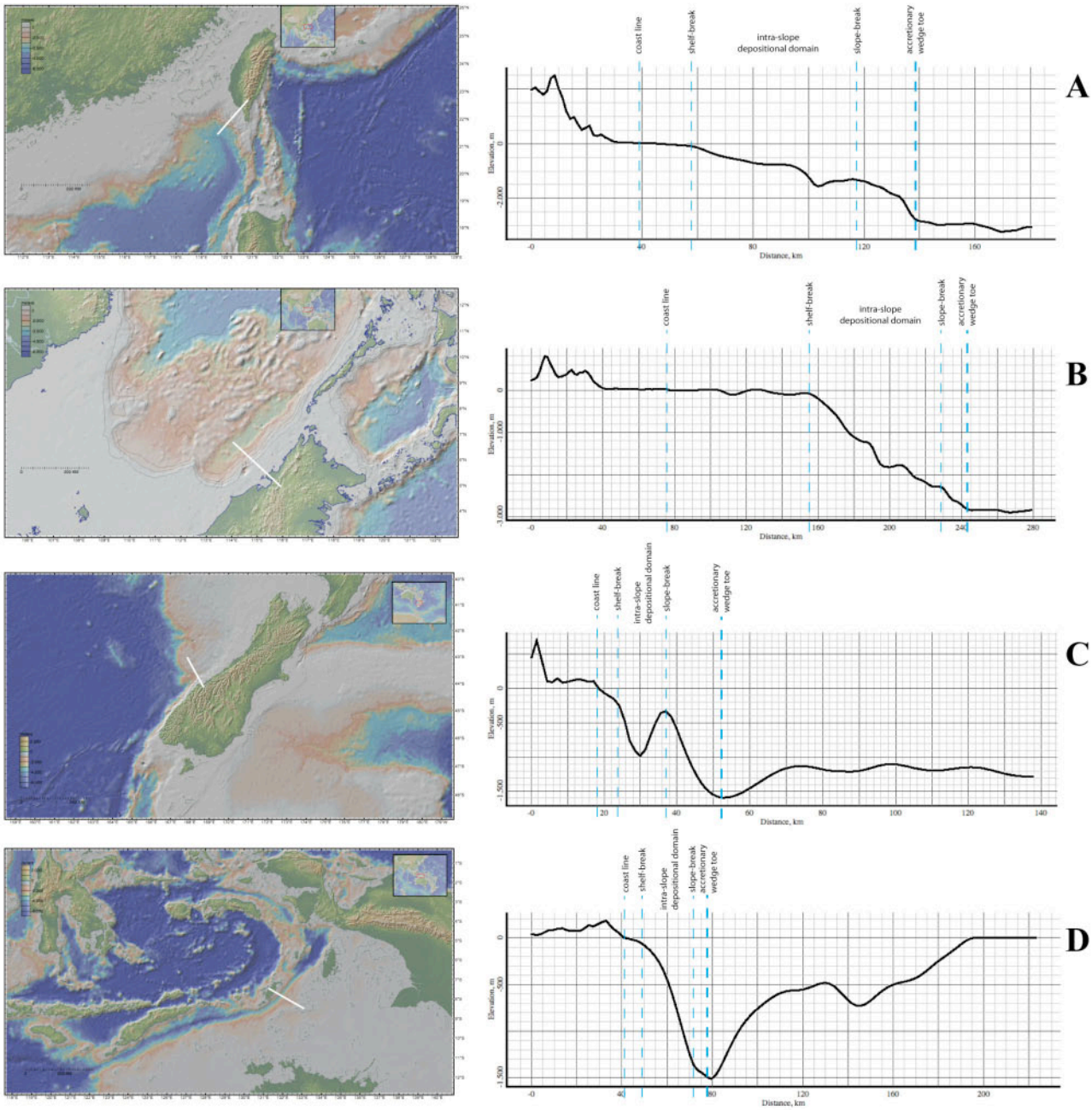
coast line
shelf-break
intra-slope depositional domain
slope-break
accretionary wedge toe
Elevation, m
Distance, km
A
B
C
D

Figure 8.21 - Morpho-bathymetric maps and topographic profiles of the selected active continental subduction zones, with location of the superficial structural features and major bathymetric domains. Elaborated with GeoMapApp (2009). **A**: SW Taiwan (*i.e.* Hengchun Ridge/Manila accretionary wedge). **B**: NW Borneo (Brunei continental slope/Crocker thrust belt). **C**: SW New Zealand (Fjordland/Westland area). **D**: SE Indonesia (Banda Arc).

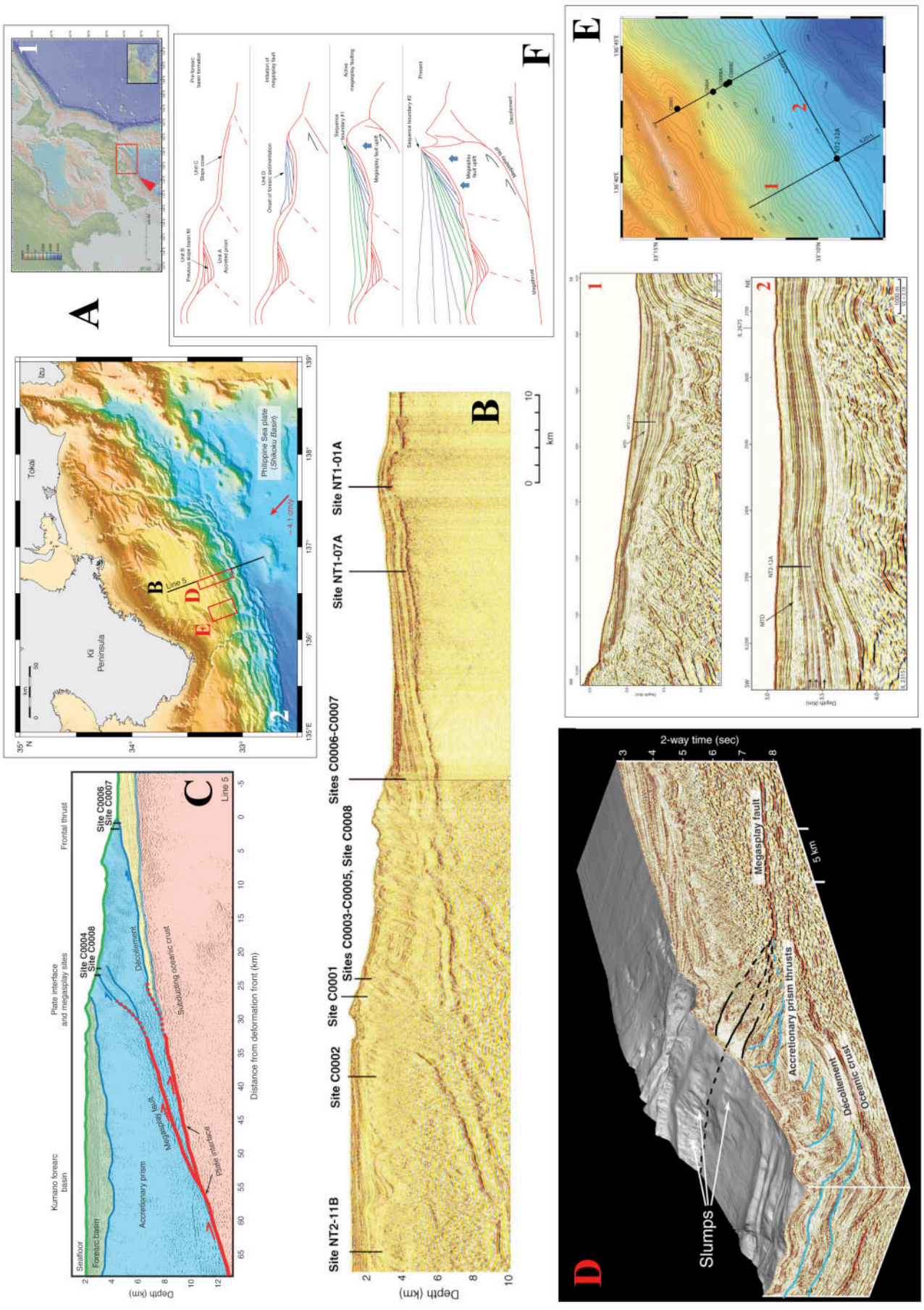
A
B
C
D
E
F
Site NT2-11B
Site C0002
Site C0001
Sites C0003-C0005, Site C0008
Sites C0006-C0007
Site NT1-07A
Site NT1-01A
Depth (km)
Site C0006
Site C0007
Site C0004
Site C0008
Frontal thrust
Plate interface and megasplay sites
Kumano forearc basin
Seafloor
Forearc basin
Accretionary prism
Megasplay fault
Plate interface
Décollement
Subducting oceanic crust
Distance from deformation front (km)
2-way time (sec)
Megasplay fault
5 km
Accretionary prism thrusts
Oceanic crust
Décollement
Slumps
Philippine Sea plate (Shikoku Basin)
Tokai
Izu
Kii Peninsula
Line 5

Figure 8.22 - A: (**1**) Morpho-bathymetric map of Japan with location of the Nankai subduction zone. Elaborated with GeoMapApp (2009). (**2**) Bathymetric map of part of the Nankai subduction zone (*i.e.* Kumano Basin region) with location of B, D and E. Slightly modified from Kinoshita *et al*. (2007).

B: Sismic line (n. KR0108-5; prestack, depth migration) across the frontal part of the Nankai accretionary complex in the Kumano Basin region. From Saito *et al.* (2009), after Park *et al.* (2002).

C: Interpretation of seismic line shown in B, displaying main structural features, bathymetric domains and depositional sites. From Kinoshita *et al*. (2007), after Park *et al.* (2002).

D: 3D seismic data volume depicting the location of the megasplay fault (black lines) and its relationships with older in-sequence thrusts of the frontal accretionary prism (blue lines). Steep sea-floor topography and numerous slumps above the splay fault are shown. From Moore *et al*. (2007).

E: Bathymetric map of outer part of the Kumano forearc basin, with location of seismic lines shown in 1 and 2. (**1**) Down-slope seismic profile with identification of a small-scale MTD, located in front of (and probalbly originated from) a buried intrabasinal high. (**2)** Along-slope seismic profile showing the same small-scale MTD of (1). Note the sudden lateral wedging-out of the slide body. From Nantro SLIDE / IODP proposal #738-APL.

F: Conceptual model of forearc basin development at the seaward edge (*i.e.* trench-slope break) of the Kumano Basin based on the seismic reflection data. Basin formation and development is significantly governed by megasplay fault activity. Dashed line = inactive thrust fault, dotted lines = sequence boundaries, black arrows = direction of coseismic slip, blue arrows = uplift associated with the fault slip. From Kimura *et al*. (2007).

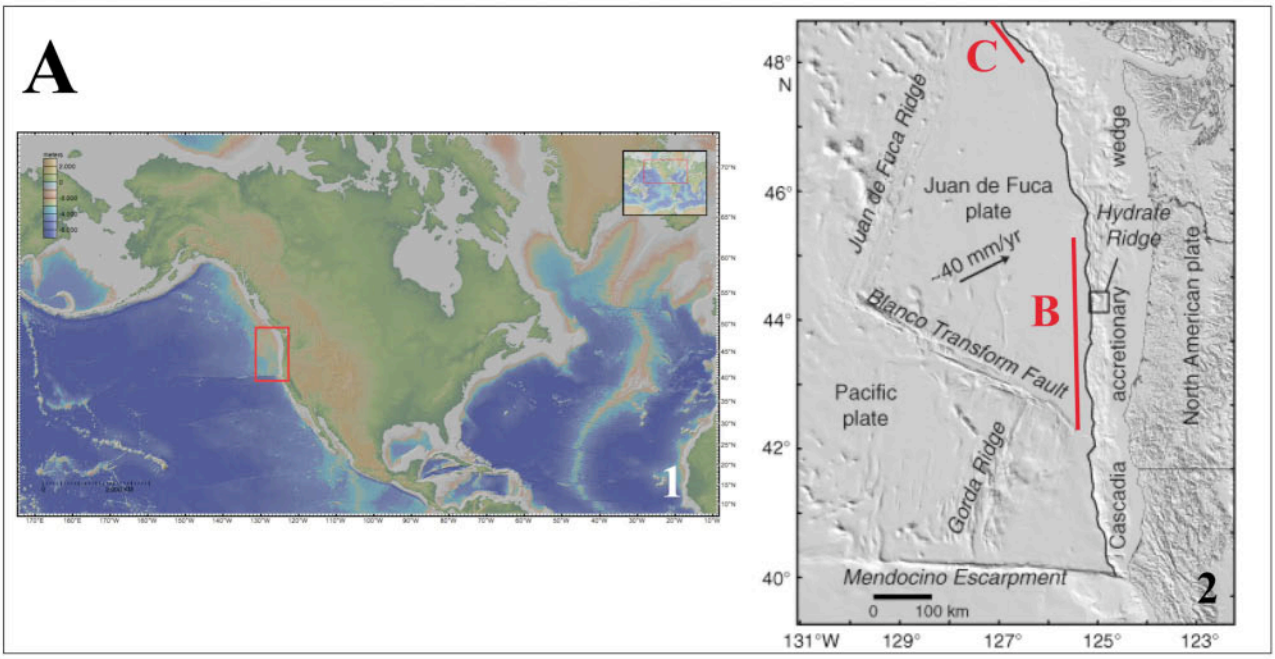
A
1
2
C
B
Juan de Fuca Ridge
Juan de Fuca plate
40 mm/yr
Hydrate Ridge
wedge
accretionary
North American plate
Blanco Transform Fault
Pacific plate
Gorda Ridge
Cascadia
Mendocino Escarpment
0 100 km
48° N
46°
44°
42°
40°
131°W
129°
127°
125°
123°

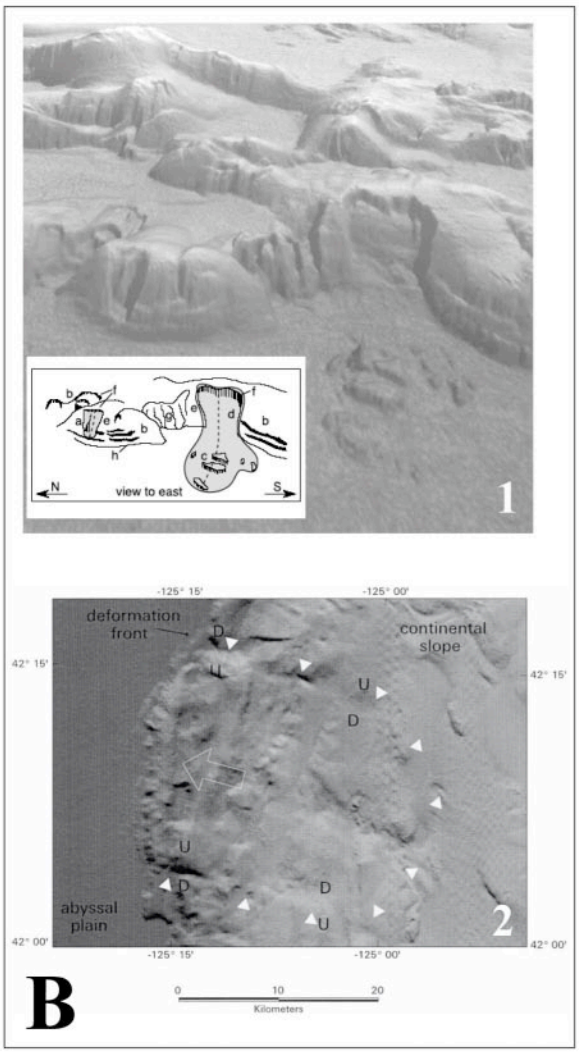
1
view to east
N
S
2
deformation front
continental slope
abyssal plain
D
U
-125° 15'
-125° 00'
42° 15'
42° 00'
0 10 20
Kilometers
B

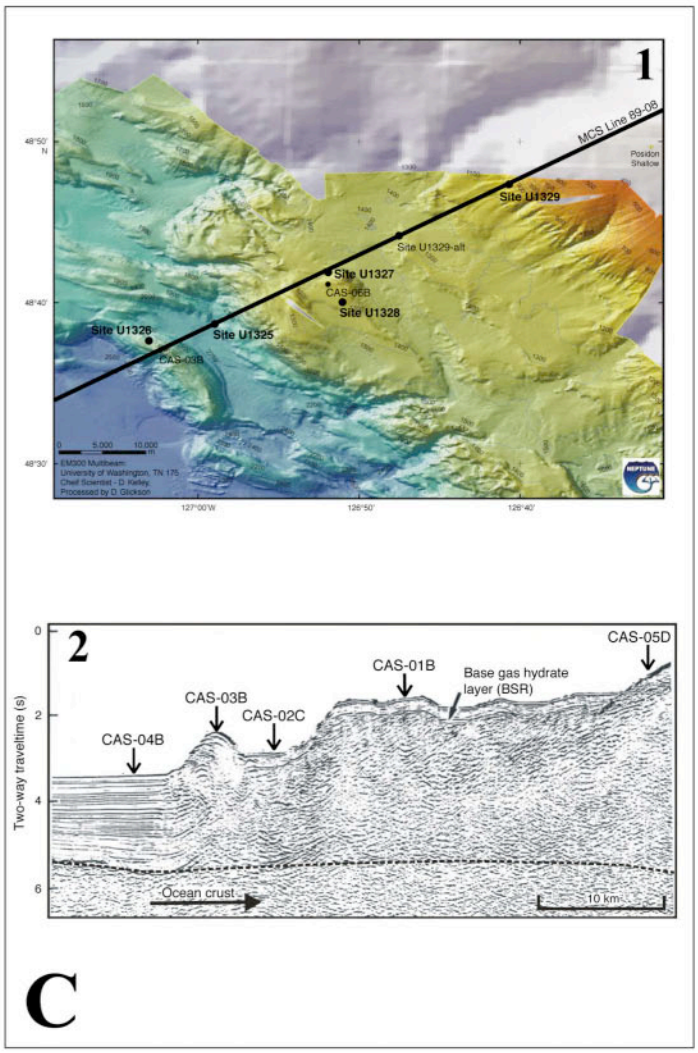
1
MCS Line 89-08
Site U1329
Site U1329-alt
Site U1327
CAS-06B
Site U1328
Site U1326
Site U1325
CAS-03B
48°50' N
48°40'
48°30'
127°00'W
126°50'
126°40'
2
CAS-05D
CAS-01B
Base gas hydrate layer (BSR)
CAS-03B
CAS-02C
CAS-04B
Two-way traveltime (s)
0
2
4
6
Ocean crust
10 km
C

Figure 8.23 - A: (**1**) Morpho-bathymetric map of the North America with location of the Cascadia subduction zone shown in 2. Elaborated with GeoMapApp (2009). (**2)** Shaded relief map (bathymetry and topography) of the Cascadia margin showing the Hydrate Ridge tectonic setting in the Cascadia accretionary wedge. Approximate location of B and C are labeled in red. From Haugerud (1999); available at: http://www-odp.tamu.edu/publications/204_SR/125/125_f1.htm.

B: (**1**) Three-dimensional perspective image of the base of the Oregon continental slope (southern Cascadia accretionary prism), approximately 3x vertical exaggeration. View is looking east; north is to the left. Scale varies with distance in the perspective, however the field of view at the slope base is approximately 30 km. Inset is a line drawing of figure, with labels (a to h) referred to below. Disintegrative landslides (a and b) have characteristic scar morphology, but lack bathymetric evidence of failed material at the base of the failure. The slope failure deposits for cohesive landslides (c) are associated with a particular scar directly up gradient (d). The gray shaded regions represent the measured landslide area, and the dashed lines the run-out distance. The angle of the non-failed slope adjacent to the failure scar (e) is used as a proxy for the pre-failure slope. Landslide headscarps (f) are the steep upslope regions at the top of the scar. 'Eroded slope' (g) refers to regions of the seafoor where material has been removed, however no evidence of discrete landslide events (*i.e.* a distinct headscarp) is present. A series of curious terraces (h) rim the very base of the slope, and often coincide with the lowermost terminus of the landslides, resulting in a 'hanging slide' (a) that does not reach to the bottom of the slope. Notice the seafloor with little visible evidence of erosion between landslide scars on the westernmost ridge (closest) and on the other background ridges. From McAdoo and Watts (2004). (**2**) Shaded-relief bathymetry of the southernmost Oregon continental slope, showing a possible incipient slump measuring about 20 × 20 km. The toe of the slide has moved 3.5 km seaward of the deformation front along WNW-trending tear faults (indicated by arrows). The detached block appears to have rotated seaward along a listric basal detachment, so that the eastern part is down and the western part is up relative to the adjacent continental slope, shown by U/D symbols. From Goldfinger *et al.* (2000).

C: (**1**) Multibeam bathymetry map along the transect across the northern Cascadia accretionary prism, offshore Vancouver Island. MCS = multichannel seismic. From Expedition 311 Scientists (2005). (**2**) Seismic section (line 89-08 shown in 1) showing proposed Expedition 311 sites. Few small-scale MTDs have been observed in this area, commonly located closed to the deformational front. BSR = bottom-simulating reflector. Form Collett *et al*. (2005).

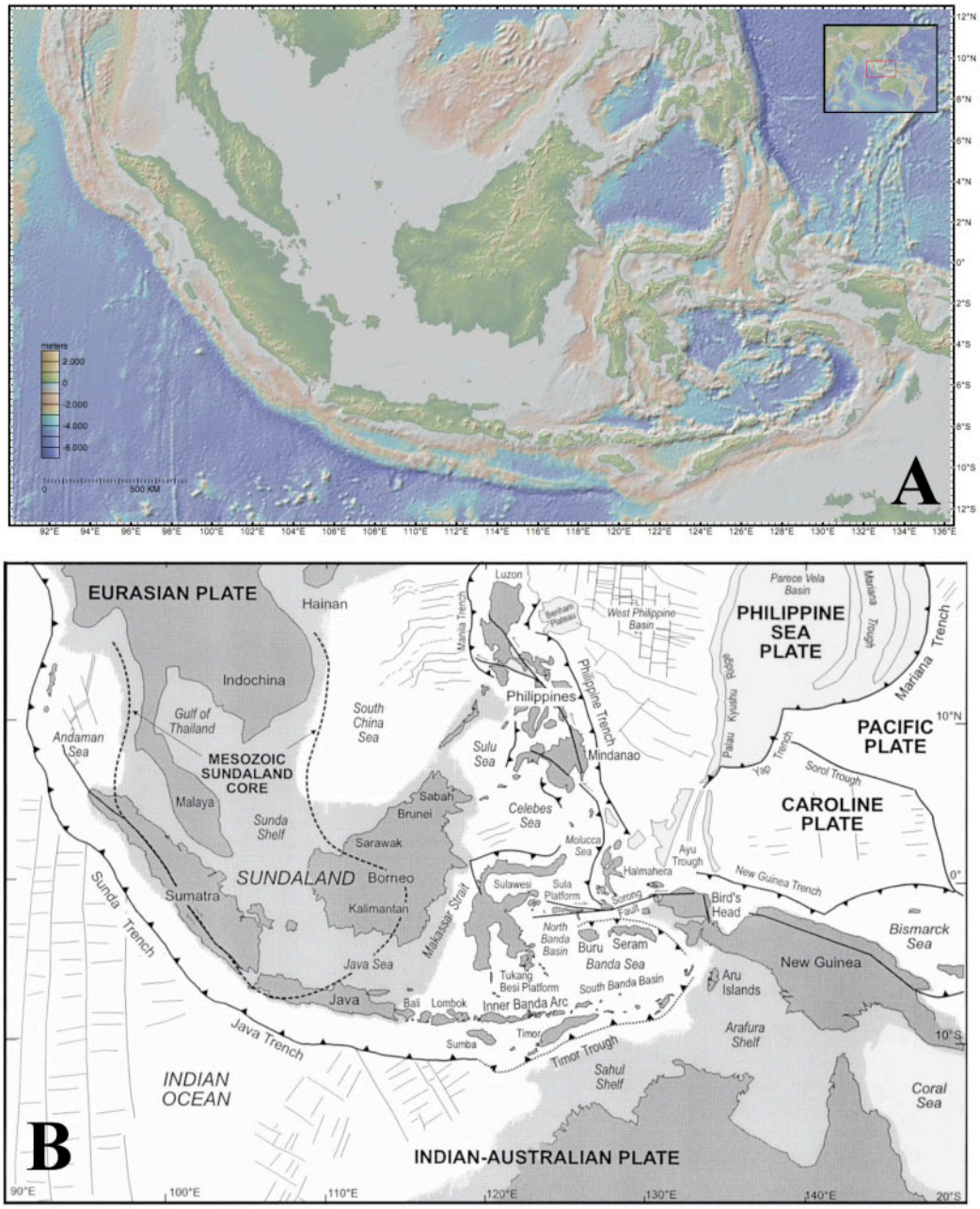

Figure 8.24 - A: Morpho-bathymetric map of Indonesia (SE Asia). Elaborated with GeoMapApp.

B: Principal geographical features of Indonesia (SE Asia). The light shaded areas are the continental shelves of Eurasia and Australia drawn at the 200 m isobath. From Hall and Wilson (2000).

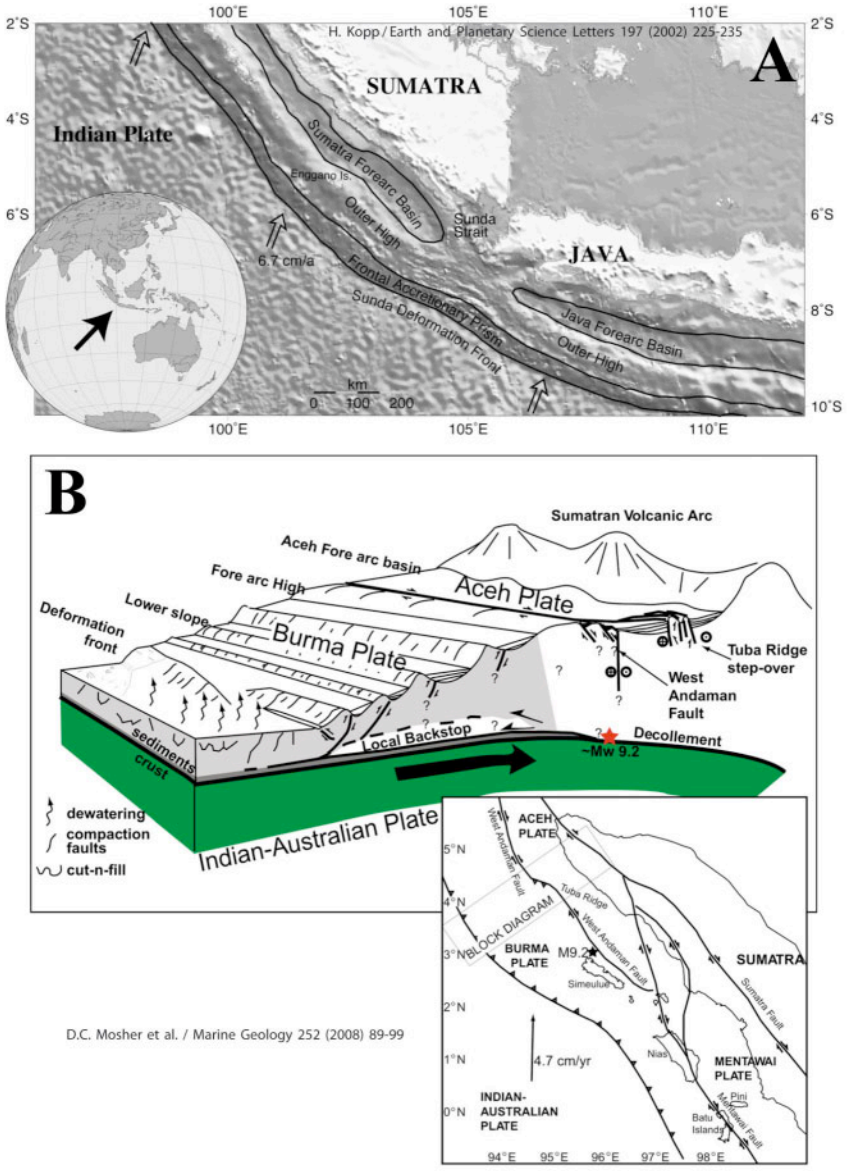

Figure 8.25 - **A**: Bathymetric map of the central Sunda Arc of Indonesia indicating the main structural elements of the margin. The Indian Plate is thrust underneath Eurasia along the Sunda deformation front where active subduction accretion forms a frontal prism. The Outer High (*i.e.* trench-slope break) is composed of old consolidated accreted material and subaerially emerges as a chain of is lands offshore Sumatra. The adjacent forearc domain consists of large basins of Sumatra and of Java, both carrying more than 4 km of sediment infill. Water depth increases to the east. South of the Sunda Strait, a distinct basin is missing and the deformation front, as well as the Outer High, show a concave curvature, resulting from the transtensional regime of the Sunda Strait. Similar amounts of sediment as in the adjoining basins have also accumulated here. From Kopp (2002).

B: Summary schematic interpretation of the tectonic framework of this part of the Sumatra convergent margin, as discerned from previous work and the SEATOS single-channel seismic profiles. Oblique convergence leads to strain partitioning predominantly in the form of landward-vergent deformation within the upper part of the accretionary prism from 3°– 4.5°N, with right-lateral strike-slip faulting localized along the West Andaman and Mentawai fault zones which together form the seaward flank of the forearc basins. Inset: Note the location of the hypocenter of the 2004 great earthquake; rupture propagation and subsequent references, stayed seaward of the seaward boundary of the Aceh Plate, entirely within the Burma Plate. From Mosher *et al.* (2008).

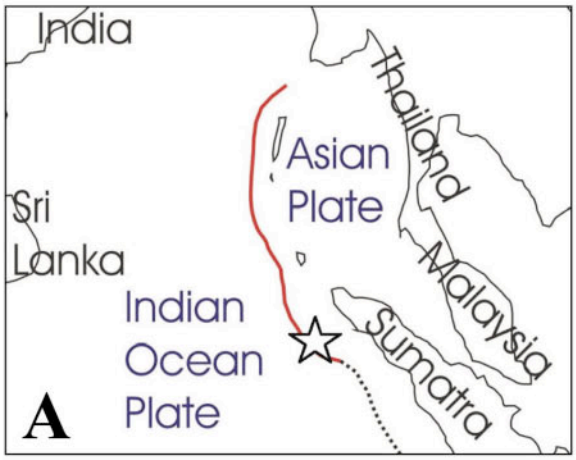
India
Thailand
Asian
Plate
Sri
Lanka
Malaysia
Indian
Ocean
Plate
Sumatra
A

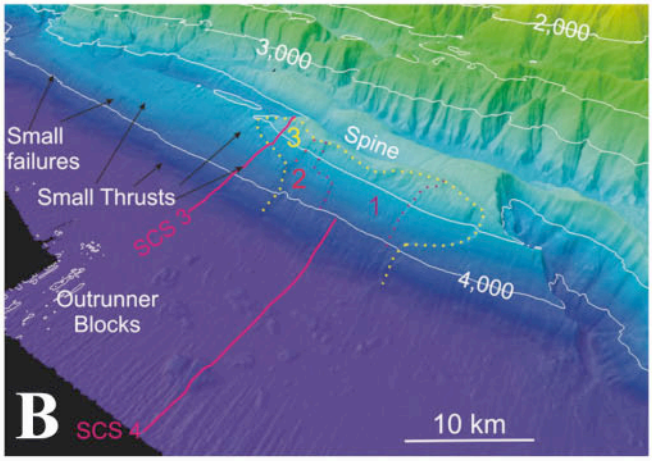
2,000
3,000
Small
failures
Spine
Small Thrusts
SCS 3
Outrunner
Blocks
4,000
B
SCS 4
10 km

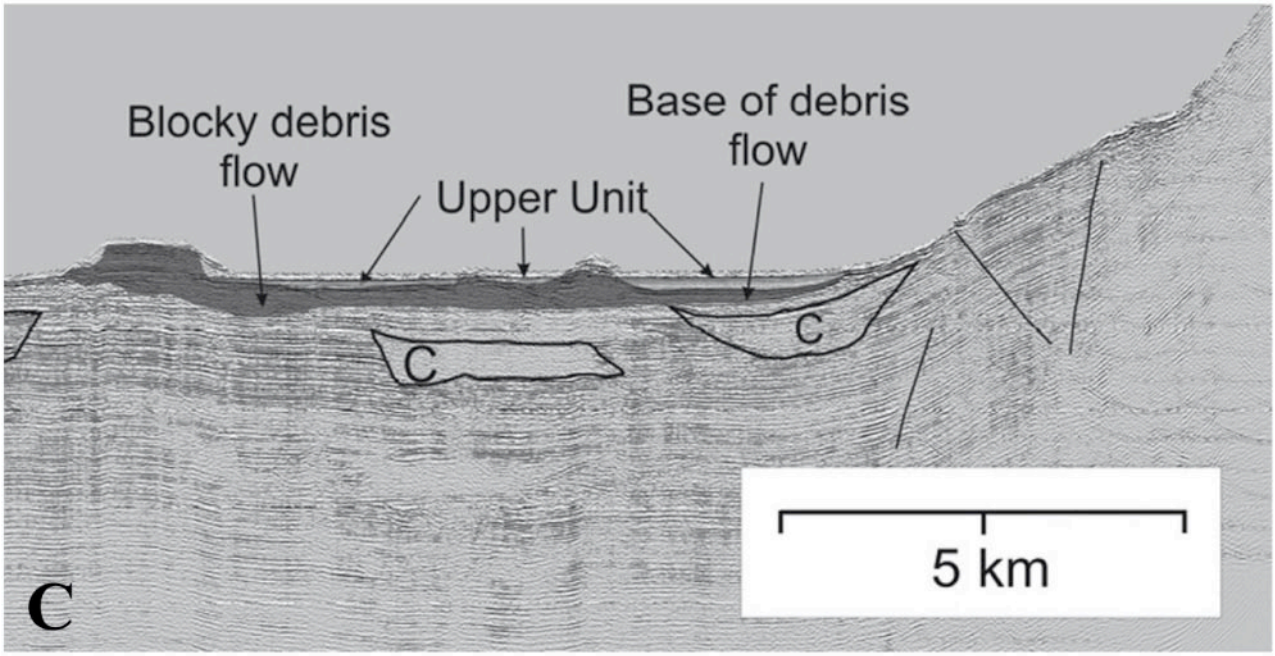
Blocky debris
flow
Upper Unit
Base of debris
flow
C
C
5 km
C

Figure 8.26 - **A**: Sketch map showing the location of the landslide site. The Sumatra margin is shown by the red/dashed lines and the landslide location is indicated with a star.

B: Multibeam bathymetry looking northward showing the debris avalanche slide.

C: Seismic transect through the slide and lower slope. Note the other buried small-scale MTDs (labeled with c) and the overall bipartition of the slide body, with an upper irregularly reflective, blocky portion and a lower transparent debris flow-like portion.

From Bradshaw *et al.* (2009), after Tappin *et al.* (2007).

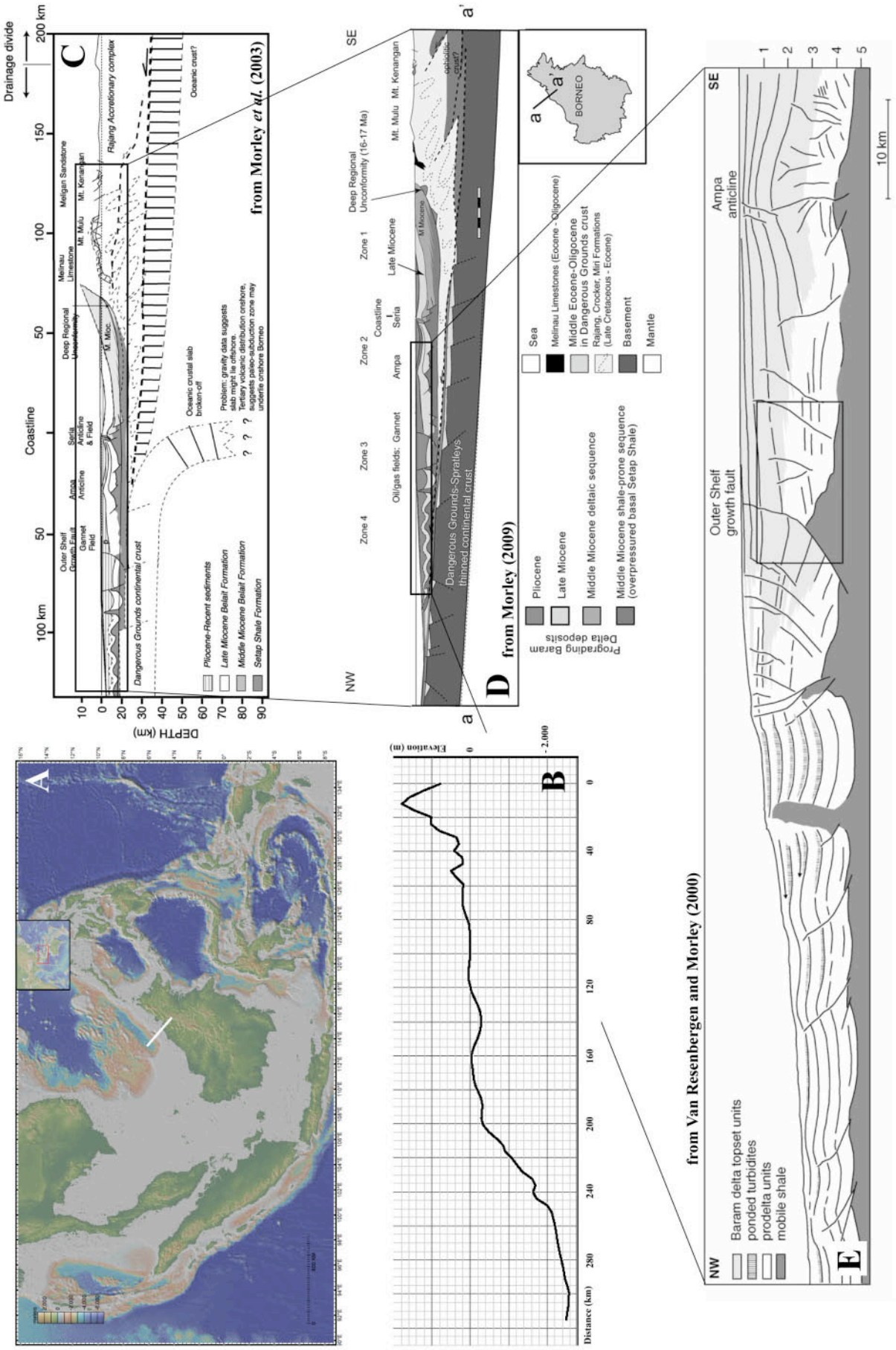
A
B
Elevation (m)
Distance (km)
C
Drainage divide
Coastline
DEPTH (km)
from Morley et al. (2003)
Dangerous Grounds continental crust
Pliocene-Recent sediments
Late Miocene Belait Formation
Middle Miocene Belait Formation
Setap Shale Formation
Oceanic crustal slab broken-off
Problem: gravity data suggests slab might lie offshore. Tertiary volcanic distribution onshore, suggests paleo-subduction zone may underlie onshore Borneo
Oceanic crust?
Rajang Accretionary complex
D
from Morley (2009)
NW
SE
Dangerous Grounds-Spratleys thinned continental crust
Oligas fields: Gannet
Deep Regional Unconformity (16-17 Ma)
Sea
Pliocene
Late Miocene
Middle Miocene deltaic sequence
Middle Miocene shale-prone sequence (overpressured basal Setap Shale)
Prograding Baram Delta deposits
Melinau Limestones (Eocene - Oligocene)
Middle Eocene-Oligocene in Dangerous Grounds crust
Rajang, Crocker, Mirri Formations (Late Cretaceous - Eocene)
Basement
Mantle
BORNEO
E
from Van Resenbergen and Morley (2000)
Outer Shelf growth fault
Ampa anticline
Baram delta topset units
ponded turbidites
prodelta units
mobile shale
10 km

Figure 8.27 - **A**: Morpho-bathymetric map of Indonesia with location of profile path (B) across the northwestern continental margin of Borneo (*i.e.* Brunei continental slope).

B: Topographic profile of the continental slope offshore Brunei. Elaborated with GeoMapApp (2009).

C: Regional geological cross-section through Brunei and Sarawak. From Morley *et al*. (2003).

D: Regional cross-section illustrating the large-scale structural setting and geometry of the Baram Delta province. Inset: Borneo sketch map and location of the profile. The Baram Delta province displays the following structural zones passing from onshore to offshore: 1) Zone 1, N–S trending folds and thrusts. The steeply dipping beds display large-scale progradational geometries in the Belait Formation on satellite images. This zone is not affected by gravity related normal faults or diapirs. 2) Zone 2, mixed growth faults and anticlines. From about 25 km inland to the mid-shelf is a zone of NE–SW striking growth faults, together with N–S and NE–SW striking folds related to episodes of inversion during the Miocene–Pliocene. 3) Zone 3, young growth faults. The outer shelf tends to be dominated by young, offshore dipping (regional) growth faults and some mud pipes. 4) Zone 4, the slope-deepwater fold and thrust belt. Most of the structures above with the likely exception of the N–S striking folds in zone 1, are developed above a basal detachment zone in the Setap Formation. From Morley (2009a).

E: Line drawing of a seimic section through the Baram delta at the western part of the Brunei shelf. Note the strong structural control operated by subsurface mud/shale remobilization. From Van Resenbergen and Morley (2000).

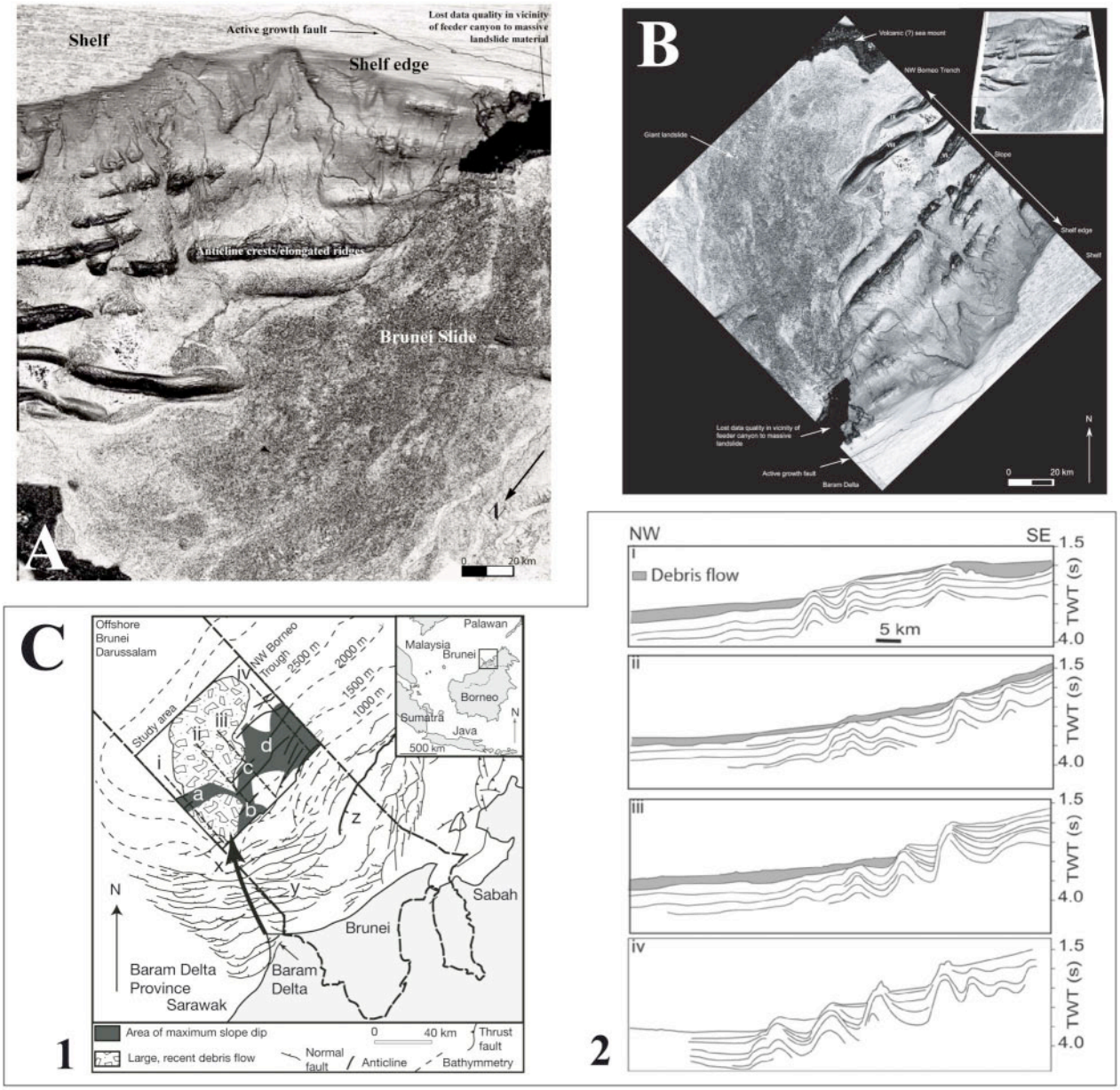
A
Shelf
Active growth fault
Lost data quality in vicinity of feeder canyon to massive landslide material
Shelf edge
Anticline crests/elongated ridges
Brunei Slide
0 20 km
B
Volcanic (?) sea mount
NW Borneo Trench
Giant landslide
Slope
Shelf edge
Shelf
Lost data quality in vicinity of feeder canyon to massive landslide
Active growth fault
Baram Delta
N
0 20 km
C
Offshore Brunei Darussalam
NW Borneo trough
2500 m
2000 m
1500 m
1000 m
Study area
i
ii
iii
iv
a
b
c
d
x
y
z
N
Palawan
Malaysia
Brunei
Borneo
Sumatra
Java
500 km
Sabah
Brunei
Baram Delta Province Sarawak
Baram Delta
1
Area of maximum slope dip
Large, recent debris flow
0 40 km
Normal fault
Anticline
Thrust fault
Bathymmetry
2
NW
SE
Debris flow
5 km
TWT (s)
1.5
4.0

Figure 8.28 - A: Perspective view elaborated from an edge map of the water bottom reflection mapped from 3-D seismic reflection data, for the outer shelf and slope region of offshore Brunei Darussalam. The Brunei Slide occupies the entire right-hand side of the map. From Morley (2007).

B: Plan view of the edge map shown in A. Note how the Brunei Slide, roughly originating from the shelf edge, reaches the basin plain breacking anticline crest ridges, and filling intra-slope basins in a longitudinal direction. From Morley (2009a).

C: (**1**) Regional location map for deep-water Brunei (roughly the same area shown in A and B). Labels i, ii, iii, and iv are lines of section shown in (2). Labels a, b, c, and d are provinces with different surface slope physiographic characteristics. x—province dominated by sediment input from the Baram Delta; y—inboard area of inverted normal faults; z—Perdana/Frigate fault depocentre. From Morley (2007). (**2**) Four regional NW-SE cross sections based on upper 1 s of data from regional three-dimensional survey, illustrating change in slope and fold geometry across continental slope. For location see (1). From Morley (2007).

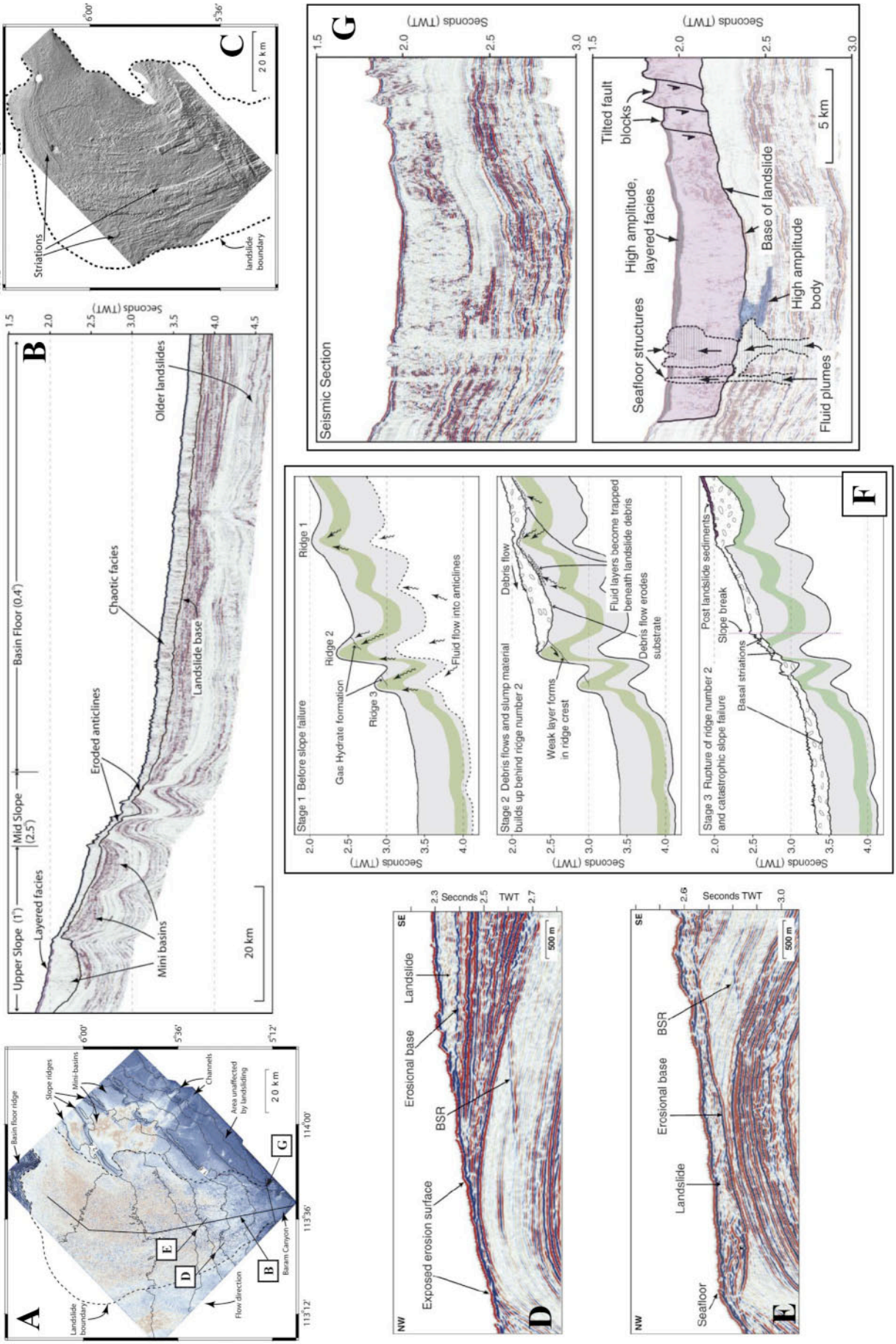
A
Basin floor ridge
Slope ridges
Mini-basins
Channels
Area unaffected by landsliding
20 km
Landslide boundary
Flow direction
Baram Canyon
B
C
Striations
landslide boundary
20 km
B
Upper Slope (1°)
Mid Slope (2.5°)
Basin Floor (0.4°)
Layered facies
Mini basins
Eroded anticlines
Chaotic facies
Landslide base
Older landslides
Seconds (TWT)
20 km
G
Seismic Section
Seconds (TWT)
Tilted fault blocks
High amplitude, layered facies
Base of landslide
5 km
Seafloor structures
High amplitude body
Fluid plumes
F
Stage 1 Before slope failure
Ridge 1
Ridge 2
Ridge 3
Gas Hydrate formation
Fluid flow into anticlines
Stage 2 Debris flows and slump material builds up behind ridge number 2
Debris flow
Fluid layers become trapped beneath landslide debris
Debris flow erodes substrate
Weak layer forms in ridge crest
Stage 3 Rupture of ridge number 2 and catastrophic slope failure
Post landslide sediments
Slope break
Basal striations
Seconds (TWT)
D
SE
NW
Seconds TWT
500 m
Landslide
Erosional base
BSR
Exposed erosion surface
E
SE
NW
Seconds TWT
500 m
BSR
Erosional base
Landslide
Seafloor

Figure 8.29 - A: Brunei Slide visualized in RMS (*i.e.* root mean square) amplitudes mapped from 3D seismic data from a 20 ms interval at the seafloor. Blue colour represents lower amplitudes. Location of B, D, E and G are labeled.

B: Long-composite profile seismic section across the entire length of the Brunei Slide, from the upper and middle slope, to the basin floor. For location see A.

C: Gradient map of the basal surface of the Brunei Slide showing striations extending 120 km across the slopes and basin of the NW Borneo Trough. Artificial illumination is from the north east.

D and **E**: Seismic sections showing eroded anticline crests and BSRs in the subsurface. For location see A.

F: A schematic model of the Brunei Slide develpoment, which describes a two stage failure event involving the weakening and catastrophic failure of anticline crests (*i.e.* dam-breakage effect of the Ridge 2) to release a bulk of landslide material into the basin.

G: Transversal seimic profile and interpretation across the proximal zone. Fluid escapes are observed at the seafloor as small mud volcanoes. The landslide unit shows significant thickess and tilted fault blocks are observable to the east. A fluid plume appears to have spread out beneath the landslide. The high amplitude body below the slide indicates gas charged sediments related to the fluid plumes. A thin (50 m) layered, high amplitude facies overlies the landslide deposit. For location see A.

From Gee *et al*. (2007).

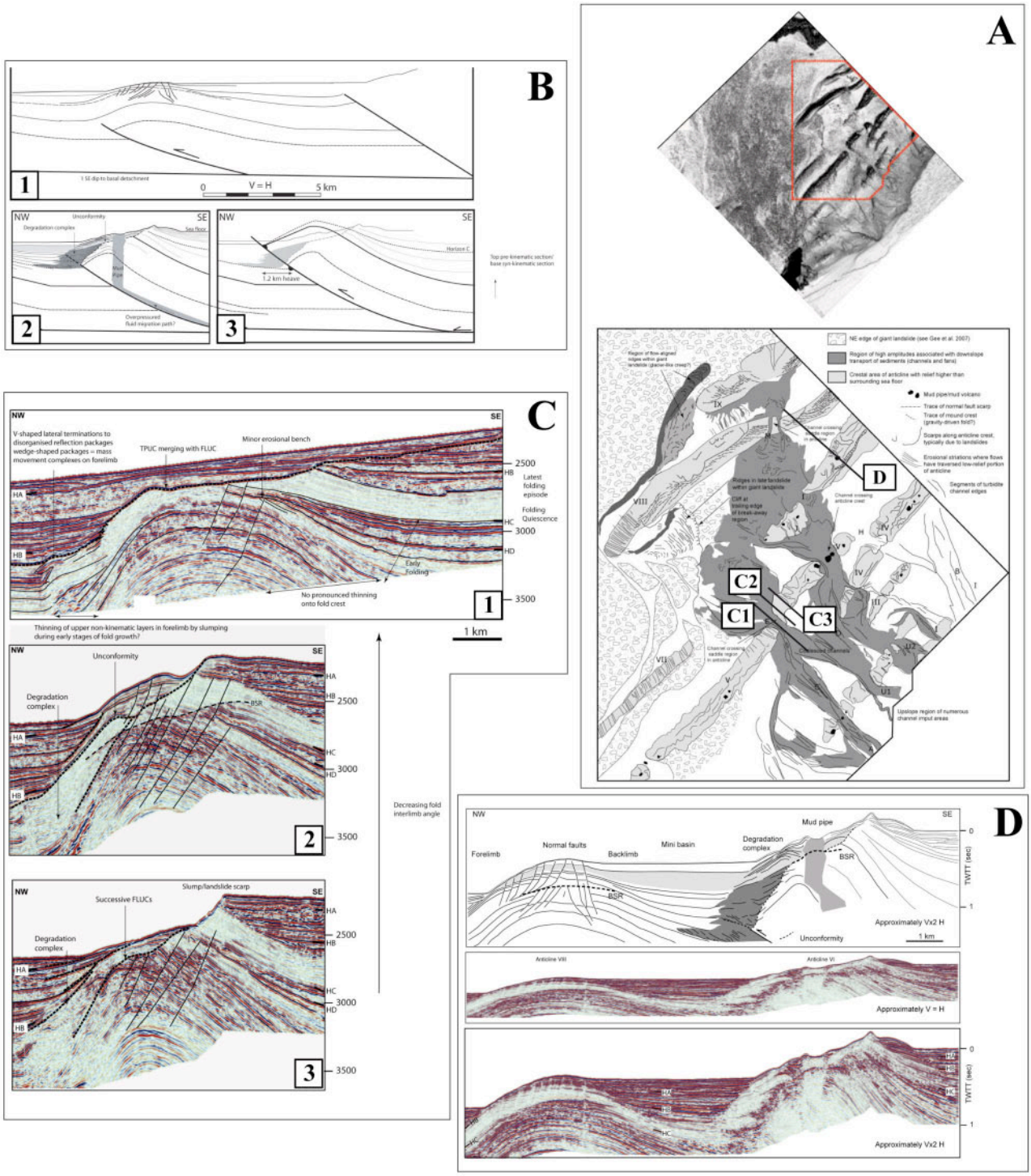
A
B
1
2
3
C
D
C1
C2
C3
NW
SE
V = H
5 km
1.2 km heave
Unconformity
Degradation complex
Sea floor
Mud pipe
Overpressured fluid migration path?
Horizon C
Top pre-kinematic section/ base syn-kinematic section
V-shaped lateral terminations to disorganised reflection packages wedge-shaped packages = mass movement complexes on forelimb
TPUC merging with FLUC
Minor erosional bench
Latest folding episode
Folding Quiescence
Early Folding
No pronounced thinning onto fold crest
1 km
Thinning of upper non-kinematic layers in forelimb by slumping during early stages of fold growth?
Decreasing fold interlimb angle
Successive FLUCs
Slump/landslide scarp
HA
HB
HC
HD
2500
3000
3500
BSR
Forelimb
Normal faults
Backlimb
Mini basin
Mud pipe
Approximately Vx2 H
Approximately V = H
TWTT (sec)
Anticline VIII
Anticline VI
NE edge of giant landslide (see Gee et al. 2007)
Region of high amplitudes associated with downslope transport of sediments (channels and fans)
Crestal area of anticline with relief higher than surrounding sea floor
Mud pipe/mud volcano
Trace of normal fault scarp
Trace of mound crest (gravity-driven fold?)
Scarps along anticline crest, typically due to landslides
Erosional striations where flows have traversed low-relief portion of anticline
Segments of turbidite channel edges
Ridges in late landslide within giant landslide
Cliff at trailing edge of break-away region
Channel crossing anticline crest
Channel crossing saddle region in anticline
Upslope region of numerous channel input areas

Figure 8.30 - A: Interpretation of the main structural and sedimentary features observable RMS amplitude maps, with location of C and D. Inset: shaded relief map with location of the interpreted RMS amplitude map slice (red contour); compare with edge maps represented in fig. 8.28 and fig. 8.29.

B: Relationship of shallow structure determined from 3D seismic data (C) and the deeper fold geometry (based on regional 2D seismic lines). The folds are represented by modified fault propagation folds with a listric imbricate fault geometry.

C: Examples of lateral changes in unconformity geometry along an anticline trend (*i.e.* anticline V axis), going from SW (1) to NE (3). Note the common occurrence of small-scale MTDs on the forelimb (*i.e.* degradation complex). See A for location.

D: Example of two anticlines (VIII and V), whose geometry at the seafloor is strongly modified by mass wasting and mass movement processes. The northwestern fold (VIII) is a simple fold with normal faults, the southeastern fold (V) is affected by erosion, forelimb degradation complexes and a mud pipe in the core zone. See A for location.

From Morley (2009a).

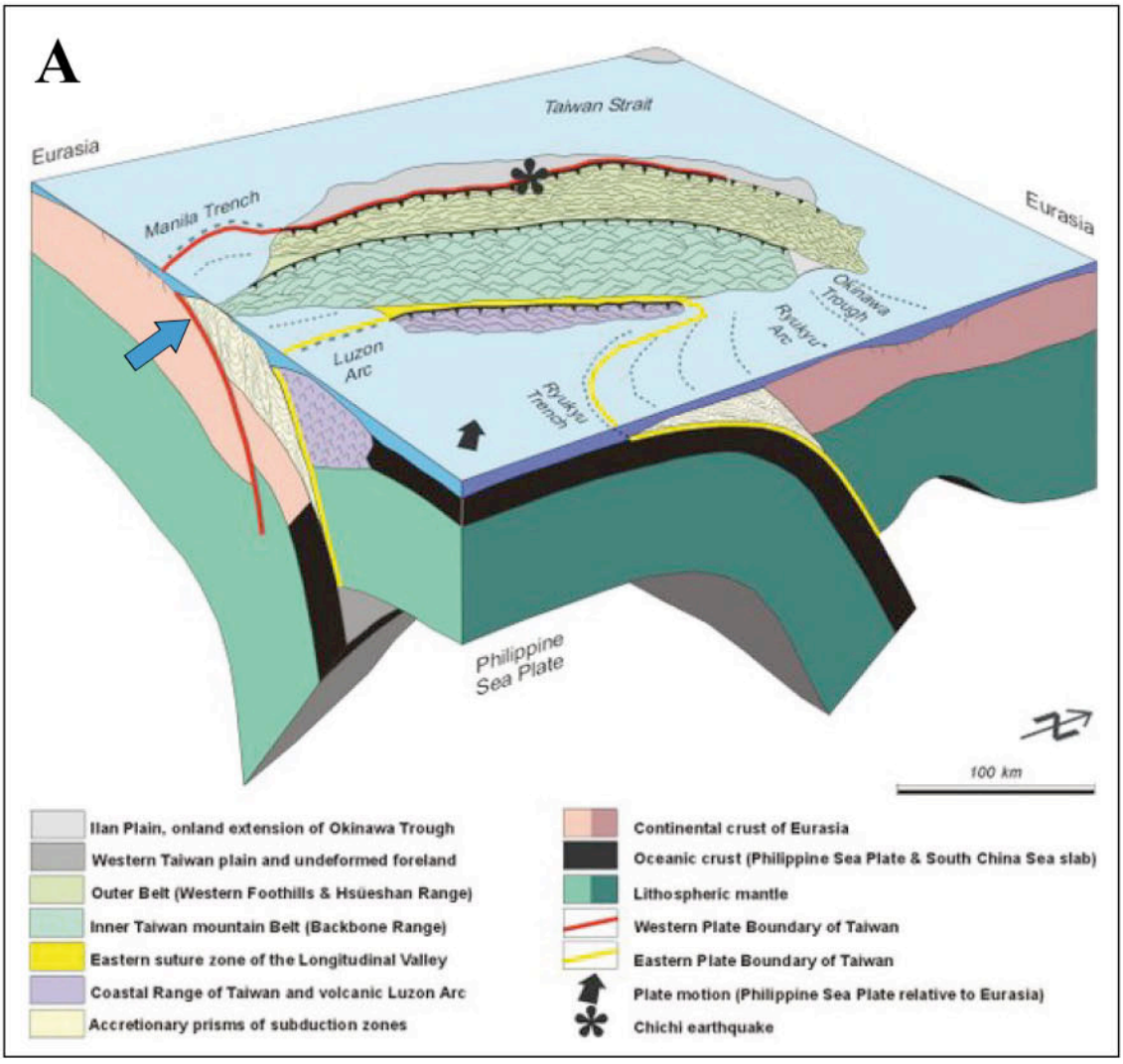
A
Taiwan Strait
Eurasia
Manila Trench
Eurasia
Okinawa Trough
Ryukyu Arc
Luzon Arc
Ryukyu Trench
Philippine Sea Plate
100 km
Ilan Plain, onland extension of Okinawa Trough
Western Taiwan plain and undeformed foreland
Outer Belt (Western Foothills & Hsüeshan Range)
Inner Taiwan mountain Belt (Backbone Range)
Eastern suture zone of the Longitudinal Valley
Coastal Range of Taiwan and volcanic Luzon Arc
Accretionary prisms of subduction zones
Continental crust of Eurasia
Oceanic crust (Philippine Sea Plate & South China Sea slab)
Lithospheric mantle
Western Plate Boundary of Taiwan
Eastern Plate Boundary of Taiwan
Plate motion (Philippine Sea Plate relative to Eurasia)
Chichi earthquake

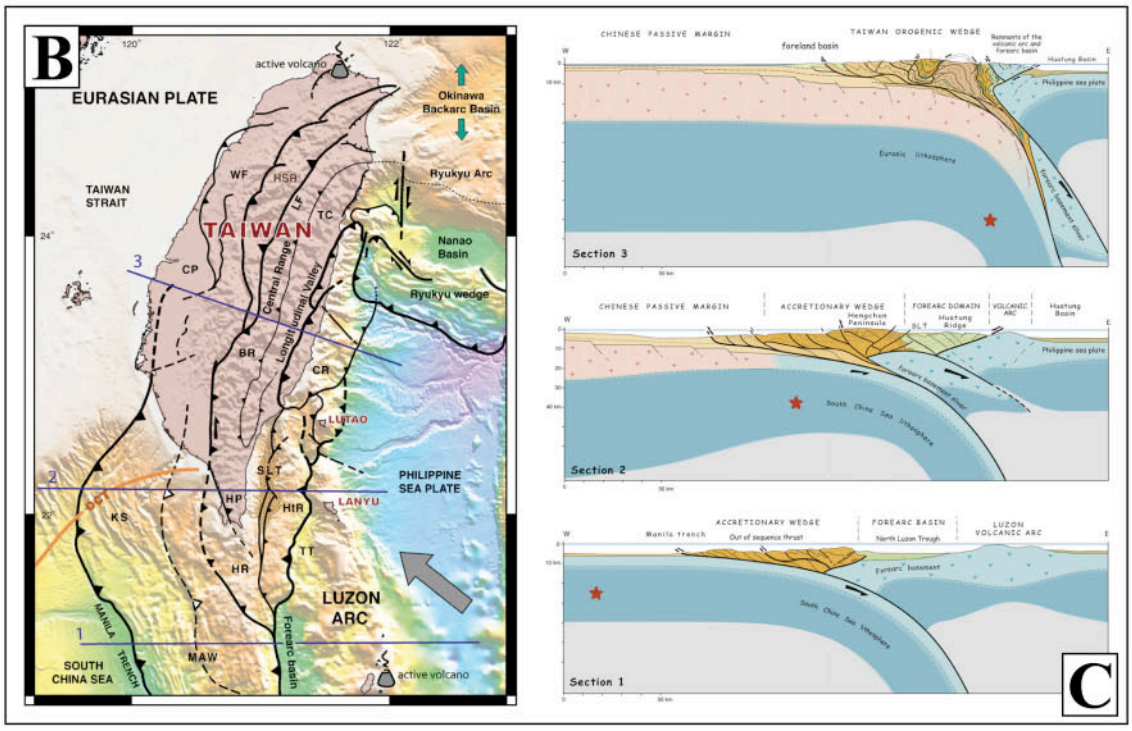
B
EURASIAN PLATE
active volcano
Okinawa Backarc Basin
Ryukyu Arc
TAIWAN STRAIT
TAIWAN
Nanao Basin
Ryukyu wedge
Central Range
Longitudinal Valley
LUTAO
LANYU
PHILIPPINE SEA PLATE
LUZON ARC
SOUTH CHINA SEA
MANILA TRENCH
Forearc basin
active volcano
WF
HSR
LF
TC
CP
BR
CR
SLT
HP
HTR
KS
TT
HR
MAW
CHINESE PASSIVE MARGIN
TAIWAN OROGENIC WEDGE
foreland basin
Section 3
ACCRETIONARY WEDGE
FOREARC DOMAIN
Section 2
FOREARC BASIN
LUZON VOLCANIC ARC
Manila trench
Section 1
C

Figure 8.31 - A: Schematic block-diagram illustrating the lithospheric structure of Taiwan. View from southeast to northwest. Blue arrow roughly indicate the position of the Hengchun Ridge/Manila accretionary wedge. From Angelier *et al*. (2001).

B: Morphostructural map of the Taiwan area showing the main tectonic units which characterizes the transition from oceanic to continental subduction. Sections of C are displayed as blue lines. CP, Coastal Plain; WF, Western Foothills; HSR, Hsueshan Range; LF, Lishan Fault; TC, Tananao Complex; BR, Backbone Range; CR, Coastal Range; SLT, "Southern Longitudinal Trough" orogenic basin; HP, Hengchun Peninsula; HR, Hengchun Ridge; HtR, Huatung Ridge; KS, Kaoping Slope; TT, Taitung Trough; MAW, Manila Accretionary Wedge; FB, Forearc Basin; OCT, inferred Ocean Continent Transition. From Malaveille and Trullenque (2007).

C: General interpretative sections showing the tectonic evolution of the orogenic wedge. Section 1, oceanic subduction and growth of a sedimentary wedge south of Taiwan; Section 2, incipient subduction of the continental margin and subduction of a slice of forearc basement inducing intense shortening of the forearc sedimentary units; Section 3, mature continental subduction and growth of the Taiwan orogenic wedge. See C for location. From Malaveille and Trullenque (2007).

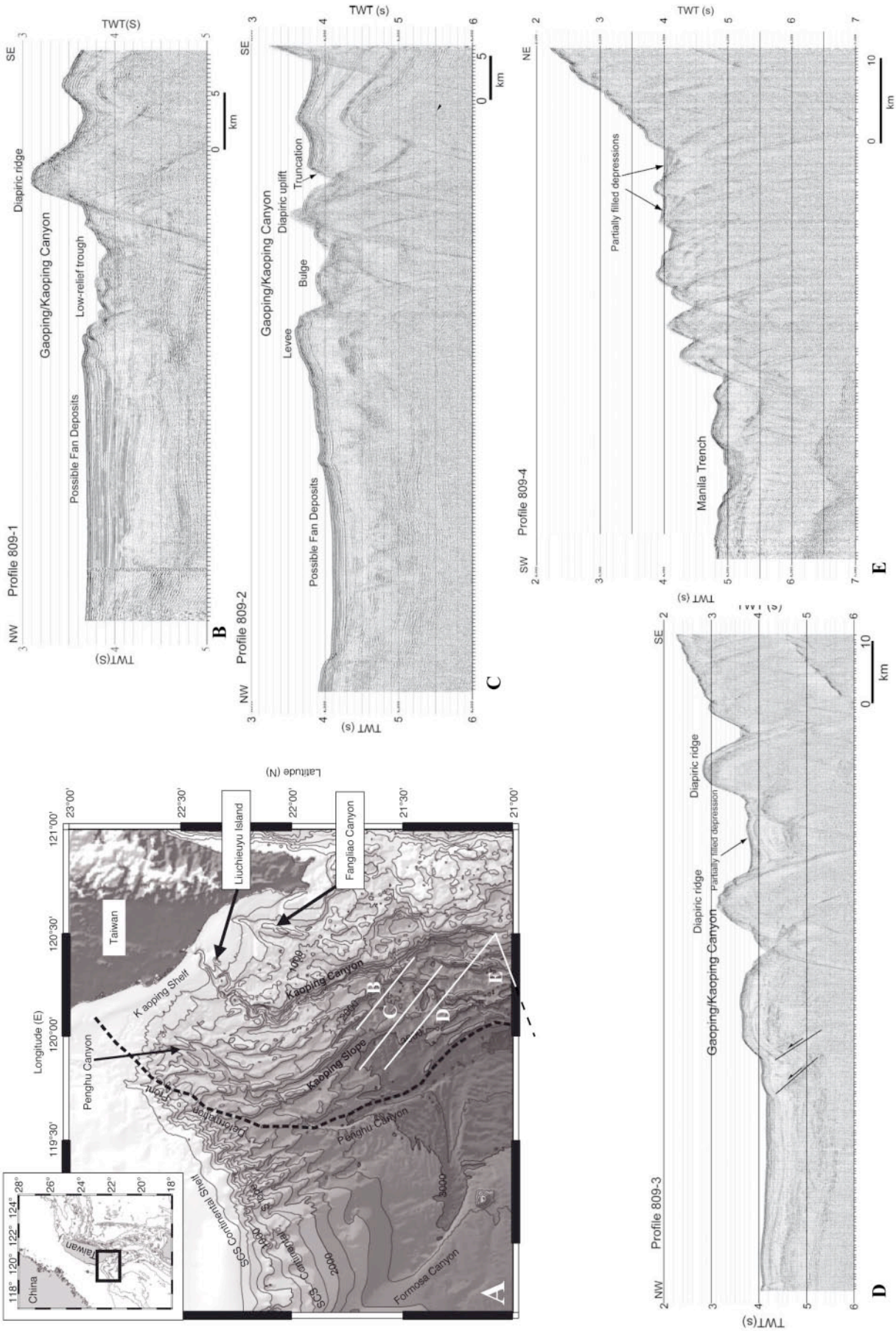
Profile 809-1
Diapiric ridge
Gaoping/Kaoping Canyon
Low-relief trough
Possible Fan Deposits
Profile 809-2
Diapiric uplift
Truncation
Levee
Bulge
Possible Fan Deposits
Profile 809-4
Partially filled depressions
Manila Trench
Profile 809-3
Diapiric ridge
Partially filled depression
Gaoping/Kaoping Canyon
Taiwan
Liuchieuyu Island
Fangliao Canyon
Kaoping Shelf
Kaoping Canyon
Kaoping Slope
Penghu Canyon
Formosa Canyon
SCS Continental Shelf
SCS Continental Slope
Longitude (E)
Latitude (N)
China
TWT(S)
TWT (s)
km

Figure 8.32 - **A**: Morpho-bathymetric map of the northern Kaoping Slope offshore SW Taiwan. The black dashed line represents the deformation front separating the passive South China Sea (SCS) continental margin from the active submarine Taiwan orogenic wedge. Bathymetry contours are at 250 m intervals. Traces of seimic sections shown in B, C, D and E are labeled. Inset: geographic location. From Chiu and Liu (2008).

B: Seismic line crossing the lower segment of the Kaoping canyon. The cross-sectional morphology of the canyon is represented by an asymmetrical broad low-relief trough with steeper wall to the southeast. The steep canyon wall is the flank of an uprising mud diapiric ridge. The canyon floor is irregular probably resulting from alternating episodes of deposition and erosion.

C: Seismic section farther down-canyon respect to the seismic profile 809-1 shown in B. Note that in the middle part of the canyon floor there is a small bulge that may be an expression of mild uplift of mud diapirism, suggesting significant interveining of structural disturbance in sedimentary processes. Truncation of parallel reflectors against a sharp steep sloping surface is observed southeast of the small bulge in the center of canyon floor, suggesting relatively intense down-cutting. The sea floor northwest of canyon wall and beyond are characterized by tilted parallel reflections that could be interpreted as overbank levees. Seismic characteristics shown on profile 809-2 indicate complex features of overbank deposition, intense local canyon floor erosion and structural disturbance.

D: Seismic profile farther down-canyon respect to the seimic profile 809-2 shown in C. a small trough with an asymmetrical V-shaped cross section with steeper wall to the southeast. There is no sediment accumulation in the canyon floor, suggesting erosion or sediments being removed. Parallel reflections beneath the sea floor northwest of the canyon are interpreted as a result of hemipelagic deposition in the lower slope. Note that the depression between two uprising mud diapiric ridges northeast of the canyon is partially filled, implying sediments from the upper slope region transported down-slope to the lower Gaoping Slope and trapped in depressions before reaching the Kaoping submarine canyon.

E: Seismic profile 809-4 across the axis of the northern Manila Trench shows that the trench is represented by a small shallow depression, partially filled with sediments. Note that some depressions (small intraslope basins) on the lower Gaoping Slope northeast of the Manila Trench are partially filled with sediment. Other depressions at the slope toe are empty. Sediments derived from the Gaoping Shelf and upper Gaoping Slope must infill depressions on the lower slope and then excess sediments can overspill the filled depressions reaching to the Manila Trench.

All seimic lines are from Yu *et al.* (2008).

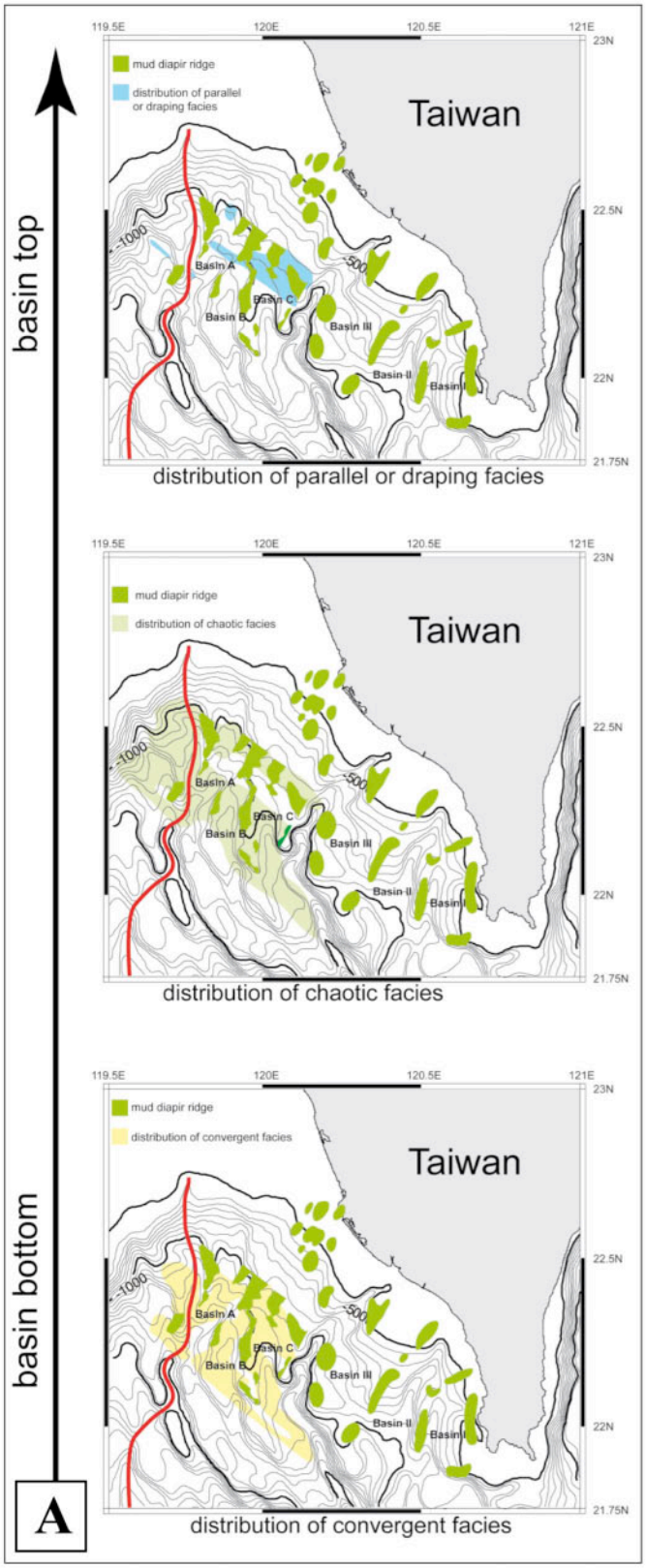
basin top
basin bottom
A
119.5E
120E
120.5E
121E
23N
22.5N
22N
21.75N
mud diapir ridge
distribution of parallel or draping facies
Taiwan
-1000
-500
Basin A
Basin C
Basin B
Basin III
Basin II
Basin I
distribution of parallel or draping facies
mud diapir ridge
distribution of chaotic facies
Taiwan
distribution of chaotic facies
mud diapir ridge
distribution of convergent facies
Taiwan
distribution of convergent facies

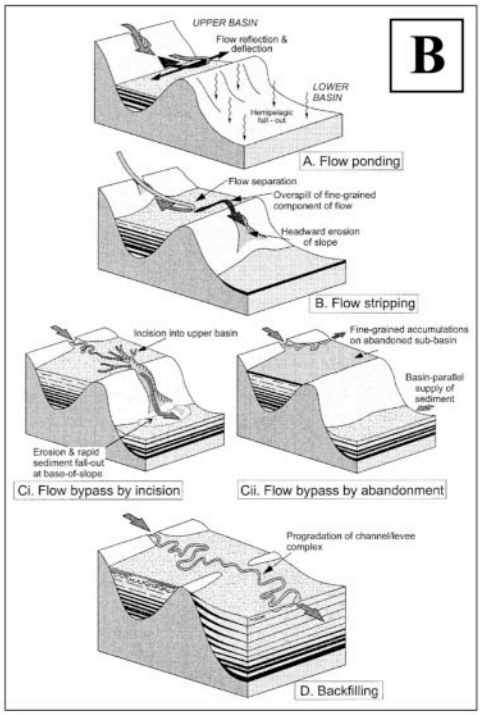
B
UPPER BASIN
Flow reflection & deflection
LOWER BASIN
Hemipelagic fall - out
A. Flow ponding
Flow separation
Overspill of fine-grained component of flow
Headward erosion of slope
B. Flow stripping
Incision into upper basin
Erosion & rapid sediment fall-out at base-of-slope
Ci. Flow bypass by incision
Fine-grained accumulations on abandoned sub-basin
Basin-parallel supply of sediment
Cii. Flow bypass by abandonment
Progradation of channel/levee complex
D. Backfilling

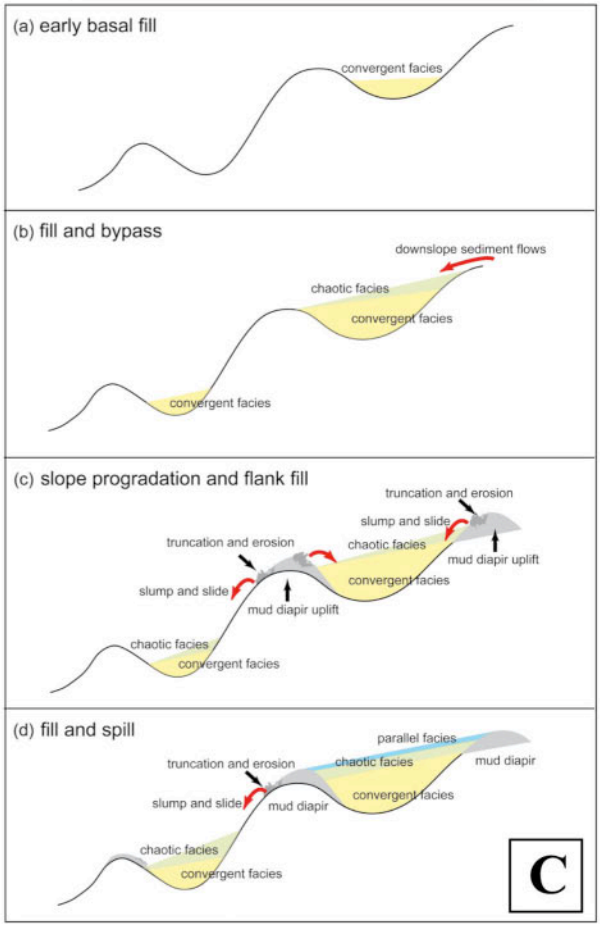
(a) early basal fill
convergent facies
(b) fill and bypass
downslope sediment flows
chaotic facies
convergent facies
convergent facies
(c) slope progradation and flank fill
truncation and erosion
slump and slide
chaotic facies
mud diapir uplift
truncation and erosion
slump and slide
convergent facies
mud diapir uplift
chaotic facies
convergent facies
(d) fill and spill
parallel facies
truncation and erosion
chaotic facies
mud diapir
slump and slide
mud diapir
convergent facies
chaotic facies
convergent facies
C

Figure 8.33 - A: Lateral distribution of three major types of seismic facies characterizing the Kaoping slope depositional style: convergent, chaotic and parallel. The basal convergent facies is the most common one and is distributed from upper slope to lower slope areas and the chaotic facies is the less common one. The parallel and draping facies is the least common one and is restricted to the upper slope region. From Yu and Huang (2006).

B: Four stage depositional model for the progressive infill of a confined turbidite basin and associated deposits at the base of the slope of a lower basin. From Sinclair and Tomasso (2002).

C: Simplified schematic sedimentation model of downslope fill and spill depositional style for development of the intraslope basins in the Kaoping Slope. From Yu and Huang (2006).

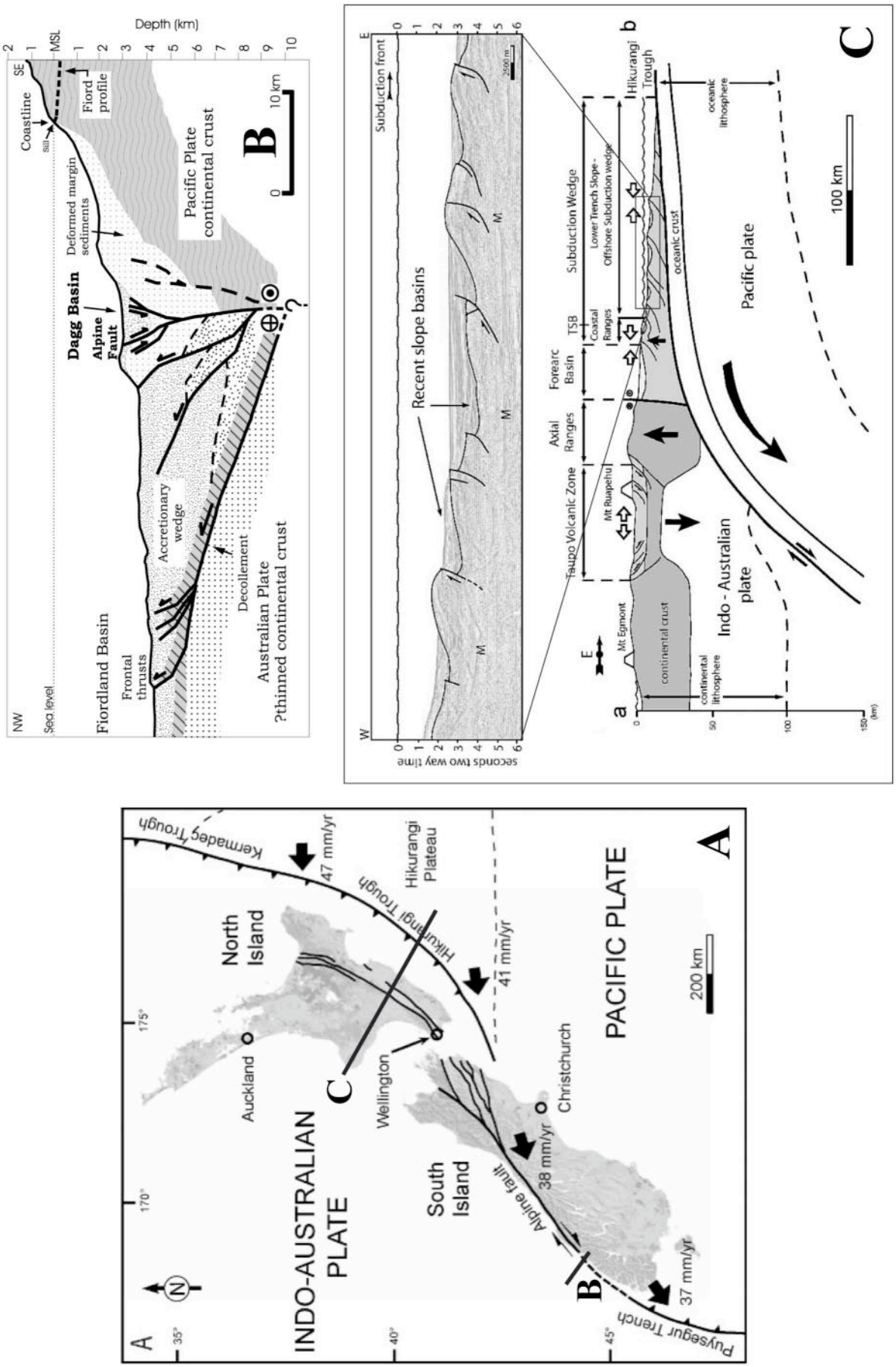
Depth (km)
NW
SE
MSL
Coastline
Sea level
Fiord profile
Deformed margin sediments
Dagg Basin
Alpine Fault
Pacific Plate continental crust
B
10 km
Fiordland Basin
Frontal thrusts
Accretionary wedge
Decollement
Australian Plate
?thinned continental crust
W
E
Subduction front
Recent slope basins
seconds two way time
Subduction Wedge
Lower Trench Slope - Offshore Subduction wedge
Hikurangi Trough
oceanic lithosphere
oceanic crust
Forearc Basin
TSB
Coastal Ranges
Axial Ranges
Taupo Volcanic Zone
Mt Ruapehu
Mt Egmont
continental crust
continental lithosphere
Pacific plate
Indo - Australian plate
100 km
a
b
C
Kermadec Trough
47 mm/yr
Hikurangi Plateau
Hikurangi Trough
41 mm/yr
North Island
Auckland
Wellington
C
INDO-AUSTRALIAN PLATE
PACIFIC PLATE
200 km
A
South Island
Christchurch
Alpine fault
38 mm/yr
37 mm/yr
B
Puysegur Trench
N
35°
40°
45°
170°
175°

Figure 8.34 - A: General tectonic setting of New Zealand with location of interpretative sections shown in B and C. From Bailleul *et al*. (2007).

B: Upper crustal schematic section through SW New Zealand (*i.e.* Dagg Basin and the lower margin of the Fjordland/Westland accretionary wedge). Aproximative location shown in A. From Barnes *et al.* (2005).

C: General cross section through Northern Island and the Hikurangi subduction complex, (TSB: Trench–Slope Break), with location of a seismic line (inset), showing the position and the geometry of offshore Quaternary trench-slope basins near the subduction front. From Bailleul *et al*. (2007) after Lewis and Pettinga (1993).

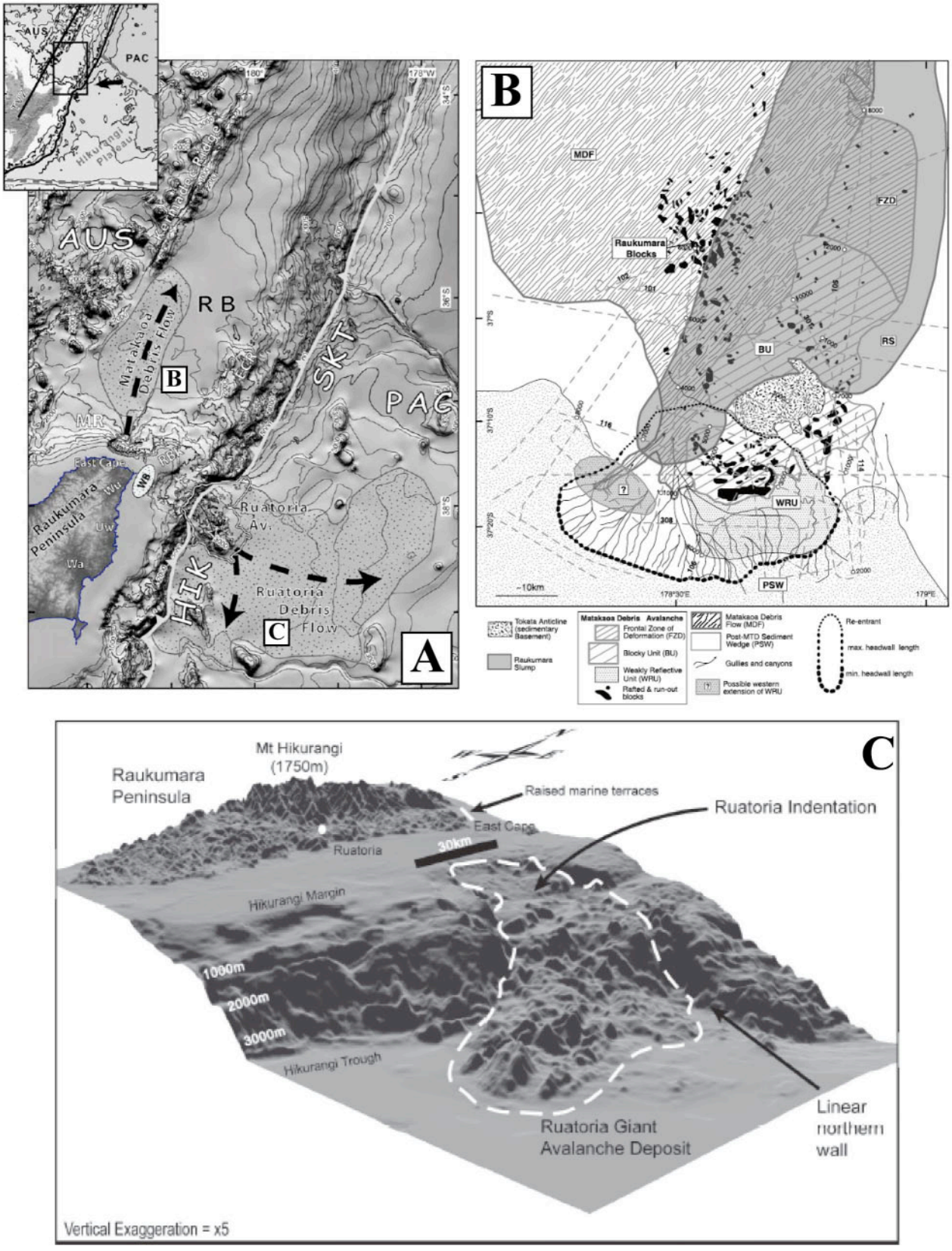
AUS
PAC
Hikurangi Plateau
AUS
RB
Matakaoa Debris Flow
B
SKT
PAC
MR
East Cape
Raukumara Peninsula
Wu
Uw
Wa
WB
Ruatoria Av.
HTK
Ruatoria Debris Flow
C
A
B
MDF
FZD
Raukumara Blocks
BU
RS
WRU
PSW
~10km
Tokata Anticline (sedimentary Basement)
Raukumara Slump
Matakaoa Debris Avalanche
Frontal Zone of Deformation (FZD)
Blocky Unit (BU)
Weakly Reflective Unit (WRU)
Rafted & run-out blocks
Matakaoa Debris Flow (MDF)
Post-MTD Sediment Wedge (PSW)
Gullies and canyons
Possible western extension of WRU
Re-entrant
max. headwall length
min. headwall length
C
Mt Hikurangi (1750m)
Raukumara Peninsula
Raised marine terraces
Ruatoria Indentation
East Cape
Ruatoria
30km
Hikurangi Margin
1000m
2000m
3000m
Hikurangi Trough
Ruatoria Giant Avalanche Deposit
Linear northern wall
Vertical Exaggeration = x5

Figure 8.35 - A: Shaded relief map of the northeasternmost part of the Northern Island (New Zealand) showing the location of the Ruatoria slide complex (Hikurangi margin deformation front) and the Matakaoa slide complex (south Kermadec fore-arc basin), labeled with C and B, respectively. Inset: geographic location of the map. From Lamarche *et al.* (2008).

B: Interpretation map of the Matakaoa slide complex. This large-scale MTC has been originated from the collapse of the NW flank of a regional anticline. From Lamarche *et al.* (2008).

C: Perspective view terrain model of the Ruatoria Indentation and Giant Avalanche deposit (location shown in A). The indentation's linear northern wall is inferred to have formed as part of a subducting seamount's "impact scar" or "wake trough". This large scale MTC is thought to be the product of the oblique subduction of a seamount. From Lewis *et al.* (2004).

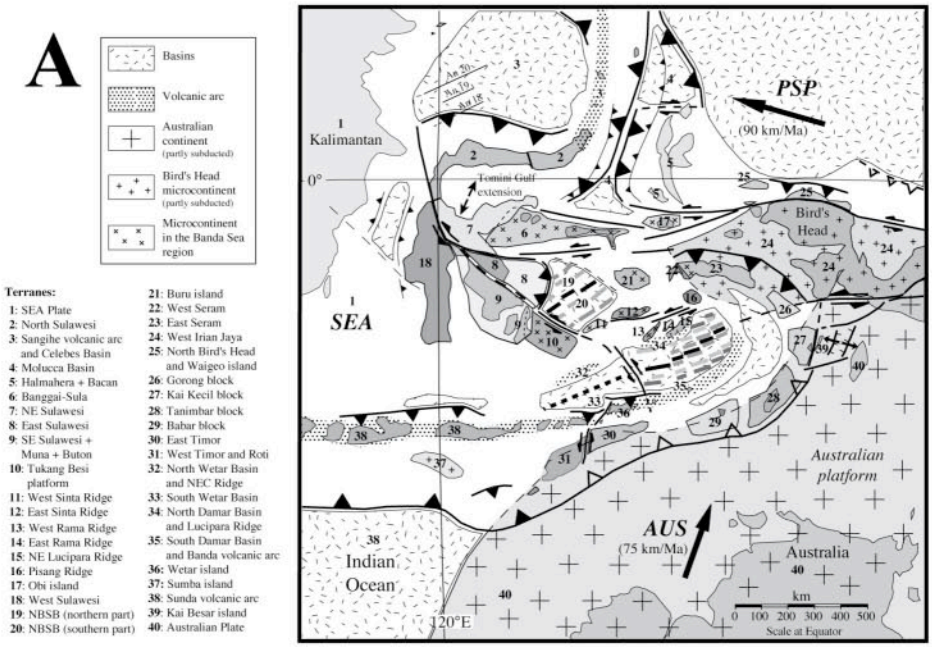
A
Basins
Volcanic arc
Australian continent (partly subducted)
Bird's Head microcontinent (partly subducted)
Microcontinent in the Banda Sea region
Terranes:
1: SEA Plate
2: North Sulawesi
3: Sangihe volcanic arc and Celebes Basin
4: Molucca Basin
5: Halmahera + Bacan
6: Banggai-Sula
7: NE Sulawesi
8: East Sulawesi
9: SE Sulawesi + Muna + Buton
10: Tukang Besi platform
11: West Sinta Ridge
12: East Sinta Ridge
13: West Rama Ridge
14: East Rama Ridge
15: NE Lucipara Ridge
16: Pisang Ridge
17: Obi island
18: West Sulawesi
19: NBSB (northern part)
20: NBSB (southern part)
21: Buru island
22: West Seram
23: East Seram
24: West Irian Jaya
25: North Bird's Head and Waigeo island
26: Gorong block
27: Kai Kecil block
28: Tanimbar block
29: Babar block
30: East Timor
31: West Timor and Roti
32: North Wetar Basin and NEC Ridge
33: South Wetar Basin
34: North Damar Basin and Lucipara Ridge
35: South Damar Basin and Banda volcanic arc
36: Wetar island
37: Sumba island
38: Sunda volcanic arc
39: Kai Besar island
40: Australian Plate
Kalimantan
SEA
PSP
(90 km/Ma)
Tomini Gulf extension
Bird's Head
Australian platform
AUS
(75 km/Ma)
Australia
Indian Ocean
120°E
km
Scale at Equator

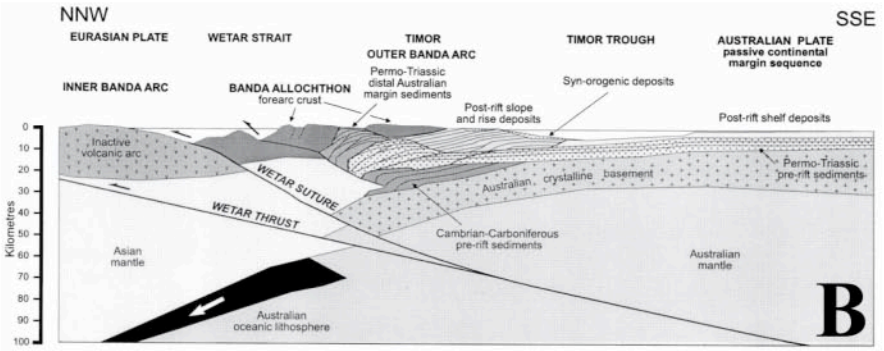
NNW
SSE
EURASIAN PLATE
WETAR STRAIT
TIMOR
OUTER BANDA ARC
TIMOR TROUGH
AUSTRALIAN PLATE
passive continental margin sequence
INNER BANDA ARC
BANDA ALLOCHTHON
forearc crust
Permo-Triassic distal Australian margin sediments
Syn-orogenic deposits
Post-rift slope and rise deposits
Post-rift shelf deposits
Inactive volcanic arc
WETAR SUTURE
WETAR THRUST
Australian crystalline basement
Permo-Triassic pre-rift sediments
Cambrian-Carboniferous pre-rift sediments
Asian mantle
Australian mantle
Australian oceanic lithosphere
Kilometres
B

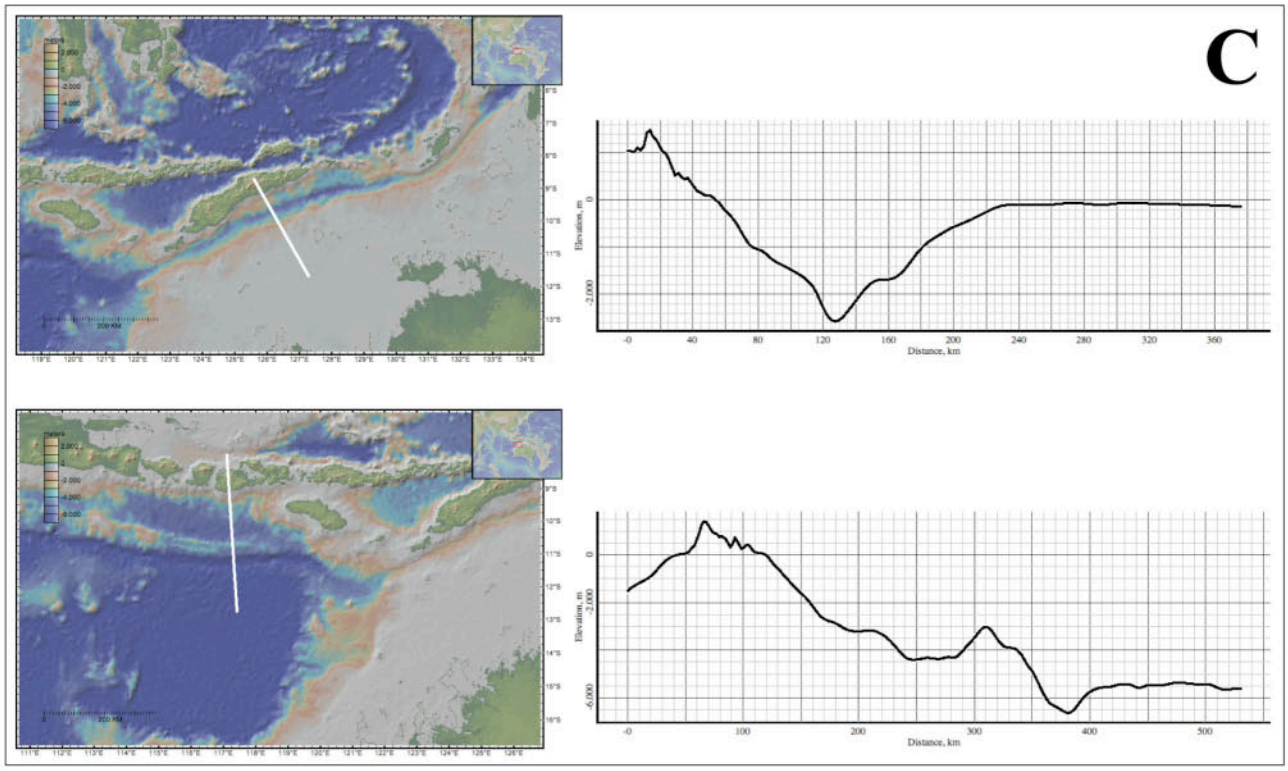
C
Elevation, m
Distance, km

Figure 8.36 - A: Map of the plates, microplates and terrane units of the Eastern Indonesia. The major tectonic structures are indicated. For the clartity of the map, all the boundaries of plates and microplates are not represented. From Hinschberger *et al*. (2005).

B: Schematic cross section across the Banda Suture at the same vertical and horizontal scales. The Wetar Thrust is interpreted as the active plate boundary between the Australian and Eurasian plates. Suggested positions for the suture at different stages in the collision are: (1) the base of the Banda allochthon; (2) the deformation front in the Timor Trough (now inactive); (3) the Wetar suture (now inactive); and (4) the Wetar Thrust. From Hall and Wilson (2000).

C: Morpho-bathymetric maps and topographic profiles taken across adjacent ocenic and incipient contienental subductions, characterizing the Sunda Arc - Banda Arc transition. Note the significant physiographic differences between the two. Elaborated with GeoMapApp (2009).

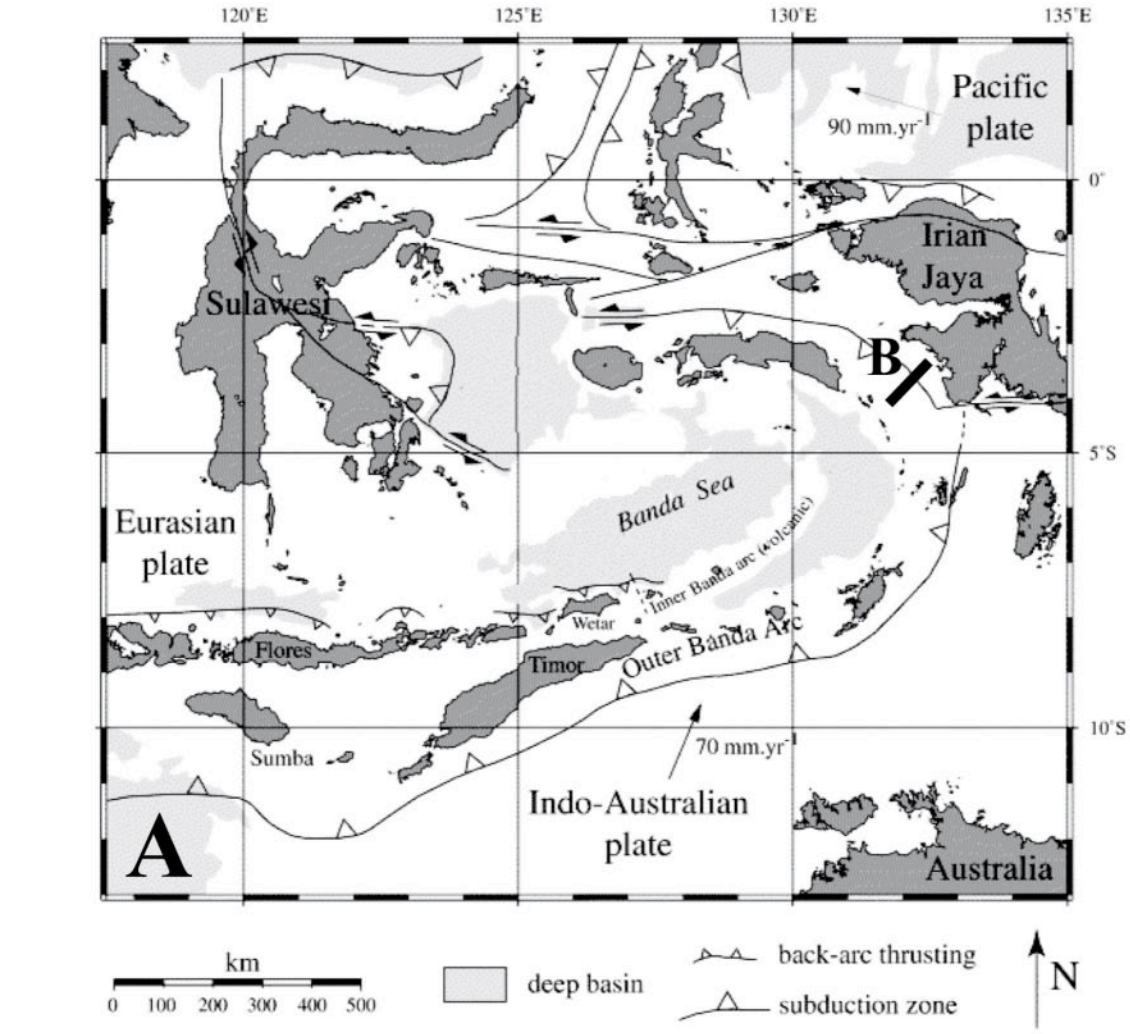
120°E
125°E
130°E
135°E
0°
5°S
10°S
Pacific plate
90 mm.yr-1
Irian Jaya
Sulawesi
B
Banda Sea
Eurasian plate
Inner Banda arc (volcanic)
Wetar
Flores
Timor
Outer Banda Arc
Sumba
70 mm.yr-1
Indo-Australian plate
A
Australia
km
0 100 200 300 400 500
deep basin
back-arc thrusting
subduction zone
N

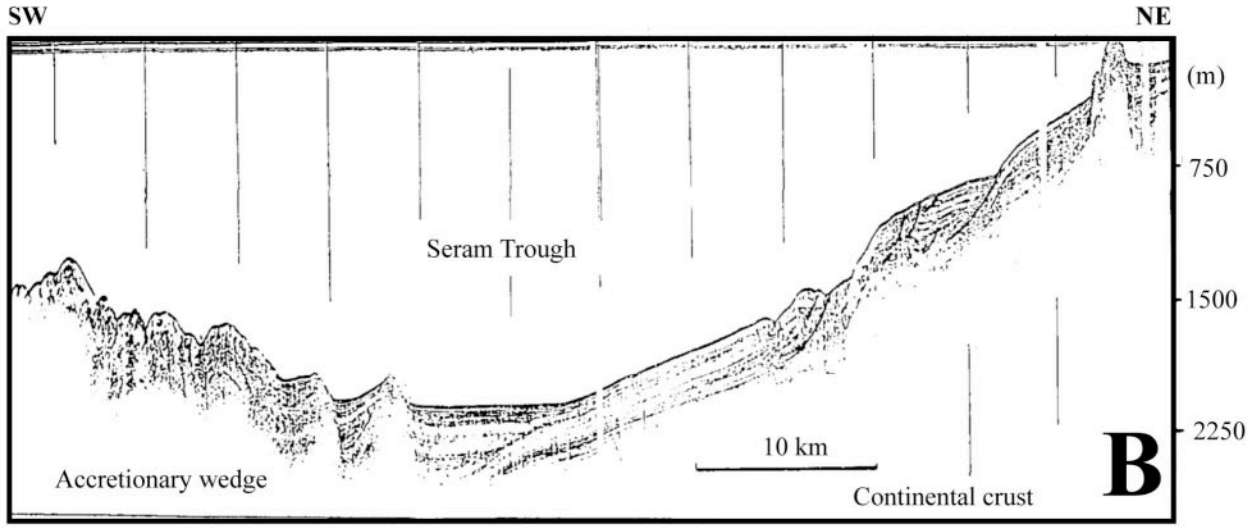
SW
NE
(m)
750
1500
2250
Seram Trough
10 km
Accretionary wedge
Continental crust
B

Figure 8.37 - A: The Banda Arc lies at the intersection of the Pacific, Eurasian and Indo-Australian plates. This map shows the position of the inner and outer Banda Arcs, the plates and their direction of movement relative to the Eurasian plate. Position of the seismic line shown in B is labeled. From Hamson (2004) after Hinschberger *et al.* (2001).

B: Single channel seismic line crossing the Seram Trough. Accretionary wedge and the colidin continental slabs are identified. Nonetheless the poor quality of data it is possible to slightly appreciate curved reflectors interpreted as potential gravity-induced movements characterizing the outer trough regions (*i.e.* tilted foreland). Form Nietzche (1989).

9. RESULTS AND DISCUSSION

The data presented in this work has been utilized to solve 3 main objectives:

1. The first one is that to give a better characterization of the Specchio Unit (R2) sedimentary chaotic complex, highlighting the structural and stratigraphic characteristics of large-scale MTDs (comparable to those occurring on modern continental margins) developed in structurally-controlled and confined basins.
2. The second objective is that to better define the general morphology of the local Ranzano Unit depocenters where the R2 Unit occurs (*i.e.* analyzed outliers), through the integrated analysis of its relationships with the substrate and the depositional style of the background sediments.
3. The third objective regards the possible contribution for a general palaeogeographic reconstruction of the Ranzano unit basin system through the integration of the palaeo-transport directions and sedimentary material provenance data from the R2 unit, inferred palaeotopography and despositional styles of R1-R3 units depocenters and the classically accepted interpretations from the inherent literature.

9.1 Kinematic models of emplacement for the R2 Specchio Unit

The R2 unit mass transport complex is thought to represent the depositional stacking of at least 3 (and possibly 5) mass transport deposits, roughly represented by the recognized internal subdivisions (see chap. 7), produced by older localized event(s) with transport direction toward the N-NE (recorded only in the Pessola Valley outlier; R2/a and R2/b subdivisions) and 2 (and possibly 3) younger, basin-wide events coming from an almost opposite direction, toward the S-SE, with the uppermost one(s) recognized in all the analyzed outliers (R2/c, R2/d and R2/e subdivisions).

These deposit are thought having been accumulated during a relatively short time, without clear evidence of intervening inter-bedded background sedimentation. Nonetheless, in place, some minor thin veneer of sediments (both hemipelagic and turbiditic) may have deposited within localized depressions on the upper uneven surface of each MTD, but the strong disturbance operated by subsequent mass transport events and early post-depositional rearrangement are likely to have remolded this drape, incorporating it in the over- and underlying deposits, almost completely masking the original features. The occurrence of strongly plastically deformed, usually m-sized fragments thin-bedded (and rarely thick-bedded) mudstone-sandstone single beds or

bedsets, roughly aligned along the inferred contact surfaces between sub-units seems to support this hypothesis.

These deposits show different internal associations of structures reflecting a confined flow-like kinematics, influenced by the structural control of the mini-basins margins and by the upper morphology of the preceding MTDs.

9.1.1 Matrix significance and blocky-flow deposits

All of these deposits are characterized by relatively strong development of matrix, which in some cases represents the major component of the entire units (see chap. 7). This significant amount of matrix forecasts strong overpressured conditions achieved by fast-moving events (*i.e.* catastrophic). This character seems also to be better developed in the upper S-directed units, which share longer run-out distances in respect to lower ones.

The internal organization of each recognized MTD, particularly R2/c and R2/d sub-units, allow their interpretation as products of some kind of bi-parted mass transport events characterized by clustering of multi-sized blocks (BDPs), carried on top of an association of separated minor blocks contained in an hyper-concentrated matrix phase (MDPs), showing slump-like structures and debris flow-like characters, respectively (fig. 9.1).

These units are herein defined as *blocky-flow* deposits, following what preliminarily hypothesized by Mutti *et al.* (2006), and the inferred generating mass transport process is thought to involve both coherent sliding (*i.e.* slump-like products) and a generalized flowage (*i.e.* debris flow-like products).

The inferred element-supporting mechanism for the blocky-flow process is thought to be achieved by the combined interaction of 2 main mechanisms: 1) the development of an upper coherent-like state portion (represented by clustering of BDPs) in response to the establishment of a gradient in the velocity profile of the sliding mass ("rigid plug" effect *sensu* Middelton and Hampton, 1972), passively transported over a lower liquidized-like state portion (represented by clustering of MDPs) and 2) a buoyancy effect caused by the overall less dense packing shared by still stratified blocks in respect to the denser state characterizing the enveloping hyper-concentrated matrix (fig. 9.2).

The high efficiency of the transport potential showed by these units is thought to be recorded by production and maintenance of overpressured conditions in the lowermost portions of the sliding body (*i.e.* overpressured basal carpet) trough the entrainment of water from both saturated seafloor sediments and surrounding environment, according to an hydro-planing process.

The overpressured conditions in the basal shear layer are thought to be maintained by the cohesive-like state of lower MDPs coupled with the coherent-like state of the upper BDPs, preventing the dissipation of fluid overpressure and thus enhancing slide mobility.

The upper R2/d, R2/e and the associated R3 basal sandstone layer, maintain their vertical organization in almost all the analyzed situations, conceptually resembling the internal subdivisions already proposed for other large-scale MTDs (*i.e.* slide/slump-debris flow-turbidite tri-partition; Johns *et al.*, 1981; Labaume *et al*., 1987; Kleverlaan, 1987), and thus, seems to share mutual genetic-evolutionary relationships.

These observations support what proposed by Mutti *et al.* (2006) about the blocky flow deposit in the conceptual evolution from slump to debris flow deposits, and thus representing a possible facies-tract of the broad mass transport facies continuum (fig. 9.3).

9.1.2 Confining effects on MTD emplacement

The R2 unit mass transport events are strongly influenced by the structurally confined nature of the depocenters and by the interaction with previously emplaced MTDs. The more direct evidences of such conditions recorded by the R2 unit components are expressed by: i) strong lateral thickness variations on short distances, with maximum values reached within the main depositional zones, due to mass transport blocking against depocentral margins, ii) generalized buckling and transpression of the slide mass margins, iii) structural overprinting of overridden MTDs and localized thickening of the overlying MTDs against the superficial asperities of the underlying ones, iv) generalized erosion of slide base and margins.

Moreover, the different deformational style shown by structure association characterizing longitudinal and transversal cross sections of the slide body is herein thought to develop in response to an overall constriction of the mass transport event.

As observed in few modern examples (*e.g.* Brunei slide; Gee *et al*., 2007), mass transport events generated in topographically complex settings tend to move following local slope gradients, translating in a parallel way to the mini-basins long axis, showing high angles (up to ~ 90°) with the main transport direction from the generating failure zone.

This forced confinement is thought to cause a generalized compression orthogonal to the main palaeo-direction, from margins to the axial part, resulting in a distinctive structure association characterized by double-vergent folds, box folds, sheath folds, pop up- and flower structure-like features, and low-angle shear zones sharing opposite shearing direction, also on the same surface. In associated longitudinal directions, these kinds of structures are less common, showing instead a general shearing sense in accord to the mean transport direction.

These structure associations are herein thought to represent a diagnostic character of MTDs emplaced within structurally confined settings (fig. 9.4).

Moreover, a general verticalization of structures (*i.e.* shear surfaces and fold axial planes) is observed close to the inferred intrabasinal high (*e.g.* previous MTD accumulation) and margins of the local depocenter.

Each MTD observed within the R2 unit share an irregular base, sometimes clearly cutting into the underlying sediments and showing a roughly scale-invariant flat-ramp geometry.

The erosive character of these events is also testified by the addiction of depocentral material ripped up from the seafloor during the last stage of movement and emplacement.

The bed erosion process operated by a MTE needs a significant coupling between the sliding mass and the overridden substratum. Given the supposed overpressured conditions necessary for the slide mass movement, this process unlikely develop during the transfer/transport phase, when the bulk of the acceleration is thought to be achieved.

Significant bed erosion is thus interpreted develop at slide margins and to characterize the early post-failure stages (*i.e.* first block detachment and seafloor scouring) and during early accumulation stages, when the arresting slide mass begins to transfer its momentum to the underlying seafloor. Generally speaking this latter process may occur where the sliding mass transfer path is characterized by local changes in the general slope gradient profile (*i.e.* topographic highs and lows, morphologic constrictions, and an overall base-of-slope settings) (fig. 9.5).

These aspects are quite well confirmed by geophysical observations on modern continental margins, where large groove-like striations have been observed to characterize the upper translational domain of submarine slides (Gee *et al.*, 1999) and erosive truncations have been recognized at slide base and margins (Diviacco *et al.*, 2006; Rebesco and Camerlenghi, 2008; Bull *et al.*, 2008). Some very high-resolution seismic lines collected in modern lacustrine environments evidenced remobilizations of seafloor sediments operated by relatively small-scale mass transport events, at the transitional zone between the lower slope and the basin plain (Schnellmann *et al.*, 2005).

Moreover, as confirmed by numerical and experimental modeling (Major, 2000), density-driven cohesive hyper-concentrated flows (mainly composed of granular slurry) are thought to maintain excess pore pressure also relatively long time after the deposition, and thus, the friction concentrated at the slide margins seem to be exert a major control on the slide mass arrest and emplacement. This fact seems to be quite well represented in the R2 unit, where the constituent MTDs share a relatively thick hyper-concentrated and liquefied lower portion (MDPs) and an upper

coherent one characterized by concentrations of blocks (BDPs), where the structures tend to be rearranged in a parallel way to the inferred basin margins.

9.2 Local basin characterization

The R2 unit vertical stacking, composed of more amalgamated MTDs, is more or less recognizable in every analyzed outlier.

In the following I will mainly discuss about the implications of this study on the basin analysis, focusing on the characterization of the Pessola Valley outlier, where the data regarding the R2 unit are integrated with a detailed stratigraphic characterization of the hosting sedimentary succession. These observations are then utilized to make some considerations on the other analyzed outliers.

9.2.1 Basin characteristics and MTDs significance

Regarding the Pessola Valley area, the lower N-NE-directed mass transport deposits are thought to represent the denudation/degradation complex (*sensu* Morley, 2009b) of a syn-sedimentary growing structure, which is recorded by the N-NW-verging tectonic stacking of the southeastern sector (*i.e.* Ricodalle thrust system).

Particularly the R2/a sub-unit, mainly composed of intrabasinal sediments from the depocentral zones of the R1 Unit, is interpreted as the first event, remobilizing the sediments uplifted by the growing structural high and deeply eroding the seafloor toward the northern sectors. The R2/b sub-unit, sharing the same lithologies of the underlying with the significant addiction of material from the MMP, BAI and AVV, is herein thought to represent a second event affecting the same failure zone, as confirmed by its erosive base on the underlying sub-units roughly ramping to the N-NE.

This latter event involves older epiligurian sediments (also belonging to the Ligurian substrate) and is therefore thought to develop through a basal rupture surface cutting down into the core of the structural high.

The brecciated nature and the mélange-like appearance of the Ligurian-derived material (*i.e.* patches of mud-breccias with indurated angular elements, autobrecciated and boudinated limestones already enclosed within a shaly matrix with evidences of primary scaly fabric), similar to the lithologies observed along the boundaries of the outlier, may suggest their provenance from diapiric structures rooted in the shaly chaotic complexes of the Ligurian substratum, which possibly affect the core zones of positive thrusting-related structures representing the mini-basin margins, as

hypothesized for some present-day examples coming from active continental margins (Deville *et al.*, 2003, 2006; Morley, 2009b).

Another possible explanation for the origin of these lower MTDs should be their close genetic relationship with an extrabasinal MTD (*i.e.* olistostrome) of Ligurian origin, which impacts from the south on a positive structure (Ricodalle thrust stacking), eroding its apex in accord to what observed by Gee *et al.* (2007) for the Brunei slide, and causing the development of intrabasinal counterparts (*i.e.* R2/a and R2/b), as proposed by Lucente and Pini (2003).

These MTDs are thought being progressive involved in the N-NW advancement of the thrust systems, as suggested by the complete lacking of the upper sub-units (*i.e.* R2/c, R2/d and R2/e sub-units) and the apparent overriding of the uppermost thrust sheets over the Rb/c sub-unit observable in the southeastern sectors.

Taking into account the necessary scaling differences, this situation seems well comparable with that classically proposed for mass wasting in collisional setting (Elter and Trevisan, 1973; Vollmer and Bosworth, 1984) and recently confirmed by analogical modeling of thrusting-related submarine landslides by Yamada *et al.* (2009).

The Ricodalle thrust stacking and the frontal accumulation of the lower MTDs are thought to have formed an intrabasinal high against which the subsequent MTEs (*i.e.* R2/c, R2/d and R2/e sub-units), directed in the opposite direction, have possibly "impacted".

These MTDs have likely temporarily filled the local depocenter, relatively leveling the topography, and thus favoring the wider development of the following uppermost S-SE-directed mass transport events (*i.e.* R2/d and R2/e sub-units).

The subsequent event (R2/c) crops out in the Mt. Barigazzo and Pessola Valley outliers, and it is characterized by generally S-directed palaeo-transport directions and materials mainly composed of fine-grained deposits of R1 unit, MMP, PZO and intermediate terms. This MTD is interpreted to be generated by a relatively far-traveled event, originated from the collapse of a intrabasinal positive structure covered by a relatively thin interval of R1 unit equivalents, localized to the N of its cropping out areas. Given its complete lacking and the significant erosional gap observed in the Mt. Roccone outlier (confirmed by observations also from the Mt. Piattello outlier), this sector should be considered as the original failure zone of this MTE.

The overlying R2/d and R2/e sub-units are interpreted as the products of a blocky- and a debris-flow process, respectively, closely associated and possibly representing two phases of the same generating event coming from NE sectors, close to the internal deformation front separating the apenninic Epiligurian succession from the one belonging to the TPB (*i.e.* Villavernia-Varzi-Ottone-Levanto tectonic lineament).

These subdivisions are recognizable in every analyzed outlier, testifying the basin-wide character of the generating event, and are composed of material coming from shallow-water (*i.e.* proximal) equivalent deposits of the PZO-R1 units, as confirmed by observations taken from blocks still bearing evidence of shelfal, fan delta, delta-slope and pro-delta environments.

Regarding the Pessola Valley outlier (and partly the Mt. Roccone one) the contact between the MMP-Ranzano Unit succession and the Ligurian substratum is quite well underlined by the discontinuous presence of mud-breccia lenticular bodies, sharing high-angle complex contacts with the MMP unit and the shale-rich Ligurian chaotic complexes. These units mark the boundary of the outlier, and are thought to roughly mimic the original margins of the depocenter.

Given the stratigraphic and sedimentological observations taken from the R1 and R3 unit, coupled with the recognition of lateral stratigraphic expansions (probably operated by growth strata-like structures and progressive unconformities development) (see below), and the lithologies and confining-related features of the R2 unit (see above), I have tentatively interpreted these basin-bounding structures as diapiric-induced structural highs, related to remobilization of Ligurian shale-rich chaotic complexes.

These kinds of structures are commonly observed in present-day analogue situations (Deville *et al.*, 2003; Yu and Huang, 2006; Morley *et al.*, 1998; Morley 2009a), and are mainly related to differential loading of susceptible lithologies through sedimentay overloading, shallow-level and gravity-related slope tectonics. Similar process may have take place ate the top the proto-apenninic submarine wedge during the time interval comprised between the Late Lutetian and the Late Oligocene regional tectonic phases (*i.e.* Ligurian Phase *Auctt.* and the continental collision/foreland flexure, respectively).

These structures affecting the Epiligurian succession (and particularly its base) are somehow related to deep-rooted Ligurian deformations, as the Mt. Dosso-Mt. Pareto-Mt. S. Antonio structure and the Mt. Sporno culmination (*i.e.* Vianino tectonic window), which are thought to be already active at the MMP-Ranzano Unit deposition time, separating the Pessola Valley depocenter from the Mt. Barigazzo and Pellegrino Parmense-Varano de'Melegari ones, respectively.

In the Enza Valley outlier, Ottria (2000) recognized at least 2 shallow-level NE-directed thrusting events affecting the basal portion of the Epiligurian succession. Particularly this author suggest the origin of a first Lower Oligocene event as related to the incipient emplacement of the Ligurian Units over the innermost Subligurian Units, which complete closure took place during a Late Oligocene thrusting event (*i.e.* continental collision).

These deformations have been instead attributed by Costa and Frati (1995) to a post-oligocenic reactivation of distensive structures, achieved during a progressive (and transitive?)

extensional regime, as recognized in the more internal sectors by Artoni *et al.* (1992, 2006). Moreover, some hypothesis regarding possible gravity tectonics contributions to the inner Northern Apennine development was anticipated by Page (1963).

Summarizing all of these observations, the possibly emerging framework is that of a complex episutural basin system, roughly detached from the original substratum along a shale-rich sole, and involved in a NE-directed large-scale gravity-induced slope tectonics, with generalized extension in the inner sectors and an overall compression in the outer ones, as more or less observable in modern gravitationally deforming continental margins (*i.e.* Gulf of Cadìz, Nigeria, Gulf of Mexico).

9.2.2 Hosting sedimentary successions depositional style

Stratigraphic and sedimentologic features of the R1 and, subordinately, R3 units' successions of the Pessola Valley outlier confirm the confining nature of this mini-basin, as already suggest by Ghibaudo and Mutti (1973), and Mutti *et al.* (1994). The most evident characteristics of a structurally controlled depositional setting are shown by the R1:

- Outcrop- to cartographic-scale south-southeastern ward stratigraphic expansion of the sandstone bodies (*i.e.* growth strata-like structures), progressive unconformity development and related onlap relationships, highlighting the progressive uplift of the northern margin (*i.e.* Vianino tectonic window);
- Cartographic-scale evidence of stratigraphic closure of the R1 unit roughly toward the E and, subordinately, toward the W;
- Outcrop- to cartographic-scale evidence of an uplifting structure affecting the southeastern sector (*i.e.* Ricodalle thrust system);
- Lenticular, channelized-like appearance and generalized evidences of bypass, flow blocking effects and compensation cycles shared by the R1 coarse-grained deposits;
- Sedimentologic evidence of discrepancies between paleao-current directions of the primary flow (erosive bottom structures) in respect to those of the associated flow (traction plus fallout structures):
- Development of an high-frequency cyclicity (probably of climatic origin, complicated by tectonism) expressed by m-thick thinning-upward stacking patterns.

The overall vertical thinning- and fining-upward trend of these deposits seems to record a gradual healing of the depositional profile, abruptly interrupted by the R2 unit emplacement.

Consequently to the deposition of this mass transport complex (more than ~ 400 m of remolded sediments accumulated in a relatively short period of time), the overall depositional

profile of the depocenter suddenly shifts upward, causing a significant change in the depositional style and clastic provenance from R1 to R3 units.

Even if some confinement conditions were maintained (R2 unit emplacement-related, syn-depositional, isostatic uplift of the margins?; see Dykstra, 2005a, 2005b), the R3 unit show the following characteristics:

- Alternations of relatively laterally continuous lenticular to roughly tabular sandstone bodies;
- Fine-grained lithologies predominance;
- Overall confining effect-related features seem to be restricted in the lower portions of the succession (related to local asperities characterizing the upper surface of the R2 unit;
- Sedimentologic and stratigraphic evidences of morphologically-induced deceleration of the generating flows;
- Significant carbonate, plant fragment and fossiliferous content increasing;
- Widespread evidence of bioturbation;
- Development of an evident high-frequency cyclicity expressed by m-thick thickening-upward stacking patterns, clearly different from those shared by R1 unit ones, probably highlighting a significant fluvio-deltaic influence on the deposits;
- Diffused presence of reworked volcanoclastic-rich layers.

These observations support the interpretation of an overall forestepping-like trend of the depositional system, caused by the sudden depocentral infilling of the R2 unit, recorded by a abrupt shift from strongly-confined to weakly-confined conditions, and probably from relatively open-marine conditions toward more shallow-water, fluvial-influenced environments.

From a wider point of view, this kind of arrangement of the deposits and their vertical organization is similar to that observed in the infilling of some modern intra-slope mini-basins, especially those characterized by a direct clastic input (*e.g.* offshore SW Taiwan), with a basal convergent-base lapping portion (R1 unit type), a chaotic intermediate portion (R2 unit type) and an upper parallel-draping portion (R3 unit type) (see chap. 8).

Given the provenance directions, the stratigraphic closure of the R1 unit toward NE (with the R3 unit directly resting upon the MMP Unit), and the inferred relative position of distal and proximal domains from the external to the internal outliers alignment, respectively, the R3 unit seems to be fed, at least in part, from a source zone located roughly to the E, highlighting the likely presence of relatively extended emerging lands (capable to develop high-gradient alluvial and fan-delta systems), possibly located close to an unknown more external deformation front representing

the separation line with the Subligurian domain (see Carrapa *et al.*, 2004). The proximal character shared by R3 unit deposits in the external outlier alignment has been also documented by Bonazzi (1971) and Papani (1971), for the Enza Valley outlier.

9.3 Regional implications for the Epiligurian succession

The study of major components of the R2 unit is a useful tool for the characterization of the basin margins, because entire portions of laterally equivalent sedimentary successions have been preserved as blocks within the mass transport complex.

In a situation where only the main depocenters are cropping out, these blocks, which still contain primary signatures about the original depositional environment (*i.e.* sedimentary facies associations, ichnofacies, fossils, authigenic minerals, etc.), may give important information on the marginal contexts, presently being completely eroded away.

This, coupled with an estimation of the palaeo-transport directions and the characterization of the palaeo-morphology of the depocenters, allow some consideration on the whole basinal setting of the Ranzano unit.

The topmost subdivisions of the R2 unit (*i.e.* R2/c, and particularly, R2/d and R2/e) are characterized by a basin-wide character and by relatively well-defined stratigraphic relationships, thus giving important information on the regional depositional setting.

The vertical arrangement shared by these sub-units, expressed by the stacking of relatively more distal elements at the base and proximal ones to the top, coupled with the upward shifting from poorly lithified components to completely un-lithified ones and the overall increasing in plant fragments, is thought to represent possible evidences of a slope failure developed in a retrogressive-like way, cutting back from upper-slope/shelf-break settings to more shallow-water environments, possibly close to the coastline.

Integrating the presented observations with that classically proposed in the concerning literature (particularly Principi and Treves 1984; Castellarin *et al.*, 1992; Mutti *et al*., 1995; Martelli *et al.*, 1998; Catanzariti *et al.*, 1997; Cibin *et al.*, 1998, 2003) the more reasonable depositional environment for the Epiligurian Ranzano Unit sedimentary succession should be interpreted as a complex basin developed in an above-grade slope (*sensu* Prather *et al.*, 1998) characterized by several connected intra-slope sub-basins, localized on the leading edge of the subaqueous proto-apenninic wedge and elongated parallel to 2 main internal and external arcuate deformation fronts.

The internal deformation front can be roughly traced across the Villavernia-Varzi-Ottone Levanto Tectonic Lineament, which surface expression could be represented by some kind of

positive structure characterized by a shelf-break environment, separating eastern TPB shallow-water deposits from more open marine deposits of the Apenninic Epiligurian intermediate domain.

The external deformation front should be interpreted as the frontal ramping of the basal *décollement* of the translating Ligurian accretionary wedge. The supposed surface expression of this thrust system could be an arcuate positive structure (possibly emerging from sea surface; Carrapa *et al.*, 2004) separating Epiligurian and Subligurian domains.

The relationships with the latter domain are evidenced by the presence of andesitic volcanoclastic detritus in the R3 unit for its entire areal extension (*i.e.* Varano de' Melegari unit; Cibin *et al.*, 1998; Martelli *et al.*, 1998), and are here confirmed also in the measured R3 unit stratigraphic logs collected in the Pessola Valley outlier (see chap. 4) (fig. 9.6).

9.4 List of figures

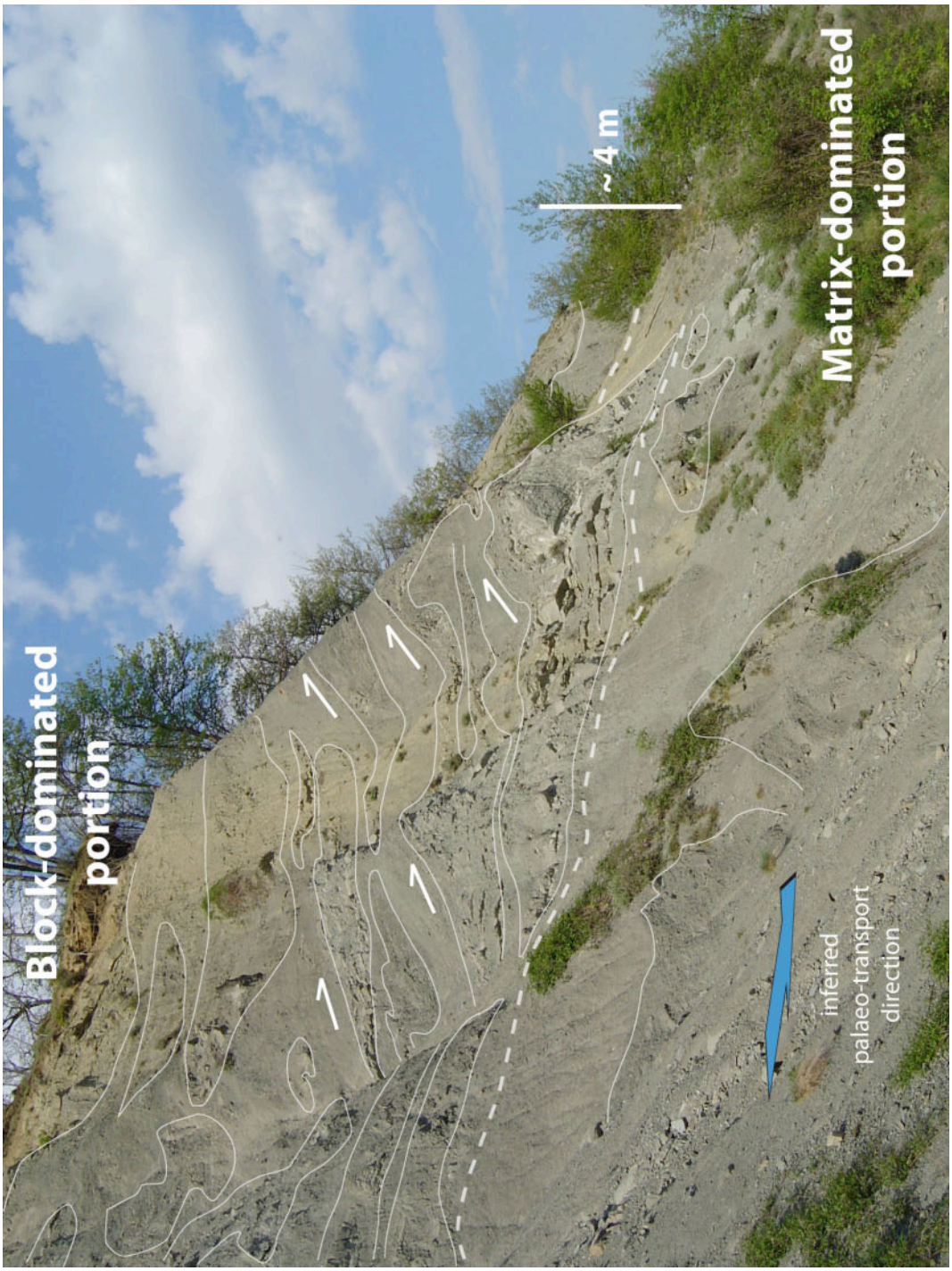

Figure 9.1 - Outcrop example of the lower part of the R2/c sub-unit in the Tintori section (for location see attached Panels n. 1 and n. 2). Here it is possible to clearly observe the distinctive internal bi-partition thought to characterize (in more or less evident way) each Specchio Unit R2 component deposits. This bi-partition is mainly due to the development of an upper block-dominated portion (BDP), characterized by slump-like facies (*i.e.* transport driven by shear surfaces) and a lower matrix-dominated portion (MDP), characterized by debris flow-like facies (*i.e.* transport driven by generalized flowage). Note that elements within the BDP are virtually separated by proto-matrix-rich portions, roughly identifying shear zones (IBTs). Such units are herein termed as blocky flow deposits, following what proposed by Mutti *et al.* (2006). Still recognizable blocks, inferred shear surfaces and indicative limit between BDP and MDP (white dashed line), are labeled.

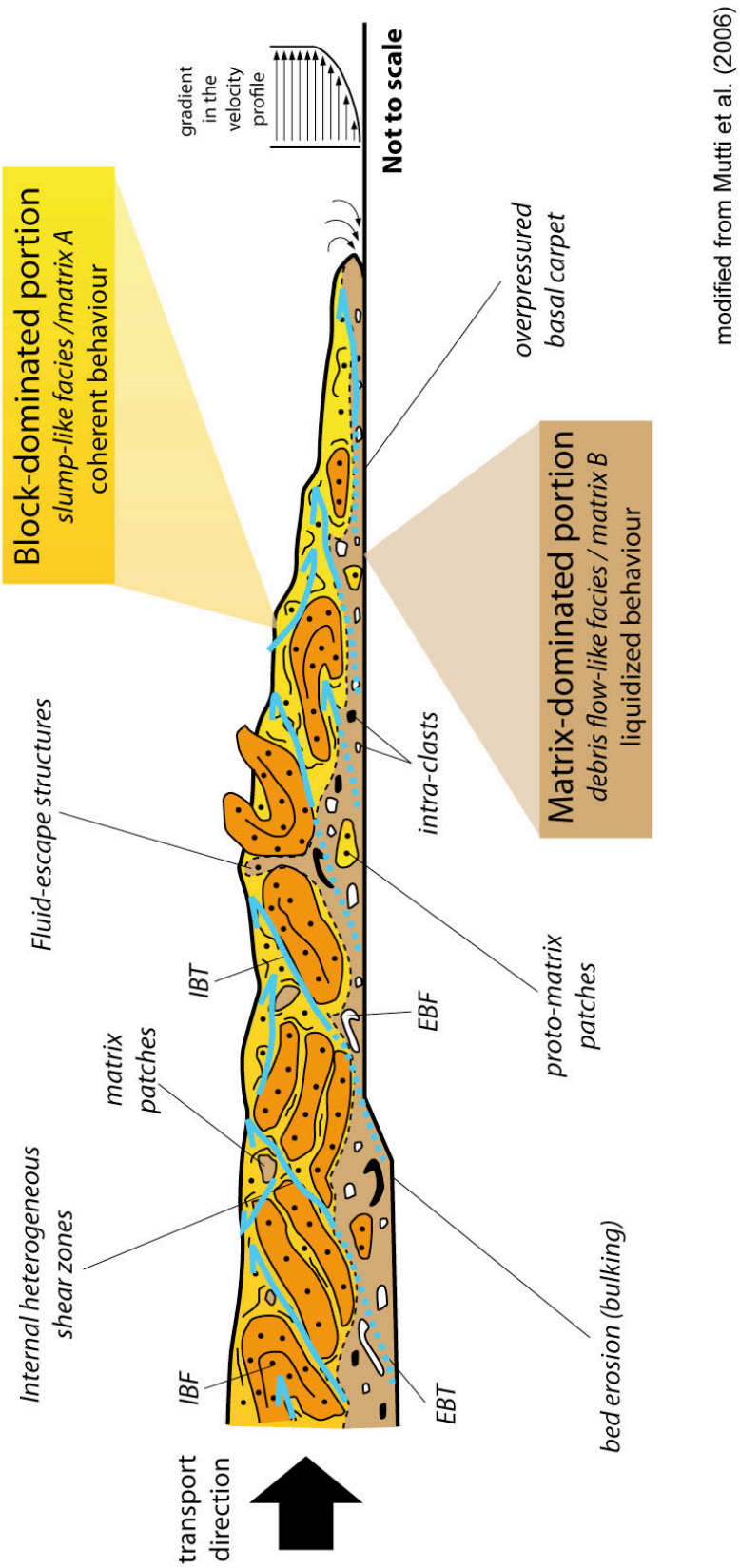

Figure 9.2 - Conceptual, schematic cartoon showing the main features of a blocky flow-type deposit (modified from Mutti *et al.*, 2006).

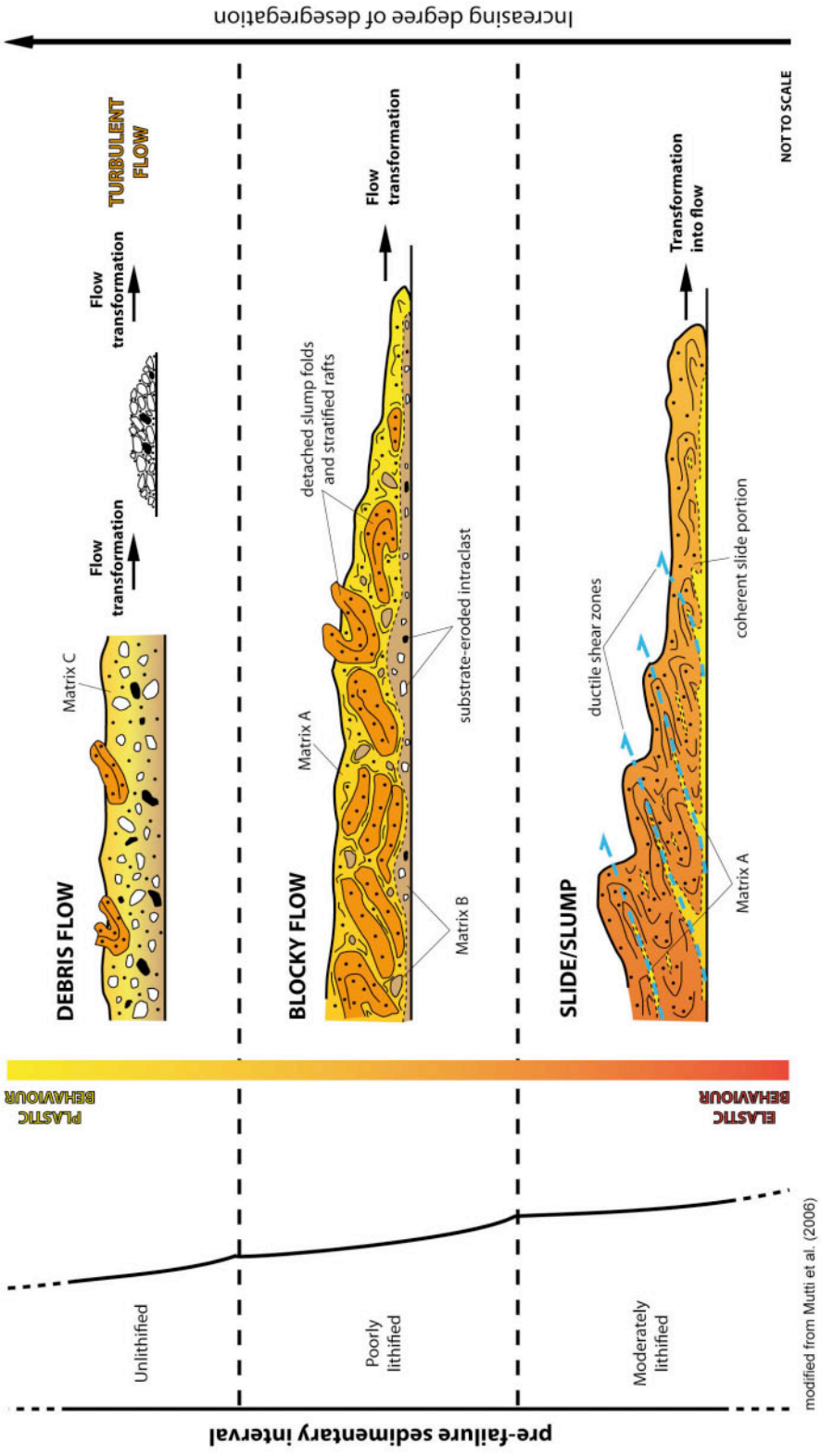

Figure 9.3 - Conceptual evolutionary scheme showing the possible relationships between slump, blocky flow and debris flow deposits (modified from Mutti *et al.*, 2006). In this scheme focuses on the structures, rheologic behaviour and disruption degree. In the left side is tentatively represented the possible linkage between the deposits and the lithification degree of the original (pre-failure) statigraphic succession.

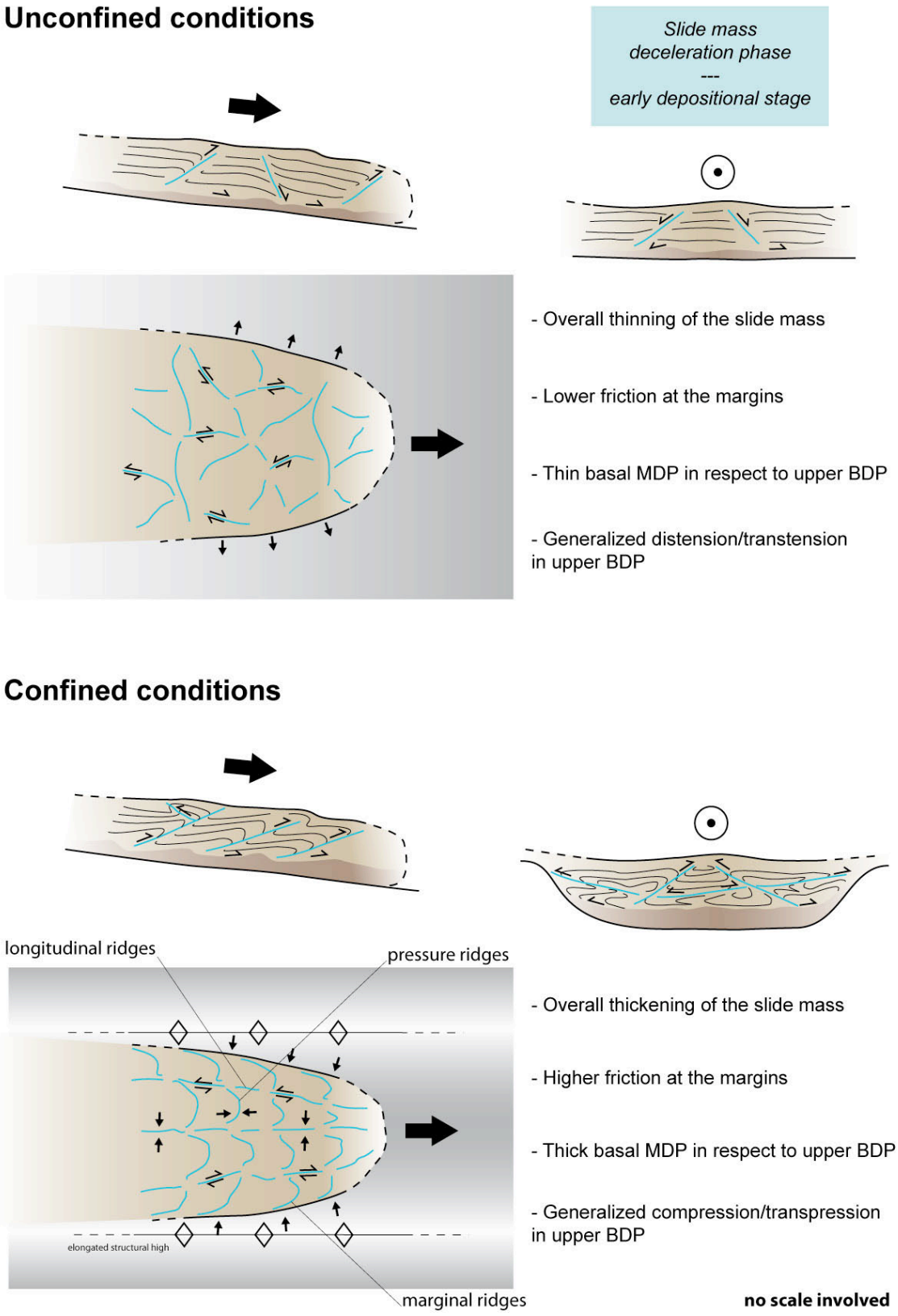

Figure 9.4 - Conceptual, highly simplified schemes showing the possible striking differences occurring between MTDs developed in confined and unconfined depositional contexts. These schemes, thought for blocky flow-type slides, are referred to the early emplacement stages, when the slide mass begins to decelerate, progressively coming to arrest. These two illustrated conditions are intended to define ideal end-members a continuum identified by different degrees of environmental confinement.

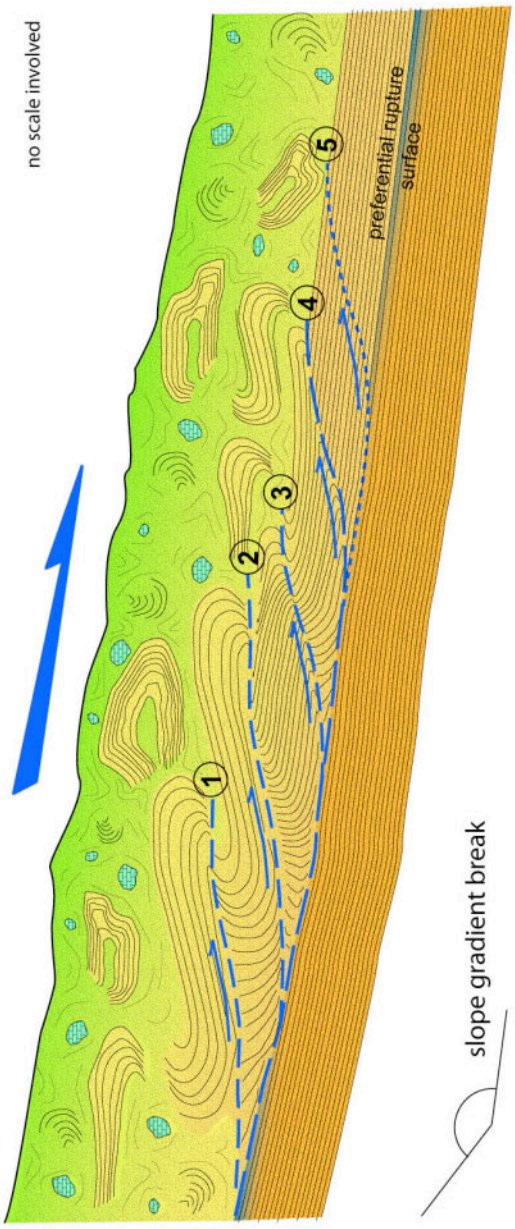

Figure 9.5 - Conceptual scheme illustrating the possible process of bed erosion (bulking) developed at the base of an overriding slide mass, through the progressive detachment of seafloor sediments along a preferential rupture surface. This kind of process is thought to develop consequently to a strong coupling between the slide mass and the overridden substratum, with a downward transfer of the landslide momentum. Such conditions are thought to be achieved where breaks in the slope gradient are likely to occur, as in the cases of incoming frontal obstacles (*e.g.* slide impacting on atopographic highs) and/or general base-of-slope settings. Morphologic constrictions may cause similar effects on slide margins, and the inferred consequent thickening of the slide body, the enhanced flow velocity, and the forced stopping may induce significant transfer of momentum from the slide body to the overridden seafloor.

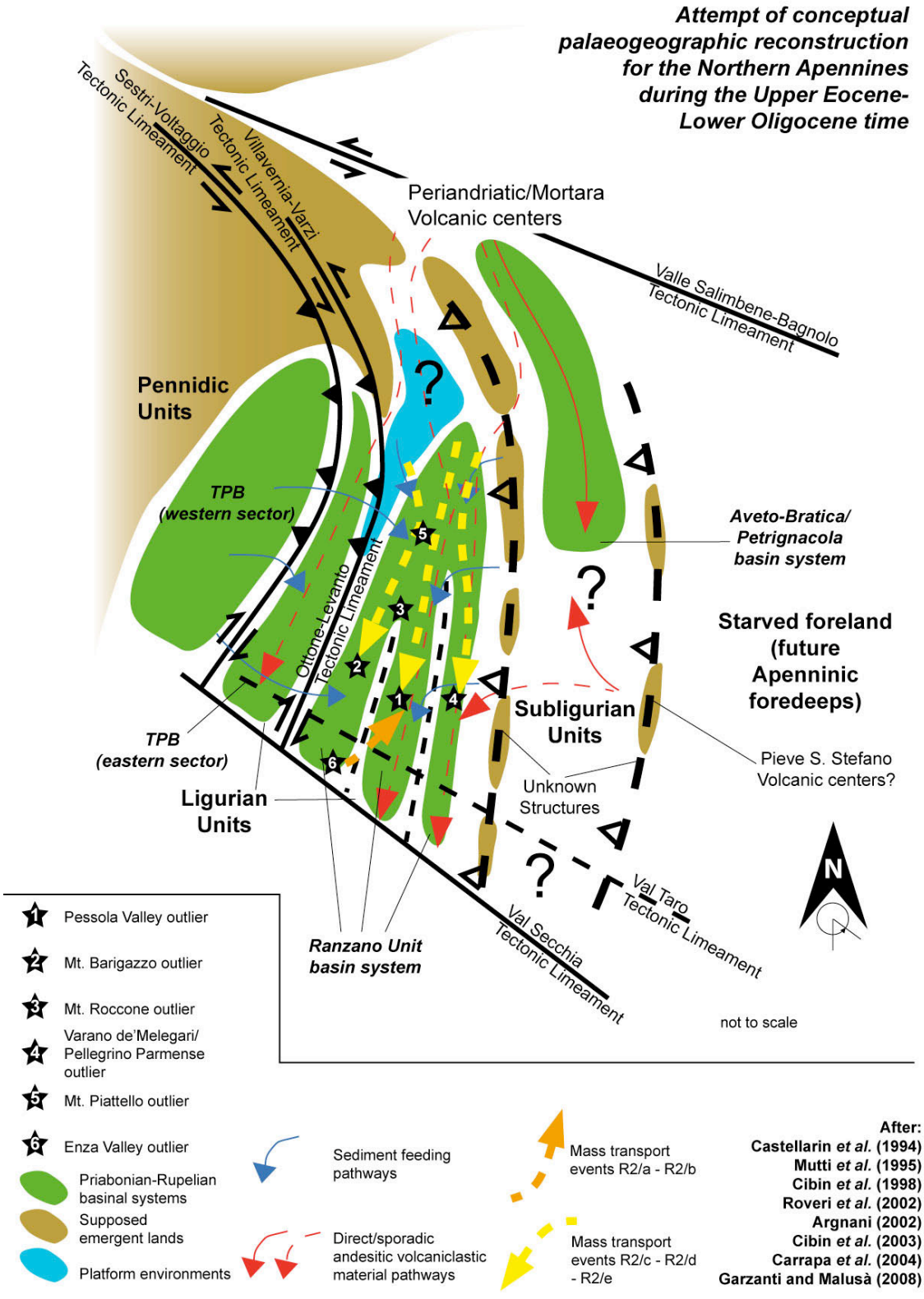

Figure 9.6 - Conceptual palaeo-geographic scheme tentatively proposed for the Northern Apennines accretionary system during the deposition of the Monte Piano-Ranzano units' sedimentary succession (upper Priabonian-lower Rupelian). This cartoon comes after a compilation of the so far accepted hypothesis available from the literature (list of references is shown in the figure explanation, in the lower-left side).

10. CONCLUSIONS

Confined intra-slope mini-basin systems (*i.e.* above-grade profile of the slope) are likely to be a typical emplacement setting for MTDs occurring on top of a deforming submarine accretionary wedge, which are so far poorly represented in the modern geophysical data set (apart some notable exceptions), mainly due to the few occurrence of present-day examples of similar geodynamic situations, and the high complex internal architecture of the tectonic prism complicating seismic interpretations.

This field-based study may contribute in this way, helping to better understand the mode of development and emplacement processes of large-scale MTDs in a structurally-controlled setting, and their important role regarding basin analysis, from a local to regional point of view, as previously done for relatively more "quiet" basin plain contexts.

The upper Priabonian-early Rupelian Ranzano Unit of the Epiligurian succession, cropping out in the eastern side of the Northern Apennines represents a perfect example of syn-orogenic siliciclastic infilling of an intra-slope mini-basin system.

These structurally confined mini-basins were located above the deforming Ligurian oceanic accretionary prism during its tectonic transport roughly toward the eastern sectors, following the complex continental convergence between African (Adria) and European plates, in a time interval comprised between the latest stages of the Alpine orogenesis and the inflection of the Apenninic foreland.

The analyzed Specchio Unit (R2) is a mass transport complex, hosted in the middle-basal part of the Ranzano Unit, with an estimated areal extent of ~ 1.500 km^2 and an average thickness of ~ 100 m. This MTC is generated by the rapid accumulation of at least 3 mass transport deposits: 1) a basal one(s) coming from the southern sectors, of mixed extra- and intrabasinal composition, originated from shallow-tectonic positive structures close to the depocentral areas), 2) a middle one coming from the northern sectors, of mainly intrabasinal composition, originated from structural highs located in a relatively distal position from the main depocenters, and 3) an upper one(s) coming from northern sectors, composed of shallow-water related sediments failed from the basin margins, in proximal position in respect to the inferred feeding areas (*i.e.* coastal areas).

The deposition of the R2 Unit took place in a relatively short period of time, accumulating in some places over 400 m of remolded sediments. The emplacement of this MTC is thought to have contributed, enhancing effects of other controlling factors (*i.e.* tectonic and eustatic), to a sudden upward shift and a relative leveling of the depositional profile, and the subsequent paleao-environmental change of these mini-basins from open-marine to fluvial-influenced conditions, as

confirmed by the different depositional styles of the lower- (Pessola unit R1) and upper- (M. Roccone unit R3) portion of the hosting Ranzano Unit sedimentary succession.

Definitively, the Specchio unit R2 accumulation is thought to represent the rapid sedimentary response to a general rearrangement of the source-depositional system, operated by the synergic effect of an active syn-sedimentary tectonism and a eustatic level fall, possibly acting together from the Early Oligocene.

The tectonic contribution is expressed by the parossistic activation/re-activation (in transpressive/transtensive regime?) of regional structures, as the Villavernia-Varzi-Ottone-Levanto tectonic lineament (*i.e.* Antola tectonic stuctureal high of Mutti *et al.*, 1995), and the likely consequent enucleation of Ligurian-related features as the Mt. Dosso-Mt. Pareto-Mt. S. Antonio and Vianino tectonic structures, thought to be indirectly responsible for the generation of intrabasinal highs affecting the Ranzano unit mini-basins system. The presence of an active calcalkaline volcanism, even if relatively distant, and shallow-level syn-sedimentary extensional and compressional (gravity-driven?) regimes, may support these interpreations.

As already evidenced by Catanzariti *et al.* (1997), these geodynamic context evolved in concomitance with the Eocene-Oligocene major climatic shift (*i.e.* Oi-1 event; Miller *et al.*, 1987; 1991; Zachos *et al.*, 1996), recording the passage from "green-house" to "ice-house" global conditions. This event is thought to be caused by the first enucleation of the circum-Antarctic oceanic circulation and the consequent growth of its land-based ice cover, resulting in a generalized, very rapid sea-level fall (Kominz *et al.*, 1998) and an increasing of climate-related erosion of the relieves (Séranne, 1999). This early Oligocene glaciation has been recently attributed to positive climatic feedbacks, synergically forced by exogenic factors (*i.e.* Late Eocene bolide impacts; Farley *et al.*, 1998; Dalai *et al.*, 2006).

Given these consideration, and underlining the "auto-cyclic" character of the Specchio unit R2 components emplacement (*i.e.* each event may contribute in the generation of the following one), inferred triggering mechanisms (apart from the classical seismic-shock contribution) should be attributed to the combined effect of: 1) sedimentary overloading (*i.e.* enhanced fluvial discharge), 2) tectonically-related progressive slope oversteepening, and 3) severe climatic events (*i.e.* flood-related failures and/or storm-wave cyclic loading). Although a generalized and rapid sea-level fall may suggest the gas hydrates dissociation as one of the main possible triggers, the shift toward a cold climate increase their stability field in the sedimentary column, acting in some kind of negative feedback relationship.

The present-day "active" continental margin settings are characterized by the generalized occurrence of several recurrent small-scale mass transport deposits, mainly developed close to the main deformational front (*i.e.* at the toe of the accretionary prism).

The inferred small size and low mobility of such MTDs have been classically taken as proofs of relatively low-risk events in term of geohazards (*i.e.* low tsunamigenic potential).

These interpretations are quite in contrast with the herein presented observations under 2 main aspects: 1) the amount of remobilized material and 2) the catastrophic character of the event.

The largest MTD recognized within the R2 unit is represented by the R2/d subdivision, showing an overall volume of ~ 75 km^3, calculated in a conservative way taking into account the mean distances among cropping out areas and its average thickness. By size and areal extent, this unit can be compared to those observable in present-day continental margins, and thus can be defined as a large-scale MTD.

These MTDs are thought to originate from intrabasinal highs and marginal shallow-water settings bordering mini-basins depocenters, in more internal portions respecting to the main deformation front of the accretionary wedge, where the vast majority of modern MTD have been observed to occur.

Another main objective of this work is that to expand the concept of blocky flow deposit proposed by Mutti *et al.* (2006), evidencing the role of mass transport-related soft sediment deformation in the some possible from slump to debris-flow deposits. The R2 Unit MTDs share the common occurrence of blocky flow-related sedimentary facies, with the generalized presence of significant amount of fine-grained unsorted matrix, thought to record overpressured conditions, and interpreted as evidence of catastrophic mass transport mechanisms.

This task has been also useful for putting in light the different processes acting inside a sliding mass emplaced within tectonically-controlled confined settings, in respect to those developed in virtually unconfined settings (*e.g.* foredeep basin plain), evidencing constriction- and forced blocking-related structures and their characteristics.

All of these considerations highlight the infrequent punctual occurrence of large-scale and fast-moving mass transport events even in convergent/collisional margin settings. These events are not only confined to the base of slope (*i.e.* toe of the accretionary wedge), but may characterize the upper- and middle-slope portions, also possibly involving near-shore areas.

Given the amount of involved material, the relatively high run-out distance and closely localized occurrence of such deposits within the sedimentary record testifies the infrequent and high-magnitude character of the generating events, probably developed by more controlling factors acting together. Indeed, the Ranzano Unit, and particularly, the R2 unit emplacement correspond to

a particular time interval of the Northern Apennine evolution, characterized by several concurrent events, essentially controlled by long-termed tectonic and climatic factors: the final structuration of proto-apenninic wedge and the incipient continental collision, and the Eocene-Oligocene "green-house" to "ice-house" passage (*i.e.* Oi-1 event; Miller *et al.*, 1991; Zachos *et al.*, 1996), respectively.

In conclusion, it is possible to suggest that this kind of wide-ranged, integrated field-based approach to the study of MTDs is extremely useful to solve many of the interpretative problems about submarine landslide deposits, especially when coupled with multidisciplinary observations considering the whole depositional environment, from the regional to the local point of view.

Acknowledgments

I am deeply indebted with the following person: my 1st tutor, Prof. **Emiliano Mutti**, for the given opportunities and teachings, both in geology and life *at whole*; my 2nd tutor, Prof.ssa **Elisabetta Costa**, for having played her role with honesty and comprehension; and my 3rd tutor Dr. **Roberto Tinterri**, for his precious help in every phase of the thesis work.

I want to express my gratitude to Prof. **Gian Andrea Pini**, co-tutor, *sensei* and friend, for having followed step-by-step my growth from the early beginning.

I want to sincerely thank all the following "brothers-in-arms" passed through this "geologic battlefield", for the mutual support and for having shared with me good and bad times, both inside the E55 room and on the field: **Josè Souto Oliveira, Pierre Muzzi Magalhaes, Silvia Prandin, Gustavo Basta, Davide Carè, Mario Zélic, Enrico Bonamini, Nicola Minelli** and **Simone Cau**.

To Dr. **Andrea Artoni** and Prof. **Paolo Vescovi** for their interest and the extremely useful suggestions, and Prof. **Renzo Valloni**, for the overall support and for having introduced me to the teaching experience.

Moreover, I want to thank Prof. **Yujihiro Ogawa** and Prof. **Ken-ichiro Hisada**, for their helpfulness and kindness during my brief stay in Tsukuba (Japan), and for having introduced me to the spectacular geology of the Boso Peninsula.

Last but not least, I want to express my sincere gratitude to Prof. **Angelo Camerlenghi** for having hosted me in his office in Barcelona during the autumn 2009, for the useful suggestions, the extremely stimulating discussions, and for having shown me the right way to do this job.

An overall thanks is due to the administrative and technical staff of the Earth Science Department of the University of Parma, as well as other PhD students and young researchers. Particularly to: Drs. **Andrea Comelli** and **Luca Barchi** for the rock samples preparation and the general help, **Omar Bartoli** for his help during microscopic analyses, and **Claudia Grillenzoni**, **Cristian Carli**, **Laura Pea**, **Vincenzo Santaniello**, **Rocco Gennari**, **Iago Nestola**, **Fabio Bonatti** and **Nicola Calda**, for smoking/coffee breaks and the good time. Moreover, I want to thank **Daniel Minisini**, for all the good suggestions.

Finally, an overall thanks to all the "their-own" extraordinary people that I have met during field-trips, congresses, courses and other particular situations.

The financial support for this PhD work comes entirely from research funds granted by Prof. Emiliano Mutti.

Credits

Morpho-bathymetric map slices and topographic profiles have been elaborated with **GeoMapApp**© freeware, developed by Lamont-Doherty Earth Observatory of Columbia University (available at http://www.geomapapp.org/). Global Multi-Resolution Topography (GMRT) data are from: Ryan, W. B. F., S.M. Carbotte, J. Coplan, S. O'Hara, A. Melkonian, R. Arko, R.A. Weissel, V. Ferrini, A. Goodwillie, F. Nitsche, J. Bonczkowski, and R. Zemsky (2010), Global Multi-Resolution Topography (GMRT) synthesis data set, *Geochem. Geophys. Geosyst.*, 10, Q03014, doi:10.1029/2008GC002332. Data doi: 10.1594/IEDA.0001000.

Stereoplots and rose diagrams have been compiled using the **Stereonet 6.3.3**© freeware, developed by Prof. R. W. Allmendinger of the Cornell University, New York (available at http://www.geo.cornell.edu/geology/faculty/RWA/).

Photomosaics has been elaborated with **Hugin**© freeware, developed by Pablo d'Angelo and coworkers (available at http://hugin.sourceforge.net/).

I want to express my sincere esteem to all the persons, whom with their no-profit work permit to others to do their own work.

REFERENCES

Aalto, K. R. (1981) - Multistage mélange formation in the Franciscan Complex, northernmost California - *Geology*, v. **9**, 602-607.

Abbate, E. & **Sagri, M.** (1982) - Le unità torbiditiche cretacee dell'Appennino settentrionale ed i margini continentali della Tetide - *Mem. Soc. Geol. It.*, v. **24**, 115-126.

Abbate, E., Bortolotti, V. & **Passerini, P.** (1970) - Olistostromes and olistoliths. - In. *Development of the Northern Apennines Geosyncline* (Ed. G. Sestini), *Sed. Geol.,* v. **4**, 521-557.

Abbate, E., Bortolotti, V. & **Sagri, M.** (1981) – Olistostromes in the Oligocene Macigno Formation (Florence area), Introduction: An approach to olistostrome interpretation – In Ricci Lucchi, F. (Ed.) *International Association of Sedimentologists, 2nd European Regional Meeting, Excursion N°5, Bologna, 1981*; *Excusion guidebook, Bologna, Tecnoprint*; 165-185.

Adeogba, A.A., McHargue, T.R. & **Graham, S.A.** (2005) - Transient fan architecture and depositional controls from near-surface 3-D seismic data, Niger Delta continental slope – *A.A.P.G. Bulletin*, v. **89**/5, 627 – 643.

Aiello, I.W., Hagstrum, J.T. & **Principi, G.** (2004) - Late Miocene remagnetization within the internal sector of the Northern Apennines, Italy – Tectonophysics, v. **383**, 1 – 14.

Alonso, J.L., Marcos, A. & **Suarez, A.** (2006) - Structure and organization of the Porma Mélange: progressive denudation of a submarine nappe toe by gravitational collapse. *American Journal of Science*, v. **306**, 32-65.

Alsop, G.I. & **Holdsworth, R.E.** (1999) - Vergence and facing patterns in large-scale sheath folds - *Journal of Structural Geology*, v. **21**, 1335-1349.

Alsop, G.I. & **Holdsworth, R.E.** (2004) - The geometry and topology of natural sheath folds: a new tool for structural analysis - Journal of Structural Geology, v. **26**, 1561–1589.

Amerman, R. (2004) - Distribution and character of soft-sediment structures within a paleo-submarine mass transport complex and implications for reservoir geometry prediction, Permian upper Cutoff Formation, west Texas. - *Summary of 2004 Research*, Research Partnership to Secure Energy for America.

Anelli, L. Gorza, M., Pieri, M. and **Riva, M.** (1994) - Subsurface well data in the Northern Apennines (Italy) - *Mem. Soc. Geol. It*., v. **48**/2, 461-471.

Anelli, M. (1938) – Note stratigrafiche e tettoniche sull'Appennino di Piacenza – *Atti Regia Accademia Scienze, Lettere e Arti di Modena, Serie 5*; v. **3**, 3-37.

Angelier, J., Lee, J.C., Chu, H.-T., Hu, J.-C., Lu, C.-Y., Chan, Y.-C., Lin, T.-J., Font, Y., Deffontaines B. & **Tsai, Y.-B.** (2001). - Le séisme de Chichi (1999) et sa place dans l'orogène de Taiwan - *C. R. Acad. Sci. Paris, série IIa, Earth Planet. Sci*., v. **333**/1, 5-21http://sites.google.com/site/jacquesangelier/plateconvergenceintaiwan.

Argnani, A. (2002) - The Northern Apennines and the kinematics of Africa-Europe convergente - *Boll. Soc. Geol. It., Spec. Publ.* n. **1**, 47-60.

Bader, A.G. & **Pubellier, M.** (2000) - Forearc deformation and tectonic significance of the ultramafic Molucca central ridge, Talaud islands (Indonesia) - *The Island Arc*, v. **9**, 653 – 663.

Bagnold, R.A. (1954) - Experiments on a gravity-free dispersion of large solid spheres in a Newtonian fluid under shear. - *Proc. of the Royal Soc. of London*, A, v. **225**, 49-63.

Bailleul, J., Robin, C., Chanier, F., Guillocheau, F.O., Field, B. & **Ferriére, J.** (2007) – Turbidite systems in the inner forearc domain of the Hikurangi convergent margin (New Zealand): new constraints on the development of

trench-slope basins - *Journal of Sedimentary Research*, v. **77**, 263–283. DOI: 10.2110/jsr.2007.028.

Bally, A.W. & **Snelson, S.** (1980) - Realms of subsidence - *In*: A.D. Miall (Ed.), *Facts and Principles of World Petroleum Occurrence*, *Memoir*, v. **6**, *Canadian Society of Petroleum Geologists* (1980), 9–94.

Bangs, N.L.B., Gulick, S.P.S. & **Shipley, T.H.** (2006) -Seamount subduction erosion in the Nankai Trough and its potential impact on the seismogenic zone – *Geology*, v. **34**, 701-704.doi: 10.1130/G22451.1.

Barber, J. & **Crow, M.J.** (2003) - An Evaluation of Plate Tectonic Models for the Development of Sumatra - *Gondwana Research*, International Association for Gondwana Research, Japan., v. **6**/1, 1- 28.

Barnes, P.M., Sutherland, **R.** & **Delteil, J.** (2005) - Strike-slip structure and sedimentary basins of the southern Alpine Fault, Fiordland, New Zealand - *GSA Bulletin*, v. **117**/3-4, 411–435. doi: 10.1130/B25458.1.

Beaudry, D. & **Moore, G.F.** (1981) - Seismic-stratigraphic framework of the forearc basin off central Sumatra, Sunda Arc - *Earth and Planetary Science Letters*, v. **54**/1, 17-28. doi:10.1016/0012-821X(81)90065-0.

Beavan, J., Tregoning, P., Bevis, M., Kato, T. & **Meertens, C.** (2002) - Motion and rigidity of the Pacific Plate and implications for plate boundary deformation. Journal of Geophysical Research - *Solid Earth*, v. **107**(B10), 2261.

Behrmann, J.H., Flemings, P.B., Cédric, M. J. & **IODP Expedition 308 Scientists** (2006) - Rapid Sedimentation, Overpressure, and Focused Fluid Flow, Gulf of Mexico Continental Margin - *Scientific Drilling*, v. **3**. doi:10.2204/iodp.sd.3.03.2006.

Bernini, M. & **Papani, G. (**2002) - Evoluzione plio-quaternaria ed analisi strutturale della Fossa tettonica della Lunigiana nord-occidentale (con Carta geologica alla scala 1:50.000) - *Bollettino Societa' Geologica Italiana.*

Bernini, M. & **Vescovi, P.** (2002) – La deformazione neogenica delle unità di avanfossa registrata nelle sovrastanti Liguridi della media Val Taro – *Atti del 3°Seminario sulla Cartografia Geologica, Regione Emilia-Romagna, Bologna.*

Bernini, M., **Vescovi, P.** & **Zanzucchi, G.** (1997) - Schema strutturale dell'Appennino Nord-Occidentale - *Acta Nat. Ateneo Parmense*; v. **33**, 43-54.

Bettelli, G. & **Panini, F.** (1987) - I *mélanges* dell'Appennino settentrionale dal T. Tresinaro al T. Sillaro. - *Mem. Soc. Geol. Ital*., **39**, 187-214.

Bettelli, G. & **Panini, F.** (1992) - Liguridi, mélanges e tettoniti nel Complesso caotico lungo la "Linea del Sillaro" (Appennino settentrionale, province di Firenze e Bologna) - *Mem. Descr. Carta Geol. d'It.*; **46**, 387-415.

Bettelli, G. & **Vannucchi, P.** (2003) - Structural style of the offscraped Ligurian oceanic sequences of the Northern Appennines: new hypotesis concerning the development of mélange block-in-matrix fabric - *Journ. of Struct. Geol.*; v. **25**, 371-388.

Bettelli, G., **Capitani, M.** & **Panini, F.** (1994) - The mesoscopic structures of a strongly deformed multilayered sequence: a hypothesis of the origin of the"block-in-matrix" fabric and the layer-parallel extension shown by the Ligurian dismembered formations of the Baganza Supergroup in the Reggio Emilia and Modena Appennines - *1st European congress on regional geological cartography and information systems, Bologna*; *Excursion Guidebook*, Post Congress Field Trip No.3.

Bettelli, G., **Capitani, M.** & **Panini, F.** (1996b) - Origine della struttura a "blocchi-in-pelite" e dell'estensione parallela alla stratificazione nelle formazioni smembrate liguri del Supergruppo del Baganza affiranti nel settore sudorientale dell'Appennino emiliano - *Accad. Naz. Sci. Lett. Arti di Modena, Miscellanea Geologica*; Collana di Studi **15**, 261-298.

Bettelli, G., **Capitani, M.**, **Panini, F.** & **Pizzolo, M.** (1996a) - Le rocce caotiche dell'Appennino emiliano: metodi sperimentali di rilevamento stratigrafico, esempi e nomenclatura - *Accad. Naz. Sci. Lett. Arti di Modena, Miscellanea Geologica*; Collana di Studi **15**, 189-220.

Biscontin, G., **Pestana, J.M.** & **Nadim, F.** (2004) - Seismic triggering of submarine slides in soft cohesive soil deposits - *Marine Geology*; v. **203**, 341-354.

Boccaletti, M., Coli, M., Decandia, F. *et alii* (1980) – Evoluzione dell'Appennino Settentrionale secondo un nuovo modello strutturale – *Mem. Soc. Geol. It.*, v. **21**, 359-374.

Bohannon, R.G. & **Gardner, J.V.** (2004) - Submarine landslides of San Pedro Escarpment, southwest of Long Beach, California - *Mar. Geol.*, v. **203**, 261–268.

Bohrmann, G., **Heeschen, K.**, **Jung, C.**, **Weirebe, W.**, **Baranov, B.**, **Catilleau, B.**, **Heath, R.**, **Hühnerbach, V.**, **Hart, M.**, **Masson, D.** & **Trumman, I.** (2002) - Widespread fluid expulsion along the seafloor of the Costa Rica convergent margin - *Terra Nova*; v. **14**, 69-79.

Bonazzi, U. (1971) – Le Arenarie di Ranzano: caratteristiche sedimentarie e analogie con altre arenarie paleogeniche emiliane – *Atti Soc. Nat. Mat. Modena*, v. **102**, 1-32.

Bonazzi, U. & **Fazzini, P.** (1979) - Le variazioni di facies nell'Oligo-Miocene semiautoctono del versante padano dell'Appennino Settentrionale - *Atti Soc. Nat. Mat. di Modena*, v. **104**, 285-308.

Boni, A. (1961) - Per la geologia dell'Appennino Settentrionale a W della linea La Spezia-Piacenza - *Atti Ist. Geol. Univ. Pavia,* v. **12**, 63-196.

Booth, J.S., O'Leary, D.W., Popenoe, P. & **Danforth, W.W.** (1993) - U.S. Atlantic continental slope landslides: their distribution, general attributes, and implications - In: Schwab, W.C., Lee, H.J., Twichell, D.C. (Eds.), *Submarine Landslides: Selected Studies in the U.S. EEZ*, USGS Bulletin, v. **2002**, 14–22.

Bradley, D. & **Hanson, L.** (1998) - Paleoslope Analysis of Slump Folds in the Devonian Flysch of Maine - *Journal of Geology*, v. **106**, 305–318.

Bradshaw, A.S., Tappin, D.R. & **Rugg, D.** (2009) – The kinematics of a debris avalanche on the Sumatra Margin – In: *Submarine Mass Movements and Their Consequences* (Eds. D.C. Mosher, R.C. Shipp, L. Moscardelli, J.D. Chaytor, C.D.P. Baxter, H.J. Lee, R. Urgeles), Advances in Natural and Technological Hazards Research, v. **28**, 117-126.

Braga, G. (1962) - Il Paleogene di Monte Roccone nell'Appennino di Piacenza – *Mem. Soc. Geol. It.*, v. **3**, 395 – 408.

Braga, G. (1965) - Geologia delle valli Nure e Ferino (Appennino piacentino) – *Atti 1st. Geol. Univ. Pavia*, v. **17**, 3-49.

Braga, G., Casnedi, R., Giametti, F., Marchetti, G. & **Zerbi, M.** (1975) - Elementi di granuliti basiche in livelli clastici associati a masse ofiolitiche ultrafemiche del versante appenninico padano - *Atti 1st. Geol. Univ. Pavia*, v. **25**, 89-105.

Brandon, M.T. (1989) - Deformational styles in a sequence of olistostromal mélanges, Pacific Rim Complex, western Vancouver Island, Canada - *Geological Society of America Bulletin*, v. **101**, 1520–1542. DOI: 10.1130/0016-7606(1989)101<1520:DSIASO>2.3.CO;2.

Brown, K. M. (1990) - The Nature and Hydrogeologic Significance of Mud Diapirs and Diatremes for Accretionary Systems - *J. Geophys. Res.*, v. **95**(B6), 8969–8982.

Brown, K.M. & **Behermann, J.** (1990) - Genesis and evolution of small-scale structures in the toe of the Barbados ridge accretionary wedge - In: Moore J.C., Mascle J., *et al.* (Eds.) *Proceedings of the Ocean Drilling Program, Scientific Results*, v. **110**, 229-244.

Bugge, T., Belderson, R.H. and **Kenyon, N.H.** (1988) - The Storegga slide - *Philosophical Transactions of the Royal*

Society, London, v. **325**, 357–388.

Bull, S., Cartwright, J. & Huuse, M. (2009) – A review of kinematic indicators from mass-transport complexes using 3Dseismic data - *Marine and Petroleum Geology*, v. **26**/7, 1132-1151.

Busby, C.J. & Ingersoll, R.V. (Eds.) (1995) – Tectonics of sedimentary basins – *Blackwell Science*, 580 pp..

Byrne, T. (1985) - Structural geology of mélange terranes in Ghost Rock Formation, Kodiak Islands, Alaska. - *in* Raymond, L.A., ed.; Mélange: Their nature, origin, and significance: *Geol. Soc. of America Special*; P. **198**, 21-51.

Callot, P., Odonne, F. & Sempere, T. (2008b) - Liquification and soft-sediment deformation in a limestone megabreccia: The Ayabacas giant collapse, Cretaceous, southern Peru - *Sedimentary Geology*, v. **212**, 49–69.

Callot, P., Sempere, T., Odonne, F. & Robert, E. (2008a) - Giant submarine collapse of a carbonate platform at the Turonian-Coniacian transition: The Ayabacas Formation, southern Peru - *Basin Research*, v. **20**, 333–357. doi: 10.1111/j.1365-2117.2008.00358.x.

Camerlenghi, A. and **Pini, G.A.** (2009) - Mud volcanoes, olistostromes and Argille scagliose in the Mediterranean region - *Sedimentology*

Camerlenghi, A., Cita, M.B., Della Vedova, B., Fusi, N., Mirabile, L. & Pellis, G. (1995) - Geophysical evidence of mud diapirism on the Mediterranean Ridge accretionary complex - Marine Geophysical Research, v. **17**, 115–141.

Camerlenghi, A., Urgeles, R. & Fantoni, L. (2009) – A database on submarine landslides of the Mediterranean Sea - In: Mosher, D.C., Shipp, C., Moscardelli, L., Chaytor, J., Baxter, C., Lee, H.J. & Urgeles, R. (Eds.) *Submarine Mass Movements and Their Consequences. Advances in Natural and Technological Hazard Research, Springer*, **28**, 491-501.

Camerlenghi, A., Urgeles, R., Ercilla, G. & Brückmann, W. (2007) - Scientific Ocean Drilling Behind the Assessment of Geo-Hazards from Submarine Slides - *Scientific Drilling*; v. **4**, 45-47. doi:10.2204/iodp.sd.4.14.2007

Campbell, C.V. (1967) – Lamina, laminaset, bed and bedset – *Sedimentology*, v. **8**, 7-26.

Canals, M., **Lastras, G.**, **Urgeles, R.**, **Casamor, J.L.**, **Mienert, J.**, **Cattaneo, A.**, **De Batist, M.**, **Haflidason, H.**, **Imbo, Y.**, **Laberg, J.S.**, **Locat, J.**, **Long, D.**, **Longva, O.**, **Masson, D.G.**, **Sultan, N.**, **Trincardi, F. & Bryn, P.** (2004) - Slope failure dynamics and impacts from seafloor and shallow sub-seafloor geophysical data: case studies from the COSTA project - *Marine Geology*; v. **213**, 9-72.

Carmignani, L. & Kligfield, R. (1990) – Crustal extension in the Northern Apennines: the transition from compression to extension in the Alpi Apuane core complex – *Tectonics*, v. **9**, 1275-1303.

Carrapa, B., Di Giulio, A. & Wijbrans, J. (2004) - The early stages of the Alpine collision: an image from the detrital thermochronology of Upper Eocene-Lower Oligocene sediments in the Alps-Apennines knot area - *Sedimentary Geology*, v. **171**, 181-203.

Carter, R.M. (1975) – A discussion and classification of mass-transport with particular application to grain-flow, slurry flow and fluxoturbidites – *Earth Science Reviews*; v. **11**, 145-177.

Castellarin, A., Cantelli, L.l., Fesce, A.M., Mercier, L., Picotti, V., Pini, G.A., Prosser, G. & Selli, L. (1992) - Alpine compressional tectonics in the southern Alps. Relationships with the N-Apennines – *Ann. Tectonic*, **VI**, 62-94.

Castellarin, A., **Pini, G.A.**, **Crestana, G. & Rabbi, E.** (1986) - Caratteri strutturali mesoscopici delle Argille Scagliose dell'Appennino bolognese - *Mem. di Scienze Geol.*; v. **38**, 459-477.

Catanzariti, R., Cerrina Feroni, A., Ottria, G. and **Vescovi, P.** (1999) – Lower Oligocene thrust-system in the epi-Ligurian succession: evidence from the Enza Valley (northern Apennines, Italy) - Geodinamica Acta (Paris), v. **12**/2, 81-96.

Catanzariti, R., Rio, D. & **Martelli, L.** (1997) - Late Eocene to Oligocene calcareous nannofossil biostratigraphy in Northern Apennines: the Ranzano Sandstone - *Mem. Sc. Geol. Univ. Padova*, vol. **49**, 207-253.

Cauchon-Voyer, G., Locat, J. & **St-Onge, G.** (2008) - Late-Quaternary morpho-sedimentology and submarine mass movements of the Betsiamites area, Lower St. Lawrence Estuary, Quebec, Canada – *Marine Geology*; v. **251**, 233-252.

Cauchon-Voyer, G., Locat, J. & **St-Onge, G.** (2008) - Late-Quaternary morpho-sedimentology and submarine mass movements of the Betsiamites area, Lower St. Lawrence Estuary, Quebec, Canada - *Marine Geology*, v. **251**, 233–252.

Cerrina Feroni, A., Ottria G. & **Ellero A.** (2004) - The Northern Apennine, Italy: geological structure and transpressive evolution - In Crescenti U., D'Offizi S., Merlino S., Sacchi L. (Eds.) *"Geology of Italy" Special Volume of the Italian Geological Society for the IGC 32 Florence 2004*, 15-32.

Chang, C.-P., Angelier, J. & **Huang, C.-Y.** (2000) - Origin and evolution of a me´ lange: the active plate boundary and suture zone of the Longitudinal Valley, Taiwan – *Tectonophysics*, v. **325**, 43–62.

Charlton, T.R. (2000) - Tertiary evolution of the Eastern Indonesia Collision Complex - *Journal of Asian Earth Sciences*, v. **18**, 603-631.

Chaytor, J.D., ten Brink, U.S., Solow, A.R. & **Andrews, B.D.** (2009) - Size distribution of submarine landslides along the U.S. Atlantic margin - *Marine Geology*, v. **264**, 16–27. doi: 10.1016/j.margeo.2008.08.007**.**

Chiang, C.S. & **Yu, H.S.** (2006) - Marine hyperpycnal flows in the Kaoping Canyon and Capbreton Canyon: comparisons between morphology and seismic facies **-** *Geophysical Research Abstracts*, v. **8**, 10081.

Chiu, J.K. & **Liu, C.S.** (2008) - Comparison of sedimentary processes on adjacent passive and active continental margins offshore of SW Taiwan based on echo character studies - *Basin Research*, v. **20**, 503–518. doi: 10.1111/j.1365-2117.2008.00388.x

Cibin, U. (1993) - Evoluzione composizionale delle areniti della Successione Epiligure eo-oligocenica (Appennino settentrionale) - *Giorn. di Geol*., **55** /1, 69-92.

Cibin, U., Di Giulio, A. & **Martelli, L.** (2003) - Oligocene-early Miocene tectonic evolution of the Northern Apennines (Northwestern Italy) traced through provenance of piggy-back basin fill successions - In: McCann T. & Saintot A., Eds., *Tracing tectonic deformation using the sedimentary record. Geol. Soc. London, Spec. Public.*, **208**, 269-287.

Cibin, U., Spadafora, E., Zuffa, G.G. & **Castellarin, A.** (2001) - Continental collision history from arenites of episutural basins in the Northern Apennines, Italy - *GSA Bull.*, vol. **113**/1, 4-19.

Cibin, U., Tateo, F., Catanzariti, R., Martelli, L. & **Rio, D.** (1998) - Composizione , origine ed età del vulcanismo andesitico oligocenico inferiore dell'Appennino Settentrionale: le intercalazioni vulcano-derivate nella formazione di Ranzano - *Boll. Soc. Geol. It.*, vol. **117**, 569-581.

Coleman, J.M. & **Prior, D.B.** (1988) - Mass wasting on continental margins - *Annu. Rev. Earth Planet. Sci.*; v. **16**, 101-119.

Coleman, J.M., Prior, D.B., Garrison, L.E. & **Lee, H.J.** (1988) - Slope failures in an area of high sedimentation rate: offshore Mississippi River delta - In: W.C. Schwab, H.J. Lee and D.C. Twichell (Eds.), *Submarine Landslides: Selected Studies in the U.S. Exclusive Economic Zone*, *US Geol. Surv. Bull.*, v. 2002, 79–91.

Collett, T.S., Riedel, M., Malone, M.J., & Expedition 311 Project Team (2005) – Cascadia margin gas hydrates - *IODP Sci. Prosp*., v. **311**. http://iodp.tamu.edu/publications/SP/311SP/311SP.PDF.

Collot, J-Y., Lewis, K. B., Lamarche, G. & Lallemand, S. E. (2001) - The giant Ruatoria debris avalanche on the northern Hikurangi Margin, New Zealand: result of oblique seamount subduction - *Journal of Geophysical Research*, v. **106**/9, 19271–19297.

Conti S. (2002) - Palaeogeographic implications and relations between tectonics and sedimentation in satellite basins (Northern Apennines): insights from Neogene Epiligurian arcs - *Boll. Soc. Geol. It., Spec. vol.* n. **1**, 353-364.

Costa, E. & Frati, G. (1995) – La tettonica post-oligocenica delle Unità Liguri e della successione Epiligure nella Media Val Ceno (prov. di Parma, Appennino Settentrionale) con carta geologico-strutturale 1:25.000 - *Atti Tic. Sc. Terra*; v. **39**, 31-53.

Costa, E. (1985) – Analisi delle strutture presenti nel "Tongriano" della media Val Taro e rapporti con quelle del substrato liguride – *Boll. Soc. Geol. It.*; v. **104**, 491-501.

Cowan, D.S. & Pini, G.A. (2001) - Disrupted and chaotic units - *in* Vai, G.B. & Martini, I.P., eds.; Anatomy of an Orogen: the Appennines and Adjacent Mediterranean Basins, *Kluwer Academic Publishers*; 165-176.

Cowan, D.S. (1985) - Structural styles in Mesozoic and Cenozoic mélanges in the Western Cordillera of North America - *Geol. Soc. of America Bulletin*; v. **96**, 451-462.

Coward, M.P. & Dietrich, D. (1989) – Alpine tectonics: an overview – *In*: M.P. Coward, D. Dietrich and R.G. Park (Eds.), *Alpine Tectonics, Geological Society of London*, 1-29.

Crandell, D.R., Miller, C.D., Christiansen, R.L., Glicken, H.X. & Newhall, C.G. (1984) - Catastrophic debris avalanche from ancestral Mount Shasta volcano, California. - In. *Geology of Upper Cretaceous Hornbrook Formation, Oregon and California* (Eds. T.H. Nilsen), *Soc. of Econ. Paleontol. and Mineral.*, Tulsa, Oklahoma, 197-201.

Cruden, D.M. & Varnes, D.J. (1996) - Landslides types and processes. - In. *Landslides investigation and mitigation, Spec. Rep.*, **247**, T.R.B., Natl. Res. Counc., **3**, Washington D.C., 36-75.

Curiale, J., Morelos, J., Lambiase, J. & Mueller, W. (2000) - Brunei Darussalam: Characteristics of selected petroleums and source rocks - *Organic Geochemistry*, v. **31**, 1475-1493.

Cyr, A.J. & Granger, D.E. (2008) – Dynamic equilibrium among erosion, river incision, and coastal uplift in the northern and central Apennines, Italy – *Geology*; vol. **36**/2, 103-106.

Dainelli, J. (1987) – Stratigrafia fisica e caratteristiche delle facies delle Arenarie di Ranzano della placca del M. Bargazzo (Parma) – *unpublished MSc thesis*, Università di Firenze.

Dalai, T.K., Ravizza, G.E. & Peucker-Ehrenbrink, B. (2006) –The Late Eocene $^{187}Os/^{188}Os$ excursion: chemostratigraphy, cosmic dust flux and the early Oligocene glaciation – *Earth and Planetary Science Letters*, v. **241**/1-2, 477-492.

Dallan Nardi, L. & Nardi, R. (1974) - Schema stratigrafico e strutturale dell'Appennino settentrionale - *Mem. Acc. Lunigianese "G. Capellini"*, v. **39**.

Davey, F.J. , Henyey, T., Holbrook, W.S., Okaya, D., Stern, T.A., Melhuish, A., Henry, S., Anderson, H., Eberhart-Phillips, D., McEvilly, T., Uhrhammer, R., Wu, F., Jiracek, G.R., Wannamaker, E.E., Caldwell, G. & Christensen, N. (1998) - Preliminary results from a geophysical study across a modern, continent-continent collisional plate boundary: the Southern Alps, New Zealand **-** *Tectonophysics*, **v. 28**, 221-235.

Davey, F.J., Hampton, M., Childs, J., Fisher, M.A., Lewis, K & Pettinga, J.R. (1986) – Structure of a growing accretionary prism, Hikurangi margin, New Zealand – *Geology*, v. **14**, 663-666.

De Blasio, F.V., Elverhøi, A., Engvik, L.E., Issler, D., Gauer, P. & Harbitz, C. (2006) - Understanding the high mobility of subaqueous debris flows – *Norwegian Journal of Geology*, vol. **86**, 275-284.

De Blasio, F.V., Elverhøi, A., Issler,D., Harbitz, C.B., Bryn, P. & Lien, R. (2005) - On the dynamics ofsubaqueous clay rich gravity mass flows: the giant Storegga slide, Norway - *Marine and Petroleum Geology*, v. **22**, 179-186.

DeMetz, C., Gordon, R.G., Argus, D.F. & Stein, S. (1990) - Current plate motions - *Geophysical Journal International* v. **101**, 425–478.

De Nardo, M.T., Iaccarino, S., Martelli, L., Tellini, C., Torelli, L. & Vernia, L. (1991) - Osservazioni sull'evoluzione del bacino satellite epiligure Vetto-Carpineti-Canossa (Appennino Settentrionale) - *Mem. descrittive della carta geologica d'Italia*, **XLVI**, 209-220.

Deville, E., Battani, A., Griboulard, R., Guerlais, S., Lallemant, S., Mascle, A., Prizhofer, A. & Schmitz, J. (2003) - Processes of Mud Volcanism in the Barbados-Trinidad Compressional System: New structural, Thermal and Geochemical Data - *Search and Discovery Article* #30017

Deville, E., Guerlais, S.H., Callec, Y., Griboulard, R., Huyghe, P, Lallemant, S., Mascle, A., Noble, M., Schmitz, J. & Caramba working group 2 (2006) - Liquefied vs stratified sediment mobilization processes: Insight from the South of the Barbados accretionary prism – *Tectonophysics*, v. **428**, 33 – 47.

Di Biase, D. (1994) – Stratigrafia fisica e analisi di facies della successione Monte Piano-Ranzano della Placca del M. Barigazzo - *unpublished MSc thesis*, *Università di Parma*.

Di Giulio, A. (1990) - Litostratigrafia e petrografia della successione eo-oligocenica del Bacino Terziario Ligure-Piemontese, nell'area compresa tra le valli Grue e Curone (Provincia di Alessandria, Italia Settentrionale) - *Boll. Soc. Geol. It.*, v. **109**/1, 279-298.

Di Giulio, A. (1991) – Late Eocene-Oligocene clastic deposition in Eastern Piedmont Tertiary Basin: sandstone petrography and tectono-stratigraphic evolution - *Atti Tic. Sc. Terra*, v. **34**, 21-41.

Di Giulio, A., Mancin, N. & Martelli, L. (2002) – Geohistory of the Ligurian orogenic wedge: first inferences from Epiligurian sediments - *Boll. Soc. Geol. It, Spec. vol.,* 375-384.

Díaz-del-Río, V., Somoza, L., Martínez-Frias, J., Mata, M.P., Delgado, A., Hernandez-Molina, F.J., Lunar, R., Martín-Rubí, J.A., Maestro, A., Fernández-Puga, M.C., León R., Llave E., Medialdea T. & Vázquez, J.T. (2003) - Vast fields of hydrocarbon-derived carbonate chimneys related to the accretionary wedge/olistostrome of the Gulf of Cádiz - *Marine Geology*, vol. **195**, 177-200.

Dickinson, W.R. (1995) – Forearc basins – In: *Tectonics of sedimentary basins* (Eds. C.J. Busby and R.V. Ingersoll), *Blackwell Science*, 221-261.

Dingle, R.V. (1977) - The anatomy of a large submarine slump on a sheared continental margin (southeast Africa) - *Journ. Geol. Soc. London*, **134**, 293-310.

Diviacco, P., Rebesco, M. & Camerlenghi, A. (2006) - Late Pliocene mega debris flow deposit and related fluid escapes identified on the Antarctic continental margin by seismic reflection data analysis - *Mar. Geophys. Res.*, v. **27**, 109–128.

Dott, Jr., R.H. (1963) - Dynamics of subaqueous gravity depositional processes - *A.A.P.G Bullettin*; v. **47**, 104-128.

Draganits, E., Schlaf, J., Grasemann, B. & Argles, T. (2008) - Giant submarine landslide grooves in the Neoproterozoic/Lower Cambrian Phe Formation, northwest Himalaya: Mechanisms of formation and palaeogeographic implications - *Sedimentary Geology*, v. **205**, 126–141.

Duperret, A., Bourgois, J., Lagabrielle, Y. & Suess, E. (1995) - Slope instabilities at an active continental margin: large scale polyphase submarine slides along the northern Peruvian margin, between 5"s and 6"s - *Marine*

Geology, v. **122**, 303-328.

Dykstra, M. (2005a) - Dynamics of Submarine Sediment Mass-Transport, from the Shelf to the Deep Sea – *Unpublished PhD thesis*, University of California. Available at: http://inside.mines.edu/~mdykstra/index_files/Page391.htm

Dykstra, M. (2005b) - Review of mass-transport: processes and products - *Online publication*. Available at: http://inside.mines.edu/~mdykstra/index_files/Page391.htm

Edgers, L. & **Karlsrud, K.** (1982) - Soil flows generated by submarine slides: case studies and consequences – In: Chryssostomidis, C. and Connor, J.J. (Eds.), *Proceedings of the Third International Conference on the Behaviour of Offshore Structures*, Hemisphere, Bristol, 425- 437.

Elliot, C.G. & **Williams, P.F.** (1988) - Sediment slump structures: a review of diagnostic criteria and application to an example from Newfoundland - *J. Struct. Geol.*, v. **10**, 171–182.

Elter, P. & **Marroni, M.** (1991) - Le Unità Liguri dell'Appennino Settentrionale: sintesi dei dati e nuove interpretazioni - *Mem. Descr. Carta Geol. d'It.*, **46**, 121-138.

Elter, P. & **Trevisan, L.** (1973) - Olistostromes in the tectonic evolution of the Northern Apennines - *in* De Jong, K.A. & Scholten, R., eds., *Gravity and Tectonics, New York*; *John Wiley and Sons*; 175-188.

Elter, P. (1973) – I lineamenti tettonici ed evolutivi dell'Appennino Settentrionale – In: *Moderne vedute sulla geologia dell'Appennino* (Ed. B. Accordi), *Quaderni Accademia Nazionale Lincei*, v. **183**, 97-108.

Elter, P. (1994) - Introduzione alla geologia dell'Appennino Ligure-Emiliano - *in Guide Geologiche_Regionali S.G.I., Appennino Ligure-Emiliano*; n. **6**, 17-24.

Elter, P., Catanzariti R., Ghiselli F., Marroni M., Molli G., Ottria G. & **Pandolfi, L.** (1999) – L'Unità Aveto (Appennino settentrionale): caratteristiche litostratigrafiche, biostratigrafia, petrografia delle areniti ed assetto strutturale - *Boll. Soc. Geol. It.*, vol. **118**, 41-63.

Elter, P., Grasso, M., Parotto, M. and **Vezzani, L.** (2003) - Structural setting of the Apennine–Maghrebian thrust belt - *Episodes*, v. **26**, 205–211.

Elverhøi, A., De Blasio, F.V., Butt, F.A., Issler, D., Harbitz, C., Engvik, L., Solheim, A. & **Marr, J.** (2002) - Submarine mass-wasting on glacially influenced continental slopes-processes and dynamics. In: J.A. Dowdeswell and C. Ó Cofaigh (Eds.), *Glacier-Influenced Sedimentation on High-Latitude Continental Margins*, Geological Society, London, U.K. Special Publication **203**, 73–87.

Elverhøi, A., Harbitz, C.B., Dimakis, P., Mohrig, D., Marr, J.G. & **Parker, G.** (2000) - On the dynamics of subaqueous debris flows – *Oceanography*, v. **13**/3, 109-117.

Elverhøi, A., Issler, **D., De Blasio, F. V., Ilstad**,**T., Harbitz**, **C. B.** & **Gauer**, **P.** (2005) - Emerging insights into the dynamics of submarine debris flows - *Natural Hazards and Earth System Sciences*, v. **5**, 633–648.

Embley, R.W. & **Jacobi, R.D.** (1977) - Distributions and morphology of large sediment slides and slumps on Atlantic continental margins - *Mar. Geotechnol.*, v. **2**, 205-228.

Embley, R.W. (1976) - New evidence for ocurrence of debris flow deposits in the deep sea – *Geology*, v. **4**, 371-374.

Eva, A., **Cattaneo, M.** & **Merlanti, F.** (1988) – Seimotectonics of the central segment of the Indonesian Arc – *Tectonophysics*, v. **146**, 241-259.

Evans, D., Harrison, Z., Shannon, P.M., Laberg, J.S., Nielsen, T., Ayers, S., Holmes, R., Hoult, R.J., Lindberg, B., Haflidason, H., Long, D., Kuijpers, A., Andersen, E.S. & **Bryn, P.** (2005) - Palaeoslides and other mass failures of Pliocene to Pleistocene age along the Atlantic continental margin of NW Europe - *Marine and Petroleum Geology*, v. **22**, 1131–1148.

Expedition 311 Scientists (2005) - Cascadia margin gas hydrates - *IODP Prel. Rept.*, v. **311**., doi:10:2204/ iodp.pr.311.2005.

Farley, K.A., Montanari, A., Shoemaker, E.M. & **Shoemaker, C.S.** (1998) – Geochemical evidence for a Comet Shower in the Late Eocene – *Science*, v. **280**, 1250-1253.

Farrell, S.G. (1984) - A dislocation model applied to *slump* structures, Ainsa Basin, South Central. Pyrenees – *Journ. of Struct. Geol*., v. **6**, 727–736.

Festa A., Pini G.A., Dilek Y., Codegone G., Vezzani L., Ghisetti F., Lucente C.C. & **Ogata, K.** (2009) - Peri-Adriatic melanges and their evolution in the Tethyan realm. *International Geology Review* , in press.

Finetti, I., Boccaletti, M., Bonini, M., Del Ben, A., Geletti, R., Pipan, M. & **Sani, F.** (2001) - Crustal section based on CROP seismic data across the North Tyrrhenian-Northern Apennines-Adriatic Sea - *Tectonophysics*, v. **343**, 135-163.

Fisher, M.A., Normark, W.R., Greene, H.J., Lee, H.J. & **Sliter, R.W.** (2005) - Geology and tsunamigenic potential of submarine landslides in Santa Barbara Channel, Southern California - *Marine Geology*, v. **224**/1-4, 1-22.

Flores, G. (1955) - Les résultats des études pour les recherches pétrolifères en Sicile: Discussion. - *Proc. 4th World Petr. Congr*., Carlo Colombo, Roma, sect. 1/A/2, 121-122

Flores, G. (1959) - Evidence of slump phenomena (olisthostromes) in areas of hydrocarbon exploration in Sicily. - *Proc. 5th World Petr. Congr*. Sect. 1, New York, 259-275.

Fornaciari, M. (1982) – Osservazioni litostratigrafiche sul margine sud-orientale della sinclinale Vetto-Carpineti (Reggio Emilia) – *Rend. Soc. Geol.It*., v. **5**, 117-118.

Fortuin, A.R , Roep, Th.B, Sumosusastro, P.A., van Weering, Tj.C.E. & **van der Werff, W.** (1992) - Slumping and sliding in Miocene and Recent developing arc basins, onshore and offshore Sumba (Indonesia) - *Marine Geology*, v. **108**/3-4, 345-363. doi:10.1016/0025-3227(92)90204-U.

Frey-Martinez, J., Cartwright, J. & **Hall, B.** (2005) – 3D seismic interpretation of slump complexes: examples from the continental margin of Israel – *Basin Research*; vol. **17**/1, 83-108.

Frey-Martinez, J., Cartwright, J. & **James, D.** (2006) – Frontally confined versus frontally emergent submarine landslides: a 3D seismic characterization – *Marine and Petroleum Geology*; vol. **23**, 585-604.

Fryer, G.J., Watts, P. & **Pratson, L.F**. (2004) - Source of the great tsunami of 1 April 1946: a landslide in the upper Aleutian forearc - Marine Geology, v. **203,** 201-218.

Furlong, K.P. & **Kamp, P.J.J.** (2009) - The lithospheric geodynamics of plate boundary transpression in New Zealand: Initiating and emplacing subduction along the Hikurangi margin, and the tectonic evolution of the Alpine Fault system – *Tectonophysics*, v. **474**, 449–462.

Gasperi, G., Gelati, R. & **Papani, G.** (1986) – Neogene evolution of the Northern Apennines on Po Valley side – *Giornale di Geologia*, v. **48**/1-2, 187-195.

Garcia, M.O., Sherman, S.B., Moore, G.F., Goll, R., Popova-Goll,I., Natland, J.H. & **Acton, G.** (2006) - Frequent landslides from Koolau Volcano: Results from ODP Hole 1223A - *Journal of Volcanology and Geothermal Research*, v. **151**, 251 – 268.

Gardner, J.V., Prior, D.B. & **Field, M.E.** (1999) - Humboldt Slide - a large shear-dominated retrogressive slope failure - *Marine Geology*, v. **154**/1, 323-338.

Garzanti, E. & **Malusà, M.** (2008) - The Oligocene Alps: Domal unroofing and drainage development during early orogenic growth - *Earth and Planetary Science Letters*, v. **268**, 487-500.

Gawthorpe, R.L. & **Clemmey, H.** (1985) - Geometry of submarine slides in the Bowland Basin (Dinantian) and their

relation to debris flows - *J. Geol. Soc. London*, v. **142**, 555-565.

Gazioglu, C., Yucel, Z.Y. & Dogan, E. (2005) - Morphological Features of Major Submarine Landslides of Marmara Sea Using Multibeam Data - *Journal of Coastal Research*, v. **21**/4, 664–673.

Gazzi, P. & Zuffa, G.G. (1970) - Le arenarie paleogeniche dell'Appennino emiliano - *Mineral. et Petrog. Acta*, v. **16**, 97-137.

Gee, M. J. R., Watts, A. B., Masson, D. G. & Mitchell, N. C. (2001) - Landslides and the evolution of El Hierro in the Canary islands - *Mar. Geol*., v. **177**, 271–294. (doi:10.1016/S0025-3227(01)00153-0)

Gee, M.J.R., Gawthorpe, R.L. & Friedmann, S.J. (2006) – Triggering and evolution of a giant submarine landslide, offshore Angola, revealed by 3D seismic stratigraphy and geomorphology – *Journ. of Sedimentary Research*; v. **76**, 9-19.

Gee, M.J.R., Gawthrope, R.L. & Friedmann, S.J. (2005) – Giant striations at the base of a submarine landslide – *Marine Geology*; v. **214**, 287-294.

Gee, M.J.R., Masson, D.G., Watts, A.B. and **Allen, P. A.** (1999) - The Saharan debris flow: An insight into the mechanics of long runout submarine debris flows - *Sedimentology*, v. **46**, 317–335. doi : 10. 1046/ j . 1365-3091.1999.00215.x.

Gee, M.J.R., Uy, H.S., Warren, J., Morley, C.K. & Lambiase, J.J. (2007) - The Brunei slide: A giant submarine landslide on the North West Borneo Margin revealed by 3D seismic data - *Marine Geology*; vol. **246**/1, 9-23.

Ghelardoni, R., Pieri, M. & Pirini, C. (1965) - Osservazioni stratigrafiche nell'area dei fogli 84 (Pontremoli) e 85 (Castelnuovo ne' Monti) - *Boll. Soc. Geol. It.,* v. **84**/6, 297-416.

Ghibaudo, G. & Mutti, E. (1973) - Facies ed interpretazione paleoambientale delle Arenarie di Ranzano nei dintorni di Specchio (Val Pessola, Appennino parmense) - *Mem. Soc. Geol. It.*, v. **12**, 251-265.

Goldfinger, C., Laverne, D., Kulm, L., McNeill, C. & Watts, P. (2000) - Super-scale Failure of the Southern Oregon Cascadia Margin - *Pure appl. geophys*., v. **157**, 1189 – 1226.

Greenly, E. (1919) - The Geology of Anglesey - *Geol. Survey of Great Britain*; M. **1**, 980 pp..

Haflidason, H., Lien, R., Sejrup, H.P., Forsberg, C. F. & Bryn, P. (2005) - The dating and morphometry of the Storegga slide - *Marine and Petroleum Geology*, v. **22**, 123-136.

Hall, R. & Wilson, M.E.J. (2000) - Neogene sutures in eastern Indonesia - *Journal of Asian Earth Sciences*, v. **18**, 781 – 808.

Hampton, M.A. (1972) - The role of subacqueous debris flow in generating turbidity currents - *J. Sedim. Petr*., vol. **42**, 775-793.

Hampton, M.A., **Lee, H.J. & Locat, J** (1996) - Submarine landslides - *Rewiews of Geophysics*; v. **34**/1, 33-59.

Harbitz, C. B. (1992) - Model simulations of tsunamis generated by the Storegga Slides - *Marine Geology*, v. **105**, 1-21.

Harbitz, C.B., Parker, G., Elverhoi, A., Marr, J.G., Mohrig, D. & Harff, P.A. (2003) - Hydroplaning of subaqueous debris flows and glide blocks: Analytical solutions and discussion - *Journal of Geophysical Research*, vol. **108**.

Harbury, N.A. & Kallagher, H.J. (1991) - The Sunda outer-arc ridge, North Sumatra, Indonesia - *Journal of Southeast Asian Earth Sciences*, v. **6**/3-4, 463-476. doi:10.1016/0743-9547(91)90088-F.

Harris, R. (2000) - Mélange genesis in the Banda Arc subduction-collision transition, Indonesia - *AAPG International Conference and Exhibition*, Bali, Indonesia, AAPG Search and Discovery Article #90913©2000.

Hasiotis, T., Papatheodorou, G., Bouckovalas, G., Corbau, C. & Ferentinos, G. (2002) - Earthquake-induced coastal sediment instabilities in the western Gulf of Corinth, Greece - *Mar. Geol.*, v. **186**, 319–335.

Haugerud, R.A. (1999) - Digital elevation model (DEM) of Cascadia, latitude 39N-53N, longitude 116W-133W - *U.S. Geological Survey*, Open-file Report 99-369, http://geopubs.wr.usgs.gov/open-file/of99-369/.

Heezen, B.C. & Ewing, M. (1952) - Turbidity currents and submarine slumps, and the 1929 Grand Banks earthquake. - *Am. Jourm. Sci.*, **250**, 849-873.

Heinio, P. & Davies, R.J. (2006) - Degradation of compressional fold belts: Deep-water Niger Delta - *AAPG Bulletin*, v. **90**/5, 753 – 770.

Hibbard, J.P. & Williams, H. (1979) - The regional setting of the Dunnage Mélange in the Newfoundland Appalachians - *American Journal of Science*, v. **279**, 993-1021.

Highland, L. & Johnson, M. (2004) - Landslide Types and Processes - U.S. Department of the Interior, U.S. Geological Survey Fact Sheet 2004-3072. http://pbs.usgs.gov/fs/2004/3072/.

Hinschberger, F., Malod, J.-A., Dyment, J., Honthaas, C., Rehault, J.-P. & Burhanuddin, S. (2001) - Magnetic lineations constraints for the back-arc opening of the Late Neogene South Banda Basin (eastern Indonesia) - *Tectonophysics*, v. **333**, 47-59.

Hinschberger, F., Malod, J.-A., Re´ hault, J.-P., Villeneuve, M., Royer, J.-Y. & Burhanuddin, S. (2005) - Late Cenozoic geodynamic evolution of eastern Indonesia – *Tectonophysics*, v. **404**, 91 – 118.

Hovius, N., Starck, C.P., Hao-Tsu, C. & Jiun-Chuan, L. (2000) – Supply and removal of sediment in a landslide-dominated mountain belt: Central Range, Taiwan – *Journal of Geology*, v. **108**, 73-89.

Hsü, K.J. (1968) - Principles of melanges and their bearing from on the Franciscan Knoxville paradox - *Geol. Soc. of America Bulletin*; v. **79**, 1063-174.

Hsü, K.J. (1974) - Mélanges and their distinction from olistostromes. - *in* R.H. Dott Jr. and R.H. Shaver, eds., *Modern and Ancient Geosynclinal Sedimentation* , *SEPM Spec. Publ.*, **19**, 321-333..

Hu, G., Yan, T., Liu, Z., Vanneste, M. & Dong, L. (2009) - Size Distribution of Submarine Landslides Along the Middle Continental Slope of the East China Sea - *J. Ocean Univ. China (Oceanic and Coastal Sea Research)*, v. **8**/4, 322-326. DOI 10.1007/s11802-009-0322-3.

Huang, C.Y., Yuan, P.B., Lin, C.W., Wang, T.K. & Chang, C.P. (2000) - Geodynamic processes of Taiwan arc–continent collision and comparison with analogs in Timor, Papua New Guinea, Urals and Corsica – *Tectonophysics*, v. **325**, 1–21.

Huguen, C., Mascle, J., Chaumillon, E., Woodside, J.M., Benkhelil, J., Kopf, A. & Volkonska, A. (2001) - Deformational styles of the eastern Mediterranean Ridge and surroundings from combined swath mapping and seismic reflection profiling – *Tectonophysics*, v. **343**, 21 – 47.

Huhnerbach, V. & Masson, D. G. (2004) - Landslides in the North Atlantic and its adjacent seas: an analysis of their morphology, setting and behaviour - *Marine Geology*, v. **213**, 343-362.

Hutchinson, D. R., Hart, P.E., Collett, T.S., Edwards, K.M., Twichell, D.C. & Snyder, F. (2008) - Geologic framework of the 2005 Keathley Canyon gas hydrate research well, northern Gulf of Mexico - *Marine and Petroleum Geology*, v. **25**, 906–918.

Huvenne, V.A.I., Croker, P.F. & Henriet, J.P. (2002) – A refreshing 3D view of an ancient collapse and slope failure – *Terra Nova*; v. **14**, 33-40.

I.G.G.P. (1965) - Carta geologica della Provincia di Parma e delle zone limitrofe: scala. 1:100.000 - *Ist. di Geol., Univ. di* Parma*, L.A.C., Firenze.*

Iaccarino, S., Papani, G., Rio, D. & Zanzucchi, G. (1974) - Considerazioni sul contatto flysch-tongriano dell'Appennino emiliano - *L'Ateneo Parmense-Acta Nat.*, v. **10**/3, 381-408.

Ilstad, T., De Blasio, F.V., Elverhøi, A., Harbitz, C.B., Engvik, L., Longva, O. & **Marr, J.G.** (2004) – On the frontal dynamics and morphology of submarine debris flow – *Marine geology*; v. **213,** 481-497.

Ilstad, T., Issler, D., Elverhoi, A. & **Marr, J.G.** (2004b) - Subaqueous debris flow behaviour and its dependence on the sand/clay ratio: a laboratory study using particle tracking - *Marine Geology*, vol. **213**, 415 – 438.

Ilstad, T., Marr, J.G., Elverhoi, A. & **Harbitz, C.B.** (2004a) **-** Laboratory studies of subaqueous debris flows by measurements of pore-fluid pressure and total stress - *Marine Geology*, vol. **213**, 403 – 414.

Ineson, J.R. (1985) - Submarine glide blocks from the Lower Cretaceous of the Antarctic Peninsula – *Sedimentology*, v. **32**/5, 659-670. DOI: 10.1111/j.1365-3091.1985.tb00480.x

Issler, D., De Blasio, F.V., Elverhøi, A., Brync, P. & **Lienc, R.** (2005) - Scaling behaviour of clay-rich submarine debris flows - *Marine and Petroleum Geology*, v. **22**, 187–194.

Jacobi, R.D. (1976) – Sediment slides on the northwestern continental margin of Africa. *Marine Geology*, v. **22**, 157-173.

Jenner, K.A., Piper, D.J.W., Campbell, D.C. & **Mosher, D.** (2007) - Lithofacies and origin of late Quaternary mass transport deposits in submarine canyons, central Scotian Slope, Canada - *Sedimentology*, v. **54**, 19–38. DOI: 10.1111/j.1365-3091.2006.00819.x

Jiang, L. & **LeBlond, P.H.** (1992) - The coupling of a submarine slide and the surface waves which it generates - *Journ. of Geophys. Res.*; v. **97**, 12731-12744.

Johns, D.R., Mutti, E., Rosell J. & **Seguret M.** (1981) - Origin of a thick redeposited carbonate bed in the Eocene turbidites of the Hecho Group, south central Pyrenees, Spain. - *Geology*, **9**, 161-164.

Kawamura, K., Kanamatsu, T., Kinoshita. M., Saito, S., Shibata, T., Fumino, K., Misawa, A. & **Burmeister, K.C.** (2009) – Redistribution of sediments by submarine landslides on the Eastern Nankai Accretionary Prism – In: *Submarine Mass Movements and Their Consequences* (Eds. D.C. Mosher, R.C. Shipp, L. Moscardelli, J.D. Chaytor, C.D.P. Baxter, H.J. Lee, R. Urgeles), Advances in Natural and Technological Hazards Research, v. **28**, 313-322.

Kenyon, N.H. (1987) - Mass-wasting features on the continental slope of Northwest Europe - *Marine Geology*, v. **74,** 57–77.

Kimura, G., Screaton, E.J., & **Curewitz, D.** (2007) - NanTroSEIZE Stage 1: NanTroSEIZE shallow megasplay and frontal thrusts - *IODP Sci. Prosp*., v. **316**. doi:10.2204/iodp.sp.316.2007

Kinoshita, M., Tobin, H. & **Thu, M.K.** (2007) - NanTroSEIZE Stage 1: NanTroSEIZE LWD transect - *IODP Sci. Prosp.*, v. **314**. doi:10.2204/iodp.sp.314.2007

Klaus, A. & **Taylor, B.** (1991) - Submarine canyon develop- ment in the Izu-Bonin Forearc: a SeaMARC II and seismic survey of Aoga Shima Canyon - *Mar. Geophys. Res.*, v. **13**, 131–152.

Kleverlaan, K. (1987) - Gordo megabed: a possible seismite in a Tortonian submarine fan, Tabernas basin, province Almeria, southeast Spain - *Sedimentary Geology*; v. **51**/3-4, 165-180.

Knipe, R.J. (1986) - Deformation mechanism path diagrams for sediments undergoing lithification - *Mem. Geol. Soc. Amer.* v. **166**, 151–160.

Kodaira, S., Takahashi, N., Park, J., Mochizuki, K., Shinohara, M. & **Kimura, S.** (2000) - Western Nankai Trough seismogenic zone: results from a wide-angle ocean bottom seismic survey - *J. Geophys. Res.,* v. **105**, 5887–5905.

Kominz, M.A., Miler, K.G. & **Browning, J.V.** (1998) – Long-term and short-term global Cenozoic sea-level estimates – *Geology*, v. **26**, 311-314.

Kopp, H. (2002) - BSR occurrence along the Sunda margin : evidence from seismic data - *Earth and Planetary Science Letters*, v. **197**, 225-235.

Korup, O., McSaveney, M.J. & **Davies, T.R.H.** (2004) - Sediment generation and delivery from large historic landslides in the Southern Alps, New Zealand – *Geomorphology*, v. **61**, 189 – 207.

Kotsakis, **T.** (1986) – Elementi di paleobiogeografia dei mammiferi terziari dell'Italia – *Hystrix*; vol. **1**, 25-68.

Kuijpers, A., Nielsen, T., Akhmetzhanov, A., de Haas, H., Kenyon, N.H. & **van Weering, T.C. E.** (2001) - Late Quaternary slope instability on the Faeroe margin: mass flow features and timing of events - *Geo-Marine Letters*, v. **20**, 149-159.

Kuzmichev, A. B., Bibikova, E. V. & Zhuravlev, D. Z. (2001) - Neoproterozoic (~800 Ma) orogeny in the Tuva-Mongolia Massif (Siberia) - Island arc–continent collision at the northeast Rodinia margin - *Precambrian Research,* v. 110, 109–26.

Labaume, P. & **Rio, D.** (1994) - Relationship between the Subligurian allocthon and the Tuscan foredeep turbidites in the Bobbio Window (NW Apennines) - *Mem. Soc. Geol. It.*; v. **48**, 309-315.

Labaume, P. (1992) - Evolution tectonique et sédimentaire des front de chaîne sous-marins. Exemples des Apennins du Nord, des Alpes françaises et de Sicile – *unpublished PhD thesis, Univeristy of Montpellier*; 476 pp..

Labaume, P., **Mutti, E.** & **Seguret, M.** (1987) - Megaturbidites: a depositional model from the Eocene of the SW-Pyrenean Foreland Basin, Spain - *Geo-Marine Letters*; v. **7**, 91-101.

Lajoie, J. (1972) - Slump fold axes orientations: an indication of paleoslope - *J. Sediment. Petrol.* v. **42**, 584–586.

Lamarche, G., Joanne, C. & **Collot, J.-Y.** (2008) - Successive, large mass-transport deposits in the south Kermadec fore-arc basin, New Zealand: The Matakaoa Submarine Instability Complex - *Geochem. Geophys. Geosyst.*, v. **9**, Q04001, doi:10.1029/2007GC001843.

Lamberg, J.S., Vorren, T.O., Kenyon, N.H. & **Ivanov, M.** (2006) - Frequency and triggering mechanisms of submarine landslides of the North Norwegian continental margin - *Norwegian Journal of Geology*, v. **86**, 155-161.

Lambiase, J.J., Rahim, A.A.A. & **Peng, C.Y.** (2002) - Facies distribution and sedimentary processes on the modern Baram Delta: implications for the reservoir sandstones of NW Borneo - *Marine and Petroleum Geology*, v. **19**, 69-78.

Lee, H.J. (2009) - Timing of occurrence of large submarine landslides on the Atlantic Ocean margin – *Marine Geology*, v. **264**, 53–64.

Lee, H.J., Normark, W.R., Fisher, M.A., Greene, H.G., Edwards, B.D. & **Locat, J.** (2004) – Timing and Extent of Submarine Landslides in Southern California - *Offshore Technology Conference, Houston*; paper n°16744.

Lee, S.H. & **Chough, S.K.** (2001) - High-resolution (2–7 kHz) acoustic and geometric characters of submarine creep deposits in the South Korea Plateau, East Sea – *Sedimentology*, v. **48**, 629–644.

Leigh, S. & **Hartley, A.J.** (1992) - Mega-debris flow deposits from the Oligo-Miocene Pindos foreland basin, western mainland Greece: implications for transport mechanisms in ancient deep marine basins – *Sedimentology*; v. **39**/6, 1003-1012.

Lewis, K.B. & **Pettinga, J.R.** (1993) - The emerging, imbricate frontal wedge of the Hikurangi Margin. *In*: P.F. Ballance (Ed.), *South Pacific Sedimentary Basins. Sedimentary Basins of the World, 2. Elsevier, Amsterdam*, 225-250.

Lewis, K.B., Lallemand, S.E. & **Carter**, **L**. (2004) - Collapse in a Quaternary shelf basin off East Cape, New Zealand: evidence for passage of a subducted seamount inboard of the Ruatoria giant avalanche - *New Zealand Journal of*

Geology & Geophysics, v. **47**, 415–429.

Leynaud, D., Mienert, J. & Vanneste, M. (2009) - Submarine mass movements on glaciated and non-glaciated European continental margins: A review of triggering mechanisms and preconditions to failure – *Marine and Petroleum Geology*; v. **26,** 618-632.

Li, C.F., Zhou, Z.Y., Li, J.B., Chen, H.J., Geng J.H. & Li, H. (2007) - Precollisional tectonics and terrain amalgamation offshore southern Taiwan: Characterizations from reflection seismic and potential field data – *Sci. China Ser D-Earth Sci*., v. **50**/6, 897-908.

Lipman, P.W., Normark, W.R., Moore, J.G., Wilson, J.B. & Gutmacher, C. (1988) - The giant submarine Alika debris slide, Mauna Loa, Hawaii - *J. Geophys. Res*., v. **93**, 4279-4299.

Locat, J. & Lee, H.J. (2002) - Submarine landslides: advances and challenges. - *Can. Geotech. Journal*, **39**, 193-212.

Locat, J., **Lee, H.J.**, **Locat, P. & Imran, J.** (2004) - Numerical analysis of the mobility of the Palos Verdes debris avalanche, California, and its implications for the generations of tsunamis - *Marine Geology*; v. **203**, 269-280.

Lomas, S. A. & Joseph, P. (Eds.) (2004) – Confined turbidites systems – *Geological Society*, London, Special Publications, v. **222**, 328 pp..

Loncke, L., Gaullier, V., Droz, L., Ducassou. E., Migeon, S. & Mascle, J. (2009) - Multi-scale slope instabilities along the Nile deep-sea fan, Egyptian margin: A general overview - *Marine and Petroleum Geology*, v. **26**, 633–646.

Longva, O., Janbu, N., Blikra, L.H. & Bøe, R. (2003) - The 1996 Finneid-fjord slide; seafloor failure and slide dynamics - In: J. Locat and J. Mienert (Eds.), *Submarine Mass movements and their consequences*, Kluwer, Dordrecht, 531-538.

Lowe, D.R. (1982) - Sediment gravity flows: II. Depositional models with special reference to the deposits of high-density turbidity currents - *J. Sedim. Petr*., vol. **52**/1, 279-297.

Lucente, C.C. & Pini, G.A. (2003) – Anatomy and emplacement mechanism of a large submarine slide within a Miocene foredeep in the Northern Appennines, Italy: a field perspective – *American Journ. of Science*; v. **303**, 565-602.

Lucente, C.C. & Pini, G.A. (2008) - Basin-wide mass-wasting complexes as markers of the Oligo-Miocene foredeep-accretionary wedge evolution in the Northern Apennines, Italy – *Basin Research*, v. **20**, 49 – 71.

Lucente, C.C. (2000) - Orizzonti di frana sottomarina nella Fm. Marnoso-Arenacea (Appennino tosco-romagnolo): organizzazione interna e implicazioni paleogeografiche - *Tesi di Dottorato, Univ. di Bologna*; 229 pp..

Lucente, C.C., Pini, G.A. & De Libero, C. (2006) - The role of large-scale sedimentary failures at the wedge front-foredeep boundary: a case study from the northern Apennines, Italy - *Geoacta*, **5**, 113-128.

Macdonald, D.I.M, Moncrieff, A.C.M. & Butterworth, P.J. (1993) - Giant slide deposits from a Mesozoic fore-arc basin, Alexander Island, Antarctica – *Geology*, v. **21**/11, 1047-1050. DOI: 10.1130/0091 7613(1993)021<1047:GSDFAM>2.3.CO;2

Madof, A.S., Christie-Blick, N. & Anders, M.H. (2009) - Stratigraphic controls on a salt-withdrawal intraslope minibasin, north-central Green Canyon, Gulf of Mexico: Implications for misinterpreting sea level change - *A.A.P.G. Bulletin*, v. **93**/4, 535 – 561.

Major, J.J. & Iverson, R.M. (1999) - Debris-flow deposition: effects of pore-fluid pressure and friction concentrated at flow margins - *GSA Bulletin*, v. **111**, 1424–1434.

Major, J.J. (2000) – Gravity-driven consolidation of granular slurries: implications for debris-flow deposition and deposit characteristics – *Journal of Sedimentary Research*, v. **70**/1, 64-83.

Malavieille, J. & **Trullenque, G.** (2007) - Consequences of continental subduction on forearc basin and accretionary wedge deformation in SE Taiwan: Insights from analogue modeling – Tectonophysics, v. xx, xxx – xxx.

Maltman, A., Labaume, P. & **Housen, B.** (1997) - Structural geology of the *décollement* at the toe of the Barbados accretionary prism – In: Shipley T.H., Ogawa Y., Blum P. & Bahr J.M. (Eds.), *Proceedings of the Ocean Drilling Program, Scientific Results*, v. **156**, 279-292.

Mancin, N. & **Pirini, C** (2001) - Middle Eocene to Early Miocene planktonic foraminiferal biostratigraphy in the Epiligurian succession (Northern Apennines, Italy) - *Riv. It. Paleont. Strat.*, v. **107** /3, 371-393.

Mancin, N. (1999) – Biostratigrafia delle Successioni Epiliguri tra l'Eocene medio ed il Miocene inferiore – *Unpublishced PhD thesis, Università degli Studi di Pavia*, 262 pp.

Mancin, N. (2001) - Agglutinated Foraminifera from the Epiligurian Succession (Middle Eocene/Lower Miocene, Northern Apennines, Italy): scanning electron microscopic characterisation and paleoenvironmental implications - *J. Foram. Research*, v. **31**/4, 294-308.

Mancin, N., Martelli, L. & **Barbieri, C.** (2006) - Foraminiferal Biostratigraphic and Paleobathymetric constraints in Geohistory analysis: the exemple of the Epiligurian succession of the Secchia Valley (Northern Apennines, Mid Ecocene-Late Miocene) – *Boll. Soc. Geol. It.*, v. **125**/2, 163 – 186.

Marroni, M. & **Pandolfi, L.** (2001) - Debris flow and slide deposits at the top of the Internal Liguride ophiolitic sequence (Northern Apennine, Italy): a record of frontal tectonic erosion in a fossil accretionary wedge - *The Island Arcs*, v. **10**/1. 9-21.

Marroni, M. & **Treves, B.** (1998) – Hidden terranes in the Northern Apennines, Italy: a record of Late Cretaceous-Oligocene transpressional tectonics – *Journal of Geology*, v. **106**, 149-162.

Martel, S.J. (2003) - Mechanics of landslide initiation as a shear fracture phenomenon - *Marine Geology*; v. **203**, 319-339.

Martelli, L. (2002) – La Successione Epiligure – In. *Note Illustrative del Foglio 216 "Borgo Val di Taro" della Nuova Carta Geologica d'Italia 1:50.000* (Vescovi, P. Coord.), Servizio Geologico d'Italia.

Martelli, L., Cibin, U., Di Giulio, A. & **Catanzariti, R.** (1998) - Litostratigrafia della Formazione di Ranzano (Priaboniano sup.-Rupeliano, Appennino Settentrionale e Bacino Terziario Ligure Piemontese) - *Boll. Soc. Geol. It.*, vol. **117**, 151-185.

Martinsen, O.J. & **Bakken, B.** (1990) - Extensional and compressional zones in slumps and slides in the Namurian of County Clare, Ireland - *Journal Geological Society of London*, v. **147**, 153–164.

Martinsen, O.J. (1989) - Styles of soft-deformation on a Namurian (Carboniferous) delta slope, Western Irish Namurian Basin, Ireland – *In*: M. K. G. Whateley, and K. T. Pickering (Eds.), *Deltas: sites and traps for fossil fuels. Special Publication Geological Society London*, v. **1**, 167–177.

Masini, L. & **Pecchioli, A.** (1988) – I conglomerati della Arenarie di Ranzano nella Bassa Val Ceno e nei dintorni di Viano (Appennino emiliano) – *Acta Naturalia, Parma*, v. **24**, 123-141.

Masson, D.G., Canals, M., Alonso, B., Urgeles, R. & **Huhnerbach, V.** (1998) - The Canary Debris Flow: source area morphology and failure mechanisms – Sedimentology, v. **45**, 411-432.

Masson, D.G., Harbitz C.B., Wynn R.B., Pedersen, G. & **Løvholt, F.** (2006) **-** Submarine landslides: processes, triggers and hazard prediction - *Phil. Trans. R. Soc.*, vol. **364**, 2009–2039. doi:10.1098/rsta.2006.1810.

Masson, D.G., **Watts, A.B.**, **Gee, M.J.R.**, **Urgeles, R.**, **Mitchell, N.C.**, **Le Bas, T.P.** & **Canals, M.** (2002) - Slope failures on the flanks of the western Canary Islands - *Earth Sci. Reviews*; v. **57**, 1-35.

McAdoo, B.G. & **Watts P.** (2004) -Tsunami hazard from submarine landslides on the Oregon continental slope -

Marine Geology, v. **203**, 235-245.

McAdoo, B.G., Capone, M. & Minder, J. (2004) - Seafloor geomorphology of convergent margins: Implications for Cascadia seismic hazard – *Tectonics*, v. **23**.

McAdoo, B.G., Orange, D.L., Screaton, E., Lee, H.J. & Kayen, R. (1997) - Slope basins, headless canyons, and submarine palaeoseismology of the Cascadia accretionary complex - *Basin Research*, v. **9**, 313–324.

McAdoo, B.G., Pratson, L. & Orange, D.L. (2000) - Submarine landslide geomorphology, US continental slope - *Marine Geology*, v. **169**, 103-136.

McCaffrey, R. & Abers, G.A. (1991) – Orogeny in arc-continent collision: the Banda Arc and western New Guinea – *Geology*, v. **19**, 563-566.

McCaffrey, R., Molnar, P. & Roecker, S.W. (1985) –Microearthquake seismicity and fault plane solutions related to arc-continent collision in the eastern Sunda Arc, Indonesia – *Journal of Geophysical Resarch*, v. **90**/B6, 4511-4528.

McConnico, T.S. & Bassett K.N. (2007) - Gravelly Gilbert-type fan delta on the Conway Coast, New Zealand: Foreset depositional processes and clast imbrications - *Sedimentary Geology*, v. **198** 147 – 166.

McGilvery, T.A., Haddad, G. & Cook, D.L. (2004) – Seafloor and Shallow Subsurface Examples of Mass Transport Complexes, Offshore Brunei - - *Offshore Technology Conference, Houston*; paper n°16780.

McHugh, C.M.G., Damuth, J.E. & Mountain, G.S. (2002) - Cenozoic mass-transport facies and their correlation with relative sea-level change, New Jersey continental margin - *Marine Geology*, v. **184**, 295-334.

McMurtry, G.M., Herrero-Bervera, E., Cremer, M.D., Smith, J.R., Resig, J., Sherman, C. & Torresan, M.E. (1999) - Stratigraphic constraints on the timing and emplacement of the Alika 2 giant Hawaiian submarine landslide - *Journal of Volcanology and Geothermal Research*, v. **94**, 35 – 58.

McMurtry, G.M., Watts, P., Fryer, G.J., Smith, J.R. & Imamura, F. (2004) - Giant landslides, mega-tsunamis, and paleo-sea level in the Hawaiian Islands - *Marine Geology*, v. **203**, 219-233

Medialdea, T., Vegas, R., Somoza, L., Vazquez, J.T., Maldonado, A., Diaz-del-Rio, V., Maestro, A., Cordoba, D. & Fernandez-Puga, M.C. (2004) - Structure and evolution of the ‘‘Olistostrome’’ complex of the Gibraltar Arc in the Gulf of Cadiz (eastern Central Atlantic): evidence from two long seismic cross-sections - *Marine Geology*, v. **209**, 173 – 198.

Melosh, J.H. (1987) - The mechanics of large rock avalanches. - *GSA Rev. in Engineering Geology*, v. **7**, 41-49.

Merla, G. (1951) – Geologia dell’Appennino settentrionale – *Boll. Soc. Geol. It.*; v. **70**, 95-382.

Middleton, G.V. & **Hampton, M.A.** (1973) - Sediment gravity flows: mechanics of flow and deposition. - In. *Turbidites and Deep-water Sedimentation* (Eds G.V. Middleton & A.H. Bouma), *SEPM Pacific Section, Short Course Notes*, 1-38.

Miller, K.G., Fairbanks, R.G. & Mountain, G.S. (1987) – Tertiary oxygen isotope synthesis, sea level history, and continental margin erosion – *Paleoceanography*, v. **2**/1, 1-19.

Miller, K.G., Wright, J.D. & Fairbanks, R.G. (1991) – Unlocking the ice house: Oligocene-Miocene oxygen isotopes, eustasy and margin erosion – *Journal of Geophysical Research*, v. **96**, 6829-6848.

Milsom, J. (2000) - Stratigraphic constraints on suture models for eastern Indonesia - Journal of Asian Earth Sciences, v. **18**, 761 – 779.

Minisini, D. (2007) – Mass-transport deposits on Mediterranean continental margins – *Published PhD Thesis, Università di Bologna*.

Minisini, D., Trincardi, F. & Asili, A. (2006) - Evidence of slope instability in the Southwestern Adriatic Margin - *Natural Hazards and Earth System Sciences*, v. **6**, 1–20.

Minisini, D., Trincardi, F., Asioli, A., Canu, M. & Foglini, F. (2007) - Morphologic variabilità of exposed mass-transport deposits on the eastern slope of Gela basin (Sicily channel) – *Basin Research*. doi: 10.1111/j.1365-2117.2007.00324.x

Miyazaki, S. & Heki, K. (2001) - Crustal velocity field of southwest Japan: subduction and arc-arc collision - *J. Geophys. Res.,* v. **106**(B3), 4305–4326. doi:10.1029/2000JB900312

Moernaut, J., De Batist, M., Heirman, K., Van Daele, M., Pino, M., Brümmer, R. & Urrutia, R. (2009) - Fluidization of buried mass-wasting deposits in lake sediments and its relevance for paleoseismology: Results from a reflection seismic study of lakes Villarrica and Calafquén (South-Central Chile) - *Sedimentary Geology*, vol. **213**, 121–135.

Mohrig, D. & Marr, J.G. (2003) - Constraining the efficency of turbidity current generation from submarine debris flows and slides using laboratory experiments - *Marine and Petroleum Geol.*; v. **20**, 883-899.

Mohrig, D., Whipple, K.X., Hondzo, M., Ellis, C. & Parker, G. (1998) - Hydroplaning of subaqueous debris flows. - *GSA Bulletin*, v. 110/**3**, 387-394.

Moore, D.G., Curray, J.R. & Emmel, F.J. (1976) - Large submarine slide (olistostrome) associated with Sunda Arc subduction zone, northeast Indian Ocean - *Marine Geology*, v. **21**/3, 211-226. doi:10.1016/0025-3227(76)90060-8.

Moore, G. F., Bangs, N. L., Taira, A., Kuramoto, S., Pangborn, E. & Tobin, H. J. (2007) - Three-dimensional splay fault geometry and implications for tsunami generation - *Science*, v. **318**, 1128-1131. DOI: 10.1126/science.1147195

Moore, G.F., Taira, A., Klaus, A., Becker, L., Boeckel, B., Cragg, B.A., Dean, A., Fergusson, C.L., Henry, P., Hirano, S., Hisamitsu, T., Hunze, S., Kastner, M., Maltman, A.J., Morgan, J.K., Muratami, Y., Saffer, D.M., Sánchez-Gómez, M., Screaton, E.J., Smith, D.C., Spivack, A.J., Steurer, J., Tobin, H.J., Ujiie, K., Underwood, M.B. & Wilson, M. (2001) - New insights into deformation and fluid flow processes in the Nankai Trough accretionary prism: results of Ocean Drilling Program Leg 190 - *Geochem., Geophys., Geosyst.,* v. **2**(10), doi:10.1029/2001GC000166

Moore, J.G. & Moore, G.W. (1984) - Deposit from a giant wave on the island of Lanai, Hawaii - *Science*, v. **226**, 1312–1315.

Moore, J.G., Bryan, W.B., Beeson, M.H. & Normark, W.R. (1995) - Giant blocks in the South Kona landslide, Hawaii – *Geology*, v. **23**, 125-128.

Moore, J.G., Clague, D.A., Holcomb, R.T., Lipman, P.W., Normark, W.R. & Torresan, M.E. (1989) – Prodigious submarine landslides on the Hawaiian ridge – *Journ. of Geophysical Research*; v. **94**, 17.465-17.484.

Moore, J.G., Normark, W.R. & Holcomb, R.T. (1994) - Giant Hawaiian landslides - *Ann. Rev. Earth Planet. Sci.*, v. **22**, 119-144.

Mora, S. (1992) - Stratigrafia fisica e analisi di facies della successione Monte Piano-Ranazano nel bacino epiligure di Specchio (Appennino parmense). – *Unpublished MSc thesis, Università di Parma.*

Moran, K. & Tappin, D. (2006) - SEATOS 2005 Cruise Report: Sumatra Earthquake and Tsunami Off shore Survey (SEATOS) - 92 pp.. http://ocean.oce.uri.edu/seatos.

Morgan *et al.,* (2008 submitted) Workshop Report: Addressing Geohazards Through Ocean Drilling, Scientific Drilling

Morley, C. K. & **Leong**, L.C. (2008) - Evolution of deep-water synkinematic sedimentation in a piggyback basin, determined from three dimensional seismic reflection data - *Geosphere*, v. **4**/6, 939–962. doi: 10.1130/GES00148

Morley, C. K. (2009a) - Growth of folds in a deep-water setting - *Geosphere*; v. **5**/ 2, 59-89, DOI: 10.1130/GES00186.1

Morley, C. K. (2009b) - Geometry of an oblique thrust fault zone in a deepwater fold belt from 3D seismic data - *Journal of Structural Geology*, xxx, 1–16.

Morley, C. K., **Crevello, P.** & **Ahmad. Z.H** (1998) - Shale tectonics and deformation associated with active diapirism: the Jerudong Anticline, Brunei Darussalam - *Journal of the Geological Society*; v. **155**/3, 475-490, DOI: 10.1144/gsjgs.155.3.0475

Morley, C.K. (2007) - Interaction between critical wedge geometry and sediment supply in a deep-water fold belt - *Geology*, v. **35**/2, 139–142. doi: 10.1130/G22921A.1.

Morley, C.K., Back, S., Van Rensbergen, P., Crevello, P. & **Lambiase, J.J.** (2003) - Characteristics of repeated, detached, Miocene – Pliocene tectonic inversion events, in a large delta province on an active margin, Brunei Darussalam, Borneo - Journal of Structural Geology, v. **25**, 1147–1169.

Moscardelli, L. & **Wood, L.** (2007) - New classification system for mass transport complexes in offshore Trinidad *Basin Research*, doi: 10.1111/j.1365-2117.2007.00340.x.

Moscardelli, L., Wood, L. & **Andrews, J.** (2005) - Visualization technology and quantitative morphometrics of mass transport complexes along the continental margin of Trinifidad, West Indies - *Seismic Geomorphology SEPM Research Conference*, February 2005, Houston, Texas.

Mosher, D.C., Austin, J.A. Jr., Fisher, D. & **Gulick, S.P.S.** (2008) - Deformation of the northern Sumatra accretionary prism from high-resolution seismic reflection profiles and ROV observations - *Marine Geology*, v. **252**, 89–99.

Mosher, D.C., Shipp, R.C., Moscardelli, L., Chaytor, J.D., Baxter, C.D.P., Lee, H.J. & **Urgeles, R.** (Eds.) (2009) - Submarine Mass Movements and their Consequences - *Advances in Natural and Technological Hazards Research*, v. **28**, Springer, 786 pp..

Mountjoy, J.J., McKean, J., Barnes, P.M. & **Pettinga, J.R.** (2009) - Terrestrial-style slow-moving earthflow kinematics in a submarine landslide complex - *Marine Geology*, xxx, xxx-xxx. doi: 10.1016/j.margeo.2009.09.007.

Mulder, T. & **Cochonat, P.** (1996) - Classification of offshore mass movements - *Journ. of Sed. Res.,* v. **66**/1, 43-57.

Mutti E., Ricci Lucchi F. & **Roveri M.** (2002) – Revisiting turbidites of the Marnoso-arenacea Formation and their basin-margin equivalents: problems with classic models - In "Excursion Guidebook," Parma, Italy, 21-22 May 2002.

Mutti, E & **De Rosa, E** (1965) - Caratteri sedimentologici delle arenarie di Ranzano e della Formazione di Val Luretta nel basso Appennino di Piacenza - *Riv. It. Paleont. Strat.*, v. **74**/1, 71 – 120.

Mutti, E. & **Ghibaudo, G.** (1972) - Un esempio di torbiditi di conoide sottomarina esterna: le Arenarie di S. Salvatore (Formazione di Bobbio, Miocene) nell'Appennino Piacentino - *Mem. Acc. Sci. Torino, Class. Sci. Fis. Mat. Nat., ser. 4a*; v. **16**, 40 pp..

Mutti, E. & **Tinterri, R.** (2004) – Cross-stratified coarse-grained sandstone beds: evidence of flow-margin deposition and reworking in confined turbidity currents – *AAPG Annual Meeting, Dallas, Texas*.

Mutti, E. (1963) - Confronto tra le direzioni d'apporto dei clastici entro il Macigno edil Tongriano dell'Appennino di

Piacenza – *Riv. It. Paleont. Strat.*, v. **69**/2, 235 – 258.

Mutti, E. (1964) - Schema paleogeografico del Paleogene dell'Appennino di Piacenza - *Riv. It. Paleont. Strat.*, v. **70**/4, 869 – 885.

Mutti, E. (1979) – Turbidites et cônes sous-marins profonds – *in* Homewood, P., Ed., *Sédimentation Détritique (Fluviatile, Littorale et Marine)*, Istitut de Géologie, Université de Fribour; 353-419.

Mutti, E. (1992) - Turbidite Sandstones. **-** *San Donato Milanese, Agip-Istituto di Geologia, Università di Parma*, 275 pp.

Mutti, E., Carminatti, M., Moreira, J.L.P. & Grassi, A.A. (2006) - Chaotic Deposits: examples from the Brazilian offshore and from outcrop studies in the Spanish Pyrenees and Northern Apennines, Italy. - *A.A.P.G. Annual Meeting,* April 9-12, Houston, Texas.

Mutti, E., Davoli, G., Mora, S. & Papani, L. (1994) – Internal stacking patterns of ancient turbidite systems from collisional basins – *GCSSEPM Foundation, 15th Annual Research Conference, Submarine Fans and Turbidite Systems*, 257-268.

Mutti, E., De Rosa, E. & Saccani, G. (1965) – Paleocorrenti e caratteri sedimentologici delle Arenarie di Ranzano tra la Val Tidone e la Val Taro (Appennino settentrionale) – *Riv. It. Paleont. Strat.*, v. **71**(2), 565-602.

Mutti, E., Ogata, K., Tinterri, R. & Carè, D. (2009) – Fine-grained unsorted matrix as evidence of excess pore pressure in sedimentary chaotic units – *27 th I.A.S. International Meeting*, September 20-23, Alghero (Sardinia), Italy.

Mutti, E., Papani, L., Di Biase, D., Davoli, G., Mora, S., Segadelli, S. and **Tinterri, R.** (1995) - Il Bacino Terziario Epimesoalpino e le sue implicazioni sui rapporti tra Alpi ed Appennino - *Memorie di Scienze Geologiche di Padova*, v. **47**, 217 – 244.

Mutti, E., Ricci-Lucchi, F., Séguret, M. & **Zanzucchi, G.** (1984) - Seismoturbidites: a new group of resedimented deposits. - *Mar. Geol.,* **55**, 103-116.

Mutti, E., **Tinterri, R.**, **Benevelli, G.**, **Di Biase, D.** & **Cavanna, G.** (2003) - Deltaic, mixed and turbidite sedimentation of ancient foreland basins - *Marine and Petroleum Geol.*; v. **20**, 733-755.

Mutti, E., Tinterri, R., Muzzi Magalhaes, P. & Basta, G. (2007) - Deep-Water Turbidites and Their Equally Important Shallower Water Cousins - *AAPG Annual Convention*, Long Beach, California, April 1-4, 2007. Search and Discovery Article #50057.

Mutti, E., **Tinterri, R.**, **Remacha, E.**, **Mavilla, N.**, **Angella, S.** & **Fava, L.** (1999) - An introduction to the analisys of ancient turbidite basins from an outcrop perspective - *AAPG, Continuing Education Course Note Series*; **39**, 61 pp..

Muttoni, G., Argnani, A., Kent, D.V., Abrahamsen, N. & **Cibin, U.** (1998) - Paleomagnetic evidence for Neogene tectonic rotations in the northern Apennines, Italy - *Earth and Planetary Science Letters*, v. **154**, 25 – 40.

Nardin, T.R., Hein, F.J., Gorsline, D.S. & **Edwards, B.D.** (1979) – A review of mass movement processes, sediment and acoustic characteristics, and contrasts in slope and base-of-slope systems versus canyon-fan-basin floor systems – *S.E.P.M. Special Publication*; n. **27**, 61-73.

Naylor, M.A. (1981) - Debris flows (olistostromes) and slumping on a distal passive continental margin: The Palombini limestone-shale sequence of the Northern Apennines - *Sedimentology*, v. **28**, 837-852.

Naylor, M.A. (1982) – The Casanova Complex of the Northern Appennines: a mélange formed on a distal passive margin – *Journ. Of Structural Geol.*; v. **4**/1, 1-18.

Nemec, W. (1990) - Aspects of sediment movement on steep delta slopes - *In*: Prior, D. B. (Ed.), *Coarse-Grained Deltas, International Association of Sedimentologists*, 29-73.

Niedoroda, A.W., Reed, C.W., Das, H. & **Hatchett, L.** (2007) – The general behavior of mass gravity flows in the marine environment – In. V. Lykousis, D. Sakellariou and J. Locat (eds.), *Submarine Mass Movements and Their Consequences, Springer,* 111–118.

Nisbet, E.G. & **Piper, D.J.W.** (1998) - Giant submarine landslides - *Nature*; v. **392**, 329-330.

Nisbet, E.G. (2002) - Have sudden large releases of methane from geological reservoirs occurred since the Last Glacial Maximum, and could such releases occur again? - *Phil. Trans. Royal Soc., London*; v. **360**, 581-607.

Nissen, S.E., Haskell, N.L., Steiner, C.T. & **Coterill, K.L.** (1999) - Debris flow outrunner blocks, glide tracks, and pressure ridges identified on the Nigerian continental slope using 3-D seismic coherency. *The Leading Edge*, Society of Exploration Geophysicists, v. **18**, 550-561.

Normark, W.R. & **Gutmacher, C.E.** (1988) - Sur submarine slide, Monterey Fan, central California - *Sedimentology*, v. **35**, 629-647.

Normark, W.R., McGann, M. & **Sliter, R.W. (**2004) - Age of Palos Verdes submarine debris avalanche, southern California - *Marine Geology*, v. **203**/3-4, 247-259.

Normark, W.R., Moore, J.G. & **Torresan, M.E.** (1993) – Giant volcano-related landslides and the development of the Hawaiian Islands – *in* Schwab, W.C., Lee, H.J. & Twichell, D.C., Eds., *Submarine Landslides: Selected Studies in the U.S. Exclusive Economic Zone*; *U.S. Geol. Surv. Bulletin, 2002*; 184-196.

Ogata, K., Zélic, M. & **Caré, D.** (2007) - Evidence of overpressured fluids in the thrust zone of the "Bobbio Window" (Trebbia Valley, Northern Apennines) - 10.1475/*Epitome*, **2**, 0471, Geoitalia 2007.

Ogniben, L. (Ed.) (1973) - Structural Model of Italy, scale 1:1000.000 - *CNR, 2 sheets*.

Orange, D.L. & **Underwood, M.B.** (1995) - Patterns of thermal maturity as diagnostic criteria for interpretation of melanges - *Geology*; v. 23/**12**, 1144-1148.

Ori, G.G. & **Friend, P.F.** (1984) - Sedimentary basins formed and carried piggy-back on active thrust sheets – Geology, v. **12**, 475-478.

Ori, G.G., Roveri, M. & **Vanoni, F.** (1986) - Plio-Pleistocene sedimentation in the Apenninic-Adriatic foredeep (Central Adriatic Sea, Italy) - *In*: P.A. Allen and P. Homewood (Eds.), *Foreland Basin. Spec. Pubbl. Int. Ass. Sed. Oxford* **8**, 183-198.

Ottria, G. (2000) - Polyphase thrusting in piggy-back deposits: the example of epi-Ligurian Succession (northern Apennines, Italy) - *Comptes rendus de l'Académie des sciences, Paris - Série IIa - Sciences de la Terre et des Planètes*, v. **330**, 845-852.

Ottria, G., Catanzariti, R. & **Cerrina Ferroni, A. (**2001) - The Ranzano unit boundaries in the type area: lower Oligocene events in the epi-Ligurian Succession (Northern Apennines, Italy) - *Eclogae Geol. Helv.*, vol. **94**, 185–196.

Owoyemi, A.O. & **Willis, B.J.** (2006) – Depositional patterns across syn-depositional normal faults, Niger Delta, Nigeria - *Journal of Sedimentary Research*, v. **76**, 346–363. DOI: 10.2110/jsr.2006.025

Page, B. M. (1978) - Franciscan mélange compared with olistostromes of Taiwan and Italy - *Tectonophysics*, vol. **47**, 665– 672.

Page, B.M. & **Suppe, J.** (1981) - The Pliocene Lichi melange of Taiwan; its plate-tectonic and olistostromal origin - *Amer. Jour. Sci.,* v. **281**, 193-227.

Page, B.M. (1963) - Gravity Tectonics Near Passo Della Cisa, Northern Apennines, Italy - *GSA Bulletin*; v. **74**/6, 655-671; DOI: 10.1130/0016-7606(1963)74

Pandolfi, L., Catanzariti R., Cerrina Feroni A., Marroni M. & Ottria, G. (2004) - Can the Aveto Unit (Early Oligocene, Subligurian Domain) be considered the record of the first Apenninic Foredeep? Evidence from provenance data. - *32° International Geological Congress, Florence* 20-28 August 2004, Abstract volume.

Papani, G. (1964) - Su un olistostroma di "argille scagliose" intercalato nella serie oligomiocenica del subappennino reggiano - *Boll. Soc. Geol. It.*, v. **82**, 195-202.

Papani, G. (1971) - Geologia della struttura di Viano (Reggio Emilia) - *Mem. Soc. Geol. It.*, v. **10**, 121-165.

Papani, G., Tellini, C., Torelli, L., Vernia, L. & Iaccarino, S. (1987) - Nuovi dati stratigrafici e strutturali sulla Formazione di Bismantova nella «sinclinale» Vetto-Carpineti (Appennino Reggiano-Parmense) - *Mem. Soc. Geol. It.*, vol . **39**, 245-275.

Papatheodorou, G. & Ferentinos, G. (1997) - Submarine and coastal sediment failure triggered by the 1995, Ms = 6.1 R Aegion earthquake, Gulf of Corinth, Greece - *Mar. Geol.*, v. **137**, 287–304.

Park, J.-O., Tsuru, T., Kodaira, S., Cummins, P.R. & Kaneda, Y. (2002) - Splay fault branching along the Nankai subduction zone - *Science*, v. **297**(5584), 1157–1160. doi:10.1126/sci- ence.1074111

Pestana, J.M., Biscontin, G., Nadim, F. & Andersen, K. (2000) - Modeling cyclic behavior of lightly overconsolidated clays in simple shear - *Soil Dynamics and Earthquake Engineering*, v. **19**, 501-519

Pickering, K.T. & Corregidor, J. (2005) – Mass-transport complexes (MTCs) and tectonic control on basin-floor submarine fans, Middle Eocene, South Spanish Pyrenees - *Journal of Sedimentary Research*, vol. **75**, 761–783.

Pickering, K.T. (1987) - Wet-sediment deformation in the Upper Ordovician Point Leamington Formation: an active thrust-imbricate system during sedimentation, Notre Dame Bay, north-central Newfoundland. *In*: Jones, M.E., Preston, R.M.F. (Eds.), *Deformation of Sediments and Sedimentary Rocks. Geological Society, London, Special Publications*, v. **29**, 213–239.

Pickering, K.T., Stow, D.A.V., Watson, M.P. & Hiscott, R.N. (1986) - Deep-water facies, processes and models: A review and classification scheme for modern and ancient sediments - *Earth Sci. Rev.*, v. **23**, 75–174.

Picotti, V. & Pazzaglia, F.J. (2008) – A new tectonic model for the construction of the Northern Apennine mountain front near Bologna (Italy) - *J. Geophys. Res.*; vol. **113**, B08412, doi:10.1029/2007JB005307.

Pieri, M. (1961) - Nota introduttiva al rilevamento del versante appenninico padano eseguito nel 1955-1959 dai geologi dell' AGI P Mineraria - *Boll. Soc. Geol. It.*, v. **80**/1, 3-34.

Pini, G.A. (1999) – Tectonosomes and olistostromes in the Argille Scagliose of the Northern Apennines, Italy – *Geol. Soc. of America Special*; p. **335**, 73 pp..

Piper, D. J. W. & Aksu, A.E. (1987) **-** The Source and Origin of the 1929 Grand Banks Turbidity Current Inferred from Sediment Budgets - *Geo-Marine Letters*; v. 7, 177-182.

Piper, D.J.W., Cochonat, P. & Morrison, M.L. (1999) – The sequence of events around the epicentre of the 1929 Grand Banks earthquake: initiation of debris flows and turbidity current inferred from sidescan sonar. - *Sedimentology*; v. **46**, 79-97.

Piper, D.J.W., Shor, A.N., Farre, J.A., O'Connell, S. & Jacobi, R. (1985) - Sediment slides and turbidity currents on the Laurentian Fan: Sidescan sonar investigations near the epicenter of the 1929 Grand Banks earthquake – *Geology*, v. **13**/8, 538-541. DOI: 10.1130/0091-7613(1985)13<538:SSATCO>2.0.CO;2

Plesi, G., Daniele, G., Botti, F. & Palandri, S. (2002) - Carta strutturale dell'Alto Appennino tosco-emiliano (scala 1:100.000) fra il Passo della Cisa e il Corno alle Scale - *1:100,000 Scale Geological Map, SELCA, Firenze.*

Praeg, D., Ceramicola, S., Barbieri, R., Unnithan, V. & Wardell, N. (2009) - Tectonically-driven mud volcanism since the late Pliocene on the Calabrian accretionary prism, central Mediterranean Sea - *Marine and Petroleum Geology*, xxx, 1–17.

Prather, B.B., Booth, J.R., Steffens, G.S. & Craig, P.A. (1998) - Classification, lithologic calibration, and stratigraphic successions of seismic facies of intraslope basins, deep-water Gulf of Mexico - *AAPG Bull.*, v. **82**, 701-728.

Principi G. & Treves B. (1984) - Il sistema Corso-Appenninico come prisma di accrezione. Riflessioni sul problema generale del limite Alpi Appennini - *Mem. Soc. Geol. It.*, v. **28**, 548-576.

Prior, D.B. & Coleman, J.M. (1982) - Active slides and flows in underconsolidated marine sediments on the slope of the Mississippi delta - *In*: S. Saxov & J. K. Nieuwenhuis (Eds.), *Marine slides and other mass movements, New York, Plenum Press*, 21–49.

Prior, D.B., Borhold, B.D., Coleman, J.M. & Bryant, W.R. (1982b) - Morphology ofa submarine slide, Kitimat Arm,British Columbia - Geology, v. **10**, 588-592.

Prior, D.B., Bornhold, B.D. & Johns, M.W. (1984) - Depositional characteristics of a submarine debris flow - *Jour. of Geol.*; v. **92**, 707-727.

Prior, D.B., Coleman, J.M. & Borhold, B.D. (1982a) - Results ofa known sea floor instability event - *Geo-Marine Letters*, v. **2**, 117-122.

Radrizzani, S. (1964) – Presenza di collate sottomarine nella placca oligocenica del M. Barigazzo – *Mem. Soc. Geol. It.*, v. **4**/1, 273-282.

Ramsay, J.G. (1967) - Folding and fracturing of rocks - *New York, McGraw-Hill*; 568 pp..

Ratzov, G., Collot, J.-Y., Sosson, M. & Migeon, S. (2008) - Recent debris-flows and megaturbidite in a confined basin of the North Ecuador subduction trench - *7th International Symposium on Andean Geodynamics* (ISAG 2008, Nice), Extended Abstracts, 431-434.

Raymond, L.A. (1984) - Classification of mélanges - *in* Raymond, L.A., ed.; Mélange: Their nature, origin, and significance: *Geol. Soc. of America Special*; P. **198**, 7-20.

Rebesco, M. & Camerlenghi, A. (2008) - Late Pliocene margin development and mega debris flow deposits on the Antarctic continental margins: Evidence of the onset of the modern Antarctic Ice Sheet? - Palaeogeography, Palaeoclimatology, Palaeoecology, v. **260**, 149 – 167.

Rebesco, M., Neagu, R.C., Cuppari, A., Muto, F., Accettella, D., Dominici, R., Cova, A., Romano, C. & Caburlotto, A. (2009) - Morphobathymetric analysis and evidence of submarine mass movements in the western Gulf of Taranto (Calabria margin, Ionian Sea) - *Int. J. Earth Sci. (Geol. Rundsch.)*, v. **98**, 791–805. DOI 10.1007/s00531-009-0429-1

Reutter, K. J. (1981) - A trench – forearc model of the Northern Apennines - *In*: F. C. Wezel Ed.), *Sedimentary Basin of Mediterranean Margins. CNR Italian Project of Oceanography*, 433-443.

Reutter, K.J., Günther, K. & Groscurth, J. (1978) - An approach to the geodynamics of Corsica- Northern Apennines double orogene - *in Alps, Appennines, Hellenides, Inter-Union Comm. Geodyn. Sc. Rep.*; v. **38**, 577-618.

Reutter, K.J., Teichmuller, M., Teichmuller, R. & Zanzucchi, G. (1980) - Ricerche sulla carbonificazione dei frustoli vegetali nelle rocce clastiche, come contributo ai problemi di paleogeotermia e tettonica nell'Appennino settentrionale – *Mem. Soc. Geol. It.,* v. **21**, 111 – 126.

Ricci Lucchi, F. & Ori, G.G. (1985) - Field excursion D: syn-orogenic deposits of a migrating basin system in the NW

Adriatic Foreland - *In*: P.H. Allen, P. Homewood e G. Williams (Eds.) *"Excursion Guidebook". Foreland Basins Symposium. Fribourg*, 137-176.

Ricci Lucchi, F. (1975) - Depositional cycles in two turbidite formations of Northern Apennines (Italy) - *Jour. Sed. Petrology*, v. **45**, 3-43.

Ricci Lucchi, F. (1986) - The foreland basin system of the Northern Apennines and related clastic wedges: apreliminary outline - *Giornale di Geol*., v. **48**/1, 165-185.

Ricci Lucchi, F., Colalongo, M.L., Cremonini, G. *et alii* (1982) – Evoluzione sedimentaria e paleogeografica del margine appenninico – In: *Guida alla geologia del margine appenninico padano* (Eds. G. Cremonini and F. Ricci Lucchi), *Pitagora, Bologna*, 17-46.

Rodine, J.D. & **Johnson, A.M.** (1976) - The ability of debris, heavily freighted with coarse clastic material to flow on gentle slopes - *Sedimentology*, vol. **23**, 213-234.

Roosmawati, N. & **Harris, R.** (2009) - Surface uplift history of the incipient Banda arc-continent collision: Geology and synorogenic foraminifera of Rote and Savu Islands, Indonesia - *Tectonophysics*, xxx, xxx–xxx.

Rothwell, R.G., Reeder, M.S., Anastasakis, G., Stow, D.A.V., Thomson, J. & **Kahler, G.** (2000) - Low sea-level stand emplacement of megaturbidites in the western and eastern Mediterranean Sea. - *Sed. Geol.*, **135**, 75-88.

Rothwell, R.G., Thomson, J. & **Kahler, G.** (1998) - Low sea-level emplacement of a very large Late Pleistocene megaturbidite in the western Mediterranean Sea. - *Nature*, **392**, 377-380.

Rovereto, G. (1939) - Liguria geologica - *Mem. Soc. Geol. It*., v. **2**, 1-743.

Roveri, M., **Manzi, V.**, **Ricci Lucchi, F.** & **Rogledi, S.** (2003) - Sedimentary and tectonic evolution of the Vena del Gesso basin (Northern Apennines, Italy): implications for the onset of the Messinian salinity crisis - *Geol. Soc. of America Bullettin*; v. **115**, 387-405.

Rupke N. A. (1976) - Large-scale slumping in a flysch basin, southwestern Pyrenees - *Journal of the Geological Society of London*, v. **132**/2, 121-130.

Saito, S., Underwood, M.B. & **Kubo, Y.** (2009) - NanTroSEIZE Stage 2: subduction inputs - *IODP Sci. Prosp.*, v. **322**. doi:10.2204/iodp.sp.322.2009

Schnellmann, M., Anselmetti, F. Giardini, D. & **McKenzie, J.** (2005) - Mass movement-induced fold-and-thrust belt structures in unconsolidated sediments in Lake Lucerne (Switzerland) – *Sedimentology*, v. **52**, 271–289. doi: 10.1111/j.1365-3091.2004.00694.x

Scholl, D.W., von Huene, R., Vallier, T.L. & **Howell, D.G.** (1980) – Sedimentary masses and concepts about tectonic processes at underthrust ocean margins – *Geology*, v. **8**, 564-568.

Seeber, L, Mueller, C., Fujiwara, T., Arai, K, Soh, W., Djajadihardja, Y.S. & **Cormier, M.-H.** (2007) - Accretion, mass wasting, and partitioned strain over the 26 Dec 2004 Mw=9.2 rupture offshore Aceh, northern Sumatra - *Earth and Planetary Science Letters*, v. **263**, 16 – 31.

Segadelli, S. (1992) – Stratigrafia fisica ed analisi di facies della Formazione di Ranzano nel bacino epiligure di Monte Roccone (Appennino parmense-piacentino) – *Unpublished MSc Thesis, Università di Parma*.

Seno, T., Stein, S. & **Gripp, A.E.** (1993) - A model for the motion of the Philippine Sea plate consistent with NUVEL-1 and geological data - *J. Geophys. Res.,* v. **98**, 17941–17948.

Séranne, M. (1999) – Early Oligocene stratigraphic turnover on the west Africa continental margin: a signature of the Tertiary greenhouse to icehouse transition? – *Terranova*, v. **11**, 135-140.

Sestini, G. (1970) - Sedimentation of the late geosynclinal stage - *Sediment. Geol.*, v. **4**, 445–479.

Shanmugam, G., Bloch, R. B., Mitchell, S. M., Beamish, G. W. J., Hodgkinson, R. J., Damuth, J. E., Straume, T., Syvertsen, S. E. & **Shields, K. E.** (1995) Basin-floor fans in the North Sea: Sequence stratigraphic models vs. sedimentary facies - *AAPG Bulletin*, v. **79**, 477-512.

Shipp, R.C., Nott, J.A. & **Newlin, J.A.** (2004) – Physical Characteristics and Impact of Mass Transport Complexes on Deepwater Jetted Conductors and Suction Anchor Piles – *Offshore Technology Conference, Houston*; paper n°16751.

Silver, E.A. & **Beutner, E.C.** (1980) - Mélanges: Penrose conference report - *Geology*, vol. **8**, 32-34.

Sinclair, H.D. & **Tomasso, M.** (2002) – Depositional evolution of confined turbidite basins – *Journal of Sedimentary Research*, v. **72**/4, 451-456.

Sircombe, K.N. & **Kamp, P.J.J.** (1998) - The South Westland Basin: seismic stratigraphy, basin geometry and evolution of a foreland basin within the Southern Alps collision zone, New Zealand – Tectonophysics, v. **300**, 359–387.

Situmorang, M. (1989) - Lithofacies and depositional pattern of seafloor sediments in the North Banda Sea, Indonesia - *Netherlands Journal of Sea Research*, v. **24**/4, 405-413.

Spence, G.H. & **Tucker , M.E.** (1997) - Genesis of limestone megabreccias and their significance in carbonate sequence stratigraphic models: a review - *Sedimentary Geology*, v. **112**, 163-193.

Spence, W. (1986) – The 1977 Sumba earthquake series: evidente for slab pull force acting at a subduction zone – *Journal of Geophysical*, v. **91**/B7, 7225-7239.

Steffens, G.S., Biegerta, E.K., Sumner, H.S. & **Bird, D.** (2003) - Quantitative bathymetric analyses of selected deepwater siliciclastic margins: receiving basin configurations for deepwater fan systems - *Marine and Petroleum Geology*, v. **20**, 547–561.

Stow, D.A.V. (1986) - Deep Clastic Seas – *In*: Reading, H. G. (Ed.), *Sedimentary Environments and Fades*, Oxford *(Blackwell Sci. Pubi.)*, 398-444.

Strachan, L.J. & **Alsop, G.I.** (2006) - Slump folds as estimators of palaeoslope: a case study from the Fisherstreet Slump of County Clare, Ireland - *Basin Research*, v. **18**, 451-470.

Strachan, L.J. (2002) - Slump-initiated and controlled syndepositional sandstone remobilization: an example from the Namurian of County Clare, Ireland - *Sedimentology*, v. **49**, 25-41.

Strachan, L.J. (2008) – Flow transformations in slumps: a case study from the Waitemata Basin, New Zealand – *Sedimentology*, vol. **55**, 1311–1332.

Sultan, N., Cochonat, P., Canals, M., Cattaneo, A., Dannielu, B., Hafdalison, H., Lamberg, J.S., Long, D., Mienert, J., Trincardi, F., Urgeles, R., Vorren, T.O. & **Wilson, C.** (2004) - Triggering mechanisms of slope instability processes and sediment failures on continental margins: a geotechnical approach - *Marine Geology*; **213** (1-4), 291-321.

Susilohadi, S., Gaedicke, C. & **Ehrhardt, A.** (2005) - Neogene structures and sedimentation history along the Sunda forearc basins off southwest Sumatra and southwest Java - *Marine Geology*, v. **219**, 133 – 154.

Sutherland, R., Davey, F. & **Beavan, J.** (2000) - Plate boundary deformation in South Island, New Zealand, is related to inherited lithospheric structure - *Earth and Planetary Science Letters*, v. **177**, 141-151.

Swarbrick, R.E. & **Naylor, M.A.** (1980) - The Kathikas mélange, SW Cyprus: late Cretaceous submarine debris flows - *Sedimentology*, v. **27**/1, 63 – 78.

Tagliavini, S. (1968) – Particolarità sedimentarie nelle "Arenarie di Ranzano" della media Val d'Enza (con carta geologica e sezioni 1:25.000) – *Acta Naturalia*, *Parma*, v. **4**/2, 1-14.

Taira, A., Hill, I., Firth, J., Berner, U., Bruckmann, W., Byrne, T., Chabernaud, T., Fisher,A., Foucher, J.-P., Gamo, T., Gieskes, J., Hyndman, R., Karig, D., Kastner, M., Kato, Y.,Lallement, S., Lu, R., Maltman, A., Moore, G., Moran, K., Olaffson, G., Owens, W.,Pickering, K., Siena, F., Taylor, E., Underwood, M., Wilkinson, C., Yamano, M. & Zhang, J. (1992) - Sediment deformation and hydrogeology of the Nankai Trough accretionary prism:synthesis of shipboard results of ODP Leg 131 - *Earth and Planetary Science Letters*, v. **109**, 431–450.

Taira, A., Tokuyama, H. & Soh, W. (1989) – Accretion tectonics and evolution of Japan – In: *The Evolution of the Pacific Ocean Margins* (Ed. Z.B. Avraham), *Oxford University Press*, 100-123.

Talling, P.J., Wynn, R.B., Masson, D.G., Frenz, M., Cronin, B.T., Schiebel, R., Akhmetzhanov, A. M., Dallmeier-Tiessen, S., Benetti, S., Weaver, P. P. E., Georgiopoulou, A., Zuhlsdorff, C. & Amy, L.A. (2007) - Onset of submarine debris flow deposition far from original giant landslide – *Nature*, v. **450**, 541-544.

Talukder, A.R., Bialas, J., Klaeschn, D., Brueckmann, W., Reston, T. & Petersen, J. (2008) - Tectonic framework of the mud mounds, associated BSRs and submarine landslides, offshore Nicaragua Pacific margin - *Journal of the Geological Society*, London, v. **165**, 167–176.

Tarquin Teale, C. & Young, J.R. (1987) - Isolated olistoliths from the Longobucco Basin, Calabria, Southern Italy. - *in* J.K. Leggett & G.G. Zuffa, eds.; *Marine Clastic Sedimentology*, 75-88.

Tingay, M.R.P., Hillis, R.R., Swarbrick, R.E., Morley, C.K. & Damit, A.R. (2007) - 'Vertically transferred' overpressures in Brunei: Evidence for a new mechanism for the formation of high-magnitude overpressure – *Geology*, v. **35**/11, 1023–1026. doi: 10.1130/G23906A.1.

Treves, B. (1984) – Orogenic belts as accretionary prisms: the example of the Northern Apennines – *Ofioliti*, v. **9**, 577-618.

Trifunac, M.D., Hayir, A. & Todorovska, M.I. (2002) - A note on the effects of nonuniform spreading velocity of submarine slumps and slides on the near-field tsunami amplitudes - *Soil Dyn. Earthqu. Eng.*, v. **22**, 167–180.

Trincardi, F. & Argnani, A. (1990) - Gela submarine slide; a major basin-wide event in the Plio-Quaternary foredeep of Sicily - *Geo-Mar. Lett.*, v. **10**, 13–21.

Trincardi, F. & Normark, W.R. (1989) - Pleistocene Suvero slide, Paola basin, southern Italy - *Marine and Petroleum Geology*, v. **6**/4, 324-335.

Tripsanas, E.K., Piper, D.J.W., Jenner, K.A. & Bryant, W.R. (2007) - Submarine mass-transport facies: new perspectives on flow processes from cores on the eastern North American margin – *Sedimentology*, v. **55**/1, 97-136. DOI: 0.1111/j.1365-3091.2007.00894.x

Turner, K.L. (1983) - Ft. Lauderadale, Florida to Galveston, Texas, September-November 1983, sites 614–624 - *Init. Rep. Deep Sea Drilling Proj.*, U.S. Govt. Printing Office, Washington, v. **96**, 824 pp.

Twichell, D.C., Chaytor, J.D., ten Brink, U.S. & Buczkowski, B. (2009) - Morphology of late Quaternary submarine landslides along the U.S. Atlantic continental margin - *Marine Geology*, v. **264**, 4–15.

Underwood, M.B. & Moore, G.F. (1995) – Trenches and trench-slope basins - In: *Tectonics of sedimentary basins* (Eds. C.J. Busby and R.V. Ingersoll), *Blackwell Science*, 179-219.

Underwood, M.B., Moore, G.F., Taira, A., Klaus, A., Wilson, M.E.J., Fergusson, C.L., Hirano, S., Steurer, J. & Leg 190 Shipboard Scientific Party (2003) - Sedimentary and tectonic evolution of a trench-slope basin in the Nankai subduction zone of southwest Japan - *J. Sediment. Res.*, v. **73**, 589-602.

Urgeles, R., Canals, M., Baraza, J., Alonso, B. and **Masson, D.** (1997) - The most recent megalandslides of the Canary Islands: El Golfo debris avalanche and Canary debris flow, west El Hierro island - Journal of

Geophysical Research-Solid Earth, v. **102**, 20305 – 20323.

Urgeles, R., Masson, D.G., Canals, M., Watts, A.B. and **Le Bas, T.** (1999) Recurrent large-scale landsliding on the west flank of La Palma, Canary Islands - *Journal of Geophysical Research*, v. **104**/11, 25,331-25,348.

Vai, G.B. & **Martini, I.P.** (Eds.) (2001) – Anatomy of an Orogen: The Apennines and Adjacent Mediterranean Basins – *Kluwer Academic Publishers*, 632 pp.

Van der Borch, C.C. (1978) – Continent-island arc collision in the Banda Arc – *Tectonophysics*, v. **54**, 169-193.

Van der Merwe, W. C., Hodgson, D. M. & **Flint, S.S.** (2009) - Widespread syn-sedimentary deformation on a muddy deep-water basin-floor: the Vischkuil Formation (Permian), Karoo Basin, South Africa - *Basin Research*, v. **21**, 389–406. doi: 10.1111/j.1365-2117.2009.00396.x.

Van der Werff, W. (1995) - Structure and morphotectonics of the accretionary prism along the Eastern Sunda-Western Banda Arc **-** *Journal of Southeast Asian Earth Sciences,* v. **2**/4, 309-322.

Van der Werff, W. (1996) - Variation in forearc basin development along the Sunda Arc, Indonesia **-** *Journal of Southeast Asian Earth Science*,. v. **14**/5, 331-349.

Van Rensbergen, P. & **Morley, C.K.** (2000) - 3D Seismic study of a shale expulsion syncline at the base of the Champion delta, offshore Brunei and its implications for the early structural evolution of large delta systems - *Marine and Petroleum Geology*, v. **17**, 861 – 872.

Vannucchi, P. & **Maltman, A.J.** (2000) - Insights into shallow-level processes of mountain building from the Northern Appennines, Italy - *Journ. of the Geol. Soc., London*; v. **157**, 105-120.

Vannucchi, P., Maltman, A., Bettelli, G. and **Clennell, B.** (2003) - On the nature of scaly fabric and scaly clay. - *J. Struct. Geol.,* **25**, 673-688.

Varnes, D.J. (1978) - Slope movement types and processes – In: Schuster, R.L., and Krizek, R.J., (Eds.), *Landslides—Analysis and control: National Research Council*, Washington, D.C., Transportation Research Board, Special Report **176**, 11–33.

Vescovi, P. & **Rio, D.** (1981) - Stratigrafia delle formazioni dell'Appennino Settentrionale. Nota I: biostratigrafia a nannofossili e cronostratigrafia della formazione delle Marne di Monte Piano nella località tipo in media Val Taro (Appennino Parmense) - *Acta Naturalia*, v. **17**/3-4, 149-168.

Vescovi, P. (1993) - Schema evolutivo per le liguridi dell'Appennino settentrionale. -*Atti.Tic.Sc.Terra*, vol. **36**, 89-112.

Vollmer, F.W. & **Bosworth, W.** (1984) - Formation of melange in a foreland basin overthrust setting: Example from the Taconic Orogen - *Geol. Soc. of America Special*; P. **198,** 53-70.

Vries Klein, G., Melo, U. & **Della Favera, J.C.** (1972) – Subaqueous Gravity Processes on the Front of Cretaceous Deltas, Recôncavo Basin, Brazil – *Geol. Soc. of America Bulletin*; v. **83**, 1.469-1.492.

Wardlaw, N.C. (1972) - Syn-Sedimentary Folds and Associated Structures in Cretaceous Salt Deposits of Sergipe, Brazil **-** *Journal of Sedimentary Research*, v. **42**, 120-132. DOI: 10.1306/74D725BD-2B21-11D7-8648000102C1865D

Weimer, P. & **Shipp, R.C.** (2004) – Mass Transport Complex: Musing on Past Uses and Suggestions for Future Directions - *Offshore Technology Conference, Houston*; paper n°16752.

Weimer, P. (1989) – Sequence stratigraphy of the Mississippi Fan (Plio-Pleistocene), Gulf of Mexico – *Geo-Marine Letters*; v. **9**, 185-272.

Weimer, P. (1990) - Sequence Stratigraphy, Facies Geometries, and Depositional History of the Mississippi Fan, Gulf of Mexico **-** *AAPG Bulletin*, v. **74**/4, 425 – 453.

Wiedicke, M., Sahling, H., Delisle, G., Faber, E., Neben, S., Beiersdorf, H., Marchig, V., Weiss, W., von Mirbach, N. & Açat, A. (2002) - Characteristics of an active vent in the fore-arc basin of the Sunda Arc, Indonesia - *Marine Geology*, v. **184**, 121-141.

Williams, P.R., **Pigram, C.J.**, & **Dow, D.B.** (1984) - Mélange production and the importance of shale diapirism in accretionary terranes - *Nature*; v. **309**, 145-146.

Wilson, C.K., Long, D. & Bulat, J. (2004) - The morphology, setting and processes of the Afen Slide - *Mar. Geol.*, v. **213**, 149–167.

Winker, C.D. & Booth, J.R. (2000) – Sedimentary dynamics of the salt-dominated continental slope, Gulf of Mexico: integration of observations from the seafloor, near-surface, and deep subsurface – GCSSEPM Foundation 20th Annual Research conferente, Deep-Water Reservoirs of the World, December 3-6, 1059-1086.

Winkler, C.D. (1996) - High resolution seismic stratigraphy of a late Pleistocene submarine fan ponded by salt withdrawal mini-basin on the Gulf of Mexico Continental Slope - *Proceedings of Offshore Technology Conference*, Houston, Texas, 6–9 May 1996, Paper OTC 8024, 619–628.

Wood, R., Herzer, R., Sutherland, R. & Melhuish, A. (2000) - Cretaceous-Tertiary tectonic history of the Fiordland margin, New Zealand - *New Zealand Journal of Geology & Geophysics,* v. **43**, 289-302.

Woodcock, N.H. (1976) - Structural style in slump sheets; Ludlow Series, Powys, Wales **-** *Journal of the Geological Society of London*, v. **132**/ 4, 399-415.

Woodcock, N.H. (1979) - The use of slump structures as palaeoslope orientation estimators – *Sedimentology*, v. **26**/1, 83 – 99.

Wynn, R.B., Masson, D.G., Stow, D.A.V. & Weaver, P.P.E. (1999) - The Northwest African slope apron: a modern analogue for deep water systems with complex seafloor topography - *Marine and Petroleum Geology*, v. **6**, 142-154.

Yamada, Y, Yamashita, Y. & Yamamoto, Y. (2009) - Submarine landslides at subduction margins: Insights from physical models - *Tectonophysics*, doi: 10.1016/j.tecto.2009.09.007

Yamamoto, Y., Ogawa, Y., Uchino, T., Muraoka, S. & Chiba, T. (2007) - Large-scale chaotically mixed sedimentary body within the Late Pliocene to Pleistocene Chikura Group, Central Japan - *Island Arc*, vol. **16**, 505–507.

Yu, H.S. & Huang, Z.Y. (2006) - Intraslope Basin, Seismic Facies and Sedimentary Processes in the Kaoping Slope, Offshore Southwestern Taiwan **-** *Terr. Atmos. Ocean. Sci.*, v. **17**/4, 659-677.

Yu, H.-S. & Song, G.-S. (1993) – Submarine physiography around Taiwan and its relation to tectonic setting - *Journal of the Geological Society of China*, v. **36**/2, 139-156.

Yu, H.-S., Chiang, C.-S. & Shen, S.-M. (2008) - Tectonically active sediment dispersal system in SW Taiwan margin with emphasis on the Gaoping (Kaoping) Submarine Canyon - *Journal of Marine Systems*, xxx, xxx–xxx.

Zachos, J.C., Quinn, T.M. & Salamy, S. (1996) - High-resolution (10^4 years) deep-sea foraminiferal stable isotope records of the Eocene-Oligocene climate transition – *Paleoceanography*; v. **11**/3, 251-266.

Zanzucchi G. (1980) - I lineamenti geologici dell'Appennino parmense. Note illustrative alla Carta Geologica e Sezioni Geologiche della Provincia di Parma e zone limitrofe (1:100.000) - *Volume dedicato a Sergio Venzo, STEP Parma.*

Zanzucchi, G. (1982) - Il substrato alloctono nell'Appennino emiliano - *In*: G. Cremonini & F. Ricci Lucchi (Eds.), *Guida alla geologia del margine appenninico-padano*, **3-8**, *Guide Geol. Reg. S.G.I., Bologna*.

Zanzucchi, G. (Ed.) (1994) – Appennino Ligure-Emiliano – *Guide Geologiche Regionali*, *Società Geologica Italiana*,

v. **6**, 382 pp..

Zuffa, G.G. (1966) – Le Arenarie "Tongriane" di Monte Barigazzo (Parma) - *unpublished MSc thesis*, Università di Bologna.